WILEY-VCH

Tharwat Tadros

Formulation of Disperse Systems

Science and Technology

Tharwat F. Tadros

Formulation of Disperse Systems

Related Titles

Norton, J.E., Fryer, P., Norton, I.

Formulation Engineering of Foods

2013

Print ISBN: 978-0-470-67290-7

Douroumis, D. (ed.)

Drug Delivery Strategies for Poorly Water-Soluble Drugs

2013

Print ISBN: 978-0-470-71197-2

Kirk-Othmer (ed.)

Kirk-Othmer Chemical Technology of Cosmetics

2013

Print ISBN: 978-1-118-40692-2

Rosen, M.J., Kunjappu, J.T.

Surfactants and Interfacial Phenomena

Fourth Edition

2012

Pensé-Lhéritier, A.

Formulation

2011

Print ISBN: 978-1-848-21259-6

Tsotsas, E., Mujumdar, A.S. (eds.)

Modern Drying Technology

Volume 3: Product Quality and Formulation

2011

Print ISBN: 978-3-527-31558-1

Jameel, F., Hershenson, S. (eds.)

Formulation and Process Development Strategies for Manufacturing Biopharmaceuticals

2010

Print ISBN: 978-0-470-11812-2

Tadros, T.F.

Rheology of Dispersions

Principles and Applications

2010

Print ISBN: 978-3-527-32003-5

Tharwat F. Tadros

Formulation of Disperse Systems

Science and Technology

WILEY-VCH
Verlag GmbH & Co. KGaA

The Author

Prof. Dr. Tharwat F. Tadros
89 Nash Grove Lane
RG40 4HE Wokingham, Berkshire
United Kingdom

Library of Congress Card No.: applied for

British Library Cataloguing-in-Publication Data
A catalogue record for this book is available from the British Library.

Bibliographic information published by the Deutsche Nationalbibliothek
The Deutsche Nationalbibliothek lists this publication in the Deutsche Nationalbibliografie; detailed bibliographic data are available on the Internet at <http://dnb.d-nb.de>.

Print ISBN: 978-3-527-33682-1
ePDF ISBN: 978-3-527-67832-7
ePub ISBN: 978-3-527-67830-3
mobi ISBN: 978-3-527-67831-0
oBook ISBN: 978-3-527-67829-7

Cover Design Adam Design, Weinheim, Germany
Typesetting Laserwords Private Limited, Chennai, India
Printing and Binding Markono Print Media Pte Ltd., Singapore

Printed on acid-free paper

Contents

Preface

Several disperse systems can be identified, including solid/liquid (suspensions), liquid/liquid (emulsions) and their mixtures (suspoemulsions), gas/liquid (foams), nanodispersions (with particle sizes in the range 20–200 nm), microemulsions, dispersions of pigments and inks, and latexes. These disperse systems exist in many industrial applications such as paints, paper coatings, dyestuffs, printing inks, agrochemicals and pharmaceuticals. The formulation of these complex multiphase systems is still an art, and in most cases they are produced by industrial chemists using simple trial-and-error techniques. Apart from being time-consuming, this approach does not provide a rational understanding on how a system is arrived at. In addition, whenever a problem arises – such as instability and separation of the formulation on storage – the formulation chemist may struggle to find a solution for the resulting instability.

This book has been written to set the fundamental basis of the formulation of the various types of disperse systems. It starts (Chapter 1) with a general introduction of the different types of disperse systems, while Chapter 2 provides a brief description of the various surfactant classes used in the formulations. Chapter 3 describes the physical chemistry of surfactant solutions, with emphasis placed on the process of micellisation, while the various dispersants and polymers used for stabilisation of disperse systems, and the criteria required for an effective dispersant are summarised in Chapter 4. Chapter 5 describes the adsorption of surfactants at the air/liquid, liquid/liquid, and solid/liquid interfaces, with details given of the adsorption process and its effect on the surface, interfacial, and solid/liquid tensions. In Chapter 6, an account is provided of the adsorption of polymeric surfactants at the solid/liquid interface, with emphasis on the general behaviour of polymer adsorption and its irreversibility. Chapter 7 describes the colloid stability of disperse systems containing electrical double layers, and the combination of electrostatic repulsion with van der Waals attraction is used to describe the theory of colloid stability. Chapter 8 describes the stability of disperse systems containing adsorbed nonionic surfactants or polymers referred to as steric stabilisation, while Chapter 9 describes the formulation of solid/liquid dispersions (suspensions). The preparation of suspensions by condensation (nucleation and growth) and dispersion methods are also described, with the stabilisation of suspensions using electrostatic and/or steric repulsion being described in terms of the various interaction forces. Chapter 10 deals with the formulation of liquid/liquid dispersions (emulsions). Here, the various methods that can be applied for selection of emulsifiers are described, and this is followed by an analysis of the stability/instability of emulsions, namely creaming or sedimentation, flocculation, Ostwald ripening, coalescence, and phase inversion. Chapter 11 describes the formulation of suspoemulsions (mixtures of suspensions and emulsions), and the application of suspoemulsions in agrochemicals, cosmetics and paints is briefly described. Chapter 12 deals with formulation of multiple emulsions: water-in-oil-in-water (W/O/W) and oil-in-water-in-oil (O/W/O) systems. The structure of multiple emulsions and their breakdown processes are described, and this is followed by a section on the preparation of multiple emulsions using a two-stage process. Chapter 13 describes the methods of preparation of nanosuspensions, and details of the application of nanosuspensions in cosmetics and drug delivery are given. The preparation of nanosuspensions, using top-up (starting from molecular units) and bottom-down (by comminution of larger particles) processes is also described. Chapter 14 deals with the formulation of nanoemulsions and the factors relating to their transparency; the advantages of nanoemulsions in personal products and healthcare products are also summarised. Chapter 15 deals with the formulation of microemulsions and the surfactant composition, with definition being provided of microemulsions and the origin of their thermodynamic stability. Theories of the stability of microemulsions are also outlined. Chapter 16 deals with the formulation of foams, starting with the factors responsible for foam formation, and the stability/instability of foams and the role of surfactants are described. Chapter 17 describes the formulation of latexes and methods of their preparation by emulsion and dispersion polymerisation, while Chapter 18 deals with the formulation of pigments and inks, and provides details of the various pigment types and their general properties. The colloid stability of pigment dispersions in terms of electrostatic, steric and electrosteric forces is also described. Chapter 19 describes the methods for evaluating formulations after dilution, starting with optical microscopy and particle size distribution using image analysis, phase contrast, differential interference contrast and polarising microscopy. This is followed by the various scattering methods, including time average light scattering, turbidity, light diffraction, dynamic light scattering and back-scattering techniques. Chapter 20 describes the methods used for the evaluation of formulations without dilution, namely rheological techniques; steady-state shear stress-shear rate measurements and the flow curves are also described, as are constant stress (creep) measurements and measurement of the residual (zero shear) viscosity. This is followed by investigations of stress relaxation after the sudden application of strain, and the dynamic (oscillatory) methods and evaluation of the elastic and viscous components are described. Finally, Chapter 21 deals with the methods that can be applied for the assessment and prediction of creaming or sedimentation, flocculation and coalescence. In addition, accelerated tests for the evaluation of stability using temperature changes and centrifugation, and their limitations, are described. The rheological methods that can be applied for the prediction of creaming or sedimentation, flocculation and coalescence are also described.

This book will be valuable for industrial scientists engaged in the formulation of disperse systems, and should provide them with a more rational approach of how to formulate a product. In addition, it should enable the formulation scientist to better understand the fundamental basis of the factors responsible for producing a stable formulation with an acceptable shelf life. The book should also be very useful for teaching the subject of formulation at academic institutions.

November 2013 *Tharwat Tadros*

1
General Introduction

Several classes of formulations of disperse systems are encountered in the chemical industry, including suspensions, emulsions, suspoemulsions (mixtures of suspensions and emulsions), nanoemulsions, multiple emulsions, microemulsions, latexes, pigment formulations, and ceramics. For the rational preparation of these multiphase systems it is necessary to understand the interaction forces that occur between the particles or droplets. Control of the long-term physical stability of these formulations requires the application of various surfactants and dispersants. It is also necessary to assess and predict the stability of these systems, and this requires the application of various physical techniques.

A brief description of the various formulation types is provided in the following sections.

1.1
Suspensions

These are by far the most commonly used systems for the formulation of insoluble solids. The solid can be hydrophobic, such as most organic materials that are used in pharmaceuticals, agrochemicals, and paints; the solid can also be hydrophilic, such as silica and clays. With some pigments and inks the particles need to be very small – that is, in the nanosize range – and these are referred to as nanosuspensions. Latexes may also be considered as suspensions, particularly if the particles are solid-like at ambient temperatures. With many of the latexes that are used in paints the particles are liquid-like at below and ambient temperature, but when applied to a surface these liquid-like particles coalesce to form a uniform film. The system may then be considered as an emulsion.

For the formulation of suspensions, the hydrophobic or hydrophilic solid is dispersed in a aqueous or nonaqueous medium to produce a system that covers a wide particle size range, typically 0.1–5 μm. This process requires the presence of a surfactant (dispersant) that satisfies four criteria: (i) wetting of the powder by the liquid; (ii) the dispersion of aggregates and agglomerates into single units; (iii) comminution of the large particles into smaller units; and (iv) stabilisation

Formulation of Disperse Systems: Science and Technology, First Edition. Tharwat F. Tadros.

of the resulting dispersion against flocculation and crystal growth. The choice of wetting/dispersing agent is crucial for achieving this control.

1.2
Latexes

As mentioned above, latexes may be considered as suspensions and are prepared using two main processes:

(i) Emulsion polymerisation: In this case the monomer, for example styrene or methylmethacrylate, is emulsified in water using an appropriate surfactant. An initiator such as potassium persulphate is then added and the system is heated to produce the polymer particles. Initiation mostly occurs in the monomer swollen micelles, and the number of particles produced and their size depends on the number of micelles.
(ii) Dispersion polymerisation: The monomer is dissolved in a solvent in which the resulting polymer particles are insoluble. An initiator that is soluble in the solvent is added to start the polymerisation process. A protective agent that strongly adsorbs onto the particle surface (or becomes incorporated in the particle) is simultaneously added to prevent aggregation of the particles. The protective agent is a block (A-B or A-B-A) or graft (Ban) copolymer. B is the ‘‘anchor’’’ chain that is chosen to be insoluble in the medium and has a strong affinity to the surface, while A is the stabilising chain that is highly soluble in the medium and is strongly solvated by its molecules. This provides a strong steric repulsion.

1.3
Emulsions

These are dispersions of liquid drops in an immiscible liquid medium. The most common systems are oil-in-water (O/W) and water-in-oil (W/O). It is also possible to disperse a polar liquid into an immiscible nonpolar liquid, and vice versa; these are referred to as oil-in-oil (O/O) emulsions. In order to disperse a liquid into another immiscible liquid, a third component is needed that is referred to as the emulsifier. Emulsifiers are surface-active molecules (surfactants) that adsorb at the liquid/liquid interface, thus lowering the interfacial tension and hence the energy required for emulsification is reduced. The emulsifier plays several other roles: (i) it prevents coalescence during emulsification; (ii) it enhances the deformation and break-up of the drops into smaller units; (iii) it prevents flocculation of the emulsion by providing a repulsive barrier that prevents close approach of the droplets to prevent van der Waals attraction; (iv) it reduces or prevents Ostwald ripening (disproportionation); (v) it prevents coalescence of the drops; and (vi) it prevents phase inversion.

1.4
Suspoemulsions

These are mixture of suspensions and emulsions that can be produced by mixing two separately prepared suspensions and emulsions. Suspoemulsions may also be produced by the emulsification of an oil into a prepared suspension, or dispersing a solid an emulsion. Several instability processes may occur in these systems: (i) homoflocculation, whereby the suspension particles and emulsion drops form separate flocs; (ii) heteroflocculation, whereby the suspension particles and emulsion drops form combined flocs; and (iii) phase transfer and crystal growth. The solid particles can enter the emulsion droplets, but when they leave the droplets they may grow to form large crystals.

1.5
Multiple Emulsions

These are complex systems of emulsions of emulsions. Two types may be identified:

(i) Water-in-Oil-in-Water (W/O/W), whereby the oil droplets of an O/W emulsion contain emulsified water droplets. These are generally produced via a two-step process: a W/O emulsion is first prepared using a low-hydrophilic–lipophilic-balance (HLB) which is then emulsified into an aqueous solution of a high-HLB surfactant.
(ii) Oil-in-Water-in-Oil (O/W/O), where an O/W emulsion that has been prepared using a high-HLB surfactant is emulsified into an oil solution of a low-HLB surfactant.

It is also possible to prepare multiple emulsions consisting of nonpolar oil droplets with emulsified polar oil droplets which are dispersed in an aqueous solution or another polar oil. With W/O/W multiple emulsions it is essential to control the osmotic balance between the internal water droplets and the external continuous phase.

Several breakdown processes may be identified with multiple emulsions:

- Expulsion of the water droplets from the multiple emulsion drop to the external phase. This may result in the production of an O/W emulsion.
- Coalescence of the water droplets in the W/O/W multiple emulsion or the oil droplets in the O/W/O system.
- Flocculation of the multiple emulsion drops that would be accompanied by an increase in the viscosity of the system.
- Coalescence of the multiple emulsion drops with the ultimate formation of a W/O emulsion.
- Diffusion of the active ingredients from the internal droplets to the external continuous phase.

1.6
Nanosuspensions

These are suspensions with a size range of 20 to 200 nm. Like suspensions, they are kinetically stable but, due to the small size of the particles, they have much longer physical stability: (i) an absence of sedimentation, as the Brownian motion is sufficient to prevent separation by gravity; and (ii) an absence of flocculation, as the repulsive forces (electrostatic and/or steric) are much larger than the weak van der Waals attraction.

Nanosuspensions can be prepared by two main process:

(i) Top-up processes, whereby one starts with molecular components that can grow by a process of nucleation and growth process.
(ii) Bottom-down processes, whereby the large particles are subdivided by application of intense energy, for example using high-pressure homogenisers or bead milling.

The resulting nanosuspensions must be maintained colloidally stable by using surfactants and/or polymers that provide an effective energy barrier against flocculation.

1.7
Nanoemulsions

These are emulsion systems with a size range of 20 to 200 nm. Like emulsions, they are only kinetically stable but, due to the very small size, they have much longer physical stability:

- The very small droplets prevent any creaming or sedimentation, as the Brownian diffusion is sufficient to prevent separation by gravity.
- The small droplets have much smaller van der Waals attraction, and flocculation is prevented. This is particularly the case with sterically stabilised systems.
- The small droplets prevent coalescence, as surface fluctuation is not possible and the liquid film between the droplets that has an appreciable thickness prevents any thinning or disruption of that film.

The major instability process of nanoemulsions is Ostwald ripening, which results from the difference in solubility between the small and larger drops. The smaller droplets with a higher curvature have a greater solubility than the larger droplets. On storage, the droplet size distribution shifts to larger sizes and, ultimately, the nanoemulsion will become an emulsion with larger sizes. Nanoemulsions can be transparent, translucent or turbid, depending on two main parameters: the droplet size distribution and the difference in refractive index between the disperse and continuous phases.

1.8
Microemulsions

These are transparent or translucent systems covering the size range from 5 to 50 nm. Unlike emulsions and nanoemulsions (which are only kinetically stable), microemulsions are thermodynamically stable as the free energy of their formation is either zero or negative. Microemulsions are better considered as swollen micelles: normal micelles can be swollen by some oil in the core of the micelle to form O/W microemulsions. Reverse micelles can be swollen by water in the core to form W/O microemulsions.

The driving force for microemulsion formation is the ultra-low interfacial tension which is normally obtained by using two surfactants: one which is predominantly oil-soluble (such as a medium-chain alcohol) and one which is predominantly water-soluble (such as an anionic surfactant). The low tension results in a low interfacial energy which can be overcompensated by the entropy of dispersion. Microemulsions require the use of a high surfactant concentration. For example, for a 20% microemulsion the surfactant concentration will be in the range 10–20%.

1.9
Pigment and Ink Dispersions

Pigments are used in many industrial applications, such as paints and dyestuffs. One of the most widely used white pigments is titanium dioxide, which is applied in white paints (undercoat and overcoat) and in sunscreens (for protection against UV light). Several dispersions of titanium dioxide are formulated that require an optimum particle size distribution for particular application. In paints, the particle size distribution is controlled to give maximum hiding power (high reflection of light), whereas for sunscreens the particle size distribution is controlled to give maximum UV adsorption. Both, aqueous and nonaqueous titanium dioxide dispersions are formulated, and these require the use of efficient dispersing agents. Several other coloured pigments of inorganic and organic materials are also formulated both for dyestuff, paint and ink jet applications. These dispersions are generally in the submicron size (nanodispersions), and they require the use of efficient wetting, dispersing and milling agents. It is also essential to control the physical stability of these nanosuspensions, both on storage and on application. Strong repulsive barriers, whether electrostatic, steric and/or electrosteric (a combination of electrostatic and steric), are essential to prevent any aggregation.

1.10
Foams

Foams are gas-in-liquid dispersions that may be obtained as either aqueous or nonaqueous forms. In some cases a highly stable foam is required, for example in fire-fighting foams and in many food products, whereas in other cases the destruction of a foam may be required, for example during the preparation of suspensions or emulsions. An antifoaming agent or a defoamer is required to prevent foam formation. Several theories are available that can describe the stability/instability of foams. One of the most acceptable of these is the production of a high interfacial elasticity (Gibbs dilational elasticity) which promotes the flow of liquid between the air bubbles (Marangoni effect). The concept of a disjoining pressure, as described by Deryaguin, has also been introduced to explain foam stability.

This book, on the formulation of disperse systems, is organised as follows. Chapter 2 will provide a brief description of the various surfactant classes that are used in the formulations, while Chapter 3 describes the physical chemistry of surfactant solutions, with emphasis placed on the process of micellisation. Chapter 4 summarises the various dispersants and polymers used for stabilisation of disperse systems, and the criteria for an effective dispersant are described. Chapter 5 describes the adsorption of surfactants at the air/liquid, liquid/liquid, and solid/liquid interfaces, together with details of the adsorption process and its effect on the surface, interfacial and solid/liquid tensions. The theoretical analysis of the adsorption process, using the Gibbs and Langmuir adsorption isotherms and area occupied by a surfactant molecule is described. Measurement of the surfactant adsorption at various interfaces is also described. Chapter 6 provides an account of the adsorption of polymeric surfactants at the solid/liquid interface, and the general behaviour of polymer adsorption and its irreversibility are also emphasised. Theories of polymer adsorption and the experimental determination of adsorption parameters are also briefly described. Chapter 7 describes the colloid stability of disperse systems containing electrical double layers. Various models of the electrical double layer at charged interfaces are described, and this is followed by a description of the interaction between particles or droplets containing electrical double layers. The van der Waals attraction between particles or droplets is analysed, and the combination of electrostatic repulsion with van der Waals attraction is used to describe the theory of colloid stability. The parameters that determine the stability/instability of disperse systems are summarised, and this is followed by a section on the flocculation of dispersions, with both fast and slow flocculation processes being described. Chapter 8 describes the stability of disperse systems containing adsorbed nonionic surfactants or polymers, referred to as steric stabilisation. The interaction between particles or droplets containing adsorbed nonionic surfactants or polymers is described in terms of mixing and elastic (entropic) interactions. A combination of the mixing and elastic terms with van der Waals attraction describes the theory of steric stabilisation and the criteria for its effectiveness. The flocculation of sterically stabilised dispersions both weak and strong is described. Chapter 9 describes the formulation of solid/liquid dispersions (suspensions), and details are provided of the preparation of suspensions by condensation (nucleation and growth) and dispersion methods. The factors affecting each process and the role of surfactants are also briefly described, and the process of powder wetting and dispersion, and their evaluation, is analysed in terms of the surface forces involved. The stabilisation of suspensions, using electrostatic and/or steric repulsion, is described in terms of the various interaction forces. The properties of concentrated suspension and their states on storage are described. Ostwald ripening (crystal growth) and its prevention is described. The distinction between colloid and physical stability is described in terms of the interaction forces and the effect of gravity. The final part of the chapter describes the process of sedimentation of suspensions and methods for its prevention. Chapter 10 deals with the formulation of liquid/liquid dispersions (emulsions), and the description of emulsion systems and their classification, depending on the nature of the emulsifier or the structure of the system, is discussed. This is followed by a section on the thermodynamics of emulsion formation and stability. The methods of emulsification and the role of the surfactant are also described, as are the various methods that can be applied for the selection of emulsifiers. This followed by analysis of the stability/instability of emulsions, namely creaming or sedimentation, flocculation, Ostwald ripening, coalescence, and phase inversion. The methods that can be applied for the prevention of emulsion instability are given. Chapter 11 describes the formulation of suspoemulsions (mixtures of suspensions and emulsions), with the application of suspoemulsions in agrochemicals, cosmetics and paints being briefly described. The various interactions in suspoemulsions, namely homoflocculation and heteroflocculation, coalescence and crystallisation are described. The reduction of heteroflocculation using polymeric surfactants, and the prevention of creaming and sedimentation and recrystallisation in suspoemulsions is also described. Chapter 12 deals with the formulation of multiple emulsions, notably W/O/W and O/W/O systems. The structure of multiple emulsions and their breakdown processes are also described, and this is followed by a section on the preparation of multiple emulsions using a two-stage process. The characterisation of multiple emulsions using droplet size analysis and rheology is also described. Chapter 13 describes the methods of preparation of nanosuspensions, and the application of nanosuspensions in cosmetics and drug delivery is outlined. The preparation of nanosuspensions by top-up (starting from molecular units) and bottom-down (by the comminution of larger particles) processes is described, with emphasis placed on the factors determining each process: nucleation and growth (top-up process), wetting, dispersion, and the comminution of larger particles (bottom-down process). The role of surfactants and dispersants in each process and maintenance of the stability of nanoparticles against flocculation and crystal growth is also described. Chapter 14 deals with the formulation of nanoemulsions and the factors that control their transparency. The advantages of nanoemulsions in personal and health care are summarised, and this is followed by a section on the preparation of nanoemulsions using high-pressure homogenisers and low-energy emulsification methods, including phase inversion composition (PIC) and phase inversion temperature (PIT) methods. The origin of the high kinetic stability of nanoemulsions is described in terms of the interaction forces between the droplets, and this is followed by a section on the Ostwald ripening of nanoemulsions, and its reduction. Examples of nanoemulsions based on nonionic and polymeric surfactants are given. Chapter 15 deals with the formulation of microemulsions and the surfactant composition. The definition of microemulsions and the origin of their thermodynamic stability is described; this is followed by a section on the phase diagrams of ternary (water-surfactant-cosurfactant) and quaternary (water-oil-surfactant-cosurfactant) systems and identification of the microemulsion region. Theories of the stability of microemulsions are also briefly described, as are the characterisation of microemulsions using scattering methods, conductivity and NMR. Chapter 16 deals with the formulation of foams, starting with the factors responsible for foam formation; the stability/instability of foams and the role of surfactants are also described. This is followed by a section on the theories of foam stability, and a description of antifoamers and defoamers is given. Applications of foam in the food industry, mineral flotation, wall insulation and enhanced oil recovery are illustrated. Chapter 17 describes the formulation of latexes and the methods of their preparation by emulsion and dispersion polymerisation; both, aqueous and oil-based latexes are described. The commonly used surfactants in emulsion and dispersion polymerisation are described, together with their role in each process. The application of latexes in paints and coatings is described, with particular reference to the factors affecting film formation. Chapter 18 deals with the formulation of pigments and inks. The various pigment types and their general properties are outlined, and the particle size and shape of pigments and the nature of the pigment surfaces are described. The wetting of pigment powders, and their deagglomeration and comminution, is described at a fundamental level, with particular reference to the role of surfactants and dispersants. The colloid stability of pigment dispersions in terms of electrostatic, steric and electrosteric forces is described. The application of pigment dispersions in paints, sunscreens and colour cosmetics is briefly described. Chapter 19 describes the methods of evaluation of formulations after dilution. The chapter starts with optical microscopy and particle size distribution using image analysis, phase contrast, differential interference contrast and polarising microscopies. A brief summary of scanning and transmission electron microscopies, confocal laser scanning microscopy, and atomic force microscopy is given. This is followed by the various scattering methods, including time average light scattering, turbidity, light diffraction, dynamic light scattering and back-scattering techniques. Chapter 20 describes the methods of evaluation of formulations without dilution, namely rheological techniques. The steady-state shear stress-shear rate measurements and the flow curves are described, together with the models that can be applied for fitting the flow curves and the evaluation of rheological parameters. The time effects during flow (thixotropy) and methods of their evaluation are described. The constant stress (creep) measurements and measurement of the residual (zero shear) viscosity are also described, followed by the investigation of stress relaxation after the sudden application of strain. The dynamic (oscillatory) methods and evaluation of the elastic and viscous components are described, with particular emphasis on calculation of the cohesive energy density of the structure formed. Chapter 21 deals with the methods that can be applied for the assessment and prediction of creaming or sedimentation, flocculation and coalescence. The accelerated tests for the evaluation of stability using temperature changes and centrifugation, and their limitations, are described. The rheological methods that can be applied for the prediction of creaming or sedimentation are described, showing a correlation of the rate with the residual (zero shear) viscosity. The prediction of formulation separation (syneresis), using modulus and cohesive energy density measurements, is described, and this is followed by the application of steady-state measurements for the prediction of formulation flocculation. The application of creep tests and dynamic (oscillatory) techniques for the prediction of flocculation is described, as is the measurement of emulsion coalescence rate by following the droplet number or average droplet size with time. The correlation of coalescence with a reduction of viscosity in the absence of flocculation and/or Ostwald ripening is also shown. Finally, the application of dynamic (oscillatory) methods for the prediction of emulsion coalescence is illustrated.

References

1. Tadros, T.F. (ed.) (1984) *Surfactants*, Academic Press, London.
2. T. Tadros (2005) *Applied Surfactants*, Wiley-VCH Verlag GmbH, Weinheim.
3. Holmberg, K., Jonsson, B., Kronberg, B., and Lindman, B. (2003) *Surfactants and Polymers in Solution*, 2nd edn, John Wiley & Sons, Ltd, Chichester.
4. Parfitt, G.D. and Rochester, C.H. (eds) (1983) *Adsorption from Solution at the Solid/Liquid Interface*, Academic Press, London.
5. Verwey, E.J.W. and Overbeek, J.T.G. (1948) *Theory of Stability of Lyophobic Colloids*, Elsevier, Amsterdam.
6. Napper, D.H. (1983) *Polymeric Stabilisation of Colloidal Dispersions*, Academic Press, London.
7. Tadros, T.F. (ed.) (1987) *Solid/Liquid Dispersions*, Academic Press, London.
8. Tadros, T. (ed.) (2013) *Emulsion Formation and Stability*, Wiley-VCH Verlag GmbH, Weinheim.
9. Exerowa, D. and Kruglyakov, P.M. (1997) *Foam and Foam Films*, Elsevier, Amsterdam.
10. Tadros, T. (2010) *Colloids in Paints*, Wiley-VCH Verlag GmbH, Weinheim.
11. Tadros, T. (2010) *Rheology of Dispersions*, Wiley-VCH Verlag GmbH, Weinheim.

2

Surfactants Used in Formulation of Dispersions

Surface-active agents (usually called surfactants) are sometimes referred to as amphiphilic molecules, which implies that they consist of at least two parts, one part which is soluble in a specific liquid (the lyophilic part) and one part which is insoluble (the lyophobic part). If the fluid is water, then one refers to the hydrophilic and hydrophobic parts, respectively. In this case, the molecule consists of a nonpolar hydrophobic portion; this is usually a straight or branched hydrocarbon or fluorocarbon chain containing between eight and 18 carbon atoms, which is attached to a polar or ionic portion (hydrophilic). The hydrophilic portion can, therefore, be nonionic, ionic, or zwitterionic, and is accompanied by counterions in the last two cases. The hydrocarbon chain interacts weakly with the water molecules in an aqueous environment, whereas the polar or ionic head group interacts strongly with water molecules via dipole or ion–dipole interactions. It is this strong interaction with the water molecules which renders the surfactant soluble in water. However, the cooperative action of dispersion and hydrogen bonding between the water molecules tends to squeeze the hydrocarbon chain out of the water, and hence these chains are referred to as hydrophobic. The balance between the hydrophobic and hydrophilic parts of the molecule gives these systems their special properties, for example their accumulation at various interfaces and their association in solution (to form micelles). In addition to the name surface-active agents, these molecules are often known by other names which include surfactants, association colloids, colloidal electrolytes, amphipathic compounds, and tensides.

The driving force for surfactant adsorption is a lowering of the free energy of the phase boundary. The interfacial free energy per unit area is the amount of work required to expand the interface. This interfacial free energy, referred to as surface or interfacial tension, γ, is given in millijoules per metre square or millinewtons per metre. The adsorption of surfactant molecules at the interface lowers γ, and the higher the surfactant adsorption (i.e., the more dense the layer is) the larger is the reduction in γ. The degree of surfactant adsorption at the interface depends on surfactant structure and the nature of the two phases that meet the interface [1, 2]. Surface-active agents also aggregate in solution-forming micelles. The driving force of micelle formation (or micellisation) is a reduction of contact between the hydrocarbon chain and water, thereby reducing the free energy of the system. In

Formulation of Disperse Systems: Science and Technology, First Edition. Tharwat F. Tadros.

the micelle, the surfactant hydrophobic groups are directed towards the interior of the aggregate, while the polar head groups are directed towards the solvent. These micelles are in dynamic equilibrium, and the rate of exchange between a surfactant molecule and the micelle may vary by orders of magnitude, depending on the structure of the surfactant molecule.

Surfactants find application in almost all disperse systems that are utilised in areas such as paints, dyestuffs, cosmetics, pharmaceuticals, agrochemicals, fibres, and plastics. Therefore, a fundamental understanding of the physical chemistry of surface-active agents, their unusual properties, and their phase behaviour is essential for most formulation chemists. In addition, an understanding of the basic phenomena involved in the application of surfactants, such as in the preparation of emulsions and suspensions and their subsequent stabilisation, in microemulsions, in wetting, spreading and adhesion, is vitally important to arrive at the correct composition and control of the system involved [1, 2]. This is particularly the case with many formulations in the chemical industry mentioned above.

It should be stated that commercially produced surfactants are not pure chemicals, and within each chemical type there can be tremendous variation. This is understandable as surfactants are prepared from various feedstocks, namely petrochemicals, natural vegetable oils and natural animal fats. It is important to realize that, in every case, the hydrophobic group exists as a mixture of chains of different lengths. The same can be applied to the polar head group, for example in the case of polyethylene oxide (PEO) (the major component of nonionic surfactants) which consists of a distribution of ethylene oxide (EO) units. Hence, products that may be given the same generic name might vary a great deal in their properties, and the formulation chemist should bear this in mind when choosing a surfactant from a particular manufacturer. It is advisable to obtain as much information as possible from the manufacturer about the properties of the surfactant chosen, such as its suitability for the job, its batch-to-batch variation, and its toxicity. The manufacturer will usually have available more information on the surfactant than is printed on the accompanying data sheet, and in most cases such extra data will be given on request.

2.1
General Classification of Surface-Active Agents

A simple classification of surfactants, based on the nature of the hydrophilic group, is commonly used, with four main classes being distinguished: anionic; cationic; amphoteric; and nonionic. A useful technical reference here is McCutcheon [3], which is produced annually to update the list of available surfactants. A recent text by van Os *et al.* [4], listing the physico-chemical properties of selected anionic, cationic and nonionic surfactants, has been published by Elsevier.

Another useful text is the *Handbook of Surfactants* by Porter [5]. It should be mentioned also that a fifth class of surfactants, usually referred to as polymeric surfactants, has been used for many years for the preparation of emulsions and suspensions, and for their stabilisation.

2.1.1
Anionic Surfactants

These are the most widely used class of surfactants in industrial applications [5–7], due mainly to their relatively low cost of manufacture, and they are used in practically every type of detergent. For optimum detergency the hydrophobic chain is a linear alkyl group with a chain length in the region of 12–16 C atoms, and the polar head group should be at the end of the chain. Linear chains are preferred as they are more effective and more degradable than are branched chains. The most commonly used hydrophilic groups are carboxylates, sulphates, sulphonates and phosphates. A general formula may be ascribed to anionic surfactants as follows:

Carboxylates: C_nH_{2n+1} $COO^- X^+$
Sulphates: C_nH_{2n+1} $OSO_3^- X^+$
Sulphonates: C_nH_{2n+1} $SO_3^- X^+$
Phosphates: C_nH_{2n+1} $OPO(OH)O^- X^+$.

where n is in the range of eight to 16 atoms and the counterion X^+ is usually Na^+.

Several other anionic surfactants are commercially available, such as sulphosuccinates, isethionates (esters of isothionic acid with the general formula $RCOOCH_2$-CH_2-SO_3Na) and taurates (derivatives of methyl taurine with the general formula $RCON(R')CH_2$-CH_2-SO_3Na), sarcosinates (with the general formula RCON(R′)COONa), and these are sometimes used for special applications. A brief description of the above-described anionic classes is provided below, together with some of their applications.

2.1.1.1 Carboxylates

These are perhaps the earliest known surfactants, as they constitute the earliest soaps, for example sodium or potassium stearate, $C_{17}H_{35}COONa$, or sodium myristate, $C_{14}H_{29}COONa$. The alkyl group may contain unsaturated portions, for example sodium oleate, which contains one double bond in the C_{17} alkyl chain. Most commercial soaps will be a mixture of fatty acids obtained from materials such as tallow, coconut oil and palm oil. The main attraction of these simple soaps is their low cost, their ready biodegradability, and low toxicity. Their main disadvantage is their ready precipitation in water containing bivalent ions such as Ca^{2+} and Mg^{2+}. In order to avoid their precipitation in hard water, the carboxylates are modified by introducing hydrophilic chains, for example ethoxy carboxylates with the general structure $RO(CH_2CH_2O)_nCH_2COO^-$, ester carboxylates containing hydroxyl or multi COOH groups, and sarcosinates which contain an amide group with the general structure $RCON(R')COO^-$. Addition of the ethoxylated groups results in an increased water solubility and enhanced chemical stability (no hydrolysis). The modified ether carboxylates are more compatible with electrolytes, and are also compatible with other nonionic, amphoteric, and sometimes even cationic, surfactants. The ester carboxylates are very soluble in water but suffer from the problem of hydrolysis. The sarcosinates are not very soluble in acid or neutral solutions but are quite soluble in alkaline media, and are compatible with other anionics, nonionics, and cationics. The phosphate esters have very interesting properties, being intermediate between ethoxylated nonionics and sulphated derivatives; they also have good compatibility with inorganic builders and they can be good emulsifiers. One specific salt of a fatty acid is lithium 12-hydroxystearic acid, which forms the major constituent of greases.

2.1.1.2 **Sulphates**

These are the largest and most important class of synthetic surfactants, which were produced by the reaction of an alcohol with sulphuric acid; that is, they are esters of sulphuric acid. In practice, however, sulphuric acid is seldom used and chlorosulphonic or sulphur dioxide/air mixtures are the most common methods used to sulphate the alcohol. Unfortunately, due to their chemical instability (hydrolysing to the alcohol, particularly in acid solutions) they have now been overtaken by the sulphonates, which are chemically stable. The properties of the sulphate surfactants depend on the nature of the alkyl chain and the sulphate group. The alkali metal salts show good solubility in water, but tend to be affected by the presence of electrolytes. The most common sulphate surfactant is sodium dodecyl sulphate (SDS, sometimes also referred to as sodium lauryl sulphate), which is used extensively not only for fundamental studies but also for many applications in industry. At room temperature (~25 °C) this surfactant is quite soluble, and 30% aqueous solutions are fairly fluid (low viscosity). However, below 25 °C the surfactant may separate out as a soft paste as the temperature falls below its Krafft point (the temperature above which the surfactant shows a rapid increase in solubility with a further increase of temperature). The latter depends on the distribution of chain lengths in the alkyl chain; that is, the wider the distribution the lower the Krafft temperature. Thus, by controlling this distribution it is possible to achieve a Krafft temperature of ~10 °C. As the surfactant concentration is increased to 30–40% (depending on the distribution of chain length in the alkyl group), the viscosity of the solution increases very rapidly with the production of a gel; subsequently, as the concentration reaches about 60–70% the solution becomes a pourable liquid, but above this concentration a gel is again formed. The concentration at which the minimum occurs varies according to the alcohol sulphate used, and also according to the presence of impurities such as unsaturated alcohol. The viscosity of the aqueous solutions can be reduced by the addition of short-chain alcohols and glycols. The critical micelle concentration (cmc) of SDS (the concentration above which the properties of the solution show abrupt changes) is 8×10^{-3} mol dm^{-3} (0.24%). The alkyl sulphates give good foaming properties with an optimum at C_{12}–C_{14}. As with the carboxylates, the sulphate surfactants are also chemically modified to change their properties; the most common modification is to introduce some EO units into the chain, at which point the sulphates are usually referred to as alcohol ether sulphates. The latter are prepared by the sulphation of ethoxylated alcohols. For example, sodium dodecyl 3 mol ether sulphate is essentially dodecyl alcohol reacted with 3 mol EO, and then sulphated and neutralised with NaOH. The presence of PEO confers an improved solubility when compared to the straight-chain alcohol sulphates. In addition, the surfactant becomes more compatible with electrolytes in aqueous solution. The ether sulphates are also more chemically stable than the alcohol sulphates. The cmc of the ether sulphates is also lower than the corresponding surfactant without the EO units. The viscosity behaviours of the aqueous solutions are similar to those of the alcohol sulphates, giving gels in the range of 30–60% ether sulphate concentration. The ether sulphates show a pronounced salt effect, with a significant increase in the viscosity of a dilute solution on the addition of an electrolyte, such as NaCl. The ether sulphates are commonly used in hand-dishwashing liquids and in shampoos, in combination with amphoteric surfactants.

2.1.1.3 **Sulphonates**

With sulphonates, the sulphur atom is directly attached to the carbon atom of the alkyl group, and this gives the molecule stability against hydrolysis when compared to the sulphates (where the sulphur atom is linked indirectly to the carbon of the hydrophobe via an oxygen atom). The alkyl aryl sulphonates are the most common type of these surfactants (e.g., sodium alkyl benzene sulphonate), and these are usually prepared by the reaction of sulphuric acid with alkyl aryl hydrocarbons, for example dodecyl benzene. One special class of sulphonate surfactants are the naphthalene and alkyl naphthalene sulphonates, which are commonly used as dispersants. As with the sulphates, some chemical modification is used by introducing EO units, for example sodium nonyl phenol 2 mol ethoxylate ethane sulphonate $C_9H_{19}C_6H_4(OCH_2CH_2)_2SO_3^-Na^+$. The paraffin sulphonates are produced by the sulpho-oxidation of normal linear paraffins with sulphur dioxide and oxygen, and catalysed with ultraviolet or gamma radiation; the resulting alkane sulphonic acid is neutralised with NaOH. These surfactants have excellent water solubility and biodegradability, and they are also compatible with many aqueous ions. The linear alkyl benzene sulphonates (LABSs) are manufactured from alkyl benzene, and the alkyl chain length can vary from C_8 to C_{15}; their properties are mainly influenced by the average molecular weight and the spread of carbon number of the alkyl side chain. The cmc of sodium dodecyl benzene sulphonate is $5 \times 10^{-3}\,\mathrm{mol\,dm^{-3}}$ (0.18%). The main disadvantages of LABS is their effect on the skin, and consequently they cannot be used in personal care formulations.

Another class of sulphonates is the α-olefin sulphonates which are prepared by reacting linear α-olefin with sulphur trioxide, typically yielding a mixture of alkene sulphonates (60–70%), 3- and 4-hydroxyalkane sulphonates (~30%), and some disulphonates and other species. The two main α-olefin fractions used as starting material are C_{12}–C_{16} and C_{16}–C_{18}. Fatty acid and ester sulphonates are produced by the sulphonation of unsaturated fatty acids or esters, a good example being sulphonated oleic acid:

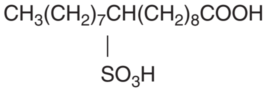

$$CH_3(CH_2)_7\underset{\displaystyle SO_3H}{\underset{|}{CH}}(CH_2)_8COOH$$

A special class of sulphonates are sulphosuccinates which are esters of sulphosuccinic acid:

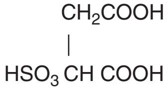

$$\begin{array}{r} \mathrm{CH_2COOH} \\ | \quad\quad\quad \\ \mathrm{HSO_3\,CH\,COOH} \end{array}$$

Both, monoesters and diesters are produced. A widely used diester in many formulations is sodium di(2-ethylhexyl)sulphosuccinate, which is sold commercially under the trade name Aerosol OT. The cmc of the diesters is very low, in the region of 0.06% for C_6-C_8 sodium salts, and they give a minimum in the surface tension of $26\ \mathrm{mN\ m^{-1}}$ for the C_8 diester; thus, these molecules are excellent wetting agents. The diesters are soluble both in water and in many organic solvents, and are particularly useful for the preparation of water-in-oil (W/O) microemulsions.

2.1.1.4 Phosphate-Containing Anionic Surfactants

Both, alkyl phosphates and alkyl ether phosphates are made by treating the fatty alcohol or alcohol ethoxylates with a phosphorylating agent, usually phosphorous pentoxide, P_4O_{10}. The reaction yields a mixture of monoesters and diesters of phosphoric acid, with the ratio of the two esters being determined by the ratio of the reactants and the amount of water present in the reaction mixture. The physico-chemical properties of the alkyl phosphate surfactants depend on the ratio of the esters. Phosphate surfactants are used in the metal-working industry, due to their anticorrosive properties.

2.1.2

Cationic Surfactants

The most common cationic surfactants are the quaternary ammonium compounds [8, 9] with the general formula $R'R''R'''R''''N^+X^-$, where X^- is usually chloride ion and R represents alkyl groups. These quaternaries are made by reacting an appropriate tertiary amine with an organic halide or organic sulphate. A common class of cationics is the alkyl trimethyl ammonium chloride, where R contains between eight and 18 C atoms, for example dodecyl trimethyl ammonium chloride, $C_{12}H_{25}(CH_3)_3NCl$. Another widely used cationic surfactant class is that containing two long-chain alkyl groups, that is dialkyl dimethyl ammonium chloride, with the alkyl groups having a chain length of between eight and 18 C atoms. These dialkyl surfactants are less soluble in water than the monoalkyl quaternary compounds, but they are commonly used in detergents as fabric softeners. A widely used cationic surfactant is alkyl dimethyl benzyl ammonium chloride (sometimes referred to as benzalkonium chloride and widely used as bactericide), having the structure:

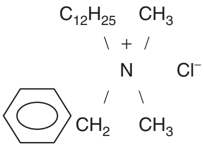

Imidazolines can also form quaternaries, the most common product being the ditallow derivative quaternise with dimethyl sulphate:

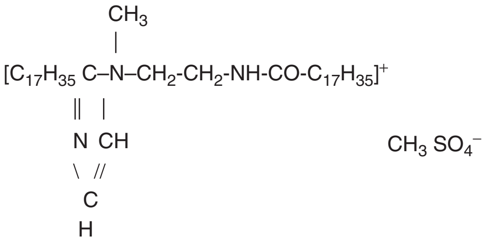

Cationic surfactants can also be modified by incorporating PEO chains, for example dodecyl methyl polyethylene oxide ammonium chloride having the structure:

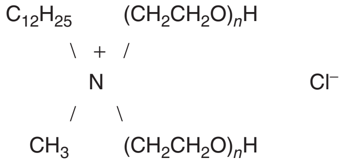

Cationic surfactants are generally water-soluble when there is only one long alkyl group. When there are two or more long-chain hydrophobes the product becomes dispersible in water and soluble in organic solvents. They are generally compatible with most inorganic ions and hard water, but are incompatible with metasilicates and highly condensed phosphates. They are also incompatible with protein-like materials. Cationics are generally stable to pH changes, both acid and alkaline. They are also incompatible with most anionic surfactants, but are compatible with nonionics. These cationic surfactants are insoluble in hydrocarbon oils. In contrast, cationics with two or more long alkyl chains are soluble in hydrocarbon solvents, but they become only dispersible in water (sometimes forming bilayer vesicle-type structures). They are generally chemically stable and can tolerate electrolytes. The cmc of cationic surfactants is close to that of anionics with the same alkyl chain length; for example, the cmc of benzalkonium chloride is 0.17%. The prime use of cationic surfactants is their tendency to adsorb at negatively charged surfaces; examples include anticorrosive agents for steel, flotation collectors for mineral ores, dispersants for inorganic pigments, antistatic agents for plastics, antistatic agents and fabric softeners, hair conditioners, anticaking agents for fertilizers, and as bactericides.

2.1.3
Amphoteric (Zwitterionic) Surfactants

These are surfactants containing both cationic and anionic groups [10]. The most common amphoterics are the *N*-alkyl betaines, which are derivatives of trimethyl glycine $(CH_3)_3NCH_2COOH$ (that was described as betaine). An example of a betaine surfactant is lauryl amido propyl dimethyl betaine $C_{12}H_{25}CON(CH_3)_2CH_2COOH$. These alkyl betaines are sometimes described as alkyl dimethyl glycinates. The main characteristics of amphoteric surfactants is their dependence on the pH of the solution in which they are dissolved. In acid pH solutions, the molecule acquires a positive charge and behaves like a cationic, whereas in alkaline pH solutions they become negatively charged and behave like an anionic. A specific pH can be defined at which both ionic groups show equal ionisation; this is the isoelectric point (i.e.p.) of the molecule, described by the following scheme:

$$N^+ \ldots COOH \leftrightarrow N^+ \ldots COO^- \leftrightarrow NH \ldots COO^-$$

$$\text{acid pH} < 3 \qquad \text{isoelectric} \qquad \text{pH} > 6\text{alkaline}$$

Amphoteric surfactants are sometimes referred to as zwitterionic molecules. They are soluble in water, but their solubility shows a minimum at the i.e.p. Amphoterics show excellent compatibility with other surfactants, forming mixed micelles; they are also chemically stable both in acids and alkalis. The surface activity of amphoterics varies widely, and depends on the distance between the charged groups. Amphoterics display a maximum in surface activity at the i.e.p.

Another class of amphoteric are the N-alkyl amino propionates having the structure $R\text{-}NHCH_2CH_2COOH$. The NH group is reactive and can react with another acid molecule (e.g., acrylic) to form an amino dipropionate $R\text{-}N(CH_2CH_2COOH)_2$. An alkyl imidazoline-based product can also be produced by reacting alkyl imidozoline with a chloro acid, but the imidazoline ring will break down during formation of the amphoteric.

The change in charge with pH of amphoteric surfactants affects their properties, such as wetting, detergency, and foaming. At the i.e.p., the properties of amphoterics resemble those of nonionics very closely, but below and above the i.e.p. the properties shift towards those of cationic and anionic surfactants, respectively. Zwitterionic surfactants have excellent dermatological properties, and also exhibit low eye irritation; consequently, they are frequently used in shampoos and other personal care products (e.g., cosmetics).

2.1.4
Nonionic Surfactants

The most common nonionic surfactants are those based on EO, referred to as ethoxylated surfactants [11–13]. Several classes can be distinguished, including alcohol ethoxylates, alkyl phenol ethoxylates, fatty acid ethoxylates, monoalkaolamide ethoxylates, sorbitan ester ethoxylates, fatty amine ethoxylates, and EO–propylene oxide copolymers (sometimes referred to as polymeric surfactants). Another important group of nonionics are the multihydroxy products such as glycol esters, glycerol (and polyglycerol) esters, glucosides (and polyglucosides) and sucrose esters. Amine oxides and sulphinyl surfactants represent nonionics with a small head group.

2.1.4.1 **Alcohol Ethoxylates**

These are generally produced by the ethoxylation of a fatty chain alcohol such as dodecanol. Several generic names have been given to this class of surfactants, including ethoxylated fatty alcohols, alkyl polyoxyethylene glycol, and monoalkyl polyethylene oxide glycol ethers. A typical example is dodecyl hexaoxyethylene glycol monoether with the chemical formula $C_{12}H_{25}(OCH_2CH_2O)_6OH$ (sometimes abbreviated as $C_{12}E_6$). In practice, the starting alcohol will have a distribution of alkyl chain lengths, and the resulting ethoxylate will have a distribution of EO chain length. Thus, the numbers listed in the literature refer to average numbers.

The cmc of nonionic surfactants is about two orders of magnitude lower than the corresponding anionics with the same alkyl chain length. At a given alkyl chain length, the cmc decreases with a decrease in the number of EO units. The solubility of the alcohol ethoxylates depend both on the alkyl chain length and the number of EO units in the molecule. Molecules with an average alkyl chain length of 12 C atoms and containing more than five EO units are usually soluble in water at room temperature; however, as the temperature of the solution is gradually raised the solution becomes cloudy (as a result of dehydration of the PEO chain and the change in conformation of the PEO chain); the temperature at which this occurs is referred to as the cloud point (CP) of the surfactant. At a given alkyl chain length, the CP increases with an increase in the EO chain of the molecule. The CP changes with change of concentration of the surfactant solution, and the trade literature usually quotes the CP of a 1% solution. The CP is also affected by the presence of an electrolyte in the aqueous solution, as most electrolytes lower the CP of a nonionic surfactant solution. Nonionics tend to have maximum surface activity near to the CP, while the CP of most nonionics increases markedly on the addition of small quantities of anionic surfactants. The surface tension of alcohol ethoxylate solutions decreases with increases in its concentration until it reaches its cmc; after this it remains constant with further increases in its concentration. The minimum surface tension reached at and above the cmc decreases with a decrease in the number of EO units of the chain (at a given alkyl chain). The viscosity of a nonionic surfactant solution increases gradually with increases in its concentration, but at a critical concentration (which depends on the alkyl and EO chain length) the viscosity show a rapid increase and, ultimately, a gel-like structure appears. This is due to the formation of a liquid crystalline structure of the hexagonal type. In many cases, the viscosity reaches a maximum, after which it shows a decrease due to the formation of other structures (e.g. lamellar phases; see below).

2.1.4.2 **Alkyl Phenol Ethoxylates**

These are prepared by the reaction of EO with an appropriate alkyl phenol. The most common surfactants of this type are those based on nonyl phenol; they are cheap to produce but suffer from problems of biodegradability and potential toxicity (the byproduct of degradation is nonyl phenol, which is considerably toxic in fish and mammals). Despite these problems, nonyl phenol ethoxylates are still used in many industrial properties, due mainly to their advantageous properties such as solubility both in aqueous and nonaqueous media, and their good emulsification and dispersion properties.

2.1.4.3 **Fatty Acid Ethoxylates**

These are produced by the reaction of EO with a fatty acid or a polyglycol, and have the general formula RCOO-$(CH_2CH_2O)_nH$. When a polyglycol is used, a mixture of monoesters and diesters (RCOO-$(CH_2CH_2O)_n$-OCOR) is produced. These surfactants are generally soluble in water, provided that there are sufficient EO units present and the alkyl chain length of the acid is not too long. The monoesters are much more soluble in water than are the diesters; in the latter case a longer EO chain is required to render the molecule soluble. The surfactants are compatible with aqueous ions, provided that not too much unreacted acid is present. However, these surfactants undergo hydrolysis in highly alkaline solutions.

2.1.4.4 **Sorbitan Esters and Their Ethoxylated Derivatives (Spans and Tweens)**

The fatty acid esters of sorbitan (which generally are referred to as Spans, an Atlas commercial trade name) and their ethoxylated derivatives (generally referred to as Tweens) are perhaps one of the most commonly used nonionics. They were first commercialised in the USA by Atlas (which has since been purchased by ICI). The sorbitan esters are produced by the reaction of sorbitol with a fatty acid at a high temperature (>200 °C). The sorbitol dehydrates to 1,4-sorbitan, after which esterification takes place. If 1 mol of fatty acid is reacted with 1 mol of sorbitol, a monoester is obtained (some diester is also produced as a byproduct). Thus, sorbitan monoester has the following general formula:

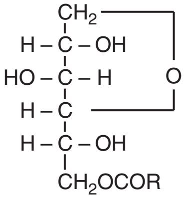

The free OH groups in the molecule can be esterified, producing diesters and triesters. Several products are available, depending on the nature of the alkyl group of the acid and whether the product is a monoester, diester, or triester. Some examples are given below:

Sorbitan monolaurate – Span 20
Sorbitan monopalmitate – Span 40
Sorbitan monostearate – Span 60
Sorbitan mono-oleate – Span 80
Sorbitan tristearate – Span 65
Sorbitan trioleate – Span 85.

The ethoxylated derivatives of Spans (Tweens) are produced by the reaction of EO on any hydroxyl group remaining on the sorbitan ester group. Alternatively, the sorbitol is first ethoxylated and then esterified, although the final product will have different surfactant properties to the Tweens. Some examples of Tween surfactants are given below:

Polyoxyethylene (20) sorbitan monolaurate – Tween 20
Polyoxyethylene (20) sorbitan monopalmitate – Tween 40
Polyoxyethylene (20) sorbitan monostearate – Tween 60
Polyoxyethylene (20) sorbitan mono-oleate – Tween 80
Polyoxyethylene (20) sorbitan tristearate – Tween 65
Polyoxyethylene (20) sorbitan tri-oleate – Tween 85.

The sorbitan esters are insoluble in water, but are soluble in most organic solvents (low hydrophilic–lipophilic-balance (HLB) number surfactants). The ethoxylated products are generally soluble in number, and have relatively high HLB numbers. One of the main advantages of the sorbitan esters and their ethoxylated derivatives is their approval as food additives. They are also used widely in cosmetics and some pharmaceutical preparations.

2.1.4.5 **Ethoxylated Fats and Oils**

A number of natural fats and oils have been ethoxylated, for example linolin (wool fat) and castor oil ethoxylates. These products are useful for applications in pharmaceutical products, for example as solubilisers.

2.1.4.6 **Amine Ethoxylates**

These are prepared by the addition of EO to primary or secondary fatty amines. With primary amines, both hydrogen atoms on the amine group react with EO, and therefore the resulting surfactant has the structure:

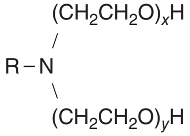

$$R-N\begin{cases}(CH_2CH_2O)_xH\\(CH_2CH_2O)_yH\end{cases}$$

The above surfactants acquire a cationic character if the EO units are small in number and if the pH is low; however, at high EO levels and neutral pH they behave very similarly to nonionics. At low EO content the surfactants are not soluble in water, but become soluble in an acid solution. At high pH, the amine ethoxylates are water-soluble, provided that the alkyl chain length of the compound is not long (usually a C_{12} chain is adequate for reasonable solubility at sufficient EO content).

2.1.4.7 **Amine Oxides**

These are prepared by oxidizing a tertiary nitrogen group with aqueous hydrogen peroxide at temperatures in the region of 60–80 °C. Several examples can be quoted, including *N*-alkyl amidopropyl-dimethyl amine oxide, *N*-alkyl bis(2-hydroxyethyl) amine oxide and *N*-alkyl dimethyl amine oxide. These have the general formula:

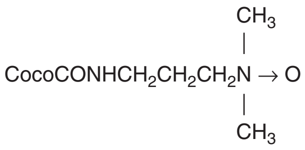

$$\mathrm{CocoCONHCH_2CH_2CH_2\overset{\displaystyle CH_3}{\underset{\displaystyle CH_3}{N}} \rightarrow O}$$

Alkyl amidopropyl-dimethyl amine oxide

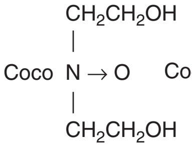

$$\mathrm{Coco\ \overset{\displaystyle CH_2CH_2OH}{\underset{\displaystyle CH_2CH_2OH}{N}} \rightarrow O}$$

Coco bis (2-hydroxyethyl) amine oxide

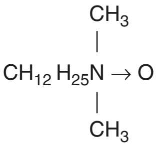

$$\mathrm{CH_{12}H_{25}\overset{\displaystyle CH_3}{\underset{\displaystyle CH_3}{N}} \rightarrow O}$$

Lauryl dimethyl amine oxide

In acid solutions, the amino group is protonated and acts as a cationic surfactant, whereas in neutral or alkaline solution the amine oxides are essentially nonionic in character. Alkyl dimethyl amine oxides are water-soluble up to C_{16} alkyl chain. Above pH 9, amine oxides are compatible with most anionics, but at pH 6.5 and below some anionics tend to interact and form precipitates. In combination with anionics, amine oxides can be used as foam boosters (e.g., in shampoos).

2.1.5
Specialty Surfactants

2.1.5.1 Fluorocarbon and Silicone Surfactants

These surfactants can lower the surface tension of water to values below 20 mN m^{-1}. By comparison, most of the surfactants described above lower the surface tension of water to values above 20 mN m^{-1}, typically in the region of 25–27 mN m^{-1}. The fluorocarbon and silicone surfactants are sometimes referred to as ''superwetters'' as they cause enhanced wetting and spreading of their aqueous solution. However, they are much more expensive than conventional surfactants and are only applied for specific applications whereby the low surface tension is a desirable property. Fluorocarbon surfactants have been prepared with various structures consisting of perfluoroalkyl chains and anionic, cationic, amphoteric and PEO polar groups. These surfactants have good thermal and chemical stabilities, and are excellent wetting agents for low-energy surfaces. Silicone surfactants, which sometimes are referred to as organosilicones, are those with polydimethylsilixane backbone. Silicone surfactants are prepared by the incorporation of a water-soluble or hydrophilic group into a siloxane backbone; the latter can also be modified by the incorporation of a paraffinic hydrophobic chain, either at the end or along the polysiloxane back bone. The most common hydrophilic groups are EO/PO (propylene oxide), and the structures produced are rather complex; in fact, most manufacturers of silicone surfactants do not reveal the exact structure of their product. The mechanism by which these molecules reduce the surface tension of water to low values is far from being well understood; nonetheless, these surfactants are widely applied as spreading agents on many hydrophobic surfaces. The incorporation of organophilic groups into the backbone of the polydimethyl siloxane backbone can yield products that exhibit surface-active properties in organic solvents.

2.1.5.2 **Gemini Surfactants**

A gemini surfactant is a dimeric molecule consisting of two hydrophobic tails and two head groups, linked together with a short spacer [14]. This is illustrated below for a molecule containing two cationic head groups (separated by two methylene groups) with two alkyl chains:

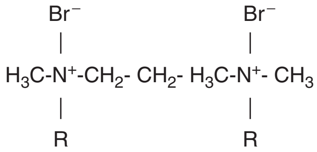

$$H_3C\text{-}\underset{\displaystyle R}{\overset{\displaystyle Br^-}{N^+}}\text{-}CH_2\text{-}\ CH_2\text{-}\ H_3C\text{-}\underset{\displaystyle R}{\overset{\displaystyle Br^-}{N^+}}\text{-}\ CH_3$$

These surfactants show several interesting physico-chemical properties, such as a very high efficiency in lowering the surface tension and a very low cmc. For example, the cmc of a conventional cationic dodecyltrimethylammonium bromide is 16 mM, whereas that of the corresponding Gemini surfactant, having a two-carbon linkage between the head groups, is 0.9 mM. In addition, the surface tension reached at and above the cmc is lower for gemini surfactants when compared to that of their corresponding conventional counterparts. Gemini surfactants are also more effective in lowering the dynamic surface tension (the time required to reach the equilibrium value is shorter). These effects are due to a better packing of the gemini surfactant molecules at the air/water interface.

2.1.5.3 **Surfactants Derived from Monosaccharides and Polysaccharides**

Several surfactants were synthesised starting from monosaccharides or oligosaccharides by reaction with the multifunctional hydroxyl groups, including alkyl glucosides, alkyl polyglucosides (APGs) [15], sugar fatty acid esters, and sucrose esters [16]. The technical problem here is one of joining a hydrophobic group to the multihydroxyl structure. Several surfactants were produced, an example being the esterification of sucrose with fatty acids or fatty glycerides to produce sucrose esters having the following structure:

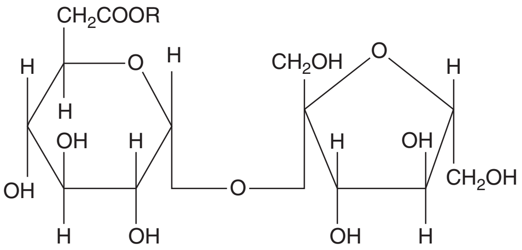

The most interesting sugar surfactants are the APGs, which are synthesised via a two-stage transacetalisation process [15]. In the first stage, the carbohydrate reacts with a short-chain alcohol such as butanol or propylene glycol, while in the second stage the short-chain alkyl glucoside is transacetalised with a relatively long-chain alcohol (C_{12-14}-OH) to form the required APG. This process is applied if oligoglucoses and polyglucoses such as starch or syrups with a low dextrose equivalent (DE) are used. In a simplified transacetalisation process, syrups with a high glucose content (DE > 96%) or solid glucose types can react with short-chain alcohols under normal pressure. The scheme for APG synthesis is shown below. Commercial APGs are complex mixtures of species that vary in their degree of polymerisation (DP, usually in the range 1.1–3) and also in the length of their alkyl chains. When the latter is shorter than C_{14} the product is water-soluble. The cmc values of APGs are comparable to those of nonionic surfactants, and they decrease as the alkyl chain length is increased.

APG surfactants have good solubility in water and have high CP values (>100 °C). Moreover, they are stable in neutral and alkaline solutions but are unstable in strong acid solutions. APG surfactants can tolerate high electrolyte concentrations, and are compatible with most types of surfactant. They are used in personal care products for cleansing formulations, for skin care and hair products, and also in hard-surface cleaners and laundry detergents. APG surfactants have also been applied in agrochemical formulations, to serve as wetting agents and penetrating agents for the active ingredient.

References

1. Tadros, T.F. (ed.) (1984) *Surfactants*, Academic Press, London.
2. Holmberg, K., Jonsson, B., Kronberg, B., and Lindman, B. (2003) *Surfactants and Polymers in Solution*, 2nd edn, John Wiley & Sons, Ltd.
3. McCutcheon. *Detergents and Emulsifiers*, Allied Publishing Co., New Jersey (published annually).
4. van Os, N.M., Haak, J.R., and Rupert, L.A.M. (1993) *Physico-Chemical Properties of Selected Anionic, Cationic and Nonionic Surfactants*, Elsevier Publishing Co., Amsterdam.
5. Porter, M.R. (1994) *Handbook of Surfactants*, Chapman & Hall, Blackie.
6. Linfield, W.M. (ed.) (1967) *Anionic Surfactants*, Marcel Dekker, New York.
7. Lucasssen-Reynders, E.H. (1981) *Anionic Surfactants – Physical Chemistry of Surfactant Action*, Marcel Dekker, New York.
8. Jungermana, E. (1970) *Cationic Surfactants*, Marcel Dekker, New York.

9. Rubingh, N. and Holland, P.M. (eds) (1991) *Cationic Surfactants – Physical Chemistry*, Marcel Dekker, New York.
10. Buestein, B.R. and Hiliton, C.L. (1982) *Amphoteric Surfactants*, Marcel Dekker, New York.
11. Schick, M.J. (ed.) (1966) *Nonionic Surfactants*, Marcel Dekker, New York.
12. Schick, M.J. (ed.) (1987) *Nonionic Surfactants: Physical Chemistry*, Marcel Dekker, New York.
13. Schonfeldt, N. (1970) *Surface Active Ethylene Oxide Adducts*, Pergamon Press, New York.
14. Zana, R.R. and Alami, E. (2003) Gemini surfactants, in *Novel Surfactants*, Chapter 12 (ed. K. Holberg), Marcel Dekker, New York.
15. von Rybinsky, W. and Hill, K. (2003) in *Novel Surfactants*, Chapter 2 (ed. K. Holmberg), Marcel Dekker, New York.
16. Drummond, C.J., Fong, C., Krodkiewska, I., Boyd, B.J., and Baker, I.J.A. (2003) in *Novel Surfactants*, Chapter 3 (ed. K. Holmberg), Marcel Dekker, New York.

3

Physical Chemistry of Surfactant Solutions and the Process of Micellisation

The physical properties of surface-active agent solutions differ from those of nonamphipathic molecule solutions (such as sugars) in one major aspect, namely the abrupt changes in their properties above a critical concentration [1]. This is illustrated in Figure 3.1, which shows the plots of several physical properties (osmotic pressure, surface tension, turbidity, solubilisation, magnetic resonance, equivalent conductivity and self-diffusion) as a function of concentration for an anionic surfactant. At low concentrations, most properties are similar to those of a simple electrolyte, the one notable exception being surface tension, which decreases rapidly with increasing surfactant concentration. Each of these properties – whether interfacial or bulk – shows an abrupt change at a particular concentration, and this is consistent with the fact that at and above this concentration, surface-active molecules or ions will associate to form larger units. These associated units are termed micelles (self-assembled structures), and the first-formed aggregates are generally approximately spherical in shape [2]. A schematic representation of a spherical micelle is shown in Figure 3.2.

The concentration at which this association phenomenon occurs is known as the critical micelle concentration (cmc). Each surfactant molecule has a characteristic cmc value at a given temperature and electrolyte concentration. The most common technique for measuring the cmc is surface tension, γ, which shows a break at the cmc, after which γ remains virtually constant with further increases in concentration. However, other techniques such as self-diffusion measurements, nuclear magnetic resonance and fluorescence spectroscopy can also be applied. A compilation of cmc values was provided in 1971 by Mukerjee and Mysels [3], and although this is clearly not an up-to-date text is an extremely valuable reference. As an illustration, the cmc values of a number of surface active agents are listed in Table 3.1, to show some of the general trends [3]. Within any class of surface-active agent the cmc decreases with increases in the chain length of the hydrophobic portion (alkyl group). As a general rule, the cmc decreases by a factor of 2 for ionics (without added salt), and by a factor of 3 for nonionics, on adding one methylene group to the alkyl chain. With nonionic surfactants, increasing the length of the hydrophilic group (polyethylene oxide; PEO) causes an increase in cmc.

In general, nonionic surfactants have lower cmc values than their corresponding ionic surfactants of the same alkyl chain length. The incorporation of a phenyl

Formulation of Disperse Systems: Science and Technology, First Edition. Tharwat F. Tadros.

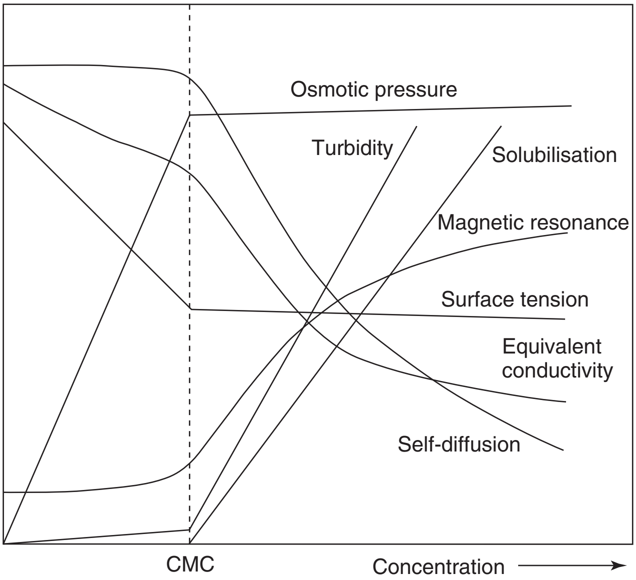

Figure 3.1 Variation of solution properties with surfactant concentration.

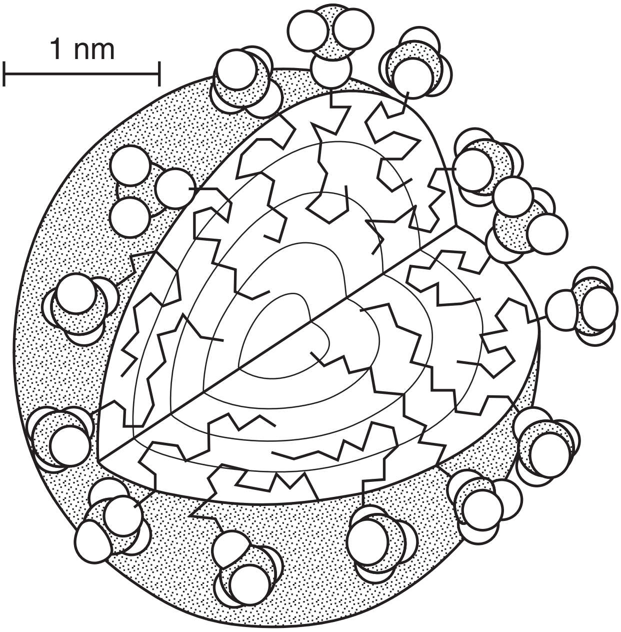

Figure 3.2 Illustration of a spherical micelle for dodecyl sulphate. (Source: Istraelachvili 1985 [2]. Reproduced with permission of Elsevier.)

Table 3.1 Critical micelle concentration (cmc) of surfactants.

Surface-active agent	cmc (mol dm^{-3})
Anionic	
Sodium octyl-l-sulphate	1.30×10^{-1}
Sodium decyl-l-sulphate	3.32×10^{-2}
Sodium dodecyl-l-sulphate	8.39×10^{-3}
Sodium tetradecyl-l-sulphate	2.05×10^{-3}
Cationic	
Octyl trimethyl ammonium bromide	1.30×10^{-1}
Decetryl trimethyl ammonium bromide	6.46×10^{-2}
Dodecyl trimethyl ammonium bromide	1.56×10^{-2}
Hexacetyltrimethyl ammonium bromide	9.20×10^{-4}
Nonionic	
Octyl hexaoxyethylene glycol monoether C_8E_6	9.80×10^{-3}
Decyl hexaoxyethylene glycol monoether $C_{10}E_6$	9.00×10^{-4}
Decyl nonaoxyethylene glycol monoether $C_{10}E_9$	1.30×10^{-3}
Dodecyl hexaoxyethylene glycol monoether $C_{12}E_6$	8.70×10^{-5}
Octylphenyl hexaoxyethylene glycol monoether C_8E_6	2.05×10^{-4}

group into the alkyl group increases its hydrophobicity to a much smaller extent than increasing its chain length with the same number of carbon atoms. The valency of the counterion in ionic surfactants has a significant effect on the cmc. For example, increasing the valency of the counterion from 1 to 2 causes a reduction of the cmc by approximately a factor of 4.

The cmc is, to a first approximation, independent of temperature. This is illustrated in Figure 3.3, which shows the variation of cmc of sodium dodecyl sulphate (SDS) with temperature. The cmc varies in a nonmonotonic way by about 10–20% over a wide temperature range. The shallow minimum around 25 °C can be compared with a similar minimum in the solubility of hydrocarbon in water [4]. However, nonionic surfactants of the ethoxylate type show a monotonic decrease [4] of cmc with increase of temperature, as illustrated in Figure 3.3 for $C_{10}E_5$. The effect of the addition of cosolutes (such as electrolytes and nonelectrolytes) on the cmc can be very striking. For example, the addition of 1 : 1 electrolyte to a solution of anionic surfactant produces a dramatic lowering of the cmc, which may amount to an order of magnitude. The effect is moderate for short-chain surfactants, but is much larger for their long-chain counterparts. At high electrolyte concentrations the reduction in cmc with the increase in number of carbon atoms in the alkyl chain is much stronger than without an added electrolyte. The rate of decrease at high electrolyte concentrations is comparable to that of nonionics. The effect of an added electrolyte also depends on the valency of the added counterions whereas, for nonionics, the addition of an electrolyte causes only a small variation in the cmc.

Nonelectrolytes such as alcohols can also cause a decrease in the cmc [5]. Alcohols are less polar than water and are distributed between the bulk solution and the

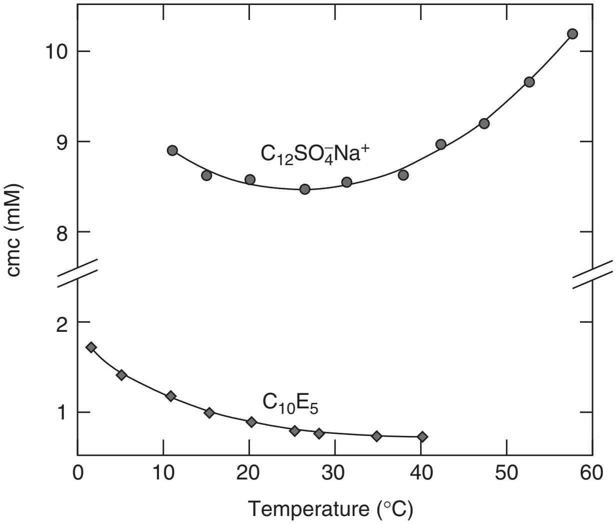

Figure 3.3 Temperature dependence of the cmc of SDS and $C_{10}E_5$ [4].

micelles; consequently, the greater the alcohols' preference for the micelles the more the micelles will be stabilised. A longer alkyl chain leads to a less favourable location in water and a more favourable location in the micelles.

The presence of micelles can account for many of the unusual properties of solutions of surface-active agents. For example, it can account for the near-constant surface tension value, above the cmc (see Figure 3.1). It can also account for the reduction in the molar conductance of the surface-active agent solution above the cmc, which is consistent with the reduction in mobility of micelles as a result of counterion association. The presence of micelles also accounts for the rapid increase in light scattering or turbidity above the cmc. The presence of micelles was originally suggested by McBain [6], who proposed that below the cmc most of the surfactant molecules would be unassociated, whereas in isotropic solutions immediately above the cmc micelles and surfactant ions (molecules) are thought to coexist, with the concentration of the latter changing very slightly as more surfactant is dissolved. However, the self-association of an amphiphile occurs in a stepwise manner, with one monomer being added to the aggregate at a time. For a long-chain amphiphile the association is strongly cooperative up to a certain micelle size, where counteracting factors became increasingly important. Typically, the micelles have a closely spherical shape in a rather wide concentration range above the cmc. Originally, it was suggested by both Adam [7] and Hartley [8] that micelles are spherical in shape and have the following properties: (i) the association unit is spherical with a radius approximately equal to the length of the hydrocarbon chain; (ii) the micelle contains about 50–100 monomeric units, and the aggregation number generally increases with an increase in alkyl chain length; (iii) with ionic surfactants, most counterions are bound to the micelle surface, thus significantly reducing the mobility from the value to be expected from a micelle with noncounterion bonding; (iv) micellisation occurs over a narrow concentration range as a result of the high association number of surfactant micelles; and (v) the interior of the surfactant micelle has essentially the properties of a liquid hydrocarbon. This is confirmed by the high mobility of the alkyl chains and the ability of micelles to solubilise many water-insoluble organic molecules, for example dyes and agrochemicals. To a first approximation micelles can, over a wide concentration range above the cmc, be viewed as microscopic liquid hydrocarbon droplets covered with polar head groups which interact strongly with water molecules. It appears that the radius of the micelle core constituted by the alkyl chains is close to the extended length of the alkyl chain, that is, in the range 1.5030 nm. As will be seen later, the driving force for micelle formation is an elimination of the contact between the alkyl chains and water. The larger a spherical micelle, the more efficient this is, since the volume-to-area ratio is increased. It should be noted that the surfactant molecules in the micelles are not all extended; rather, only one molecule needs to be extended to satisfy the criterion that the radius of the micelle core is close to the extended length of the alkyl chain. The majority of surfactant molecules are in a disordered state; in other words, the interior of the micelle is close to that of the corresponding alkane in a neat liquid oil. This explains the large solubilisation capacity of the micelle towards a broad range of nonpolar and weakly polar substances. At the surface of the micelle, associated counterions (in the region of 50–80% of the surfactant ions) are present; however, simple inorganic counterions are very loosely associated with the micelle. The counterions are very mobile (see below), and there is no specific complex formed with a definite counterion–head group distance. In other words, the counterions are associated by long-range electrostatic interactions.

A useful concept for characterizing micelle geometry is the critical packing parameter (CPP) [2]. The aggregation number N is the ratio between the micellar core volume, V_{mic} and the volume of one chain, v,

$$N = \frac{V_{\text{mic}}}{v} = \frac{(4/3)\pi\, R^3_{\text{mic}}}{v} \tag{3.1}$$

where R_{mic} is the radius of the micelle.

The aggregation number, N, is also equal to the ratio of the area of a micelle, A_{mic}, to the cross-sectional area, a, of one surfactant molecule,

$$N = \frac{A_{\text{mic}}}{a} = \frac{4\pi\, R^2_{\text{mic}}}{a} \tag{3.2}$$

Combining Equations (3.1) and (3.2),

$$\frac{v}{R_{\text{mic}}\, a} = \frac{1}{3} \tag{3.3}$$

Since R_{mic} cannot exceed the extended length of a surfactant alkyl chain, l_{max},

$$l_{\text{max}} = 1.5 + 1.265\, n_c \tag{3.4}$$

This means that, for a spherical micelle,

$$\frac{v}{l_{\max}\,a} \leq \frac{1}{3} \tag{3.5}$$

The ratio $v/(l_{\max}\,a)$ is denoted as the CPP.

Although, the spherical micelle model accounts for many of the physical properties of solutions of surfactants, a number of phenomena remain unexplained, without considering other shapes. For example, McBain [9] suggested the presence of two types of micelle – spherical and lamellar – in order to account for the drop in molar conductance of surfactant solutions. The lamellar micelles are neutral and hence they account for the reduction in conductance. Later, Harkins *et al.* [10] used McBain's model of lamellar micelles to interpret his X-ray results in soap solutions. Moreover, many modern techniques such as light-scattering and neutron-scattering indicate that, in many systems, the micelles are not spherical. For example, Debye and Anacker [11] proposed a cylindrical micelle to explain the light-scattering results on hexadecyltrimethyl ammonium bromide in water; evidence for disc-shaped micelles has also been obtained under certain conditions. A schematic representation of the spherical, lamellar and rod-shaped micelles, as suggested by McBain, Hartley and Debye, is given in Figure 3.4. Many ionic surfactants show dramatic temperature-dependent solubility, as illustrated in Figure 3.5. The solubility first increases gradually with rising temperature after which, above a certain temperature, there is a sudden increase in solubility with a further increase in temperature. The cmc increases gradually with increasing temperature, but at a particular temperature the solubility becomes equal to the cmc such that the solubility curve intersects the cmc; the temperature at this point is referred to as the Krafft temperature. At the Krafft temperature an equilibrium exists between the solid hydrated surfactant, micelles and monomers (i.e. the temperature is a "triple point"). Surfactants with ionic head groups and long straight alkyl chains have high Krafft temperatures, and the latter temperature increases with increase in the length of the alkyl chain of the surfactant molecule. The Krafft temperature can be reduced by introducing branching into the alkyl chain, and also by using alkyl chains with a wide distribution of chain length. The addition of electrolytes causes an increase in the Krafft temperature.

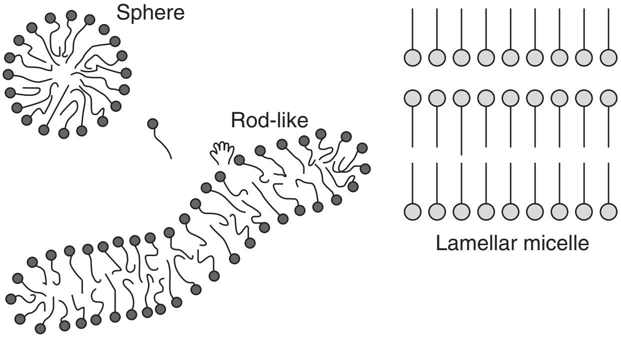

Figure 3.4 Shape of micelles.

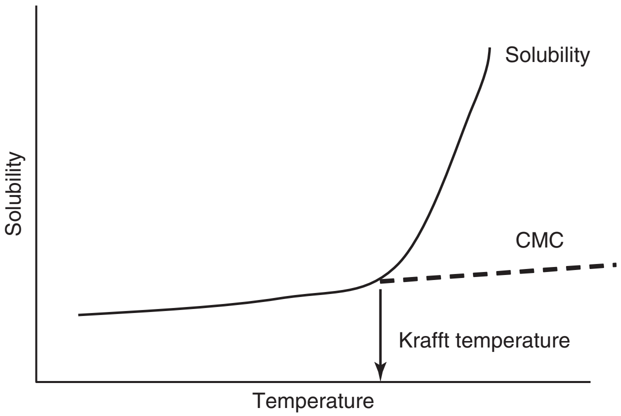

Figure 3.5 Variation of solubility and critical micelle concentration (cmc) with temperature.

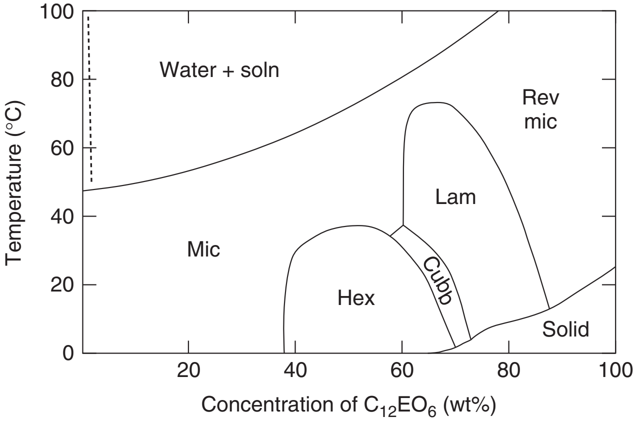

Figure 3.6 Phase diagram of $C_{12}E_6$.

With nonionic surfactants of the ethoxylate type, an increase in the temperature of a solution at a given concentration causes dehydration of the PEO chains and, at a critical temperature, the solution will become cloudy. This is illustrated in Figure 3.6, which shows the phase diagram of $C_{12}E_6$. Below the CP curve it is possible to identify the different liquid crystalline phases hexagonal–cubic–lamellar, which are shown schematically in Figure 3.7.

3.1
Thermodynamics of Micellisation

As the process of micellisation is one of the most important characteristics of surfactant solution, it is essential to understand the mechanism involved (i.e., the

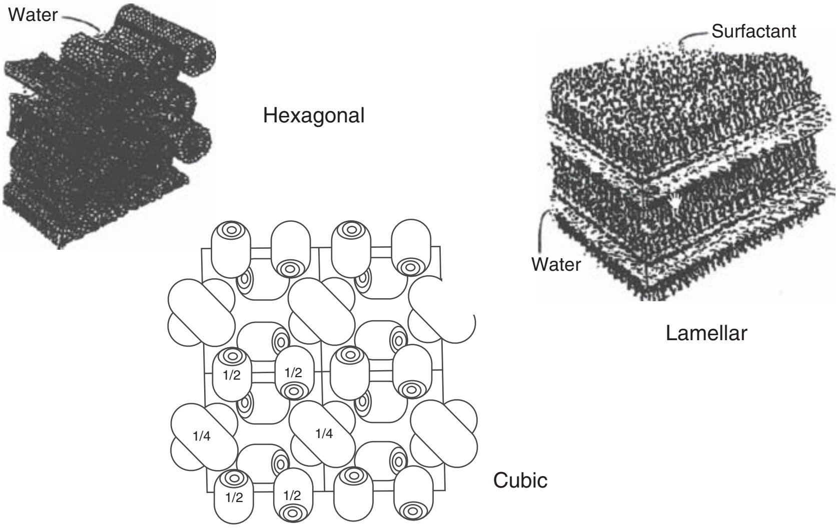

Figure 3.7 Schematic images of liquid crystalline phases.

driving force of micelle formation). This requires an analysis of the dynamics of the process (i.e., the kinetic aspects), as well as the equilibrium aspects whereby the laws of thermodynamics may be applied to obtain the free energy, enthalpy, and entropy of micellisation.

3.1.1
Kinetic Aspects

Micellisation is a dynamic phenomenon in which n monomeric surfactant molecules associate to form a micelle S_{n}; that is

$$n\,S \Leftrightarrow S_n \tag{3.6}$$

Hartley [8] envisaged a dynamic equilibrium whereby surface-active agent molecules are constantly leaving the micelles while other molecules from solution enter the micelles. The same applies to the counterions with ionic surfactants, which can exchange between the micelle surface and bulk solution. Experimental investigations using fast kinetic methods (e.g., stopped-flow, temperature and pressure-jumps) and ultrasonic relaxation measurements have shown that there are two relaxation processes for micellar equilibrium [12–18], characterised by the relaxation times τ_1 and τ_2. The first relaxation time, τ_1, is on the order of 10^{-7} s (10^{-8} to 10^{-3} s) and represents the lifetime of a surface-active molecule in a micelle; that is, it represents the association and dissociation rate for a single molecule (S) entering and leaving the micelle, which may be represented by the equation,

$$\mathrm{S} + \mathrm{S}_{n-1} \Leftrightarrow \mathrm{S}_n \tag{3.7}$$

where K^+ and K^- represent the association and dissociation rate respectively for a single molecule entering or leaving the micelle.

The slower relaxation time, τ_2, corresponds to a relatively slow process, namely the micellisation–dissolution process represented by Equation (3.6). The value of τ_2 is of the order of milliseconds (10^{-3} to 1 s), and hence can be conveniently measured by using stopped-flow methods. The fast relaxation time τ_1 can be measured using various techniques, depending on its range. For example, τ_1 values in the range of 10^{-8} to 10^{-7} s are accessible to ultrasonic absorption methods, whereas τ_1 in the range of 10^{-5} to 10^{-3} s can be measured using pressure-jump methods. The value of τ_1 depends on the surfactant concentration, chain length and temperature; typically, τ_1 increases with an increase of the chain length of surfactants – that is, the residence time increases with an increase in chain length.

The above discussion emphasizes the dynamic nature of micelles, and it is important to realize that these molecules are in continuous motion and that there is a constant interchange between micelles and solution. This dynamic nature also applies to the counterions which exchange rapidly with lifetimes in the range 10^{-9} to 10^{-8} s. Furthermore, the counterions appear to be laterally mobile and not to be associated with (single) specific groups on the micelle surfaces.

3.1.2
Equilibrium Aspects: Thermodynamics of Micellisation

Various approaches have been employed to tackle the problem of micelle formation. The most simple approach treats micelles as a single phase, and this is referred to as the phase-separation model. In this model, micelle formation is considered as a phase-separation phenomenon, and the cmc is then taken as the saturation concentration of the amphiphile in the monomeric state, whereas the micelles constitute the separated pseudophase. Above the cmc, a phase equilibrium exists with a constant activity of the surfactant in the micellar phase. The Krafft point is viewed as the temperature at which a solid-hydrated surfactant, the micelles, and a solution saturated with undissociated surfactant molecules are in equilibrium at a given pressure.

Consider an anionic surfactant, in which n surfactant anions, S^- and n counterions M^+ associate to form a micelle; that is:

$$n\,S^- + nM^+ \Leftrightarrow S_n \tag{3.8}$$

The micelle is simply a charged aggregate of surfactant ions plus an equivalent number of counterions in the surrounding atmosphere, and is treated as a separate phase. At any given temperature the chemical potential of the surfactant in the micellar state is assumed to be constant, and this may be adopted as the standard chemical potential, $\mu_m{}^\circ$, by analogy to a pure liquid or a pure solid. Considering the equilibrium between micelles and monomer, then

$$\mu_m^o = \mu_1^o + RT\ \ln\ a_1 \tag{3.9}$$

where μ_1 is the standard chemical potential of the surfactant monomer and a_1 is its activity which is equal to $f_1\ x_1$, where f_1 is the activity coefficient and x_1 the mole fraction. Therefore, the standard free energy of micellisation per mol of monomer, $\Delta G^\circ{}_\mathrm{m}$, is given by:

$$\Delta G^\mathrm{o}_\mathrm{m} = \mu^\mathrm{o}_\mathrm{m} - \mu^\mathrm{o}_1 \ = RT\ \ln\ a_1 \approx RT\ \ln\ x_1 \tag{3.10}$$

where f_1 is taken as unity (a reasonable value in very dilute solution). The cmc may be identified with x_1 so that

$$\Delta G^\mathrm{o}_\mathrm{m} = RT\ \ln\,(\mathrm{cmc}) \tag{3.11}$$

In Equation (3.10), the cmc is expressed as a mole fraction, which is equal to $C/(55.5 + C)$, where C is the concentration of surfactant in mol dm^{-3}, that is

$$\Delta G^\mathrm{o}_\mathrm{m} \ = RT\ \ln\ C - RT\ \ln\,(55.5 + C) \tag{3.12}$$

It must be stated that ΔG° should be calculated using the cmc expressed as a mole fraction, as indicated by Equation (3.12). However, most cmc values quoted in the literature are given in mol dm^{-3} and, in many cases, ΔG°-values have been quoted when the cmc was simply expressed in mol dm^{-3}. Strictly speaking, this is incorrect, as ΔG° should be based on x_1 rather than on C. The value of ΔG°, when the cmc is expressed in mol dm^{-3}, is substantially different from the ΔG° value when the cmc is expressed in mole fraction. For example, for dodecyl hexaoxyethylene glycol the quoted cmc value is 8.7×10^{-5} mol dm^{-3} at 25 °C. Therefore,

$$\Delta G^\mathrm{o} = RT\ \ln\ \frac{8.7 \times 10^{-5}}{55.5 + 8.7 \times 10^{-5}} \ = -33.1\,\mathrm{KJmol}^{-1} \tag{3.13}$$

when the mole fraction scale is used. On the other hand,

$$\Delta G^\mathrm{o} = RT\ \ln\ 8.7 \times 10^{-5} = -23.2\ \mathrm{KJ\,mol}^{-1} \tag{3.14}$$

when the molarity scale is used.

The phase-separation model has been questioned for two main reasons:

1) According to this model a clear discontinuity in the physical property of a surfactant solution, such as surface tension and turbidity, should be observed at the cmc. This is not always found experimentally and the cmc is not a sharp break point.
2) If two phases actually exist at the cmc, then equating the chemical potential of the surfactant molecule in the two phases would imply that the activity of the surfactant in the aqueous phase would be constant above the cmc. If this were the case, the surface tension of a surfactant solution should remain constant above the cmc. However, careful measurements have shown that the surface tension of a surfactant solution decreases slowly above the cmc, particularly when using purified surfactants.

A convenient solution for relating ΔG_m to (cmc.) was given by Phillips [17] for ionic surfactants, who arrived at the following expression,

$$\Delta G^\mathrm{o}_\mathrm{m} = \{2 - (p/n)\}\ RT\ \ln\,(\mathrm{cmc}) \tag{3.15}$$

where p is the number of free (unassociated) surfactant ions and n is the total number of surfactant molecules in the micelle. For many ionic surfactants, the degree of dissociation (p/n) is ~0.2, so that

$$\Delta G^{\mathrm{o}}_{\mathrm{m}} = 1.8\ \boldsymbol{RT}\ \ln(\mathrm{cmc}) \tag{3.16}$$

Comparison with Equation (3.11) clearly shows that for similar ΔG_{m}, the (cmc) is about two orders of magnitude higher for ionic surfactants when compared to a nonionic surfactant of the same alkyl chain length (see Table 3.1).

In the presence of excess added electrolyte, with mole fraction x, the free energy of micellisation is given by the expression:

$$\Delta G^{\mathrm{o}}_{\mathrm{m}} = \boldsymbol{RT}\ \ln(\mathrm{cmc}) + \{1 - (p/n)\}\ \ln\ x \tag{3.17}$$

Equation (3.17) shows that as x increases, the (cmc) decreases.

It is clear from Equation (3.15) that as $p \to 0$, that is when most charges are associated with counterions,

$$\Delta G^{\mathrm{o}}_{\mathrm{m}} = 2\ \boldsymbol{RT}\ \ln(\mathrm{cmc}) \tag{3.18}$$

whereas when $p \sim n$, that is when the counterions are bound to micelles,

$$\Delta G^{\mathrm{o}}_{\mathrm{m}} = \boldsymbol{RT}\ \ln(\mathrm{cmc}) \tag{3.19}$$

which is the same equation for nonionic surfactants.

3.2
Enthalpy and Entropy of Micellisation

The enthalpy of micellisation can be calculated from the variation of cmc with temperature. This follows from,

$$-\Delta H^{\mathrm{o}} = RT^2 \frac{\mathrm{d}ln\,(\mathrm{cmc})}{\mathrm{d}T} \tag{3.20}$$

The entropy of micellisation can then be calculated from the relationship between $\Delta G°$ and $\Delta H°$, that is

$$\Delta G^{\mathrm{o}} = \Delta H^{\mathrm{o}} - T\Delta S^{\mathrm{o}} \tag{3.21}$$

Therefore $\Delta H°$ may be calculated from the surface tension–log C plots at various temperatures. Unfortunately, the errors in locating the cmc (which in many cases is not a sharp point) leads to a large error in the value of $\Delta H°$. A more accurate and direct method of obtaining $\Delta H°$ is microcalorimetry. As an illustration, the thermodynamic parameters, $\Delta G°$, $\Delta H°$ and $T\Delta S°$ for octylhexaoxyethylene glycol monoether (C_8E_6) are given in Table 3.2.

It can be seen from Table 3.2 that $\Delta G°$ is large and negative, whereas $\Delta H°$ is positive, indicating that the process is endothermic. In addition, $T\Delta S°$ is large and positive, which implies that in the micellisation process there is a net increase in entropy. This positive enthalpy and entropy points to a different driving force for micellisation from that encountered in many aggregation processes.

Table 3.2 Thermodynamic quantities for Micellisation of octylhexaoxyethylene glycol monoether.

Temperature (°C)	**$\Delta G°$ (kJ mol^{-1})**	**$\Delta H°$ (kJ mol^{-1}) (from cmc)**	**$\Delta H°$ (kJ mol l^{-1}) (from calorimetry)**	**$T\Delta S°$ (kJ mol^{-1})**
25	-21.3 ± 2.1	8.0 ± 4.2	20.1 ± 0.8	41.8 ± 1.0
40	-23.4 ± 2.1	—	14.6 ± 0.8	38.0 ± 1.0

Table 3.3 Change of thermodynamic parameters of micellisation of alkyl sulphoxide with increasing chain length of the alkyl group.

Surfactant	**ΔG (kJ mol^{-1})**	**$\Delta H°$ (kJ mol^{-1})**	**$T\Delta S°$ (kJ mol^{-1})**
$C_6H_{13}S(CH_3)O$	−12.0	10.6	22.6
$C_7H_{15}S(CH_3)O$	−15.9	9.2	25.1
$C_8H_{17}S(CH_3)O$	−18.8	7.8	26.4
$C_9H_{19}S(CH_3)O$	−22.0	7.1	29.1
$C_{10}H_{21}S(CH_3)O$	−25.5	5.4	30.9
$C_{11}H_{23}S(CH_3)O$	−28.7	3.0	31.7

The influence of alkyl chain length of the surfactant on the free energy, enthalpy and entropy of micellisation, was demonstrated by Rosen [20], who listed these parameters as a function of alkyl chain length for sulphoxide surfactants. The results are given in Table 3.3, where it can be seen that the standard free energy of micellisation becomes increasingly negative as the chain length increases. This is to be expected as the cmc decreases with an increase in the alkyl chain length. However, $\Delta H°$ becomes less positive and $T\ \Delta S$ becomes more positive with an increase in chain length of the surfactant. Thus, the large negative free energy of micellisation is made up of a small positive enthalpy (which decreases slightly with increase of the chain length of the surfactant) and a large positive entropy term $T\Delta S°$, which becomes more positive as the chain is lengthened. As will be seen in the next section, these results can be accounted for in terms of the hydrophobic effect, which will be described in some detail.

3.2.1
Driving Force for Micelle Formation

Until recently, the formation of micelles was regarded primarily as an interfacial energy process, analogous to the process of the coalescence of oil droplets in an aqueous medium. If this was the case, micelle formation would be a highly exothermic process as the interfacial free energy has a large enthalpy component.

Table 3.4 Thermodynamic parameters for transfer of hydrocarbons from water to liquid hydrocarbon at 25 °C.

Hydrocarbon	ΔG° (kJ mol^{-1})	ΔH° (kJ mol^{-1})	ΔS° (kJ mol^{-1} K^{-1})	$\Delta C_p{}^\circ$ (kJ mol^{-1} K^{-1})	$C_p{}^{\circ,\mathrm{gas}}$ (kJ mol^{-1} K^{-1})
C_2H_6	−16.4	10.5	88.2	—	—
C_3H_8	−20.4	7.1	92.4	—	—
C_4H_{10}	−24.8	3.4	96.6	−273	−143
C_5H_{12}	−28.8	2.1	105.0	−403	−172
C_6H_{14}	−32.5	0	109.2	−441	−197
C_6H_6	−19.3	−2.1	58.8	−227	−134
$C_6H_5CH_3$	−22.7	−1.7	71.4	−265	−155
$C_6H_5C_2H_5$	−26.0	−2.0	79.8	−319	−185
$C_6H_5C_3H_8$	−29.0	−2.3	88.2	−395	—

However, as mentioned above, experimental results have shown clearly that micelle formation involves only a small enthalpy change, and is often endothermic. The negative free energy of micellisation is the result of a large positive entropy, and this led to the conclusion that micelle formation must be predominantly an entropy-driven process.

Two main sources of entropy may have been suggested. The first is related to the so-called "hydrophobic effect," which was initially established from a consideration of the free energy enthalpy and entropy of transfer of hydrocarbon from water to a liquid hydrocarbon. Some results are listed in Table 3.4; this table also includes the heat capacity change ΔC_p on transfer from water to a hydrocarbon, as well as $C_p{}^{\circ,\mathrm{gas}}$, that is the heat capacity in the gas phase. It can be seen from the data in Table 3.4 that the principal contribution to the value of ΔG° is the large positive value of ΔS°, which increases with an increase in the hydrocarbon chain length, whereas ΔH° is either positive or small and negative. To account for this large positive entropy of transfer, Tanford [19] suggested that the water molecules around a hydrocarbon chain are ordered, forming "clusters" or "icebergs." On the transfer of an alkane from water to a liquid hydrocarbon, these clusters are broken, thus releasing water molecules which now have a higher entropy, and this accounts for the large entropy of transfer of an alkane from water to a hydrocarbon medium. This effect is also reflected in the much higher heat capacity change on transfer, $\Delta C_p{}^\circ$, when compared to the heat capacity in the gas phase, $C_p{}^\circ$. This effect is also operative on the transfer of a surfactant monomer to a micelle, during the micellisation process. The surfactant monomers will also contain "structured" water around their hydrocarbon chain; on the transfer of such monomers to a micelle these water molecules are released and have a higher entropy.

The second source of entropy increase on micellisation may arise from an increase in the flexibility of hydrocarbon chains on their transfer from an aqueous to a hydrocarbon medium [19]. The orientations and bendings of an organic chain are likely to be more restricted in an aqueous phase compared to an organic phase. It should be mentioned that in the case of ionic and zwitterionic surfactants an additional entropy contribution, associated with the ionic head groups, must be considered. Upon partial neutralisation of the ionic charge by the counterions when aggregation occurs, water molecules are released. This will be associated with an entropy increase which should be added to the entropy increase resulting from the hydrophobic effect mentioned above. However, the relative contribution of the two effects is difficult to assess in a quantitative manner.

3.2.2
Micellisation in Surfactant Mixtures (Mixed Micelles)

In most industrial applications, more than one surfactant molecule is used in the formulation, and it is therefore necessary to predict the types of possible interactions and whether this will lead to certain synergistic effects. Two general cases may be considered: (i) surfactant molecules with no net interaction (with similar head groups); and (ii) systems with a net interaction [1]. The first case applies when mixing two surfactants with the same head group but with different chain lengths. In analogy with the hydrophilic–lipophilic balance (HLB) for surfactant mixtures, it can also be assumed that the cmc of a surfactant mixture (with no net interaction) will be an average of the two cmcs of the single components [1]:

$$\mathrm{cmc} = x_1\,\mathrm{cmc}_1 + x_2\,\mathrm{cmc}_2 \tag{3.22}$$

where x_1 and x_2 are the mole fractions of the respective surfactants in the system. However, the mole fractions should not be those in the whole system, but those inside the micelle. This means that Equation (3.22) should be modified as,

$$\mathrm{cmc} = x_1^m\,\mathrm{cmc}_1 + x_2^m\,\mathrm{cmc}_2 \tag{3.23}$$

The superscript m indicates that the values are inside the micelle. If x_1 and $\underline{x}_2$ are the solution composition, then,

$$\frac{1}{\mathrm{cmc}} = \frac{x_1}{\mathrm{cmc}_1} + \frac{x_2}{\mathrm{cmc}_2} \tag{3.24}$$

The molar composition of the mixed micelle is given by,

$$x_1^m = \frac{x_1\,\mathrm{cmc}_2}{x_1\,\mathrm{cmc}_2 + x_2\,\mathrm{cmc}_1} \tag{3.25}$$

Figure 3.8 shows the calculated cmc and the micelle composition as a function of solution composition, using Equations (3.24) and (3.25) for three cases where $\mathrm{cmc}_2/\mathrm{cmc}_1 = 1$, 0.1, and 0.01, respectively. As can be seen, the cmc and micellar composition change dramatically with solution composition when the cmcs of the two surfactants vary considerably – that is, when the ratio of the cmcs is far from 1. This fact is used when preparing microemulsions, where the addition of a medium-chain alcohol (e.g., pentanol or hexanol) changes the properties considerably. If component 2 is much more surface-active (i.e., $\mathrm{cmc}_2/\mathrm{cmc}_1 \ll 1$) and it is present in low concentrations (i.e., x_2 is on the order of 0.01), then from Equation (3.25)

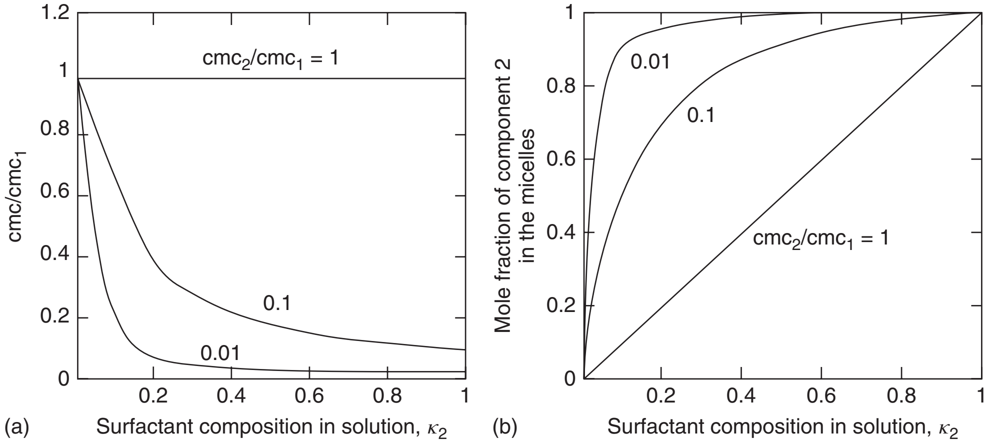

Figure 3.8 (a) Calculated cmc and (b) micellar composition as a function of solution composition for three ratios of cmc.

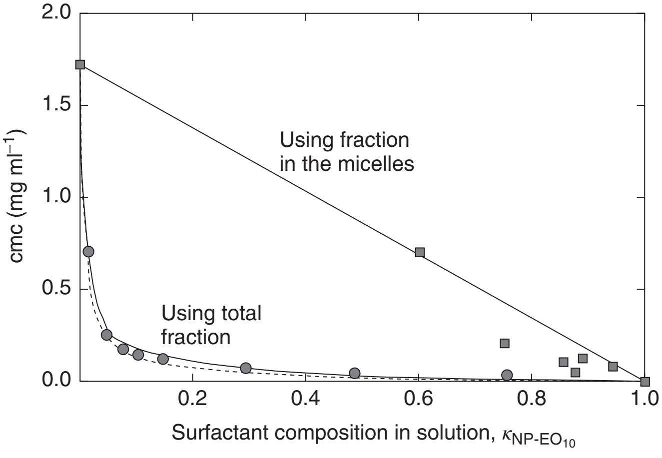

Figure 3.9 cmc as a function of surfactant composition, x_1 or micellar surfactant composition, $x_1{}^m$ for the system SDS + NP-E$_{10}$.

$x_1{}^m \sim x_2{}^m \sim 0.5$; that is, at the cmc of the systems the micelles are composed up to 50% of component 2. This illustrates the role of contaminants in surface activity, for example dodecyl alcohol in SDS.

Figure 3.9 shows the cmc as a function of molar composition of the solution and in the micelles for a mixture of SDS and nonylphenol with 10 mol ethylene oxide (NP-E$_{10}$). If the molar composition of the micelles is used as the x-axis, the cmc is more or less the arithmetic mean of the cmcs of the two surfactants. If, on the other hand, the molar composition in the solution is used as the x-axis (which at the cmc is equal to the total molar concentration), then the cmc of the mixture shows a dramatic decrease at low fractions of NP-E_{10}. This decrease is due to the preferential absorption of NP-E_{10} in the micelle. This higher absorption is due to the higher hydrophobicity of the NP-E_{10} surfactant when compared with SDS.

With many industrial formulations, surfactants of different kinds are mixed together, for example anionics and nonionics. The nonionic surfactant molecules shield the repulsion between the negative head groups in the micelle, and consequently there will be a net interaction between the two types of molecules. Another example is the case when anionic and cationic surfactants are mixed, whereby a very strong interaction will take place between the oppositely charged surfactant molecules. To account for this interaction, Equation (3.25) must be modified by introducing activity coefficients of the surfactants, $f_1{}^m$ and $f_2{}^m$ in the micelle,

$$\text{cmc} = x_1^m f_1^m \,\text{cmc}_1 + x_2^m f_2^m \,\text{cmc}_2 \tag{3.26}$$

An expression for the activity coefficients can be obtained using the regular solutions theory [1],

$$\ln f_1^m = (x_2^m)^2 \beta \tag{3.27}$$

$$\ln f_2^m = (x_2^m)^2 \beta \tag{3.28}$$

where β is an interaction parameter between the surfactant molecules in the micelle. A positive β-value means that there is a net repulsion between the surfactant molecules in the micelle, whereas a negative β-value means a net attraction.

The cmc of the surfactant mixture and the composition x_1 are given by the following equations:

$$\frac{1}{\text{cmc}} = \frac{x_1}{f_1^m \,\text{cmc}_1} + \frac{x_2}{f_2^m \,\text{cmc}_2} \tag{3.29}$$

$$x_1^m = \frac{x_1 f_2^m \,\text{cmc}_2}{x_1 f_2^m \,\text{cmc}_2 + x_2 f_2^m \,\text{cmc}_1} \tag{3.30}$$

Figure 3.10 shows the effect of increasing the β parameter on the cmc and micellar composition for two surfactant with a cmc ratio of 0.1.

This figure shows that as β becomes more negative, the cmc of the mixture decreases. β-values in the region of −2 are typical for anionic/nonionic mixtures, whereas values in the region of −10 to −20 are typical of anionic/cationic mixtures. On increasing the negative value of β, the mixed micelles tend towards a mixing ratio of 50 : 50, which reflects the mutual electrostatic attraction between the surfactant molecules. The predicted cmc and micellar composition depend both on the ratio of the cmcs as well as the value of β. When the cmcs of the single surfactants are similar, the predicted value of the cmc is very sensitive to small variation in β. On the other hand, when the ratio of the cmcs is large, the predicted value of the mixed cmc and the micellar composition are insensitive to variations of the β parameter. For mixtures of nonionic and ionic surfactants, β decreases with an increase in electrolyte concentration, due to screening of the electrostatic repulsion

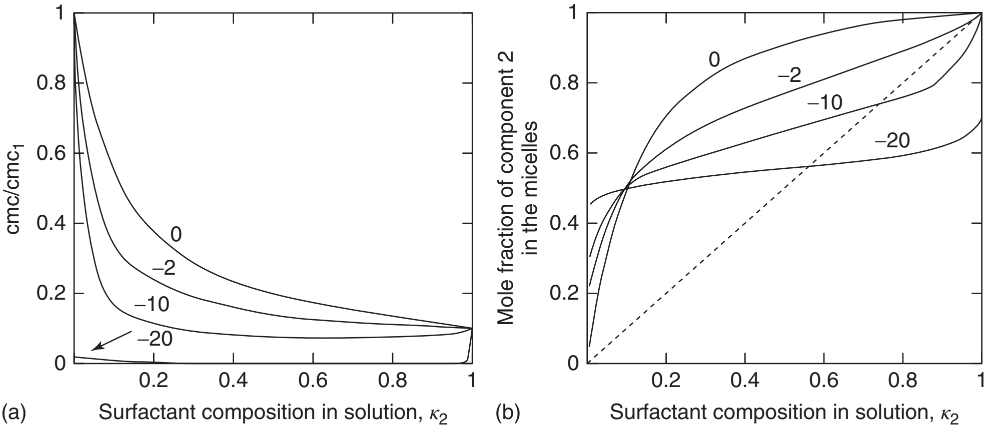

Figure 3.10 (a) cmc and (b) micellar composition for various values of β for a system with a cmc$_2$/cmc$_1$ ratio of 0.1.

on the addition of electrolyte. With some surfactant mixtures, β is decreased with an increase of temperature – that is, the net attraction decreases with an increase of temperature.

References

1. (a) Lindman, B. (1984) in *Surfactants* (ed. Th.F. Tadros), Academic Press, London, NY; (b) K. Holmberg, B. Jonsson, B. Kronberg and B. Lindman *Surfactants and Polymers in Aqueous Solution*, 2nd edn, John Wiley & Sons Ltd, Chichester (2003).
2. Istraelachvili, J. (1985) *Intermolecular and Surface Forces, with Special applications to Colloidal and Biological Systems*, Academic Press, London, p. 251.
3. Mukerjee, P. and Mysels, K.J. (1971) *Critical Micelle Concentrations of Aqueous Surfactant Systems*, National Bureau of Standards Publication, Washington, DC.
4. Elworthy, P.H., Florence, A.T., and Macfarlane, C.B. (1968) *Solubilisation by Surface Active Agents*, Chapman & Hall, London.
5. Shinoda, K., Nagakawa, T., Tamamushi, B.I., and Isemura, T. (1963) *Colloidal Surfactants, Some Physicochemical Properties*, Academic Press, London.
6. McBain, J.W. (1913) *Trans. Faraday Soc.*, **9**, 99.
7. Adam, N.K. (1925) *J. Phys. Chem.*, **29**, 87.
8. Hartley, G.S. (1936) *Aqueous Solutions of Paraffin Chain Salts*, Hermann and Cie, Paris.
9. McBain, J.W. (1950) *Colloid Science*, Heath and Company, Boston, MA.
10. Harkins, W.D., Mattoon, W.D., and Corrin, M.L. (1946) *J. Am. Chem. Soc.*, **68**, 220; *J. Colloid Sci.*, **1**, 105 (1946).
11. Debye, P. and Anaker, E.W. (1951) *J. Phys. Colloid Chem*, **55**, 644.
12. Anainsson, E.A.G. and Wall, S.N. (1974) *J. Phys. Chem.*, **78**, 1024; **79**, 857 (1975).
13. Aniansson, E.A.G., Wall, S.N., Almagren, M., Hoffmann, H., Ulbricht, W., Zana, R., Lang, J., and Tondre, C. (1976) *J. Phys. Chem.*, **80**, 905.
14. Rassing, J., Sams, P.J., and Wyn-Jones, E. (1974) *J. Chem. Soc., Faraday Trans. II*, **70**, 1247.
15. Jaycock, M.J. and Ottewill, R.H. (1964) Proceedings of the Fourth International Congress on Surface Activity, Vol. 2, p. 545.

16. Okub, T., Kitano, H., Ishiwatari, T., and Isem, N. (1979) *Proc. R. Soc.*, **A36**, 81.
17. Phillips, J.N. (1955) *Trans. Faraday Soc.*, **51**, 561.
18. Kahlweit, M. and Teubner, M. (1980) *Adv. Colloid Interface Sci.*, **13**, 1.
19. Tanford, C. (1980) *The Hydrophobic Effect*, 2nd edn, John Wiley & Sons, Inc., New York.
20. Rosen, M.L. (1978) *Surfactants and Interfacial Phenomena*, Wiley-Interscience, New York.

4

Dispersants and Polymeric Surfactants

The surfactants used for the preparation of disperse systems are seldom effective in maintaining the long-term physical stability (absence of flocculation and/or coalescence) of the formulation. This is due to their weak and reversible adsorption and lack of the presence of a high-energy barrier that prevents flocculation as a result of van der Waals attractions. For this reason, dispersants and emulsifiers of polymeric nature that are strongly and irreversibly adsorbed at the interface are required. In addition, these polymeric dispersant provide effective repulsive forces (referred to as steric repulsion) that overcomes the van der Waals attractions. The criteria for an effective dispersant are [1, 2]:

1) The particles should be completely covered by the dispersant (the amount of dispersant should correspond to the plateau value). Any bare patches may cause flocculation either by van der Waals attractions (between the bare patches) or by bridging flocculation (whereby a polymer molecule will become simultaneously adsorbed onto two or more particles).
2) The dispersant should be strongly 'anchored' to the particle surfaces, to prevent any displacement during particle approach. This is particularly important for concentrated suspensions. For this purpose, A-B, A-B-A block and BA_n graft copolymers are most suitable, where the chain B is chosen to be highly insoluble in the medium and has a strong affinity to the surface. Examples of B groups for hydrophobic particles in aqueous media are polystyrene and poly(methylmethacrylate).
3) The stabilising chain A should be highly soluble in the medium and strongly solvated by its molecules. Examples of A chains in aqueous media are poly(ethylene oxide) (PEO) and poly(vinyl alcohol) (PVA).
4) The adsorbed layer thickness δ should be sufficiently large (>5 nm) to prevent weak flocculation.

The above polymeric dispersants are essential materials for the preparation of most disperse systems, of which should be mentioned dyestuffs, paper coatings, inks, agrochemicals, pharmaceuticals, personal care products, ceramics, and detergents [1]. One of the most important applications of polymeric surfactants is in the preparation of oil-in-water (O/W) and water-in-oil (W/O) emulsions, as well as solid/liquid dispersions [2, 3]. In this case, the hydrophobic portion of the surfactant molecule should adsorb "strongly" at the O/W or become dissolved in

Formulation of Disperse Systems: Science and Technology, First Edition. Tharwat F. Tadros.

the oil phase; this will leave the hydrophilic components in the aqueous medium, whereby they become strongly solvated by the water molecules.

The other major application of polymeric dispersants is in the preparation of solid/liquid dispersions (usually referred to as suspensions). In general, two methods are used for the preparation of suspensions: condensation and dispersion methods:

- The *condensation method* begins with molecular units, and the particles are built-up by a process of nucleation typical example is the preparation of polymer lattices, in which case the monomer (e.g., styrene or methylmethacrylate) is emulsified in water using an anionic or nonionic surfactant (e.g., sodium dodecyl sulphate or alcohol ethoxylate). A polymeric surfactant is also added to ensure the long-term colloid stability of the resulting latex. An initiator such as potassium persulphate is then added and, when the temperature of the system has increased, initiation occurs that results in formation of the latex [polystyrene or poly(methylmethacrylate)].
- In the *dispersion method*, preformed particles (usually powders) are dispersed in an aqueous solution containing a surfactant. The latter is essential to ensure adequate wetting of the powder (both the external and internal surfaces of the powder aggregates and agglomerates must be wetted) [2]. A polymeric dispersant is also added to ensure the long-term colloid stability of the resulting suspension; this is followed by dispersion of the powder using high-speed stirrers. Finally, the dispersion is ‘‘milled’’ to reduce the particle size to the appropriate range.

The first section of this chapter describes the solution properties of polymers, and this is followed by a general classification of polymeric surfactants. Examples are provided of polymeric surfactants and polyelectrolytes that are used as dispersants and emulsifiers.

4.1
Solution Properties of Polymeric Surfactants

Long flexible macromolecules have a large number of internal degrees of freedom [4–6]. A typical primary structure of such molecules is a linear chain of units connected by covalent bonds that are referred to as the backbone. By rotating about the bonds in the backbone the molecule can change its shape, and this results in a wide spectrum of conformations. Unfortunately, the rotation may be hindered by the side groups, so that some of these conformations may be rather unfavourable. In some macromolecules (e.g., proteins), sequences of preferred orientations appear as helical or folded sections.

For flexible linear polymers the energy barriers associated with rotation around the bonds are small with respect to the thermal motion. Such molecules have a randomly fluctuating three-dimensional tertiary structure that is referred to as the random coil (as illustrated in Figure 4.1). The chain conformation is described as a random flight chain of N bonds of length l. The fluctuating distance between

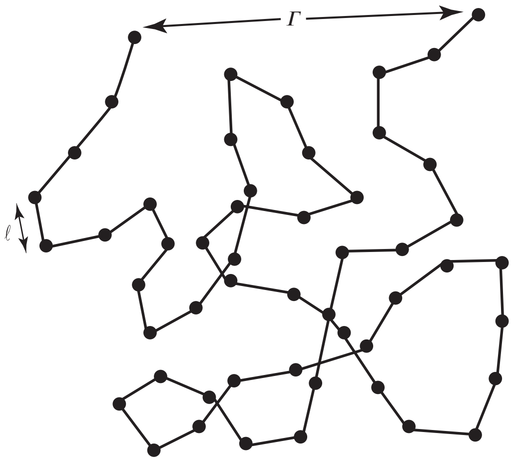

Figure 4.1 Schematic representation of the chain conformation for a random coil.

the end points is r, and the quantity $<r^2>^{1/2}$, which is referred to as the mean end-to-end distance, is a measure of the size of the chain – that is, its mean coil diameter:

$$< r^2>^{1/2} = N^{1/2}\ell \tag{4.1}$$

Another useful parameter is the radius of gyration $<s^2>^{1/2}$, which is a measure of the effective size of a polymer molecule (it is the root mean-square distance of the elements of the chain from its centre of gravity).

For linear polymers [6],

$$< s^2>^{1/2} = \frac{< r^2>^{1/2}}{6^{1/2}} \tag{4.2}$$

Although, in real polymers the bonds cannot assume arbitrary directions, there are fixed angles between them. In addition, rotation about bonds is not entirely free, because the potential energy shows maxima and minima as a function of the rotation angle. Consequently, to account for these effects the above equations are modified by introducing a rigidity parameter p (stiffness ''persistence'') which depends on the architecture of the chain:

$$< r^2>^{1/2} = 6^{1/2}p^{1/2}N^{1/2}\ell \tag{4.3}$$

$$< s^2>^{1/2} = p^{1/2}N^{1/2}\ell \tag{4.4}$$

where $p = 1/6$ for a (hypothetically) fully flexible chain and increases as the chain becomes less flexible, for example when the side groups are bulky. Typical p-values for real chains are in the range of 0.5 to 4.

A useful parameter, called the characteristic ratio, was introduced by Flory [6] and is defined as

$$C_\infty = \frac{< r^2 >}{N\ell_b^2} \tag{4.5}$$

where $l_b{}^2$ represents the sum of the squares of the lengths of the backbone bonds of one monomer unit,

$$\ell_b^2 = \sum_i a_i^2 \tag{4.6}$$

The main consequence of the above equations is that, for ideal chains, the dimensions (root mean-square end-to-end distance and radius of gyration) are proportional to $N^{1/2}$. This is only valid for ideal chains where the volume of the segments and solvency effects are entirely ignored; in other words, a walk may return to its origin without any hindrance. This is unrealistic for segments which occupy a volume, and in good solvents where the chains swell the excluded volume will become important as the segments cannot overlap and there is an exclusion volume that automatically leads to coil expansion. In very good solvents, where the segments repel each other, the excluded volume is larger than the exclusion volume. In contrast, in a poor solvent the segments experience a net attraction such that the effective excluded volume is small and the ideal chain model provides a reasonable description.

The effect of solvency for the polymer chain has been considered in the thermodynamic treatment of Flory and Huggins [6], usually referred to as the Flory–Huggins theory. This theory considers the free energy of mixing of a pure polymer with a pure solvent, ΔG_{mix}, in terms of two contributions, namely the enthalpy of mixing, ΔH_{mix} and the entropy of mixing, ΔS_{mix}, that is using the Second Law of Thermodynamics:

$$\Delta G_{\text{mix}} = \Delta H_{\text{mix}} - T\,\Delta S_{\text{mix}} \tag{4.7}$$

Assuming that the polymer chain adopts a configuration on a lattice (provided by solvent molecules), and considering that the mixing is "random," then the entropy of mixing ΔS_{mix} is given by the following expression:

$$\Delta S_{\text{mix}} = -k\,[n_1 \ln \varphi_1 + n_2 \ln \varphi_2] \tag{4.8}$$

where k is the Boltzmann constant, n_1 is the number of solvent molecules with a volume fraction φ_1, and n_2 is the number of polymer molecules with a volume fraction φ_2.

The enthalpy of mixing, ΔH_{mix}, is given by the following expression:

$$\Delta H_{\text{mix}} = n_1\,\varphi_2\,\chi\,kT \tag{4.9}$$

where χ is a dimensionless interaction parameter and χ^{kT} expresses the difference in energy of a solvent molecule in pure solvent compared to its immersion in pure polymer. χ is usually referred to as the Flory–Huggins interaction parameter.

By combining Equations (4.7–4.9), one obtains

$$\Delta G_{\text{mix}} = kT\,[n_1 \ln \varphi_1 + n_2 \ln \varphi_2 + \chi\,n_1\,\varphi_2] \tag{4.10}$$

The mixing of a pure solvent with a polymer solution creates an osmotic pressure, π, which can be expressed in terms of the polymer concentration c_2 and the volume fraction of the polymer:

$$\frac{\pi}{C_2} = RT\left[\frac{1}{M_2} + \left(\frac{v_2^2}{V_1}\right)\left(\frac{1}{2} - \chi\right) c_2 + \ldots\ldots\right] \tag{4.11}$$

where v_2 is the partial specific volume of the polymer ($v_2 = V_2/M_2$) and V_1 is the molar volume of the solvent.

The second term in Equation (4.11) is the second virial coefficient, B_2, that is

$$\frac{\pi}{c_2} = RT\left[\frac{1}{M_2} + B_2 + \ldots\ldots\right] \tag{4.12}$$

$$B_2 = \left(\frac{v_2^2}{V_1}\right)\left(\frac{1}{2} - \chi\right) \tag{4.13}$$

It should be noted that $B_2 = 0$ when $\chi = 1/2$ – that is, the polymer behaves as ideal in mixing with the solvent; this condition was termed by Flory [6] as the θ-point. Under these conditions the polymer chains in solution has no repulsion or attraction, or they adopt their unperturbed dimension. Clearly, when $\chi < 1/2$, B_2 is positive and mixing is non-ideal, leading to a positive deviation (repulsion); this occurs when the polymer chains are in ‘‘good’’ solvent conditions. In contrast, when $\chi > 1/2$, $\mathbf{B}_2$ will be negative and mixing is non-ideal, leading to a negative deviation (attraction); this occurs when the polymer chains are in ‘‘poor’’ solvent conditions (precipitation of the polymer may occur under these conditions). As the polymer solvency depends on temperature, a θ- temperature can also be defined at which $\chi = 1/2$.

The function $[(1/2) - \chi]$ can also be expressed in terms of two mixing parameters, an enthalpy parameter κ_1 and an entropy parameter ψ_1; that is

$$\left(\frac{1}{2} - \chi\right) = \kappa_1 - \psi_1 \tag{4.14}$$

The θ-temperature can also be defined in terms of κ_1 and ψ_1,

$$\theta = \frac{\kappa_1 T}{\psi_1} \tag{4.15}$$

Alternatively, it is possible to write,

$$\left(\frac{1}{2} - \chi\right) = \psi_1\left(1 - \frac{\theta}{T}\right) \tag{4.16}$$

Although the Flory–Huggins theory is sound in principle, several experimental results cannot be accounted for. For example, it was found that the χ parameter depends on the polymer concentration in solution. Most serious is the fact that many polymer solutions (e.g., PEO) show phase separation on heating, when theory predicts that this should occur only on cooling. Another complication arises from specific interactions with the solvent, for example hydrogen bonding between the polymer and solvent molecules (e.g. with PEO and PVA in water). Aggregation in solution (a lack of complete dissolution) may also present another problem.

The derivation of the Flory–Huggins equation was carried out under the assumption that the volume changes occurring on mixing the polymer and solvent are negligible. As discussed above, the free volume concept must be considered, as this predicts that close to the critical point – where phase separation occurs – there are no bonds between the molecules to constrain separation of the solvent molecules. Such bonds are present, however, for the segments of polymer molecules. Hence, on heating a polymer solution the increase in free volume for the solvent will be large, and much larger than that for the polymer. This difference in free volume will create a large difference in the coefficient of expansion between the polymer and solvent, and this leads to phase separation on heating.

The solution properties of copolymers are much more complicated. This is due mainly to the fact that the two copolymer components A and B behave differently in different solvents, and only when the two components are soluble in the same solvent will they exhibit similar solution properties. This is the case, for example for a nonpolar copolymer in a nonpolar solvent. It should also be emphasised that the Flory–Huggins theory was developed for ideal linear polymers. Indeed, with branched polymers with a high monomer density (e.g. star-branched polymers), the θ-temperature will depend on the length of the arms, and is in general lower than that of a linear polymer with the same molecular weight.

4.2
General Classification of Polymeric Surfactants

Perhaps the simplest type of a polymeric surfactant is a homopolymer, that is formed from the same repeating units, such as PEO or poly(vinyl pyrrolidone). These homopolymers have minimal surface activity at the O/W interface, as the homopolymer segments (e.g., ethylene oxide or vinylpyrrolidone) are highly water-soluble and have little affinity to the interface. However, such homopolymers may adsorb significantly at the solid/liquid (S/L) interface. Even if the adsorption energy per monomer segment to the surface is small (fraction of kT, where k is the Boltzmann constant and T is absolute temperature), the total adsorption energy per molecule may be sufficient to overcome the unfavourable entropy loss of the molecule at the S/L interface.

Clearly, homopolymers are not the most suitable emulsifiers or dispersants. A small variant is to use polymers that contain specific groups that have a high affinity to the surface. This is exemplified by partially hydrolysed poly(vinyl acetate) (PVAc), which is referred to technically as poly(vinyl alcohol). The polymer is prepared by the partial hydrolysis of PVAc, leaving some residual vinyl acetate groups. Most commercially available PVA molecules contain 4–12% acetate groups which are hydrophobic and give the molecule its amphipathic character. On a hydrophobic surface such as polystyrene, the polymer adsorbs with preferential attachment of the acetate groups on the surface, leaving the more hydrophilic vinyl alcohol segments dangling in the aqueous medium. These partially hydrolysed PVA molecules also exhibit surface activity at the O/W interface [1].

The most convenient polymeric surfactants are those of the block and graft copolymer type. A block copolymer is a linear arrangement of blocks of variable monomer composition. The nomenclature for a diblock is poly-A-block-poly-B, and for a triblock it is poly-A-block-poly-B-poly-A [7]. One of the most widely used triblock polymeric surfactants are the “Pluronics” (BASF, Germany), which consist of two poly-A blocks of PEO and one block of poly(propylene oxide) (PPO):

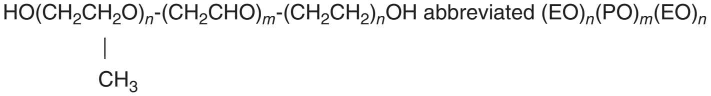

$$HO(CH_2CH_2O)_n\text{-}(CH_2\underset{\underset{CH_3}{|}}{C}HO)_m\text{-}(CH_2CH_2)_nOH \text{ abbreviated } (EO)_n(PO)_m(EO)_n$$

Various molecules are available, where n and m are varied systematically.

Trifunctional products are also available where the starting material is glycerol; these have the structure:

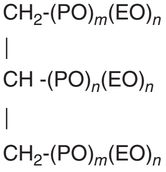

$$\begin{array}{l} CH_2\text{-}(PO)_m(EO)_n \\ | \\ CH\ \text{-}(PO)_n(EO)_n \\ | \\ CH_2\text{-}(PO)_m(EO)_n \end{array}$$

Tetrafunctional products are available where the starting material is ethylene diamine; these have the structures:

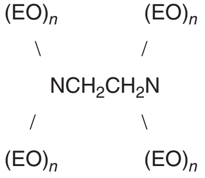

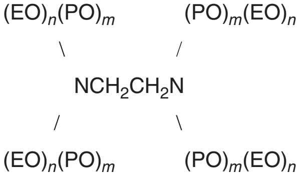

The above polymeric triblocks can be applied as dispersants, whereby the assumption is made that the hydrophobic PPO chain resides at the hydrophobic surface, leaving the two PEO chains dangling in aqueous solution and hence providing steric repulsion. Although these triblock polymeric surfactants have been widely used in various applications suspensions, some doubt has arisen as to how effective these can be. It is generally accepted that the PPO chain is not sufficiently hydrophobic to provide a strong “anchor” to a hydrophobic surface.

Several other diblock and triblock copolymers have been synthesised, although these are of limited commercial availability [7]. Typical examples are diblocks of polystyrene-block-PVA, triblocks of poly(methyl methacrylate)-block PEO-block poly(methyl methacrylate), diblocks of polystyrene block-PEO, and triblocks of PEO-block polystyrene-PEO. An alternative – and perhaps more efficient – polymeric surfactant is the amphipathic graft copolymer consisting of a polymeric backbone B [polystyrene or poly(methylmethacrylate)] and several A chains (''teeth'') such as PEO. This graft copolymer is sometimes referred to as a ''comb'' stabiliser, and is usually prepared by grafting a macromonomer such methoxy polyethylene oxide methacrylate with poly(methylmethacrylate). The ''grafting-onto'' technique has also been used to synthesize polystyrene-PEO graft copolymers.

Recently, graft copolymers based on polysaccharides have been developed for the stabilisation of disperse systems. One of the most useful graft copolymers is based on inulin obtained from chicory roots [8–10]. Inulin is a linear polyfructose chain with a glucose end which, when extracted from chicory roots, has a wide range of chain lengths ranging from two to 65 fructose units. Inulin is fractionated to obtain a molecule with a narrow molecular weight distribution with a degree of polymerisation >23, and is commercially available as INUTEC® N25. The latter molecule has been used to prepare a series of graft copolymers by a random grafting of alkyl chains (using alky isocyanate) onto the inulin backbone. The first molecule of this series was INUTEC® SP1 (Beneo-Remy, Belgium), obtained by a random grafting of C_{12} alkyl chains. This has an average molecular weight of ~5000 Da; the structure is shown in Figure 4.2 and the molecule is illustrated schematically in Figure 4.3. The structure shows clearly the hydrophilic polyfructose chain (backbone) and the randomly attached alkyl chains. The main advantages of INUTEC® SP1 as a stabiliser for disperse systems are:

- Its strong adsorption to the particle or droplet by multipoint attachment with several alkyl chains; this ensures a lack of desorption and displacement of the molecule from the interface.
- A strong hydration of the linear polyfructose chains, both in water and in the presence of high electrolyte concentrations and high temperatures. This ensures an effective steric stabilisation.

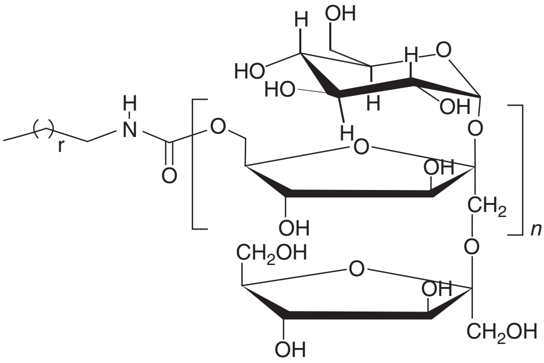

(GFn)

1a

Figure 4.2 Structure of INUTEC® SP1.

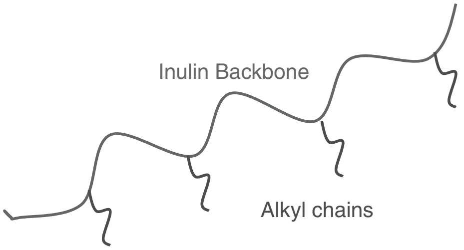

Figure 4.3 Schematic representation of INUTEC® SP1 polymeric surfactant.

4.3
Polyelectrolytes

A good example of polyelectrolytes is sulphonated alkyl naphthalene formaldehyde condensates:

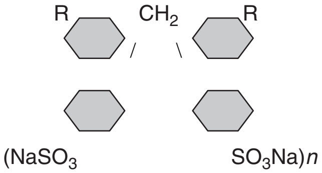

The polyelectrolyte molecule has a wide distribution of molecular weights, and is a good dispersant for many hydrophobic solids. In some cases a wetter is not needed as the low-molecular-weight species can diffuse rapidly to the interface.

Another group of polyelectrolytes that are used in many suspensions are the lignosulphonates. These are isolated from the waste liquor produced during wood pulping by the sulphite process, and during which lignin is sulphonated. Lignosulphonates may also be produced by sulphonating lignin during the alkaline pulping of wood, using the Krafft process. Lignosulphonates as dispersants are mixtures of polyelectrolytes with molecular weights ranging from 2000 to 10 000 Da. The exact structure of lignosulphonates is not completely known, but guaiacylpropyl groups with sulphate groups attached to the aliphatic chains of lignin have been identified. The degree of sulphonation varies from 0.3 to 1.0 per phenyl unit. The commercial products, namely Polyfon (Wesvaco, USA) and Ufoxane (Borregard, Norway), are described by their degree of sulphonation per 840 units of lignin; for example, Polyfon H has a degree of sulphonation of 0.5, and Polyfon T a degree of 2.0. The most effective lignosulphonates for hydrophobic solids in aqueous solution are those with a lower degree of sulphonation, as these produce a higher level of adsorption.

References

1. Tadros, Th.F. (2005) *Applied Surfactants*, Wiley-VCH Verlag GmbH, Weinheim.
2. Tadros, Th.F. (2012) *Dispersion of Powders in Liquids and Stabilisation of Suspensions*, Wiley-VCH Verlag GmbH, Weinheim.
3. Tadros, Th.F. (ed.) (2013) *Emulsion Formation and Stability*, Wiley-VCH Verlag GmbH, Weinheim.
4. Tadros, Th.F. (1999) in *Principles of Polymer Science and Technology in Cosmetics and Personal Care* (eds E.D. Goddard and J.V. Gruber), Marcel Dekker, New York.
5. Tadros, Th.F. (2003) in *Novel Surfactants* (ed. K. Holmberg), Marcel Dekker, New York.
6. Flory, P.J. (1953) *Principles of Polymer Chemistry*, Cornell University Press, New York.
7. Piirma, I. (1992) *Polymeric Surfactants*, Surfactant Science Series, vol. 42, Marcel Dekker, New York.
8. Stevens, C.V., Meriggi, A., Peristerpoulou, M., Christov, P.P., Booten, K., Levecke, B., Vandamme, A., Pittevils, N. and Tadros, Th.F. (2001) *Biomacromolecules*, **2**, 1256.
9. Hirst, E.L., McGilvary, D.I., and Percival, E.G. (1950) *J. Chem. Soc.*, 1297.
10. Suzuki, M. (1993) in *Science and Technology of Fructans* (eds M. Suzuki and N.J. Chatterton), CRC Press, Boca Raton, FL, p. 21.

5

Adsorption of Surfactants at the Air/Liquid, Liquid/Liquid, and Solid/Liquid Interfaces

5.1

Introduction

Surfactants play a major role in the formulation of most disperse systems. They are used for the stabilisation of emulsions, nanoemulsions, microemulsions and suspensions. The surfactant needs to accumulate at the interface, a process that is generally described as adsorption. The simplest interface is that of the air/liquid (A/L), and in this case the surfactant will adsorb with the hydrophilic group pointing towards the polar liquid (water), leaving the hydrocarbon chain pointing towards the air; this process results in a lowering of the surface tension, γ. Typically, surfactants show a gradual reduction in γ until the critical micelle concentration (cmc) is reached, above which the surface tension remains virtually constant. Hydrocarbon surfactants of the ionic, nonionic or zwitterionic ionic type lower the surface tension to limiting values, reaching 30–40 $\mathrm{mN\,m^{-1}}$ depending on the nature of the surfactant. Lower values, typically on the order of 20 $\mathrm{mN\,m^{-1}}$, may be achieved using fluorocarbon surfactants. It is, therefore, essential to understand the adsorption and conformation of surfactants at the A/L interface. This is especially important in the process of wetting of solids in liquids, as it is a prerequisite for the dispersion of powder aggregates and agglomerates into single units.

With emulsions, nanoemulsions and microemulsions, the surfactant adsorbs at the oil/water (O/W) interface, with the hydrophilic head group immersed in the aqueous phase and leaving the hydrocarbon chain in the oil phase. Again, the mechanism of stabilisation of emulsions, nanoemulsions and microemulsions depends on the adsorption and orientation of the surfactant molecules at the liquid/liquid (L/L) interface. Surfactants consist of a small number of units and are mostly reversibly adsorbed, which in turn allows some thermodynamic treatments to be applied. In this case, it is possible to describe adsorption in terms of various interaction parameters such as chain/surface, chain solvent and surface solvent. Moreover, the configuration of the surfactant molecule can be simply described in terms of these possible interactions.

The adsorption of surfactants at the solid/liquid (S/L) interface determines their efficiency in powder wetting and dispersion. A reduction of the S/L interfacial tension by surfactant adsorption leads to a reduction of the contact angle, which in turn ensures complete wetting of the powder by the liquid. In addition, the

Formulation of Disperse Systems: Science and Technology, First Edition. Tharwat F. Tadros.

adsorption of surfactants (ionic, nonionic and zwitterionic) allows the stability behaviour of suspensions to be controlled, which is of considerable technological importance. Surfactants are used in the formulation of most disperse system such as dyestuffs, paints, paper coatings, agrochemicals, pharmaceuticals, ceramics, and printing inks. They represent a particularly robust form of stabilisation which is useful at high disperse volume fractions and high electrolyte concentrations, as well as under extreme conditions of high temperature, pressure, and flow. In particular, surfactants are essential for the stabilisation of suspensions in nonaqueous media, where electrostatic stabilisation is less successful. The key to understanding how surfactants function as stabilisers is to recognize the mechanism(s) of their adsorption and their conformation at the S/L interface.

5.2
Adsorption of Surfactants at the Air/Liquid (A/L) and Liquid/Liquid (L/L) Interfaces

Before describing surfactant adsorption at A/L and L/L interfaces, it is essential first to define the interface. The surface of a liquid is the boundary between two bulk phases, namely liquid and air (or the liquid vapour). Similarly, an interface between two immiscible liquids (oil and water) may be defined, provided that a dividing line is introduced as the interfacial region is not a layer of one-molecule thickness; rather, it usually has a thickness δ with properties that are different from the two bulk phases α and β [1]. However, Gibbs [2] introduced the concept of a mathematical dividing plane Z_σ in the interfacial region (Figure 5.1)

In this model the two bulk phases α and β are assumed to have uniform thermodynamic properties up to Z_σ. This situation applies for both A/L and L/L interfaces (with A/L interfaces, one of the phases is air-saturated with the vapour of the liquid).

By using the Gibbs model, it is possible to obtain a definition of the surface or interfacial tension γ, starting from the Gibbs–Duhem equation [2], that is

$$dG^\sigma = -S^\sigma\, dT + A\, d\gamma + \sum n_i\, d\mu_i \tag{5.1}$$

where G^σ is the surface free energy, S^σ is the entropy, A is the area of the interface, and n_i is the number of moles of component i with chemical potential μ_i at the

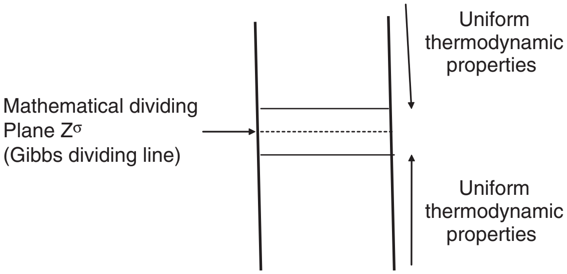

Figure 5.1 Gibbs convention for an interface.

interface. At a constant temperature and composition of the interface (i.e., in the absence of any adsorption):

$$\gamma = \left(\frac{\partial G^{\sigma}}{\partial A}\right)_{T,n_i} \tag{5.2}$$

It is obvious from Equation (5.2) that for a stable interface, γ should be positive. In other words, the free energy should increase if the area of the interface increases; otherwise, the interface will become convoluted, increasing the interfacial area, until the liquid evaporates (for the A/L case) or the two "immiscible" phases dissolved in each other (for the L/L case).

It is also clear from Equation (5.2) that surface or interfacial tension – that is, the force per unit length tangential to the surface, measured in units of millinewtons per metre – is dimensionally equivalent to an energy per unit area measured in millijoules per square metre. For this reason, it has been stated that the excess surface free energy is identical to the surface tension, but this is true only for a single-component system – that is, a pure liquid (where the total adsorption is zero).

There are generally two approaches for treating surfactant adsorption at the A/L and L/L interfaces. The first approach, adopted by Gibbs, treats adsorption as an equilibrium phenomenon whereby the Second Law of Thermodynamics may be applied using surface quantities. The second approach, referred to as the equation of state approach, treats the surfactant film as a two-dimensional layer with a surface pressure π that may be related to the surface excess Γ (the amount of surfactant adsorbed per unit area). These two approaches are summarised below.

5.3
The Gibbs Adsorption Isotherm

Gibbs [2] derived a thermodynamic relationship between the surface or interfacial tension γ and the surface excess Γ (adsorption per unit area). The starting point of this equation is the Gibbs–Duhem equation, as given above [see Eq. (5.1)]. At equilibrium, where the rate of adsorption is equal to the rate of desorption, $\mathrm{d}G^{\sigma} = 0$. Hence, at a constant temperature, but in the presence of adsorption,

$$\mathrm{d}G^{\sigma} = -S^{\sigma}\,\mathrm{d}T + A\,\mathrm{d}\gamma + \sum n_i\,\mathrm{d}\mu_i = 0$$

or

$$\mathrm{d}\gamma = -\sum \frac{n_i^{\sigma}}{A}\,\mathrm{d}\mu_i = -\sum \Gamma_i\,\mathrm{d}\mu_i \tag{5.3}$$

where $\Gamma_i = n_i^{\sigma}/A$ is the number of moles of component i adsorbed per unit area.

Equation (5.3) is the general form for the Gibbs adsorption isotherm. The simplest case of this isotherm is a system of two components in which the solute [Eq. (5.2)] is the surface-active component – that is, it is adsorbed at the surface of the solvent [Eq. (5.1)]. For such a case, Equation (5.3) may be written as:

$$-\mathrm{d}\gamma = \Gamma_1^{\sigma}\,\mathrm{d}\mu_1 + \Gamma_2^{\sigma}\,\mathrm{d}\mu_2 \tag{5.4}$$

and if the Gibbs dividing surface is used, $\Gamma_1 = 0$ and,

$$-\mathrm{d}\gamma = \Gamma_{1,2}^{\sigma}\ \mathrm{d}\mu_2 \tag{5.5}$$

where $\Gamma_{2,1}{}^{\sigma}$ is the relative adsorption of Equation (5.2) with respect to Equation (5.1). Since,

$$\mu_2 = \mu_2^{o} + RT\ \ln\ a_2^{L} \tag{5.6}$$

or,

$$\mathrm{d}\mu_2 = RT\ \mathrm{dln}\ a_2^{L} \tag{5.7}$$

then,

$$-\mathrm{d}\gamma = \Gamma_{2,1}^{\sigma}\ RT\ \mathrm{dln}\ a_2^{L} \tag{5.8}$$

or

$$\Gamma_{2,1}^{\sigma} = -\frac{1}{RT}\left(\frac{\mathrm{d}\gamma}{\mathrm{dln}\ a_2^{L}}\right) \tag{5.9}$$

where $a_2{}^{L}$ is the activity of the surfactant in bulk solution that is equal to $C_2 f_2$ or $x_2 f_2$, where C_2 is the concentration of the surfactant in mol dm^{-3} and x_2 is its mole fraction.

Equation (5.9) allows the surface excess (abbreviated as Γ_2) to be obtained from the variation of surface or interfacial tension with surfactant concentration. Note that $a_2 \sim C_2$, since in dilute solutions $f_2 \sim 1$. This approximation is valid since most surfactants have a low cmc (usually $<10^{-3}$ mol dm^{-3}) and adsorption is complete at or just below the cmc.

The surface excess Γ_2 can be calculated from the linear portion of the γ–log C_2 curves before the cmc. Such γ–log C curves are illustrated in Figure 5.2 for the air/water (A/W) and O/W interfaces; (C_{SAA}) denotes the concentration of surface active agent in bulk solution. It can be seen that, for the A/W interface, γ decreases from the value for water (72 mN m^{-1} at 20 °C) and reaches about 25–30 mN m^{-1} near the cmc; this is clearly schematic as the actual values depend on the surfactant nature. For the O/W case, γ decreases from a value of about 50 mN m^{-1} (for a pure

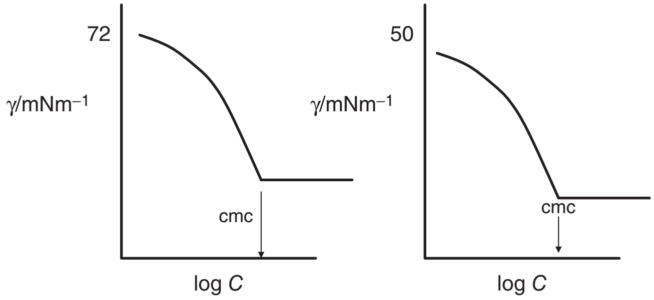

Figure 5.2 Variation of surface and interfacial tension with log (C_{SAA}) at the air/water and oil/water interface.

hydrocarbon-water interface) to ~1–5 mN m^{-1} near the cmc (again, depending on the nature of the surfactant).

As mentioned above, Γ_2 can be calculated from the slope of the linear position of the curves shown in Figure 5.2, just before the cmc is reached. The area per surfactant ion or molecule can be calculated from Γ_2, since

$$\text{Area/molecule} = \frac{1}{\Gamma_2\, N_{\text{Av}}}\ \text{m}^2 = \frac{10^{18}}{\Gamma_2 N_{\text{Av}}}\ \text{nm}^2 \tag{5.10}$$

where N_{Av} is Avogadro's constant. Determining the area per surfactant molecule is very useful as it provides information on the surfactant orientation at the interface. For example, in the case of ionic surfactants such as alkyl sulphates the area per surfactant is determined by the area occupied by the alkyl chain and head group if these molecules lie flat at the interface. In this instance, the area per molecule increases with increases in the alkyl chain length. For vertical orientation, the area per surfactant ion is determined by that occupied by the charged head group, which at low electrolyte concentrations will be in the region of 0.40 nm^2. Such an area is larger than the geometric area occupied by a sulphate group, as a result of the lateral repulsion between the head groups. However, on the addition of electrolytes this lateral repulsion is reduced and the area/surfactant ion for vertical orientation will be less than 0.4 nm^2 (reaching in some cases 0.2 nm^2).

Another important point can be made from the γ–log C curves. At a concentration just before the break point there is a condition of constant slope, which indicates that saturation adsorption has been reached:

$$\left(\frac{\partial \gamma}{\partial \ln\ a_2}\right)_{p,T} = \text{constant} \tag{5.11}$$

while just above the break point

$$\left(\frac{\partial \gamma}{\partial \ln\ a_2}\right)_{p,T} = 0 \tag{5.12}$$

indicating the constancy of γ with log C above the cmc. Integration of Equation (5.12) gives

$$\gamma = \text{constant}\ x\ \ln\ a_2 \tag{5.13}$$

Since γ is constant in this region, a_2 must also remain constant, which means that the addition of surfactant molecules above the cmc must result in an association to form units (micellar) with low activity.

As mentioned above, the hydrophilic head group may be unionised [e.g., alcohols or poly(ethylene oxide) (PEO) alkane or alkyl phenol compounds], weakly ionised (e.g., carboxylic acids), or strongly ionised (e.g., sulphates, sulphonates, and quaternary ammonium salts). The adsorption of these different surfactants at the A/W and O/W interfaces depends on the nature of the head group. With nonionic surfactants, repulsion between the head groups is small and these surfactants are usually strongly adsorbed at the surface of water from very dilute solutions. Nonionic surfactants have much lower cmc values when compared to ionic surfactants with the same alkyl chain length; typically, the cmc is in the region of

10^{-5} to 10^{-4} mol dm^{-3}. Such nonionic surfactants form closely packed adsorbed layers at concentrations lower than their cmc values. The activity coefficient of such surfactants is close to unity and is only slightly affected by the addition of moderate amounts of electrolytes (or a change in the pH of the solution). Thus, nonionic surfactant adsorption is the simplest case as the solutions can be represented by a two-component system and the adsorption can be accurately calculated, using Equation (5.9).

In contrast, with ionic surfactants the adsorption process is relatively more complicated as the repulsion between the head groups and the effect of presence of any indifferent electrolyte must be considered. Moreover, the Gibbs adsorption equation must be solved, taking into account the surfactant ions, the counterion and any indifferent electrolyte ions present. For a strong surfactant electrolyte such as $Na^+ R^-$:

$$\Gamma_2 = \frac{1}{2RT}\frac{\partial\gamma}{\partial \ln a\pm} \tag{5.14}$$

The factor of 2 in Equation (5.14) arises because both the surfactant ion and the counterion must be adsorbed to maintain neutrally, and $d\gamma/d\ln a\pm$ is twice as large as for an unionised surfactant.

If a nonadsorbed electrolyte (such as NaCl) is present in a large excess, then any increase in concentration of Na^+R^- will produce a negligible increase in Na^+ ion concentration, and therefore $d\mu_{Na}$ becomes negligible. Moreover, $d\mu_{Cl}$ is also negligible, so that the Gibbs adsorption equation reduces to

$$\Gamma_2 = -\frac{1}{RT}\left(\frac{\partial\gamma}{\partial \ln C_{NaR}}\right) \tag{5.15}$$

That is, the equation becomes identical to that for a nonionic surfactant.

The above discussion clearly illustrates that, in order to calculate Γ_2 from the γ–log C curve it is important to consider the nature of the surfactant and the composition of the medium. For nonionic surfactants the Gibbs adsorption equation [Eq. (5.9)] can be used directly but for an ionic surfactant, in the absence of electrolytes, the right-hand side of Equation (5.9) should be divided by 2 to account for surfactant dissociation. This factor disappears in the presence of a high concentration of an indifferent electrolyte.

5.4
Equation of State Approach

In this approach, the surface pressure π is related to the surface excess $\underline{\Gamma_2}$ and defined by the equation:

$$\pi = \gamma_o - \gamma \tag{5.16}$$

where γ_o is the surface or interfacial tension before adsorption and γ is that after adsorption.

For an ideal surface film, behaving as a two-dimensional gas, the surface pressure π is related to the surface excess Γ_2 by the equation,

$$\pi\ A = n_2\ RT \tag{5.17}$$

or

$$\pi = (n_2/A)\ RT = \Gamma_2\ RT \tag{5.18}$$

Differentiating Equation (5.17) at constant temperature,

$$d\pi = RT\ d\Gamma_2 \tag{5.19}$$

Using the Gibbs equation,

$$\mathrm{d}\pi = -\mathrm{d}\gamma = \Gamma_2\ RT\ \mathrm{dln}a_2 \approx \Gamma_2\ RT\ \mathrm{dln}C_2 \tag{5.20}$$

Combining Equations (5.19) and (5.20)

$$\mathrm{dln}\Gamma_2 = \mathrm{dln}C_2 \tag{5.21}$$

or

$$\Gamma_2 = K\ C_2^{\alpha} \tag{5.22}$$

Equation (5.22), which is referred to as Henry's law isotherm, predicts a linear relationship between Γ_2 and C_2.

It is clear that Equations (5.16) and (5.19) are based on an idealised model in which the lateral interaction between the molecules has not been considered. Moreover, in this model the molecules are considered to be dimensionless. This model can only be applied at very low surface coverage where the surfactant molecules are so far apart that lateral interaction may be neglected. Moreover, under these conditions the total area occupied by the surfactant molecules is relatively small compared to the total interfacial area.

At a significant surface coverage the above equations must be modified to take into account any lateral interactions between the molecules, as well as the area occupied by them. Lateral interactions may cause a reduction in π if there is an attraction between the chains (e.g., with most nonionic surfactant), or it may cause an increase in π as a result of the repulsion between head groups, as in the case of ionic surfactants.

Various equation of state have been proposed, taking into account the above two effects, in order to fit the π-A data. The two-dimensional van der Waals equation of state is probably the most convenient for fitting these adsorption isotherms, that is:

$$\left(\pi + \frac{(n_2)^2\alpha}{A_2}\right)(A - n_2 A_2^{\mathrm{o}}) = n_2\ RT \tag{5.23}$$

where $A_2°$ is the excluded area or co-area of type 2 molecule in the interface and α is a parameter which allows for lateral interaction.

Equation (5.23) leads to the following theoretical adsorption isotherm, using the Gibbs equation:

$$C_2^\alpha = K_1 \left(\frac{\theta}{1-\theta}\right) \exp \left(\frac{\theta}{1-\theta} - \frac{2\alpha\theta}{a_2^\mathrm{o}\ RT}\right) \tag{5.24}$$

where θ is the surface coverage ($\theta = \Gamma_2/\Gamma_{2,\max}$), K_1 is a constant related to the free energy of adsorption of surfactant molecules at the interface ($K_1 \propto \exp(-\Delta G_\mathrm{ads}/kT)$), and $a_2{}^\circ$ is the area/molecule.

For a charged surfactant layer, Equation (5.21) must be modified to take into account the electrical contribution from the ionic head groups, that is:

$$C_2^\alpha = K_1 \left(\frac{\theta}{1-\theta}\right) \exp \left(\frac{\theta}{1-\theta}\right) \exp \left(\frac{e\psi_\mathrm{o}}{kT}\right) \tag{5.25}$$

where Ψ_o is the surface potential. Equation (5.47) shows how the electrical potential energy (Ψ_o/kT) of adsorbed surfactant ions affects the surface excess. Assuming that the bulk concentration remains constant, then Ψ_o will increase as θ increases; this means that $[\theta/(1-\theta)] \exp [\theta/(1-\theta)]$ will increase less rapidly with C_2, and in turn the adsorption will be inhibited as a result of ionisation.

5.5
The Langmuir, Szyszkowski, and Frumkin Equations

In addition to the Gibbs equation, three other equations have been suggested that relate the surface excess Γ_1, surface or interfacial tension and equilibrium concentration in the liquid phase C_1. The Langmuir equation [3] relates Γ_1 to C_1 by,

$$\Gamma_1 = \frac{\Gamma_m C_1}{C_1 + a} \tag{5.26}$$

where Γ_m is the saturation adsorption at monolayer coverage by surfactant molecules, and a is a constant that is related to the free energy of adsorption $\Delta G^\circ{}_\mathrm{ads}$:

$$a = 55.3 \exp \left(\frac{\Delta G^\mathrm{o}_\mathrm{ads}}{RT}\right) \tag{5.27}$$

where R is the gas constant and T is the absolute temperature.

A linear form of the Gibbs equation is,

$$\frac{1}{\Gamma_1} = \frac{1}{\Gamma_m} + \frac{a}{\Gamma_m C_1} \tag{5.28}$$

Equation (5.28) shows that a plot of $1/\Gamma_1$ versus $1/C_1$ gives a straight line from which Γ_m and a can be calculated from the intercept and slope of the line.

The Szyszkowski equation [4], which indicates a relationship between the surface pressure π and bulk surfactant concentration C_1, is a form of equation of state:

$$\gamma_\mathrm{o} - \gamma = \pi = 2.303 RT \Gamma_m \log \left(\frac{C_1}{a} + 1\right) \tag{5.29}$$

The Frumkin equation [5] is another equation of state:

$$\gamma_o - \gamma = \pi = -2.303RT\Gamma_m \log\left(1 - \frac{\Gamma_1}{\Gamma_m}\right) \quad (5.30)$$

5.6
Interfacial Tension Measurements

These methods may be classified into two categories: (i) those in which the properties of the meniscus are measured at equilibrium, for example the pendant drop or sessile drop profile and Wilhelmy plate methods; and (ii) those where the measurement is made under nonequilibrium or quasi-equilibrium conditions such as the drop volume (weight) or the de Nouy ring method. Although the latter methods are faster, they suffer from the disadvantage of premature rupture and expansion of the interface, causing adsorption depletion. For the measurement of low interfacial tensions ($<0.1\,\text{mN}\,\text{m}^{-1}$), the spinning drop technique is applied. Brief descriptions of each of these techniques are provided in the following sections.

5.6.1
The Wilhelmy Plate Method

In this method [6] a thin plate made from glass (e.g., a microscope cover slide) or platinum foil is either detached from the interface (nonequilibrium condition) or its weight is measured statically, using an accurate microbalance. In the detachment method, the total force F is given by the weight of the plate W and the interfacial tension force:

$$F = W + \gamma\, p \quad (5.31)$$

where p is the "contact length" of the plate with the liquid – that is the plate perimeter. Provided that the contact angle of the liquid is zero, no correction will be required for Equation (5.31), and therefore the Wilhelmy plate method can be applied in the same manner as du Nouy's technique (see below).

The static technique may be applied for following the interfacial tension as a function of time (to follow the kinetics of adsorption) until equilibrium is reached. In this case, the plate is suspended from one arm of a microbalance and allowed to penetrate the upper liquid layer (usually the oil) into the aqueous phase to ensure wetting of the plate. The whole vessel is then lowered to bring the plate into the oil phase. At this point the microbalance is adjusted to counteract the weight of the plate (i.e., its weight now becomes zero), after which the vessel is raised until the plate touches the interface. The increase in weight, ΔW, is given by the following equation:

$$\Delta W = \gamma\, p \cos\theta \quad (5.32)$$

where θ is the contact angle. If the plate is completely wetted by the lower liquid as it penetrates, $\theta = 0$ and γ may be calculated directly from ΔW. Care should always be taken that the plate is completely wetted by the aqueous solution, and for that purpose a roughened platinum or glass plate is used to ensure a zero contact angle. However, if the oil is more dense than water, a hydrophobic plate should be used so that when the plate penetrates the upper aqueous layer and touches the interface it will be completely wetted by the oil phase.

5.6.2
The Pendant Drop Method

If a drop of oil is allowed to hang from the end of a capillary that is immersed in the aqueous phase, it will adopt an equilibrium profile as shown in Figure 5.3. This is a unique function of the tube radius, the interfacial tension, its density, and the gravitational field.

The interfacial tension is given by the following equation [7]:

$$\gamma = \frac{\Delta\rho\, g\, d_e^2}{H} \tag{5.33}$$

where $\Delta\rho$ is the density difference between the two phases, d_e is the equatorial diameter of the drop (see Figure 5.3), and H is a function of d_s/d_e, where d_s is the diameter measured at a distance d from the bottom of the drop (see Figure 5.3). The relationship between H and the experimental values of d_s/d_e has been obtained empirically by using pendant drops of water, with accurate values of H having been obtained by Niederhauser and Bartell [8].

5.6.3
The Du Nouy's Ring Method

The basis of this method is to measure the force required to detach a ring or loop of wire from the L/L interface [9]. As a first approximation, the detachment force is taken to be equal to the interfacial tension γ, multiplied by the perimeter of the ring:

$$F = W + 4\,\pi\,R\,\gamma \tag{5.34}$$

where W is the weight of the ring. Harkins and Jordan [10] introduced a correction factor f (that is a function of the meniscus volume, V, and the radius of the wire, r)

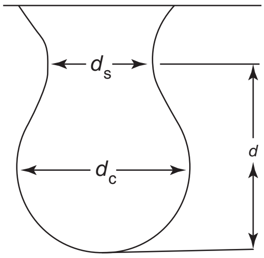

Figure 5.3 Schematic representation of the profile of a pendant drop.

for more accurate calculation of γ from F, that is:

$$f = \frac{\gamma}{\gamma_{\text{ideal}}} = f\left(\frac{R^3}{V}, \frac{R}{r}\right) \tag{5.35}$$

Values of the correction factor f were tabulated by Harkins and Jordan [see Eq. (5.7)], and a theoretical account of f was given by Freud and Freud [11].

When using the du Nouy method for determining γ, it is essential that the ring is kept horizontal during the measurements. Moreover, the ring should be free from any contaminant; this is usually achieved by using a platinum ring that is flamed before use.

5.6.4
The Drop Volume (Weight) Method

The aim here is to determine the volume V (or weight W) of a drop of liquid (immersed in a second, less-dense liquid) which becomes detached from a vertically mounted capillary tip having a circular cross-section of radius r. The ideal drop weight W_{ideal} is given by the expression,

$$W_{ideal} = 2\,\pi\,r\,\gamma \tag{5.36}$$

In practice, a weight W is obtained which is less than W_{ideal} because a portion of the drop remains attached to the tube tip. Thus, Equation (5.36) should include a correction factor φ, that is a function of the tube radius r and some linear dimension of the drop, that is $V^{1/3}$. Thus,

$$W = 2\,\pi\,r\,\gamma\,\varphi\left(\frac{r}{V^{1/3}}\right) \tag{5.37}$$

Values of $(r/V^{1/3})$ have been tabulated by Harkins and Brown [12]. Lando and Oakley [13] used a quadratic equation to fit the correction function to $(r/V^{1/3})$, but a better fit was provided by Wilkinson and Kidwell [14].

5.6.5
The Spinning Drop Method

This method is particularly useful for the measurement of very low interfacial tensions ($<10^{-1}$ mN m^{-1}) that are particularly important in applications such as spontaneous emulsification and the formation of microemulsions. Such low interfacial tensions may also be achieved with emulsions, particularly when mixed surfactant films are used. In this case, a drop of the less-dense liquid A is suspended in a tube containing the second liquid, B. On rotating the whole mass (see Figure 5.4) the drop of the liquid moves to the centre and, with an increasing speed of revolution, the drop elongates as the centrifugal force opposes the interfacial tension force that tends to maintain the spherical shape, which is that having a minimum surface area.

An equilibrium shape is reached at any given speed of rotation. At moderate speeds of rotation, the drop approximates to a prolate ellipsoid, whereas at very

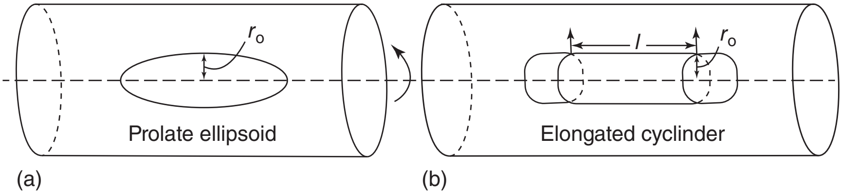

Figure 5.4 Schematic representation of a spinning drop. (a) Prolate ellipsoid; (b) Elongated cylinder.

high speeds of revolution the drop approximates to an elongated cylinder, as shown schematically in Figure 5.4.

When the shape of the drop approximates a cylinder, the interfacial tension is given by the following expression [15]:

$$\gamma = \frac{\omega_2 \, \Delta\rho \, r_o^4}{4} \tag{5.38}$$

where ω is the speed of rotation, $\Delta\rho$ is the density difference between the two liquids A and B, and r_o is the radius of the elongated cylinder. Equation (5.38) is valid when the length of the elongated cylinder is much larger than r_o.

5.7
Adsorption of Surfactants at the Solid/Liquid (S/L) Interface

As mentioned above, surfactants consist of a small number of units and are mostly reversibly adsorbed, which in turn allows thermodynamic treatments to be applied. In this case it is possible to describe adsorption in terms of the various interaction parameters, namely chain–surface, chain–solvent, and surface–solvent. Moreover, the conformation of the surfactant molecules at the interface can be deduced from these simple interaction parameters. However, in some cases the interaction parameters may involve ill-defined forces, such as hydrophobic bonding, solvation forces and chemisorption. In addition, the adsorption of ionic surfactants involves electrostatic forces, particularly in the case of polar surfaces containing ionogenic groups. For that reason, the adsorption of ionic and nonionic surfactants will be treated separately. The surfaces (substrates) can be also hydrophobic or hydrophilic, and these may also be treated separately. Thus, four cases can be considered: (i) the adsorption of ionic surfactants on hydrophobic (nonpolar) surfaces; (ii) the adsorption of ionic surfactants on polar (charged) surfaces); (iii) the adsorption of nonionic surfactants on hydrophobic surfaces; and (iv) the adsorption of nonionic surfactants on polar surfaces. Cases (i) and (iii) are governed by hydrophobic interaction between the alkyl chain and hydrophobic surface, where the charge plays a minor role, while cases (ii) and (iv) are determined by charge and/or polar interaction.

At the S/L interface, the main interest is in determining the following parameters:

- The amount of surfactant adsorbed Γ per unit mass or unit area of the solid adsorbent at a given temperature.

- The equilibrium concentration of the surfactant C (mole dm^{-3} or mole fraction $x = C/55.51$) in the liquid phase required to produce a given value of Γ at a given temperature.
- The surfactant concentration at full saturation of the adsorbent Γ_{sat}.
- The orientation of the adsorbed surfactant ion or molecule that can be obtained from the area occupied by the ion or molecule at full saturation.
- The effect of adsorption on the properties of the adsorbent (nonpolar, polar, or charged).

The general equation for calculating the amount of surfactant adsorbed onto a solid adsorbent from a binary solution containing two components (surfactant component 1 and solvent component 2) is given by [16]:

$$\frac{n_o \Delta x_1}{m} = n_1^s x_2 - n_2^s x_1 \tag{5.39}$$

where n_o is the number of moles of solution before adsorption, $\Delta x_1 = x_{1,0} - x_1$, $x_{1,0}$ is the mole fraction of component 1 before adsorption, x_1 and x_2 are the mole fractions of components 1 and 2 at adsorption equilibrium, m is the mass of adsorbent (in grams), and $n_1{}^{\text{s}}$ and $n_2{}^{\text{s}}$ are the number of components 1 and 2 adsorbed per gram of adsorbent at adsorption equilibrium.

When the liquid phase is a dilute solution of surfactant (component 1) that is much more strongly adsorbed onto the solid substrate than the solvent (component 2), then $n_o \Delta x_1 = \Delta n_1$ where $\Delta n_1 =$ change in number of moles of component 1 in solution, $n_2{}^{\text{s}} \approx 0$, and $x_2 \approx 1$. In this case, Equation (5.39) reduces to

$$n_1^{\text{s}} = \frac{\Delta n_1}{m} = \frac{\Delta C_1 V}{m} \tag{5.40}$$

where $\Delta C_1 = C_{1,0} - C_1$, $C_{1,0}$ is the molar concentration of component 1 before adsorption, C_1 is the molar concentration of component 1 after adsorption, and V is the volume of the liquid phase (in litres).

The surface concentration Γ_1 (in mol m^{-2}) can be calculated from a knowledge of surface area A (m^2 g^{-1}):

$$\Gamma_1 = \frac{\Delta C_1 V}{mA} \tag{5.41}$$

The adsorption isotherm is represented by a plot of Γ_1 versus C_1. In most cases, the adsorption increases gradually with increase of C_1, and a plateau $\Gamma_1{}^{\infty}$ is reached at full coverage corresponding to a surfactant monolayer. The area per surfactant molecule or ion at full saturation can be calculated from:

$$a_1^s = \frac{10^{18}}{\Gamma_1^{\infty} N_{\text{Av}}} \text{nm}^2 \tag{5.42}$$

where N_{Av} is Avogadro's number.

5.7.1
Adsorption of Ionic Surfactants on Hydrophobic Surfaces

The adsorption of ionic surfactants on hydrophobic surfaces such as carbon black, polymer surfaces and ceramics (e.g., silicon carbide or silicon nitride) is governed by hydrophobic interactions between the alkyl chain of the surfactant and the hydrophobic surface. In this case, electrostatic interaction will play a relatively smaller role. However, if the surfactant head group is of the same sign of charge as that on the substrate surface, electrostatic repulsion may oppose adsorption. In contrast, if the head groups are of opposite sign to the surface, adsorption may be enhanced. As the adsorption depends on the magnitude of the hydrophobic bonding free energy, the amount of surfactant adsorbed is increased directly with an increase in the alkyl chain length, in accordance with Traube's rule.

The adsorption of ionic surfactants on hydrophobic surfaces may be represented by the Stern–Langmuir isotherm [17]. Consider a substrate containing N_s sites (mol m^{-2}) on which Γ mol m^{-2} of surfactant ions are adsorbed. The surface coverage θ is (Γ/N_s), and the fraction of uncovered surface is $(1-\theta)$. The rate of adsorption is proportional to the surfactant concentration expressed in mole fraction, $(C/55.5)$, and the fraction of free surface $(1-\theta)$, that is

$$\text{Rate of adsorption} = k_{\text{ads}} \left(\frac{C}{55.5}\right)(1-\theta) \tag{5.43}$$

where k_{ads} is the rate constant for adsorption.

The rate of desorption is proportional to the fraction of surface covered θ,

$$\text{Rate of desorption} = k_{\text{des}}\, \theta \tag{5.44}$$

At equilibrium, the rate of adsorption is equal to the rate of desorption, and the ratio of $(k_{\text{ads}}/k_{\text{des}})$ is the equilibrium constant K, that is

$$\frac{\theta}{(1-\theta)} = \frac{C}{55.5} K \tag{5.45}$$

The equilibrium constant K is related to the standard free energy of adsorption by,

$$-\Delta G^{\text{o}}_{\text{ads}} = RT \ln K \tag{5.46}$$

where R is the gas constant and T is the absolute temperature. Equation (5.46) can be re-written in the form, or

$$K = \exp\left(-\frac{\Delta G^{\text{o}}_{\text{ads}}}{RT}\right) \tag{5.47}$$

By combining Equations (5.45) and (5.47),

$$\frac{\theta}{1-\theta} = \frac{C}{55.5} \exp\left(-\frac{\Delta G^{\text{o}}_{\text{ads}}}{RT}\right) \tag{5.48}$$

Equation (5.48) applies only at low surface coverage ($\theta < 0.1$), where lateral interaction between the surfactant ions can be neglected.

At high surface coverage ($\theta > 0.1$) the lateral interaction between the chains must be taken into account, by introducing a constant A, for example using the Frumkin–Fowler–Guggenheim (FFG) equation [17]:

$$\frac{\theta}{(1-\theta)} \exp(A\theta) = \frac{C}{55.5} \exp\left(-\frac{\Delta G^{\text{o}}_{\text{ads}}}{RT}\right) \tag{5.49}$$

The value of A can be estimated from the maximum slope $(\mathrm{d}\theta/\ln C)_{\max}$ of the isotherm which occurs at $\theta = 0.5$. Furthermore, at $\theta = 0.5$, substitution of A into Equation (5.49) gives the value of $\Delta G^{\circ}{}_{\text{ads}}$.

The above treatment using the FFG isotherm has two limitations. First, it is assumed that A is constant and independent of surface coverage although, in reality, A could change in sign as well as increase in θ. At low coverages, A would reflect repulsive (electrostatic) interaction between adsorbed surfactant ions. At higher coverage, attractive chain–chain interaction becomes more important. The apparent adsorption energy becomes more favourable at a high surface coverage, and this could lead to the formation of "hemimicelles." Second, electrostatic interactions are strongly affected by the level of supporting electrolyte.

Various authors [18, 19] have used the Stern–Langmuir equation in a simple form to describe the adsorption of surfactant ions on mineral surfaces:

$$\Gamma = 2\, r\, C \exp\left(-\frac{\Delta G^{\text{o}}_{\text{ads}}}{RT}\right) \tag{5.50}$$

Various contributions to the adsorption free energy may be envisaged, and to a first approximation these may be considered to be additive. In the first instance, ΔG_{ads} may be taken to consist of two main contributions, that is

$$\Delta G_{\text{ads}} = \Delta G_{\text{elec}} + \Delta G_{\text{spec}} \tag{5.51}$$

where ΔG_{elec} accounts for any electrical interactions (coulombic as well as polar) and ΔG_{spec} is a specific adsorption term which contains all contributions to the adsorption free energy that are dependent on the "specific"(nonelectrical) nature of the system [20]. Several authors have subdivided ΔG_{spec} into supposedly separate independent interactions [20, 21]; for example:

$$\Delta G_{\text{spec}} = \Delta G_{\text{cc}} + \Delta G_{\text{cs}} + \Delta G_{\text{hs}} + \ldots \tag{5.52}$$

where ΔG_{cc} is a term that accounts for the cohesive chain–chain interaction between the hydrophobic moieties of the adsorbed ions, ΔG_{cs} is the term for chain/substrate interaction, whereas ΔG_{hs} is a term for the head group/substrate interaction. Several other contributions to ΔG_{spec} may be envisaged, for example ion–dipole, ion-induced–dipole or dipole-induced–dipole interactions.

As there is no rigorous theory that can predict adsorption isotherms, the most suitable method for investigating the adsorption of surfactants is to determine the adsorption isotherm. The measurement of surfactant adsorption is fairly straightforward: a known mass m (in grams) of the particles (substrate) with known specific surface area A_s ($\text{m}^2\,\text{g}^{-1}$) is equilibrated at constant temperature with surfactant solution with initial concentration C_1. The suspension is kept stirred for sufficient time to reach equilibrium, after which the particles are removed from the suspension by centrifugation and the equilibrium concentration C_2 is determined using a suitable analytical method. The amount of adsorption Γ (mol m^{-2}) is calculated as follows:

$$\Gamma = \frac{(C_1 - C_2)V}{m\,A_s} \tag{5.53}$$

The adsorption isotherm is represented by plotting Γ versus C_2. A range of surfactant concentrations should be used to cover the whole adsorption process – that is, from the initial low values to the plateau values. In order to obtain accurate results the solid should have a high surface area (usually >1 m^2).

Several examples may be quoted from the literature to illustrate the adsorption of surfactant ions onto solid surfaces. For a model hydrophobic surface, carbon black has been chosen [22, 23], and Figure 5.5 shows the typical results for the adsorption of sodium dodecyl sulphate (SDS) onto two carbon black surfaces, namely Spheron 6 (untreated) and Graphon (graphitised), which also describes the effect of surface treatment.

The adsorption of SDS on untreated Spheron 6 tends to show a maximum that is removed on washing. This suggests the removal of impurities from the carbon black, which becomes extractable at high surfactant concentration. The plateau adsorption value was ~2×10^{-6} mol m^{-2} (~2 μmol m^{-2}); this plateau value was reached at ~8 m mol dm^{-3} SDS, which was close to the cmc of the surfactant in bulk solution. The area per surfactant ion in this case was ~0.7 nm^2. Graphitisation (Graphon) removes the hydrophilic ionisable groups (e.g., –C=O or –COOH), producing a surface that is more hydrophobic. The same occurs by heating Spheron 6 to 2700 °C; this leads to a different adsorption isotherm (Figure 5.5) that shows a step (inflection point) at a surfactant concentration in the region of ~6 m mol dm^{-3}. The first plateau value was ~2.3 μmol m^{-2}, whereas the second plateau value (which occurred at the cmc of the surfactant) was ~4 μmol m^{-2}. It is likely in this case

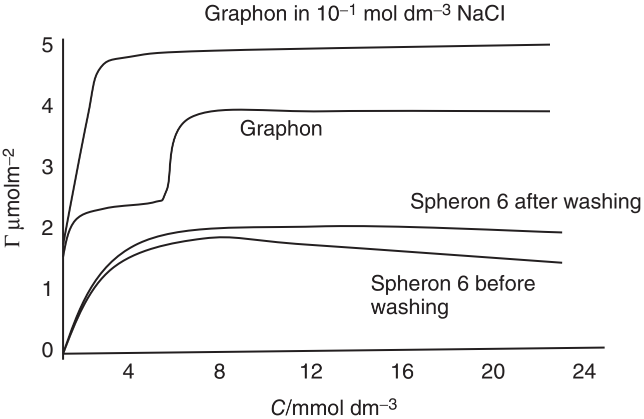

Figure 5.5 Adsorption isotherms for sodium dodecyl sulphate on carbon substrates.

that the surfactant ions had adopted different orientations at the first and second plateaus. In the first plateau region, a more ''flat'' orientation (alkyl chains adsorbed parallel to the surface) was obtained, whereas at the second plateau a vertical orientation was more favourable, with the polar head groups being directed towards the solution phase. The addition of electrolyte (10^{-1} mol dm^{-3} NaCl) had enhanced the surfactant adsorption, this increase being due to a reduction in lateral repulsion between the sulphate head groups, which in turn enhanced the adsorption.

The adsorption of ionic surfactants onto hydrophobic polar surfaces resembles that for carbon black [24, 25]. For example, Saleeb and Kitchener [24] found a similar limiting area for cetyltrimethyl ammonium bromide on Graphon and polystyrene (~0.4 nm^2). As with carbon black, the area per molecule depended on the nature and amount of the added electrolyte. This can be accounted for in terms of the reduction in head group repulsion and/or counterion binging.

Surfactant adsorption close to the cmc may appear Langmuirian, but this does not automatically imply a simple orientation. For example, rearrangement from a horizontal to a vertical orientation or electrostatic interaction and counterion binding may be masked by simple adsorption isotherms. It is essential, therefore, to combine the adsorption isotherms with other techniques such as microcalorimetry and various spectroscopic methods in order to obtain a full picture of surfactant adsorption.

5.7.2
Adsorption of Ionic Surfactants on Polar Surfaces

The adsorption of ionic surfactants onto polar surfaces that contain ionisable groups may show characteristic features due to additional interactions between the head group and substrate, and/or possible chain–chain interaction. This is best illustrated by the results of the adsorption of sodium dodecyl sulphonate (SDSe) on alumina at pH 7.2, as obtained by Fuerestenau [26] and shown in Figure 5.6. At pH 7.2 the alumina is positively charged (the isoelectric point of alumina is

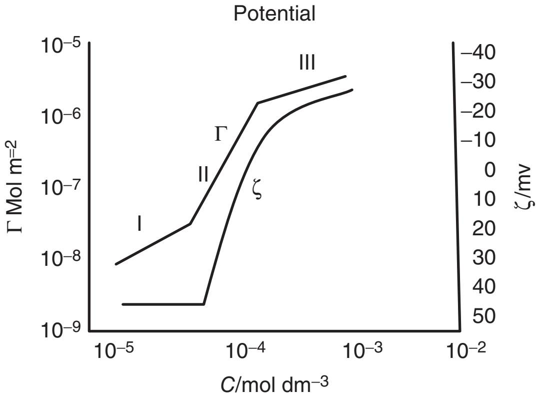

Figure 5.6 Adsorption isotherm for sodium dodecyl sulphonate on alumina and corresponding zeta (ζ).

at pH ~ 9) and the counterions are Cl^- from the added supporting electrolyte. In Figure 5.6, the saturation adsorption Γ_1 is plotted versus the equilibrium surfactant concentration C_1 on logarithmic scales; the figure also shows the results of zeta potential (ζ) measurements (these are a measure of the magnitude sign of charge on the surface). Both, the adsorption and zeta-potential results showed three distinct regions. In region I there was a gradual increase of adsorption with increases in concentration, with virtually no change in the value of the zeta-potential corresponding to an ion-exchange process [27]. In other words, the surfactant ions had simply exchanged with the counterions (Cl^-) of the supporting electrolyte in the electrical double layer. At a critical surfactant concentration, the desorption increased dramatically, with further increases in surfactant concentration (region II). In this region, the positive zeta-potential was gradually decreased, reaching a zero value (charge neutralisation) after which a negative value was obtained that increased rapidly with an increase in surfactant concentration. The rapid increase in region II could be explained in terms of ''hemi-micelle formation,'' as originally postulated by Gaudin and Fuerestenau [28]. In other words, at a critical surfactant concentration (to be denoted the cmc of ''hemi-micelle formation'' or, better, the critical aggregation concentration; CAC), the hydrophobic moieties of the adsorbed surfactant chains were ''squeezed out'' from the aqueous solution by forming two-dimensional aggregates on the adsorbent surface. This was analogous to the process of micellisation in bulk solution. However, the fact that the CAC was lower than the cmc indicated that the substrate had promoted surfactant aggregation. At a certain surfactant concentration in the hemi-micellisation process, the isoelectric point was exceeded and, thereafter, the adsorption was hindered by electrostatic repulsion between the hemi-micelles, such that the slope of the adsorption isotherm was reduced (region III).

5.7.3
Adsorption of Nonionic Surfactants

Several types of nonionic surfactants exist, depending on the nature of the polar (hydrophilic) group. The most common type is that based on a poly(oxyethylene) glycol group, that is $(CH_2CH_2O)_nOH$ (where n can vary from as little as two units to 100 or more units) linked either to an alkyl (C_xH_{2x+1}) or alkyl phenyl (C_xH_{2x+1}-C_6H_4-) group. These surfactants may be abbreviated as C_xE_n or $C_x\varphi E_n$ (where C refers to the number of C atoms in the alkyl chain, φ denotes C_6H_4, and E denotes ethylene oxide; EO). These ethoxylated surfactants are characterised by a relatively large head group compared to the alkyl chain (when $n > 4$). However, there are nonionic surfactants with a small head group such as amine oxide ($-N \rightarrow O$) head group, phosphate oxide ($-P \rightarrow O$), or sulphinyl-alkanol ($-SO-(CH_2)_n-OH$). Most adsorption isotherms in the literature are based on ethoxylated-type surfactants.

The adsorption isotherm of nonionic surfactants are in many cases Langmuirian, much like those of most other highly surface active solutes adsorbing from dilute solutions, and the adsorption is generally reversible. However, several other adsorption types are produced [29], and these are illustrated in Figure 5.7. The steps

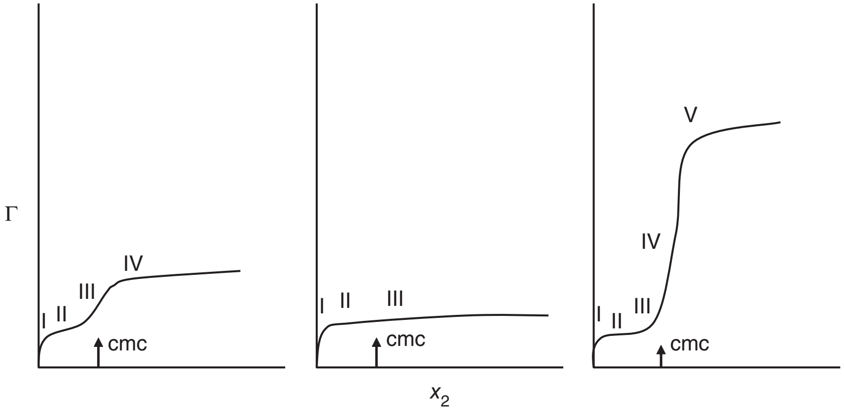

Figure 5.7 Adsorption isotherms corresponding to the three adsorption sequences shown in Figure 5.6.

in the isotherm may be explained in terms of the various adsorbate–adsorbate, adsorbate–adsorbent, and adsorbate–solvent interactions.

These orientations are illustrated schematically in Figure 5.8. In the first stage of adsorption (denoted by I in Figures 5.7 and 5.8), the surfactant–surfactant interaction is negligible (low coverage) and adsorption occurs mainly by van der Waals interactions. On a hydrophobic surface, however, the interaction is dominated by the hydrophobic portion of the surfactant molecule; this is mostly the case with agrochemicals, which have hydrophobic surfaces. However, if the chemical is hydrophilic in nature the interaction will be dominated by the EO chain. The approach to monolayer saturation with the molecules lying flat is accompanied by a gradual decrease in the slope of the adsorption isotherm (region II in Figure 5.7). An increase in the size of the surfactant molecule, for example by increasing the length of the alkyl or EO chain, will decrease the adsorption (when expressed in moles per unit area). On the other hand, increasing the temperature will cause an increase in adsorption as a result of desolvation of the EO chains, which reduces their size. Increasing the temperature will also reduce the solubility of the nonionic surfactant, and this in turn will enhance adsorption.

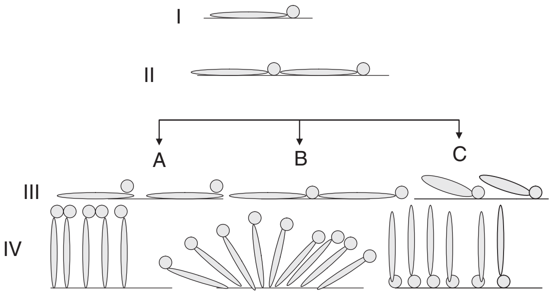

Figure 5.8 Model for the adsorption of nonionic surfactants.

The subsequent stages of adsorption (regions III and IV) are determined by surfactant–surfactant interactions, although surfactant–surface interaction initially determines adsorption beyond stage II. This interaction depends on the nature of the surface and the hydrophilic–lipophilic balance (HLB) of the surfactant molecule. For a hydrophobic surface, adsorption occurs via the alkyl group of the surfactant and, for a given EO chain, the adsorption will increase in line with increases in alkyl chain length. On the other hand, for a given alkyl chain length the adsorption is increased with a decrease in the PEO chain length.

As the surfactant concentration approaches the cmc, there is a tendency for the alkyl groups to aggregate, which will in turn cause a vertical orientation of the surfactant molecules (stage IV). This will compress the head group and, for an EO chain, this will result in a less-coiled and more-extended conformation. In fact, the larger the surfactant alkyl chain, the greater will be the cohesive forces and hence the smaller the cross-sectional area; this may explain why saturation adsorption increases in line with increasing alkyl chain length.

The interactions occurring in the adsorption layer during the fourth and subsequent stages of adsorption are similar to those that occur in bulk solution. In this case, aggregate units (as shown in Figure 5.8 V (hemi-micelles or micelles) may be formed. This proposed scheme was supported by Kleminko *et al.* [30], who found a close agreement between saturation adsorption and adsorption calculated based on the assumption that the surface was covered with close-packed hemi-micelles. Kleminko [31] also developed a theoretical model for the three stages of adsorption of nonionic surfactants. In the first stage (flat orientation), a modified Langmuir adsorption equation was used, while in the second stage of horizontal orientation the surface concentration was increased by an amount that was determined by the displacement of the ethoxy chain by the alkyl group. Finally, in the region of hemi-micelle formation the adsorption could be described by a simple Langmuir equation of the form:

$$C_2\ K_a^* = \frac{\Gamma_2}{(\Gamma_2^{\text{infinity}} - \Gamma_2)} \tag{5.54}$$

where $\Gamma_2{}^{\infty}$ is the maximum surface excess, that is the surface excess when the surface is covered with close-packed hemi-micelles, $K_a{}^*$ is a constant that is inversely proportional to the cmc, and C_2 is the equilibrium concentration.

References

1. Guggenheim, E.A. (1967) *Thermodynamics*, 5th edn, North Holland, Amsterdam, p. 45.
2. Gibbs, J.W. (1928) *Collected Works*, vol. **1**, Longman, New York, p. 219.
3. Langmuir, I. (1917) *J. Am. Chem. Soc.*, **39**, 1848.
4. Szyszkowski, B. (1908) *Z. Phys. Chem.*, **64**, 385.
5. Frumkin, A. (1925) *Z. Phys. Chem.*, **116**, 466.
6. Wilhelmy, L. (1863) *Ann. Phys.*, **119**, 177.
7. Bashforth, F. and Adams, J.C. (1883) *An Attempt to Test the Theories of Capillary Action*, Cambridge University Press, Cambridge.
8. Niederhauser, D.O. and Bartell, F.E. (1950) *Report of Progress, Fundamental*

Research on Occurrence of Petroleum, Publication of the American Petroleum Institute, Lord Baltimore Press, Baltimore, MD, p. 114.

9. Du Nouy, P.L. (1919) *J. Gen. Physiol.*, **1**, 521.
10. Harkins, W.D. and Jordan, H.F. (1930) *J. Am. Chem. Soc.*, **52**, 1715.
11. Freud, B.B. and Freud, H.Z. (1930) *J. Am. Chem. Soc.*, **52**, 1772.
12. Harkins, W.D. and Brown, F.E. (1919) *J. Am. Chem. Soc.*, **41**, 499.
13. Lando, J.L. and Oakley, H.T. (1967) *J. Colloid Interface Sci.*, **25**, 526.
14. Wilkinson, M.C. and Kidwell, R.L. (1971) *J. Colloid Interface Sci.*, **35**, 114.
15. Vonnegut, B. (1942) *New Sci. Intrum.*, **13**, 6.
16. Aveyard, R. and Haydon, D.A. (1973) *An Introduction to the Principles of Surface Chemistry*, Cambridge University Press, Cambridge.
17. Hough, D.B. and Randall, H.M., in *Adsorption from Solution at the Solid/Liquid Interface*, (eds G.D. Parfitt and C.H. Rochester), London, Academic Press, 1983, p.247.
18. Fuerstenau, D.W. and Healy, T.W., in *Adsorptive Bubble Separation Techniques*, (ed. R. Lemlich), London, Academic Press, 1972, p. 91.
19. Somasundaran, P. and Goddard, E.D. (1979) *Mod. Aspects Electrochem.*, **13**, 207.
20. Healy, T.W. (1974) *J. Macromol. Sci. Chem.*, **118**, 603.
21. Somasundaran, P. and Hannah, H.S., *Improved Oil Recovery by Surfactant and Polymer Flooding*, (eds D.O. Shah and R.S. Schechter), London, Academic Press, 1979, p.205.
22. Greenwood, F.G., Parfitt, G.D., Picton, N.H., and Wharton, D.G. (1968) *Adv. Chem. Ser.*, **79**, 135.
23. Day, R.E., Greenwood, F.G. and Parfitt, G.D. (1967) 4th International Congress of Surface Active Substances, Vol. 18, p. 1005.
24. Saleeb, F.Z. and Kitchener, J.A. (1965) *J. Chem. Soc.*, 911.
25. Conner, P. and Ottewill, R.H. (1971) *J. Colloid Interface Sci.*, **37**, 642.
26. Fuerestenau, D.W., in *The Chemistry of Biosurfaces*, (ed. M.L. Hair), New York, Marcel Dekker, 1971, p.91.
27. Wakamatsu, T. and Fuerstenau, D.W. (1968) *Adv. Chem. Ser.*, **71**, 161.
28. Gaudin, A.M. and Fuertsenau, D.W. (1955) *Trans. AIME*, **202**, 958.
29. Clunie, J.S. and Ingram, B.T. (1983) in *Adsorption from Solution at the Solid/Liquid Interface* (eds G.D. Parfitt and C.H. Rochester), Academic Press, London, p. 105.
30. Klimenko, N.A., Tryasorukova, A.A., and Permilouskayan, A.A. (1974) *Kolloid Zh.*, **36**, 678.
31. Kleminko, N.A. (1978) *Kolloid Zh.*, **40**, 1105; 1979, **41**, 78.

6

Adsorption of Polymeric Surfactants at the Solid/Liquid Interface

Understanding the adsorption and conformation of polymeric surfactants at interfaces is key to knowing how these molecules act as stabilisers for disperse systems. Most basic ideas on the adsorption and conformation of polymers have been developed for the solid/liquid (S/L) interface [1]. The first theories on polymer adsorption were developed during the 1950s and 1960s, with extensive developments later in the 1970s. The process of polymer adsorption is fairly complicated. In addition to the usual adsorption considerations such as polymer–surface, polymer–solvent and surface–solvent interactions, one of the principal problems to be resolved is the configuration (conformation) of the polymer at the S/L interface. This was recognised in 1951 by Jenkel and Rumbach [2], who found that the amount of polymer adsorbed per unit area of the surface would correspond to a layer more than 10 molecules thick if all the segments of the chain were attached. These authors suggested a model in which each polymer molecule is attached in sequences separated by bridges which extended into solution. In other words, not all of the segments of a macromolecule would be in contact with the surface. Those segments which are in direct contact with the surface are termed ‘‘trains’’; those which are in between and are extended into solution are termed ‘‘loops’’; while the free ends of the macromolecule also extending into solution are termed ‘‘tails.’’ This is illustrated in Figure 6.1a for a homopolymer. Examples of homopolymers that are formed from the same repeating units are poly(ethylene oxide) (PEO) or poly(vinyl pyrrolidone). Such homopolymers may adsorb significantly at the S/L interface. Even if the adsorption energy per monomer segment to the surface is small (fraction of kT, where k is the Boltzmann constant and T is the absolute temperature), the total adsorption energy per molecule may be sufficient to overcome the unfavourable entropy loss of the molecule at the S/L interface. Clearly, homopolymers are not the most suitable emulsifiers or dispersants. A small variant is to use polymers that contain specific groups that have a high affinity to the surface. This is exemplified by partially hydrolysed poly(vinyl acetate) (PVAc), which is referred to technically as poly(vinyl alcohol) (PVA). The polymer is prepared by a partial hydrolysis of PVAc, leaving some residual vinyl acetate groups. Most commercially available PVA molecules contain 4–12% acetate groups which are hydrophobic and give the molecule its amphipathic character. On a hydrophobic surface such as polystyrene (PS), the PVA adsorbs with a preferential attachment of the acetate groups on

Formulation of Disperse Systems: Science and Technology, First Edition. Tharwat F. Tadros.

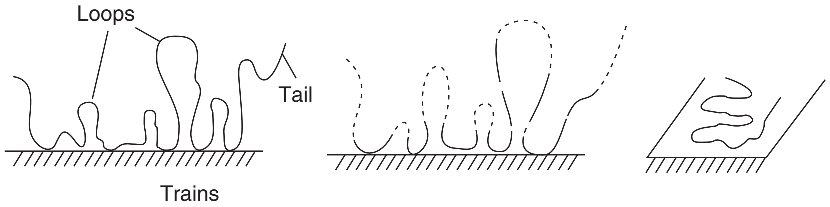

(a) Homopolymer sequence of loops-tails and trains

(b) Chains with "blocks" that have higher affinity to the surface

(c) Chain lying flat on the surface

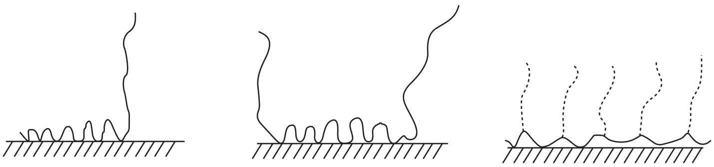

(d) A-B block B forms small loops and A are tails

(e) A-B-A block

(f) BA_n graft one B chain (small loops) and several A chains

Figure 6.1 (a–f) Various conformations of macromolecules on a plane surface.

the surface, leaving the more hydrophilic vinyl alcohol segments dangling in the aqueous medium. The configuration of such ''blocky'' copolymers is illustrated in Figure 6.1b. Clearly, if the molecule is made fully from hydrophobic segments the chain will adopt a flat configuration, as illustrated in Figure 6.1c. The most convenient polymeric surfactants are those of the block and graft copolymer type. A block copolymer is a linear arrangement of blocks of variable monomer composition. The nomenclature for a diblock is poly-A-block-poly-B, and for a triblock is poly-A-block-poly-B-poly-A. An example of an A-B diblock is polystyrene block-PEO, and its conformation is represented in Figure 6.1d. The most widely used triblock polymeric surfactants are the ''Pluronics'' (BASF, Germany), which consist of two poly-A blocks of PEO and one block of poly(propylene oxide) (PPO). Several chain lengths of PEO and PPO are available. As mentioned in Chapter 5, these polymeric triblocks can be applied as dispersants, whereby the assumption is made that the hydrophobic PPO chain resides at the hydrophobic surface, leaving the two PEO chains dangling in aqueous solution and hence providing steric repulsion. As also mentioned in Chapter 5, several other triblock copolymers have been synthesised, although these are of limited commercial availability; typical examples are triblocks of poly(methyl methacrylate)-block PEO-block poly(methyl methacrylate). The conformation of these triblock copolymers is illustrated in Figure 6.1e. An alternative (and perhaps more efficient) polymeric surfactant is the amphipathic graft copolymer consisting of a polymeric backbone B [polystyrene or poly(methyl methacrylate)] and several A chains (''teeth''), such as PEO. This graft copolymer is sometimes referred to as ''comb'' stabiliser, and is configuration is illustrated in Figure 6.1f.

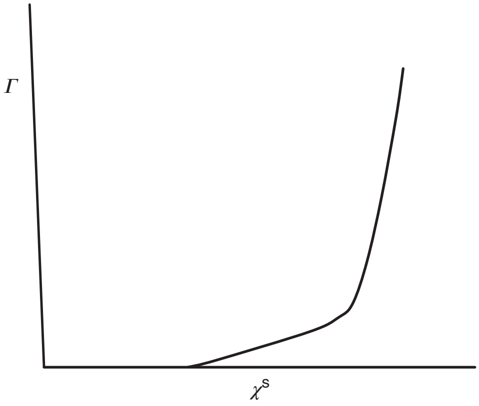

Figure 6.2 Variation of adsorption amount Γ with adsorption energy per segment χ_s.

The polymer–surface interaction is described in terms of adsorption energy per segment χ_s. The polymer–solvent interaction is described in terms of the Flory–Huggins interaction parameter χ, and in order for adsorption to occur a minimum energy of adsorption per segment, χ_s, is required. When a polymer molecule adsorbs onto a surface it loses its configurational entropy, and this must be compensated by an adsorption energy χ_s per segment. This is shown schematically in Figure 6.2, where the adsorbed amount Γ is plotted versus χ_s The minimum value of χ_s can be very small (<0.1 kT) as a large number of segments per molecule are adsorbed. In the case of a polymer with 100 segments, 10% of which are in trains, the adsorption energy per molecule may reach 1 kT (with $\chi_s = 0.1$ kT). For 1000 segments, the adsorption energy per molecule is now 10 kT.

As mentioned above, homopolymers are not the most suitable vehicle for the stabilisation of dispersions. For strong adsorption, the molecule must be "insoluble" in the medium and to have a strong affinity ("anchoring") to the surface, whereas for stabilisation the molecule must be highly soluble in the medium and strongly solvated by its molecules; this requires a Flory–Huggins interaction parameter of <0.5. The above opposing effects can be resolved by introducing "short" blocks into the molecule that are insoluble in the medium and have a strong affinity to the surface; an example is partially hydrolysed PVAc (88% hydrolysed, i.e. with 12% acetate groups), usually referred to as PVA:

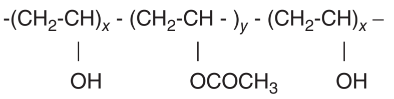

$$-(CH_2\text{-}\underset{\displaystyle OH}{\underset{|}{C}H})_x - (CH_2\text{-}\underset{\displaystyle OCOCH_3}{\underset{|}{C}H} -)_y - (CH_2\text{-}\underset{\displaystyle OH}{\underset{|}{C}H})_x -$$

As mentioned above, these requirements are better satisfied using A-B, A-B-A and BA_n graft copolymers. B is chosen to be highly insoluble in the medium, and should also have high affinity to the surface; this is essential to ensure a strong "anchoring" to the surface (irreversible adsorption). A is chosen to be highly soluble in the medium and strongly solvated by its molecules; the Flory–Huggins χ parameter can be applied in this case. For a polymer in a good solvent χ must be <0.5; indeed, the smaller the χ-value the better the solvent for polymer chains. Examples of B for a hydrophobic particles in aqueous media are polystyrene and poly(methylmethacrylate), while examples of A in aqueous media include PEO, polyacrylic acid, poly(vinyl pyrollidone) and polysaccharides. For nonaqueous media, such as hydrocarbons, the A chain(s) may be poly(12-hydroxystearic acid).

In order to acquire a full description of polymer adsorption, it is necessary to obtain information on the following points:

- The amount of polymer adsorbed Γ (in mg or mol) per unit area of the particles. It is essential to know the surface area of the particles in the suspension. Nitrogen adsorption on the powder surface may provide such information, by application of the Brunauer–Emmett–Teller (BET) equation, provided that no change will occur in area when the particles are dispersed in the medium For many practical systems, a change in surface area may occur on dispersing the powder, in which case it would be necessary to use dye adsorption to measure the surface area (some assumptions must be made in this case).
- The fraction of segments in direct contact with the surface – that is the fraction of segments in trains, p (where p is the number of segments in direct contact with the surface/total number).
- The distribution of segments in loops and tails, $\rho(z)$, which extend in several layers from the surface. $\rho(z)$ is usually difficult to obtain experimentally, although recently the application of small-angle neutron scattering has been used to obtain such information. An alternative and useful parameter for assessing ‘‘steric stabilisation’’ is the hydrodynamic thickness, δ_h (the thickness of the adsorbed or grafted polymer layer plus any contribution from the hydration layer). Several methods can be applied to measure δ_h, as will be discussed below.

6.1
Theories of Polymer Adsorption

Two main approaches have been developed to treat the problem of polymer adsorption:

1) The random walk approach, which is based on Flory’s treatment of the polymer chain in solution; in this case the surface was considered as a reflecting barrier.
2) The statistical mechanical approach, in which the polymer configuration is treated as being composed of three types of structure – trains, loops, and tails – with each having a different energy state.

The random walk approach is based on the random-walk concept, which was originally applied to the problem of diffusion and later adopted by Flory [3] to deduce the conformations of macromolecules in solution. The earliest analysis was by Simha *et al.* [4], who neglected volume effects and treated the polymer as a random walk. Basically, the solution was represented by a three-dimensional lattice, and the surface by a two-dimensional lattice. The polymer was represented by the realisation of a random walk on the lattice, and the probabilities of performing steps in different directions were considered to be the same except at the interface, which acts as a reflecting barrier. The polymer molecules were, therefore, effectively assumed to be adsorbed with large loops protruding into the solvent and with few segments actually attached to the surface, unless the segment–surface attractive forces were very high. This theory predicts an isotherm for flexible macromolecules that is considerably different from the Langmuir-type isotherm. The number of attached segments per chain is proportional to $n^{1/2}$, where n is the total number of segments. Increasing the molecular weight results in an increased adsorption, except for strong chain interaction with the surface.

This approach has been criticised by Silberberg [5] and by Di Marzio [6], with one of the major problems being the use of a reflecting barrier as the boundary condition, which meant the number of distinguishable conformations might be overcounted. In order to overcome this problem, Di Marzio and McCrackin [7] used a Monte Carlo method to calculate the average number of contacts of the chain with the surface, the end-to-end length and distribution of segments $\rho(z)$ with respect to the distance z from the surface, as a function of chain length of the polymer and the attractive energy of the surface. The same method was also used by Clayfield and Lumb [8, 9].

The is a more realistic model for the problem of polymer adsorption as it takes into account the various interactions involved. This approach was first used by Silberberg [5], who treated separately the surface layer which contains adsorbed units (trains) and the adjacent layer in solution (loops or tails). The units in each layer were considered to be in two different energy states and partition functions were used to describe the system. The units close to the surface were adsorbed with an internal partition function determined by the short-range forces between the segments and the surface, whereas the units in loops and tails were considered to have an internal partition function equivalent to the segments in the bulk. By equating the chemical potential of macromolecules in the adsorbed state and in bulk solution, the adsorption isotherm could be determined. In this treatment, Silberberg [5] assumed a narrow distribution of loop sizes and predicted small loops for all values of the adsorption energy. Later, the loop size distribution was introduced by Hoeve *et al.* [10], and this theory predicted large loops for small adsorption free energies and small loops and more units adsorbed for larger adsorption free energies when the chains are sufficiently flexible. Most of these theories considered the case of an isolated polymer molecule at an interface – that is, under conditions of low surface coverage, θ. These theories were extended by Silberberg [11] and Hoeve [12, 13] to take into account the lateral interaction between the molecules on the surface, that is high surface coverage. These theories also considered the excluded volume effect, which reduces the number of configurations available for interacting chains near the surface. Excluded volume effects are heavily dependent on the solvent, as is the case for chains in solution. Some progress has been made in the analysis of the problem of multilayer adsorption [14].

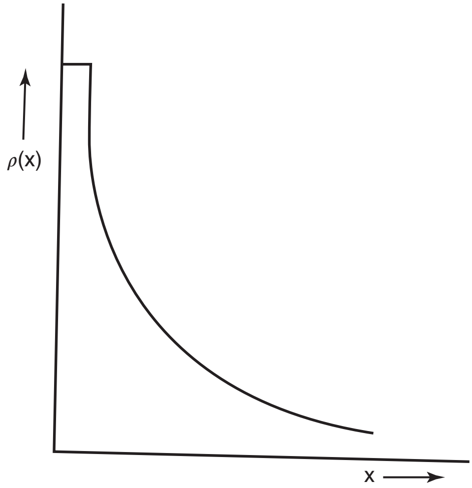

Figure 6.3 Segment density–distance distribution.

One feature of an adsorbed layer that is important in the theory of steric stabilisation is the actual segment distribution normal to the interface. Hoeve [15, 16] was the first to calculate this quantity for an adsorbed homopolymer of loops and tails, using random flight statistics. Hoeve showed that, at a distance from the interface corresponding to the thickness of the trains, there was a discontinuity in the distribution, but beyond this the segment density falls exponentially with distance, as shown schematically in Figure 6.3. Similarly, Meier [17] developed an equation for the segment density distribution of a single terminally adsorbed tail. Hesselink [18, 19] has developed Meier's theory and given the segment density distribution for single tails, single loops, homopolymers, and random copolymers.

A useful model for treating polymer adsorption and configuration was suggested by Roe [20] Scheutjens and Fleer (SF theory) [21–24] that is referred to as the step-weighted random walk approach. In order to be able to describe all possible chain conformations, Scheutjens and Fleer [21–23] used a model of a quasi-crystalline lattice with lattice layers parallel to the surface. Starting from the surface the layers are numbered $I = 1,2,3 \ldots M$, where M is a layer in bulk solution. All lattice sites within one layer were considered to be energetically equivalent. The probability of finding any lattice site in layer I occupied by a segment was assumed to be equal to the volume fraction ϕ_I in this layer. The conformation probability and the free energy of mixing were calculated with the assumption of random mixing within each layer (the Brag–Williams or mean field approximation). The energy for any segment is only determined by the layer number, and each segment can be assigned a weighting or Boltzmann factor p_i which depends only on the layer number. The partition functions were derived for the mixture of free and adsorbed polymer molecules, as well as for the solvent molecules. As mentioned before, all chain conformations were described as step-weighted random walks on a quasi-crystalline lattice which extends in parallel layers from the surface; this is

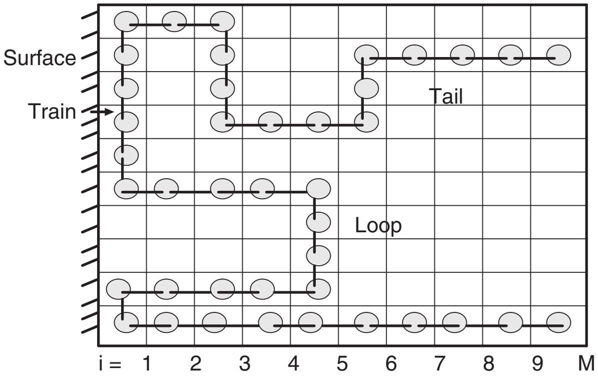

Figure 6.4 Schematic representation of a polymer molecule adsorbing on a flat surface-quasi-crystalline lattice with segments filling layers that are parallel to the surface (random mixing of segments and solvent molecules in each layer is assumed).

shown schematically in Figure 6.4. The partition function is written in terms of a number of configurations; these were treated as connected sequences of segments. In each layer, random mixing between segments and solvent molecules was assumed (mean field approximation). Each step in the random walk was assigned a weighting factor p_i that consisted of three contributions: (i) an adsorption energy χ_s (which exists only for the segments that are near the surface); (ii) configurational entropy of mixing (that exists in each layer); and (iii) a segment–solvent interaction parameter χ (the Flory–Huggins interaction parameter; note that $\chi = 0$ for an athermal solvent; $\chi = 0.5$ for a θ-solvent). The adsorption energy gives rise to a Boltzmann factor exp χ_s in the weighting factor for the first layer, provided that χ_s is interpreted as the adsorption energy difference (in units of kT) between a segment and a solvent molecule. The configurational entropy for the segment, as a part of the chain, is accounted for in the matrix procedure in which all possible chain conformations are considered. However, the configurational entropy loss of the solvent molecule, going from a layer I with low solvent concentration to the bulk solution with a higher solvent concentration, has to be introduced in p_i. According to the Flory–Huggins theory [3], this entropy loss can be written as $\Delta s^\circ = k \ln \phi_*{}^\circ/\phi_i{}^\circ$ per solvent molecule, where $\phi_i{}^\circ$ and $\phi_*{}^\circ$ are the solvent volume fractions in layer I and in bulk solution respectively. This change is equivalent to introducing a Boltzmann factor $\exp(-\Delta s^\circ/k) = \phi_i{}^\circ/\phi_*{}^\circ$ in the weighting factor p_i. The last contribution stems from the mixing energy of the exchange process. The transfer of a segment from the bulk solution to layer I is accompanied by an energy change (in units of kT) $\chi(\phi_i{}^\circ - \phi_*{}^\circ)$, where χ is the Flory–Huggins segment solvent interaction parameter.

Figure 6.5 shows typical adsorption isotherms plotted as surface coverage (in equivalent monolayers) versus polymer volume fraction ϕ_* in bulk solution (ϕ_* was taken to vary between 0 and 10^{-3}, which is the normal experimental range). The results in Figure 6.6 show the effect of increasing the chain length r and effect of solvency (athermal solvent with $\chi = 0$ and theta solvent with $\chi = 0.5$). The

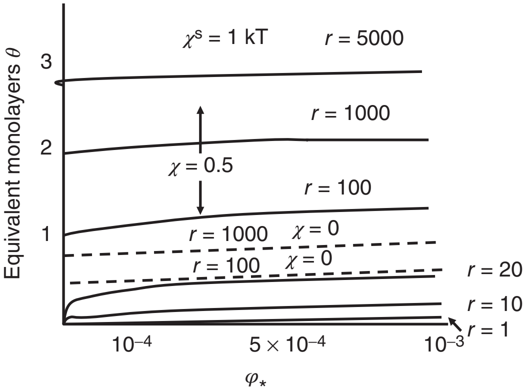

Figure 6.5 Adsorption isotherms for oligomers and polymers in the dilute region based on SF theory. For full curves $\chi = 0.5$; for dashed curves, $\chi = 0$.

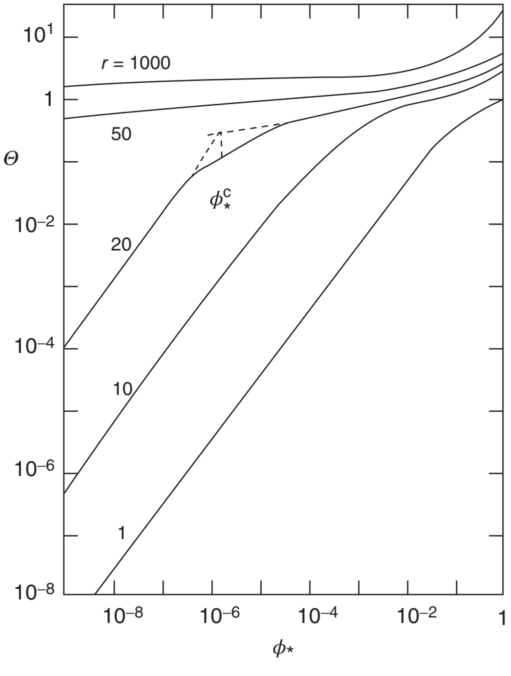

Figure 6.6 Log–log presentation of adsorption isotherms of various r-values. $\chi_s = 1$ and $\chi = 0.5$. Hexagonal lattice.

adsorption energy χ_s was taken to be the same and equal to 1 kT. When $r = 1$, θ is very small and the adsorption increases linearly with any increase of ϕ^* (Henry-type isotherm). On the other hand, when $r = 10$ the isotherm deviates much from a straight line and approaches a Langmuirian type. However, when $r \geq 20$ high-affinity isotherms are obtained, which implies that the first added polymer chains are completely adsorbed and this results in an extremely low polymer concentration in solution (approaching zero). This explains the irreversibility of adsorption of polymeric surfactants with $r > 100$. The adsorption isotherms with $r = 100$ and above are typical of those observed experimentally for most polymers that are not too polydisperse – that is, showing a steep rise followed by a near-horizontal plateau (which only increases a few percent per decade increase of ϕ^*). In these dilute solutions, the effect of solvency is most clearly seen, with poor solvents giving the highest adsorbed amounts. In good solvents, θ will be much smaller and will level off for long chains to attain an adsorption plateau which is essentially independent of molecular weight.

Some general features of the adsorption isotherms over a wide concentration range can be illustrated by using logarithmic scales for both θ and φ_* which highlight the behaviour in extremely dilute solutions. Such a presentation [23] is shown in Figure 6.6, where the results show a linear Henry region followed by a pseudoplateau region. A transition concentration, $\varphi_*{}^{1c}$, can be defined by extrapolation of the two linear parts. $\varphi_*{}^{c}$ decreases exponentially with increasing chain length and when $r = 50$, $\varphi_*{}^{c}$ is so small (10^{-12}) that it does not appear within the scale shown in Figure 6.6. With $r = 1000$, $\varphi_*{}^{c}$ reaches the ridiculously low value of 10^{-235}. The region below $\varphi_*{}^{c}$ is the Henry region, where the adsorbed polymer molecules behaves essentially as isolated molecules. The representation in Figure 6.7 also answers the question of reversibility versus irreversibility for polymer adsorption. When $r > 50$, the pseudoplateau region extends down to very low concentration ($\varphi_*{}^{c} = 10^{-12}$), and this explains why no desorption can easily be detected upon dilution. Clearly, if such an extremely low concentration can be reached, desorption of the polymer may take place. Thus, the lack of desorption (sometimes referred to as irreversible adsorption) is due to the fact that the equilibrium between the adsorbed and free polymer is shifted far in favour of the surface because of the high number of possible attachments per chain.

Another point that emerges from the SF theory is the difference in shape between the experimental and theoretical adsorption isotherms in the low concentration region. The experimental isotherms are usually rounded, whereas those predicted from theory are flat. This is accounted for in terms of the molecular weight distribution (polydispersity) which is encountered with most practical polymers. This effect has been explained by Cohen-Stuart *et al.* [25]. With polydisperse polymers, the larger molecular-weight fractions adsorb preferentially over the smaller ones. At low polymer concentrations nearly all polymer fractions are adsorbed, leaving a small fraction of the polymer with the lowest molecular weights in solution. As the polymer concentration is increased, the higher-molecular-weight fractions displace their lower molecular-weight counterparts on the surface; the latter are now released

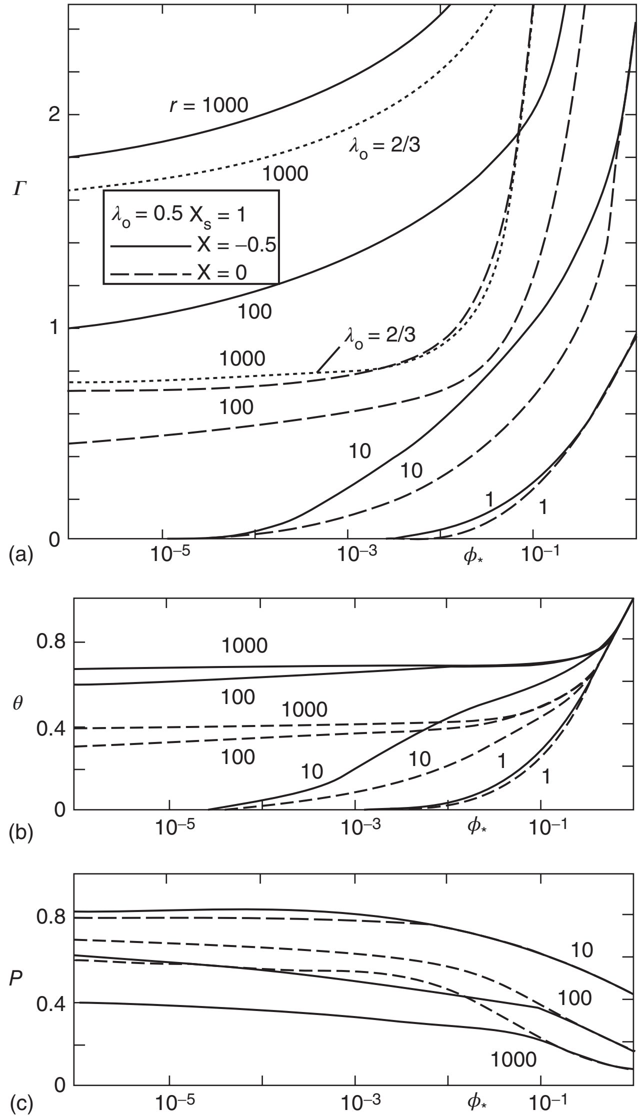

Figure 6.7 (a) Adsorbed amount (Γ), (b) surface coverage (θ), and (c) fraction of adsorbed segments $p = \theta/\Gamma$ as a function of volume fraction ϕ_*. Full lines indicate θ-solvent ($\chi = 0.5$); dashed lines indicate athermal solvent ($\chi = 0$).

in solution, thus shifting the molecular weight distribution in solution to lower values. This process continues with further increases in polymer concentration leading to fractionation, whereby the higher-molecular-weight fractions are adsorbed at the expense of the lower-molecular-weight fractions, which are released to the bulk solution. However, in very concentrated solutions, monomers are adsorbed preferentially with respect to polymers, and short chains with respect to larger chains. This is due to the fact that, in this region, the conformational entropy term predominates the free energy, disfavouring the adsorption of long chains.

According to the SF theory, the bound fraction p and the direct surface coverage θ_1 depend on the chain length for the same volume fraction. This is illustrated in Figure 6.7, which shows the adsorbed amount Γ (Figure 6.7a), surface coverage θ (Figure 6.7b) and fraction of adsorbed segments $p = \theta/\Gamma$ (Figure 6.7c) as a function of volume fraction ϕ_*.

In the Henry region ($\phi_* < \phi_*^c$), p is rather high and independent of chain length for $r \geq 20$. In this region the molecules lie nearly flat on the surface, with 87% of segments in trains. At the other end of the concentration range ($\phi_* = 1$), p is proportional to $r^{-1/2}$, while at intermediate concentrations p is within these two extremes. With increasing polymer concentration the adsorbed molecules become gradually more extended (lower p) until at very high ϕ_* values they become Gaussian at the interface. In better solvents the direct surface coverage is lower, due to the stronger repulsion between the segments; this effect is more pronounced if the surface concentration differs strongly from the solution concentration. If the adsorption is small, the effect of the excluded volume effect (and therefore of χ) is rather weak; the same applies if both the concentrations in the bulk solution and near the surface are high. Both, θ_1 and θ decrease with increasing solvent power (decreasing χ), but the effect is stronger for θ than for $\theta_{1,}$ resulting in a higher bound fraction (thus flatter chains) from better solvents at the same solution concentration.

The structure of the adsorbed layer is described in terms of the segment density distribution. As an illustration, Figure 6.8 shows some calculations using the SF theory for loops and tails with $r = 1000$, $\phi^* = 10^{-6}$, and $\chi = 0.5$. In this example, 38% of the segments are in trains, 55.5% in loops, and 6.5% in tails. This theory demonstrates the importance of tails which dominate the total distribution in the outer region.

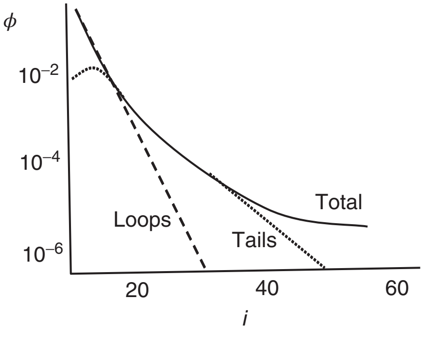

Figure 6.8 Loop, tail, and total segment profile according to SF theory.

6.2
Experimental Techniques for Studying Polymeric Surfactant Adsorption

As mentioned above, in order to fully characterize polymeric surfactant adsorption, three parameters must be determined: (i) the adsorbed amount Γ (mg m^{-2} or mol m^{-2}) as a function of the equilibrium concentration C_{eq}, that is, the adsorption isotherm; (ii) the fraction of segments in direct contact with the surface p (the number of segments in trains relative to the total number of segments); and (iii) the segment density distribution $\rho(z)$ or the hydrodynamic adsorbed layer thickness δ_h.

It is important to obtain the adsorption parameters as a function of the important variables of the system:

- Solvency of the medium for the chain which can be affected by temperature, the addition of salt, or a nonsolvent. The Flory–Huggins interaction parameter χ could be separately measured.
- The molecular weight of the adsorbed polymer.
- The affinity of the polymer to the surface, as measured by the value of χ_s, the segment–surface adsorption energy.
- The structure of the polymer; this is particularly important for block and graft copolymers.

6.2.1
Measurement of the Adsorption Isotherm

This is by far the easiest parameter to obtain. The polymeric surfactant concentration is measured before (C_{initial}, C_1) and after ($C_{\text{equilibrium}}$, C_2):

$$\Gamma = \frac{(C_1 - C_2)V}{A} \tag{6.1}$$

where V is the total volume of the solution and A is the specific surface area (m^2 g^{-1}). It is necessary in this case to separate the particles from the polymer solution after adsorption, and this may be carried out by centrifugation and/or filtration, ensuring that all particles have been removed. To obtain this isotherm a sensitive analytical technique must be developed to determine the polymeric surfactant concentration in the ppm range. It is essential to follow the adsorption as a function of time to determine the time required to reach equilibrium. For some polymer molecules, such as PVA and PEO (or blocks containing PEO), analytical methods based on complexation with iodine/potassium iodide or iodine/boric acid potassium iodide have been established. For some polymers with specific functional groups, spectroscopic methods may be applied, including ultraviolet (UV), infrared (IR), or fluorescence spectroscopy. One possible method involves measuring changes in the refractive index of the polymer solution before and after adsorption, but this requires very sensitive refractometers. High-resolution NMR has been recently applied as the polymer molecules in the adsorbed state are in a different environment from those in the bulk. The chemical shift of functional groups within the chain are different in these two environments, but this has the attraction of measuring the amount of adsorption without separating the particles.

6.2.2
Measurement of the Fraction of Segments, p

The fraction of segments in direct contact with the surface can be measured directly using spectroscopic techniques:

- IR if there is specific interaction between the segments in trains and the surface, for example PEO on silica from nonaqueous solutions [26, 27].
- Electron spin resonance (ESR); this requires labelling of the molecule.
- NMR, pulse gradient or spin-echo NMR; this method is based on the fact that the segments in trains are "immobilised" and hence will have a lower mobility than those in loops and tails [28, 29].

An indirect method of determining p is to measure the heat of adsorption ΔH, using microcalorimetry [30]. The heat of adsorption of a monomer H_m (or molecule representing the monomer (e.g., ethylene glycol for PEO) should then be determined; p is then given by the equation:

$$p = \frac{\Delta H}{H_m n} \tag{6.2}$$

where n is the total number of segments in the molecule.

The above-described indirect method is not very accurate and can only be used in a qualitative sense. It also requires very sensitive enthalpy measurements (e.g., by using an LKB microcalorimeter).

6.3
Determination of Segment Density Distribution ρ(z) and Adsorbed Layer Thickness δ_h

The segment density distribution $\rho(z)$ is given by the number of segments parallel to the surface in the z-direction. Three direct methods can be applied to determine the adsorbed layer thickness: ellipsometry; attenuated total reflection (ATR); and neutron scattering. Both ellipsometry and ATR [31] depend on the difference in the refractive indices between the substrate, the adsorbed layer and bulk solution, and they require a flat reflecting surface. Ellipsometry [31] is based on the principle that light undergoes a change in polarisability when it is reflected at a flat surface (whether the surface is covered or not with a polymer layer).

The above limitations when using ellipsometry or ATR can be overcome by applying the technique of neutron scattering, which can be used for both flat surfaces and particulate dispersions. The basic principle of neutron scattering is to measure the scattering due to the adsorbed layer, when the scattering length density of the particle is matched to that of the medium (the so-called "contrast-matching" method). The contrast matching of particles and medium can be achieved by changing the isotopic composition of the system (using deuterated particles and a mixture of D_2O and H_2O). The technique was used to measure the adsorbed layer thickness of polymers, for example PVA or PEO on polystyrene latex [32]. Apart from obtaining δ, it is also possible to determine the segment density distribution $\rho(z)$.

Neutron scattering provides a clear quantitative picture of the adsorbed polymer layer, but its application in practice is limited as there is a need to prepare deuterated particles or polymers for the contrast matching procedure. Practical methods for determining adsorbed layer thicknesses are mostly based on hydrodynamic techniques. Indeed, several methods may be applied to determine the hydrodynamic thickness of adsorbed polymer layers, with viscosity, sedimentation coefficient (using an ultracentrifuge) and dynamic light-scattering measurements being the most convenient. A less-accurate method involves zeta-potential measurements.

The viscosity method [33] depends on measuring increases in the volume fraction of the particles as a result of the presence of an adsorbed layer of thickness δ_h. The volume fraction of the particles φ plus the contribution of the adsorbed layers is usually referred to as the effective volume fraction, φ_{eff}. Assuming that the particles behave as hard spheres, the measured relative viscosity η_r is related to the effective volume fraction by Einstein's equation, that is:

$$\eta_r = 1 + 2.5\ \varphi_{\text{eff}} \tag{6.3}$$

where φ_{eff} and φ are related from simple geometry by,

$$\varphi_{\text{eff}} = \varphi \left[1 + \left(\frac{\delta_h}{R}\right)\right]^3 \tag{6.4}$$

where R is the particle radius. Thus, from a knowledge of η_r and φ it is possible to obtain δ_h, using the above equations.

The sedimentation method depends on measuring the sedimentation coefficient (by ultracentrifugation) of the particles, S_o' (extrapolated to zero concentration), in the presence of the polymer layer [34]. Assuming that the particles obey Stokes' law, S_o' is given by the expression:

$$S_{o'} = \frac{(4/3)\pi R^3\ (\rho - \rho_s) + (4/3)\pi\ [(R + \delta_h)^3 - R^3](\rho_s^{\text{ads}} - \rho_s)}{6\pi\eta\ (R + \delta_h)} \tag{6.5}$$

where ρ and ρ_s are the mass density of the solid and solution phase, respectively, and ρ^{ads} is the average mass density of the adsorbed layer which may be obtained from the average mass concentration of the polymer in the adsorbed layer.

In order to apply the above methods, a dispersion should be used with monodisperse particles of radius not much larger than δ_h. In this case, small model particles of polystyrene may be used.

One relatively simple sedimentation method for determination of δ_h is the slow-speed centrifugation applied by Garvey *et al.* [34]. Basically, a stable monodisperse dispersion is slowly centrifuged at low *g*-values (<50g) to form a close-packed (hexagonal or cubic) lattice in the sediment. From a knowledge of φ and the packing fraction (0.74 for hexagonal packing), the distance of separation between the centres of two particles R_δ may be obtained, that is:

$$R_\delta = R + \delta_h = \left(\frac{0.74\ V\ \rho_1\ R^3}{W}\right) \tag{6.6}$$

where V is the sediment volume, ρ_1 is the density of the particles, and W is their weight.

The most rapid technique for measuring δ_h is photon correlation spectroscopy (PCS; sometimes referred to as quasi-elastic light scattering), which allows the diffusion coefficients of the particles to be obtained with and without the adsorbed layer (D_δ and D, respectively). This is obtained by measuring the intensity fluctuation of scattered light as the particles undergo Brownian diffusion [35]. When a light beam (e.g., a monochromatic laser beam) passes through a dispersion, an oscillating dipole is induced in the particles, causing the light to be re-radiated. Due to the random arrangement of the particles (which are separated by a distance comparable to the wavelength of the light beam; that is, the light is coherent with the interparticle distance), the intensity of the scattered light will, at any instant, appear as random diffraction or a "speckle" pattern. As the particles undergo Brownian motion, the random configuration of the speckle pattern changes. Consequently, the intensity at any one point in the pattern will fluctuate such that the time taken for an intensity maximum to become a minimum (i.e., the coherence time) will correspond approximately to the time required for a particle to move one wavelength. By using a photomultiplier of active area about the size of a diffraction maximum (i.e., approximately one coherence area), this intensity fluctuation can be measured. A digital correlator is used to measure the photocount or intensity correlation function of the scattered light. The photocount correlation function can be used to obtain the diffusion coefficient D of the particles. For monodisperse, noninteracting particles (i.e., at sufficient dilution) the normalised correlation function $[g^{(1)}(\tau)]$ of the scattered electric field is given by the equation:

$$[g^{(1)}(\tau)] = \exp -(\Gamma\ \tau) \tag{6.7}$$

where τ is the correlation delay time and Γ is the decay rate or inverse coherence time. Γ is related to D by the equation,

$$\Gamma = D\ K^2 \tag{6.8}$$

where K is the magnitude of the scattering vector that is given by,

$$K = \left(\frac{4n}{\lambda_o}\right)\ \sin\left(\frac{\theta}{2}\right) \tag{6.9}$$

where n is the refractive index of the solution, λ is the wavelength of light in a vacuum, and θ is the scattering angle.

From D, the particle radius R is calculated using the Stokes–Einstein equation:

$$D = \frac{kT}{6\pi\eta R} \tag{6.10}$$

where k is the Boltzmann constant and T is the absolute temperature. For a polymer-coated particle, R is denoted as R_δ which is equal to $R + \delta_h$; thus, by measuring D_δ and D it is possible to obtain δ_h. It should be mentioned that the accuracy of the PCS method depends on the ratio of δ_δ/R, as δ_h is determined by difference. Since the accuracy of the measurement is ±1%, δ_h should be at least 10% of the particle radius. This method can only be used with small particles and reasonably thick adsorbed layers. Measurements of electrophoretic mobility, u, can also be applied to measure δ_h [36] since, from u, the zeta-potential ζ – that is, the potential at the slipping (shear) plane of the particles – can be calculated. The adsorption of a polymer causes a shift in the shear plane from its value in the absence of a polymer layer (which is close to the Stern plane) to a value that depends on the thickness of the adsorbed layer. Thus, by measuring ζ in the presence (ζ_δ) and absence (ζ) of a polymer layer, it is possible to estimate δ_h. Assuming that the thickness of the Stern plane is Δ, then ζ_δ may be related to ζ, which may be assumed to be equal to the Stern potential (ψ_d) by the equation:

$$\tanh\left(\frac{e\psi_\delta}{4kT}\right) = \tanh\left(\frac{e\zeta}{4kT}\right) \exp\left[-\kappa\left(\delta_h - \Delta\right)\right] \tag{6.11}$$

where κ is the Debye parameter that is related to electrolyte concentration and valency.

It should be mentioned that the value of δ_h calculated using the above simple equation shows a dependence on electrolyte concentration, and hence the method cannot be used in a straightforward manner. Cohen-Stuart *et al.* [36] showed that the measured electrophoretic thickness δ_e approaches δ_h only at low electrolyte concentrations. Thus, in order to obtain δ_h from electrophoretic mobility measurements, results should be obtained at various electrolyte concentrations and δ_e plotted versus the Debye length ($1/\kappa$) to obtain the limiting value at high ($1/\kappa$) (i.e., low electrolyte concentration) which now corresponds to δ_h.

6.4
Examples of the Adsorption Isotherms of Nonionic Polymeric Surfactants

Figure 6.9 shows the adsorption isotherms for PEO with different molecular weights on PS (at room temperature). It can be seen that the amount adsorbed (in $\mathrm{mg\,m^{-2}}$) is increased in line with increases in the polymer molecular weight [37]. Figure 6.10 shows the variation in hydrodynamic thickness δ_h with molecular weight M. δ_h shows a linear increase with log M, and increases with n, the number of segments in the chain, according to:

$$\delta_h \approx n^{0.8} \tag{6.12}$$

Figure 6.11 shows the adsorption isotherms of PVA with various molecular weights on PS latex (at 25 °C) [38]. The polymers were obtained fractionating a commercial sample of PVA with an average molecular weight of 45 000 Da (the polymer also contained 12% vinyl acetate groups). As with PEO, the amount of adsorption was increased with increases in M, and the isotherms were also of the high-affinity type. Γ at the plateau was increased linearly with $\mathrm{M}^{1/2}$.

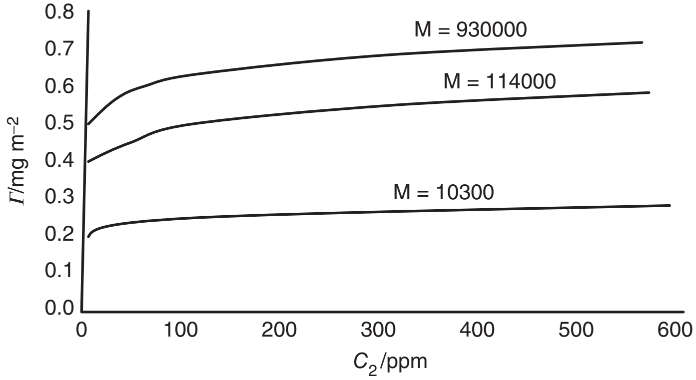

Figure 6.9 Adsorption isotherms for PEO on PS.

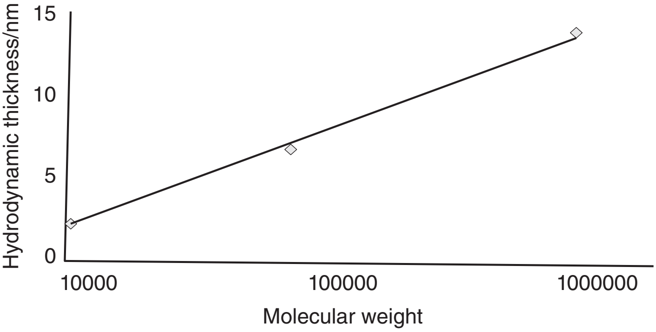

Figure 6.10 Hydrodynamic thickness of PEO on PS as a function of molecular weight.

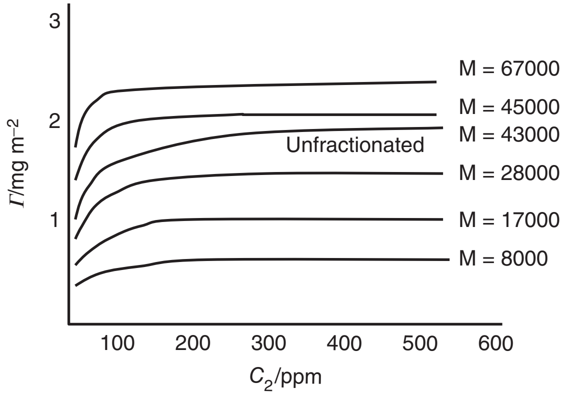

Figure 6.11 Adsorption isotherms of PVA with different molecular weights on polystyrene latex at 25 °C.

The hydrodynamic thickness was determined using PCS and the results are given below:

M (Da)	67 000	43 000	28 000	17 000	8000
δ_h (nm)	25.5	19.7	14.0	9.8	3.3

where δ_h seemed to increase linearly with increases in molecular weight.

The effect of solvency on adsorption was investigated by increasing the temperature (the PVA molecules are less soluble at higher temperature) or the addition of an electrolyte (KCl) [39, 40]. The results are shown in Figures 6.12 and 6.13 for M = 65 100 Da. As can be seen from Figure 6.12, an increase in temperature resulted in a reduction of solvency of the medium for the chain (due to the breakdown of hydrogen bonds), and this resulted in an increase in the amount adsorbed. The addition of KCl (which reduces the solvency of the medium for the chain) resulted in an increased adsorption (as predicted by theory).

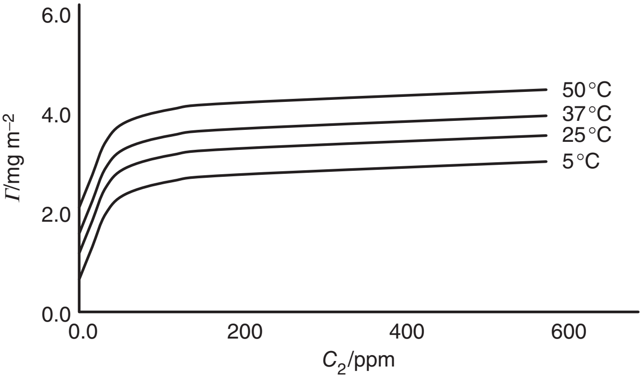

Figure 6.12 Influence of temperature on adsorption.

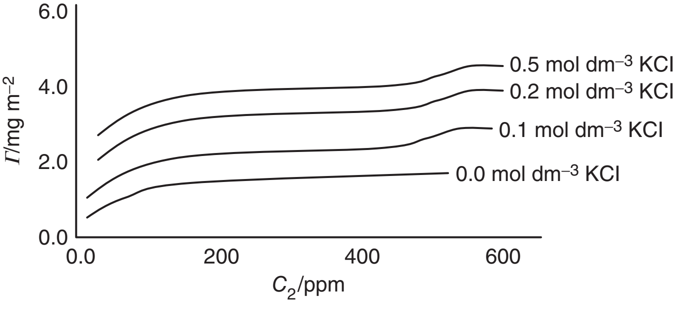

Figure 6.13 Influence of addition of KCl on adsorption.

The adsorption of block and graft copolymers is more complex, as the intimate structure of the chain will determine the extent of adsorption [37]. Random copolymers adsorb in an intermediate fashion compared to that of the corresponding homopolymers. Block copolymers retain the adsorption preference of the individual blocks. The hydrophilic block (e.g., PEO; the buoy) extends away from the particle surface into the bulk solution, while the hydrophobic anchor block (e.g., PS or PPO) provides a firm attachment to the surface. Figure 6.14 shows the theoretical prediction of diblock copolymer adsorption according to SF theory. In this case, the surface density σ was plotted versus the fraction of anchor segments ν_A, and adsorption was shown to depend on the anchor/buoy composition.

The amount of adsorption was greater than for homopolymers, and the adsorbed layer thickness was more extended and dense. For a triblock copolymer A-B-A, with two buoy chains and one anchor chain, the behaviour was similar to that of diblock copolymers; this is shown in Figure 6.15 for the PEO-PPO-PEO block (Pluronic).

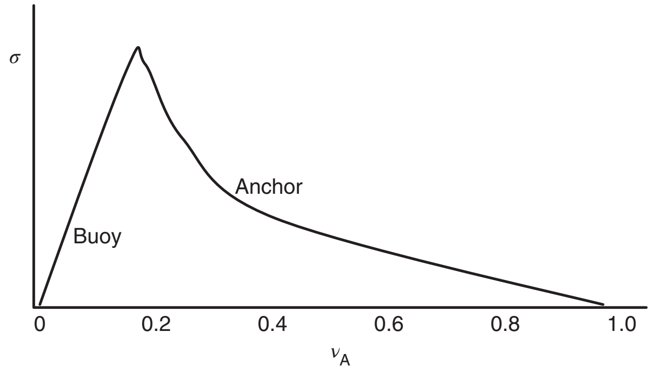

Figure 6.14 Prediction of adsorption of diblock copolymer.

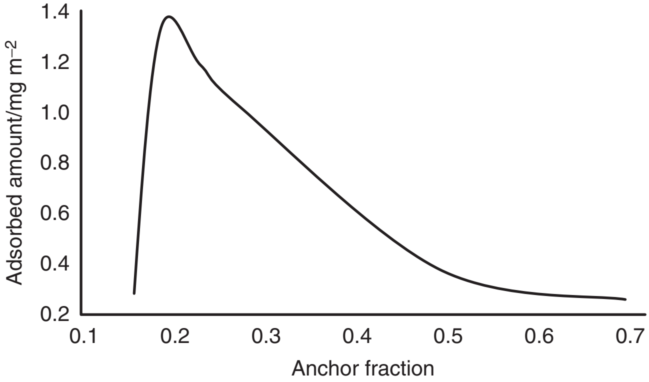

Figure 6.15 Adsorbed amount (mg m^{-2}) versus fraction of anchor segment for an A-B-A triblock copolymer (PEO-PPO-PEO).

6.4.1
Adsorbed Layer Thickness Results

Figure 6.16 shows a plot of $\rho(z)$ against z for PVA (M = 37 000 Da) adsorbed onto deuterated PS latex in D_2O/H_2O. The results shows a monotonic decay of $\rho(z)$ with distance z from the surface, and several regions may be distinguished. Close to the surface ($0 < z < 3$ nm), the decay in $\rho(z)$ was rapid and, assuming a thickness of 1.3 nm for the bound layer, p was calculated to be 0.1, which was in close agreement with results obtained using NMR measurements. In the middle region, $\rho(z)$ showed a shallow maximum, followed by a slow decay which extended to 18 nm, that was close to the hydrodynamic layer thickness δ_h of the polymer chain (see below). δ_h was determined by the longest tails, and was about 2.5-fold the radius of gyration in bulk solution (~7.2 nm). This slow decay of $\rho(z)$ with z at long distances was in qualitative agreement with SF theory [23], which predicts the presence of long tails. The shallow maximum at intermediate distances suggested that the observed segment density distribution was a summation of a fast monotonic decay due to loops and trains, together with the segment density for tails which was a maximum density away from the surface. The latter maximum was clearly observed for a sample which had PEO grafted to a deuterated polystyrene latex [32] (where the configuration is represented by tails only).

The hydrodynamic thickness of block copolymers shows a different behaviour from that of homopolymers (or random copolymers). Figure 6.17 shows the theoretical prediction for the adsorbed layer thickness δ, which is plotted as a function of ν_A.

Figure 6.18 shows the hydrodynamic thickness versus fraction of anchor segment for an ABA block copolymer of PEO-PPO-PEO [37]. The theoretical (SF) predictions of adsorbed amount and layer thickness versus fraction of anchor segment are shown in the inserts of Figure 6.18. In the presence of two buoy blocks and a central anchor block (as in the above example), the A-B-A block showed a similar

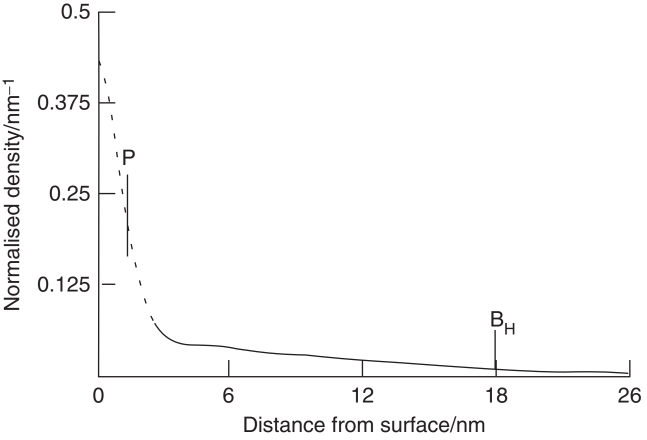

Figure 6.16 Plot of $\rho(z)$ against z for PVA (M = 37 000) adsorbed onto deuterated PS latex in D_2O/H_2O.

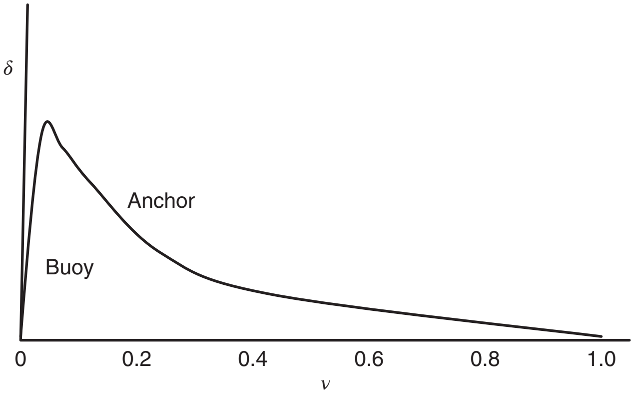

Figure 6.17 Theoretical predictions of the adsorbed layer thickness for a diblock copolymer.

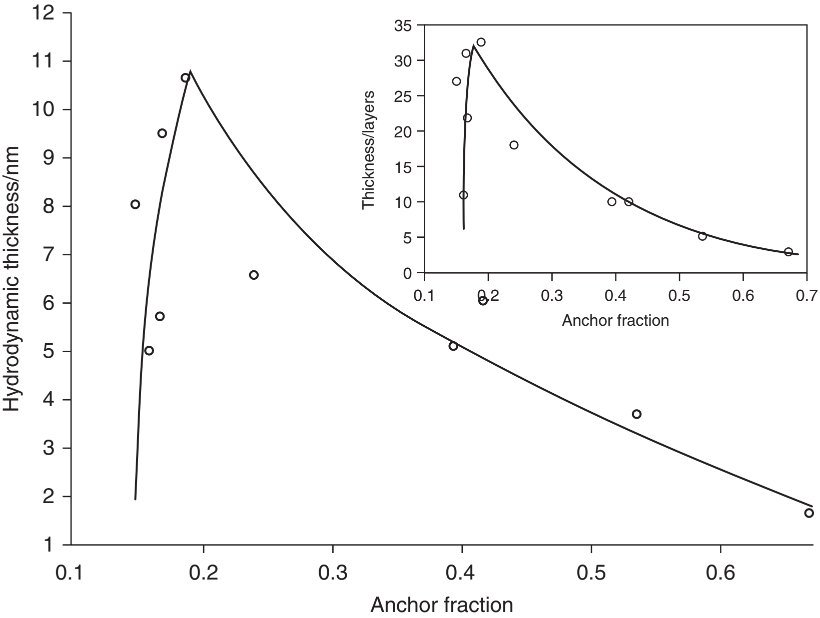

Figure 6.18 Hydrodynamic thickness versus fraction of anchor segment ν_A for PEO-PPO-PEO block copolymer onto polystyrene latex. The inset shows the mean field calculation of thickness versus anchor fraction, using SF theory.

behaviour to that of an A-B block. However, in the presence of two anchor blocks and a central buoy block, a surface precipitation of the polymer molecule at the particle surface was observed, and this was reflected in a continuous increase in adsorption in line with increases in polymer concentration, as has been shown for an A-B-A block of PPO-PEO-PPO [37].

6.4.2
Kinetics of Polymer Adsorption

The kinetics of polymer adsorption is a highly complex process, and several distinct processes can be distinguished, each with a characteristic time scale [37]. As these processes may occur simultaneously, it is difficult to separate them. The first process involves a mass transfer of the polymer to the surface, which may be due to either diffusion or convection. Having reached the surface, the polymer must then attach itself to a surface site, and this depends on any local activation energy barrier. Finally, the polymer will undergo large-scale rearrangements as it changes from its solution conformation to a ''tail-train-loop'' conformation. Once the polymer has reached the surface the amount of adsorption increases with time; the increase is initially rapid but subsequently slows as the surface becomes saturated. The initial rate of adsorption is sensitive to the bulk polymer solution concentration and molecular weight, as well as to the solution viscosity. Nevertheless, all polymer molecules that arrive at the surface will tend to be adsorbed immediately. The concentration of unadsorbed polymer around the periphery of the forming layer (the surface polymer solution) is zero, and therefore the concentration of polymer in the interfacial region will be significantly greater than the bulk polymer concentration. Mass transport is found to dominate the kinetics of adsorption until 75% of full surface coverage. However, at a higher surface coverage the rate of adsorption will decrease as the polymer molecules arriving at the surface cannot be adsorbed immediately. Consequently, over time an equilibrium will be set up between this interfacial concentration of polymer and the concentration of polymer in the bulk. Given that the adsorption isotherm is of the high-affinity type, no significant change in adsorbed amount is to be expected, even over decades of polymer concentration. If the surface polymer concentration increases towards that of the bulk solution, the rate of adsorption will be decreased because the driving force for adsorption (the difference in concentration between the surface and bulk solutions) will also be decreased. Adsorption processes tend to be very rapid, with equilibrated polymer layers forming within several thousand seconds, whereas desorption is a much slower process that can take several years!

References

1. Tadros, Th.F. (1985) in *Polymer Colloids* (eds R. Buscall, T. Corner, and J. Stageman), Elsevier Applied Sciences, London, p. 105.
2. Jenkel, E. and Rumbach, R. (1951) *Z. Elektrochem.*, **55**, 612.
3. Flory, P.J. (1953) *Principles of Polymer Chemistry*, Cornell University Press, New York.
4. Simha, R., Frisch, L., and Eirich, F.R. (1953) *J. Phys. Chem.*, **57**, 584.
5. Silberberg, A. (1962) *J. Phys. Chem.*, **66**, 1872.
6. Di Marzio, E.A. (1965) *J. Chem. Phys.*, **42**, 2101.
7. Di Marzio, E.A. and McCrakin, F.L. (1965) *J. Chem. Phys.*, **43**, 539.
8. Clayfield, E.J. and Lumb, E.C. (1966) *J. Colloid Interface Sci.*, **22** (269), 285.
9. Clayfield, E.J. and Lumb, E.C. (1968) *Macromolecules*, **1**, 133.

10. Hoeve, C.A., Di Marzio, E.A., and Peyser, P. (1965) *J. Chem. Phys.*, **42**, 2558.

11. Silberberg, A. (1968) *J. Chem. Phys.*, **48**, 2835.

12. Hoeve, C.A. (1965) *J. Chem. Phys.*, **44**, 1505; **47**, 3007 (1966).

13. Hoeve, C.A. (1970) *J. Polym. Sci.*, **30**, 361; **34**, 1 (1971).

14. Silberberg, A. (1972) *J. Colloid Interface Sci.*, **38**, 217.

15. Hoeve, C.A.J. (1965) *J. Chem. Phys.*, **44**, 1505.

16. Hoeve, C.A.J. (1966) *J. Chem. Phys.*, **47**, 3007.

17. Meier, D.J. (1965) *J. Phys. Chem.*, **71**, 1861.

18. Hesselink, F.T. (1969) *J. Phys. Chem.*, **73**, 3488.

19. Hesselink, F.T. (1971) *J. Phys. Chem.*, **75**, 65.

20. Roe, R.J. (1974) *J. Chem. Phys.*, **60**, 4192.

21. Scheutjens, J.M.H.M. and Fleer, G.J. (1979) *J. Phys. Chem.*, **83**, 1919.

22. Scheutjens, J.M.H.M. and Fleer, G.J. (1980) *J. Phys. Chem.*, **84**, 178.

23. Scheutjens, J.M.H.M. and Fleer, G.J. (1982) *Adv. Colloid Interface Sci.*, **16**, 341.

24. Fleer, G.J., Cohen-Stuart, M.A., Scheutjens, J.M.H.M., Cosgrove, T., and Vincent, B. (1993) *Polymers at Interfaces*, Chapman & Hall, London.

25. Cohen-Stuart, M.A., Scheutjens, J.M.H.M., and Fleer, G.J. (1980) *J. Polym. Sci., Polym. Phys. Ed.*, **18**, 559.

26. Killmann, E., Eisenlauer, E., and Horn, M.J. (1977) *Polym. Sci. Polym. Symp.*, **61**, 413.

27. Fontana, B.J. and Thomas, J.R. (1961) *J. Phys. Chem.*, **65**, 480.

28. Robb, I.D. and Smith, R. (1974) *Eur. Polym. J.*, **10**, 1005.

29. Barnett, K.G., Cosgrove, T., Vincent, B., Burgess, A., Crowley, T.L., Kims, J., Turner, J.D., and Tadros, Th.F. (1981) *Disc. Faraday Soc.*, **22**, 283.

30. Cohen-Staurt, M.A., Fleer, G.J., and Bijesterbosch, B. (1982) *J. Colloid Interface Sci.*, **90**, 321.

31. Abeles, F. (1964) in *Ellipsometry in the Measurement of Surfaces and Thin Films*, vol. **256** (eds E. Passaglia, R.R. Stromberg, and J. Kruger), National Bureau of Standards Miscellaneous Publications, p. 41.

32. Cosgrove, T., Crowley, T.L., and Ryan, T. (1987) *Macromolecules*, **20**, 2879.

33. Einstein, A. (1906) *Investigations on the Theory of the Brownian Movement*, Dover Publications, New York.

34. Garvey, M.J., Tadros, Th.F., and Vincent, B. (1976) *J. Colloid Interface Sci.*, **55**, 440.

35. Pusey, P.N. (1973) in *Industrial Polymers: Characterisation by Molecular Weights* (eds J.H.S. Green and R. Dietz), Transcripta Books, London.

36. Cohen-Stuart, M.A. and Mulder, J.W. (1985) *Colloids Surf.*, **15**, 49.

37. Obey, T.M. and Griffiths, P.C. (1999) in *Principles of Polymer Science and Technology in Cosmetics and Personal Care*, Chapter 2 (eds E.D. Goddard and J.V. Gruber), Marcel Dekker, New York.

38. Garvey, M.J., Tadros, Th.F., and Vincent, B. (1974) *J. Colloid Interface Sci.*, **49**, 57.

39. van den Boomgaard, T., King, T.A., Tadros, T.F., Tang, H., and Vincent, B. (1978) *J. Colloid Interface Sci.*, **61**, 68.

40. Tadros, T.F. and Vincent, B. (1978) *J. Colloid Interface Sci.*, **72**, 505.

7
Colloid Stability of Disperse Systems Containing Electrical Double Layers

7.1
Origin of Charge on Surfaces

A great variety of processes occur to produce a surface charge. and these are summarised below.

7.1.1
Surface Ions

These are ions that have such a high affinity to the surface of the particles that they may be taken as part of the surface, for example Ag^+ and I^- for AgI. For AgI in a solution of KNO_3, the surface charge σ_o is given by the following expression:

$$\sigma_p = F\,(\Gamma_{Ag^+} - \Gamma_{I^-}) = F\,\Gamma_{AgNO_3} - \Gamma_{KI} \tag{7.1}$$

where F is the Faraday constant (96 500 C mol^{-1}) and Γ is the surface excess of ions (mol m^{-2}).

Similarly for an oxide such as silica or alumina in KNO_3, H^+ and OH^- may be taken as part of the surface,

$$\sigma_o = F\,(\Gamma_{H^+} - \Gamma_{OH^-}) = F\,(\Gamma_{HCl} - \Gamma_{KOH}) \tag{7.2}$$

The ions which determine the charge on the surface are termed potential determining ions. Consider an oxide surface (Figure 7.1), where the charge depends on the pH of the solution. Below a certain pH the surface is positive, but above a certain pH the surface is negative. At a specific pH ($\Gamma_H = \Gamma_{OH}$) the surface is uncharged; this is referred to as the point of zero charge (pzc).

The pzc depends on the type of the oxide. For an acidic oxide such as silica, the pzc is ~pH 2–3, but for a basic oxide such as alumina the pzc is ~pH 9. For an amphoteric oxide such as titania, the pzc ~pH 6. Some typical values of pzc for various oxides are listed in Table 7.1.

In some cases, specifically adsorbed ions (that have a nonelectrostatic affinity to the surface) ‘‘enrich’’ the surface, but may not be considered as part of the surface;

Formulation of Disperse Systems: Science and Technology, First Edition. Tharwat F. Tadros.

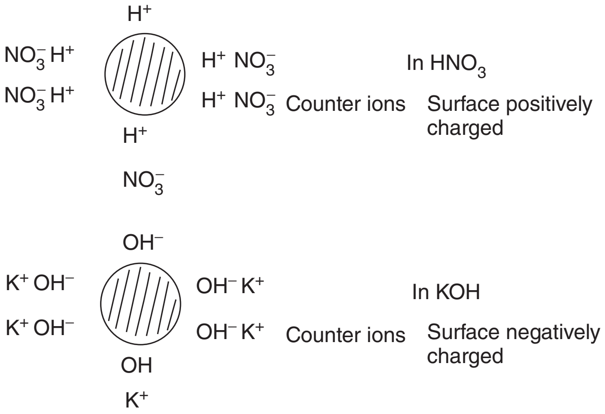

Figure 7.1 Schematic representation of an oxide surface.

Table 7.1 pzc values for some oxides.

Oxide	pzc
SiO_2 (precipitated)	2–3
SiO_2 (quartz)	3.7
SnO_2 (cassiterite)	5–6
TiO_2 (anatase)	6.2
TiO_2 (rutile)	5.7–5.8
RuO_2	5.7
α-Fe_2O_3 (hematite)	8.5–9.5
α-FeO.OH (goethite)	8.4–9.4
ZnO	8.5–9.5
γ-$Al(OH)_3$ (gibbsite)	8–9

examples include bivalent cations on oxides, and cationic and anionic surfactants on most surfaces [1].

7.1.2
Isomorphic Substitution

Isomorphic substitution (e.g., with sodium montmorillonite) involves the replacement of cations inside the crystal structure by cations of lower valency, for example Si^{4+} may be replaced by Al^{3+}. The deficit of one positive charge gives one negative charge. The surface of Na montmorillonite is negatively charged with Na^+ as counterions, as shown schematically in Figure 7.2. Here, the surface charge + counter ions from the electrical double layer.

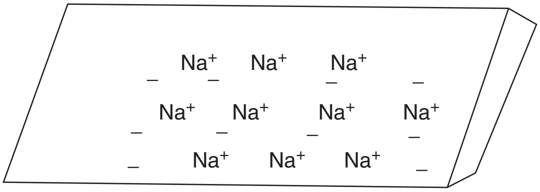

Figure 7.2 Schematic representation of a clay particle.

7.2
Structure of the Electrical Double Layer

7.2.1
Diffuse Double layer (Gouy and Chapman)

The surface charge σ_o is compensated by unequal distribution of counterions (opposite in charge to the surface) and co-ions (same sign as the surface) which extend to some distance from the surface [2, 3]. This is shown schematically in Figure 7.3, where the potential decays exponentially with distance x. At low potentials:

$$\psi = \psi_o \exp -(\kappa x) \tag{7.3}$$

Note that when $x = 1/\kappa$, $\psi_x = \psi_o/e - 1/\kappa$ is referred to as the "thickness" of the double layer.

The double-layer extension depends on electrolyte concentration and valency of the counterions,

$$\left(\frac{1}{\kappa}\right) = \left(\frac{\varepsilon_r \varepsilon_o kT}{2n_o Z_i^2 e^2}\right)^{1/2} \tag{7.4}$$

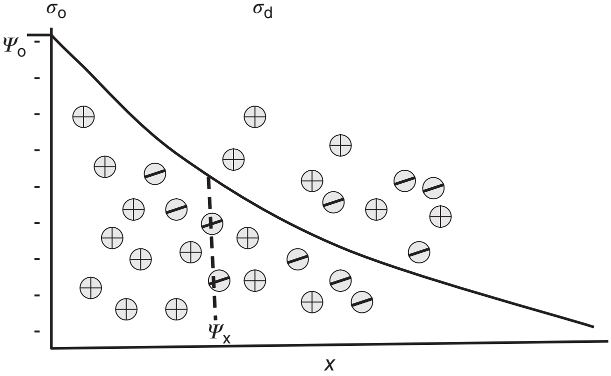

Figure 7.3 Schematic representation of the diffuse double layer, according to Gouy and Chapman.

where ε_r is the permittivity (dielectric constant; 78.6 for water at 25 °C), ε_o is the permittivity of free space, k is the Boltzmann constant, T is the absolute temperature, n_o is the number of ions per unit volume of each type present in bulk solution, Z_i is the valency of the ions, and e is the electronic charge.

For 1 : 1 electrolyte (e.g., KCl)

C (mol dm^{-3})	10^{-5}	10^{-4}	10^{-3}	10^{-2}	10^{-1}
(1/κ) (nm)	100	33	10	3.3	1

The double-layer extension increases with a decrease in electrolyte concentration.

7.3
Stern–Grahame Model of the Double Layer

Stern [4] introduced the concept of the nondiffuse part of the double layer for specifically adsorbed ions, the remainder being diffuse in nature; this is shown schematically in Figure 7.4, where the potential is seen to drop linearly in the Stern region, and then exponentially. Grahame distinguished two types of ions in the Stern plane, namely physically adsorbed counterions (outer Helmholtz plane) and chemically adsorbed ions that lose part of their hydration shell (inner Helmholtz plane).

7.4
Distinction between Specific and Nonspecific Adsorbed Ions

For the specifically adsorbed ions the range of interaction is short; that is, these ions must reside at the distance of closest approach, possibly within the hydration shell. For indifferent ions the situation is different, and these ions are subjected to either an attractive (for the counterions) or a repulsive (for the co-ions) potential (energy = $\pm ZF\psi(x)/RT$). The space charge density due to these ions is high close

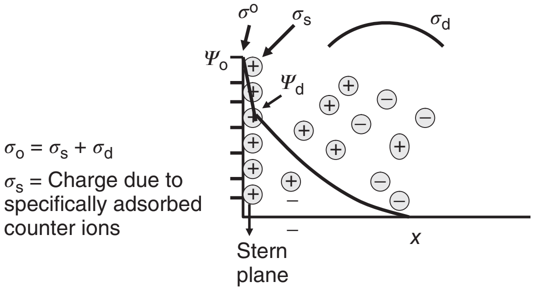

Figure 7.4 Schematic representation of the double layer, according to Stern and Grahame.

to the surface and decreases gradually with distance to its bulk value. Such a layer is the diffuse double layer described by Gouy-Chapman [2, 3]. Generally speaking, a double layer contains one part that is specifically adsorbed, and a diffuse part; however, because of the finite size of the counterions there will always be a charge-free layer close to the surface.

7.5
Electrical Double Layer Repulsion

When charged colloidal particles in a dispersion approach each other such that the double layers begin to overlap (when the particle separation becomes less than twice the double layer extension), then repulsion will occur. The individual double layers can no longer develop unrestrictedly, as the limited space does not allow complete potential decay [5].

This is illustrated in Figure 7.5 for two flat plates. The potential $\psi_{H/2}$ half-way between the plates is no longer zero (as would be the case for isolated particles at $x \to \infty$). The potential distribution at an interparticle distance H is depicted schematically by the full line in Figure 7.5. The stern potential ψ_{d} is considered to be independent of the particle distance, and the dashed curves show the potential as a function of distance x to the Helmholtz plane, had the particles been at an infinite distance.

For two spherical particles of radius R and surface potential ψ_{o} and condition $\kappa R < 3$, the expression for the electrical double layer repulsive interaction is given by Bijesterbosch [6]:

$$G_{\mathrm{el}} = \frac{4\pi\ \varepsilon_r \varepsilon_{\mathrm{o}}\ R^2\ \psi_o^2\ \exp -(\kappa h)}{2R + h} \tag{7.5}$$

where h is the closest distance of separation between the surfaces.

The above expression shows the exponential decay of G_{el} with h. The higher the value of κ (i.e., the higher the electrolyte concentration), the steeper the decay, as shown schematically in Figure 7.6. This means that, at any given distance h, the double layer repulsion decreases in lines with increases of electrolyte concentration.

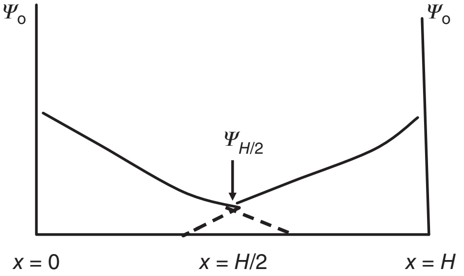

Figure 7.5 Schematic representation of double layer interaction for two flat plates.

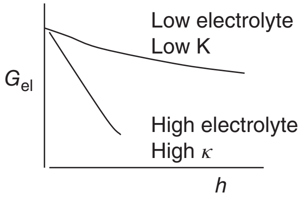

Figure 7.6 Variation of G_{el} with h at different electrolyte concentrations.

An important aspect of the double layer repulsion is the situation during particle approach. If, at any stage, the assumption is made that the double layers adjust to new conditions, so that equilibrium is always maintained, then the interaction will take place at a constant potential. This would be the case if the relaxation time of the surface charge were to be much shorter than the time that the particles are in each other's interaction sphere as a result of Brownian motion. However, if the relaxation time of the surface charge is appreciably longer than the time particles are in each other's interaction sphere, the charge rather than the potential will be the constant parameter. The constant charge leads to larger repulsion than the constant potential case.

7.6
van der Waals Attraction

It is well known that atoms or molecules always attract each other at short distances of separation. The attractive forces are of three different types: dipole–dipole interaction (Keesom); dipole-induced dipole interaction (Debye); and London dispersion force. Of these, the London dispersion force is the most important, as it occurs for both polar and nonpolar molecules, and arises from fluctuations in electron density distribution.

At small distances of separation r in a vacuum, the attractive energy between two atoms or molecules is given by,

$$G_{aa} = -\frac{\beta_{11}}{r^6} \tag{7.6}$$

where β_{11} is the London dispersion constant.

For colloidal particles which are made of atom or molecular assemblies, the attractive energies must be compounded. In this process, only the London interactions need to be considered as large assemblies have neither a net dipole moment nor a net polarisation. The result relies on the assumption that the interaction energies between all molecules in one particle with all others are simply additive [7]. The interaction between two identical half-infinite plates at a distance H in vacuum is given by,

$$G_A = -\frac{A_{11}}{12\pi h^2} \tag{7.7}$$

whereas for two spheres in vacuum the result is,

$$G_A = -\frac{A_{11}}{6}\left(\frac{2}{s^2-4}+\frac{2}{s^2}+\ln\frac{s^2-4}{s^2}\right) \tag{7.8}$$

A_{11} is known as the Hamaker constant and is defined by,

$$A_{11} = \pi^2\, q_{11}^2\, \beta_{ii} \tag{7.9}$$

where q_{11} is the number of atoms or molecules of type 1 per unit volume, and $s = (2R + h)/R$. Equation (7.9) shows that A_{11} has the dimension of energy.

For very short distances ($h \ll R$), Equation (7.8) may be approximated by,

$$G_A = -\frac{A_{11}\, R}{12\, h} \tag{7.10}$$

When the particles are dispersed in a liquid medium, the van der Waals attraction has to be modified to take into account the medium effect. When two particles are brought from infinite distance to h in a medium, an equivalent amount of medium must be transported in the other direction. Hamaker forces in a medium are excess forces.

Consider two identical spheres 1 at a large distance apart in a medium 2, as illustrated in Figure 7.7a; in this case the attractive energy is zero. Figure 7.7b shows the same situation, with arrows indicating the exchange of 1 against 2, while Figure 7.7c shows the complete exchange which now indicates the attraction between the two particles 1 and 1 and equivalent volumes of the medium 2 and 2.

The effective Hamaker constant for two identical particles 1 and 1 in a medium 2 is given by,

$$A_{11(2)} = A_{11} + A_{22} - 2A_{12} = \left(A_{11}^{1/2} - A_{22}^{1/2}\right)^2 \tag{7.11}$$

Equation (7.11) shows that two particles of the same material attract each other unless their Hamaker constant exactly matches each other. Equation (7.10) now becomes,

$$G_A = -\frac{A_{11(2)}\, R}{12\, h} \tag{7.12}$$

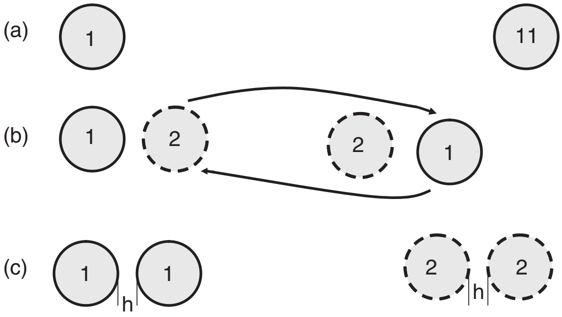

Figure 7.7 (a–c) Schematic representations of interaction of two particles in a medium.

Table 7.2 Hamaker constant (A_{22}) of some liquids.

Liquid	$A_{22} \times 10^{20}$ J
Water	3.7
Ethanol	4.2
Decane	4.8
Hexadecane	5.2
Cyclohexane	5.2

Table 7.3 Effective Hamaker constant $A_{11(2)}$ of some particles in water.

System	$A_{11(2)} \times 10^{20}$ J
Fused quartz/water	0.83
Al_2O_3/water	5.32
Copper/water	30.00
Poly(methylmethacrylate/water)	1.05
Poly(vinylchloride)/water	1.03
Poly(tetrafluoroethylene)/water	0.33

where $A_{11(2)}$ is the effective Hamaker constant of two identical particles with Hamaker constant A_{11} in a medium with Hamaker constant A_{22}.

In most cases, the Hamaker constant of the particles is higher than that of the medium. Examples of Hamaker constant for some liquids are listed in Table 7.2, while Table 7.3 contains values of the effective Hamaker constant for some particles in some liquids. Generally speaking, the effect of the liquid medium is to reduce the Hamaker constant of the particles below its value in vacuum (air).

G_A decreases with increase of h, as shown schematically in Figure 7.8. In this case, V_A can be seen to increase very sharply with h, at small h values. A capture distance can be defined at which all the particles become strongly attracted to each other (coagulation); at very short distances the Born repulsion appears.

The Hamaker approach, which his referred to as a ‘‘microscopic’’ theory, is based on the interactions between pairs of atoms or molecules. In contrast, the more accurate ‘‘macroscopic’’' approach, as originally suggested by Lifshitz and described in detail by Mahanty and Ninham [8], is based on the principle that the spontaneous electromagnetic fluctuations in two particles become correlated when the latter approach each other, causing a decrease in the free energy of the system. The elaboration of this theory is rather complex, and its application requires extensive data on the electromagnetic interaction energies. Nevertheless, the theory allows the important conclusion to be drawn that the most qualitative aspects of the ‘‘microscopic’’ theory given by Equations (7.7–7.12) are fully confirmed. The only

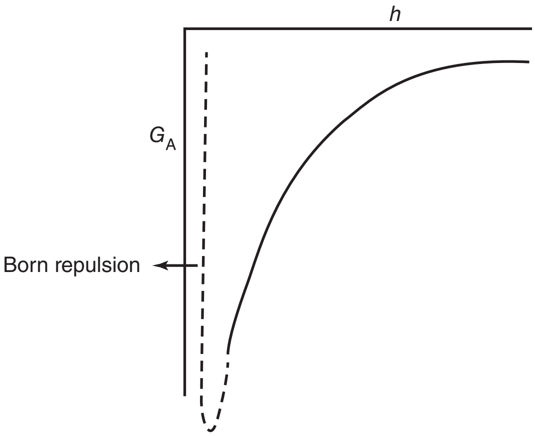

Figure 7.8 Variation of G_A with h.

exception concerns the decay of G_A with h at large separations. Owing to the time required for electromagnetic waves to cover the distance between the particles, the h^{-2} dependence in Equation (7.7) gradually changes to h^{-3} dependence at large separations, a phenomenon known as ''retardation.''

7.7
Total Energy of Interaction

7.7.1
Deryaguin–Landau–Verwey–Overbeek (DLVO) Theory

The combination of G_{el} and G_A results in the well-known theory of stability of colloids, that is the Deryaguin–Landau–Verwey–Overbeek (DLVO) theory [8–11],

$$G_T = G_{el} + G_A \tag{7.13}$$

A plot of G_T versus h is shown in Figure 7.9, which represents the case at low electrolyte concentrations – that is, a strong electrostatic repulsion between the particles. G_{el} decays exponentially with h, that is $G_{el} \rightarrow 0$ as h becomes large. G_A is $\infty 1/h$, such that G_A does not decay to 0 at large h.

At long distances of separation, $G_A > G_{el}$, which results in a shallow minimum (secondary minimum), whereas at very short distances, $G_A \gg G_{el}$, the results is a deep primary minimum.

At intermediate distances, $G_{el} > G_A$, the result would be an energy maximum, G_{max}, the height of which would depend on ψ_o (or ψ_d), and also on the electrolyte concentration and valency.

At low electrolyte concentrations ($<10^{-2}$ mol dm^{-3} for a 1 : 1 electrolyte), G_{max} is high ($>25\,kT$) and this prevents particle aggregation into the primary minimum.

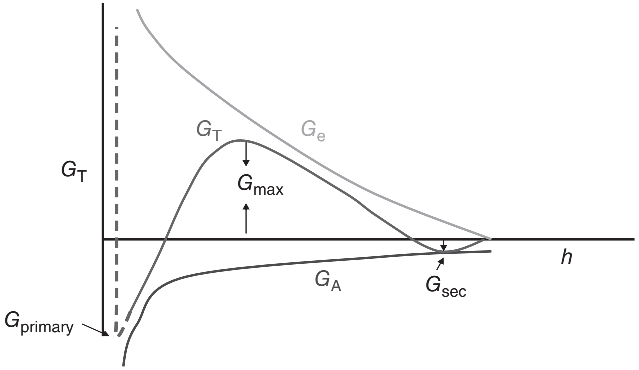

Figure 7.9 Schematic representation of the variation of G_T with h, according to DLVO theory.

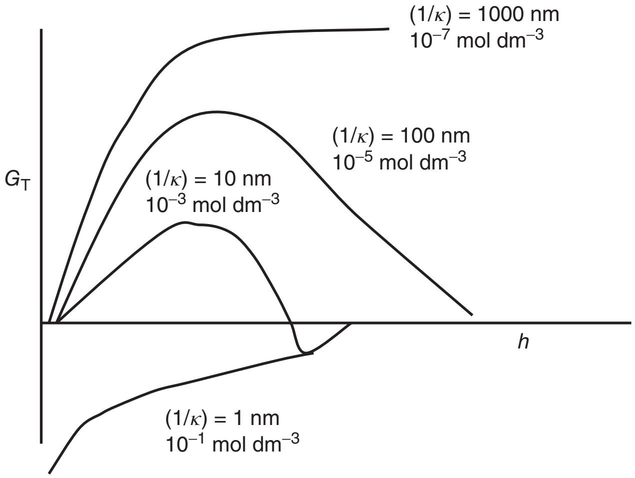

Figure 7.10 Variation of G_T with h at various electrolyte concentrations.

The higher the electrolyte concentration (and the higher the valency of the ions), the lower will be the energy maximum.

Under some conditions (depending on electrolyte concentration and particle size), flocculation into the secondary minimum may occur, although such flocculation is weak and reversible. On increasing the electrolyte concentration G_{max} decreases until, at a given concentration, it vanishes and particle coagulation occurs. This is illustrated in Figure 7.10, which shows the variation of G_T with h at various electrolyte concentrations.

As approximate formulas are available for G_{el} and G_A, quantitative expressions for $G_T(h)$ can also be created and used to derive expressions for the coagulation concentration (the latter is the concentration that causes every encounter between two colloidal particles to lead to destabilisation). Verwey and Overbeek [10] introduced the following criteria for transition between stability and instability:

$$G_T (= G_{el} + G_A) = 0 \tag{7.14}$$

$$\frac{dG_T}{dh} = 0 \tag{7.15}$$

$$\frac{dG_{el}}{dh} = -\frac{dG_A}{dh} \tag{7.16}$$

By using the equations for G_{el} and G_A, the critical coagulation concentration (ccc) could be calculated, as will be shown below. Theory predicts that the ccc is directly proportional to the surface potential ψ_o, and is inversely proportional to the Hamaker constant A and the electrolyte valency Z. As will be shown below, the ccc is inversely proportional to Z^6 at high surface potential, and inversely proportional to Z^6 at low surface potential.

7.8
Flocculation of Suspensions

As discussed above, the condition for kinetic stability is $G_{max} > 25\,kT$, but when $G_{max} < 5\,kT$ then flocculation will occur. Two types of flocculation kinetics may be distinguished: (i) fast flocculation with no energy barrier; and (ii) slow flocculation, where an energy barrier exists.

The fast flocculation kinetics was investigated by Smoluchowski [12], who considered the process to be represented by second-order kinetics and the process to be simply diffusion-controlled. The number of particles n at any time t may be related to the initial number n_o (at $t = 0$) by the following expression:

$$n = \frac{n_o}{1 + k\, n_o\, t} \tag{7.17}$$

where k is the rate constant for fast flocculation that is related to the diffusion coefficient of the particles D, that is,

$$k = 8\pi\, D\, R \tag{7.18}$$

where D is given by the Stokes–Einstein equation,

$$D = \frac{kT}{6\pi\,\eta\, R} \tag{7.19}$$

Combining Equations (7.12) and (7.13),

$$k = \frac{4}{3}\,\frac{kT}{\eta} = 5.5 \times 10^{-18}\ \mathrm{m^3 s^{-1}} \text{ for water at } 25\,^{\circ}\mathrm{C} \tag{7.20}$$

The half-life $t_{1/2}$ ($n = (1/2)\, n_o$) can be calculated at various values of n_o or volume fraction φ, as listed in Table 7.4

Table 7.4 Half-life of suspension flocculation.

R (μm)	φ			
	10^{-5}	10^{-2}	10^{-1}	5×10^{-1}
0.1	765 s	76 ms	7.6 ms	1.5 ms
1.0	21 h	76 s	7.6 s	1.5 s
10.0	4 mo	21 h	2 h	25 m

The slow flocculation kinetics was investigated by Fuchs [13], who related the rate constant k to the Smoluchowski rate by the stability constant W,

$$W = \frac{k_o}{k} \tag{7.21}$$

where W is related to $G_{\max}$ by the following expression,

$$W = \frac{1}{2}\, k \, \exp\left(\frac{G_{\max}}{kT}\right) \tag{7.22}$$

Since $G_{\max}$ is determined by the salt concentration C and valency, it is possible to derive an expression relating W to C and Z [14],

$$\log\, W = -2.06 \times 10^{9} \left(\frac{R\,\gamma^{2}}{Z^{2}}\right) \log\, C \tag{7.23}$$

where γ is a function that is determined by the surface potential ψ_o,

$$\gamma = \left[\frac{\exp\,\left(Ze\psi_o/kT\right) - 1}{\exp\,(Ze\psi_o/kT) + 1}\right] \tag{7.24}$$

Plots of log W versus log C are shown in Figure 7.11. The condition log $W = 0$ ($W = 1$) is the onset of fast flocculation, and the electrolyte concentration at this point defines the critical coagulation concentration (ccc). Above the ccc, W will be less than 1 (due to the contribution of van der Waals attraction which accelerates the rate above the Smoluchowski value), whereas below the ccc, W will be greater than 1, and will increase in line with a decrease in electrolyte concentration. The data in Figure 7.11 also shows that the ccc decreases with an increase of valency. At low surface potentials, ccc $\infty\ 1/Z^2$; this referred to as the Schultze–Hardy rule.

Another mechanism of flocculation is that involving the secondary minimum ($G_{\min}$) which is few kT units. In this case, the flocculation is weak and reversible and hence both the rate of flocculation (forward rate k_f) and deflocculation (backward rate k_b) must be considered. In this case, the rate or decrease of particle number with time is given by the expression:

$$-\frac{dn}{dt} = -k_f\, n^2 + k_b\, n \tag{7.25}$$

The backward reaction (break-up of weak flocs) reduces the overall rate of flocculation.

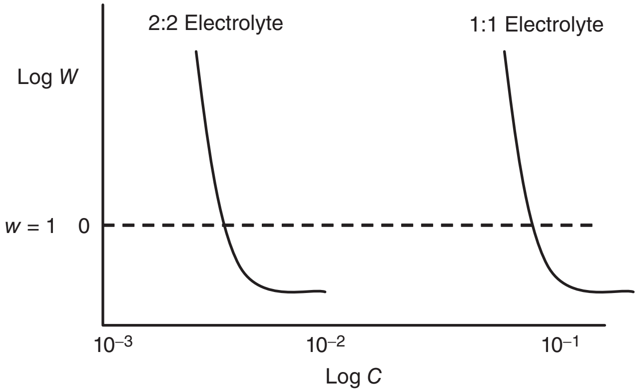

Figure 7.11 Log W–log C curves for electrostatically Stabilised emulsions.

Another process of flocculation that occurs under shearing conditions is referred to as orthokinetic, to distinguish it from the diffusion-controlled perikinetic process. In this case, the rate of flocculation is related to the shear rate by the expression:

$$-\frac{dn}{dt} = \frac{16}{3}\alpha^2\dot{\gamma}R^3 \tag{7.26}$$

where α is the collision frequency, that is the fraction of collisions that result in permanent aggregates.

7.9
Criteria for Stabilisation of Dispersions with Double Layer Interaction

The two main criteria for Stabilisation are:

- A high surface or Stern potential (zeta-potential), and high surface charge. As shown in Equation (7.5), the repulsive energy G_{el} is proportional to ${\psi_o}^2$. In practice, ψ_o cannot be measured directly and, therefore the measurable zeta-potential is used instead, as discussed in Chapter 5.
- A low electrolyte concentration and low valency of counterions and co-ions. As shown in Figure 7.11, the energy maximum increases with a decrease in electrolyte concentration. The latter should be less than 10^{-2} mol dm^{-3} for a 1 : 1 electrolyte, and less than 10^{-3} mol dm^{-3} for a 2 : 2 electrolyte. It should also be ensured that an energy maximum in excess of 25 kT exists in the energy–distance curve. When $G_{max} \gg kT$, the particles in the dispersion cannot overcome the energy barrier, and this prevents coagulation. However, in some cases – particularly with large and asymmetric particles – flocculation into the secondary minimum may occur. Although such flocculation is usually weak and reversible, it may be advantageous for preventing the formation of hard sediments.

References

1. Lyklema, J. (1987) Structure of the solid/liquid interface and the electrical double layer, in *Solid/Liquid Dispersions* (ed. T.F. Tadros), Academic Press, London.
2. (a) Gouy, G. (1910) *J. Phys.*, **9**, 457; (b) Gouy, G. (1917) *Ann. Phys.*, **7**, 129.
3. Chapman, D.L. (1913) *Philos. Mag.*, **25**, 475.
4. Stern, O. (1924) *Z. Electrochem.*, **30**, 508.
5. Grahame, D.C. (1947) *Chem. Rev.*, **41**, 44.
6. Bijesterbosch, B.H. (1987) Stability of solid/liquid dispersions, in *Solid/Liquid Dispersions* (ed. T.F. Tadros), Academic Press, London.
7. Hamaker, H.C. (1937) *Physica (Utrecht)*, **4**, 1058.
8. Mahanty, J. and Ninham, B.W. (1976) *Dispersion Forces*, Academic Press, London.
9. Deryaguin, B.V. and Landau, L. (1941) *Acta Physicochem. USSR*, **14**, 633.
10. Verwey, E.J.W. and Overbeek, J.T.G. (1948) *Theory of Stability of Lyophobic Colloids*, Elsevier, Amsterdam.
11. Kruyt, H.R. (ed.) (1952) *Colloid Science*, vol. **I**, Elsevier, Amsterdam.
12. Smoluchowski, M.V. (1927) *Z. Phys. Chem.*, **92**, 129.
13. Fuchs, N. (1936) *Z. Phys.*, **89**, 736.
14. Reerink, H. and Overbeek, J.T.G. (1954) *Discuss. Faraday Soc.*, **18**, 74.

8

Stability of Disperse Systems Containing Adsorbed Nonionic Surfactants or Polymers: Steric Stabilisation

8.1

Introduction

Nonionic surfactants and both natural and synthetic polymers (which are collectively referred to as polymeric surfactants), when used to stabilise solid/liquid (suspensions) and liquid/liquid (emulsions) disperse systems, play important roles in many industrial applications including paints, cosmetics, agrochemicals, and ceramics. Nonionic surfactants and polymers are particularly important for the preparation of concentrated dispersions – that is, with a high volume fraction φ of the disperse phase,

$$\phi = (\text{volume of all particles})/(\text{total volume of dispersion})$$

Polymers are also essential for the stabilisation of nonaqueous dispersions, since in this case electrostatic stabilisation is not possible (due to the low dielectric constant of the medium). In order to understand the role of nonionic surfactants and polymers in dispersion stability, it is essential to consider the adsorption and conformation of the surfactant and macromolecule at the solid/liquid interface (this point was discussed in detail in Chapters 5 and 6). With nonionic surfactants of the alcohol ethoxylate-type (which may be represented as A-B structures), the hydrophobic chain B (the alkyl group) becomes adsorbed onto the hydrophobic particle or droplet surface so as to leave the strongly hydrated poly(ethylene oxide) (PEO) chain A dangling in solution The latter provides not only the steric repulsion but also a hydrodynamic thickness δ that is determined by the number of ethylene oxide (EO) units present. The polymeric surfactants used for steric stabilisation are mostly of the A-B-A type, with the hydrophobic B chain [e.g., poly(propylene oxide)] forming the ''anchor'' as a result of its being strongly adsorbed onto the hydrophobic particle or oil droplet. The A chains consist of hydrophilic components (e.g., EO groups), and these provide the effective steric repulsion.

In some cases, a graft copolymer of one B chain with several A chains attached to the B backbone (i.e., BA_n) is used and, again, the hydrodynamic thickness of the layer δ is determined by the number of EO units in the A chains.

Formulation of Disperse Systems: Science and Technology, First Edition. Tharwat F. Tadros.

In this chapter, two main topics will be addressed:

1) The interaction between particles containing adsorbed nonionic surfactants or polymer and the theory of steric stabilisation. Particular attention will be given to the solvency of the medium for the stabilising chains that determines the magnitude of steric repulsion.
2) The flocculation of sterically stabilised dispersions, including weak, incipient, and depletion flocculation.

8.2
Interaction between Particles Containing Adsorbed Nonionic and Polymeric Surfactant Layers (Steric Stabilisation)

When two particles, each with a radius R and containing an adsorbed surfactant or polymer layer with a hydrodynamic thickness δ_H, approach each other to a surface-surface separation distance h that is smaller than $2\delta_H$, the surfactant or polymer layers interact with each other, with two main outcomes [1]: (i) the surfactant or polymer chains may overlap with each other; or (ii) the surfactant or polymer layer may undergo some compression. In both cases, there will be an increase in the local segment density of the surfactant or polymer chains in the interaction region; this is shown schematically in Figure 8.1. The real-life situation perhaps lies between the above two cases, however, with the surfactant or polymer chains undergoing some interpenetration and some compression.

Provided that the dangling chains (the A chains in A-B, A-B-A block or BA_n graft copolymers) are in a good solvent, this local increase in segment density in the interaction zone will result in a strong repulsion as the result of two main effects [1]:

1) An increase in the osmotic pressure in the overlap region as a result of the unfavourable mixing of the A chains, when these are in good solvent conditions; this is referred to as osmotic repulsion or mixing interaction, and is described by a free energy of interaction G_{mix}.
2) A reduction in the configurational entropy of the chains in the interaction zone; this results from a decrease in the volume available for the A chains when these are either overlapped or compressed. This is referred to as volume restriction

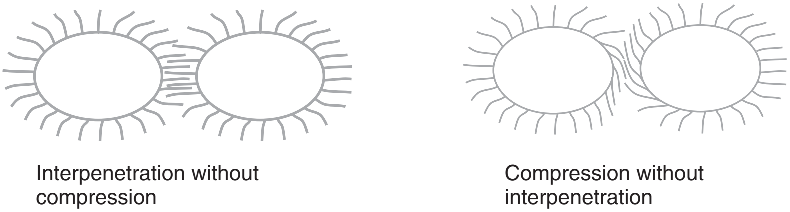

Figure 8.1 Schematic representation of the interaction between particles containing adsorbed polymer layers.

interaction, entropic interaction or elastic interaction, and is described by a free energy of interaction G_{el}.

The combination of G_{mix} and G_{el} is usually referred to as the steric interaction free energy, G_{s}, that is,

$$G_{\mathrm{s}} = G_{\mathrm{mix}} + G_{\mathrm{el}} \tag{8.1}$$

The sign of G_{mix} depends on the solvency of the medium for the A chains. If in a good solvent – that is, the Flory–Huggins interaction parameter χ is <0.5 – then G_{mix} will be positive and the mixing interaction will lead to repulsion (see below). In contrast, if $\chi > 0.5$ (i.e., the chains are in a poor solvent condition) then G_{mix} will be negative and the mixing interaction will become attractive. G_{el} is always positive, and hence in some cases stable dispersions can be produced in a relatively poor solvent (enhanced steric stabilisation).

8.3
Mixing Interaction G_{mix}

This results from the unfavourable mixing of the polymer chains, when these are in a good solvent condition; this is shown schematically in Figure 8.2. Consider two spherical particles with the same radius and each containing an adsorbed hydrated layer with thickness δ. Before overlap, it is possible to define in each layer a chemical potential for the solvent, $\mu_{\mathrm{i}}^{\alpha}$, and a volume fraction for the chains in the layer, ϕ_2. In the overlap region (volume element dV), the chemical potential of the solvent is reduced to μ_{i}^{β}; this results from the increase in A segment concentration in this overlap region.

In the overlap region, the chemical potential of the hydrated chains is now higher than in the remainder of the layer (with no overlap). This amounts to an increase in the osmotic pressure in the overlap region, and as a result solvent will diffuse from the bulk to the overlap region; this causes the particles to be separated and a strong repulsive energy arises from this effect. Such repulsive energy can be calculated

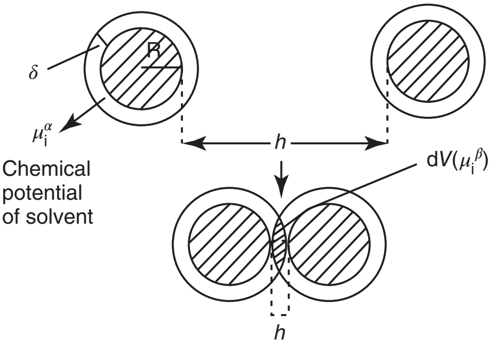

Figure 8.2 Schematic representation of polymer layer overlap.

by considering the free energy of mixing of two polymer solutions, as treated by Flory and Krigbaum [2]. The free energy of mixing is given by two terms: (i) an entropy term that depends on the volume fraction of polymer and solvent; and (ii) an energy term that is determined by the Flory–Huggins interaction parameter,

$$\delta(G_{\mathrm{mix}}) = kT\ (n_1\ \ln\ \varphi_1 + n_2\ \ln\ \varphi_2 + \chi\ n_1\ \varphi_2) \tag{8.2}$$

where n_1 and n_2 are the number of moles of solvent and polymer with volume fractions φ_1 and φ_2, respectively, k is the Boltzmann constant, and T is the absolute temperature.

The total change in free energy of mixing for the whole interaction zone, V, is obtained by summing over all the elements in V,

$$G_{\mathrm{mix}} = \frac{2kT\ V_2^2}{V_1}\ \nu_2\ \left(\frac{1}{2} - \chi\right)\ R_{\mathrm{mix}}(h) \tag{8.3}$$

where V_1 and V_2 are the molar volumes of the solvent and polymer, respectively, ν_2 is the number of chains per unit area, and $R_{\mathrm{mix}}(h)$ is geometric function which depends on the form of the segment density distribution of the chain normal to the surface, $\rho(z)$. In addition, k is the Boltzmann constant and T is the absolute temperature.

Using the above theory it is possible to derive an expression for the free energy of mixing of two hydrated layers (assuming a uniform segment density distribution in each layer) surrounding two spherical particles as a function of the separation distance h between the particles [3, 4].

The expression for G_{mix} is,

$$G_{\mathrm{mix}} = \left(\frac{2V_2^2}{V_1}\right)\ \nu_2\ \left(\frac{1}{2} - \chi\right)\ \left(\delta - \frac{h}{2}\right)^2\ \left(3R + 2\delta + \frac{h}{2}\right) \tag{8.4}$$

The sign of G_{mix} depends on the value of the Flory–Huggins interaction parameter χ: if $\chi < 0.5$, then G_{mix} will be positive and the interaction repulsive, but if $\chi > 0.5$, then G_{mix} will be negative and the interaction attractive. The condition $\chi = 0.5$ and $G_{\mathrm{mix}} = 0$ is termed the θ-condition. The latter corresponds to the case where the chain mixing behaves as ideal – that is, mixing of the chains does not lead to an increase or decrease of the free energy.

8.4
Elastic Interaction G_{el}

This arises from the loss in configurational entropy of the chains on the approach of a second particle. As a result of such an approach the volume available for the chains becomes restricted, which results in a loss of the number of configurations. This can be illustrated by considering a simple molecule, represented by a rod that rotates freely in a hemisphere across a surface (Figure 8.3). When the two surfaces are separated by an infinite distance, ∞, the number of configurations of the rod is $\Omega(\infty)$, which is proportional to the volume of the hemisphere. When a second

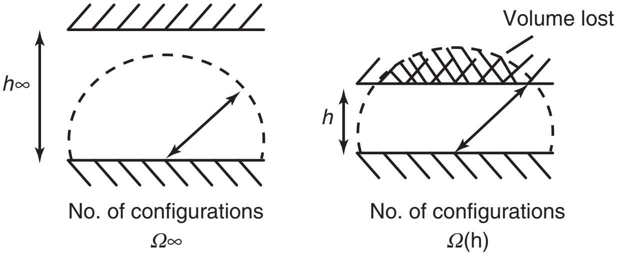

Figure 8.3 Schematic representation of configurational entropy loss on the approach of a second particle.

particle approaches to a distance h such that it cuts the hemisphere (losing some of its volume), the volume available to the chains is reduced and the number of configurations become $\Omega(h)$, which is less than $\Omega(\infty)$. For two flat plates, G_{el} is given by the following expression [5]:

$$\frac{G_{\text{el}}}{kT} = 2\nu_2 \ln\left[\frac{\Omega(h)}{\Omega(\infty)}\right] = 2\nu_2 R_{\text{el}}(h) \tag{8.5}$$

where $R_{\text{el}}(h)$ is a geometric function whose form depends on the segment density distribution. It should be stressed that G_{el} is always positive and could play a major role in steric stabilisation. In particular, it becomes very strong when the separation distance between the particles becomes comparable to the adsorbed layer thickness, δ.

8.5
Total Energy of Interaction

The combination of G_{mix} and G_{el} with G_{A} gives the total energy of interaction, G_{T} (assuming that there is no contribution from any residual electrostatic interaction), that is [6]:

$$G_{\text{T}} = G_{\text{mix}} + G_{\text{el}} + G_{\text{A}} \tag{8.6}$$

A schematic representation of the variation of G_{mix}, G_{el}, G_{A}, and G_{T} with surface-surface separation distance h is shown in Figure 8.4. G_{mix} increases very sharply with a decrease in h, when $h < 2\delta$; likewise, G_{el} increases very sharply with a decrease in h, when $h < \delta$; and G_{T} versus h shows a minimum, G_{min}, at separation distances comparable to 2δ. When $h < 2\delta$, G_{T} shows a rapid increase with decrease in h. The depth of the minimum depends on the Hamaker constant A, the particle radius R, and the adsorbed layer thickness δ. G_{min} increases with increases of A and R and, at a given A and R, also increases with a decrease in δ (i.e., with decrease in the molecular weight, M_{w}, of the stabiliser). This is illustrated in Figure 8.5, which shows the energy–distance curves as a function of δ/R. The larger the value of δ/R, the smaller the value of G_{min}; in this case, the system may approach thermodynamic stability, as occurs with nanodispersions.

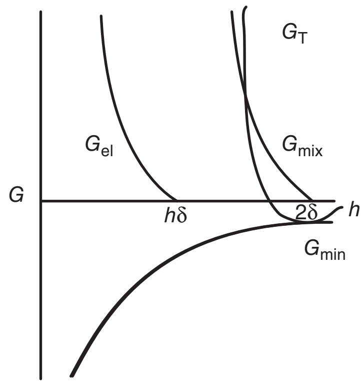

Figure 8.4 Energy–distance curves for sterically stabilised systems.

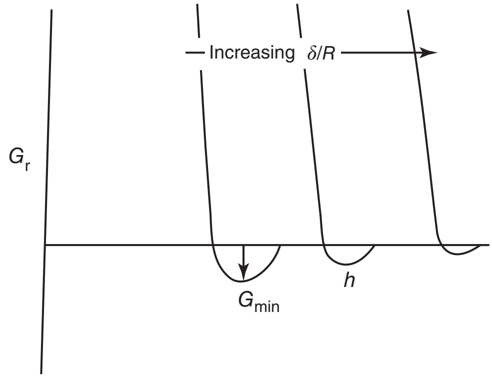

Figure 8.5 Variation of G_{min} with δ/R.

8.6
Criteria for Effective Steric Stabilisation

1) The particles should be completely covered by the surfactant or polymer (the amount of surfactant or polymer should correspond to the plateau value). Any bare patches may cause flocculation, either by van der Waals attraction (between the bare patches) or by bridging flocculation (whereby a polymer molecule will become simultaneously adsorbed onto two or more particles).
2) The chain should be strongly ‘‘anchored’’ to the particle surfaces, to prevent any displacement during particle approach; this is particularly important for concentrated suspensions. For this purpose, A-B, A-B-A block and BA_n graft copolymers are the most suitable, where the chain B is chosen to be highly insoluble in the medium and has a strong affinity to the surface. Examples of B groups for hydrophobic particles in aqueous media are polystyrene and poly(methylmethacrylate).

3) The stabilising chain A should be highly soluble in the medium and strongly solvated by its molecules. Examples of A chains in aqueous media are poly(ethylene oxide) and poly(vinyl alcohol).
4) δ should be sufficiently large (>5 nm) to prevent weak flocculation.

8.7
Flocculation of Sterically Stabilised Dispersions

Three main types of flocculation may be distinguished:

8.7.1
Weak Flocculation

This occurs when the thickness of the adsorbed layer is small (usually <5 nm), and particularly when the particle radius and Hamaker constant are large. The minimum depth required to cause weak flocculation depends on the volume fraction of the suspension: the higher the volume fraction the lower the minimum depth required for weak flocculation. This can be understood by considering the free energy of flocculation that consists of two terms: (i) an energy term determined by the depth of the minimum (G_{min}); and (ii) an entropy term that is determined by reduction in configurational entropy on aggregation of particles,

$$\Delta G_{\text{flocc}} = \Delta H_{\text{flocc}} - T\,\Delta S_{\text{flocc}} \tag{8.7}$$

With dilute suspensions the entropy loss on flocculation is larger than with concentrated suspensions. Hence, for the flocculation of a dilute suspension a higher energy minimum will be required when compared to the case with concentrated suspensions.

The above flocculation is weak and reversible; that is, on shaking the container a redispersion of the suspension will occur, but on standing the dispersed particles will aggregate to form a weak "gel." This process (which is referred to as sol–gel transformation) leads to a reversible time dependence of viscosity (thixotropy). On shearing the suspension the viscosity is decreased such that, when the shear is removed, the viscosity is recovered. This phenomenon is applied in paints; when a paint is applied (by brush or roller) the gel is fluidised, which allows a uniform coating of the paint. However, when shearing is stopped the paint film recovers its viscosity, avoiding any dripping.

8.7.2
Incipient Flocculation

This occurs when the solvency of the medium is reduced to become worse than θ-solvent (i.e., $\chi > 0.5$). This is illustrated in Figure 8.6, where χ was increased from <0.5 (good solvent) to >0.5 (poor solvent).

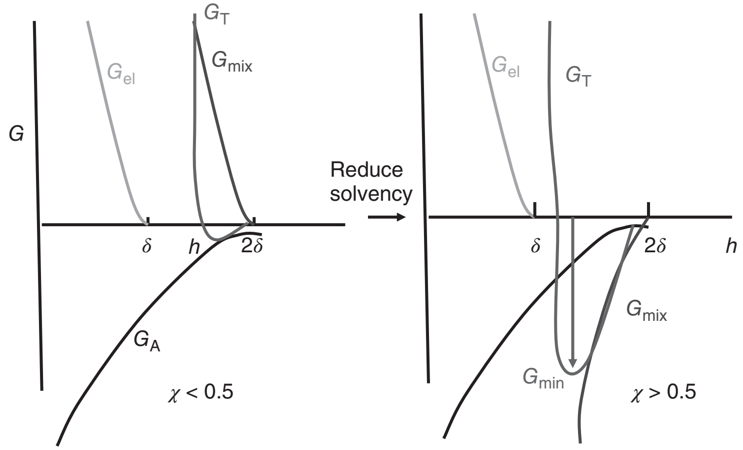

Figure 8.6 Influence of reduction in solvency on the energy–distance curve.

When $\chi > 0.5$, G_{mix} becomes negative (attractive) this, combined with the van der Waals attraction at this separation distance, produces a deep minimum causing flocculation. In most cases, there is a correlation between the critical flocculation point and the θ-condition of the medium. A good correlation is found in many cases between the critical flocculation temperature (CFT) and the θ-temperature of the polymer in solution (with both block and graft copolymers the θ-temperature of the stabilising chains A should be considered) [2]. A good correlation was also found between the critical volume fraction (CFV) of a nonsolvent for the polymer chains and their θ-point under these conditions. In some cases, however, such correlation may break down, and this is particularly the case for polymers that adsorb by multipoint attachment. This situation has been described by Napper [2], who referred to it as ‘‘enhanced’’ steric stabilisation.

Thus, by measuring the θ-point (CFT or CFV) for the polymer chains (A) in the medium under investigation (which could be obtained from viscosity measurements), it is possible to establish the stability conditions for a dispersion, before its preparation. This procedure is also helpful when designing effective steric stabilisers such as block and graft copolymers.

8.7.3
Depletion Flocculation

Depletion flocculation is produced by addition of a ‘‘free’’ nonadsorbing polymer [7]. In this case, the polymer coils cannot approach the particles to a distance Δ (this is determined by the radius of gyration of free polymer, R_G), as the reduction in entropy on close approach of the polymer coils is not compensated by an adsorption energy. The suspcakesension particles or emulsion droplets will be surrounded by a depletion zone with thickness Δ. Above a critical volume fraction of the free polymer, $\varphi_p{}^+$, the polymer coils will be ‘‘squeezed out’’ from between the particles

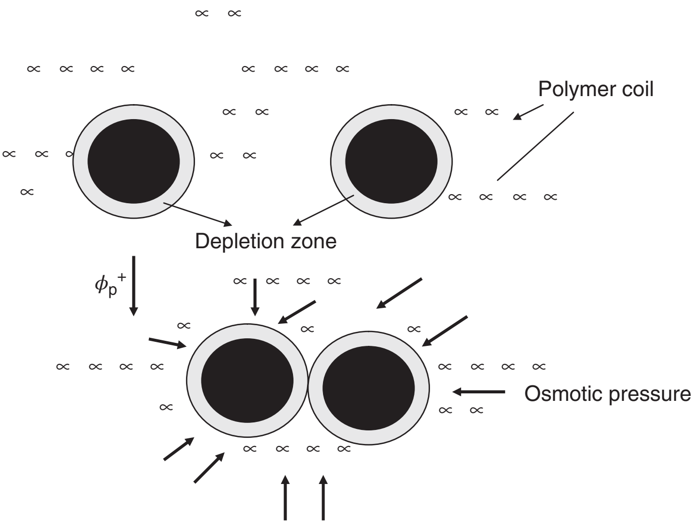

Figure 8.7 Schematic representation of depletion flocculation.

and the depletion zones will begin to interact. As a consequence, the interstices between the particles will become free from the polymer coils such that an osmotic pressure is exerted outside the particle surface (the osmotic pressure outside is higher than in between the particles), and this results in a weak flocculation [7]. A schematic representation of depletion flocculation is shown in Figure 8.7.

The magnitude of the depletion attraction free energy, G_{dep}, is proportional to the osmotic pressure of the polymer solution, which in turn is determined by φ_p and the molecular weight M. The range of depletion attraction is proportional to the thickness of the depletion zone, Δ, which is roughly equal to the radius of gyration, R_G, of the free polymer. A simple expression for G_{dep} is [7],

$$G_{\text{dep}} = \frac{2\pi\ R\,\Delta^2}{V_1}\,(\mu_1 - \mu_1^{\circ})\left(1 + \frac{2\Delta}{R}\right) \tag{8.8}$$

where V_1 is the molar volume of the solvent, μ_1 is the chemical potential of the solvent in the presence of free polymer with volume fraction φ_p and $\mu_1{}^{\circ}$ is the chemical potential of the solvent in the absence of free polymer. $(\mu_1 - \mu_1{}^{\circ})$ is proportional to the osmotic pressure of the polymer solution.

References

1. Tadros, T.F. (1981) Polymer adsorption and dispersion stability, in *The Effect of Polymers on Dispersion Properties* (ed. T.F. Tadros), Academic Press, London.
2. Napper, D.H. (1981) *Polymeric Stabilisation of Colloidal Dispersions,* Academic Press, London.
3. Flory, P.J. and Krigbaum, W.R. (1950) *J. Chem. Phys.*, **18**, 1086.

4. Fischer, E.W. (1958) *Kolloid Z.*, **160**, 120.
5. Mackor, E.L. and van der Waals, J.H. (1951) *J. Colloid Sci.*, **7**, 535.
6. Hesselink, F.T., Vrij, A., and Overbeek, J.T.G. (1971) *J. Phys. Chem.*, **75**, 2094.
7. (a) Asakura, A. and Oosawa, F. (1954) *J. Chem. Phys.*, **22**, 1235; (b) Asakura, A. and Oosawa, F. (1958) *J. Polym. Sci.*, **93**, 183.

9

Formulation of Solid/Liquid Dispersions (Suspensions)

9.1

Introduction

Suspensions are solid/liquid dispersions that find application in almost every industrial preparation, including paints, dyestuffs, paper coatings, printing inks, agrochemicals, pharmaceuticals, cosmetics, food products, detergents, and ceramics. The powder particles can be hydrophobic (e.g., organic pigments, agrochemicals, ceramics) or hydrophilic (e.g., silica, titania and clays), while the liquid can be either aqueous or nonaqueous. It is essential to understand the process of dispersion of powders in liquids (to prepare suspensions) at a fundamental level: ''Dispersion is a process whereby aggregates and agglomerates of powders are dispersed into 'individual' units, usually followed by a wet milling process (to subdivide the particles into smaller units) and stabilisation of the resulting dispersion against aggregation and sedimentation'' [1, 2].

In this chapter, the main procedures for preparing solid/liquid dispersions (suspensions) will be described. This will be followed by sections on the origin of charge in suspension particles, the electrical double layer, and the concept of the zeta-potential. The adsorption of surfactants and polymers at the solid/liquid interface is described, and the stabilisation of suspensions by surfactants, both electrostatically and sterically, will be outlined at a fundamental level. This will be followed by a section on the different states of suspensions on standing, and how the three-dimensional structures formed can be accounted for in terms of the various interaction forces that occur between the particles. A summary of the various procedures that may be used to characterize suspensions will be provided, with particular attention being paid to the application of rheological techniques used to assess and predict the long-term stability of suspensions. This will be followed by a section on the settling of suspensions and prevention of the formation of compact sediments (clays or cakes); methods that can be applied to prevent settling will be briefly described. The fundamental principles involved in each of the above processes will be outlined as far as possible.

Formulation of Disperse Systems: Science and Technology, First Edition. Tharwat F. Tadros.

9.2
Preparation of Suspensions

Two main processes are utilised for the preparation of solid/liquid dispersions:

- The ‘‘condensation’’ method: this depends on the ‘‘build-up’’ of particles from molecular units, and involves two main processes of nucleation and growth. In this case, it is necessary first to prepare a molecular (ionic, atomic or molecular) distribution of the insoluble substances; then, by changing the conditions, a precipitation is caused that leads to the formation of nuclei which grow to form the particles in question.
- The ‘‘dispersion’’ method: in this case larger ‘‘lumps’’ of the insoluble substances are created and then subdivided by mechanical or other means into smaller units.

The role of surfactants in the preparation of suspensions using these two methods will be described separately.

9.3
Condensation Methods: Nucleation and Growth

Nucleation is the spontaneous process of the appearance of a new phase from a metastable (supersaturated) solution of the material in question [3]. The initial stages of nucleation result in the formation of small nuclei, where the surface-to-volume ratio is very large and hence the role of specific surface energy is very important. With a progressive increase in the size of the nuclei, the ratio becomes smaller and eventually large crystals appear, with a corresponding reduction in the role played by the specific surface energy. The addition of surfactants can be used to control the process of nucleation and the size of the resulting nucleus.

According to Gibbs [4] and Volmer [5], the free energy of formation of a spherical nucleus, ΔG, is given by the sum of two contributions: (i) a positive surface energy term ΔG_s which increases with increase in the radius of the nucleus r; and (ii) a negative contribution ΔG_v due to the appearance of a new phase, which also increases with increases in r,

$$\Delta G = \Delta G_s + \Delta G_v \tag{9.1}$$

where ΔG_s is given by the product of area of the nucleus and the specific surface energy, solid/liquid interfacial tension σ; ΔG_v is related to the relative supersaturation (S/S_o),

$$\Delta G = 4\pi\, r^2\, \sigma - \left(\frac{4\pi\, r^3\, \rho}{3M}\right)\, RT\; \ln\left(\frac{S}{S_o}\right) \tag{9.2}$$

where ρ is the density, R is the gas constant, and T is the absolute temperature.

In the initial stages of nucleation, ΔG_s increases faster with increases in r when compared to ΔG_v and ΔG remains positive, reaching a maximum at a critical radius r^*, after which it decreases and eventually becomes negative. This occurs because

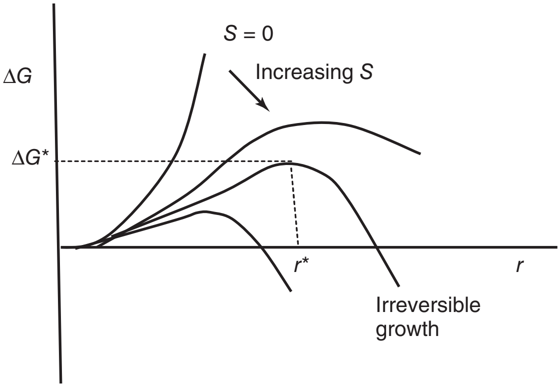

Figure 9.1 Schematic representation of the effect of supersaturation on particle growth.

the second term in Equation (9.2) rises faster with increases in r than does the first term (r^3 versus r^2). When ΔG becomes negative, growth becomes spontaneous and the cluster grows very fast. This is illustrated in Figure 9.1, which shows the effect of increasing the supersaturation; this figure also shows the critical size of the nucleus r^* above which growth becomes spontaneous. The free energy maximum ΔG^* at the critical radius represents the barrier that must be overcome before growth becomes spontaneous. Both, r^* and ΔG^* can be obtained by differentiating Equation (9.2) with respect to r and equating the result to zero. This gives the following expressions,

$$r^* = \frac{2\,\sigma\,M}{\rho\,RT\,\ln(S/S_o)} \tag{9.3}$$

$$\Delta G^* = \frac{16}{3}\,\frac{\pi\,\sigma^3\,M^2}{(\rho\,RT)^2\,[(\ln(S/S_o)]^2} \tag{9.4}$$

It is clear from Equations (9.1) to (9.4) that the free energy of formation of a nucleus and the critical radius r^*, above which the cluster formation grows spontaneously, depend on two main parameters, namely σ and (S/S_o), both of which are influenced by the presence of surfactants. σ is influenced in a direct way by the adsorption of surfactant onto the surface of the nucleus; this adsorption lowers γ and this in turn reduces r^* and ΔG^*; in other words, spontaneous cluster formation will occur at a smaller critical radius. In addition, surfactant adsorption stabilises the nuclei against any flocculation. The presence of micelles in solution also affects the processes of nucleation and growth, both directly and indirectly. For example, the micelles can act as ''nuclei'' on which growth may occur, and may also solubilize the molecules of the material; this can affect the relative supersaturation and, in turn, may have an effect on nucleation and growth.

9.4
Dispersion Methods

Dispersion methods are used to prepare suspensions of preformed particles. The term dispersion is used when referring to the complete process of incorporating a solid into a liquid, such that the final product consists of fine particles distributed throughout the dispersion medium. The role of surfactants (or polymers) in dispersion can be appreciated from a consideration of the three stages involved [1–3]: (i) wetting of the powder by the liquid; (ii) breaking the aggregates and agglomerates; and (iii) comminution (milling) of the resultant particles into smaller units.

Wetting is a fundamental process in which one fluid phase is displaced completely or partially by another fluid phase from the surface of a solid. One useful parameter to describe wetting is the contact angle θ of a liquid drop on a solid substrate [6]. If the liquid makes no contact with the solid, then $\theta = 180°$ and the solid is referred to as being nonwettable by the liquid in question. This may be the case for a perfectly hydrophobic surface with a polar liquid such as water. However, when $180° > \theta > 90°$, a case of poor wetting may be referred to. When $0° < \theta < 90°$, partial (incomplete) wetting is the case, whereas when $\theta = 0°$ complete wetting occurs and the liquid spreads on the solid substrate, forming a uniform liquid film.

The use of contact angle measurements depends on equilibrium thermodynamic arguments (static measurements) using the well-known Young's equation [6]. The value of θ will depend on: (i) the history of the system; and (ii) whether the liquid is tending to advance across or recede from the solid surface (advancing angle θ_A, receding angle θ_R; usually $\theta_A > \theta_R$). Under equilibrium, the liquid drop takes the shape that minimizes the free energy of the system. Three interfacial tensions can be identified: γ_{SV}, Solid/Vapour area A_{SV}; γ_{SL}, Solid/Liquid area A_{SL}; and γ_{LV}, Liquid/Vapour area A_{LV}. A schematic representation of the balance of tensions at the solid/liquid/Vapour interface is shown in Figure 9.2. The contact angle is that formed between the planes tangent to the surfaces of the solid and liquid at the wetting perimeter. Here, solid and liquid are simultaneously in contact with each other and the surrounding phase (air or vapour of the liquid). The wetting perimeter is referred to as the three-phase line or wetting line. In this region there is an equilibrium between vapour, liquid, and solid [6].

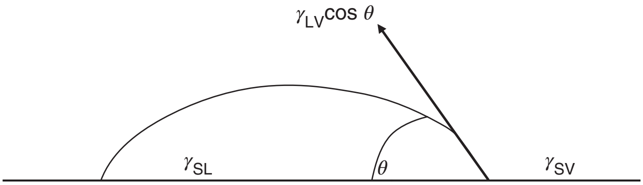

Figure 9.2 Schematic representation of the contact angle.

$\gamma_{SV} A_{SV} + \gamma_{SL} A_{SL} + \gamma_{LV} A_{LV}$ should be a minimum at equilibrium, and this leads to the well-known Young's equation:

$$\gamma_{SV} = \gamma_{SL} + \gamma_{LV} \cos\theta \tag{9.5}$$

$$\cos\theta = \frac{\gamma_{SV} - \gamma_{SL}}{\gamma_{LV}} \tag{9.6}$$

The contact angle θ depends on the balance between the solid/Vapour (γ_{SV}) and solid/liquid (γ_{SL}) interfacial tensions. The angle which a drop assumes on a solid surface is the result of the balance between the adhesion force between solid and liquid and the cohesive force in the liquid,

$$\gamma_{LV} \cos\theta = \gamma_{SV} - \gamma_{SL} \tag{9.7}$$

9.4.1
Wetting of Powders by Liquids

Wetting of powders by liquids is very important in their dispersion, for example in the preparation of concentrated suspensions. The particles in a dry powder form either aggregates (where the particles are joined by their crystal faces forming compact structures) or agglomerates (where the particles are joined by their edges or corners forming loose structures). It is essential in the dispersion process to wet both the external and internal surfaces and to displace the air entrapped between the particles. Wetting is achieved by the use of surface-active agents (wetting agents) of the ionic or nonionic type which are capable of diffusing quickly (i.e., reduce the dynamic surface tension) to the solid/liquid interface and displace the air entrapped by rapid penetration through the channels between the particles and inside any "capillaries." For the wetting of hydrophobic powders into water, anionic surfactants (e.g., alkyl sulphates or sulphonates) or nonionic surfactants of the alcohol or alkyl phenol ethoxylates are normally used.

A useful concept for choosing wetting agents of the ethoxylated surfactants is the hydrophilic–lipophilic balance (HLB) concept,

$$\text{HLB} = \frac{\%\text{ of hydrophilic groups}}{5} \tag{9.8}$$

Most wetting agents of this class have an HLB number in the range 7–9.

The process of wetting of a solid by a liquid involves three types of wetting: adhesion wetting, W_a; immersion wetting, W_i; and spreading wetting, W_s. In every step, Young's equation can be applied:

$$W_a = \gamma_{SL} - (\gamma_{SV} + \gamma_{LV}) = -\gamma_{LV}(\cos\theta + 1) \tag{9.9}$$

$$W_i = 4\,\gamma_{SL} - 4\,\gamma_{SV} = -4\,\gamma_{LV} \cos\theta \tag{9.10}$$

$$W_s = (\gamma_{SL} + \gamma_{LV}) - \gamma_{SV} = -\gamma_{LV}(\cos\theta - 1) \tag{9.11}$$

The work of dispersion W_d is the sum of W_a, W_i, and W_s:

$$W_d = W_a + W_i + W_s = 6\,\gamma_{SV} - \gamma_{SL} = -6\,\gamma_{LV}\ \cos\ \theta \tag{9.12}$$

Wetting and dispersion depends on γ_{LV}, the liquid surface tension and θ, the contact angle between the liquid and solid. W_a, W_i and W_s are spontaneous when $\theta < 90°$, and W_d is spontaneous when $\theta = 0$. Since surfactants are added in sufficient amounts ($\gamma_{dynamic}$ is lowered sufficiently), spontaneous dispersion is the rule rather than the exception.

Wetting of the internal surface requires penetration of the liquid into channels between and inside the agglomerates, a process which is similar to forcing a liquid through fine capillaries. In order to force a liquid through a capillary with radius r, a pressure p is required that is given by Rideal [7] and Washburn [8],

$$p = -\frac{2\,\gamma_{LV}\ \cos\ \theta}{r} = \left[\frac{-2\ \left(\gamma_{SV} - \gamma_{SL}\right)}{r\,\gamma_{LV}}\right] \tag{9.13}$$

γ_{SL} must be made as small as possible, there must be a rapid surfactant adsorption to the solid surface, and a low θ. When $\theta = 0$, $p \propto \gamma_{LV}$; thus, for penetration into the pores a high γ_{LV} is required. Consequently, wetting of the external surface requires a low contact angle θ and a low surface tension $\underline{\gamma}_{LV}$. Wetting of the internal surface (i.e., penetration through pores) requires a low θ but a high γ_{LV}. These two conditions are incompatible and a compromise must be made: $(\gamma_{SV} - \gamma_{SL})$ must be kept at a maximum, and γ_{LV} should be kept as low as possible, but not too low. These conclusions illustrate the problem of choosing the best dispersing agent for a particular powder. This requires measurement of the above parameters, as well as testing the efficiency of the dispersion process.

The rate of liquid penetration has been investigated by Rideal and Washburn [7, 8]. For horizontal capillaries (gravity-neglected), the depth of penetration l in time t is given by the Rideal–Washburn equation [7, 8]:

$$l = \left[\frac{r\,t\,\gamma_{LV}\ \cos\ \theta}{2\,\eta}\right]^{1/2} \tag{9.14}$$

To enhance the rate of penetration, γ_{LV} has to be made as high as possible, θ as low as possible, and η as low as possible. For the dispersion of powders into liquids, surfactants should be used that lower θ but do not reduce γ_{LV} too much; the viscosity of the liquid should also be kept at a minimum. Thickening agents (such as polymers) should not be added during the dispersion process. It is also necessary to avoid foam formation during the dispersion process. For a packed bed of particles, r may be replaced by K, which contains the effective radius of the bed and a tortuosity factor, which takes into account the complex path formed by the channels between the particles, that is:

$$l^2 = \frac{k\,t\,\gamma_{LV}\ \cos\ \theta}{2\,\eta} \tag{9.15}$$

Thus, a plot of l^2 versus t gives a straight line, from the slope of which θ can be obtained. The Rideal–Washburn [7, 8] equation can be applied to obtain the contact angle of liquids (and surfactant solutions) in powder beds. K should first be obtained using a liquid that produces a zero contact angle. A packed bed of powder is prepared, perhaps in a tube fitted with a sintered glass at the end (to retain the powder particles), the essential point being to pack the powder uniformly in the tube (a plunger may be used in this case). The tube containing the bed is then immersed in a liquid that provides spontaneous wetting (e.g., a lower alkane) – that is, the liquid gives a zero contact angle and $\cos\theta = 1$. By measuring the rate of penetration of the liquid (this can be carried out gravimetrically using, for example, a microbalance or a Kruss instrument), K can be obtained. The tube is then removed from the lower-alkane liquid and left to stand so that the liquid evaporates. The tube is then immersed in the liquid in question and the rate of penetration measured again as a function of time. By using Equation (9.25) it is possible to calculate $\cos\theta$, and hence θ.

9.4.2
Structure of the Solid/Liquid Interface and the Electrical Double Layer

A great variety of processes can be described that cause charge separation and the formation of electrical double layers. As these processes have been described in detail in Chapter 7, only a brief summary is given here. For example, charge separation can be produced by the ionisation of surface groups (e.g., on oxides) or by the adsorption of ionic surfactants. The resulting surface charge and the compensating diffuse charges in the bulk (counterions and co-ions) then form the electrical double layer. The most acceptable models of the double layer are due to Gouy–Chapman–Stern and Grahame. In the Gouy–Chapman theory [9], the compensating ions form a diffuse layer whose extension ($1/\kappa$) – that is, the Debye length – is determined by electrolyte concentration and valency, as given by the following equation:

$$\left(\frac{1}{\kappa}\right) = \left(\frac{\varepsilon_r \varepsilon_o \, kT}{2\, n_o \, Z_i^2 \, e^2}\right)^{1/2} \tag{9.16}$$

where ε_r is the permittivity (dielectric constant; 78.6 for water at 25 °C), ε_o is the permittivity of free space, k is the Boltzmann constant, T is the absolute temperature, n_o is the number of ions per unit volume of each type present in bulk solution, Z_i is the valency of the ions, and e is the electronic charge.

For 1 : 1 electrolyte (e.g., KCl)

C (mol dm^{-3})	10^{-5}	10^{-4}	10^{-3}	10^{-2}	10^{-1}
($1/\kappa$) (nm)	100	33	10	3.3	1

The double layer extension increases with decreases in electrolyte concentration.

Stern [9] introduced the concept of the nondiffuse part of the double layer for specifically adsorbed ions, the remainder being diffuse in nature. The potential drops linearly in the Stern region and then exponentially. Grahame [9] distinguished two types of ion in the Stern plane: physically adsorbed counterions (outer Helmholtz plane); and chemically adsorbed ions (that lose part of their hydration shell) (inner Helmholtz plane).

9.4.2.1 Electrical Double Layer Repulsion

When charged colloidal particles in a dispersion approach each other such that the double layers begin to overlap (i.e., the particle separation becomes less than twice the double layer extension), then repulsion will occur. The individual double layers can no longer develop unrestrictedly, as the limited space does not allow complete potential decay [10]; this is illustrated in Figure 9.3 for two flat plates.

The potential $\psi_{\mathrm{H}/2}$ half-way between the plates is no longer zero (as would be the case for isolated particles at $x \to \infty$). For two spherical particles of radius R and surface potential ψ_{o} and condition $\kappa R < 3$, the expression for the electrical double layer repulsive interaction is given by,

$$G_{\mathrm{el}} = \frac{4\pi\, \varepsilon_r \varepsilon_{\mathrm{o}}\, R^2\, \psi_{\mathrm{o}}^2\, \exp -(\kappa h)}{2R + h} \tag{9.17}$$

where h is the closest distance of separation between the surfaces. This expression shows the exponential decay of G_{el} with h. The higher the value of κ (i.e., the higher the electrolyte concentration), the steeper the decay.

9.4.2.2 van der Waals Attraction

As is well known, atoms or molecules always attract each other at short distances of separation. The attractive forces are of three different types: dipole–dipole interaction (Keesom); dipole-induced dipole interaction (Debye); and London dispersion force. Of these forces, the London dispersion is the most important as it occurs for polar and nonpolar molecules. It arises from fluctuations in the electron density distribution, and at small distances of separation r in vacuum, the attractive energy between two atoms or molecules is given by,

$$G_{\mathrm{aa}} = -\frac{\beta_{11}}{r^6} \tag{9.18}$$

where β_{11} is the London dispersion constant.

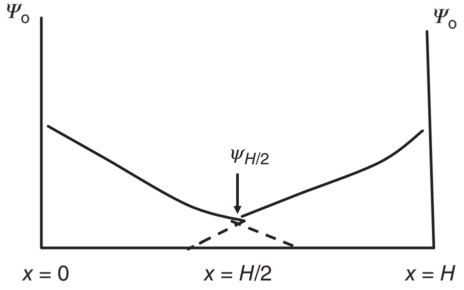

Figure 9.3 Schematic representation of double layer interaction for two flat plates.

For colloidal particles which are made of atom or molecular assemblies, the attractive energies may be added and this results in the following expression for two spheres (at small h),

$$G_A = -\frac{A\,R}{12\,h} \tag{9.19}$$

where A is the effective Hamaker constant,

$$A = (A_{11}^{1/2} - A_{22}^{1/2})^2 \tag{9.20}$$

where A_{11} is the Hamaker constant between particles in vacuum and A_{22} is the Hamaker constant for equivalent volumes of the medium.

$$A = \pi^2\, q^2\, \beta_{11} \tag{9.21}$$

where q is number of atoms or molecules per unit volume.

G_A decreases with increases of h and becomes very large at short distances of separation, whilst at very short distances the Born repulsion appears.

9.4.2.3 **Total Energy of Interaction**

According to Deryaguin–Landua–Verwey–Overbeek (DLVO) theory [11, 12], a combination of G_{el} and G_A results in the well-known theory of stability of colloids (DLVO theory) [13, 14],

$$G_T = G_{el} + G_A \tag{9.22}$$

A plot of G_T versus h is shown in Figure 9.4, which represents the case at low electrolyte concentrations – that is, a strong electrostatic repulsion between the particles. G_{el} decays exponentially with h, such that $G_{el} > 0$ as h becomes large. G_A is ∞ $1/h$, such that G_A does not decay to 0 at large h.

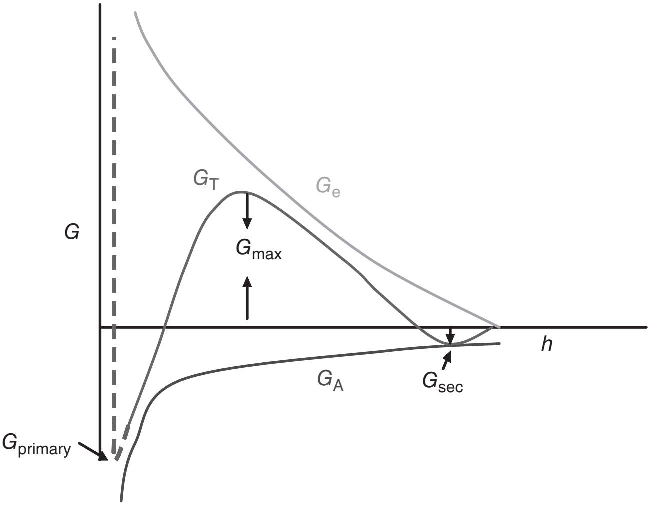

Figure 9.4 Total energy–distance curve according to DLVO theory.

At long distances of separation, $G_A > G_{el}$ which results in a shallow minimum (secondary minimum), but at very short distances, $G_A \gg G_{el}$ which results in a deep primary minimum. At intermediate distances, $G_{el} > G_A$ which results in an energy maximum, G_{max}, the height of which depends on ψ_o (or ψ_d) and the electrolyte concentration and valency. At low electrolyte concentrations ($<10^{-2}$ mol dm^{-3} for a 1 : 1 electrolyte), G_{max} is high (>25 kT) and this prevents particle aggregation into the primary minimum. The higher the electrolyte concentration (and the higher the valency of the ions), the lower the energy maximum.

Under certain conditions (depending on the electrolyte concentration and particle size), flocculation into the secondary minimum may occur. This flocculation is weak and reversible. However, by increasing the electrolyte concentration, G_{max} will be decreased until, at a given concentration, it vanishes and particle coagulation occurs. This is illustrated in Figure 9.5, which shows the variation of G_T with h at various electrolyte concentrations.

Coagulation occurs at a critical electrolyte concentration, the critical coagulation concentration (ccc), which in turn depends on the electrolyte valency. At low surface potentials, ccc ∞ $1/Z^2$; this referred to as the Schultze–Hardy rule. A rate constant for flocculation can be defined as: k_o = rapid rate of flocculation (in the absence of an energy barrier) and k = slow rate of flocculation (in the presence of an energy barrier)

$$\frac{k_o}{k} = W \text{ (the stability ratio)} \tag{9.23}$$

Note that W increases as G_{max} increases. The stability of colloidal dispersions can be quantitatively assessed from plots of log W versus log C, as illustrated in Figure 9.6.

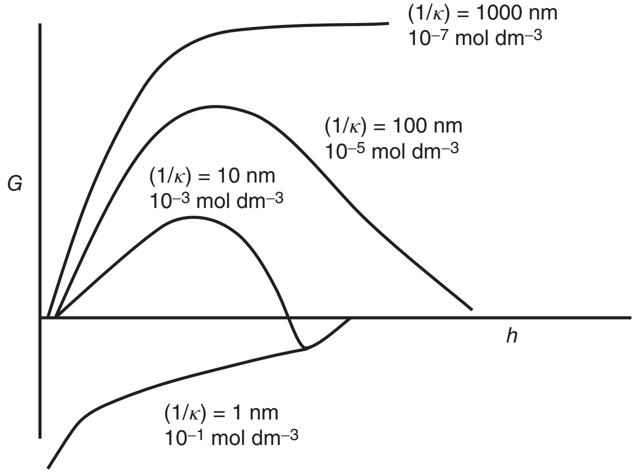

Figure 9.5 Energy–distance curves at various 1 : 1 electrolyte concentrations.

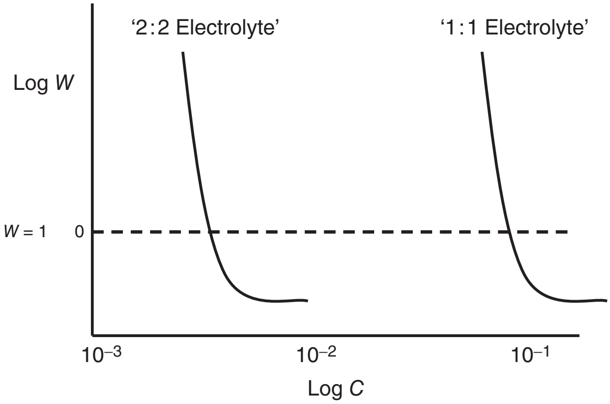

Figure 9.6 Log–log C curves.

9.4.2.4 Criteria for Stabilisation of Suspensions with Double Layer Interaction

The two main criteria for stabilisation are: (i) a high surface or Stern potential (zeta-potential) and a high surface charge; and (ii) a low electrolyte concentration and a low valency of counterions and co-ions. It should be ensured that an energy maximum in excess of 25 kT exists in the energy–distance curve. When $G_{max} \gg$ kT, the particles in the dispersion cannot overcome the energy barrier, thus preventing coagulation In some cases – particularly with large and asymmetric particles – flocculation into the secondary minimum may occur. Typically, this flocculation is weak and reversible, but may be advantageous for preventing the formation of hard sediments.

9.4.2.5 Electrokinetic Phenomena and the Zeta-Potential

As mentioned above, one of the main criteria for electrostatic stability is the high surface potential, but this can only be measured experimentally for systems containing ionogenic groups, such as oxides. For most practical systems that are stabilised by surfactants, the surface potential cannot be directly measured. In this case, the surface potential can be replaced by the measured zeta-potential (calculated from the particle electrophoretic mobility), which is the value close to the Stern potential and is referred to as the electrokinetic potential [15]. Electrokinetic effects are the direct result of charge separation at the interface between two phases. Consider a negatively charged surface where the positive ions (counterions) are attracted to the surface whereas the negative ions (co-ions) are repelled. The accumulation of excess positive ions will cause a gradual reduction in the potential, from its value ψ_o at the surface to 0 in bulk solution. At a point p from the surface, a potential ψ_x can be defined. Electrokinetic effects arise when one of the two phases is caused to move tangentially past the second phase. Such tangential motion can be caused conveniently by the application of an electric field, a process referred to as electrophoresis. Subsequently, the particle velocity v can be measured, from which the electrophoretic mobility u can be calculated:

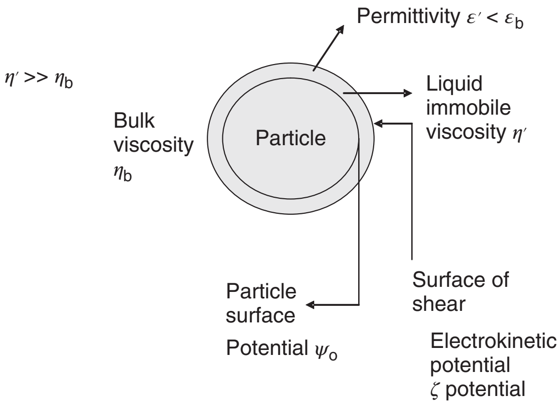

Figure 9.7 Surface (plane) of shear.

$$u = \frac{v}{(E/l)} \quad m^2 V^{-1} s^{-1} \tag{9.24}$$

where E is the applied potential and l is the distance between the two electrodes; E/l is the field strength. In all electrokinetic phenomena [15], a fluid moves with respect to a solid surface; hence, there is a need to derive a relationship between the fluid velocity (which varies with distance from the solid) and the electric field in the interfacial region. The most important concept here is the surface of shear, which is an imaginary surface close to the surface within which the fluid is stationary. This is illustrated in Figure 9.7, which shows the position of the surface potential ψ_o, the shear plane, and zeta potential (that is close to the Stern potential ψ_d).

9.4.2.6 **Calculation of the Zeta-Potential**

Calculation of the zeta-potential from particle mobility depends on the particle size and shape, as well as the electrolyte concentration, and several theories are available for this purpose.

Von Smoluchowski (Classical) Treatment The von Smoluchowski treatment [16] applies to the case where the particle radius R is much larger than the double layer thickness $(1/\kappa)$, that is $\kappa R \gg 1$. This generally applies to particles that are greater than 0.5 mμ (when the 1 : 1 electrolyte concentration is lower than 10^{-3} mol dm^{-3}, that is $\kappa R > 10$),

$$u = \frac{\varepsilon_r \varepsilon_o \zeta}{\eta} \tag{9.25}$$

where ε_r is the relative permittivity of the medium (78.6 for water at 25 °C), ε_o is the permittivity of free space (8.85×10^{-12} Fm^{-1}), η is the viscosity of the medium (8.9×10^{-4} Pa·s for water at 25 °C), and ζ is the zeta-potential (in volts).

For water at 25 °C,

$$\zeta = 1.282 \times 10^6\, u \tag{9.26}$$

where u is expressed in m^2 V^{-1} s^{-1}.

The Hückel Equation The Hückel equation [17] applies for the case $\kappa R < 1$,

$$u = \frac{2}{3} \frac{\varepsilon_r \varepsilon_o \zeta}{\eta} \tag{9.27}$$

The above equation applies for small particles (<100 nm) and thick double layers (low electrolyte concentration).

Henry's Treatment Henry's treatment [18] applies to intermediate cases where κR is not too small or too large, Henry derived the following expression (which can be applied at all κR values),

$$u = \frac{2}{3} \frac{\varepsilon_r \varepsilon_o \zeta}{\eta} f\,(\kappa R) \tag{9.28}$$

The function $f\,(\kappa R)$ depends also on the particle shape. Values of $f\,(\kappa R)$ at various values of κR are given in the following table as Henry's correction factor $f\,(\kappa R)$:

κR	0	1	2	3	4	5	10	25	100	∞
$f\,(\kappa R)$	1.0	1.027	1.066	1.101	1.133	1.160	1.239	1.370	1.460	1.500

Henry's calculations are based on the assumption that the external field can be superimposed on the field due to the particle, and hence it can only be applied for low potentials ($\zeta < 25$ mV). It also does not take into account the distortion of the field induced by the movement of the particle (relaxation effect). Wiersema, Loeb and Overbeek [19] introduced two corrections for the Henry's treatment, namely the relaxation and retardation (movement of the liquid with the double layer ions) effects. A numerical tabulation of the relationship between mobility and zeta-potential has been provided by Ottewill and Shaw [20]. Such tables are useful for converting u to ζ at all practical values of κR.

9.4.2.7 Measurement of the Zeta-Potential

Two main procedures can be applied for measuring the zeta potential [15]:

1) *Ultramicroscopic technique (microelectrophoresis)*: This is the most commonly used method as it allows direct observation of the particles using an ultramicroscope (suitable for particles that are larger than 100 nm). Basically, a dilute suspension is placed in a cell consisting of a thin-walled (~100 µm) glass tube that is attached to two larger-bore tubes with sockets for placing the electrodes. The cell is immersed in a thermostatic bath (accurate to +0.1 °C) that contains an attachment for illumination and a microscope objective for observing the particles. It is also possible to use a video camera for directly observing the particles. As the glass walls are charged (usually negative at practical pH measurements), the solution in the cell will in general experience electro-osmotic flow. Only where the electro-osmotic flow is zero – that is, at the stationary level – can the electrophoretic mobility of the particles be measured.

The stationary level is located at a distance of 0.707 of the radius from the centre of the tube, or 0.146 of the internal diameter from the wall. By focusing the microscope objective at the top and bottom of the walls of the tube, it is easy to locate the position of the stationary levels. The average particle velocity is measured at the top and bottom stationary levels by averaging at least 20 measurements in each direction (the eyepiece of the microscope is fitted with a graticule). Several commercial instruments are available (e.g., Rank Brothers, Bottisham, Cambridge, UK; Pen Kem in USA). For large particles (>1 μm and high density), sedimentation may occur during the measurement. In this case, a rectangular cell can be used and the particles observed horizontally from the side of the glass cell. Microelectrophoresis has many advantages as the particles can be measured in their normal environment. It is preferable to dilute the suspension with the supernatant liquid, which can be produced by centrifugation.

2) *Laser velocimetry technique*: This method is more suitable for small particles that undergo Brownian motion. The light scattered by small particles will show an intensity fluctuation as a result of the Brownian diffusion (Doppler shift). By applying an electric field as the particles undergo Brownian motion and measuring the fluctuation in the intensity of the scattered light (using a correlator), it is possible to measure the particle mobility. Two laser beams of equal intensity are allowed to cross at a particular point within the cell containing the suspension of particles. At the intersection of the beam, which is focused at the stationary level, interferences of known spacing are formed. The particles moving through the fringes under the influence of the electric field scatter light, the intensity of which fluctuates with a frequency that is related to the mobility of the particles. The photons are detected by a photomultiplier and the signal is fed to the correlator. The resulting correlation function is analysed to determine the frequency (Doppler) spectrum and this is converted to the particle velocity v,

$$v = \Delta v \, s \tag{9.29}$$

where Δv is the Doppler shift frequency and s is the spacing between the interference fringes in the region where the beams cross. s is given by the relationship,

$$s = \frac{\lambda}{2\ \sin(\alpha/2)} \tag{9.30}$$

where λ is the laser wavelength and α is the angle between the crossing laser beams. The velocity spectrum is then converted to a mobility spectrum (allowing the mobility distribution to be obtained), and the mobility is then converted to zeta-potential using Hückel's equation. Several commercial instruments are available for this procedure, including the Malvern Zeta Sizer and the Coulter Delsa Sizer.

9.4.3
Dispersing Agents for Formulation of Suspensions

As mentioned above, for dispersing powders into liquids, the addition of a dispersing agent is usually needed which satisfies the following requirements: (i) it lowers the surface tension of the liquid to aid wetting of the powder; (ii) it adsorbs at the solid/liquid interface to lower the solid/liquid interfacial tension; (iii) it lowers the contact angle of the liquid on the solid surface (zero contact angle is very common); (iv) it helps to break up the aggregates and agglomerates, as well as in the subdivision of particles into smaller units; and (v) it stabilises the particles formed against any aggregation (or rejoining). All dispersing agents are surface-active and can be simple surfactants (anionic, cationic, zwitterionic or nonionic), polymers, or polyelectrolytes. The dispersing agent should be soluble (or at least dispersible) in the liquid medium, and it should adsorb at the solid/liquid interface. As lists of surfactants and dispersants (polymers and polyelectrolytes) were provided in Chapters 2 and 4, respectively, only a summary is given at this point.

- *Surfactants*: Ionic, anionic (e.g., sodium dodecyl sulphate, $C_{12}H_{25}OSO_3^-\ Na^+$), cationic (e.g., cetyl trimethyl ammonium chloride, $C_{16}H_{33}\text{-}N^+(CH_3)_3Cl^-$), zwitterionic [e.g., 3-dimethyldodecylamine propane sulphonate (betaine $C_{12}H_{25}\text{-}N^+(CH_3)_2\text{-}CH_2\text{-}CH_2\text{-}CH_2\text{-}SO_3$)], nonionic, alcohol ethoxylates $C_nH_{2n+1}\text{-}O\text{-}(CH_2\text{-}CH_2\text{-}O)_n\text{-}H$, alkyl phenol ethoxylates $C_nH_{2n+1}\text{-}C_6H_4\text{-}O\text{-}(CH_2\text{-}CH_2\text{-}O)_n\text{-}H$, amine oxides (e.g., decyl dimethyl amine oxide, $C_{10}H_{21}\text{-}N\ (CH_3)_2{\rightarrow}O$), and amine ethoxylates.
- *Nonionic polymers*: Polyvinyl alcohol (with polyvinyl acetate blocks, usually 4–12%). $\text{-}(CH_2\text{-}CH\text{-}OH)_x\text{-}(CH_2\text{-}CH(OCOCH_3)\text{-}OH)_y\text{-}(CH_2\text{-}CH\text{-}OH)_x\text{-}$. Block copolymers of ethylene oxide-propylene oxide (ABA block of PEO-PPO-PEO), Pluronics (BASF), Synperonic PE (ICI), $H\text{-}(O\text{-}CH_2\text{-}CH_2)_n\text{-}(CH_2\text{-}CH\ (CH_3)\text{-}O)_m\text{-}(CH_2\text{-}CH_2\text{-}O)_n\text{-}H$. Graft copolymers, for example a poly(methylmethacrylate) (PMMA) backbone (with some polymethacrylic acid) with grafted PEO chains (Atlox 4913, Hypermer CG6; ICI).
- *Polyelectrolytes*: Polyacrylic acid, $\text{-}(CH_2\text{-}CH\text{-}COOH)_n\text{-}$. At $pH > 5$, ionisation of the carboxylic acid groups occurs forming an anionic polyelectrolyte. Polyacrylic acid/polymethacrylic acid, $(CH_2\text{-}CH\text{-}COO^-)_n\text{-}\ (CH_2\text{-}C\ (CH_3)\text{-}COO^-)_m$. Naphthalene formaldehyde sulphonated condensates, lignosulphonates.

9.4.4
Adsorption of Surfactants at the Solid/Liquid Interface

As this subject was covered in detail in Chapter 5, only a summary will be provided at this point. Surfactant adsorption is usually reversible, and hence thermodynamics can be applied for deriving the adsorption isotherm. For example, the adsorption of ionic surfactants onto hydrophobic surfaces may be represented by the Stern–Langmuir isotherm [13]. Consider a substrate containing N_s sites (mol m^{-2}) on which Γ mol m^{-2} of surfactant ions are adsorbed. The surface coverage θ is (Γ/N_s) and the fraction of uncovered surface is $(1-\theta)$. The Stern–Langmuir equation is given by Equation (9.31):

$$\frac{\theta}{1\text{-}\theta} = \frac{C}{55.5} \exp\left(-\frac{\Delta G^{\mathrm{O}}_{\mathrm{ads}}}{RT}\right) \tag{9.31}$$

Equation (9.31) applies only at low surface coverage ($\theta < 0.1$) where lateral interaction between the surfactant ions can be neglected. At high surface coverage ($\theta > 0.1$) one should take the lateral interaction between the chains into account, by introducing a constant A, for example using the Frumkin–Fowler–Guggenheim equation [13],

$$\frac{\theta}{(1-\theta)} \exp(A\theta) = \frac{C}{55.5} \exp\left(-\frac{\Delta G^{o}_{ads}}{RT}\right) \tag{9.32}$$

Various authors [14] have used the Stern–Langmuir equation in a simple form to describe the adsorption of surfactant ions on mineral surfaces,

$$\Gamma = 2\, r\, C \exp\left(-\frac{\Delta G^{\mathrm{o}}_{\mathrm{ads}}}{RT}\right) \tag{9.33}$$

Various contributions to the adsorption free energy may be envisaged. To a first approximation, these contributions may be considered to be additive. In the first instance, ΔG_{ads} may be taken to consist of two main contributions, that is

$$\Delta G_{\mathrm{ads}} = \Delta G_{\mathrm{elec}} + \Delta G_{\mathrm{spec}} \tag{9.34}$$

where ΔG_{elec} accounts for any electrical interactions and ΔG_{spec} is a specific adsorption term which contains all contributions to the adsorption free energy that are dependent on the "specific" (nonelectrical) nature of the system [21, 22]. Several authors have subdivided ΔG_{spec} into supposedly separate independent interactions [23, 24], for example

$$\Delta G_{\mathrm{spec}} = \Delta G_{\mathrm{cc}} + \Delta G_{\mathrm{cs}} + \Delta G_{\mathrm{hs}} + \ldots\ldots\ldots\ldots \tag{9.35}$$

where ΔG_{cc} is a term that accounts for the cohesive chain–chain interaction between the hydrophobic moieties of the adsorbed ions and ΔG_{cs} is the term for chain/substrate interaction, whereas ΔG_{hs} is a term for the head group/substrate interaction. Several other contributions to ΔG_{spec} may be envisaged, for example ion–dipole, ion-induced dipole or dipole-induced dipole interactions.

Since there is no rigorous theory that can predict adsorption isotherms, the most suitable method to investigate the adsorption of surfactants is actually to determine the adsorption isotherms directly. The measurement of surfactant adsorption is fairly straightforward: a known mass m (in grams) of the particles (substrate) with known specific surface area A_{s} ($\mathrm{m}^2\,\mathrm{g}^{-1}$) is equilibrated at constant temperature with a surfactant solution of initial concentration C_1. The suspension is kept stirred for sufficient time to reach equilibrium, after which the particles are removed from the suspension by centrifugation and the equilibrium concentration C_2 is determined using a suitable analytical method. The amount of adsorption Γ ($\mathrm{mol\,m}^{-2}$) is calculated as:

$$\Gamma = \frac{(C_1 - C_2)}{m\, A_{\mathrm{s}}} \tag{9.36}$$

The adsorption isotherm is represented by plotting Γ versus C_2. A range of surfactant concentrations should be used to cover the whole adsorption process – that is, from the initial low values to the plateau values. To obtain accurate results, the solid should have a high surface area (usually $>1\,\mathrm{m}^2$).

The adsorption of ionic surfactants on polar surfaces that contain ionizable groups may show characteristic features due to additional interactions between the head group and substrate and/or possible chain–chain interactions. Three distinct regions can be identified as the surfactant concentration is increased. The first region shows a gradual increase of adsorption with increase in concentration, with virtually no change in the value of the zeta-potential, and this corresponds to an ion-exchange process whereby the surfactant ions exchange with the counterions [24, 25] of the supporting electrolyte in the electrical double layer. At a critical surfactant concentration, the adsorption increases dramatically with a further increase in surfactant concentration (region II), and this was explained in terms of the ''hemi-micelle formation'' as originally postulated by Gaudin and Fuerestenau [24–26]. In other words, at a critical surfactant concentration [to be denoted the critical micelle concentration (cmc) of hemi-micelle formation or, better, the critical aggregation concentration (CAC)], the hydrophobic moieties of the adsorbed surfactant chains are ''squeezed out'' from the aqueous solution by forming two-dimensional aggregates on the adsorbent surface. This is analogous to the process of micellisation in bulk solution. However, the CAC is lower than the cmc, indicating that the substrate promotes surfactant aggregation. At a certain surfactant concentration in the hemi-micellisation process, the adsorption is hindered by the electrostatic repulsion between the hemi-micelles, and hence the slope of the adsorption isotherm is reduced (region III).

The adsorption of nonionic surfactants, such as the alcohol ethoxylates, are in many cases Langmuirian, like those of most other highly surface active solutes adsorbing from dilute solutions, and the adsorption is generally reversible. However, several other adsorption types are produced [27] giving several steps that may be explained in terms of the various adsorbate–adsorbate, adsorbate–adsorbent and adsorbate–solvent interactions forming bilayers, hemi-micelles, and micelles on the particle surface.

The adsorption of polymeric surfactants is more complex, since in this case the process is irreversible and produces a high-affinity isotherm with a steep rise in the adsorption value at low polymer concentrations (in this region most of the molecules are completely adsorbed). Subsequently, the adsorbed amount remains virtually constant, giving a plateau value that depends on the molecular weight, temperature and solvency of the medium for the chains (this topic was discussed in detail in Chapter 6).

9.4.5
Steric Stabilisation of Suspensions

As this subject was covered in detail in Chapter 8, only a brief summary will be given at this point. When two particles each with a radius R and containing an adsorbed polymer layer with a hydrodynamic thickness δ_h, approach each other to a surface–surface separation distance h that is smaller than 2 δ_h, the polymer layers interact with each other and this results in two main situations [28, 29]: (i) the polymer chains may overlap with each other; and/or (ii) the polymer layer may undergo some compression. In both cases there will be an increase in the local segment density of the polymer chains in the interaction region. Provided that the dangling chains (the A chains in A-B, A-B-A block or BA_n graft copolymers) are in a good solvent, this local increase in segment density in the interaction zone will result in a strong repulsion as a result of two main effects:

1) An increase in the osmotic pressure in the overlap region as a result of the unfavourable mixing of the polymer chains, when these are in good solvent conditions [28, 29]. This is referred to as osmotic repulsion or mixing interaction, and is described by a free energy of interaction, $G_{\text{mix.}}$
2) A reduction of the configurational entropy of the chains in the interaction zone; this entropy reduction results from the decrease in the volume available for the chains when these are either overlapped or compressed. This is referred to as volume restriction interaction, entropic or elastic interaction, and is described by a free energy of interaction, G_{el}.

A combination of G_{mix} and G_{el} is usually referred to as the steric interaction free energy, G_{s}, that is

$$G_{\text{s}} = G_{\text{mix}} + G_{\text{el}} \tag{9.37}$$

The sign of G_{mix} depends on the solvency of the medium for the chains. If in a good solvent – that is, the Flory–Huggins interaction parameter χ is less than 0.5 – then G_{mix} will be positive and the mixing interaction will lead to repulsion. In contrast, if $\chi > 0.5$ – that is, if the chains are in a poor solvent condition – then G_{mix} will be negative and the mixing interaction becomes attractive. G_{el} is always positive, and hence in some cases stable dispersions can be produced in a relatively poor solvent (enhanced steric stabilisation) [29].

The combination of G_{mix} and G_{el} with G_{A} gives the total energy of interaction G_{T} (assuming that there is no contribution from any residual electrostatic interaction), that is

$$G_{\text{T}} = G_{\text{mix}} + G_{\text{el}} + G_{\text{A}} \tag{9.38}$$

A schematic representation of the variation of G_{mix}, G_{el}, G_{A} and G_{T} with surface–surface separation distance h is shown in Figure 9.8. Here, G_{mix} is seen to increase very sharply with a decrease of h, when $h < 2\delta$, while G_{el} increases very sharply with a decrease of h, when $h < \delta$. G_{T} versus h shows a minimum, G_{min}, at separation distances comparable to 2δ; when $h < 2\delta$, G_{T} shows a rapid increase with a further decrease in h [29]. Unlike the G_{T}–h curve predicted by the DLVO theory (which shows two minima and one energy maximum), the G_{T}–h curve for systems that are sterically stabilised shows only one minimum, G_{min}, followed by a sharp increase in G_{T} with a decrease of h (when $h = 2\delta$). The depth of the minimum depends on A, R, and the adsorbed layer thickness δ, while G_{min} increases with

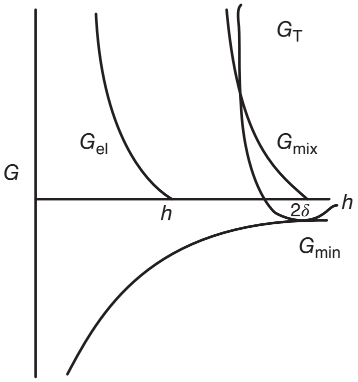

Figure 9.8 Energy–distance curves for sterically stabilised systems.

increases of both A and R. At given values of A and R, G_{min} increases with a decrease in δ (i.e., with a decrease of the molecular weight, M_w, of the stabiliser).

Several criteria can be established for the effective steric stabilisation of suspensions:

- The particles should be completely covered by the polymer (the amount of polymer should correspond to the plateau value). Any bare patches may cause flocculation, either by van der Waals attractions (between the bare patches) or by bridging flocculation (whereby a polymer molecule will become simultaneously adsorbed onto two or more particles).
- The polymer should be strongly ‘‘anchored’’ to the particle surfaces, to prevent any displacement during particle approach. This is particularly important for concentrated suspensions. For this purpose, A-B, A-B-A block and BA_n graft copolymers are the most suitable, where the chain B is chosen to be highly insoluble in the medium and has a strong affinity to the surface. Examples of B groups for hydrophobic particles in aqueous media are polystyrene and PMMA.
- The stabilising chain A should be highly soluble in the medium and strongly solvated by its molecules. Examples of A chains in aqueous media are poly(ethylene oxide) and poly(vinyl alcohol).
- δ should be sufficiently large (>5 nm) to prevent weak flocculation.

9.4.6
Flocculation of Sterically Stabilised Suspensions

Two main types of flocculation may be distinguished:

- Weak flocculation: this occurs when the thickness of the adsorbed layer is small (usually <5 nm), particularly when the particle radius and Hamaker constant are large.
- Incipient flocculation: this occurs when the solvency of the medium is reduced to become worse than θ-solvent (i.e., $\chi > 0.5$). This is illustrated in Figure 9.9, where χ was increased from <0.5 (good solvent) to >0.5 (poor solvent).

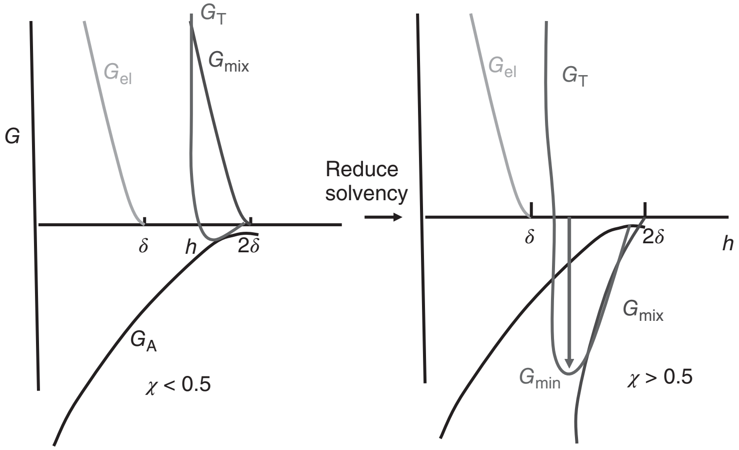

Figure 9.9 Influence of reduction in solvency on the energy–distance curve.

When $\chi > 0.5$, G_{mix} becomes negative (attractive) which, when combined with the van der Waals attraction at this separation distance, gives a deep minimum causing flocculation. In most cases there is a correlation between the critical flocculation point and the θ-condition of the medium. A good correlation is found in many cases between the critical flocculation temperature (CFT) and θ-temperature of the polymer in solution (with block and graft copolymers, the θ-temperature of the stabilising chains A should be considered) [29]. A good correlation is also found between the critical volume fraction (CFV) of a nonsolvent for the polymer chains and their θ-point under these conditions. However, in some cases such correlation may break down, which is particularly the case for polymers which adsorb by multipoint attachment. This situation has been described by Napper [29], who referred to it as ‘‘enhanced’’ steric stabilisation. Thus, by measuring the θ-point (CFT or CFV) for the polymer chains (A) in the medium under investigation (which could be obtained from viscosity measurements), it is possible to establish the stability conditions for a dispersion, before its preparation. This procedure is also helpful when designing effective steric stabilisers, such as block and graft copolymers.

9.4.7
Properties of Concentrated Suspensions

One of the main features of concentrated suspensions is the formation of three-dimensional structure units, which determine their properties and, in particular, their rheology. The formation of these units is determined by the interparticle interactions, which need to be clearly defined and quantified. It is useful to define the concentration range above which a suspension may be considered as concentrated. The particle number concentration and volume fraction, φ, above which a suspension may be considered to be concentrated, is best defined in terms of the balance between the particle translational motion and interparticle interaction. At one extreme, a suspension may be considered dilute if the thermal motion (Brownian diffusion) of the particles predominate over the imposed interparticle interaction [30–32]. In this case, the particle translational motion is large and only occasional contacts will occur between the particles; that is, the particles do not ''see'' each other until a collision occurs, giving a random arrangement of particles. In this case the particle interactions can be represented by two-body collisions. In such ''dilute'' systems gravity effects may be neglected, and if the particle size range is within the colloid range (1 nm to 1 μm) then no settling will occur. The properties of the suspension are time-independent and, therefore, any time-average quantity such as viscosity or scattering may be extrapolated to infinite dilution. As the particle number concentration is increased in a suspension, the volume of space occupied by the particles increases relative to the total volume; thus, a proportion of the space is excluded in terms of its occupancy by a single particle. Moreover, the particle–particle interaction increases and the forces of interaction between the particles play a dominant role is determining the properties of the system. With further increases in particle number concentration, the interactive contact between the particles is increased until a situation is reached where the interaction produces a specific order between the particles, and a highly developed structure is reached. With solid-in-liquid dispersions, such a highly ordered structure – which is close to the maximum packing fraction ($\varphi = 0.74$ for hexagonally closed packed array of monodisperse particles) – is referred to as a ''solid'' suspension. In such a system, any particle in the system interacts with many neighbours and the vibrational amplitude is small relative to particle size; thus, the properties of the system are essentially time-independent [30–32]. In between the random arrangement of particles in ''dilute'' suspensions and the highly ordered structure of ''solid'' suspensions, ''concentrated'' suspensions may be easily defined. In this case, the particle interactions occur by many body collisions and the translational motion of the particles is restricted. However, this reduced translational motion is less than with ''solid'' suspensions – that is, the vibrational motion of the particles is large compared to the particle size. Consequently, a time-dependent system arises in which there will be both spatial and temporal correlation.

On standing, concentrated suspensions reach various states (structures) that are determined by:

- The magnitude and balance of the various interaction forces, electrostatic repulsion, steric repulsion and van der Waals attraction.
- The particle size and shape distribution.
- The density difference between the disperse phase and the medium, which determines the sedimentation characteristics.
- The conditions and prehistory of the suspension, for example agitation which determines the structure of the flocs formed (chain aggregates, compact clusters, etc.).
- The presence of additives, such as high-molecular-weight polymers that may cause bridging or depletion flocculation.

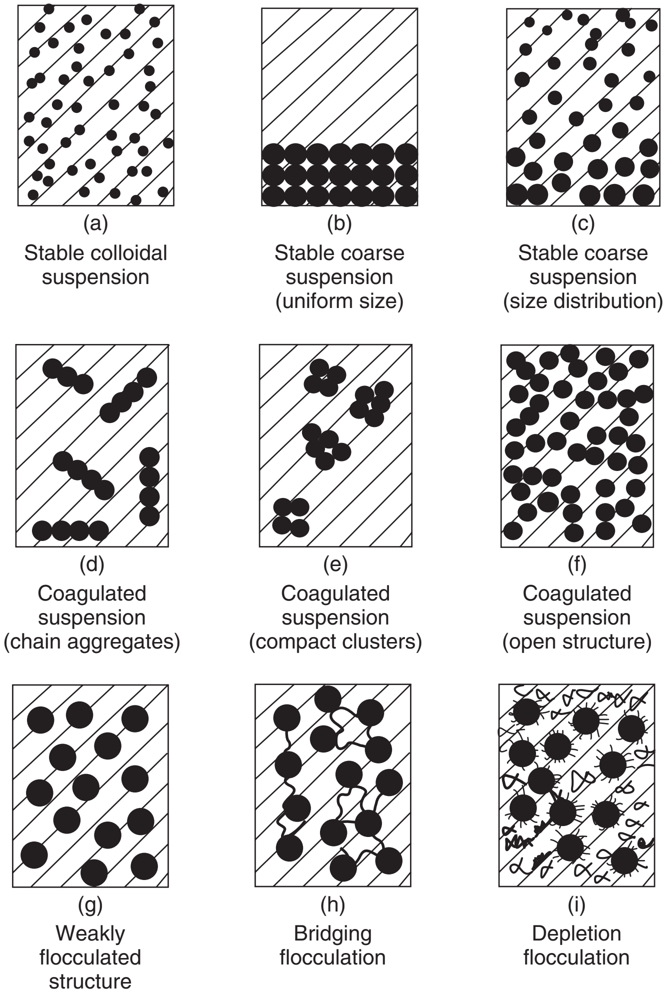

Figure 9.10 States of the suspension.

An illustration of some of the various states that may be produced is provided in Figure 9.10. These states may be described in terms of three different energy–distance curves as: (i) electrostatic, produced for example by the presence of ionogenic groups on the surface of the particles, or the adsorption of ionic surfactants; (ii) steric, produced for example by the adsorption of nonionic surfactants or polymers; and (iii) electrostatic + steric (electrosteric), as for example produced by polyelectrolytes.

A brief description of the various states shown in Figure 9.10 is given as follows [33, 34]: States (a)–(c) correspond to a suspension that is stable in the colloid sense, with stability being obtained as a result of net repulsion due to the presence of extended double layers (i.e., at low electrolyte concentration), the result of steric repulsion-produced adsorption of nonionic surfactants or polymers, or the result of a combination of double layer and steric repulsion (electrosteric). State (a) represents the case of a suspension with small particle size (submicron), whereby the Brownian diffusion overcomes the gravity force producing uniform distribution of the particles in the suspension, that is:

$$kT \ll (4/3)\,\pi\, R^3\, \Delta\rho\, g\, h \tag{9.39}$$

where k is the Boltzmann constant, T is the absolute temperature, R is the particle radius, $\Delta\rho$ is the buoyancy (the difference in density between the particles and the medium), g is acceleration due to gravity, and h is the height of the container. A good example of this case is a latex suspension with particle size well below 1 μm that is stabilised by ionogenic groups, by an ionic surfactant or nonionic surfactant or polymer. This suspension will show no separation on storage for long periods of time.

States (b) and (c) represent the case of suspensions, whereby the particle size range is outside the colloid range (>1 μm). In this case, the gravity force exceeds the Brownian diffusion. With state (b), the particles are uniform and will settle under gravity to form a hard sediment (technically referred to a ''clay'' or a ''cake.'' The repulsive forces between the particles allow them to move past each other until they reach small distances of separation (these are determined by the location of the repulsive barrier). Due to the small distances between the particles in the sediment it is very difficult to redisperse the suspension by simple shaking. With state (c) consisting of a wide distribution of particle sizes, the sediment may contain larger proportions of the larger size particles, but a hard ''clay'' will still be produced. These ''clays'' are dilatant (i.e., shear thickening) and can be easily detected by inserting a glass rod into the suspension, though penetration of the glass rod into these hard sediments is very difficult. States (d)–(f) represent the cases for coagulated suspensions in which the repulsive energy barrier is either small or is completely absent. State (d) represents the case of coagulation under no stirring conditions, in which situation chain aggregates are produced that will settle under gravity to form a relatively open structure. State (e) represents the case of coagulation under stirring conditions whereby compact aggregates are produced that will settle faster than the chain aggregates and the sediment produced will be more compact. State (f) represents the case of coagulation at a high volume fraction of the particles, φ. In this case, the whole particles will form a ''one-floc'' structure from chains and cross chains that extend from one wall to the other in the container. Such a coagulated structure may undergo some compression (consolidation) under gravity, leaving a clear supernatant liquid layer at the top of the container; this phenomenon is referred to as syneresis.

State (g) represents the case of weak and reversible flocculation. This occurs when the secondary minimum in the energy distance curve is deep enough to cause flocculation. This situation can occur at moderate electrolyte concentrations, in particular with larger particles; the same occurs with sterically and electrosterically stabilised suspensions. It also occurs when the adsorbed layer thickness is not very large, particularly with large particles. The minimum depth required to cause weak flocculation depends on the volume fraction of the suspension: the higher the volume fraction the lower the minimum depth required for weak flocculation. This can be understood by considering the free energy of flocculation that consists of two terms: an energy term determined by the depth of the minimum (G_{min}); and an entropy term that is determined by reduction in configurational entropy on aggregation of particles,

$$\Delta G_{\text{flocc}} = \Delta H_{\text{flocc}} - T\,\Delta S_{\text{flocc}} \tag{9.40}$$

With a dilute suspension the entropy loss on flocculation is larger than with a concentrated suspension; consequently, for flocculation of a dilute suspension a higher energy minimum is required when compared to the case with concentrated suspensions. This flocculation is weak and reversible such that, on shaking the container, a redispersion of the suspension will occur; however, on standing the dispersed particles will aggregate to form a weak "gel." This process (which is referred to as sol ↔ gel transformation) leads to a reversible time dependence of viscosity (thixotropy). On shearing the suspension the viscosity decreases, but when the shear is removed the viscosity recovers. This phenomenon is applied in paints, whereby when a paint is applied (by a brush or roller) the gel is fluidised and this allows a uniform coating of the paint. However, when the shearing is stopped the paint film recovers its viscosity, which prevents the paint from dripping.

State (h) represents the case whereby the particles are not completely covered by the polymer chains. In this situation, the simultaneous adsorption of one polymer chain onto more than one particle occurs, leading to bridging flocculation. If the polymer adsorption is weak (low adsorption energy per polymer segment), the flocculation may be weak and reversible, but if the adsorption of the polymer is strong then tough flocs will be produced and the flocculation will be irreversible. The latter phenomenon is used for solid/liquid separation, for example in water and effluent treatment.

State (i) represents a phenomenon that is referred to as depletion flocculation and is caused by the addition of a "free" nonadsorbing polymer [35]. In this case, the polymer coils cannot approach the particles to a distance Δ (this is determined by the radius of gyration of free polymer R_G), as the reduction in entropy on close approach of the polymer coils is not compensated by an adsorption energy. Thus, the suspension particles will be surrounded by a depletion zone with thickness Δ. Above a CFV of the free polymer, $\varphi_p{}^{+}$, the polymer coils are "squeezed out" from between the particles and the depletion zones begin to interact. At this point the interstices between the particles are free from polymer coils, such that an osmotic pressure is exerted outside the particle surface (the osmotic pressure outside is higher than in between the particles), and this results in a weak flocculation [35]. A schematic representation of depletion flocculation is shown in Figure 9.11.

The magnitude of the depletion attraction free energy, G_{dep}, is proportional to the osmotic pressure of the polymer solution, which in turn is determined by φ_p and molecular weight M. The range of depletion attraction is proportional to the thickness of the depletion zone, Δ, which is roughly equal to the radius of gyration,

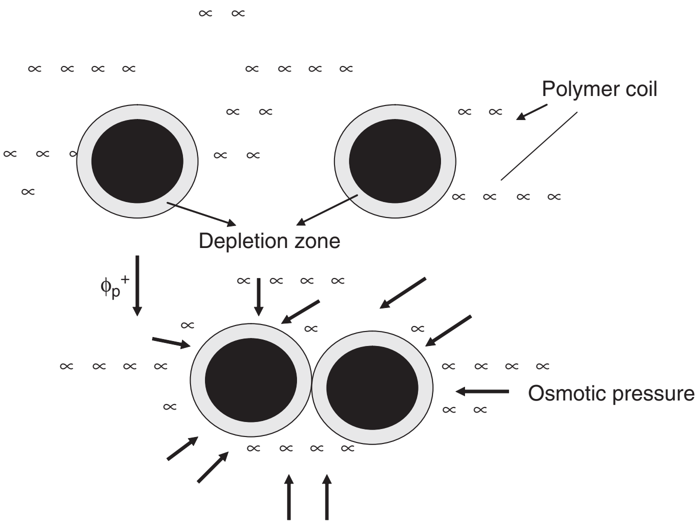

Figure 9.11 Schematic representation of depletion flocculation.

R_G, of the free polymer. A simple expression for G_{dep} is [35],

$$G_{dep} = \frac{2\pi\ R\,\Delta^2}{V_1}\ (\mu_1 - \mu_1^o)\ \left(1 + \frac{2\Delta}{R}\right) \tag{9.41}$$

where V_1 is the molar volume of the solvent, μ_1 is the chemical potential of the solvent in the presence of free polymer with volume fraction φ_p, and $\mu_1{}^o$ is the chemical potential of the solvent in the absence of free polymer. $(\mu_1 - \mu_1{}^{\circ})$ is proportional to the osmotic pressure of the polymer solution.

9.4.8
Characterisation of Suspensions and Assessment of their Stability

Two main procedures can be applied for the characterisation of suspensions and assessment of their stability (such as flocculation). The first method depends on the measurement of particle size distribution and the rate of flocculation and/or Ostwald ripening after dilution of the suspension with the dispersion medium, while the second procedure depends on measurement of the state of suspension without dilution, using rheological techniques. As both methods are described in detail in Chapters 19 and 20, only a summary will be provided here.

In all of these methods, care should be taken when sampling the suspension, with as little disturbance as possible being caused for when the ‘‘structure’’ is investigated. For example, when investigating the flocculation of a concentrated suspension, dilution of the system for microscopic investigation may lead to a breakdown of the flocs such that a false assessment will be obtained. The same applies when investigating the rheology of a concentrated suspension, as transferring the system from its container to the rheometer may lead to a breakdown of the structure. For these reasons it is important to establish well-defined procedures for every technique, and this requires a great deal of skill and experience. It is advisable in all cases to develop standard operating procedures for these investigations.

9.4.8.1 Optical Microscopy

Optical microscopy is by far the most valuable tool for qualitative or quantitative examinations of the suspension. A drop of the suspension is placed on a glass microscopy slide and covered with a coverslip. If the suspension has to be diluted the dispersion medium (which can be obtained by centrifugation and/or filtration of the suspension) should be used as the diluent in order to avoid aggregation. Information on the size, shape, morphology and aggregation of particles can be conveniently obtained, with minimum time required for sample preparation. As individual particles can be directly observed and their shape examined, optical microscopy is considered to be the only absolute method for particle characterisation. Unfortunately, optical microscopy has some limitations in terms of the minimum size that can be detected. The practical lower limit for the accurate measurement of particle size is 1.0 μm, although some detection may be obtained down to 0.3 μm. Image contrasting may be insufficient for observation, particularly when using a video camera (this is mostly for convenience). The contrast can be improved by decreasing the aperture of the iris diaphragm, but this reduces the resolution. As the contrast of the image depends on the refractive index of the particles relative to that of the medium, the contrast can be improved by increasing the difference between the refractive index of the particles and the immersion medium. However, changing the medium for the suspension is generally not practical as this may affect the state of the dispersion. Fortunately, water with a refractive index of 1.33 is a suitable medium for most organic particles with a refractive index usually >1.4.

Three main developments of optical microscopy are possible:

- *Phase-contrast microscopy*, which utilizes the difference between the diffracted waves from the main image and the direct light from the light source.
- *Differential interference contrast* (DIC) *microscopy*, which provides a better contrast than the phase-contrast method. This utilizes a phase difference to improve contrast, but the separation and recombination of a light beam into two beams is accomplished by prisms.
- *Polarised light microscopy*, in which the sample is illuminated with linearly or circularly polarised light, either in a reflection or transmission mode. One polarising element, located below the stage of the microscope, converts the illumination to polarised light, while a second polariser is located between the objective and the ocular and is used to detect polarised light. Various characteristics of the specimen can be determined, including anisotropy, polarisation colours, birefringence, and polymorphism.

The optical microscope can be used to observe dispersed particles and flocs, with particle sizing carried out using manual, semiautomatic, or automatic image analysis techniques.

9.4.8.2 Electron Microscopy

Detailed information on particle size and shape can be obtained using electron microscopy, which utilizes an electron beam to illuminate the sample. Due to the very short wavelength of electrons, the resolving power of an electron microscope exceeds that of an optical microscope about 200-fold. In transmission electron microscopy (TEM), the sample is deposited on a Formvar (polyvinyl formal) film that is resting on a grid in order to prevent the sample becoming charged. The sample is usually observed as a replica by coating with an electron-transparent material (e.g., gold or graphite). In scanning electron microscopy (SEM), the particle topography is obtained by scanning a very narrowly focused beam across the particle surface. The electron beam is directed either normally or obliquely at the surface, and the back-scattered or secondary electrons are detected in a raster pattern and displayed on a monitor screen.

9.4.8.3 Confocal Laser Scanning Microscopy

Confocal laser scanning microscopy (CLSM) is a very useful technique for the identification of suspensions. It uses a variable pinhole aperture or variable-width slit to illuminate only the focal plane by the apex of a cone of laser light. Out-of-focus items are dark and do not distract from the contrast of the image. As a result of extreme depth discrimination (optical sectioning), the resolution is considerably improved (up to 40% compared to optical microscopy). The CLSM technique acquires images by laser scanning or uses computer software to subtract any out-of-focus details from the in-focus image. The images are stored as the sample is advanced through the focal plane in elements as small as 50 nm. Three-dimensional images can be constructed to show the shape of the particles.

9.4.8.4 Scattering Techniques

These are by far the most useful methods for the characterisation of suspensions, and in principle they can provide quantitative information on the particle size distribution, floc size, and shape. The only limitation of these methods is the need to use sufficiently dilute samples to avoid interference, such as multiple scattering, which makes interpretation of the results difficult. However, back-scattering methods have recently been designed to allow measurements of the sample without dilution. In principle, any electromagnetic radiation can be used such as light, X-ray or neutrons, but in most industrial laboratories only light scattering is applied (using lasers).

Light-Scattering Techniques These can be conveniently divided into the following classes:

- Time-averaged light scattering, static or elastic scattering.
- Turbidity measurements, which can be carried out using a simple spectrophotometer.
- Light diffraction techniques.
- Dynamic (quasi-elastic) light scattering that is usually referred as photon correlation spectroscopy; this is a rapid technique that is especially suited to measuring submicron particles (nanosize range).
- Back-scattering techniques that are suitable for measuring concentrated samples.

The application of any of these methods depends on the information required and the availability of the instrument. These methods are described in detail in Chapter 19.

9.5
Bulk Properties of Suspensions

A qualitative method for assessing the bulk properties of suspensions involves measuring the equilibrium sediment volume (or height) and redispersion. For a ‘‘structured’’ suspension, obtained by ‘‘controlled flocculation’’ or the addition of ‘‘thickeners’’ (e.g., polysaccharides, clays or oxides), the ‘‘flocs’’ sediment at a rate depending on their size and porosity of the aggregated mass. After this initial sedimentation, compaction and rearrangement of the floc structure occurs; this phenomenon is referred to as ‘‘consolidation’’. Normally, in sediment volume measurements the initial volume V_o (or height H_o) is compared to the ultimately reached value of V (or H). A colloidally stable suspension gives a ‘‘close-packed’’ structure with a relatively small sediment volume (a dilatant sediment is referred to as a clay), whereas a weakly ‘‘flocculated’’ or ‘‘structured’’ suspension gives a more open sediment and hence a higher sediment volume. Thus, by comparing the relative sediment volume V/V_o or height H/H_o, it is possible to distinguish between a clayed and flocculated suspension.

9.5.1
Rheological Measurements

Three different rheological measurements may be applied [36–39]: (i) steady-state shear stress–shear rate measurements, using a controlled shear rate instrument; (ii) constant stress (creep) measurements, carried out using a constant stress instrument; and (iii) dynamic (oscillatory) measurements, preferably carried out using a constant strain instrument. These rheological techniques can be used to assess the sedimentation and/or flocculation of suspensions, and are described in detail in Chapters 20 and 21.

9.5.2
Sedimentation of Suspensions and Prevention of Formation of Dilatant Sediments (Clays)

As discussed previously, most suspensions undergo separation on standing as a result of the density difference between the particles and the medium, unless the particles are small enough for Brownian motion to overcome gravity.

For a very dilute suspension of rigid noninteracting particles, the rate of sedimentation v_o can be calculated by the application of Stokes' law, whereby the hydrodynamic force is balanced by the gravitational force,

$$\text{Hydrodynamic force} = 6\pi\ \eta\ R\ v_o \tag{9.42}$$

$$\text{Gravity force} = (4/3)\ \pi\ R^3\ \Delta\ \rho\ g \tag{9.43}$$

$$v_o = \frac{2}{9}\ \frac{R^2\ \Delta\rho\ g}{\eta} \tag{9.44}$$

where η is the viscosity of the medium (water).

When v_o was calculated for three particle sizes (0.1, 1, and 10 μm) for a suspension with density difference $\Delta\rho = 0.2$, the values of v_o were 4.4×10^{-9}, 4.4×10^{-7} and $4.4 \times 10^{-5}\ \mathrm{m\,s^{-1}}$, respectively. The times needed for complete sedimentation in a 0.1 m container were 250 days, 60 h, and 40 min, respectively.

For moderately concentrated suspensions, $0.2 > \varphi > 0.01$, the sedimentation is reduced as a result of hydrodynamic interaction between the particles, which no longer sediment independently of each other. The sedimentation velocity, v, can be related to the Stokes' velocity v_o by the following equation,

$$v = v_o\ (1 - 6.55\ \varphi) \tag{9.45}$$

This means that for a suspension with $\varphi = 0.1$, $v = 0.345\ v_o$; that is, the rate is reduced by a factor of approximately 3.

For more concentrated suspensions ($\varphi > 0.2$), the sedimentation velocity becomes a complex function of φ. At $\varphi > 0.4$, a hindered settling regime is usually entered whereby all of the particles sediment at the same rate (independent of size). A schematic representation for the variation of v with φ is shown in Figure 9.12, which also shows the variation of relative viscosity with φ. It can be seen from these data that v decreases exponentially with increase in φ, and ultimately approaches zero when φ approaches a critical value φ_p (the maximum packing fraction). The relative viscosity shows a gradual increase with increase in φ such that, when $\varphi = \varphi_p$, the relative viscosity approaches infinity.

The maximum packing fraction φ_p can be easily calculated for monodisperse rigid spheres. For an hexagonal packing $\varphi_p = 0.74$, whereas for a random packing $\varphi_p = 0.64$. The maximum packing fraction increases with polydisperse suspensions; for example, for a bimodal particle size distribution (with a ratio of ~10 : 1), $\varphi_p > 0.8$.

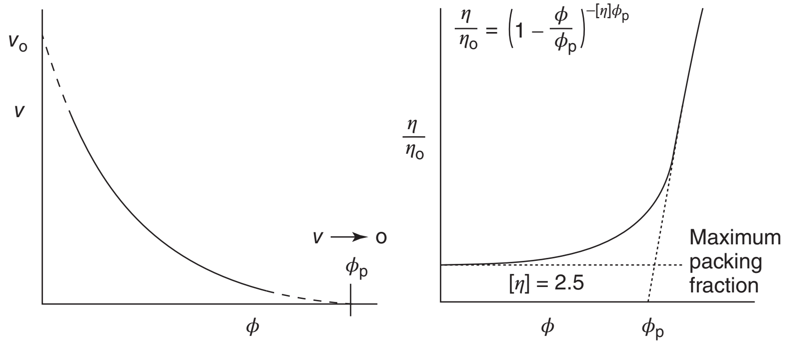

Figure 9.12 Variation of sedimentation velocity and relative viscosity with φ.

It is possible to relate the relative sedimentation rate (v/v_o) to the relative viscosity η/η_o,

$$\left(\frac{v}{v_o}\right) = \alpha \left(\frac{\eta_o}{\eta}\right) \tag{9.46}$$

The relative viscosity is related to the volume fraction φ by the Dougherty–Krieger equation [40] for hard spheres,

$$\frac{\eta}{\eta_o} = \left(1 - \frac{\varphi}{\varphi_p}\right)^{-[\eta]\,\varphi_p} \tag{9.47}$$

where $[\eta]$ is the intrinsic viscosity (2.5 for hard-spheres).

Combining Equations (9.45) and (9.46),

$$\frac{v}{v_o} = \left(1 - \frac{\varphi}{\varphi_p}\right)^{\alpha\,[\eta]\,\varphi_p} = \left(1 - \frac{\varphi}{\varphi_p}\right)^{k\,\varphi_p} \tag{9.48}$$

The above empirical relationship was tested for the sedimentation of polystyrene latex suspensions with $R = 1.55\ \mu m$ in 10^{-3} mol dm^{-3} NaCl; the results are shown in Figure 9.13. In this case the circles are the experimental points, whereas the solid line is calculated using Equation (9.48) with $\varphi_p = 0.58$ and $k = 5.4$ [41].

The sedimentation of particles in non-Newtonian fluids, such as aqueous solutions containing high-molecular-weight compounds such as hydroxyethyl cellulose (HEC) or xanthan gum, is not simple as these non-Newtonian solutions are shear thinning such that the viscosity decreases with increases in shear rate. As discussed above, these solutions show a Newtonian region at low shear rates or shear stresses, which is usually are referred to as the residual or zero shear viscosity, $\eta(0)$. As discussed above, the stress exerted by the particles is very small, in the region of 10^{-3} to 10^{-1} Pa, depending on the particle size and the density of the particles. Clearly, in order to predict sedimentation it is necessary to measure the viscosity at this low stresses, and this is illustrated for solutions of ethyl hydroxy ethyl cellulose (EHEC) in Figure 9.14.

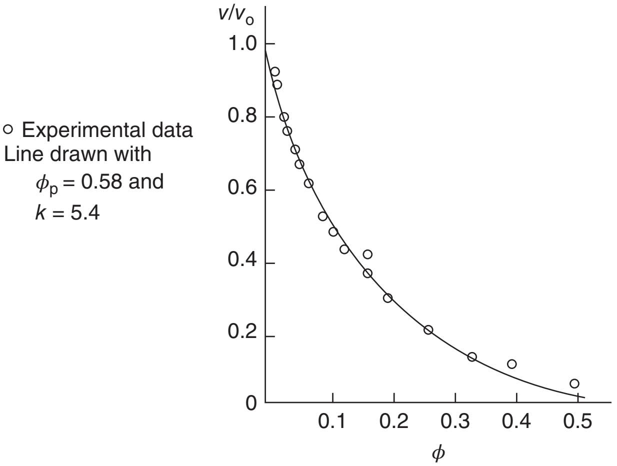

Figure 9.13 Variation of ν/ν_o with φ for polystyrene latex suspensions ($R = 1.55\,\mu m$).

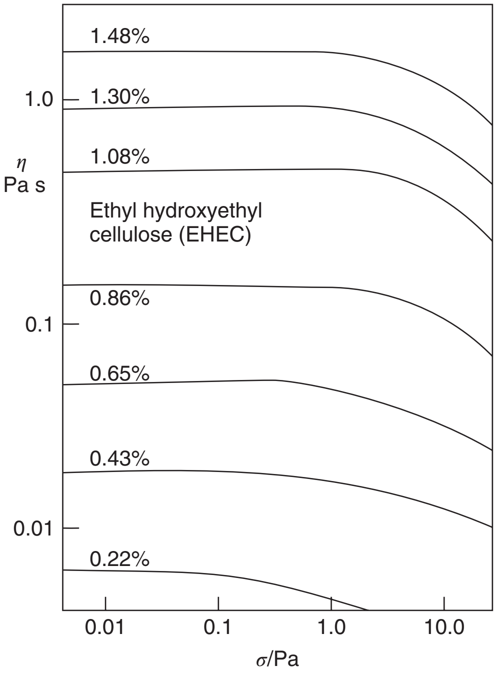

Figure 9.14 Variation of viscosity with applied stress for solutions of EHEC at various concentrations.

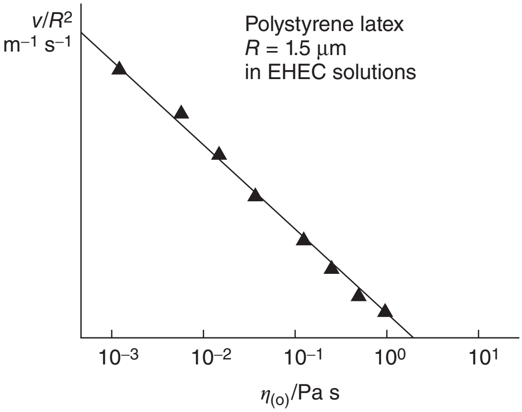

Figure 9.15 Variation of v/R^2 with $\eta(0)$ for polystyrene latex suspensions ($R = 1.55$).

A good correlation was found between the rate of sedimentation for polystyrene latex and $\eta(0)$ [41], as shown in Figure 9.15. Although, for the above suspension, no sedimentation occurred when $\eta(0)$ was greater than 10 Pa·s, the situation with more practical dispersions is more complex due to interactions between the thickener and the particles. Most practical suspensions show some weak flocculation, and the "gel" produced between the particles and thickener may undergo some contraction as a result of the force due to the gravitational force exerted on the whole network. One useful method to describe separation in these concentrated suspensions is to follow the relative sediment volume V_t/V_0 or relative sediment height h_t/h_0 (where the subscripts t and 0 refer to time t and zero time, respectively) with storage time. For good physical stability, the values of V_t/V_0 or h_t/h_0 should be as close as possible to unity (i.e., minimum separation), and this can be achieved by balancing the gravitational force exerted by the gel network with the bulk "elastic" modulus of the suspension. The latter is related to the high-frequency modulus, G'.

9.5.3
Prevention of Sedimentation and Formation of Dilatant Sediments

Several methods may be applied to prevent sedimentation and the formation of clays or cakes in a suspension [42, 43]:

- Balance the density of the disperse phase and the medium: It is clear from Stokes' law that if $\Delta\rho = 0$, then $v_0 = 0$. This method can be applied only when the density of the particles is not much larger than that of the medium (e.g., $\Delta\rho \sim 0.1$). By dissolving an inert substance in the continuous phase density matching may be achieved; however, apart from being limited to particles with a density not much larger than the medium, the method is not very practical as density matching can only occur at one temperature.

- A reduction of particle size: As mentioned above, if R is significantly reduced (to values below 0.1 μm), the Brownian diffusion can overcome the gravitational force and no sedimentation will occur. This is the principle of the formation of nanosuspensions.
- The use of high-molecular-weight thickeners: As discussed above, high-molecular-weight materials such as HEC or xanthan gum, when added above a critical concentration (at which polymer coil overlap occurs), will produce very high viscosity at low stresses or shear rates (usually in excess of several hundred Pa·s), and this will prevent sedimentation of the particles.
- The use of ‘‘inert’’ fine particles: Several fine particulate inorganic material produce ‘‘gels’’ when dispersed in aqueous media; examples include sodium montmorillonite and silica. These particulate materials produce three-dimensional structures in the continuous phase as a result of interparticle interaction. For example, sodium montmorillonite (referred to as ‘‘swellable clays’’) form gels at low electrolyte concentrations by simple double layer interaction. At intermediate electrolyte concentrations, the clay particles produce gels by ‘‘face-to-edge’’ association as the faces of the platelets are negatively charged whereas the edges are positively charged. At sufficient particle concentration, the T-junctions produce a continuous gel network in the continuous phase, preventing sedimentation of the coarse suspension particles. Finely divided silica such as Aerosil 200 (product of Degussa) produce gel structures by simple association (by van der Waals attraction) of the particles into chains and cross chains. When incorporated in the continuous phase of a suspension, these gels prevent sedimentation.
- The use of mixtures of polymers and finely divided particulate solids: By combining thickeners such as HEC or xanthan gum with particulate solids such as sodium montmorillonite, a more robust gel structure can be produced. This gel structure may be less temperature-dependent and could be optimised by controlling the ratio of the polymer and the particles.
- Depletion flocculation: As discussed above, the addition of a free nonadsorbing polymer can produce weak flocculation above a CFV of the free polymer, φ_p. This weak flocculation produces a ‘‘gel’’ structure that reduces sedimentation. As an illustration, results were obtained for a sterically stabilised suspension (using a graft copolymer of PMMA with polyethylene oxide side chains) to which HEC with various molecular weights was added to the suspension. The weak flocculation was studied using oscillatory measurements. Figure 9.16 shows the variation of the complex modulus G^* with A above a critical φ_p value (that depends on the molecular weight of HEC), whereby G^* increases very rapidly with further increases in φ_p. When φ_p reaches an optimum concentration, sedimentation is prevented. This situation is illustrated in Figure 9.17, which shows the sediment volume in 10 cm cylinders as a function φ_p for various volume fractions of the suspension φ_s. At a sufficiently high volume fraction of the suspensions φ_s and high volume fraction of free polymer φ_p, a 100% sediment volume is reached and this is effective in eliminating sedimentation and the formation of dilatant sediments.

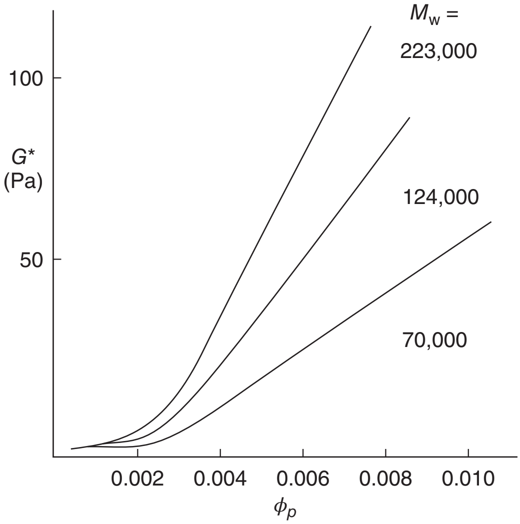

Figure 9.16 Variation of G^* with φ_p for EHEC with various molecular weights.

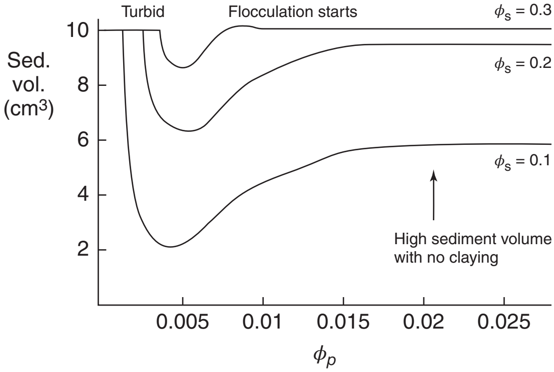

Figure 9.17 Variation of sediment volume with φ_p.

- Use of liquid crystalline phases: Surfactants produce liquid crystalline phases at high concentrations. Three main types of liquid crystals can be identified: hexagonal phase (sometimes referred to as middle phase); cubic phase; and lamellar (neat phase). All of these structures are highly viscous and also show elastic responses. If produced in the continuous phase of suspensions, they can eliminate sedimentation of the particles. These liquid crystalline phase are particularly useful for application in liquid detergents which contain high surfactant concentrations. Their presence reduces sedimentation of the coarse builder particles (phosphates and silicates).

References

1. Parfitt, G.D. (1977) in *Dispersion of Powders in Liquids* (ed.), Applied Science Publishers, London.
2. Tadros, Th. (2012) *Dispersions of Powders in Liquids and Stabilisation of Suspensions*, Wiley-VCH Verlag GmbH, Weinheim.
3. Parfitt, G.D. (1973) Fundamental aspects of dispersions, in *Dispersion of Powders in Liquids* (ed. G.D. Parfitt), Applied Science Publishers, London.
4. Gibbs, J.W. (1906) *Scientific Papers*, Vol. 1, Longman Green, London.
5. Volmer, M. (1939) *Kinetik der Phase Buildung*, Stemkopf, Dresden.
6. Blake, T. (1984) Wetting, in *Surfactants* (ed. T.F. Tadros), Academic Press, London.
7. Rideal, E.K. (1922) *Philos. Mag.*, **44**, 1152.
8. Washburn, E.D. (1921) *Phys. Rev.*, **17**, 273.
9. Lyklema, J. (1987) Structure of the solid/liquid interface and the electrical double layer, in *Solid/Liquid Dispersions* (ed. T.F. Tadros), Academic Press, London.
10. Bijesterbosch, B.H. (1987) Stability of solid/liquid dispersions, in *Solid/Liquid Dispersions* (ed. T.F. Tadros), Academic Press, London.
11. Deryaguin, B.V. and Landau, L. (1941) *Acta Physicochem. USSR*, **14**, 633.
12. Verwey, E.J.W. and Overbeek, J.T.G. (1948) *Theory of Stability of Lyophobic Colloids*, Elsevier, Amsterdam.
13. Hough, D.B. and Randall, H.M. (1983) in *Adsorption from Solution at the Solid/Liquid Interface* (eds G.D. Parfitt and C.H. Rochester), Academic Press, London, p. 247.
14. Fuerstenau, D.W. and Healy, T.W. (1972) in *Adsorptive Bubble Separation Techniques* (ed. R. Lemlich), Academic Press, London, p. 91.
15. Hunter, R.J. (1981) *Zeta Potential in Colloid science; Principles and Applications*, Academic Press, London.
16. von Smoluchowski, M.V. (1914) *Handbuch der Electricitat und des Magnetismus*, Vol. II, Barth, Leipzig.
17. Hückel, E. (1924) *Phys. Z.*, **25**, 204.
18. Henry, D.C. (1948) *Proc. R. Soc., London*, **A133**, 106.
19. Wiersema, P.H., Loeb, A.L., and Overbeek, J.T.G. (1967) *J. Colloid Interface Sci.*, **22**, 78.
20. Ottewill, R.H. and Shaw, J.N. (1972) *J. Electroanal. Interfacial Electrochem.*, **37**, 133.
21. Somasundaran, P. and Goddard, E.D. (1979) *Mod. Aspects Electrochem.*, **13**, 207.
22. Healy, T.W. (1974) *J. Macromol. Sci. Chem.*, **118**, 603.
23. Somasundaran, P. and Hannah, H.S. (1979) in *Improved Oil Recovery by Surfactant and Polymer Flooding* (eds D.O. Shah and R.S. Schechter), Academic Press, London, p. 205.
24. Fuerestenau, D.W. (1971) in *The Chemistry of Biosurfaces* (ed. M.L. Hair), Marcel Dekker, New York, p. 91.
25. Wakamatsu, T. and Fuerstenau, D.W. (1968) *Adv. Chem. Ser.*, **71**, 161.
26. Gaudin, A.M. and Fuertsenau, D.W. (1955) *Trans. AIME*, **202**, 958.
27. Clunie, J.S. and Ingram, B.T. (1983) in *Adsorption from Solution at the solid/Liquid Interface* (eds G.D. Parfitt and C.H. Rochester), Academic Press, London, p. 105.
28. Tadros, Th.F. (1981) Polymer adsorption and dispersion stability, in *The Effect of Polymers on Dispersion Properties* (ed. T.F. Tadros), Academic Press, London.
29. Napper, D.H. (1981) *Polymeric Stabilisation of Colloidal Dispersions*, Academic Press, London.
30. Ottewill, R.H. (1982) in *Concentrated Dispersions*, Chapter 9, Royal Society of Chemistry Publication No. 43 (ed. J.W. Goodwin), RSC, London.
31. Ottewill, R.H. (1983) in *Science and Technology of Polymer Colloids*, Vol. II (eds G.W. Poehlein, R.H. Ottewill, and J.W. Goodwin), Martinus Nishof Publishing, Boston, MA, The Hague, p. 503.
32. Ottewill, R.H. (1987) Properties of concentrated suspensions, in *Solid/Liquid Dispersions* (ed. T.F. Tadros), Academic Press, London.
33. Tadros, Th.F. (1980) *Adv. Colloid Interface Sci.*, **12**, 141.

34. Tadros, Th.F. (1983) in *Science and Technology of Polymer Colloids*, Vol. II (eds G.W. Poehlein and R.H. Ottewill), Martinus Nishof Publishing, Boston, MA, The Hague.
35. Asakura, A. and Oosawa, F. (1954) *J. Chem. Phys.*, **22**, 1235; *J. Polymer Sci.*, **93**, 183 (1958).
36. Ferry, J.D. (1980) *Viscoelastic Properties of Polymers*, John Wiley & Sons, Inc., New York.
37. Whorlow, R.W. (1980) *Rheological Techniques*, Ellis Horwood, Chichester.
38. Goodwin, J.W. and Hughes, R. (2000) *Rheology for Chemists*, Royal Society of Chemistry Publication, Cambridge.
39. Tadros, Th. (2010) *Rheology of Dispersions*, Wiley-VCH Verlag GmbH, Weinheim.
40. Krieger, I.M. (1972) *Adv. Colloid Interface Sci.*, **3**, 111.
41. Buscall, R., Goodwin, J.W., Ottewill, R.H., and Tadros, Th.F. (1982) *J. Colloid Interface Sci.*, **85**, 78.
42. Tadros, Th.F. (1993) *Adv. Colloid and Interface Sci.*, **46**, 1.
43. Tadros, Th.F. (1996) *Adv. Colloid and Interface Sci.*, **68**, 91.

10
Formulation of Liquid/Liquid Dispersions (Emulsions)

10.1
Introduction

Emulsions are a class of disperse systems consisting of two immiscible liquids [1–3], whereby the liquid droplets (the disperse phase) are dispersed in a liquid medium (the continuous phase). Several classes of emulsion may be distinguished, namely Oil-in-Water (O/W), Water-in-Oil (W/O), and Oil-in-Oil (O/O). The latter class may be exemplified by an emulsion consisting of a polar oil (e.g., propylene glycol) dispersed in a nonpolar oil (paraffinic oil), and vice versa. In order to disperse two immiscible liquids a third component is needed, namely the emulsifier. The choice of the emulsifier is crucial in the formation of an emulsion and its long-term stability [1–3].

The various breakdown processes in emulsions are illustrated in Figure 10.1. The physical phenomena involved in each breakdown process are not simple, and analyses of the various surface forces involved are required. In addition, the above processes may take place simultaneously rather than consecutively, and this in turn complicates the analysis. A summary of the methods of prevention of each breakdown process is provided in the following sections.

10.1.1
Creaming and Sedimentation

This process results from external forces, usually gravitational or centrifugal. When such forces exceed the thermal motion of the droplets (Brownian motion), a concentration gradient builds up in the system such that the larger droplets move faster either to the top (if their density is lower than that of the medium) or to the bottom (if their density is larger than that of the medium) of the container. In the limiting cases, the droplets may form a close-packed (random or ordered) array at the top or bottom of the system, with the remainder of the volume occupied by the continuous liquid phase.

Formulation of Disperse Systems: Science and Technology, First Edition. Tharwat F. Tadros.

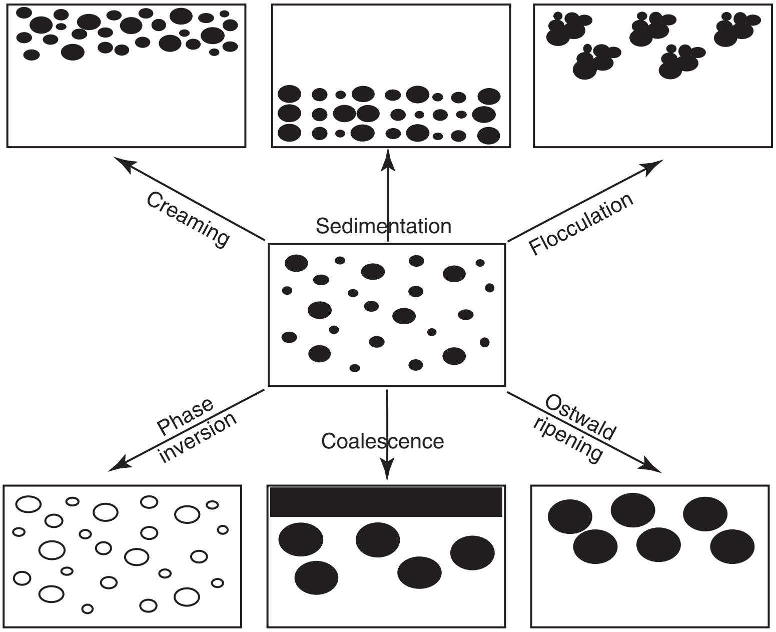

Figure 10.1 Schematic representation of the various breakdown processes in emulsions.

10.1.2
Flocculation

This process refers to aggregation of the droplets (without any change in primary droplet size) into larger units. It is the result of the van der Waals attractions that are universal with all disperse systems. Flocculation occurs when there is insufficient repulsion to keep the droplets apart at distances where the van der Waals attractions are weak. Flocculation may be either ''strong'' or ''weak,'' depending on the magnitude of the attractive energy involved.

10.1.3
Ostwald Ripening (Disproportionation)

This results from the finite solubility of the liquid phases. Liquids which are referred to as being immiscible often have mutual solubilities which are not negligible. In the case of emulsions, which are usually polydisperse, the smaller droplets will have a greater solubility compared to the larger droplets (due to curvature effects). With time, however, the smaller droplets will disappear and their molecules will diffuse to the bulk and become deposited on the larger droplets. With time, the droplet size distribution will shift to a larger value.

10.1.4
Coalescence

This refers to the process of thinning and disruption of the liquid film between the droplets, with the result that two or more droplets fuse into a larger droplet. The limiting case for coalescence is the complete separation of the emulsion into two distinct liquid phases. The driving force for coalescence is the surface or film fluctuations; this results in a close approach of the droplets whereby the van der Waals forces are strong and prevent their separation.

10.1.5
Phase Inversion

This refers to the process when an exchange occurs between the disperse phase and the medium. For example, an O/W emulsion may, with time or change of conditions, invert to a W/O emulsion. In many cases phase inversion passes through a transition state whereby multiple emulsions are produced.

10.2
Industrial Applications of Emulsions

Several industrial systems involve emulsions, of which the following are worthy of mention. Food emulsions include mayonnaise, salad creams, deserts, and beverages, while personal care and cosmetics emulsions include hand creams, lotions, hair sprays, and sunscreens. Agrochemical emulsions include self-emulsifiable oils that produce emulsions on dilution with water, emulsion concentrates with water as the continuous phase, and crop oil sprays. Pharmaceutical emulsions include anaesthetics (O/W emulsions), lipid emulsions, and double and multiple emulsions, while paints may involve emulsions of alkyd resins and latex. Some dry-cleaning formulations may contain water droplets emulsified in the dry cleaning oil that is necessary to remove soils and clays, while bitumen emulsions are prepared stable in their containers but coalesce to form a uniform film of bitumen when applied with road chippings. In the oil industry, many crude oils (e.g., North sea oil) contain water droplets that must be removed by coalescence followed by separation. In oil slick dispersion, the oil spilled from tankers must be emulsified and then separated, while the emulsification of waste oils is an important process for pollution control.

The above-described importance of emulsion in many industries justifies the extensive research that has been carried out to understand the origins of emulsion instability and methods to prevent their breakdown. Unfortunately, fundamental research with emulsions is not easy, as model systems (e.g., with monodisperse droplets) are difficult to produce. In many cases, theories on emulsion stability are not exact and semi-empirical approaches must be used.

10.3
Physical Chemistry of Emulsion Systems

10.3.1
The Interface (Gibbs Dividing Line)

An interface between two bulk phases, for example liquid and air (or liquid/vapour) or two immiscible liquids (oil/water) may be defined provided that a dividing line is introduced (Figure 10.2). The interfacial region is not a layer that is one molecule thick; rather, it is a region with thickness δ and properties which differ from those of the two bulk phases α and β.

Using the Gibbs model, it is possible to obtain a definition of the surface or interfacial tension γ. The surface free energy $\mathrm{d}G^\sigma$ comprises three components: (i) an entropy term $S^\sigma \mathrm{d}T$; (ii) an interfacial energy term $A\mathrm{d}\gamma$, and (iii) a composition term $\Sigma\ n_i \mathrm{d}\mu_i$ (where n_i is the number of moles of component i with chemical potential μ_i). The Gibbs–Duhem equation is,

$$\mathrm{d}G^\sigma = -S^\sigma \mathrm{d}T + A\mathrm{d}\gamma + \sum n_i \mathrm{d}\mu_i \tag{10.1}$$

At constant temperature and composition,

$$\mathrm{d}G^\sigma = A\mathrm{d}\gamma$$

$$\gamma = \left(\frac{\partial G^\sigma}{\partial A}\right)_{T,n_i} \tag{10.2}$$

For a stable interface γ is positive; that is, if the interfacial area increases G^σ increases. Note that γ is energy per unit area (mJ m^{-2}), which is dimensionally equivalent to force per unit length (mN m^{-1}), the unit usually used to define surface or interfacial tension.

For a curved interface the effect of the radius of curvature should be considered. Fortunately, γ for a curved interface is estimated to be very close to that of a planer surface, unless the droplets are very small (<10 nm). Curved interfaces produce some other important physical phenomena which affect emulsion properties, such as the Laplace pressure Δp, which is determined by the radii of curvature of the droplets,

$$\Delta p = \gamma\left(\frac{1}{r_1} + \frac{1}{r_2}\right) \tag{10.3}$$

where r_1 and r_2 are the two principal radii of curvature.

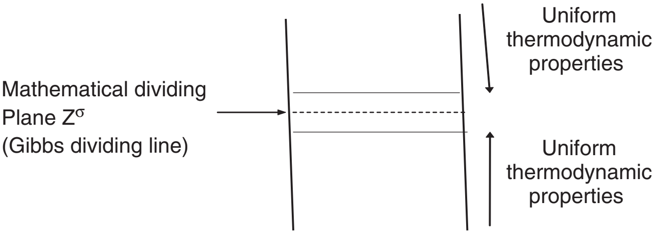

Figure 10.2 The Gibbs dividing line.

For a perfectly spherical droplet $r_1 = r_2 = r$ and

$$\Delta p = \frac{2\gamma}{r} \tag{10.4}$$

For a hydrocarbon droplet with radius 100 nm, and $\gamma = 50\,\mathrm{mN\,m^{-1}}$, Δp is approximately 10^6 Pa (10 atm).

10.3.2
Thermodynamics of Emulsion Formation and Breakdown

Consider a system in which an oil is represented by a large drop 2 of area A_1 immersed in a liquid 2, which is now subdivided into a large number of smaller droplets with total area A_2 ($A_2 \gg A_1$), as shown in Figure 10.3. The interfacial tension γ_{12} is the same for the large and smaller droplets as the latter are generally in the region of 0.1 to few micrometres.

The change in free energy in going from state I to state II is made from two contributions: (i) a surface energy term (that is positive) that is equal to $\Delta A\ \gamma_{12}$ (where $\Delta A = A_2 - A_1$); and (ii) an entropy of dispersions term which is also positive (since the production of a large number of droplets is accompanied by an increase in configurational entropy) which is equal to $T\,\Delta S^{\mathrm{conf}}$.

From the Second law of Thermodynamics,

$$\Delta G^{\mathrm{form}} = \Delta A \gamma_{12} - T \Delta S^{\mathrm{conf}} \tag{10.5}$$

In most cases $\Delta A\gamma_{12} \gg T\,\Delta S^{\mathrm{conf}}$, which means that ΔG^{form} is positive; that is, the formation of emulsions is nonspontaneous and the system is thermodynamically unstable. In the absence of any stabilisation mechanism, the emulsion will break by flocculation, coalescence, Ostwald ripening, or a combination of all these processes. This is illustrated in Figure 10.4, which shows several pathways for emulsion breakdown processes.

In the presence of a stabiliser (surfactant and/or polymer), an energy barrier is created between the droplets, and therefore the reversal from state II to state I becomes noncontinuous as a result of the presence of these energy barriers; this is illustrated in Figure 10.5. In the presence of the above energy barriers, the system becomes kinetically stable.

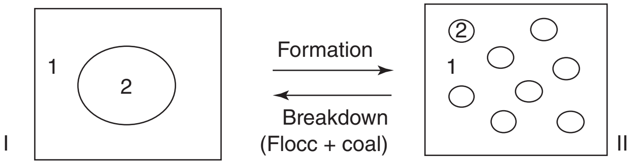

Figure 10.3 Schematic representation of emulsion formation and breakdown.

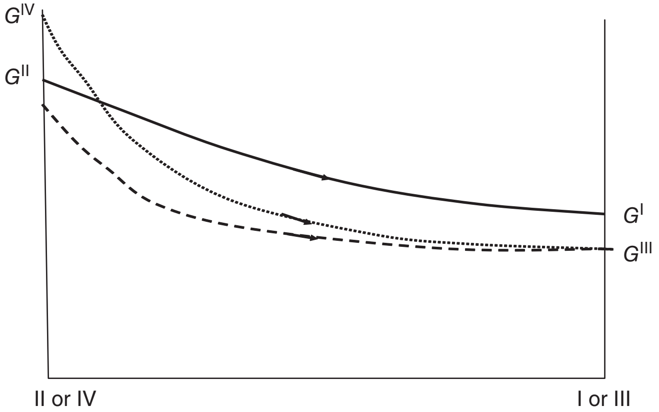

Figure 10.4 Free energy path in emulsion breakdown. The solid line indicates flocculation + coalescence; the dashed line indicates flocculation + coalescence + sedimentation; the dotted line indicates flocculation + coalescence + sedimentation + Ostwald ripening.

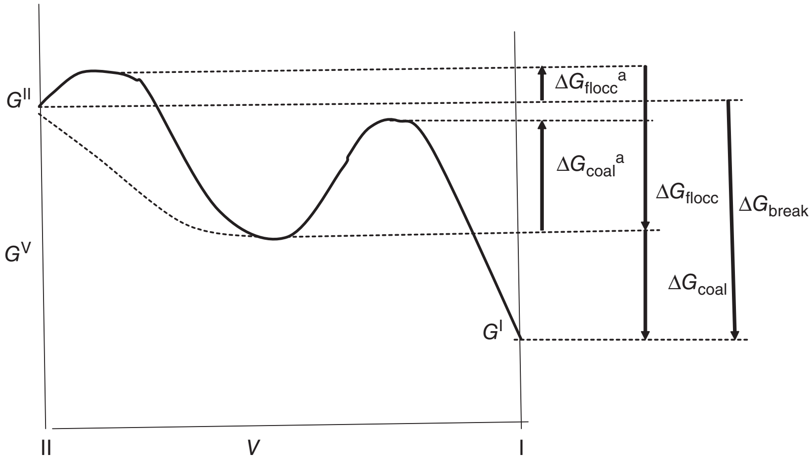

Figure 10.5 Schematic representation of free energy path for breakdown (flocculation and coalescence) for systems containing an energy barrier.

10.3.3
Interaction Energies (Forces) between Emulsion Droplets and Their Combinations

Generally speaking, there are three main interaction energies (forces) between emulsion droplets and these are discussed below.

10.3.3.1 van der Waals Attractions

The van der Waals attractions between atoms or molecules are of three different types: dipole–dipole (Keesom), dipole-induced dipole (Debye), and dispersion (London) interactions. The Keesom and Debye attraction forces are vectors, and although dipole–dipole or dipole-induced dipole attractions are large they tend to cancel due to the different orientations of the dipoles. Thus, the most important are the London dispersion interactions which arise from charge fluctuations. With atoms or molecules consisting of a nucleus and electrons that are continuously rotating around the nucleus, a temporary dipole is created as a result of charge fluctuations. This temporary dipole induces another dipole in the adjacent atom or molecule. The interaction energy between two atoms or molecules G_a is short range and is inversely proportional to the sixth power of the separation distance r between the atoms or molecules,

$$G_a = -\frac{\beta}{r^6} \tag{10.6}$$

where β is the London dispersion constant that is determined by the polarisability of the atom or molecule.

Hamaker [4] suggested that the London dispersion interactions between atoms or molecules in macroscopic bodies (such as emulsion droplets) can be added, resulting in strong van der Waals attractions, particularly at close distances of separation between the droplets. For two droplets with equal radii, R, at a separation distance h, the van der Waals attraction G_{A} is given by the following equation (due to Hamaker):

$$G_{\mathrm{A}} = -\frac{AR}{12h} \tag{10.7}$$

where A is the effective Hamaker constant,

$$A = \left(A_{11}^{1/2} - A_{22}^{1/2}\right)^2 \tag{10.8}$$

where A_{11} and A_{22} are the Hamaker constants of the droplets and dispersion medium, respectively.

The Hamaker constant of any material depends on the number of atoms or molecules per unit volume q and the London dispersion constant β,

$$A = \pi^2 q^2 \beta \tag{10.9}$$

G_{A} increases very rapidly with decrease of h (at close approach), and this is illustrated in Figure 10.6, which shows the van der Waals energy–distance curve for two emulsion droplets with separation distance h.

In the absence of any repulsion, flocculation is very fast and produces large clusters. In order to counteract the van der Waals attractions, it is necessary to create a repulsive force. Two main types of repulsion can be distinguished, depending on the nature of the emulsifier used, namely electrostatic (due to the creation of double layers) and steric (due to the presence of adsorbed surfactant or polymer layers).

10.3.3.2 Electrostatic Repulsion

This can be produced by the adsorption of an ionic surfactant, as illustrated in Figure 10.7, which shows a schematic image of the structure of the double layer according to Gouy–Chapman and Stern [3]. The surface potential ψ_{o} decreases

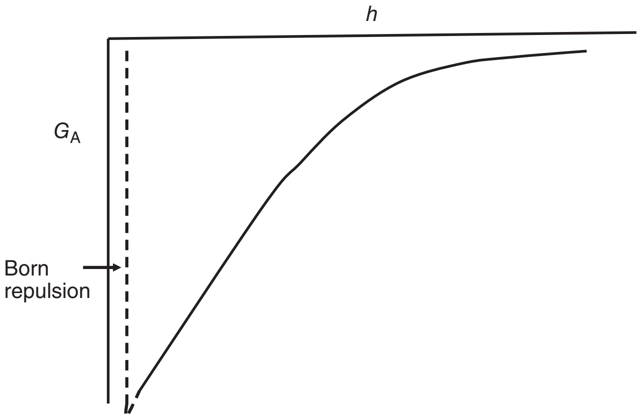

Figure 10.6 Variation of the van der Waals attraction energy with separation distance.

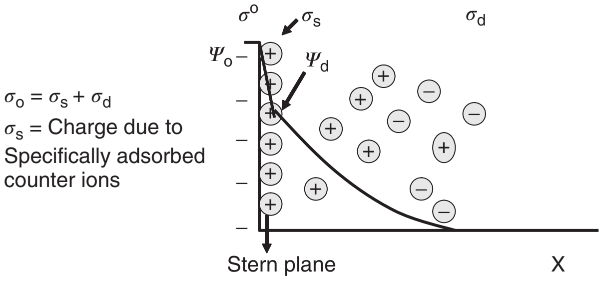

Figure 10.7 Schematic representation of double layers produced by adsorption of an ionic surfactant.

linearly to ψ_d (Stern or zeta-potential) and then exponentially with increase of the distance x. The double layer extension depends on electrolyte concentration and valency (the lower the electrolyte concentration and the lower the valency, the more extended the double layer is).

When charged colloidal particles in a dispersion approach each other such that the double layer begins to overlap (when particle separation becomes less than twice the double layer extension), then repulsion will occur. The individual double layers can no longer develop unrestrictedly, as the limited space does not allow complete potential decay [3]. This is illustrated in Figure 10.8 for two flat plates, and shows clearly shows that when the separation distance h between the emulsion droplets become less than twice the doubly layer extension, the potential at the mid plane between the surfaces is not equal to zero (which would be the case if h were more than twice the double layer extension) plates.

The repulsive interaction G_{el} is given by the following expression,

$$G_{el} = 2\pi R\varepsilon_r\varepsilon_o\psi_o^2 \ln[1 + \exp(-\kappa h)] \tag{10.10}$$

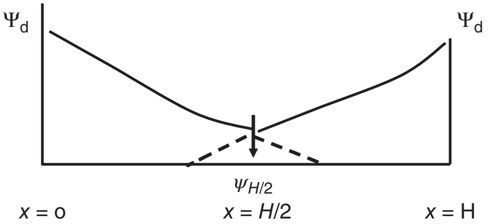

Figure 10.8 Schematic representation of double layer overlap.

where ε_r is the relative permittivity and ε_o is the permittivity of free space, κ is the Debye–Hückel parameter, and $1/\kappa$ is the extension of the double layer (double layer thickness) that is given by the expression,

$$\left(\frac{1}{\kappa}\right) = \left(\frac{\varepsilon_r \varepsilon_o kT}{2n_o Z_i^2 e^2}\right) \tag{10.11}$$

where k is the Boltzmann constant, T is the absolute temperature, n_o is the number of ions per unit volume of each type present in bulk solution, Z_i is the valency of the ions, and e is the electronic charge.

Values of $(1/\kappa)$ at various 1 : 1 electrolyte concentrations are given below:

C (mol dm^{-3})	10^{-5}	10^{-4}	10^{-3}	10^{-2}	10^{-1}
$(1/\kappa)$ (nm)	100	33	10	3.3	1

The double layer extension decreases with increase of electrolyte concentration. This means that the repulsion decreases with increase of electrolyte concentration, as is illustrated in Figure 10.9.

Combination of van der Waals attraction and double layer repulsion results in the well-known theory of colloid stability due to Deryaguin–Landau–Verwey–Overbeek (DLVO) theory [5, 6]:

$$G_T = G_{el} + G_A \tag{10.12}$$

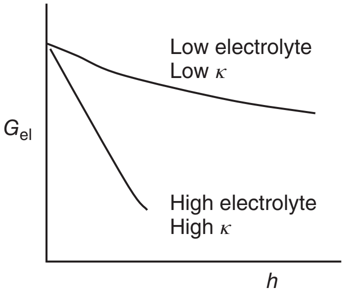

Figure 10.9 Variation of G_{el} with h at low and high electrolyte concentrations.

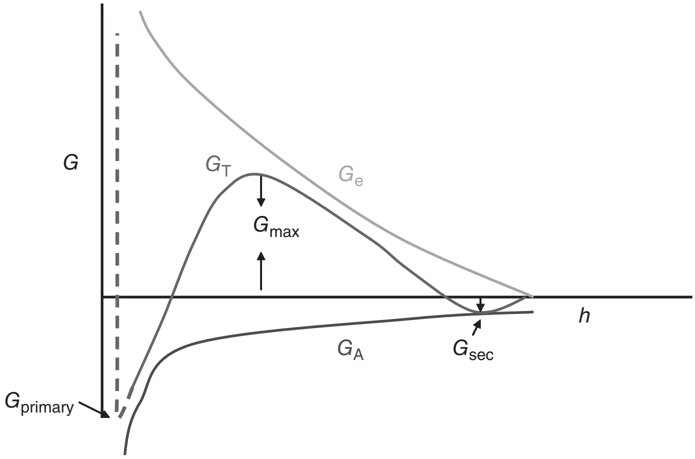

Figure 10.10 Total energy–distance curve according to DLVO theory.

A schematic representation of the force (energy)–distance curve, according to DLVO theory, is shown in Figure 10.10.

The above presentation is for a system at low electrolyte concentration. At large *h*, attraction prevails resulting in a shallow minimum (G_{sec}) on the order of few kT units. At very short *h*, $V_A \gg G_{el}$, resulting in a deep primary minimum (several hundred kT), while at intermediate *h*, $G_{el} > G_A$, resulting in a maximum (energy barrier) whose height depends on ψ_o (or ζ) and electrolyte concentration and valency; the energy maximum is usually kept at >25 kT. The energy maximum prevents close approach of the droplets, and flocculation into the primary minimum is also prevented. The higher the value of ψ_o and the lower the electrolyte concentration and valency, the higher the energy maximum. At intermediate electrolyte concentrations, weak flocculation into the secondary minimum may occur.

10.3.3.3 **Steric Repulsion**

This is produced by using nonionic surfactants or polymers, for example alcohol ethoxylates, or A-B-A block copolymers PEO-PPO-PEO (where PEO refers to polyethylene oxide and PPO refers to polypropylene oxide), as illustrated in Figure 10.11.

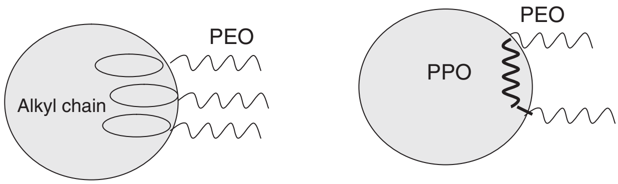

Figure 10.11 Schematic representation of adsorbed layers.

The "thick" hydrophilic chains (PEO in water) produce repulsion as a result of two main effects [7]:

- Unfavourable mixing of the PEO chains: When these are in good solvent conditions (moderate electrolyte and low temperatures), this is referred to as the osmotic or mixing free energy of interaction, that is given by the expression,

$$\frac{G_{\text{mix}}}{kT} = \left(\frac{4\pi}{V_1}\right) \varphi_2^2 N_{\text{av}} \left(\frac{1}{2} - \chi\right) \left(\delta - \frac{h}{2}\right)^2 \left(3R + 2\delta + \frac{h}{2}\right) \tag{10.13}$$

  where V_1 is the molar volume of the solvent, φ_2 is the volume fraction of the polymer chain with a thickness δ, and χ is the Flory–Huggins interaction parameter. When $\chi < 0.5$, G_{mix} is positive and the interaction is repulsive, but when $\chi > 0.5$, G_{mix} is negative and the interaction is attractive. When $\chi = 0.5$ and $G_{\text{mix}} = 0$, this is referred to as the θ-condition.
- Entropic, volume restriction or elastic interaction, G_{el}: This results from the loss in configurational entropy of the chains on significant overlap. Entropy loss is unfavourable and, therefore, G_{el} is always positive. A combination of G_{mix}, G_{el} with G_A gives the total energy of interaction G_T (theory of steric stabilisation),

$$G_T = G_{\text{mix}} + G_{\text{el}} + G_A \tag{10.14}$$

A schematic representation of the variation of G_{mix}, G_{el} and G_A with h is given in Figure 10.12. G_{mix} increases very sharply with a decrease of h when the latter becomes less than 2δ, while G_{el} increases very sharply with a decrease of h when the latter becomes smaller than δ. G_T increases very sharply with a decrease of h when the latter becomes less than 2δ.

Figure 10.12 shows that there is only one minimum (G_{min}) whose depth depends on R, δ and A. At a given droplet size and Hamaker constant, the larger the adsorbed layer thickness, the smaller the depth of the minimum. If G_{min} is made sufficiently small (large δ and small R), then thermodynamic stability may be approaching.

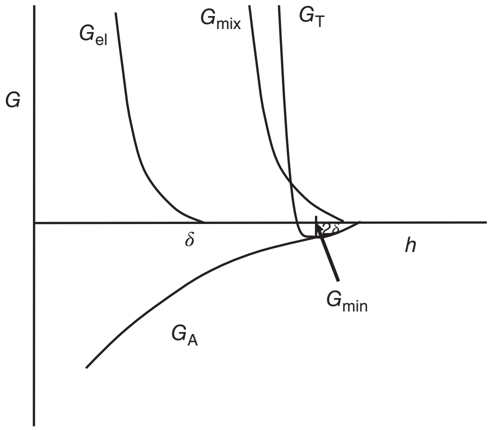

Figure 10.12 Schematic representation of the energy–distance curve for a sterically stabilised emulsion.

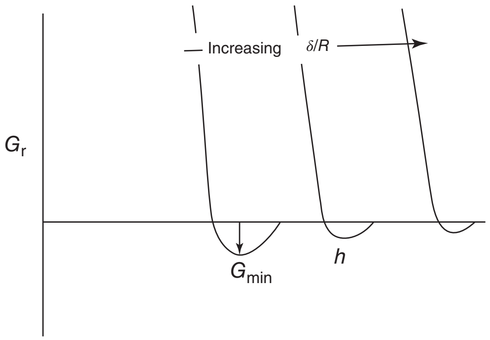

Figure 10.13 Variation of G_T with *h* at various δ/R values.

This is illustrated in Figure 10.13, which shows the energy–distance curves as a function of δ/R. The larger the value of δ/R, the smaller the value of G_{min}. In this case, the system may approach thermodynamic stability, as is the case with nanodispersions.

10.4
Adsorption of Surfactants at the Liquid/Liquid Interface

Surfactants accumulate at interfaces, a process described as adsorption. The simplest interfaces are the air/water (A/W) and oil/water (O/W). The surfactant molecule orients itself at the interface, with the hydrophobic portion orienting towards the hydrophobic phase (air or oil) and the hydrophilic portion orienting at the hydrophilic phase (water); this is shown schematically in Figure 10.14. As a result of adsorption, the surface tension of water is reduced from its value of 72 mN m^{-1} before adsorption to ~30–40 mN m^{-1}, while the interfacial tension for the O/W system decreases from a value of 50 mN m^{-1} (for an alkane oil) before adsorption to a value of 1–10 mN m^{-1}, depending on the nature of the surfactant.

Two approaches can be applied to treat surfactant adsorption at the A/L and L/L interfaces [3]. In the "Gibbs approach" the process is treated as an equilibrium phenomenon, and it is possible to apply the Second Law of Thermodynamics. Alternately, in the "Equation of state approach" the surfactant film is treated as a two-dimensional layer with a surface pressure π. The Gibbs approach allows the

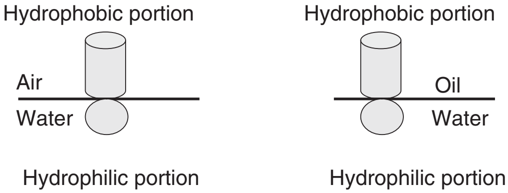

Figure 10.14 Schematic representation of orientation of surfactant molecules.

surfactant adsorption to be determined from surface tension measurements, while the equation of state approach allows the surfactant orientation at the interface to be studied. Although both approaches were described in detail in Chapter 5, at this point only the Gibbs approach will be summarised here, as it provides a relationship between the reduction in interfacial tension on increasing the surfactant adsorption ($\mathrm{d}\gamma/\mathrm{dlog}C_2$) with the amount of surfactant adsorbed at the interface Γ_2 ($\mathrm{mol\,m^{-2}}$):

$$\frac{\mathrm{d}\gamma}{\mathrm{d}\ln C_2} = -\Gamma_2 RT \tag{10.15}$$

where Γ_2 can be calculated from the linear portion of the γ–log C curve just before the critical micelle concentration (cmc):

$$\text{slope} = -\frac{\mathrm{d}\gamma}{\mathrm{d}\log C_2} = -2.303\Gamma_2 RT \tag{10.16}$$

From Γ_2 the area per molecule of surfactant (or ion) can be calculated,

$$\text{Area/molecule} = \frac{1}{\Gamma_2 N_{\mathrm{Av}}}(\mathrm{m}^2) = \frac{10^{18}}{\Gamma_2 N_{\mathrm{Av}}}(\mathrm{nm}^2) \tag{10.17}$$

where N_{Av} is the Avogadro's constant, equal to 6.023×10^{23}.

The area per surfactant ion or molecule provides information on the orientation of the ion or molecule at the interface. The area depends on whether the molecules lie flat or vertical at the interface, and also on the length of the alkyl chain length (if the molecules lie flat) or the cross-sectional area of the head group (if the molecules lie vertical). For example, for an ionic surfactant such as sodium dodecyl sulphate (SDS), the area per molecule depends on the orientation. If the molecule lies flat, the area is determined by the area occupied by the alky chain and that by the sulphate head group. In this case, the area per molecule increases with increases in the alkyl chain length and will be in the range 1–2 nm^2. In contrast, for vertical orientation the area per molecule is determined by the cross-sectional area of the sulphate group, which is ~0.4 nm^2 and virtually independent of the alkyl chain length. The addition of electrolytes screens the charge on the head group, and hence the area per molecule is decreased. For nonionic surfactants such as alcohol ethoxylates the area per molecule for flat orientation is determined by the length of the alkyl chain and the number of ethylene oxide (EO) units. For vertical orientation, the area per molecule is determined by the cross-sectional area of the PEO chain, and this increases with increase in line with the number of EO units.

At concentrations just before the break point, the slope of the γ–log C curve is constant,

$$\left(\frac{\partial\gamma}{\partial\log C_2}\right) = \text{constant} \tag{10.18}$$

This indicates that saturation of the interface occurs just below the cmc.

Above the break point ($C >$ cmc), the slope is zero,

$$\left(\frac{\partial\gamma}{\partial\log C_2}\right) = 0 \tag{10.19}$$

or

$$\gamma = \text{constant } x \log C_2 \tag{10.20}$$

Since γ remains constant above the cmc, then C_2 or a_2 of the monomer must remain constant.

The addition of surfactant molecules above the cmc must result in an association to form micelles which have low activity, and hence a_2 will remain virtually constant.

The hydrophilic head group of the surfactant molecule can also affect its adsorption. Such head groups can be unionised, for example alcohol or PEO (weakly ionised such as COOH, or strongly ionised such as sulphates $-O-SO_3^-$, sulphonates $-SO_3^-$ or ammonium salts $-N^+(CH_3)_3$-). The adsorption of the different surfactants at the A/W and O/W interfaces depends on the nature of the head group. With nonionic surfactants, repulsion between the head groups is less than with ionic head groups and adsorption occurs from dilute solutions; in this case the cmc is low, typically 10^{-5} to 10^{-4} mol dm^{-3}. Nonionic surfactants with medium PEO form closely packed layers at $C <$ cmc, when adsorption will be slightly affected by the moderate addition of electrolytes or by a change in the pH. Nonionic surfactant adsorption is relatively simple and can be described using the Gibbs adsorption equation.

With ionic surfactants, adsorption is more complicated depending on the repulsion between the head groups and the addition of indifferent electrolytes. The Gibbs adsorption equation must be solved to take into account the adsorption of the counterions and any indifferent electrolyte ions.

For a strong surfactant electrolyte such as $R-O-SO_3^-\ Na^+$ ($R^-\ Na^+$):

$$\Gamma_2 = -\frac{1}{2RT}\left(\frac{\partial \gamma}{\partial \ln a\pm}\right) \tag{10.21}$$

The factor of 2 in Equation (10.21) arises because both surfactant ion and counterion must be adsorbed to maintain neutrality. ($\partial\gamma/\mathrm{dln}\ a\pm$) is twice as large for an unionised surfactant molecule.

For a nonadsorbed electrolyte such as NaCl, any increase in $Na^+\ R^-$ concentration produces a negligible increase in Na^+ concentration ($d\mu_{Na}{}^+$ is negligible and $d\mu_{Cl}{}^-$ is also negligible.

$$\Gamma_2 = -\frac{1}{RT}\left(\frac{\partial \gamma}{\partial \ln C_{NaR}}\right) \tag{10.22}$$

which is identical to the case of nonionics.

The above analysis shows that many ionic surfactants may behave like nonionics in the presence of a large concentration of an indifferent electrolyte such as NaCl.

10.4.1
Mechanism of Emulsification

As mentioned previously, the requirements to prepare an emulsion include oil, water, surfactant, and energy, and this can be considered from the energy required to expand the interface, $\Delta A\gamma$ (where ΔA is the increase in interfacial area when the bulk oil with area A_1 produces a large number of droplets with area A_2; $A_2 \gg A_1$, and γ is the interfacial tension). As γ is positive, the energy needed to expand the interface is large and positive, and cannot be compensated by the small entropy of dispersion $T\Delta S$ (which is also positive); moreover, the total free energy of formation of an emulsion, ΔG, given by Equation (10.5), is positive. Thus, emulsion formation is nonspontaneous and energy is required to produce the droplets.

The formation of large droplets (a few micrometres in size), as is the case for macroemulsions, is fairly easy and high-speed stirrers such as the UltraTurrax or Silverson mixer are sufficient to produce such emulsions. In contrast, the formation of small drops (submicron, as is the case with nanoemulsions) is difficult and this requires a large amount of surfactant and/or energy. The high energy required for formation of nanoemulsions can be understood from a consideration of the Laplace pressure Δp (the difference in pressure between the inside and outside of the droplet), as given by Equations (10.3) and (10.4).

In order to break up a drop into smaller units it must be strongly deformed, and this deformation increases Δp. Surfactants play major roles in the formation of emulsions [8]; by lowering the interfacial tension Δp is reduced, and hence the stress needed to break up a drop is reduced. Surfactants also prevent the coalescence of newly formed drops.

To describe emulsion formation two main factors must be considered, namely hydrodynamics and interfacial science. In hydrodynamics, consideration must be given to the type of flow, whether laminar or turbulent, and this depends on the Reynolds number (as will be discussed later).

To assess emulsion formation, the normal approach is to measures the droplet size distribution using, for example laser diffraction techniques. A useful average diameter d is,

$$d_{nm} = \left(\frac{S_m}{S_n}\right)^{1/(n-m)} \tag{10.23}$$

In most cases d_{32} (the volume/surface average or Sauter mean) is used, while the width of the size distribution can be given as the variation coefficient c_m . The latter is the standard deviation of the distribution weighted with d_m divided by the corresponding average d. Generally C_2 will be used which corresponds to $d_{32.}$

An alternative way to describe the emulsion quality is to use the specific surface area A (the surface area of all emulsion droplets per unit volume of emulsion),

$$A = \pi s^2 = \frac{6\phi}{d_{32}} \tag{10.24}$$

10.4.2
Methods of Emulsification

Several procedures may be applied for emulsion preparation, ranging from simple pipe flow (low agitation energy, L), static mixers and general stirrers (low to medium energy, L-M), high-speed mixers such as the UltraTurrax (M), colloid mills and high-pressure homogenisers (high energy, H), ultrasound generators (M-H). In addition, the method of preparation can be either continuous or batch-wise: typically, pipe flow and static mixers are continuous; stirrers and UltraTurrax are batchwise and continuous; colloid mill and high-pressure homogenisers are continuous; and ultrasound is both batchwise and continuous.

In all methods there is liquid flow with unbounded and strongly confined flow. In the unbounded flow, any droplets are surrounded by a large amount of flowing liquid (the confining walls of the apparatus are far away from most droplets), while the forces can be either frictional (mostly viscous) or inertial. Viscous forces cause shear stresses to act on the interface between the droplets and the continuous phase (primarily in the direction of the interface). The shear stresses can be generated by either laminar flow (LV) or turbulent flow (TV); this depends on the Reynolds number R_e,

$$R_e = \frac{vl\rho}{\eta} \tag{10.25}$$

where ν is the linear liquid velocity, ρ is the liquid density, η is its viscosity, and l is a characteristic length that is given by the diameter of flow through a cylindrical tube and by twice the slit width in a narrow slit.

For laminar flow $R_e < \sim 1000$, whereas for turbulent flow $R_e > \sim 2000$. Thus, whether the regime is linear or turbulent depends on the scale of the apparatus, the flow rate, and the liquid viscosity [9–12].

If the turbulent eddies are much larger than the droplets they exert shear stresses on the droplets; however, if the turbulent eddies are much smaller than the droplets then inertial forces will cause disruption (turbulent/inertial).

In bounded flow other relationships hold; for example, if the smallest dimension of the part of the apparatus in which the droplets are disrupted (e.g., a slit) is comparable to the droplet size, the flow will always be laminar. A different regime prevails, however, if the droplets are injected directly through a narrow capillary into the continuous phase (injection regime), namely membrane emulsification.

Within each regime, one essential variable is the intensity of the forces which are acting; the viscous stress during laminar flow σ_{viscous} is given by,

$$\sigma_{\text{viscous}} = \eta G \tag{10.26}$$

where G is the velocity gradient.

The intensity in turbulent flow is expressed by the power density ε (the amount of energy dissipated per unit volume per unit time); for laminar flow,

$$\varepsilon = \eta G^2 \tag{10.27}$$

The most important regimes are laminar/viscous (LV), turbulent/viscous (TV), and turbulent/inertial (TI). With water as the continuous phase the regime is always TI, but when the viscosity of the continuous phase is higher ($\eta_C = 0.1$ Pa·s) the regime will be TV. For a still higher viscosity or a small apparatus (small l), the regime will be LV, and for very small apparatus (as is the case with most laboratory homogenisers) the regime is nearly always LV.

For the above regimes, a semi-quantitative theory is available that can provide the time scale and magnitude of the local stress σ_{ext}, the droplet diameter d, the time scale of droplet deformation τ_{def}, the time scale of surfactant adsorption, τ_{ads}, and the mutual collision of droplets.

An important parameter that describes droplet deformation is the Weber number $\mathrm{W_e}$ (which gives the ratio of the external stress over the Laplace pressure),

$$\mathrm{W}_e = \frac{G\eta_C R}{2\gamma} \tag{10.28}$$

The viscosity of the oil plays an important role in the break-up of droplets; the higher the viscosity, the longer it will take to deform a drop. The deformation time τ_{def} is given by the ratio of oil viscosity to the external stress acting on the drop,

$$\tau_{\mathrm{def}} = \frac{\eta_D}{\sigma_{\mathrm{ext}}} \tag{10.29}$$

The viscosity of the continuous phase η_{C} plays an important role in some regimes; for the TI regime η_{C} has no effect on droplets size, but for the TV regime a larger value of ηC leads to smaller droplets, and for LV the effect is even stronger.

10.4.3
Role of Surfactants in Emulsion Formation

Surfactants lower the interfacial tension γ, which in turn causes a reduction in droplet size; typically, the latter will decrease with a decrease in γ. For laminar flow, the droplet diameter is proportional to γ, but for a TI regime the droplet diameter is proportional to $\gamma^{3/5}$.

The effect of reducing γ on droplet size is illustrated in Figure 10.15, which shows a plot of the droplet surface area A and mean drop size d_{32} as a function of the surfactant concentration m for various systems.

The amount of surfactant required to produce the smallest drop size will depend on its activity a (concentration) in the bulk which in turn determines the reduction in γ, as given by the Gibbs adsorption equation as discussed before,

$$-\mathrm{d}\gamma = RT\Gamma \mathrm{d}\ln a \tag{10.30}$$

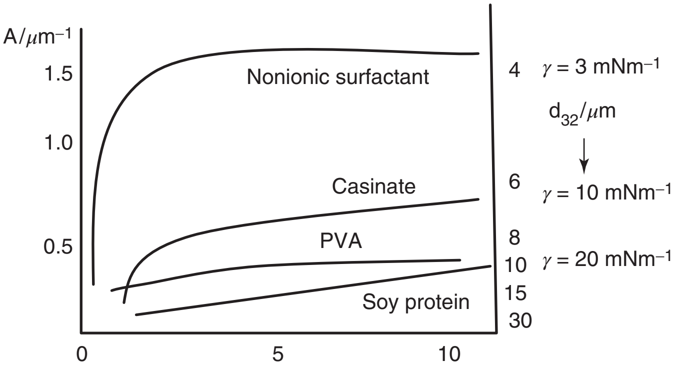

Figure 10.15 Variation of A and d_{32} with m for various surfactant systems.

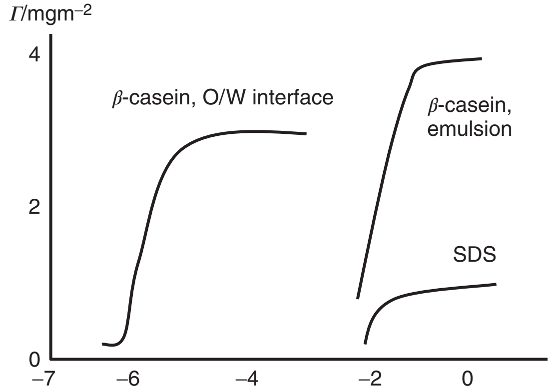

Figure 10.16 Variation of Γ (mg m^{-2}) with log C_{eq} (wt%). The oils are β-casein (O/W interface), toluene, β-casein (emulsions), soybean, SDS benzene.

where R is the gas constant, T is the absolute temperature, and Γ is the surface excess (number of moles adsorbed per unit area of the interface).

Γ increases with increases in surfactant concentration, and eventually reaches a plateau value (saturation adsorption); this is illustrated in Figure 10.16 for various emulsifiers.

The value of γ obtained depends on the nature of the oil and surfactant used; small molecules such as nonionic surfactants lower γ more than polymeric surfactants such as PVA.

Another important role of the surfactant is its effect on the interfacial dilational modulus ε,

$$\varepsilon = \frac{d\gamma}{d\ln A} \tag{10.31}$$

During emulsification an increase in the interfacial area A takes place and this causes a reduction in Γ. The equilibrium is restored by the adsorption of surfactant from the bulk, but this takes time (shorter times occur at higher surfactant activity). Thus, ε is small whether a is small or large. Because of the lack or slowness of equilibrium with polymeric surfactants, ε will not be the same for expansion and compression of the interface.

In practice, surfactant mixtures are used that may have pronounced effects on γ and ε. Some specific surfactant mixtures produce lower γ-values than either of the two individual components, while the presence of more than one surfactant molecule at the interface tends to increase ε at high surfactant concentrations. The various components vary in surface activity; those with the lowest γ tend to predominate at the interface, although if these are present at low concentrations it may take a long time before the lowest value is reached. Polymer–surfactant mixtures may also show some synergetic surface activity.

10.4.4
Role of Surfactants in Droplet Deformation

Apart from their effect on reducing γ, surfactants play major roles in the deformation and break-up of droplets, and this is summarised as follows. Surfactants allow the existence of interfacial tension gradients which is crucial for the formation of stable droplets [8]. In the absence of surfactants (clean interface), the interface cannot withstand a tangential stress, and the liquid motion will be continuous (Figure 10.17a).

If a liquid flows along the interface with surfactants, the latter will be swept downstream, causing an interfacial tension gradient (Figure 10.17b). Thus, a balance of forces will be established,

$$\eta\left[\frac{dV_x}{dy}\right]_{y=0} = -\frac{dy}{dx} \tag{10.32}$$

If the γ-gradient can become large enough, it will arrest the interface. If the surfactant is applied at one site of the interface, a γ-gradient is formed that will cause the interface to move roughly at a velocity given by,

$$v = 1.2[\eta\rho z]^{-1/3}|\Delta\gamma|^{2/3} \tag{10.33}$$

The interface will then drag some of the bordering liquid with it (Figure 10.17c).

Interfacial tension gradients are very important in stabilising the thin liquid film that is located between the droplets and which is very important at the start of emulsification (films of the continuous phase may be drawn through the disperse phase and collision is very large). The magnitude of the γ-gradients and of the Marangoni effect depends on the surface dilational modulus ε, which for a plane

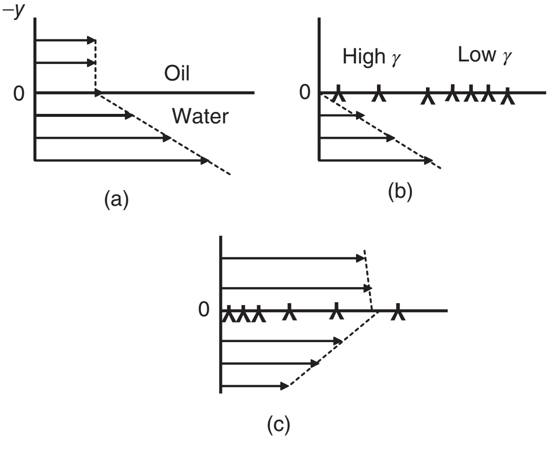

Figure 10.17 Interfacial tension gradients and flow near an oil/water interface. (a) No surfactant; (b) Velocity gradient causes an interfacial tension gradient; (c) Interfacial tension gradient causes flow (Marangoni effect).

interface with one surfactant-containing phase, is given by the expression,

$$\varepsilon = \frac{-\mathrm{d}\gamma/\mathrm{d}\ln\Gamma}{(1+2\xi+2\xi^2)^{1/2}} \tag{10.34}$$

$$\xi = \frac{\mathrm{d}m_C}{\mathrm{d}\Gamma}\left(\frac{D}{2\omega}\right)^{1/2} \tag{10.35}$$

$$\omega = \frac{\mathrm{d}\ln A}{\mathrm{d}t} \tag{10.36}$$

where D is the diffusion coefficient of the surfactant and ω represents a time scale (the time needed to double the surface area) that is roughly equal to τ_{def}.

During emulsification, ε is dominated by the magnitude of the denominator in Equation (10.34) because ζ remains small. The value of $\mathrm{d}m_C/\mathrm{d}\Gamma$ tends to go to very high values when Γ reaches its plateau value; ε goes to a maximum when m_C is increased.

For conditions that prevail during emulsification, ε increases with m_C, and is given by the relationship,

$$\varepsilon = \frac{\mathrm{d}\pi}{\mathrm{d}\ln\Gamma} \tag{10.37}$$

where π is the surface pressure ($\pi = \gamma_o - \gamma$). Figure 10.18 shows the variation of π with ln Γ; ε is given by the slope of the line.

Typically, SDS shows a much higher ε-value when compared with β-casein and lysosome, mainly because the value of Γ is higher for SDS. The two proteins show a difference in their ε-values which may be attributed to the conformational change that occurs upon adsorption.

The presence of a surfactant means that, during emulsification, the interfacial tension need not to be the same everywhere (see Figure 10.17). This has two consequences: (i) the equilibrium shape of the drop is affected; and (ii) any

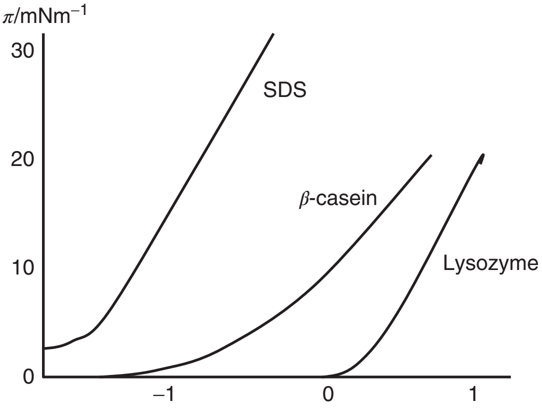

Figure 10.18 π versus ln Γ for various emulsifiers.

γ-gradient formed will slow down the motion of the liquid inside the drop (this diminishes the amount of energy needed to deform and break-up the drop).

Another important role of the emulsifier is to prevent coalescence during emulsification. This is certainly not due to the strong repulsion between the droplets, as the pressure at which two drops are pressed together is much greater than the repulsive stresses. Rather, the counteracting stress must be due to the formation of γ-gradients. When two drops are pushed together, liquid will flow out from the thin layer between them, and the flow will induce a γ-gradient [13–17], as shown in Figure 10.17c This produces a counteracting stress given by,

$$\tau_{\Delta\gamma} \approx \frac{2|\Delta\gamma|}{(1/2)d} \tag{10.38}$$

The factor 2 follows from the fact that two interfaces are involved. Taking a value of $\Delta\gamma = 10\,\mathrm{mN\,m^{-1}}$, the stress amounts to 40 kPa (which is of the same order of magnitude as the external stress).

Closely related to the above mechanism is the Gibbs–Marangoni effect [13–17], which is represented schematically in Figure 10.19. The depletion of surfactant in the thin film between approaching drops results in a γ-gradient without liquid flow being involved. This results in an inward flow of liquid that tends to drive the drops apart.

The Gibbs–Marangoni effect also explains the Bancroft rule, which states that the phase in which the surfactant is most soluble forms the continuous phase [8]. If the surfactant is in the droplets, a γ-gradient cannot develop and the drops would be prone to coalescence. Thus, surfactants with HLB > 7 tend to form O/W emulsions, while those with HLB < 7 tend to form W/O emulsions.

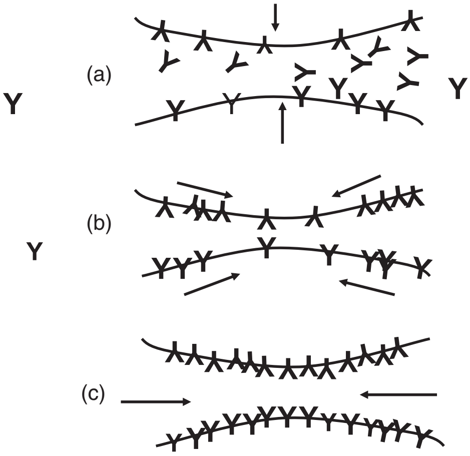

Figure 10.19 Schematic representation of the Gibbs–Marangoni effect for two approaching drops.

The Gibbs–Marangoni effect also explains the difference between surfactants and polymers for emulsification. When compared to surfactants, polymers produce larger drops and also give a smaller value of ε at low concentrations (Figure 10.19).

Among various other factors that should be considered for emulsification must be included the disperse phase volume fraction ϕ. An increase in ϕ leads to increase in droplet collision and hence coalescence during emulsification. Moreover, with an increase in ϕ the viscosity of the emulsion increases, and this may change the flow from being turbulent to being laminar (LV regime).

The presence of many particles results in a local increase in velocity gradients, which means that G is increased. In turbulent flow, an increase in ϕ will induce turbulence depression and this will result in larger droplets. Turbulence depression caused by added polymers tend to remove the small eddies and result in the formation of larger droplets.

If the mass ratio of the surfactant to the continuous phase is kept constant, an increase in ϕ will result in a decrease in surfactant concentration and hence an increase in γ_{eq}, resulting in larger droplets. However, if the mass ratio of the surfactant to the disperse phase is kept constant, the above changes will be reversed.

At this point, general conclusions cannot be drawn since several of the above-mentioned mechanisms may come into play. Experiments using high-pressure homogenisation at various φ-values and constant initial m_C (with TI regime changing to TV at higher ϕ) showed that, with increasing ϕ (>0.1), the resulting droplet diameter was increased and the dependence on energy consumption became weaker. Figure 10.20 shows a comparison of the average droplet diameter versus power consumption, using different emulsifying machines. The data show

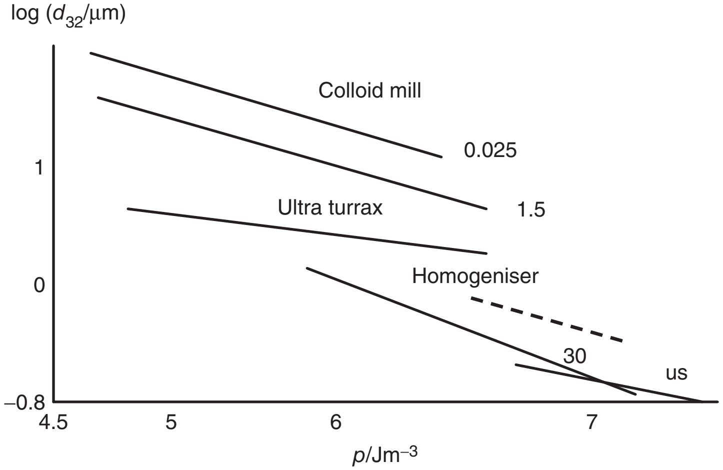

Figure 10.20 Average droplet diameters obtained in various emulsifying machines as a function of energy consumption (p). Numbers near the curves denote the viscosity ratio (λ). Results for the homogeniser are for $\phi = 0.04$ (solid line) and $\phi = 0.3$ (broken line). us, ultrasonic generator.

that the smallest droplet diameters were obtained when using high-pressure homogenisation.

10.5
Selection of Emulsifiers

10.5.1
The Hydrophilic–Lipophilic Balance (HLB) Concept

The selection of different surfactants in the preparation of either O/W or W/O emulsions is often still made on an empirical basis. A semi-empirical scale for selecting surfactants, the hydrophilic–lipophilic balance (HLB number) was developed by Griffin [18]. This scale is based on the relative percentage of hydrophilic to lipophilic (hydrophobic) groups in the surfactant molecule(s). For an O/W emulsion droplet the hydrophobic chain resides in the oil phase, whereas the hydrophilic head group resides in the aqueous phase. In contrast, for a W/O emulsion droplet the hydrophilic group(s) reside in the water droplet while the lipophilic groups reside in the hydrocarbon phase.

A guide to the selection of surfactants for particular applications is provided in Table 10.1. As the HLB number depends on the nature of the oil, the HLB numbers required to emulsify various oils are listed in Table 10.2, as an illustration.

The relative importance of the hydrophilic and lipophilic groups was first recognised when using mixtures of surfactants containing varying proportions of

Table 10.1 Summary of HLB ranges and their applications.

HLB range	Application
3–6	W/O emulsifier
7–9	Wetting agent
8–18	O/W emulsifier
13–15	Detergent
15–18	Solubiliser

Table 10.2 Required HLB numbers to emulsify various oils.

Oil	W/O emulsion	O/W emulsion
Paraffin oil	4	10
Beeswax	5	9
Linolin, anhydrous	8	12
Cyclohexane	—	15
Toluene	—	15

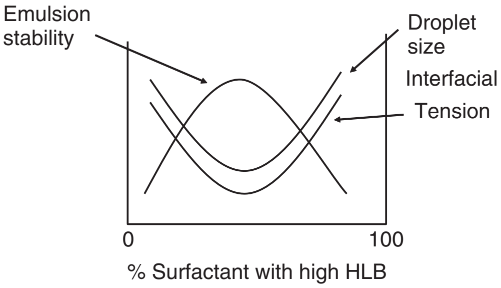

Figure 10.21 Variation of emulsion stability, droplet size and interfacial tension with % surfactant with high HLB number.

low and high HLB numbers. The efficiency of any combination (as judged by phase separation) was found to pass a maximum when the blend contained a particular proportion of the surfactant with the higher HLB number. This is illustrated in Figure 10.21, which shows the variation of emulsion stability, droplet size and interfacial tension with percentage surfactant with a high HLB number.

The average HLB number may be calculated from additivity,

$$\text{HLB} = x_1\text{HLB}_1 + x_2\text{HLB}_2 \tag{10.39}$$

where x_1 and x_2 are the weight fractions of the two surfactants with HLB_1 and HLB_2.

Griffin developed simple equations for calculating the HLB number of relatively simple nonionic surfactants. For example, for a polyhydroxy fatty acid ester:

$$\text{HLB} = 20\left(1 - \frac{S}{A}\right) \tag{10.40}$$

where S is the saponification number of the ester and A is the acid number. For a glyceryl monostearate, $S = 161$ and $A = 198$; the HLB is 3.8 (suitable for W/O emulsion).

For a simple alcohol ethoxylate, the HLB number can be calculated from the weight percentage of EO (E) and polyhydric alcohol (P):

$$\text{HLB} = \frac{\text{E} + \text{P}}{5} \tag{10.41}$$

If the surfactant contains PEO as the only hydrophilic group, the contribution from one OH group is neglected,

$$\text{HLB} = \frac{\text{E}}{5} \tag{10.42}$$

For a nonionic surfactant $C_{12}H_{25}$–O–$(CH_2$–CH_2–$O)_6$, the HLB is 12 (suitable for O/W emulsion).

The above simple equations cannot be used for surfactants containing propylene oxide or butylene oxide; neither can they be applied for ionic surfactants. Davies [19, 20] devised a method for calculating the HLB number for surfactants from their chemical formulae, using empirically determined group numbers that are assigned to various component groups. A summary of the group numbers for some surfactants is provided in Table 10.3.

Table 10.3 HLB group numbers.

	Group number
Hydrophilic	
$-SO_4Na^+$	38.7
$-COO^-$	21.2
–COONa	19.1
N(tertiary amine)	9.4
Ester (sorbitan ring)	6.8
–O–	1.3
CH–(sorbitan ring)	0.5
Lipophilic	
$(-CH-)$, $(-CH_2-)$, CH_3	0.475
Derived	
$-CH_2-CH_2-O$	0.33
$-CH_2-CH_2-CH_2-O-$	−0.15

The HLB is given by the following empirical equation:

$$\text{HLB} = 7 + \sum(\text{hydrophilic group Nos}) - \sum(\text{lipohilic group Nos}) \qquad (10.43)$$

Davies has shown that the agreement between HLB numbers calculated from the above equation and those determined experimentally is quite satisfactory.

Various other procedures were developed to obtain a rough estimate of the HLB number. Griffin found good correlation between the cloud points of 5% solutions of various ethoxylated surfactants and their HLB numbers. Davies [19, 20] also attempted to relate the HLB values to the selective coalescence rates of emulsions. Such correlations were not realised, however, as it was found that the emulsion stability – and even its type – depend to a large extent on the method of dispersing the oil into the water, and vice versa. At best, the HLB number can only be used as a guide for selecting the optimum compositions of emulsifying agents.

Any pair of emulsifying agents that fall at opposite ends of the HLB scale – for example, Tween 80 (sorbitan monooleate with 20 mol EO, HLB = 15) and Span 80 (sorbitan monooleate, HLB = 5) – can be taken and used in various proportions to cover a wide range of HLB numbers. The emulsions should be prepared in the same fashion, with a few percent of the emulsifying blend. The stability of the emulsions can then be assessed at each HLB number, either from the rate of coalescence or qualitatively by measuring the rate of oil separation. In this way it should be possible to determine the optimum HLB number for a given oil. Subsequently, having found the most effective HLB value, various other surfactant pairs can be compared at this HLB value to identify the most effective pair.

10.5.2
The Phase Inversion Temperature (PIT) Concept

Shinoda and coworkers [21, 22] found that many O/W emulsions stabilised with nonionic surfactants undergo a process of inversion at a critical temperature, termed the phase inversion temperature (PIT). The PIT can be determined by following the emulsion conductivity (a small amount of electrolyte is added to increase the sensitivity) as a function of temperature. The conductivity of the O/W emulsion increases with an increase of temperature until the PIT is reached, above which there will be a rapid reduction in conductivity (a W/O emulsion is formed). Shinoda and coworkers found that the PIT is influenced by the HLB number of the surfactant. In addition, the size of the emulsion droplets was found to depend on the temperature and the HLB number of the emulsifiers, with the droplets being less stable towards coalescence when close to the PIT. However, a rapid cooling of the emulsion allows the production of a stable system. Relatively stable O/W emulsions were obtained when the PIT of the system was 20–65 °C higher than the storage temperature. Emulsions prepared at a temperature just below the PIT, followed by rapid cooling, generally have smaller droplet sizes. This effect can be understood by considering the change in interfacial tension with temperature, as illustrated in Figure 10.22. The interfacial tension decreases with an increase of temperature to reach a minimum when close to the PIT, after which the tension increases.

Thus, droplets prepared close to the PIT will be smaller than those prepared at lower temperatures. These droplets are relatively unstable towards coalescence near the PIT, although by rapid cooling of the emulsion the smaller size can be retained. This procedure may be applied to prepare mini (nano) emulsions.

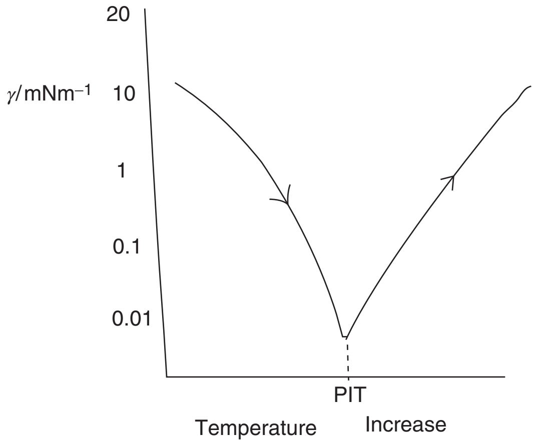

Figure 10.22 Variation of interfacial tension with temperature increase for an O/W emulsion.

Whilst the optimum stability of the emulsion was found to be relatively insensitive to changes in the HLB value or the PIT of the emulsifier, its instability was very sensitive to the PIT of the system.

It is essential, therefore to measure the PIT of the emulsion as a whole (with all other ingredients).

At a given HLB value, the stability of emulsions against coalescence is increased markedly as the molar mass of both the hydrophilic and lipophilic components is increased. An enhanced stability using high-molecular-weight (polymeric) surfactants can be understood by considering the steric repulsion, which produces more stable films. Films produced using macromolecular surfactants resist thinning and disruption, thus reducing the possibility of coalescence. The emulsions showed maximum stability when the distribution of the PEO chains was broad. The cloud point was lower but the PIT was higher than in the corresponding case for narrow size distributions. Hence, the PIT and HLB number are directly related parameters.

As the addition of electrolytes reduces the PIT, an emulsifier with a higher PIT value will be required when preparing emulsions in the presence of electrolytes. Electrolytes cause dehydration of the PEO chains which, in effect, reduces the cloud point of the nonionic surfactant; this must be compensated for by using a surfactant with a higher HLB. The optimum PIT of the emulsifier is fixed if the storage temperature is fixed.

Measurement of the PIT can at best be used as a guide for the preparation of stable emulsions. Any assessments of stability should be evaluated by following the droplet size distribution as a function of time, using a Coulter counter or light-diffraction techniques. Following the rheology of the emulsion as a function of time and temperature may also be used to assess the stability against coalescence. Care should be taken when analysing the rheological results as coalescence leads to an increase in droplet size that is usually followed by a reduction in the viscosity of the emulsion. This trend is only observed if the coalescence is not accompanied by flocculation of the emulsion droplets (which results in an increase in the viscosity). Ostwald ripening can also complicate the analysis of rheological data.

10.6
Creaming or Sedimentation of Emulsions

This is the result of gravity, when the density of the droplets and the medium are not equal. When the density of the disperse phase is lower than that of the medium, creaming occurs, whereas if the density of the disperse phase is higher than that of the medium, sedimentation occurs. A schematic representation for the creaming of emulsions in three cases is shown in Figure 10.23 [1–3].

Case (a) represents the situation for small droplets ($<0.1\,\mu\text{m}$, i.e., nanoemulsions), whereby the Brownian diffusion kT (where k is the Boltzmann constant and T is the absolute temperature) exceeds the force of gravity (mass × acceleration due to gravity, g):

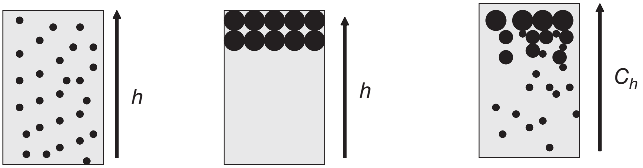

(a) $kT > (4/3)\pi R^3 \Delta\rho gh$ (b) $kT < (4/3)\pi R^3 \Delta\rho gh$ (c) $C_h = C_o \exp(-mgh/kT)$

C_o = conc. At $t = 0$

C_h = conc. At time t and height h

$m = (4/3)\pi R^3 \Delta\rho$

Figure 10.23 Representation of creaming of emulsions. See text for details.

$$kT >> \frac{4}{3}\pi R^3 \Delta\rho g L \tag{10.44}$$

where R is the droplet radius, $\Delta\rho$ is the density difference between the droplets and the medium, and L is the height of the container.

Case (b) represents emulsions consisting of "monodisperse" droplets with radius >1 μm. In this case, the emulsion separates into two distinct layers with the droplets forming a cream or sediment and leaving the clear supernatant liquid; this situation is seldom observed in practice.

Case (c) is that for a polydisperse (practical) emulsions, in which case the droplets will cream or sediment at various rates. In this last case a concentration gradient build-up occurs, with the larger droplets staying at the top of the cream layer or the bottom of the sediment:

$$C(h) = C_o \exp\left(-\frac{mgh}{kT}\right) \tag{10.45}$$

where $C(h)$ is the concentration (or volume fraction ϕ) of droplets at height h, and C_o is the concentration at the top or bottom of the container.

10.6.1
Creaming or Sedimentation Rates

10.6.1.1 Very Dilute Emulsions ($\phi < 0.01$)

In this case, the rate can be calculated using Stokes' law, which balances the hydrodynamic force with gravity force:

$$\text{Hydrodynamic force} = 6\pi\eta_o R v_o \tag{10.46}$$

$$\text{Gravity force} = \frac{4}{3}\pi R^3 \Delta\rho g \tag{10.47}$$

$$v_o = \frac{2}{9}\frac{\Delta\rho g R^2}{\eta_o} \tag{10.48}$$

where v_o is the Stokes' velocity and η_o is the viscosity of the medium.

For an O/W emulsion with $\Delta\rho = 0.2$ in water ($\eta_o \sim 10^{-3}$ Pa·s), the rate of creaming or sedimentation is $\sim 4.4 \times 10^{-5}$ m s^{-1} for 10 μm droplets, and $\sim 4.4 \times 0^{-7}$ m s^{-1} for 1 μm droplets. This means that in a 0.1 m container, creaming or sedimentation of the 10 μm droplets will be complete in ~0.6 h, whereas for the 1 μm droplets this will take ~60 h.

10.6.1.2 **Moderately Concentrated Emulsions ($0.2 < \varphi < 0.1$)**

In this case, account must be taken of the hydrodynamic interaction between the droplets, which reduces the Stokes velocity to a value v given, by the following expression [23]:

$$v = v_o(1 - k\varphi) \tag{10.49}$$

where k is a constant that accounts for hydrodynamic interaction. k is on the order of 6.5, which means that the rate of creaming or sedimentation is reduced by about 65%.

10.6.1.3 **Concentrated Emulsions ($\varphi > 0.2$)**

The rate of creaming or sedimentation becomes a complex function of ϕ, as illustrated in Figure 10.24, which also shows the change of relative viscosity η_r with ϕ.

As can be seen from Figure 10.24, v decreases with the increase in ϕ and ultimately approaches zero when ϕ exceeds a critical value, φ_p, which is the so-called "maximum packing fraction." The value of ϕ_p for monodisperse "hard-spheres" ranges from 0.64 (for random packing) to 0.74 for hexagonal packing, but exceeds 0.74 for polydisperse systems. For emulsions which are deformable, ϕ_p can be much larger than 0.74.

The data in Figure 10.24 also show that when ϕ approaches ϕ_p, η_r approaches ∞. In practice, most emulsions are prepared at ϕ-values well below ϕ_p (usually in the range of 0.2–0.5), and under these conditions creaming or sedimentation is the rule rather than the exception. Several procedures may be applied to reduce or eliminate creaming or sedimentation, and these are discussed below.

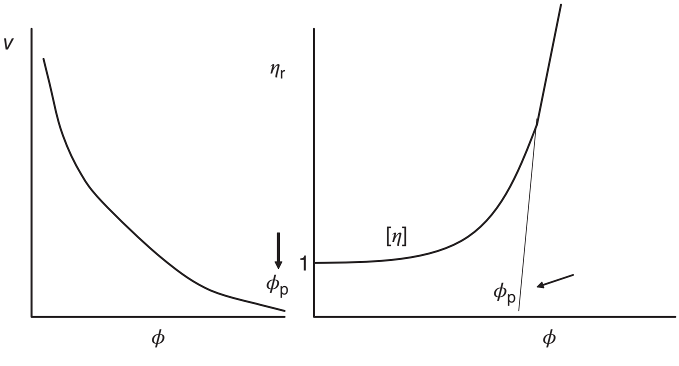

Figure 10.24 Variation of v and η_r with φ.

10.6.2
Prevention of Creaming or Sedimentation

10.6.2.1 Matching the Density of Oil and Aqueous Phases

Clearly, if $\Delta\rho = 0$, $v = 0$; however, this method is seldom practical. Density matching, if possible, only occurs at one temperature.

10.6.2.2 Reduction of Droplet Size

Since the gravity force is proportional to R^3, then if R is reduced by a factor of 10, the gravity force is reduced by 1000. Below a certain droplet size (which also depends on the density difference between oil and water), the Brownian diffusion may exceed gravity and creaming or sedimentation is prevented. This is the principle of formulation of nanoemulsions (with size range 20–200 nm) that may show very little or no creaming or sedimentation. The same applies for microemulsions (size range 5–50 nm).

10.6.2.3 Use of 'Thickeners'

These are high-molecular-weight polymers, either natural or synthetic, such as xanthan gum, hydroxyethyl cellulose, alginates, and carrageenans. In order to understand the role of these "thickeners," the gravitational stresses exerted during creaming or sedimentation should be considered:

$$\text{stress} = \text{mass of drop} \times \text{acceleration due to gravity} = \frac{4}{3}\pi R^3 \Delta\rho g \qquad (10.50)$$

To overcome such stress, needs a restoring force is needed:

$$\text{Restoring force} = \text{area of drop} \times \text{stress of drop} = 4\pi R^2 \sigma_p \qquad (10.51)$$

Thus, the stress exerted by the droplet σ_p is given by,

$$\sigma_p = \frac{\Delta\rho R g}{3} \qquad (10.52)$$

Simple calculation shows that σ_p is in the range 10^{-3} to 10^{-1} Pa, which implies that for prediction of creaming or sedimentation it is necessary to measure the viscosity at such low stresses. This can be achieved by using constant stress or creep measurements.

The above-described "thickeners" satisfy the criteria for obtaining very high viscosities at low stresses or shear rates. This can be illustrated from plots of shear stress σ and viscosity η versus shear rate γ (or shear stress), as shown in Figure 10.25. These systems are described as "pseudoplastic" or shear thinning. The low shear (residual or zero shear rate) viscosity $\eta(0)$ can reach several thousand Pa·s, and such high values prevent creaming or sedimentation [24, 25].

The above-described behaviour is obtained above a critical polymer concentration (C^*), which can be located from plots of log η versus log C, as is illustrated in Figure 10.26. Below C^*, the log η–log C curve has a slope in the region of 1, whereas above C^* the slope of the line exceeds 3. In most cases a good correlation between the rate of creaming or sedimentation and $\eta(0)$ is obtained.

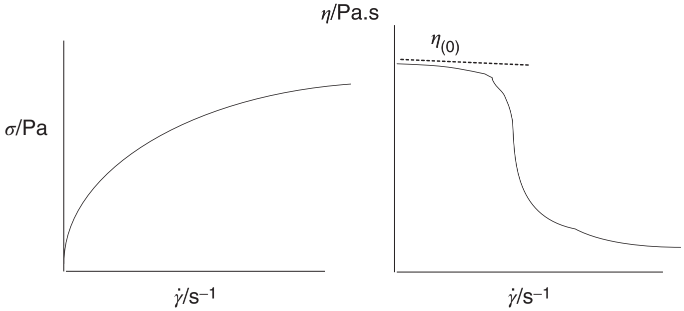

Figure 10.25 Variation of (stress) σ and viscosity η with shear rate γ.

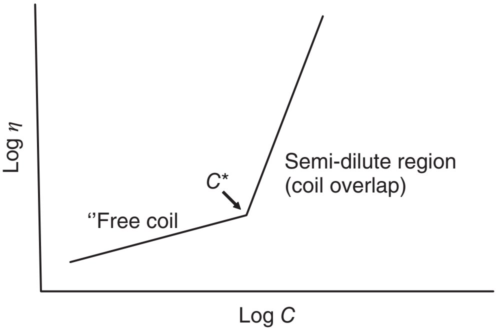

Figure 10.26 Variation of log η with log C for polymer solutions.

10.6.2.4 **Controlled Flocculation**

As discussed above, the total energy–distance of separation curve for electrostatically stabilised shows a shallow minimum (secondary minimum) at a relatively long distance of separation between the droplets. However, by adding small amounts of electrolyte, such minima can be made sufficiently deep for weak flocculation to occur. The same applies to sterically stabilised emulsions, which show only one minimum, but whose depth can be controlled by reducing the thickness of the adsorbed layer. This can be achieved by reducing the molecular weight of the stabiliser and/or the addition of a nonsolvent for the chains (e.g., an electrolyte).

The above phenomenon of weak flocculation may be applied to reduce creaming or sedimentation, although in practice this is not easy as the droplet size has also to be controlled.

10.6.2.5 **Depletion Flocculation**

This is achieved by the addition of ''free'' (nonadsorbing) polymer in the continuous phase [26]. At a critical concentration, or volume fraction of free polymer, $\phi_p{}^+$, weak flocculation occurs as the free polymer coils become ''squeezed-out'' from between the droplets. This is illustrated in Figure 10.27, which shows the situation when the polymer volume fraction exceeds the critical concentration.

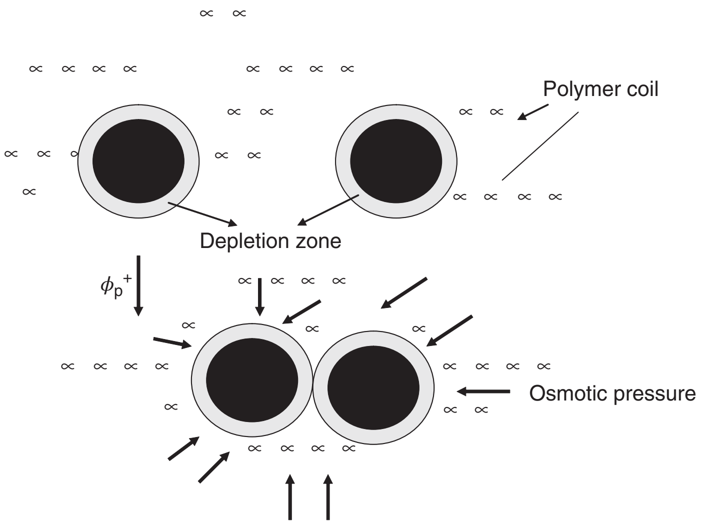

Figure 10.27 Schematic representation of depletion flocculation.

The osmotic pressure outside the droplets is higher than in between the droplets, and this results in an attraction the magnitude of which depends on the concentration of the free polymer and its molecular weight, as well as the droplet size and ϕ. The value of $\phi_p{}^+$ decreases with increase of the molecular weight of the free polymer, and also decreases as the volume fraction of the emulsion increases.

The above weak flocculation can be applied to reduce creaming or sedimentation, although it suffers from the following drawbacks:

- Temperature dependence; as the temperature increases, the hydrodynamic radius of the free polymer decreases (due to dehydration) and hence more polymer will be required to achieve the same effect at lower temperatures.
- If the free polymer concentration is increased above a certain limit, phase separation may occur and the flocculated emulsion droplets may cream or sediment faster than in the absence of the free polymer.

10.7
Flocculation of Emulsions

Flocculation is the result of van der Waals attraction that is universal for all disperse systems. The van der Waals attraction G_A was described previously and, as shown in Figure 10.6, it is inversely proportional to the droplet–droplet distance of separation h; it also depends on the effective Hamaker constant A of the emulsion system. One way to overcome the van der Waals attractions is by electrostatic stabilisation using ionic surfactants; this results in the formation of electrical double layers that introduce a repulsive energy that overcomes the attractive energy. Emulsions stabilised by electrostatic repulsion become flocculated at intermediate electrolyte concentrations (see below). The second and most effective method of overcoming flocculation is by ''steric stabilisation'' using nonionic surfactants or polymers. Stability may be maintained in electrolyte solutions (as high as 1 mol dm^{-3}, depending on the nature of the electrolyte) and up to high temperatures (in excess of 50 °C), provided that the stabilising chains (e.g., PEO) are still in better than θ-conditions ($\chi < 0.5$).

10.7.1
Mechanism of Emulsion Flocculation

This can occur if the energy barrier is small or absent (for electrostatically stabilised emulsions) or when the stabilising chains reach poor solvency (for sterically stabilised emulsions, that is if $\chi > 0.5$). For convenience, the flocculation of electrostatically and sterically stabilised emulsions will be discussed separately.

10.7.1.1 Flocculation of Electrostatically Stabilised Emulsions

As discussed above, the condition for kinetic stability is $G_{\text{max}} > 25\,\text{kT}$ since, when $G_{\text{max}} < 5\,\text{kT}$ flocculation will occur. Two types of flocculation kinetics may be distinguished: fast flocculation with no energy barrier; and slow flocculation when an energy barrier exists.

The fast flocculation kinetics was treated by Smoluchowski [27], who considered the process to be represented by second-order kinetics and to be simply diffusion-controlled. The number of particles n at any time t may be related to the final number n_o (at $t = 0$) by the following expression:

$$n = \frac{n_o}{1 + kn_o t} \tag{10.53}$$

where k is the rate constant for fast flocculation that is related to the diffusion coefficient of the particles D, that is,

$$k = 8\pi DR \tag{10.54}$$

where D is given by the Stokes–Einstein equation,

$$D = \frac{kT}{6\pi\eta R} \tag{10.55}$$

Combining Equations (10.54) and (10.55),

$$k = \frac{4}{3}\frac{kT}{\eta} = 5.5 \times 10^{-18}\,\text{m}^3\,\text{s}^{-1}\,\text{for water at } 25^\circ\text{C} \tag{10.56}$$

The half-life $t_{1/2}$ ($n = (1/2)\, n_o$) can be calculated at various n_o or volume fraction ϕ, as given in Table 10.4.

The slow flocculation kinetics was treated by Fuchs [28] who related the rate constant k to the Smoluchowski rate by the stability constant W:

$$W = \frac{k_o}{k} \tag{10.57}$$

Table 10.4 Half-life of emulsion flocculation.

R (μm)	ϕ			
	10^{-5}	10^{-2}	10^{-1}	5×10^{-1}
0.1	765 s	76 ms	7.6 ms	1.5 ms
1.0	21 h	76 s	7.6 s	1.5 s
10.0	4 mo	21 h	2 h	25 m

where W is related to G_{max} by the following expression [29],

$$W = \frac{1}{2}\exp\left(\frac{G_{\text{max}}}{kT}\right) \tag{10.58}$$

Since G_{max} is determined by the salt concentration C and valency, it is possible to derive an expression relating W to C and Z,

$$\log W = -2.06\times10^{9}\left(\frac{R\gamma^{2}}{Z^{2}}\right)\log C \tag{10.59}$$

where γ is a function that is determined by the surface potential ψ_{o},

$$\gamma = \left[\frac{\exp\left(Ze\psi_o/kT\right)-1}{\exp(ZE\psi_o/kT)+1}\right] \tag{10.60}$$

Plots of log W versus log C are shown in Figure 10.28. The condition log $W=0$ ($W=1$) is the onset of fast flocculation. The electrolyte concentration at this point defines the critical flocculation concentration (CFC). Above the CFC, $W<1$ (due to the contribution of van der Waals attractions which accelerate the rate above the Smoluchowski value). Below the CFC, $W>1$ and it increases with a decrease

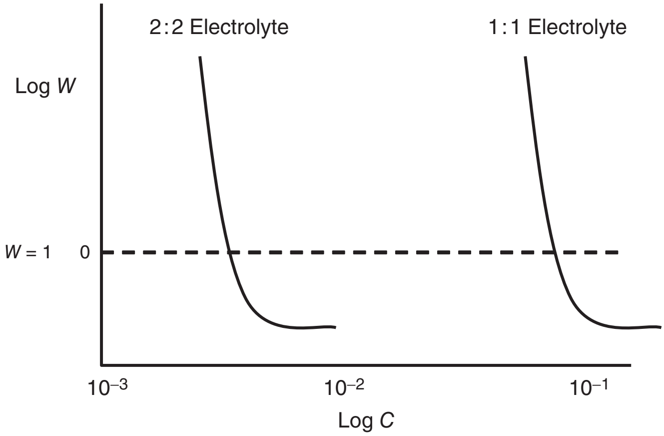

Figure 10.28 Log W–log C curves for electrostatically stabilised emulsions.

of electrolyte concentration. The data in Figure 10.28 also show that the CFC decreases with increase of valency, in accordance to the Schultze–Hardy rule.

Another mechanism of flocculation is that involving the secondary minimum (G_{min}), which typically is a few kT units. In this case the flocculation is weak and reversible, and hence both the rate of flocculation (forward rate k_{f}) and deflocculation (backward rate k_{b}) must be considered. The rate of decrease of particle number with time is given by the expression,

$$-\frac{\mathrm{d}n}{\mathrm{d}t} = -k_{\mathrm{f}}n^2 + k_{\mathrm{b}}n \qquad (10.61)$$

The backward reaction (break-up of weak flocs) reduces the overall rate of flocculation.

10.7.1.2 Flocculation of Sterically Stabilised Emulsions

This occurs when the solvency of the medium for the chain becomes worse than a θ-solvent ($\chi > 0.5$). Under these conditions, G_{mix} becomes negative (i.e., attractive) and a deep minimum is produced that results in catastrophic flocculation (this is referred to as incipient flocculation). This is shown schematically in Figure 10.29. With many systems a good correlation between the flocculation point and the θ-point is obtained.

For example, the emulsion will flocculate at a temperature (referred to as the critical flocculation temperature; CFT) that is equal to the θ-temperature of the stabilising chain. The emulsion may flocculate at a critical volume fraction (CFV) of a nonsolvent, which is equal to the volume of nonsolvent that brings it to a θ-solvent.

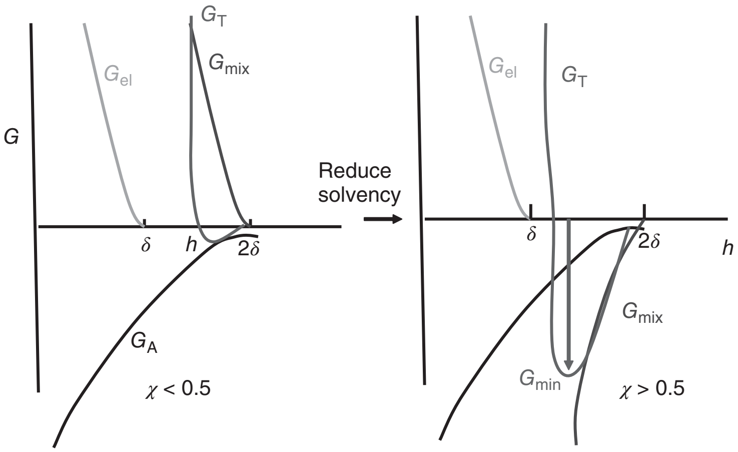

Figure 10.29 Schematic representation of flocculation of sterically stabilised emulsions.

10.8
General Rules for Reducing (Eliminating) Flocculation

10.8.1
Charge-Stabilised Emulsions (e.g., Using Ionic Surfactants)

The most important criterion is to make $G_{\max}$ as high as possible; this is achieved by three main conditions: (i) high surface or zeta-potential; (ii) low electrolyte concentration; and (iii) low valency of ions.

10.8.2
Sterically Stabilised Emulsions

Four main criteria are necessary:

- Complete coverage of the droplets by the stabilising chains.
- A firm attachment (strong anchoring) of the chains to the droplets. This requires the chains to be insoluble in the medium and soluble in the oil. However, this is incompatible with stabilisation which requires a chain that is soluble in the medium and strongly solvated by its molecules. These conflicting requirements are solved by the use of A-B, A-B-A block or BA_n graft copolymers (B is the ‘‘anchor’’ chain and A is the stabilising chain(s)). Examples of the B chains for O/W emulsions are polystyrene, PMMA, PPO and alkyl PPO. For the A chain(s), PEO or polyvinyl alcohol are good examples. For W/O emulsions, PEO can form the B chain, whereas the A chain(s) could be polyhydroxy stearic acid (PHS) which is strongly solvated by most oils.
- Thick adsorbed layers; the adsorbed layer thickness should be in the region of 5–10 nm. This means that the molecular weight of the stabilising chains could be in the region of 1000–5000 Da.
- The stabilising chain should be maintained in good solvent conditions ($\chi < 0.5$) under all conditions of temperature changes on storage.

10.9
Ostwald Ripening

The driving force for Ostwald ripening is the difference in solubility between the small and large droplets (the smaller droplets have a higher Laplace pressure and a higher solubility than the larger droplets). This is illustrated in Figure 10.30, where R_1 decreases and R_2 increases as a result of diffusion of molecules from the smaller to the larger droplets.

The difference in chemical potential between different sized droplets was given by Lord Kelvin [30],

$$S(r) = S(\infty)\exp\left(\frac{2\gamma V_m}{rRT}\right) \tag{10.62}$$

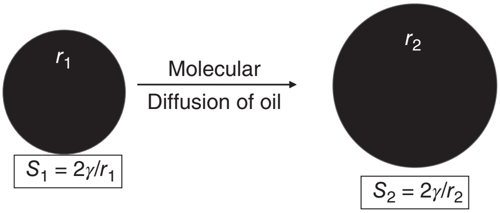

Figure 10.30 Schematic representation of Ostwald ripening.

where $S(r)$ is the solubility surrounding a particle of radius r, $S(\infty)$ is the bulk solubility, V_m is the molar volume of the dispersed phase, R is the gas constant, and T is the absolute temperature.

The quantity $(2\gamma V_m/RT)$ is termed the characteristic length, and has an order of ~1 nm or less, indicating that the difference in solubility of a 1 μm droplet is of the order of 0.1%, or less. In theory, Ostwald ripening should lead to the condensation of all droplets into a single drop; however, this does not occur in practice as the rate of growth decreases with increases in droplet size.

For two droplets with radii r_1 and r_2 $(r_1 < r_2)$,

$$\frac{RT}{V_m}\ln\left[\frac{S(r_1)}{S(r_2)}\right] = 2\gamma\left[\frac{1}{r_1} - \frac{1}{r_2}\right] \tag{10.63}$$

Equation (10.63) shows that the larger the difference between r_1 and r_2, the higher the rate of Ostwald ripening.

Ostwald ripening can be quantitatively assessed from plots of the cube of the radius versus time t [31, 32],

$$r^3 = \frac{8}{9}\left[\frac{S(\infty)\gamma V_m D}{\rho RT}\right] t \tag{10.64}$$

where D is the diffusion coefficient of the disperse phase in the continuous phase and ρ is the density of the disperse phase.

Several methods may be applied to reduce Ostwald ripening [33–35]:

(i) The addition of a second disperse phase component which is insoluble in the continuous medium (e.g., squalane). In this case, partitioning between different droplet sizes occurs, with the component having a low solubility expected to be concentrated in the smaller droplets. During Ostwald ripening in a two-component system, equilibrium is established when the difference in chemical potential between different size droplets (which results from curvature effects) is balanced by the difference in chemical potential resulting from partitioning of the two components. This effect reduces further growth of droplets.

(ii) Modification of the interfacial film at the O/W interface. According to Equation (10.64), a reduction in γ will result in a reduction of the Ostwald ripening rate. By using surfactants that are strongly adsorbed at the O/W interface (i.e., polymeric surfactants), and which do not desorb during ripening (by choosing a molecule that is insoluble in the continuous phase), the rate could be significantly reduced. An increase in the surface dilational modulus ε ($= \mathrm{d}\gamma/\mathrm{d}\ln A$) and a decrease in γ would be observed for the shrinking drop, and this would tend to reduce further growth.

A-B-A block copolymers such as PHS-PEO-PHS (which is soluble in the oil droplets, but insoluble in water) can be used to achieve the above effect. Similar effects can also be obtained using a graft copolymer of hydrophobically modified inulin, namely INUTEC® SP1 (ORAFTI, Belgium). This polymeric surfactant adsorbs with several alkyl chains (which may dissolve in the oil phase), leaving loops and tails of strongly hydrated inulin (polyfructose) chains. The molecule has a limited solubility in water and hence it resides at the O/W interface. These polymeric emulsifiers enhance the Gibbs elasticity, thus significantly reducing the Ostwald ripening rate.

10.10
Emulsion Coalescence

When two emulsion droplets come into close contact in a floc or creamed layer, or during Brownian diffusion, thinning and disruption of the liquid film may occur that results in eventual rupture. On close approach of the droplets, film thickness fluctuations may occur; alternatively, the liquid surfaces may undergo some fluctuations to form surface waves, as illustrated in Figure 10.31. These surface waves may grow in amplitude and the apices may join as a result of the strong van der Waals attractions (at the apex, the film thickness is the smallest). The same applies if the film thins to a small value (critical thickness for coalescence)

A very useful concept was introduced by Deryaguin [36], who suggested that a ‘‘Disjoining Pressure’’ $\pi(h)$ is produced in the film which balances the excess normal pressure,

$$\pi(h) = P(h) - P_\mathrm{o} \tag{10.65}$$

where $P(h)$ is the pressure of a film with thickness h, and P_o is the pressure of a sufficiently thick film such that the net interaction free energy is zero.

$\pi(h)$ may be equated to the net force (or energy) per unit area acting across the film,

$$\pi(h) = -\frac{\mathrm{d}G_\mathrm{T}}{\mathrm{d}h} \tag{10.66}$$

where G_T is the total interaction energy in the film.

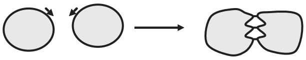

Figure 10.31 Schematic representation of surface fluctuations.

$\pi(h)$ is composed of three contributions due to electrostatic repulsion (π_E), steric repulsion (π_s) and van der Waals attractions (π_A),

$$\pi(h) = \pi_E + \pi_s + \pi_A \tag{10.67}$$

In order to produce a stable film $\pi_E + \pi_s > \pi_A$, and this is the driving force for the prevention of coalescence, which can be achieved by two mechanisms and their combination: (i) increased repulsion, both electrostatic and steric; and (ii) dampening of the fluctuation by enhancing the Gibbs elasticity. In general, smaller droplets are less susceptible to surface fluctuations and hence coalescence is reduced; this explains the high stability of nanoemulsions.

Several methods may be applied to achieve the above effects:

- Use of mixed surfactant films: In many cases the used of mixed surfactants (e.g., anionic and nonionic or long chain alcohols) can reduce coalescence as a result of several effects: a high Gibbs elasticity; high surface viscosity; and hindered diffusion of surfactant molecules from the film.
- Formation of lamellar liquid crystalline phases at the O/W interface: This mechanism, as suggested by Friberg and coworkers [37], proposed that surfactant or mixed surfactant film can produce several bilayers that "wrap" the droplets. As a result of these multilayer structures, the potential drop is shifted to longer distances, thus reducing the van der Waals attractions. A schematic representation of the role of liquid crystals is shown in Figure 10.32, which illustrates the difference between having a monomolecular layer and a multilayer, as is the case with liquid crystals.

For coalescence to occur, these multilayers have to be removed 'two-by-two' and this forms an energy barrier preventing coalescence.

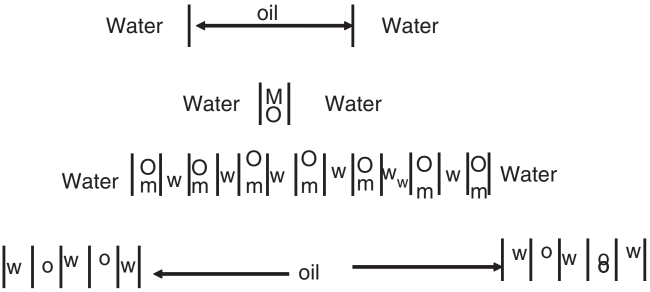

Upper part monomolecular layer

Lower part presence of liquid crystalline phases

Figure 10.32 Schematic representation of the role of liquid crystalline phases.

10.10.1
Rate of Coalescence

Since film drainage and rupture is a kinetic process, coalescence is also a kinetic process. If the number of particles n (flocculated or not) is measured at time t,

$$n = n_t + n_v m \tag{10.68}$$

where n_t is the number of primary particles remaining, and n is the number of aggregates consisting of m separate particles.

For studying emulsion coalescence, it is important to consider the rate constant of flocculation and coalescence. If coalescence is the dominant factor, then the rate K follows a first-order kinetics,

$$n = \frac{n_o}{Kt}[1 + \exp(-Kt)] \tag{10.69}$$

which shows that a plot of log n versus t should give a straight line from which K can be calculated.

10.11
Phase Inversion

The phase inversion of emulsions can be one of two types: (i) transitional inversion, which is induced by changing facers which affect the HLB of the system (e.g., temperature and/or electrolyte concentration); and (ii) catastrophic inversion, which is induced by increasing the volume fraction of the disperse phase.

Catastrophic inversion is illustrated in Figure 10.33, which shows the variation of viscosity and conductivity with the oil volume fraction ϕ. As can be seen, inversion occurs at a critical ϕ, which may be identified with the maximum packing fraction.

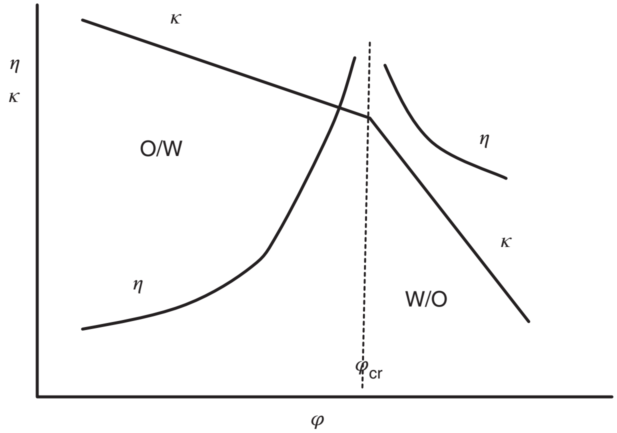

Figure 10.33 Variation of conductivity and viscosity with volume fraction of oil.

At ϕ_{cr}, η suddenly decreases as the inverted W/O emulsion has a much lower volume fraction. κ also decreases sharply at the inversion point as the continuous phase is now oil.

Earlier theories of phase inversion were based on packing parameters. When φ exceeds the maximum packing (~0.64 for random packing and ~0.74 for hexagonal packing of monodisperse spheres; for polydisperse systems, the maximum packing exceeds 0.74), inversion occurs. However, these theories are inadequate as many emulsions invert at φ values well below the maximum packing as a result of the change in surfactant characteristics with variation of conditions. For example, when using a nonionic surfactant based on PEO the latter chain changes its solvation by increase of temperature and/or the addition of electrolyte. Many emulsions show phase inversion at a critical temperature (the PIT) that depends on the HLB number of the surfactant as well as the presence of electrolytes. By increasing temperature and/or addition of electrolyte, the PEO chains become dehydrated and finally more soluble in the oil phase. Under these conditions, the O/W emulsion will invert to a W/O emulsion. The above dehydration effect amounts to a decrease in the HLB number, and when the latter reaches a value that is more suitable for a W/O emulsion then inversion will occur. At present, however, there is no quantitative theory that accounts for phase inversion of emulsions.

References

1. Tadros, T.F. and Vincent, B. (1983) in *Encyclopedia of Emulsion Technology* (ed. P. Becher), Marcel Dekker, New York.
2. Tadros, T. (ed.) (2013) *Emulsion Formation and Stability*, Wiley-VCH Verlag GmbH, Weinheim.
3. Tadros, T. (2005) *Applied Surfactants*, Wiley-VCH Verlag GmbH, Weinheim.
4. Hamaker, H.C. (1937) *Physica (Utrecht)*, **4**, 1058.
5. Deryaguin, B.V. and Landau, L. (1941) *Acta Physicochem. USSR*, **14**, 633.
6. Verwey, E.J.W. and Overbeek, J.T.G. (1948) *Theory of Stability of Lyophobic Colloids*, Elsevier, Amsterdam.
7. Napper, D.H. (1983) *Polymeric Stabilisation of Dispersions*, Academic Press, London.
8. Walstra, P. and Smolders, P.E.A. (1998) in *Modern Aspects of Emulsions* (ed. B.P. Binks), The Royal Society of Chemistry, Cambridge.
9. Stone, H.A. (1994) *Annu. Rev. Fluid Mech.*, **226**, 95.
10. Wierenga, J.A., van Dieren, F., Janssen, J.J.M., and Agterof, W.G.M. (1996) *Trans. Inst. Chem. Eng.*, **74-A**, 554.
11. Levich, V.G. (1962) *Physicochemical Hydrodynamics*, Prentice-Hall, Englewood Cliffs, NJ.
12. Davis, J.T. (1972) *Turbulent Phenomena*, Academic Press, London.
13. Lucasses-Reynders, E.H. (1996) in *Encyclopedia of Emulsion Technology* (ed. P. Becher), Marcel Dekker, New York.
14. Graham, D.E. and Phillips, M.C. (1979) *J. Colloid Interface Sci.*, **70**, 415.
15. Lucassen-Reynders, E.H. (1994) *Colloids Surf.*, **A91**, 79.
16. Lucassen, J. (1981) in *Anionic Surfactants* (ed. E.H. Lucassen-Reynders), Marcel Dekker, New York.
17. van den Tempel, M. (1960) *Proc. Int. Congr. Surf. Activity*, **2**, 573.
18. Griffin, W.C. *J. Cosmet. Chemists*, **1**, 311(1949); **5**, 249 (1954).
19. Davies, J.T. (1959) *Proc. Int. Congr. Surf. Activity*, **1**, 426.
20. Davies, J.T. and Rideal, E.K. (1961) *Interfacial Phenomena*, Academic Press, New York.
21. Shinoda, K. (1967) *J. Colloid Interface Sci.*, **25**, 396.

22. Shinoda, K. and Saito, H. (1969) *J. Colloid Interface Sci.*, **30**, 258.

23. Batchelor, G.K. (1972) *J. Fluid. Mech.*, **52**, 245.

24. Buscall, R., Goodwin, J.W., Ottewill, R.H., and Tadros, T.F. (1982) *J. Colloid Interface Sci.*, **85**, 78.

25. Tadros, T. (2010) *Rheology of Dispersions*, Wiley-VCH Verlag GmbH, Weinheim.

26. Asakura, S. and Osawa, F. (1954) *J. Phys. Chem.*, **22**, 1255; *J. Polym. Sci.*, 1958, **33**, 183.

27. Smoluchowski, M.V. (1927) *Z. Phys. Chem.*, **92**, 129.

28. Fuchs, N. (1936) *Z. Phys.*, **89**, 736.

29. Reerink, H. and Overbeek, J.T.G. (1954) *Disc. Faraday Soc.*, **18**, 74.

30. Thompson, W. (Lord Kelvin) (1871) *Philos. Mag.*, **42**, 448.

31. Lifshitz, I.M. and Slesov, V.V. (1959) *Sov. Phys. JETP*, **35**, 331.

32. Wagner, C. (1961) *Z. Electrochem.*, **35**, 581.

33. Kabalanov, A.S. and Shchukin, E.D. (1992) *Adv. Colloid Interface Sci.*, **38**, 69.

34. Kabalanov, A.S. (1994) *Langmuir*, **10**, 680.

35. Weers, J.G. (1998) in *Modern Aspects of Emulsion Science* (ed. B.P. Binks), Royal Society of Chemistry Publication, Cambridge.

36. Deryaguin, B.V. and Scherbaker, R.L. (1961) *Kolloid Zh.*, **23**, 33.

37. Friberg, S., Jansson, P.O., and Cederberg, E. (1976) *J. Colloid Interface Sci.*, **55**, 614.

11
Formulation of Suspoemulsions (Mixtures of Suspensions and Emulsions)

11.1
Introduction

Suspoemulsions are mixtures of suspensions and emulsions [1] that are applied in many formulations such as paints, personal care products and agrochemicals. In aqueous paint formulations, the latex dispersion – which is liquid-like at room temperature (to provide a minimum film-forming temperature below room temperature) – is mixed with particulate dispersions (e.g., titanium dioxide) which must remain in the dispersed state with particle sizes in the region of 200–400 nm in order to provide maximum opacity. Other coloured pigments such as iron oxide are also included in the formulation to provide a coloured paint on application. In personal care product applications, the main formulations that consist of suspoemulsions are sunscreens and colour cosmetics. In the case of sunscreens, titanium dioxide or zinc oxide are incorporated into an oil-in-water (O/W) or water-in-oil (W/O) emulsion. In order to provide maximum UV protection, the particle size of the titanium dioxide or zinc oxide must be maintained in the region of 20–40 nm. In agrochemicals, suspoemulsions are applied to formulate two active ingredients with one as an aqueous suspension and the other as an oil/water emulsion.

A schematic representation of suspoemulsions is shown in Figure 11.1, where two main types can be distinguished: (i) a system whereby the solid particles and emulsion droplets remain as separate entities; and (ii) a system whereby the solid particles are dispersed in the oil droplets. Of these two systems, the first is the most commonly applied when preparing formulations [1].

The formulation of suspoemulsions is not an easy task; although it is quite easy to produce a stable suspension and an emulsion separately, when the two are mixed they become unstable due to the following interactions [1]:

- *Homoflocculation of the suspension particles*: This can occur if the dispersing agent used to prepare the suspension is not strongly adsorbed and becomes displaced by the emulsifier, which is more strongly adsorbed but not a good stabiliser for the suspension particles.
- *Emulsion coalescence*: This can occur if the emulsifier is not strongly adsorbed at the O/W or W/O interface, and results in its partial or complete displacement by the suspension dispersant which is not a good emulsion stabiliser. This in turn

Formulation of Disperse Systems: Science and Technology, First Edition. Tharwat F. Tadros.

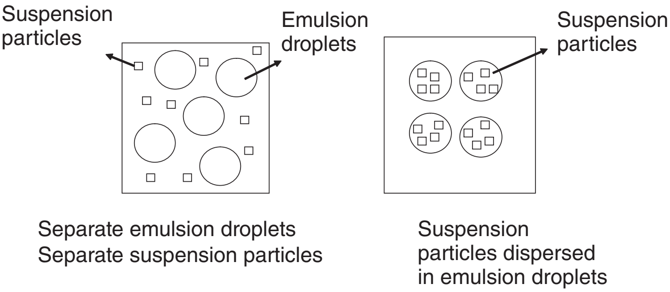

Figure 11.1 Schematic representation of suspoemulsions.

results in a coalescence of the emulsion droplets with ultimate separation of oil (for O/W) or water (for W/O).

- *Heteroflocculation between the oil droplets and suspension particles*: The latter may be partially wetted by the oil and may reside at the O/W interface (this is particularly the case if the oil droplets are much larger than the suspension particles). Heteroflocculation can also occur with suspension particles dispersed in a W/O emulsion.
- *Phase transfer and crystallisation*: This occurs when the suspension particles have a limited solubility in the oil phase. Small suspension particles which are more soluble than their larger counterparts (due to curvature effects) may dissolve in the oil phase and then recrystallize onto the larger suspension particles (this is a form of Ostwald ripening). Large and sometimes needle-shaped crystals may be produced as a result of crystal habit modification (this sometimes occurs with Ostwald ripening).

Several methods can be applied to study interactions in suspoemulsions, including microscopy (both optical and electron) and rheology. The latter in particular allows investigations of the stability/instability of suspoemulsions, without dilution.

In this chapter, the creation of suspoemulsions using three different formulation, namely paints, sunscreens/colour cosmetics and agrochemicals, will be described.

11.2
Suspoemulsions in Paints

Most paint formulations consist of disperse systems (solid in liquid dispersions) [2]. The disperse phase consists of primary pigment particles (organic or inorganic) which provide the opacity, colour and other optical effects; these are usually in the submicron range. Other coarse particles (mostly inorganic) are used in primers and undercoats to seal the substrate and enhance adhesion of the top coat. The continuous phase consists of a solution of polymer or resin which provides the basis for a continuous film that seals the surface and protects it from the outside environment. Most modern paints contain latexes which are used as film formers. These latexes – which typically have a glass transition temperature (T_g) below ambient temperature – coalesce on the surface and form a strong and durable film. Other components may be present in the paint formulation such as corrosion inhibitors, driers, and fungicides [2].

It is clear from the above description that a paint is essentially a suspoemulsion consisting mainly of solid particles of pigments and ''liquid'' droplets of latex. An understanding of the colloidal interactions occurring between the various components helps to determine the flow characteristics of the paint, and in turn to determine its long-term stability, application, and the final formation of the paint coatings. The primary pigment particles (which normally are in the submicron range) are responsible for the opacity, colour and anticorrosive properties. Today, the principal pigment used is titanium dioxide, which has a high refractive index and is employed in the production of white paints in particular [2]. To produce maximum scattering, the particle size distribution of titanium dioxide must be controlled within narrow limits. Typically, rutile with a refractive index of 2.76 is preferred over anatase, which has a lower refractive index of 2.55. Thus, rutile not only provides the possibility of a higher opacity than anatase but it is also more resistant to chalking on exterior exposure. In order to obtain maximum opacity, the particle size of rutile should be between 220 and 140 nm. The surface of rutile is photoactive, and it is surface-coated with silica and alumina in various proportions to reduce its photoactivity.

Coloured pigments may consist of either inorganic or organic particles. For a black pigment it is possible to use carbon black, copper carbonate, manganese dioxide (inorganic) or aniline black (organic), while yellow pigments require the use of lead, zinc, chromates, cadmium sulphide, iron oxides (inorganic) or nickel azo yellow (organic). The best blue/violet pigments include ultramarine, Prussian blue, cobalt blue (inorganic) or phthalocyanine, indanthrone blue, carbazol violet (organic), while for red pigments iron oxide, cadmium selenide, red lead, chrome red (inorganic) or toluidine red, quinacridones (organic) are best used.

The colour of a pigment is determined by the selective absorption and reflection of the various wavelengths of visible light (400–700 nm) which impinge on it [2]. For example, a blue pigment appears so because it reflects the blue wavelengths in the incident white light and absorbs the other wavelengths. Black pigments absorb all wavelengths of incident light almost totally, whereas a white pigment reflects all visible wavelengths.

Surface-active agents are added to aid wetting of the pigment powder, while dispersing agents (mostly polymeric surfactants) are also added to stabilise the particles against aggregation. Both materials can affect the viscosity and yield value of the final paint dispersion by adsorption at the solid/liquid interface. The main purpose of wetters and dispersants is to produce a ''better dispersion'' by causing deaggregation and deflocculation. Deaggregation refers to the mechanical or chemical separation of single particles in an aggregate. The aggregate consisting of these unit particles is ''glued'' together, which prevents the liquid from penetrating into the aggregated mass and surrounding each unit particle. Deflocculation, on the other hand, can only be affected by the use of a dispersing agent. A mechanical force cannot change the state of flocculation as a flocculate is a ''loose'' but connected structure of particles in which the particles are far enough apart to permit the liquid to surround them. However, as the particles are sufficiently close to each other due to strong van der Waals attractions, the dispersion will not flow until sufficient shearing stress is applied to overcome these attractive forces. This shearing stress is proportional to the yield value. A dispersant that is strongly adsorbed to the particle surface and provides sufficient repulsive forces can overcome the van der Waals attractions, causing a marked reduction in the yield value [2].

It should be mentioned that the controlled flocculation of a pigment dispersion may be desirable to prevent settling and the formation of hard sediments, and also to control the surface finish of a coating. For pigments dispersed in oil, small quantities of a polar liquid (e.g., alcohol, glycerol or butanol) can be used as flocculating agents. In the case of hydrophilic pigments suspended in an aqueous medium, oils and oil-soluble agents (e.g., lecithin) can induce flocculation.

The dispersion of a pigment into single particles is aided by grinding and mixing [2]. In general, an increase in the viscosity of a dispersion will result in an increase in the efficiency of milling. In ball milling, the viscosity of the dispersion also plays an important role. A practical viscosity for good operation depends on the nature of the balls. When using steel ball mills, a high viscosity (up to 20 Pa·s) can be used, but with pebble and porcelain ball mills a lower viscosity is required as the weight of the grinding medium will be lower. It should also be noted that the viscosity measured before mixing is substantially different from that existing during the mixing operation. The flow properties of the dispersion during the process of grinding are changed as a result of increases in temperature, increases in wetting, an increased degree of aggregation, and an improved interaction between the solid and liquid phases.

Microscopic investigations have demonstrated increases in deaggregation during milling, and this is accompanied by increases in colour strength [2]. Because the shear rate is much higher during milling than the maximum value measured in a rotational viscometer (usually on the order of $1000\,\text{s}^{-1}$), the viscosity of a pseudoplastic plastic material will decrease substantially during milling, while its yield value may increase. The viscosity of a thixotropic dispersion will decrease substantially, and its yield value may increase during milling. Thus, in order to evaluate grinding performance the consistency of the dispersion at the operational grinding conditions and at different steps of processing must be determined. This may require measurements of the viscosity at a much higher shear rate than would be encountered with rotational viscometers, as for example determined using a capillary viscometer (which can operate at much higher shear rates).

Emulsion polymers (latexes) are the most commonly used film formers in the coating industry; this is particularly the case with aqueous emulsion paints that are used for home decoration. These aqueous emulsion paints are applied at room temperature, when the latexes coalesce on the substrate to form a thermoplastic film. Occasionally, functional polymers are used for crosslinking in the coating system. The polymer particles are typically in the submicron range (0.1–0.5 μm).

Generally speaking, three methods are used to prepare polymer dispersions [3]:

- *Emulsion polymerisation*: in this case the monomer is emulsified in a nonsolvent (commonly water), usually in the presence of a surfactant. A water-soluble initiator is then added, whereupon particles of polymer form and grow in the aqueous medium as the monomer reservoir in the emulsified droplets is gradually used up.
- *Dispersion polymerisation*: this is usually applied to the preparation of nonaqueous polymer dispersions, and is commonly referred to as nonaqueous dispersion (NAD) polymerisation. In this case, the monomer, initiator, stabiliser (referred as the protective agent) and the solvent initially form a homogeneous solution, and the polymer particles precipitate when the solubility limit of the polymer is exceeded. The particles continue to grow until the monomer is consumed.
- *Suspension polymerisation*: in this case the monomer is emulsified in the continuous phase, using a surfactant or polymeric suspending agent. The initiator (which is oil-soluble) is dissolved in the monomer droplets and the droplets are converted into insoluble particles, but no new particles are formed.

In a paint film, the pigment particles need to undergo a process of deposition to the surfaces (which is governed by long-range forces such as van der Waals attractions and electrical double layer repulsion or attraction). This process of deposition is also affected by polymers (nonionic, anionic or cationic) which can enhance or prevent adhesion. Once the particles reach surface they must adhere strongly to the substrate; this process of adhesion is governed by short-range forces (chemical or nonchemical). The same applies to latex particles, which also undergo a process of deposition, adhesion and coalescence. The ability to control the flow characteristics of a paint is essential for its successful application [2]. The components of the paint interact with each other such that the final formulation becomes non-Newtonian and shows a complex rheological behaviour. The paint is usually applied in three stages: (i) transfer of the paint from a bulk container; (ii) transfer from the applicator (brush or roller) to the surface to form a thin, even film; and (iii) flow-out from the film surface, coalescence of the polymer particles (latexes) and loss of the medium by evaporation. During each of these processes the flow characteristics of the paint and its time relaxation produce interesting rheological responses. This shows that the formulation of a paint suspoemulsion requires an understanding of the various interactions between the pigment particles, the latex, and other components in the paint such as rheology modifiers (thickeners) and colours.

11.2.1
Suspoemulsions in Sunscreens and Colour Cosmetics

The formulation of suspoemulsions for sunscreens and colour cosmetics remains a challenge for the chemist due to the complex interactions between the particles and droplets that may result in heteroflocculation [4]. One of the main challenges here is to ensure that the small submicron particles remain individually dispersed in the formulation in order to achieve maximum UV protection for sunscreens and optimum colour properties for make-up products. To achieve maximum dispersion it is necessary to add an optimum wetting agent that can disperse the aggregates and agglomerates into single particles. It is essential to wet both the external and internal surface of the aggregates and agglomerates, and this process is aided by the application of mechanical energy that can be supplied, for example, by high-speed mixers, bead milling, and ultrasonics. In order to maintain the resulting submicron particles as individual units it is necessary to use an effective dispersing agent that provides an effective repulsive barrier between the particles. In addition, the dispersing agent can prevent interaction with the emulsion droplets, thus eliminating any possibility of heteroflocculation. A brief summary of how this can be achieved when using pigments is provided in the following sections.

Pigments are the primary ingredient of any colour cosmetic, and the way in which these particulate materials are distributed within the product will determine many aspects of product quality, including not only its functional activity (colour, opacity, UV protection) but also its stability, rheology, and skin feel. Currently, several colour pigments are used in cosmetic formulations, ranging from inorganic pigments (e.g., iron oxide) to organic pigments of various types. The formulation of these pigments in colour cosmetics requires a great deal of skill as the pigment particles are dispersed in an emulsion (O/W or W/O). The pigment particles may be dispersed in the continuous medium, in which case flocculation with the oil or water droplets should be avoided. In some cases the pigment may be dispersed in an oil, which is then emulsified in an aqueous medium. Several other ingredients might then be added (e.g., humectants, thickeners and preservatives), but the interaction between the various components may then become very complex.

Although particulate distribution depends on many factors including particle size and shape, surface characteristics, processing and other formulation ingredients, ultimately it is determined by the interparticle interactions. The fundamental principles of preparing pigment dispersions (as described briefly at this point) include wetting, dispersion (or wet milling, including comminution), and stabilisation. In the following sections, dispersion stability for both aqueous and nonaqueous media will be outlined, as will the interactions with other formulation ingredients when the particulate is incorporated within a suspoemulsion.

The process of wetting involves replacing the solid/vapour interface (with interfacial tension γ_{SV}) with a solid/liquid interface (with interfacial tension γ_{SL}). Wetting can be described in equilibrium thermodynamics in terms of the contact angle θ by Young's equation at the wetting line [5].

$$\gamma_{SV} = \gamma_{SL} + \gamma_{LV}\cos\theta \tag{11.1}$$

$$\cos\theta = \frac{\gamma_{SV} - \gamma_{SL}}{\gamma_{LV}} \tag{11.2}$$

The energy required to achieve dispersion wetting, W_d is given by the product of the external area of the powder, A and the difference between γ_{SL} and γ_{SV},

$$W_d = A(\gamma_{SL} - \gamma_{SV}) \tag{11.3}$$

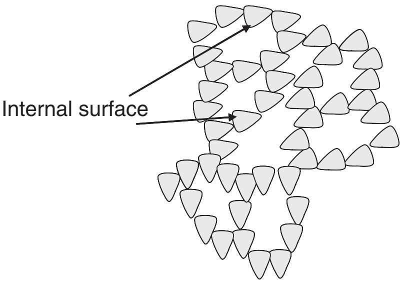

Figure 11.2 Schematic representation of an agglomerate.

Using Young's equation,

$$W_{\mathrm{d}} = -A\gamma_{\mathrm{LV}} \cos\theta \tag{11.4}$$

Thus, wetting of the external surface of the powder depends on the liquid surface tension and the contact angle. If $\theta < 90°$, $\cos\theta$ is positive and the work of dispersion is negative – that is, wetting will be spontaneous.

For agglomerates (as represented in Figure 11.2), which are found in all powders, wetting of the internal surface between the particles in the structure requires liquid penetration through the pores. Assuming that the pores behave as simple capillaries of radius r, Δp is given by the following equation:

$$\Delta p = \frac{2\gamma_{\mathrm{LV}} \cos\theta}{r} \tag{11.5}$$

In order for liquid penetration to occur, Δp must be positive and hence θ should be less than 90°.

The maximum capillary pressure is obtained when $\theta = 0$ and Δp is proportional to γ_{LV}, which means that a high γ_{LV} is required. Thus, to achieve wetting of the internal surface a compromise is needed since the contact angle only goes down as γ_{LV} goes down. Hence, there is a need to make θ as close as possible to 0 while not having a too- low liquid surface tension.

The rate of penetration of a liquid by a distance l through capillaries with radius r has been described by the Rideal–Washburn equation,

$$\frac{\mathrm{d}l}{\mathrm{d}t} = \frac{r\gamma_{\mathrm{LV}} \cos\theta}{4\eta l} \tag{11.6}$$

where η is the viscosity of the liquid.

Integration of Equation (11.6) gives,

$$l^2 = \left(\frac{r\gamma_{\mathrm{LV}} \cos\theta}{2\eta}\right) t \tag{11.7}$$

Equation (11.7) shows that a plot of l^2 versus t gives a straight line, and this forms the basis of measuring the contact angle on the surface of a powder, as will be discussed below.

For an agglomerate, the liquid pathway through the pores is complex and a simple radius cannot be used; in this case a tortuosity factor k must be introduced in Equation (11.7),

$$l^2 = \frac{r\gamma_{\mathrm{LV}} \cos\theta}{2\eta k^2} t \tag{11.8}$$

where $k = 1$ for cylindrical capillaries, though for a more complex pathway it can reach values as high as 2.5.

The most effective wetter will be the one that gives $\theta = 0°$ at the lowest concentration.

For $\theta = 0°$ or $\cos\theta = 1$, γ_{SL} and γ_{LV} must be as low as possible, and this requires a quick reduction of γ_{SL} and γ_{LV} under dynamic conditions during powder dispersion (this reduction should normally be achieved in less than 20 s). This requires a rapid adsorption of the surfactant molecules both at the L/V and S/L interfaces. It should be noted that a reduction in γ_{LV} is not always accompanied by a simultaneous reduction of γ_{SL}, and hence it is necessary to have information on both interfacial tensions, which means that measurement of the contact angle is essential in the selection of wetting agents. Measurements of γ_{SL} and γ_{LV} should be carried out under dynamic conditions (i.e., at very short times). In the absence of such measurements, the sinking time described above could be applied as a guide for wetting agent selection.

To achieve rapid adsorption, the wetting agent should be either a branched chain with central hydrophilic group or a short hydrophobic chain with hydrophilic end group. The most commonly used wetting agent for hydrophobic solids in aqueous media is Aerosol OT (diethylhexyl sulphosuccinate). This molecule has a low critical micelle concentration (cmc) of 0.7 g dm^{-3}, above which the water surface tension is reduced to ~25 mN m^{-1} in less than 15 s. Several nonionic surfactants (e.g., alcohol ethoxylates) can also be used as wetting agents; these molecules consist of a short hydrophobic chain (mostly C_{10}) which is also branched, and a medium chain polyethylene oxide (PEO) that mostly consists of six EO units or fewer. These molecules also reduce the dynamic surface tension within a short time (<20 s), and have reasonably low cmc-values. In all cases, the minimum amount of wetting agent should be used to avoid interference with the dispersant added (the latter is required to maintain colloid stability during dispersion and on storage).

The above-mentioned wetting agents consist of small molecules and are seldom effective in stabilising suspensions against flocculation, due to the small energy barrier produced by these molecules. For an effective stabilisation of the suspension against flocculation, a dispersing agent is required that will normally replace the wetting agent at the S/L interface and produce an effective repulsive barrier on close approach of the particles. This can be achieved in two main ways, by either electrostatic repulsion [6, 7] or steric repulsion [8], as illustrated in Figure 11.3a,b (or with a combination of the two; see Figure 11.3c).

The efficiency of steric stabilisation depends on both architecture and the physical properties of the stabilising molecule. Steric stabilisers should have an adsorbing anchor with a high affinity for the particles and/or be insoluble in the medium. The stabiliser should be soluble in the medium and highly solvated by its molecules. For aqueous or highly polar oil systems, the stabiliser block can be ionic or hydrophilic

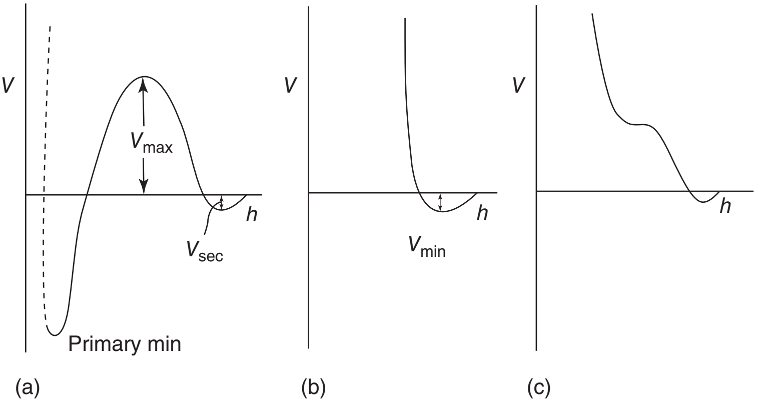

Figure 11.3 Energy-distance curves for three stabilisation mechanisms: (a) electrostatic; (b) steric and (c) electrosteric.

(e.g., polyalkylene glycols), and for oils it should resemble the oil in character. In the case of silicone oils, silicone stabilisers are best, while other oils could use a long-chain alkane, fatty ester or polymers such as poly(methylmethacrylate) (PMMA) or polypropylene oxide (PPO).

Various types of surface–anchor interactions are responsible for the adsorption of a dispersant to the particle surface. These include: ionic or acid/base interactions; sulphonic acid, carboxylic acid or phosphate with a basic surface (e.g., alumina); amine or quaternary with an acidic surface (e.g., silica); H-bonding; surface esters, ketones, ethers, hydroxyls; multiple anchors-polyamines and polyols (H-bond donor or acceptor) or polyethers (H-bond acceptor). Polarizing groups (e.g., polyurethanes) can also provide sufficient adsorption energies and, in nonspecific cases, lyophobic bonding (via van der Waals attractions) driven by insolubility (e.g., PMMA). It is also possible to use chemical bonding, for example by reactive silanes.

For relatively reactive surfaces, specific ion pairs may interact to produce particularly good adsorption to a powder surface. An ion pair may even be formed *in situ*, particularly if in a low-dielectric medium. Some surfaces are actually heterogeneous and can have both basic and acidic sites, especially near the isoelectric point. Although hydrogen bonding is weak, it is particularly important for polymerics which may have multiple anchoring.

The adsorption strength is measured in terms of the segment/surface energy of adsorption χ^s. The total adsorption energy is given by the product of the number of attachment points n and χ^s. For polymers, the total value of $n\chi^s$ can be sufficiently high for strong and irreversible adsorption, even though the value of χ^s may be small (less than $1\,kT$, where k is the Boltzmann constant and T is the absolute temperature). However, this situation may be inadequate, particularly in the presence of an appreciable concentration of wetter and/or in the presence of other surfactants used as adjuvants. If the χ^s of the individual wetter and/or other surfactant molecules is higher than the χ^s of one segment of the B chain of the dispersant, these small molecules can displace the polymeric dispersant particularly at high wetter concentrations and/or the presence of other surfactant molecules, and this could result in flocculation of the suspension. It is, therefore, essential to ensure that the χ^s per segment of the B chain is higher than that of wetter and/or surfactant adsorption, and that the wetter concentration is not excessive.

In order to optimise the steric repulsion, the steric potential as expressed by Napper can be considered [8]:

$$V(h) = 2\pi kTR\Gamma^2 N_{\text{Av}} \left[\frac{V_{\text{p}}^2}{V_{\text{s}}}\right] [0.5 - \chi] \left(1 - \frac{h}{2\delta}\right)^2 + V_{\text{elastic}} \tag{11.9}$$

where k is the Boltzmann constant, T is temperature, R is the particle radius, Γ is the adsorbed amount, N_{Av} is Avogadro's constant, V_{p} is the specific partial volume of the polymer, V_{s} the molar volume of the solvent, χ is the Flory–Huggins parameter, and δ is the maximum extent of the adsorbed layer. V_{elastic} takes account of the compression of polymer chains on close approach.

It is instructive to examine the terms in this relationship:

- The adsorbed amount Γ: Higher adsorbed amounts will result in more interaction/repulsion.
- Solvent conditions as determined by χ, the Flory–Huggins chain–solvent interaction parameter: Two very distinct cases emerge; a maximum interaction is apparent on overlap of the stabilising layers when the chain is in good solvent conditions ($\chi < 0.5$). Osmotic forces cause solvent to move into the highly concentrated overlap zone, forcing the particles apart. If $\chi = 0.5$, a θ-solvent, the steric potential goes to zero and for poor solvent conditions ($\chi > 0.5$) the steric potential becomes negative and the chains will attract, enhancing flocculation. It should be noted that a poorly solvated dispersant can enhance flocculation/aggregation.
- Adsorbed layer thickness δ: The steric interaction starts at $h = 2\delta$ as the chains begin to overlap and increases as the square of the distance. Here, the important point is not the size of the steric potential but rather the distance h at which it begins.
- The final interaction potential is the superposition of the steric potential and the van der Waal's attractions, as shown in Figure 11.3b.

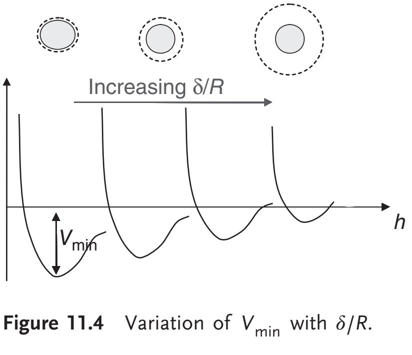

Figure 11.4 Variation of V_{min} with δ/R.

For sterically stabilised dispersions, the resulting energy–distance curve often shows a shallow minimum $V_{\min}$ at particle–particle separation distance h comparable to twice the adsorbed layer thickness δ. For a given material, the depth of this minimum depends upon the particle size R, and adsorbed layer thickness δ; consequently, $V_{\min}$ decreases with increase in δ/R, as illustrated in Figure 11.4. This occurs because, as the layer thickness is increased the van der Waals attraction is weakened, so that the superposition of attraction and repulsion will have a smaller minimum. For very small steric layers, $V_{\min}$ may become deep enough to cause weak flocculation that would result in a weak attractive gel. Hence, it becomes apparent exactly how the interaction energies can also determine the dispersion rheology.

In contrast, if the layer thickness is too large the viscosity will also be increased as a result of repulsion; this occurs due to the much higher effective volume fraction ϕ_{eff} of the dispersion compared to the core volume fraction. If the effective volume fraction of particles plus dispersant layer is calculated geometrically, it can be seen to depend on the thickness of that adsorbed layer, as illustrated in Figure 11.5. The effective volume fraction increases with a relative increase of the dispersant layer thickness. Even at 10% volume fraction, a maximum packing ($\phi = 0.67$) is soon reached, with an adsorbed layer thickness that is comparable to the particle radius. In this case, overlap of the steric layers will result in significant increases in viscosity. Such considerations may help to explain why solids loading can be severely limited, especially with small particles. In practice, solids loading curves can be used to characterize the system, and take the form of those illustrated in Figure 11.6

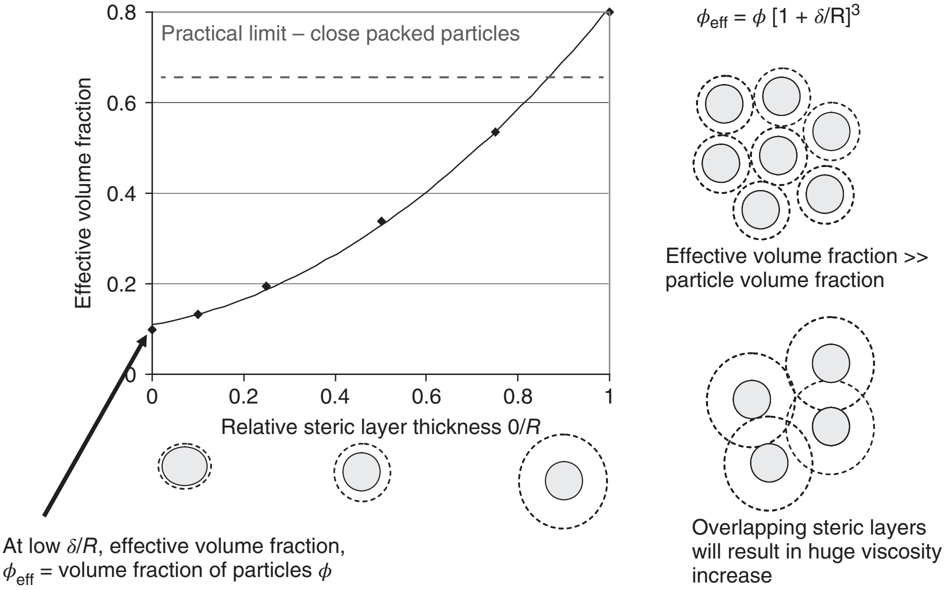

At low δ/R, effective volume fraction, ϕ_{eff} = volume fraction of particles ϕ

Effective volume fraction >> particle volume fraction

Overlapping steric layers will result in huge viscosity increase

Figure 11.5 Schematic representation of the effective volume fraction.

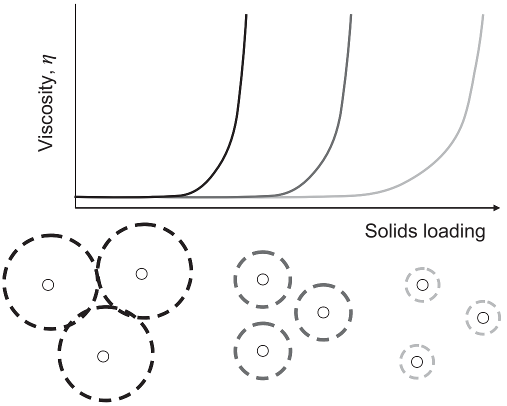

Figure 11.6 Dependence of solids loading on adsorbed layer thickness.

A higher solids loading may be achieved with thinner adsorbed layers, but this may also result in interparticle attraction resulting in particle aggregation. Clearly, a compromise is needed such that an appropriate steric stabiliser is chosen for the particle size of the pigment.

Some of the most frequently used dispersants for aqueous media are nonionic surfactants, the most common being alcohol ethoxylates R-O-$(CH_2{-}CH_2{-}O)_n$-H (e.g., $C_{13/15}(EO)_n$, where n is 7, 9, 11, or 20). These nonionic surfactants are not the most effective dispersants as adsorption by the $C_{13/15}$ chain is not very strong. Consequently, in order to enhance the adsorption on hydrophobic surfaces a PPO chain is introduced in the molecule, giving R–O–$(PPO)_m$–$(PEO)_n$–H. These nonionic surfactants can also be used for the stabilisation of polar solids in nonaqueous media; in this case the PEO chain adsorbs onto the particle surface leaving the alkyl chains in the nonaqueous solvent. Provided that these alkyl chains are sufficiently long and strongly solvated by the molecules of the medium, they can provide sufficient steric repulsion to prevent flocculation.

A better dispersant for polar solids in nonaqueous media is poly(hydroxystearic acid) (PHS), which has a molecular weight in the region of 1000–2000 Da. In the case of PHS, the carboxylic group adsorbs strongly onto the particle surface, leaving the extended chain in the nonaqueous solvent. With most hydrocarbon solvents the PHS chain is strongly solvated by its molecules and an adsorbed layer thickness in the region of 5–10 nm can be produced. This layer thickness prevents any flocculation, and the suspension can remain fluid up to a high solids content. The most effective dispersants are those of the A-B, A-B-A block and BA_n types. A schematic representation of the architecture of block and graft copolymers is shown in Figure 11.7.

In this case, B (the "anchor" chain, in red) is chosen to be highly insoluble in the medium and has a strong affinity to the surface. Examples of B chains for hydrophobic solids are polystyrene (PS), PMMA, PPO or alkyl chains, provided that these have several attachments to the surface. The A-stabilising (blue) chain must be soluble in the medium and strongly solvated by its molecules. In addition,

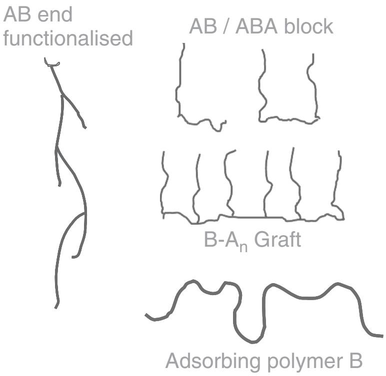

Figure 11.7 Schematic representation of the architecture of block and graft copolymers.

the A chain/solvent interaction should be strong, giving a Flory–Huggins χ-parameter <0.5 under all conditions. Examples of A chains for aqueous media are PEO, polyvinyl alcohol (PVA) and polysaccharides (e.g., polyfructose), whereas for nonaqueous media the A chain may be PHS.

Some of the most commonly used A-B-A block copolymers for aqueous dispersions are those based on PEO (A) and PPO (B). Several molecules of PEO-PPO-PEO are available with various proportions of PEO and PPO; for these materials, the commercial name is followed by a letter L (Liquid), P (Paste) or F (Flake), and this is followed by two numbers that represent the composition. The first digits represent the PPO molar mass and the last digit represents the % PEO. Examples of this are: F68 (PPO molecular mass 1508–1800 + 80% or 140 mol EO), and L62 (PPO molecular mass 1508–1800 + 20% or 15 mol EO). In many cases two molecules with high and low EO contents are used together to enhance the dispersing power.

An example of a BA$_n$ graft copolymer is based on PMMA backbone (with some polymethacrylic acid) onto which are grafted several PEO chains with an average molecular weight of 750 Da (Atlox 4913); this is a very effective dispersant, particularly for high solids-content suspensions. The graft copolymer is adsorbed strongly onto hydrophobic surfaces with several attachment points along the PMMA backbone, and a strong steric barrier is obtained by the highly hydrated PEO chains in aqueous solutions.

Another effective graft copolymer is hydrophobically modified inulin; this is a linear polyfructose chain A (with degree of polymerisation >23) onto which several alkyl chains have been grafted. The polymeric surfactant adsorbs onto several alkyl chains via multipoint attachment.

The optimisation of functionality can often depend heavily on the state of dispersion. The opacity and UV attenuation of TiO_2, for example, is heavily dependent on particle size [9] (Figure 11.8). A TiO_2 pigment, designed to provide opacity in a formulation, will not realize its maximum "hiding" power unless it is dispersed and remains dispersed in its constituent particles of 200–300 nm. On the other hand, a UV-attenuating grade of TiO_2 must be dispersed down to its primary

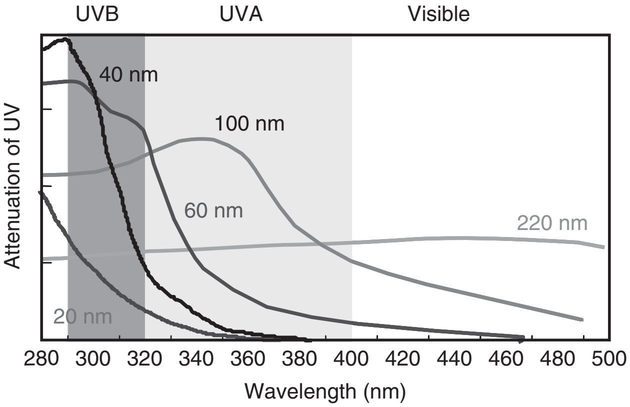

Figure 11.8 Attenuation of UV versus wavelength for TiO_2 dispersion.

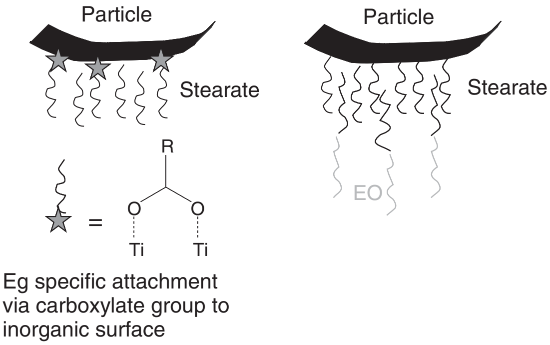

Figure 11.9 Schematic representation of specific interaction of stearate to TiO_2 (a) and effect of addition of alcohol ethoxylate (b).

particle size of 50–100 nm in order to be optimally functional as a sunscreen agent. Notably, both materials are supplied as powders (to aid their handling) and have similar agglomerate sizes of several microns.

As mentioned above, the primary task is to obtain a complete wetting of the powder, with both the external and internal surfaces of the agglomerates being adequately wetted by using a suitable surfactant. For aqueous dispersions, the above-mentioned wetting agents such as Aerosol OT or alcohol ethoxylates are generally efficient. For hydrophilic pigments in oil, coated particles (with a hydrophobic coating) can be used or, alternatively, sodium stearate which binds strongly to the hydroxyl surface. A schematic representation for the binding of stearate to hydrophilic TiO_2 is shown in Figure 11.9, whereby the pigment is easily wetted and dispersed in oils. The data in this figure also show the effect of adding an alcohol ethoxylate to the coated TiO_2, which can then be dispersed in an aqueous medium.

This process is followed by complete dispersion and/or comminution and adequate stabilisation of the resultant single particles, as illustrated in Figure 11.10.

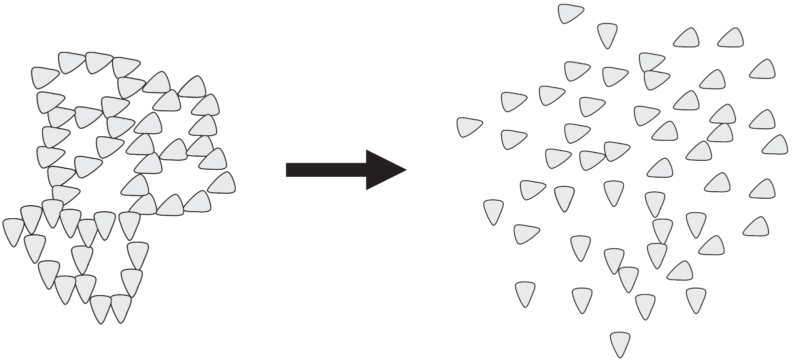

Figure 11.10 Schematic representation of the dispersion process.

The simple mixing of inorganic powders can produce a fluid dispersion even at high solids content. However, this is not necessarily an indication of a ''well-dispersed'' material and, indeed, a particle size analysis (and for UV attenuators, spectral analysis) demonstrates that the particle dispersion is not optimised. Particulate powders are supplied in an aggregated state, but must be milled down to their individual units in order to provide their designed function. This process must allow transport of the dispersant to the particle surface, and its adsorption there. Finally, the dispersion must remain stable to dilution or to the addition of further formulation components. The presence of a suitable dispersant/stabiliser at the correct level can be critical in achieving a usable and stable dispersion and preventing reaggregation on standing. In practice, the dispersion chemist may use some simple laboratory tools to assess dispersion quality and arrive at an appropriate dispersion recipe. Having assessed wetting as previously described, a dispersant demand curve will often be plotted in order to establish the optimum dispersant loading. The pigment is processed (by milling or grinding) in the presence of the carrier oil and wetting agent, with varying levels of dispersant. The state of dispersion can be effectively monitored by rheology and/or some functional measurement (e.g., colour strength, UV attenuation). The results of some fine-particle TiO_2 in isopropyl isostearate as the dispersing fluid and PHS as the dispersant are shown in Figure 11.11 [10].

Dispersions were produced at 30 wt% solids so that they could be prepared on a bead mill at all dispersant loadings, and their UV attenuation properties compared. Zero shear viscosities give an indication of the interparticle interactions, and were found to be minimal at around 5% dispersant. UV attenuation was used as an indicator of particle size.

The unmilled dispersions appeared very fluid, but UV measurement revealed poor attenuation properties that implied the particles were still aggregated; subsequently, the solid particles quickly settled out of suspension to form a sediment at the bottom of the beaker. An improvement of the UV attenuation properties, along with an increase in viscosity, was observed upon milling. The aggregates were broken down into their constituent particles in the mill but, in the absence of

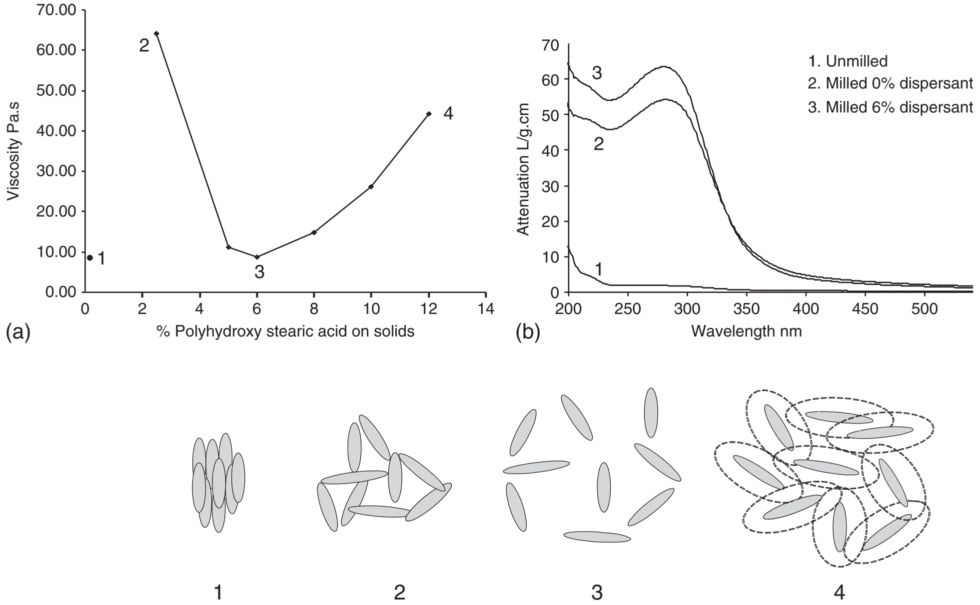

Figure 11.11 (a,b) Zero shear viscosity (dispersant demand curve), UV attenuation curves, and a schematic of the milling process.

a dispersant, they quickly reaggregated by van der Waals attractions in a more open structure, which caused the mill to block. Further improvements in UV properties were observed when the dispersion was milled in the presence of the dispersant, but the viscosity remained high.

The addition of sufficient dispersant allowed the particles to disperse to single particulates which were well stabilised and the viscosity fells This was an optimised dispersion, and the UV properties were well developed. On adding further dispersant, however, the particles gained an extended stabilisation layer that caused a potential overlap of the stabilisation layers sufficient to produce a weak repulsive gel. The viscosity again rose and the dispersion had a measurable yield value. The UV properties were still well developed but the solids loading became very limited.

These dispersant demand curves and particle size monitoring, in combination with solids loading curves, serve as very useful tools for optimising pigment dispersion in practice.

When colour cosmetic pigments are added to O/W or W/O emulsions, the resulting system is referred to as a suspoemulsion. The particles can be in either the internal or external phases, or both, as illustrated in Figure 11.12. An understanding of competitive interactions is also important when optimising the formulation stability and performance of these materials.

Possible instabilities which might arise in the final formulations are: (i) heteroflocculation of particles with differing charges; (ii) electrolyte intolerance of electrostatically stabilised pigments; (iii) competitive adsorption/desorption of a

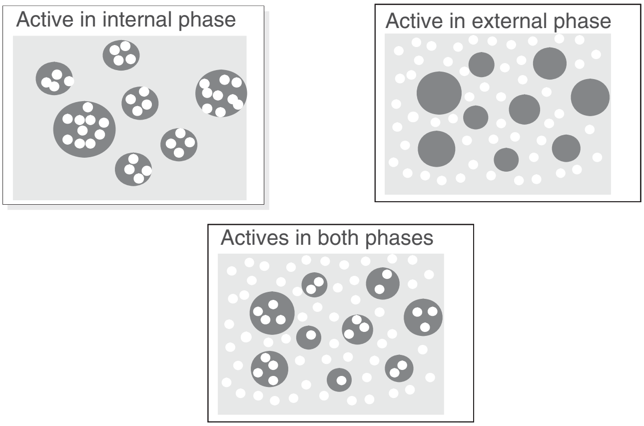

Figure 11.12 Schematic representation of suspoemulsions.

weakly anchored stabiliser (homoflocculation and emulsion coalescence); and (iv) interaction between thickeners and charge-stabilised pigments.

Several steps can be made to improve the stability of suspoemulsions, and these are in fact very similar to the steps used for optimal steric stabilisation:

- The use of a strongly adsorbed (''anchored'') dispersant, for example by multipoint attachment of a block or graft copolymer.
- The use of a polymeric stabiliser for the emulsion (also with multipoint attachment).
- The preparation of suspensions and emulsions separately, allowing sufficient time for complete adsorption (equilibrium).
- The use of low shear when mixing the suspension and emulsion.
- The use of rheology modifiers.
- Increasing the dispersant and emulsifier concentrations to ensure that the lifetime(s) of any bare patches produced during collision is/are very short.
- Using the same molecule for the emulsifier and the dispersant.
- Reducing the emulsion droplet size.

11.3
Suspoemulsions in Agrochemicals

With suspoemulsions, two active ingredients are formulated together, which not only offers convenience to the farmer but also may result in synergistic biological efficacy. As a consequence, a wider spectrum of disease control may be achieved, particularly when using many fungicides and herbicides. For many suspoemulsions an adjuvant is also added that enhances biological efficacy.

1) Practical agrochemical suspoemulsions: Chlorothalonil (density $\rho = 1.85$ g cm^{-3}) and dichlobutrazol (density $\rho = 1.25$ g cm^{-3}) suspensions were

prepared by bead milling (using Synperonic NP1800), nonyl phenol with 13 mol PPO and 27 mol PEO. Tridemorph (density $\rho = 0.87\ \mathrm{g\,cm^{-3}}$) emulsions are prepared using the same surfactants (emulsification was carried out using a Silverson mixer).

2) Model suspoemulsions of polystyrene latex (mean volume diameter 1.84 μm) were prepared using the surfactant-free method, and then stabilised with Synperonic PE P94 (an ABA block of PEO-PPO-PEO with 47 PPO units and 42 PEO units) and isoparaffinic O/W emulsion (stabilised with Synperonic PE L92 with 47 PPO units and 16 PEO units).
3) Model suspoemulsions of polystyrene containing grafted PEO chains (with molecular weight ~2000 Da) were prepared using the ‘‘aquersamer method’’ having a Z-average particle radius of 310 ± 10 nm and hexadecane-in-water emulsions (stabilised with Synperonic PE L92) having a Z-average particle radius of 310 ± 10 nm.

The particle size was determined using dynamic light scattering (also termed photon correlation spectroscopy; PCS), using a Malvern PCS instrument. The equilibrium sediment and cream volumes were recorded using measuring cylinders at room temperature, and viscoelastic measurements were made using a Bohlin VOR rheometer.

Assuming that a stable suspoemulsion (in the colloid sense) could be prepared – for example, by using a polymeric dispersant and emulsifier – the creaming and/or sedimentation behaviour of the suspoemulsion showed different patterns depending on the density difference between the oil droplets and suspension particles, as well as the total volume fraction ϕ of the whole systems.

The above behaviour could be illustrated by using agrochemical suspoemulsions consisting of an oil (namely tridemorph, see above) and two different suspensions, namely dichlobutrazol ($\rho = 1.25\ \mathrm{g\,cm^{-3}}$) and chlorothalonil ($\rho = 1.85\ \mathrm{g\,cm^{-3}}$). To ensure colloid stability and an absence of heteroflocculation, both the emulsion and suspension were prepared using an A-B-C block copolymer (Synperonic NPE 1800) which consisted of an anchor chain (B-C) of propylene oxide (13 mol) and nonyl phenol and a stabilising chain of PEO (23 mol). Synperonic NPE 1800 is an excellent emulsifier for tridemorph, and is also an excellent dispersant for both dichlobutrazol and chlorothalonil. The colloid stability of both emulsion and suspensions was confirmed by optical microscopy, which showed no coalescence of the emulsion or flocculation of the suspensions In addition, when mixing the emulsion and suspension there was no heteroflocculation. The suspoemulsions were prepared by simple mixing of the emulsion and suspension, keeping the total volume fraction ϕ constant while varying the ratio of suspension to emulsion. Two ϕ-values were investigated (<0.2 and >0.2), and a comparison was made between systems with small density difference (dichlobutrazol/tridemorph) and large density difference (chlorothalonil/tridemorph). The results are illustrated in Figures 11.2–11.4.

When the density difference between the suspension particles and emulsion droplets was not large and $\phi < 0.2$, the emulsion creamed and the suspension

Low volume fractions $\phi < 0.2$

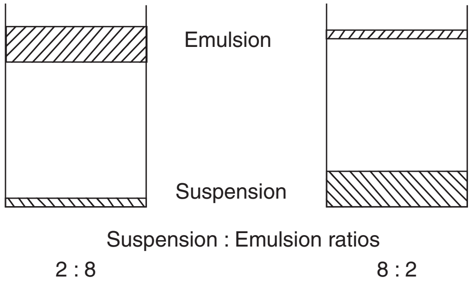

Figure 11.13 Chlobutrazol/tridemorph ($\phi < 0.2$).

High volume fractions $\phi > 0.2$

WHEN ρ mixture < 1 the emulsion and the suspension both cream
WHEN ρ mixture > 1 the emulsion and the suspension both sediment

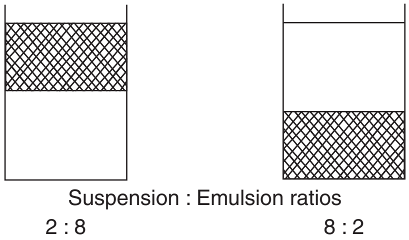

Figure 11.14 Chlobutrazol/tridemorph ($\phi > 0.2$).

sedimented separately (Figure 11.13). When the density difference between the suspension particles and emulsion droplets was small but $\phi > 0.2$, the system formed a cream layer when the suspension : emulsion ratio was 2 : 8, and formed a sediment layer when the ratio was 8 : 2 (Figure 11.14). When the density difference between the suspension particles and emulsion droplets was large, then the average density of the suspension particle/emulsion droplet was > 1, and in this case sedimentation was observed when the ratio was 2 : 8, though some creaming occurred when the ratio was 8 : 2 (Figure 11.15).

The above-described creaming/sedimentation behaviour indicated some interaction between the emulsion droplets and suspension particles.

One particularly useful method of illustrating the interactions in suspoemulsions is to compare the total observed sediment plus cream height with that based on simple additivity. This is illustrated for chlorothalonil/tridemorph suspoemulsions in Figure 11.16, from which it can be observed that the sediment + cream heights were smaller than would be expected from simple additivity. It is possible that the small suspension particles had become trapped between the larger oil droplets in the cream layer, and that the small suspension particles had become entrapped between the larger suspension particles. Some deformation of the oil droplets may also have occurred in the sedimented layer.

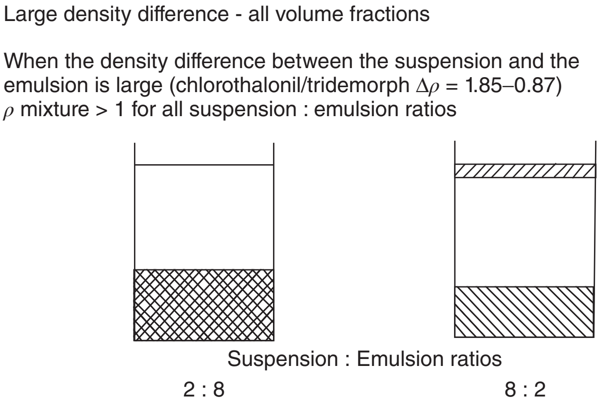

Figure 11.15 Chlorothalonil/tridemorph (all volume fractions).

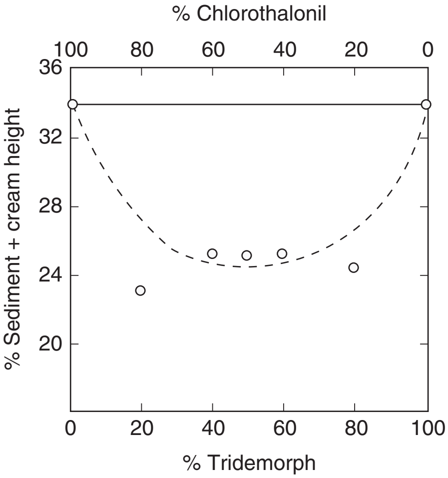

Figure 11.16 Comparison of experimental, ------- and predicted (based on additivity), sediment + cream heights for chlorothalonil/tridemorph suspoemulsions.

Optical microscopic investigations of some other suspoemulsions showed heteroflocculation, but this could be reduced or eliminated by using Atlox 4913 (an acrylic graft copolymer of PMMA backbone and PEO Chains), as discussed below.

The use of strongly "anchored" dispersants and emulsifiers is crucial for reducing the interaction between the particles and droplets. The interaction can also be significantly reduced by the addition of rheology modifiers such hydroxyethyl cellulose (HEC) or xanthan gum.

The above-described thickeners produce a "three-dimensional" gel network by the overlap of the polymer coils of HEC or the double helices of xanthan gum. Apart from their effect in reducing creaming and sedimentation by producing a high residual viscosity (at low shear rates), these polymers will also prevent the trapping of oil droplets into the suspension and of suspension particles into the emulsion.

Heteroflocculation results from the competitive adsorption between the dispersant and emulsifier, particularly when these are not strongly anchored to the surfaces. The displacement of some or all of the dispersant by the emulsifier, and vice versa, may result in an attraction between the particles and droplets and the repulsive barrier is weakened in both cases. If the particles are partially wetted by the oil they may reside at the O/W interface if the oil droplets are sufficiently large.

The above processes of attraction may continue for long periods of time such that, ultimately, the suspoemulsion becomes physically unstable. Any flocculation will result in an entrapment of the liquid between the particles in the floc structure, and this causes a significant increase in the viscosity of the system.

Competitive adsorption may be reduced by using the same surfactant for dispersing the solid and emulsifying the oil. This was demonstrated above by using Synperonic NPE 1800; however, as this molecule shows some reversible adsorption, the interaction between the particles and droplets is not completely prevented.

A better method for reducing competitive adsorption is to use a polymeric surfactant that is strongly and irreversibly adsorbed onto the suspension particles and emulsion droplets, such as the graft copolymer of PMMA backbone with several PEO chains grafted onto the backbone [9]. This graft copolymer (Atlox 4913), which has a weight average molecular weight of ~20 000 Da, adsorbs strongly and irreversibly onto hydrophobic particles such as polystyrene latex and most agrochemical suspensions. By using the above graft copolymer as dispersant, and an A-B-A block copolymer of PEO (A) and PPO (B) as emulsifier, very stable suspoemulsions can be obtained. A good polymeric stabiliser is INUTEC® SP1 (ORAFTI, Belgium); this consists of an inulin (linear polyfructose with degree of polymerisation >23) chain onto which several alky chains are grafted [10]. This polymeric surfactant adsorbs onto hydrophobic particles and emulsion droplets by multipoint attachment with several alky groups, leaving strongly hydrated loops and tails of polyfructose that provide an effective steric barrier.

The coalescence of emulsion droplets on storage accelerates the instability of the suspoemulsion. Large oil droplets can induce heteroflocculation with the suspension particles residing at the O/W interface. Emulsion coalescence can be reduced by one or more of the following methods: (i) a reduction of droplet size by using high-pressure homogenisation; (ii) the use of an effective emulsion stabiliser such as INUTEC SP1; and (iii) the incorporation of an oil-soluble polymeric surfactant such as Atlox 4912 (Arlacel P135 can be used in cosmetics), which is an A-B-A block copolymer of PHS (A) and PEO (B).

In order to produce a stable suspoemulsion of agrochemicals, the following criteria must be applied:

1) The use of a strongly adsorbed (‘‘anchored’’) dispersant by multipoint attachment of a block or graft copolymer.
2) The use of a polymeric stabiliser for the emulsion (also with multipoint attachment), for example INUTEC SP1.

3) Preparation of the suspension and emulsion separately, and allowing sufficient time for complete adsorption (equilibrium).
4) The use of low shear when mixing the suspension and emulsion.
5) When dissolving an active in an oil (e.g., with many agrochemicals), an oil should be chosen in which the suspension particles are insoluble, and the oil should not wet the particles.
6) Increasing the dispersant and emulsifier concentrations to ensure that the lifetime of any bare patches produced during collision is very short.
7) Reducing the emulsion droplet size by using high-pressure homogenisation. The smaller droplets are less deformable and coalescence is prevented. In addition, the accumulation of suspension particles at the O/W interface is prevented.
8) The use of a rheology modifier such as HEC or xanthan gum that produces a viscoelastic solution which prevents not only creaming or sedimentation but also entrapment of the oil droplets in between the suspension particles, or the suspension particles in between the emulsion droplets.
9) If possible, it is preferable to use a higher volume fraction of the oil when compared with the suspension. In many cases, flocculation occurs more rapidly at higher solid volume fractions. The emulsion oil phase volume can be increased by the incorporation of an inert oil.

When there is a need to prepare a suspoemulsion with a high volume fraction ϕ of suspension and emulsion (e.g., $\phi > 0.4$), it is preferable to emulsify the oil directly into a prepared suspension. In this case the suspension is prepared first (e.g., by bead milling), using the polymeric dispersant, and left to equilibrate for a sufficient time (preferably overnight) to ensure complete adsorption of the polymer. The polymeric emulsifier is then added and the oil is emulsified into the suspension concentrate (SC) using, for example a Silverson or UltraTurrax blender. Overmixing, which may result in orthokinetic (or shear) flocculation and dialatancy, must be avoided and the whole system should be cooled as much as possible during emulsification.

Crystallisation, which is by far the most serious instability problem with suspoemulsions (particularly with many agrochemicals), arises from the partial solubility of the suspension particles into the oil droplets. The process is accelerated at higher temperatures and also on temperature cycling. The smaller particles will have a higher solubility than their larger counterparts, due to the fact that the higher the curvature the higher the solubility, as described by the Kelvin equation [11],

$$S(r) = S(\infty)\exp\left(\frac{2\gamma V_{\mathrm{m}}}{rRT}\right) \tag{11.10}$$

where $S(r)$ is the solubility of a particle with radius r and $S(\infty)$ is the solubility of a particle with infinite radius (the bulk solubility), γ is the S/L interfacial tension, R is the gas constant, and T is the absolute temperature.

On storage, the smaller particles will dissolve in the oil and recrystallize on any larger particles which may be in the vicinity of the O/W interface. Some crystal habit modification may be produced and large plates or needles are formed which can reach several micrometers in size. Several procedures may be applied to inhibit recrystallisation:

1) Diluting the oil phase with another inert oil in which the particles are insoluble.
2) The use of a strongly adsorbed polymeric surfactant such as Atlox 4913 or INUTEC SP1 that prevents entry of the suspension particles into the oil droplets.
3) The addition of electrolytes in the continuous phase; this has the effect of enhancing the polymeric surfactant adsorption and thus preventing particle entry into the oil droplets.
4) The use of crystal growth inhibitors; for example, flat dye molecules which are insoluble in the oil are strongly adsorbed onto the particle surface, and this prevents particle entry into the oil droplets.
5) The use of analogues of the solid active ingredient (having the same basic structure) that are insoluble in the oil and become incorporated onto the surface of the solid particles.
6) The use of thickeners such as HEC and xanthan gum; this will increase the low shear rate viscosity of the medium and hence slow down the diffusion of the small particles, preventing their entry into the oil droplets. These thickeners can produce gels in the continuous phase that is viscoelastic, and this can prevent particle diffusion.

11.3.1

Model Suspoemulsion of Polystyrene Latex and Isoparaffinic Oil stabilised with Synperonic PE (PEO–PPO–PEO A-B-A Block Copolymer)

The interaction was investigated using viscoelastic measurements [12, 13]. As an illustration, Figure 11.17 shows typical plots of G^* (complex modulus), G' (storage or elastic modulus), G'' (loss or viscous modulus) and η' (dynamic viscosity) as a function of frequency (Hz) for 90% emulsion and 10% latex, both stabilised with Synperonic PE block copolymer. The results of Figure 11.17 were obtained at low strain amplitudes (i.e., in the linear viscoelastic region). Both, G^* and G' showed a rapid increase with increase in frequency above 0.1 Hz; however, G'' which was higher than G' at frequencies below 1 Hz began to decrease with an increase in frequency above 1 Hz. The dynamic viscosity showed a decrease with increase of frequency, as expected (shear thinning system).

A well-defined cross-over point ($G' = G''$) can be identified from which the relaxation time of the system can be calculated:

$$\tau = \frac{1}{\omega^*} \tag{11.11}$$

where ω^* is the characteristic frequency (rad s^{-1}) at the cross-over point. Note that $\omega = 2\pi\upsilon$, where υ is the frequency in hertz.

Similar results were obtained for other suspoemulsions containing various emulsion : latex ratios. The same trend was also obtained for the emulsion and

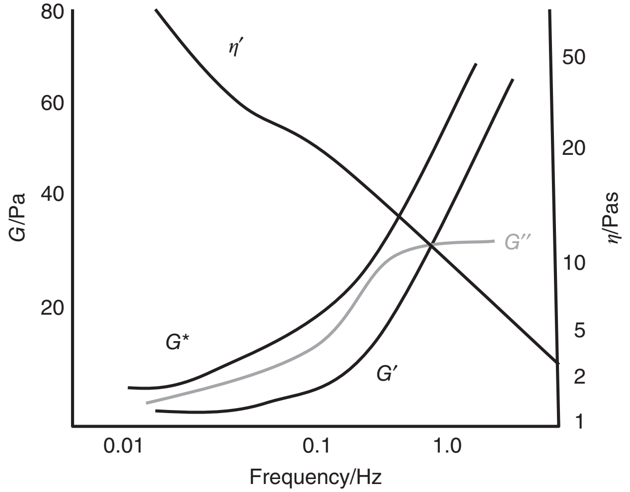

Figure 11.17 Variation of G^*, G', G'' and η' with frequency for a suspoemulsion of 90% isoparaffinic oil in water emulsion and 10% polystyrene latex.

latex dispersions alone. The addition of a latex to the emulsion caused a shift in τ values to higher frequencies, indicating a stronger interaction between the latex particles and the emulsion droplets.

Figure 11.18 shows the variation of G^*, G' and G'' at $\phi = 0.57$ and $\upsilon = 1$ Hz with % emulsion and latex in the suspoemulsion. The emulsion had much higher moduli than the latex at the same volume fraction. Although the emulsion had a VMD (0.98 μm) that was close to the latex (1.18 μm), the former was much more polydisperse than the latter. The much smaller emulsion droplets present may have accounted for the higher moduli of the emulsion when compared to the latex. As the

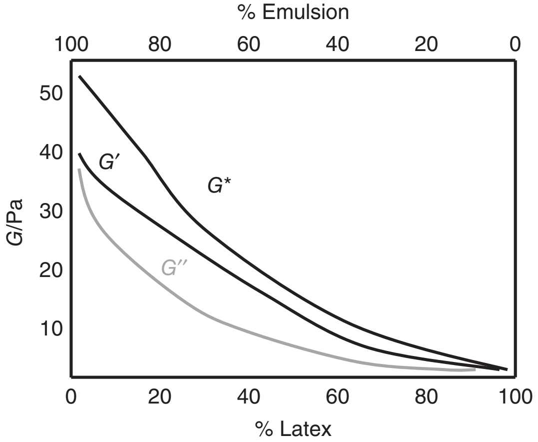

Figure 11.18 Variation of G^*, G' and G'' with % emulsion and latex; $\phi = 0.5$.

proportion of the latex in the suspoemulsion was increased, the moduli decreased. Replacement of the emulsion with latex would mean replacing a proportion of the smaller emulsion droplets with larger latex particles, and this would result in a reduction of the moduli values. It should be mentioned, however, that the mixture of emulsion and latex became relatively more elastic than viscous, indicating a stronger interaction between the emulsion droplets and the latex particles.

11.3.2
Model Systems of Polystyrene Latex with Grafted PEO Chains and Hexadecane Emulsions

It is clear from the above discussion that the interaction between suspension particles and emulsion droplets depends on the nature of the stabiliser used for the particles and droplets. For that reason, model systems were investigated whereby the latex particles contained grafted PEO chains (with no possible desorption) and the emulsion was based on hexadecane stabilised with Pluronic PE L92 (containing 20% PEO). The particle and droplet radii were very similar (315 and 280 nm, respectively) in order to avoid complications arising from the change in particle size distribution on mixing the suspension and emulsion.

Steady-state shear stress–shear rate curves were used to obtain the relative viscosity (η_r)-volume fraction (ϕ) relationship for the latex and emulsion. The results are shown in Figure 11.19 which also contains the theoretically predicted curve based on the Dougherty–Krieger equation [14],

$$\eta_r = \left[1 - \left(\frac{\varphi}{\varphi_\mathrm{p}}\right)\right]^{-[\eta]\varphi_\mathrm{p}} \tag{11.12}$$

where ϕ_p is the maximum packing fraction and $[\eta]$ is the intrinsic viscosity that is equal to 2.5 for hard-spheres. Two values for ϕ_p were used, namely 0.60 and 0.61 for the emulsion and latex, respectively. Reasonable agreement between the

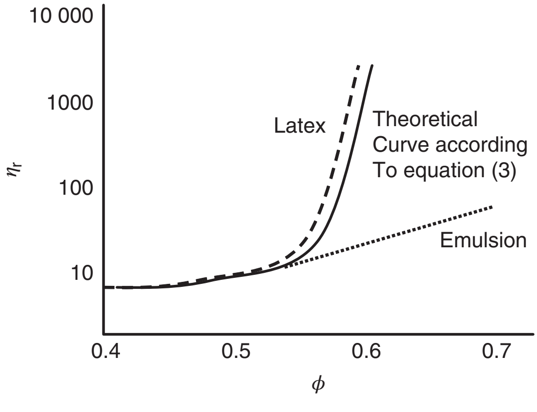

Figure 11.19 η_r–ϕ curves for latexes and emulsions.

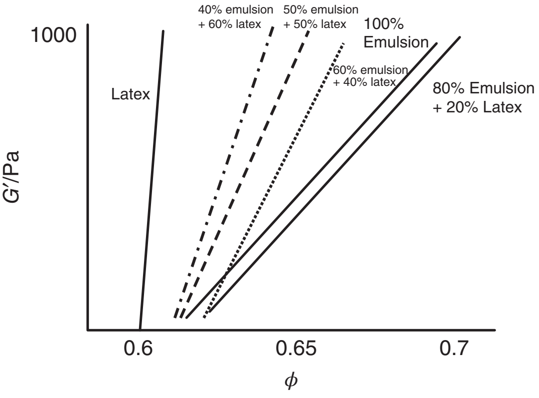

Figure 11.20 Log–log plots of G' versus ϕ for latexes, emulsions and their mixtures.

experimental η_r–ϕ curve and the theoretical curve based on Equation (11.12) for the latex dispersions was obtained, indicating that this system behaves as near hard-spheres. However, the results for the emulsion deviated from the theoretical curves as the emulsion droplets were deformable.

Figure 11.20 shows log–log plots of the elastic modulus G' (measured at low strain amplitudes to ensure the linear viscoelastic region and frequency of 1 Hz) versus volume fraction of the latex, emulsion and various mixtures of emulsion–latex systems. All results were similar for a volume fraction below ~0.62, indicating that the interactions between the emulsion droplets and latex particles were of the same nature, and both particles and droplets behaved as near hard-spheres. However, at $\phi > 0.62$, the behaviour of the latexes and emulsions differed significantly, as indicated by the much reduced slope of the log G'–log ϕ curve for the emulsions when compared with the latexes. Above this volume fraction the interaction between the emulsion droplets was quite high, but the system could reduce this interaction by deformation of the emulsion droplets. This situation was not possible with the latexes, however, where the particles were rigid. A similar behaviour was observed for the suspoemulsion when the percentage of emulsion in the mixture exceeded 60%; this implied that the behaviour of emulsions and suspoemulsions with >60% emulsion was close to its rheological behaviour in concentrated emulsions, and this has implications in the formulation of suspoemulsions.

The G'–ϕ curves can be analysed using the model suggested by Princen and Kiss [15], who assumed a system of cylinders arranged in a hexagonal array. When such an arrangement is strained, the total interface is increased; this creates a restoring force that is proportional to the interfacial tension γ. By using this model, Princen derived an expression relating the shear modulus G_o (which can be replaced by the high-frequency modulus G') to the volume fraction ϕ,

$$G' = a\left(\frac{\gamma}{R_{32}}\right)\varphi^{1/3}(\varphi - b) \qquad (11.13)$$

Table 11.1 Parameters of the fit of Equation (11.4) for the emulsion, latex, and their mixtures.

% Emulsion	$a\gamma/R_{32}$	b
100	9 896 ± 690	0.63 ± 0.01
80	9 900 ± 1700	0.63 ± 0.01
60	17 500 ± 2000	0.63 ± 0.03
50	20 700 ± 2200	0.63 ± 0.01
40	23 700 ± 2200	0.62 ± 0.02
20	~100 000	0.61 ± 0.01
0	~1 000 000	0.62 ± 0.02

where a and b are constants equal to 1.7 and 0.71, respectively. The origin of constant b is the value of the maximum packing of undistorted cylinders in the array. R_{32} is the average volume-to-surface ratio of the radius R (the Sauter radius).

For the latex–emulsion systems studied, R_{32} for the emulsion was constant and, due to the excess surfactant in the emulsion, γ was expected to be minimally dependent on the composition. The values of the parameters to fit the data of Figure 11.20 are listed in Table 11.1. The parameter b corresponds to the volume fraction at the onset of elasticity.

The mixture of latex and emulsion may be regarded as two elastic elements in series with the appropriate volume fractions,

$$\frac{1}{G_m} = \frac{f_e}{G_e} + \frac{(1 - f_e)}{G_L} \tag{11.14}$$

where G_m, G_e and G_L are the elastic moduli of the mixture, emulsion and latex, respectively, and f_e is the weight fraction of the emulsion in the mixture.

A plot of the linear lines of Figure 11.20 (which is equal to $a\gamma/R_{32}$) is shown in Figure 11.21, together with the predicted line based on Equation (11.14). The

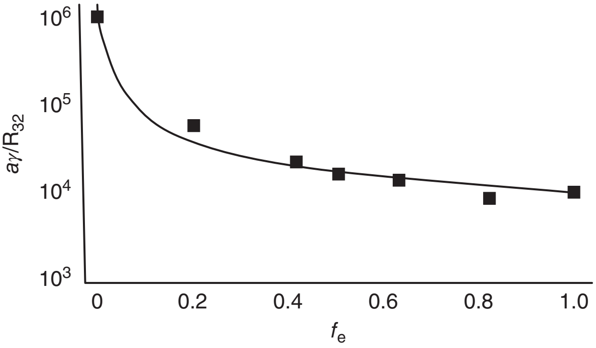

Figure 11.21 $(a\gamma/R_{32})$ versus f_e. The line was drawn using Equation (11.5).

agreement between the values of the slopes and those predicted using Equation (11.14) is good.

References

1. Tadros, Th.F. (2009) *Colloids in Agrochemicals*, Wiley-VCH Verlag GmbH, Weinheim.
2. Tadros, Th.F. (2010) *Colloids in Paints*, Wiley-VCH Verlag GmbH, Weinheim.
3. Balkely, D.C. (1975) *Emulsion Polymerisation*, Elsevier Applied Sciences, London.
4. Tadros, Th.F. (ed.) (2008) *Colloids in Cosmetics and Personal Care*, Wiley-VCH Verlag GmbH, Weinheim.
5. Blake, T. (1984) in *Surfactants* (ed. T. Tadros), Academic Press, London.
6. Deryaguin, B.V. and Landau, L. (1941) *Acta Physicochem. USSR*, **14**, 633.
7. Verwey, E.J.W. (1948) in *Theory of Stability of Lyophobic Colloids* (ed. J.T.G. Overbeek), Elsevier, Amsterdam.
8. Napper, D.H. (1983) *Polymeric Stabilisation of Dispersions*, Academic Press, London.
9. Heath, D., Knott, R.D., Knowles, D.A., and Tadros, Th.F. (1984) *ACS Symp. Ser.*, **254**, 2.
10. Tadros, Th.F., Vandamme, A., Levecke, B., Booten, K., and Stevens, C.V. (2004) *Adv. Colloid Interface Sci.*, **108–109**, 207.
11. Thompson, W. (Lord Kelvin) (1871) *Philos. Mag.*, **42**, 448.
12. Pons, R., Rossi, P., and Tadros, Th.F. (1995) *J. Phys. Chem.*, **99**, 12624.
13. Tadros, Th.F., Cutler, J., Pons, R., and Rossi, P. (1998) Investigations of the interactions between suspensions and emulsions (Suspoemulsions), in *Modern Aspects of Colloidal Dispersions* (eds R.H. Ottewill and A.R. Rennie), Kluwer Academic Publishers, Dordrecht.
14. Krieger, I.M. (1972) *Adv. Colloid Interface Sci.*, **3**, 111.
15. Princen, H.M. and Kiss, A.D. (1986) *J. Colloid Interface Sci.*, **112**, 427.

12
Formulation of Multiple Emulsions

12.1
Introduction

Multiple emulsions are complex systems of ‘‘emulsions of emulsions.’’ Both water-in-oil-in-water (W/O/W) and oil-in-water-in-oil (O/W/O) multiple emulsions have potential applications in various fields. The W/O/W multiple emulsion may be considered as a water/water emulsion whereby the internal water droplets are separated by an ‘‘oily layer’’ (membrane). The internal droplets might also consist of a polar solvent such as glycol or glycerol, which may contain a dissolved or dispersed active ingredient (a.i.). The O/W/O multiple emulsion can be considered as an oil/oil emulsion separated by an ‘‘aqueous layer’’ (membrane).

Multiple emulsions are ideal systems for application in several fields, among which can be mentioned pharmaceuticals, cosmetics, the food industry, and agrochemicals. Due to the oily liquid or aqueous membrane formed, multiple emulsions ensure complete protection of the entrapped drug, controlled release of the drug from the internal to the external phase, and possibly also drug targeting due to the vesicular character of these systems. In the field of cosmetics, multiple emulsions offer several advantages such as the protection of fragile ingredients, the separation of incompatible ingredients, prolonged hydration of the skin and, in some cases, the formation of a firm gelled structure. In addition, a pleasant skin feel similar to that obtained with oil-in-water (O/W) emulsions, combined with the well-known moisturizing properties of water-in-oil (W/O) emulsions, can be achieved with W/O/W multiple emulsions. In the food industry, the existence of an encapsulated water (or oil) phase in a W/O/W (or O/W/O) multiple emulsion allows the protection of reactive food ingredients or volatile flavours, as well as control of their release. Since less oil phase is required to produce a W/O/W multiple emulsion compared to an O/W emulsion with the same disperse volume fraction, multiple emulsions can be used in the development of low calorie, reduced-fat food products such as dressings, mayonnaises, or spreads. In the agrochemical industry, multiple emulsions allows three a.i.s to be included in one formulation, and to incorporate adjuvants in three compartments. Multiple emulsions can be usefully applied for controlled release by controlling the rate of the breakdown process of the multiple emulsion on application. Initially, a stable multiple emulsion (with a shelf-life of two years) is prepared which, on dilution, breaks down in a

Formulation of Disperse Systems: Science and Technology, First Edition. Tharwat F. Tadros.

controlled manner thus releasing the a.i. also in a controlled manner (termed slow- or sustained-release). As will be discussed later, the formulated W/O/W multiple emulsion is osmotically balanced, but on dilution the system will break down as a result of the lack of this balance.

12.2
Preparation of Multiple Emulsions

These multiple emulsions are usually prepared in a two-stage process. For example, a W/O/W multiple emulsion is formulated by first preparing a W/O emulsion using a surfactant with a low HLB number (5–6) and a high-speed mixer (e.g., an UltraTurrax or Silverson). The resulting W/O emulsion is further emulsified in aqueous solution containing a surfactant with a high HLB number (9–12), using a low-speed stirrer (e.g., a paddle stirrer). A schematic representation of the preparation of multiple emulsions is shown in Figure 12.1.

The yield of the multiple emulsion can be determined using dialysis for W/O/W multiple emulsions. A water-soluble marker is used and its concentration in the outside phase is determined.

$$\%\ \text{Multiple emulsion} = \frac{C_\mathrm{i}}{C_\mathrm{i} + C_\mathrm{e}} \times 100 \tag{12.1}$$

where C_i is the amount of marker in the internal phase and C_e is the amount in the external phase. It has been suggested that if a yield of more than 90% is required, the lipophilic (low-HLB) surfactant used to prepare the primary emulsion must be about 10-fold higher in concentration than the hydrophilic (high-HLB) surfactant.

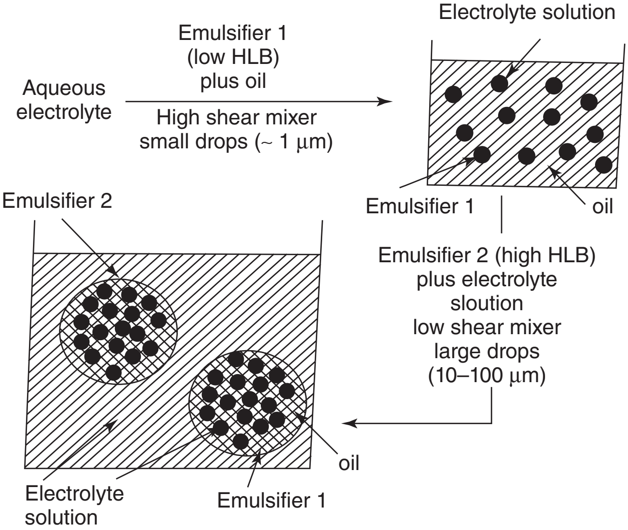

Figure 12.1 Scheme for preparation of W/O/W multiple emulsion.

12.3
Types of Multiple Emulsions

Florence and Whitehill [1] classified multiple emulsions into three main categories, namely A, B and C, as illustrated in Figure 12.2:

- Type A emulsions contain one large internal droplet similar to that described by Matsumoto *et al.* [2]. This type was produced when polyoxyethylene (EO = 4) lauryl ether (Brij 30) was used as emulsifier at 2%.
- Type B emulsions contains several small internal droplets. These were prepared using 2% polyoxyethylene (EO = 16.5) nonyl phenyl ether (Triton X-165).
- Type C emulsions contain drops entrapped in a very large number of small internal droplets, and were prepared using a 3 : 1 Span 80 : Tween 80 mixture.

It should be noted that type A multiple emulsions are not encountered much in practice, while type C is difficult to prepare as a large number of small water internal droplets (which are produced in the primary emulsification process) results in a large increase in viscosity. Thus, the most common multiple emulsions used in practice are those represented by type B.

12.4
Breakdown Processes of Multiple Emulsions

Florence and Whitehill [1] identified several types of breakdown process. The external oil drops may coalesce with other oil drops (which may or may not contain internal aqueous droplets); alternatively, the internal aqueous droplets may be individually expelled, more than one may be expelled, or they may be less frequently expelled in one step. The internal droplets may coalesce before being

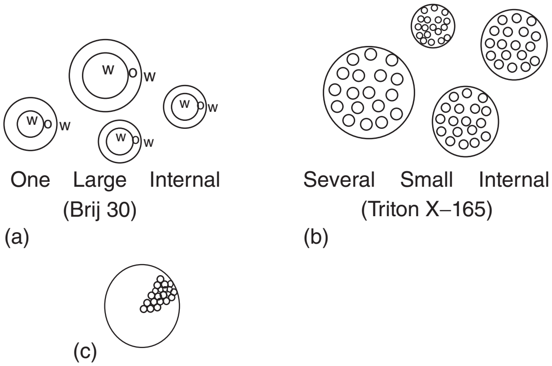

- (A) One large internal (Brij 30) ; (B) Several small internal (Triton X-165)
- (C) Large number of very small droplets (3:1 Span 80:Tween 80).

Figure 12.2 (a–c) Schematic representation of three structures of W/O/W multiple emulsions.

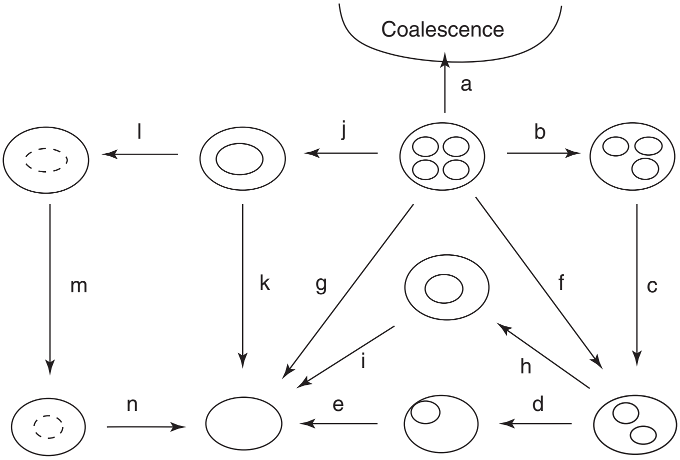

Figure 12.3 Schematic representation of the possible breakdown pathways in W/O/W multiple emulsions. (a) Coalescence; (b–e) Expulsion of one or more internal aqueous droplets; (g) Less-frequent expulsion; (h,i) Coalescence of water droplets before expulsion; (j,k) Diffusion of water through the oil phase; (l–n) Shrinking of the internal droplets.

expelled or water may pass by diffusion through the oil phase, resulting in a shrinkage of the internal droplets. A schematic image of the breakdown processes in multiple emulsions [1] is shown in Figure 12.3.

All of the above processes are influenced by the nature of the two emulsifiers used to prepare the multiple emulsion. Most reports on multiple emulsions are based on conventional nonionic surfactants, but unfortunately most of these surfactant systems produce multiple emulsions with limited shelf-lives, particularly if the system is subjected to large temperature variations. During the past few years, multiple emulsions have been formulated using polymeric surfactants for both the primary and multiple emulsion preparation. These polymeric surfactants proved to be superior over conventional nonionic surfactants in maintaining the physical stability of the multiple emulsion, such that today they may be applied successfully to the formulation of agrochemical multiple emulsions. The results obtained using these polymeric surfactants offer several potential applications in formulations. The key in the latter cases is to use polymeric surfactants that are approved by the FDA for pharmacy and food, by the CTA for cosmetics, and by the EPA for agrochemicals.

One of the main instabilities of multiple emulsions is the osmotic flow of water from the internal to the external phase, or vice versa, which leads to shrinkage or swelling of the internal water droplets, respectively. This process assumes the oil layer to act as a semi-permeable membrane (permeable to water, but not to solute).

The volume flow of water, J_W, may be equated with the change of droplet volume with time dv/dt,

$$J_W = \frac{dv}{dt} = -L_p\, ART\, (g_2 c_2 - g_1 c_1) \tag{12.2}$$

where L_p is the hydrodynamic coefficient of the oil "membrane," A is the cross-sectional area, R is the gas constant, and T is the absolute temperature.

The flux of water ϕ_W is,

$$\varphi_W = \frac{J_W}{V_m} \tag{12.3}$$

where V_m is the partial molar volume of water.

An osmotic permeability coefficient P_o can be defined,

$$P_o = \frac{L_p\, RT}{V_m} \tag{12.4}$$

Combining Equations (12.2–12.4),

$$\varphi_W = -P_o\, A\, (g_2 c_2 - g_1 c_1) \tag{12.5}$$

The diffusion coefficient of water D_W can be obtained from P_o and the thickness of the diffusion layer Δx,

$$-P_o = \frac{D_W}{\Delta x} \tag{12.6}$$

For isopropyl myristate W/O/W emulsions, Δx is ~8.2 μm and $D_W \sim 5.15 \times 10^{-8}\ \text{cm}^2\ \text{s}^{-1}$, the value expected for the diffusion of water in reverse micelles.

12.5
Factors Affecting Stability of Multiple Emulsions, and Criteria for Their Stabilisation

It is clear that the stability of the resulting multiple emulsion depends on a number of factors:

- The nature of the emulsifiers used for preparation of the primary and multiple emulsion.
- The osmotic balance between the aqueous droplets in the multiple emulsion drops and that in the external aqueous phase.
- The volume fractions of the disperse water droplets in the multiple emulsion drops and the final volume fraction of the multiple emulsions.
- The temperature range to which the multiple emulsion is subjected.
- The process used to prepare the system.
- The rheology of the whole system, which can be modified by the addition of thickeners in the external aqueous phase.

The main criteria for the preparation of a stable multiple emulsion are:

- Two emulsifiers, one with a low HLB number (emulsifier I) and one with a high number (emulsifier II)
- Emulsifier I should provide a very effective barrier against coalescence of the water droplets in the multiple emulsion drop. Emulsifier II should also provide an

effective barrier against flocculation and/or coalescence of the multiple emulsion drops.
- The amount of emulsifiers used in the preparation of primary and multiple emulsion is critical. Excess emulsifier I in the oil phase may result in further emulsification of the aqueous phase into the multiple emulsion, with the ultimate production of a W/O emulsion. Excess emulsifier II in the aqueous phase may result in solubilisation of the low-HLB surfactant, with the ultimate formation of an O/W emulsion.
- Optimum osmotic balance of the internal and external aqueous phases. If the osmotic pressure of the internal aqueous droplets is higher than the external aqueous phase, water will flow to the internal droplets and result in ''swelling'' of the multiple emulsion drops with the ultimate production of a W/O emulsion. In contrast, if the osmotic pressure in the outside external phase is higher, water will diffuse in the opposite direction and the multiple emulsion will revert to an O/W emulsion.

Various formulation variables must also be considered:

- The primary W/O emulsifier: various low-HLB surfactants are available of which the following may be mentioned: decaglycerol decaoleate; mixed triglycerol trioleate and sorbitan trioleate; ABA block copolymers of polyethylene oxide (PEO) and polyhydroxystearic acid (PHS).
- The primary volume fraction of the W/O or O/W emulsion: Usually, volume fractions between 0.4 and 0.6 are produced, depending on the requirements.
- The nature of the oil phase: various paraffinic oils (e.g., heptamethyl nonane), silicone oil, soybean and other vegetable oils may be used.
- Secondary O/W emulsifiers: High-HLB surfactants or polymers may be used, such as Tween 20, polyethylene oxide–polypropylene oxide (PPO) block copolymers (Pluronics) may be used.
- Secondary volume fraction: This may be varied between 0.4 and 0.8, depending on the consistency required.
- Electrolyte nature and concentration: Examples include NaCl, $CaCl_2$, $MgCl_2$, or $MgSO_4$.
- Thickeners and other additives: In some cases a gel coating for the multiple emulsion drops may be beneficial, for example polymethacrylic acid or carboxymethyl cellulose. Gels in the outside continuous phase for a W/O/W multiple emulsion may be produced using xanthan gum (Keltrol or Rhodopol), Carbopol or alginates.
- The process employed: For the preparation of a primary emulsion, high-speed mixers (e.g., Elado (Ystral), UltraTurrax or Silverson) may be used. For the secondary emulsion preparation, a low-shear mixing regime is required, in which case paddle stirrers are probably the most convenient. The mixing times, speed, and order of addition need to be optimised.

In this chapter, the formulation of multiple emulsions with particular reference to the use of polymeric surfactants to prepare W/O/W multiple emulsions for the above applications will be covered. The first section will provide a brief description of polymeric surfactants, followed by the fundamental principles of stabilisation of emulsions using polymeric surfactants. Finally, some examples will be given of formulations prepared using these polymeric surfactants.

It should be noted that the above-listed principles apply to the preparation of stable O/W and W/O emulsions as well as to other related applications.

12.6
General Description of Polymeric Surfactants

The most convenient polymeric surfactants are those of the block (A-B or A-B-A) and graft (BA_n) types, which exhibit considerable surface activity. For an O/W emulsifier, the B chain is chosen to have a high affinity to the oil phase (or soluble in it), whereas the A chain is chosen to be highly soluble in the aqueous medium and strongly solvated by the water molecules. This configuration is the most suitable for effective stabilisation, as will be discussed below. The high affinity of the B chain to the oil phase ensures strong ‘‘anchoring’’ of the chain to the surface, and this prevents any displacement of the molecule on the approach of two oil droplets, thus preventing any flocculation and/or coalescence. Examples of the A-B-A block copolymers for stabilising O/W emulsions are the Pluronics (trade name of BASF); these are shown schematically in Figure 12.4, which also shows the adsorption and conformation of the polymer. These triblock copolymers consist of two poly-A blocks of PEO and one poly-B block of PPO. Several chain lengths of PEO and PPO are available. The PPO chain which is hydrophobic adsorbs at the oil surface, due either to its high affinity to the oil molecules or as result of ‘‘rejection anchoring’’ (as the PPO chain is insoluble in water). The two PEO chains reside in the aqueous medium and become strongly solvated by the water molecules (as a result of hydrogen bonding with water molecules). These PEO chains provide the strong repulsion on close approach of two emulsion droplets, as will be discussed later.

For W/O emulsions, the B chain should have a high affinity to the water droplets (or be water-soluble), whereas the A chains should be soluble in the oil phase

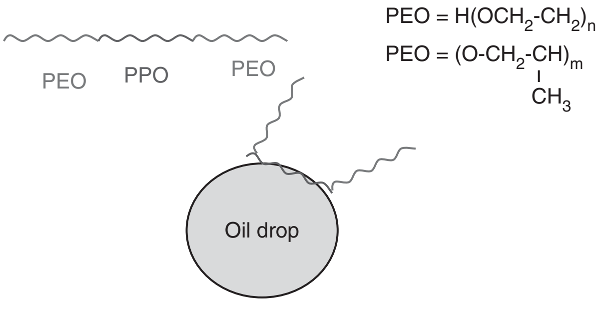

$PEO = H(OCH_2\text{-}CH_2)_n$

$PEO = (O\text{-}CH_2\text{-}\underset{\displaystyle CH_3}{\underset{|}{CH}})_m$

Figure 12.4 Schematic representation of the structure of ‘‘Pluronics,’’ and their adsorption at the O/W interface.

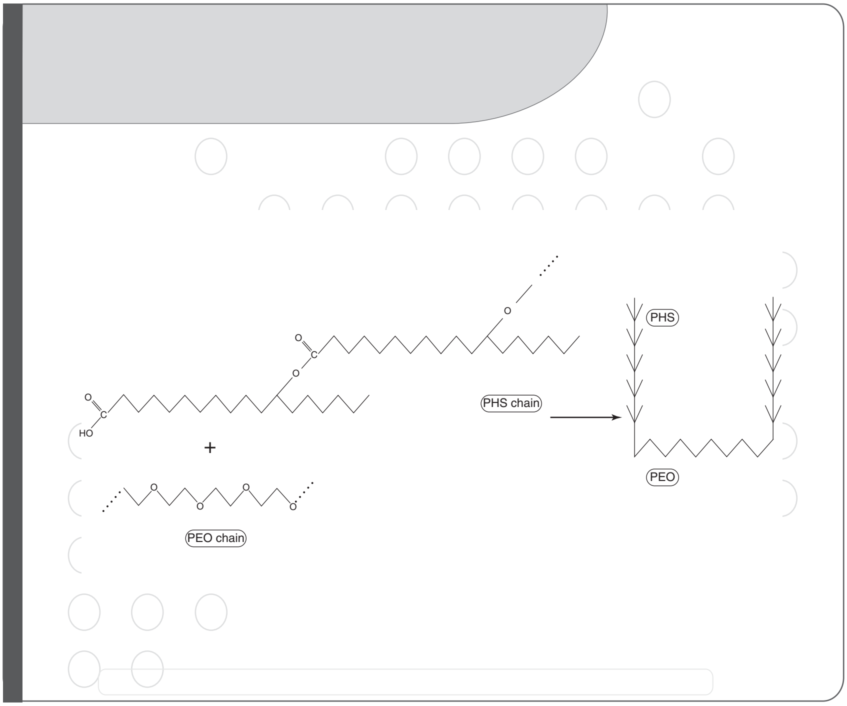

Figure 12.5 Structure of PHS-PEO-PHS block copolymer.

and strongly solvated by the oil molecules. A good example of such a triblock is poly(hydroxystearic acid)–poly(ethylene oxide)–poly(hydroxystearic acid) (PHS-PEO-PHS). A schematic representation of the structure of this block copolymer is shown in Figure 12.5, and its adsorption and conformation at the W/O interface is shown in Figure 12.6. The PEO chain is soluble in the water droplets and provides a strong ''anchor'' to the interface, whereas the PHS chains are highly soluble in most hydrocarbon solvents as well as some of the polar solvents. These PHS chains provide the strong repulsion on approach of the water droplets. The PHS-PEO-PHS molecules also lower the interfacial tension of the W/O interface to very low values (approaching zero); a consequence of this is that the emulsification of water in oil is very efficient, allowing the preparation of highly concentrated W/O emulsions that have low viscosity.

12.7
Interaction between Oil or Water Droplets Containing an Adsorbed Polymeric Surfactant: Steric Stabilisation

Consider the case of two water droplets containing an adsorbed polymeric surfactant such as PHS-PEO-PHS (the molecule used to prepare the primary W/O emulsion).

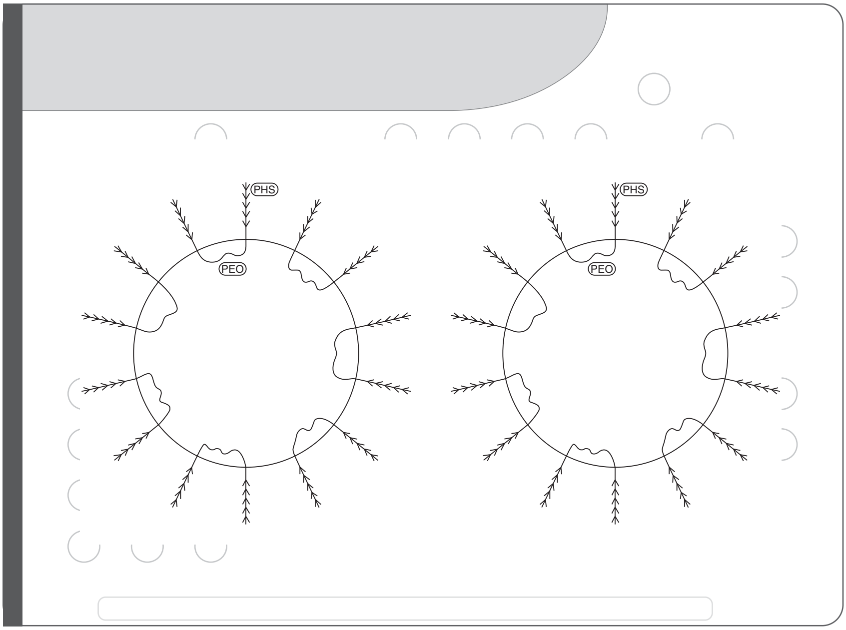

Figure 12.6 Conformation of PHS-PEO-PHS block copolymer at the W/O interface.

As discussed above, this molecule has a very high surface activity at the W/O interface. This is due to the fact that the PEO chain (of molecular weight ~1500 Da) resides in the water droplets, leaving the two PHS chains (each of molecular weight ~1000 Da) in the oil phase. Surface pressure (π)–area per molecule (A) isotherms at the water/air (W/A) and water/oil (W/O) interfaces obtained using a semiautomatic Langmuir trough [3] are shown in Figure 12.7. The W/O isotherm is more expanded than the W/O isotherm, although the two curves tend to approach each other as

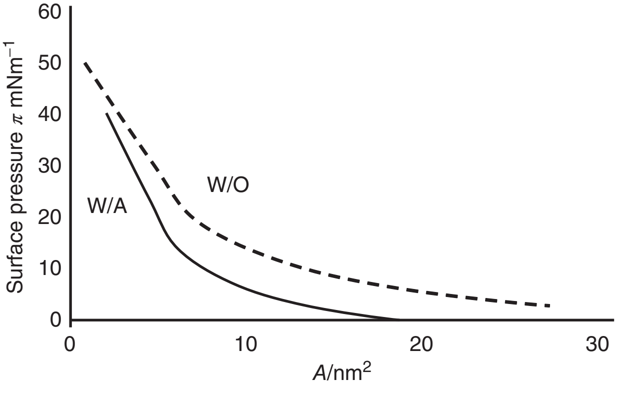

Figure 12.7 π–A curves (25 °C) for PHS-PEO-PHS block copolymer at the air/water and oil/water interfaces.

the surface pressure is increased. The W/O monolayer would be expected to be more expanded as the oil will reduce the van der Waals attractions between the hydrocarbon chains. Collapse at the W/A interface was well defined, occurring at a surface pressure of 38.5 mN m^{-1}. This possibly involved the formation of bilayers of PHS-PEO-PHS at the surface, particularly in view of the lamellar liquid crystalline structure of the bulk material.

For the W/O case, the maximum surface pressure approached 51 mN m^{-1}, implying an interfacial pressure approaching zero. These interfacial tension results show that the PHS-PEO-PHS block copolymer is an excellent W/O emulsifier. Indeed, W/O emulsions with a water volume fraction ϕ of 0.9 can be prepared using this block copolymer.

The PHS chains are highly solvated by the oil molecules and extend at the W/O interface, giving a layer thickness on the order of 7–8 nm, as confirmed using film thickness measurements [3]. A thin film consisting of oil plus surfactant was formed between two aqueous droplets when they were brought into contact, and the thickness of the film was measured using light reflectance; a film thickness of 14.2 nm indicated a layer thickness of the PHS chains on the order of 7 nm. The layer thickness could also be measured using rheological measurements. When shear stress (τ)–shear rate (γ) curves were obtained for W/O emulsions at various volume fractions of water, the results indicated a change from Newtonian to non-Newtonian flow behaviour as the volume fraction of the water in the emulsion was increased. The non-Newtonian flow reflects the droplet–droplet interaction as these approach to closer distances. The data were analysed using the Bingham model [4],

$$\tau = \tau_\beta + \eta_{\text{pl}}\,\gamma \tag{12.7}$$

In Figure 12.8, plots of η_{pl} versus ϕ show that η_{pl} increases gradually with an increase in ϕ; however, above $\phi = 0.6$ there is a rapid increase in both parameters, with further increases in the volume fraction. Such behaviour is typical of concentrated dispersions [5, 6], which show rapid increases in their rheological parameters when the distance of separation between the particles become comparable to the range of repulsive interaction.

Assuming that the W/O emulsion behaves as a near "hard-sphere" dispersion, it is possible to apply the Dougherty–Krieger equation [7, 8] to obtain the effective volume fraction, ϕ_{eff}. The assumption that the W/O emulsion behaves as a near hard sphere dispersion is reasonable as the water droplets are stabilised with a block copolymer with relatively short PHS chains (of the order of 10 nm and less). Any lateral displacement of the polymer will be opposed by the high Gibbs elasticity of the adsorbed polymer layer, and the droplets will maintain their spherical shape up to high volume fractions.

For hard-sphere dispersions, the relative viscosity, η_{r}, is related to the effective volume fraction by the following expression,

$$\eta_{\text{r}} = \left[1 - \left(\frac{\varphi_{\text{eff}}}{\varphi_{\text{p}}}\right)\right]^{-[\eta]\varphi_{\text{p}}} \tag{12.8}$$

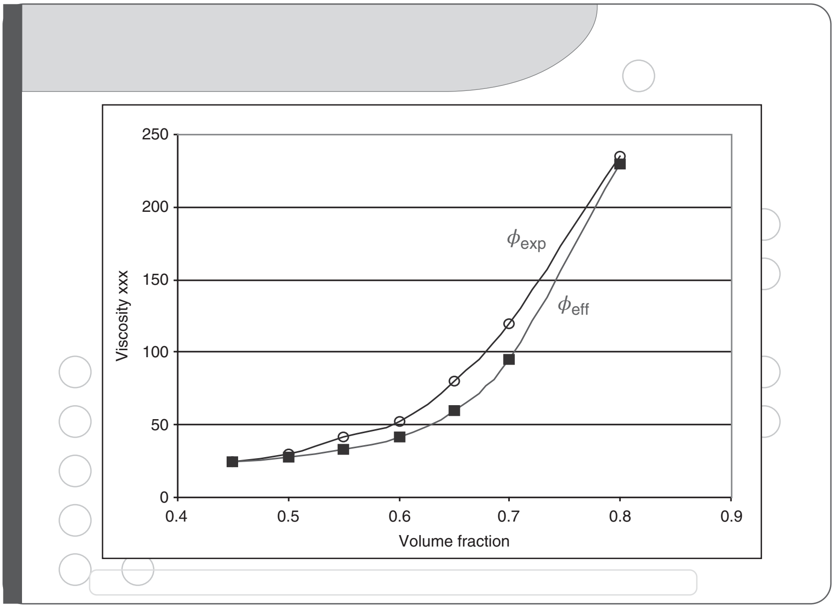

Figure 12.8 Viscosity–volume fraction curves for W/O emulsions stabilised with PHS-PEO-PHS block copolymer.

In Equation (12.8), ϕ is replaced by ϕ_{eff} which includes the contribution from the adsorbed layer, [η] is the intrinsic viscosity (which for hard spheres is equal to 2.5), and ϕ_{p} is the maximum packing fraction. It was shown that a plot of $1/\eta_{\text{r}}{}^{1/2}$ versus ϕ is linear with an intercept that is equal to ϕ_{p}. For the present W/O emulsion, such a plot gave a ϕ_{p} value of 0.84, which was higher than the theoretical maximum packing fraction for monodisperse spheres (0.74 for hexagonal packing). However, this high value is not unreasonable considering the polydispersity of the W/O emulsion. The high ϕ_{p} value shows, without doubt, that the PHS-PEO-PHS block copolymer is very suitable for preparation of high-volume fraction W/O emulsions.

Using ϕ_{p} and the measured η_{r}, ϕ_{eff} was calculated at each ϕ value using Equation (12.3), and the results are plotted in Figure 12.8. From ϕ_{eff}, the adsorbed layer thickness, δ, was calculated using the following equation,

$$\varphi_{\text{eff}} = \varphi\left[1+\left(\frac{\delta}{R}\right)\right]^3 \tag{12.9}$$

where R is the droplet size (which could be determined using dynamic light scattering).

A plot of δ versus ϕ showed a linear decrease of δ with increase in ϕ. The value of δ at $\phi = 0.4$ was ~10 nm, which is a measure of the fully extended PHS chains. At such a low ϕ-value there will be no interpenetration of the PHS chains as the distance between the droplets is relatively large. The reduction in δ with increase in ϕ is due to the possible interpenetration and/or compression of the PHS chains on close approach of the droplets. This is also possible in thin liquid film studies, which showed a layer thickness in the region of 7–8 nm.

When two water droplets each containing adsorbed copolymers of PHS-PEO-PHS approach to a distance of separation h that is smaller than twice the fully extended PHS chains – that is, h becomes less than ~20 nm – repulsion occurs as a result of two main effects [9]. The first repulsive force arises from the unfavourable mixing of the PHS chains when these are in a good solvent. The PHS chains are soluble in most hydrocarbon solvents and are strongly solvated by their molecules over a wide range of temperatures. The unfavourable mixing of polymer chains in good solvent conditions was considered by Flory and Krigbaum [10], whose theory could be applied to the present case of mixing two PHS chains in a hydrocarbon solvent.

Before overlap, the chains have a volume fraction ϕ_2 and the solvent has a chemical potential $\mu_1{}^{\alpha}$. In the overlap region, the volume fraction of the chains is $\phi_2{}'$ which is higher than ϕ_2, and the solvent has a chemical potential $\mu_1{}^{\beta}$ which is lower than $\mu_1{}^{\alpha}$. This is equivalent to an increase in the osmotic pressure in the overlap region. As a result, solvent diffuses from the bulk to the overlap region and the two water droplets are separated, and this results in strong repulsion; the latter is referred to as mixing or osmotic repulsion.

Using the Flory–Krigbaum theory [10], it is possible to calculate the free energy of mixing, G_{mix}, due to this unfavourable overlap; that is,

$$\frac{G_{\text{mix}}}{kT} = \frac{4\pi}{3V_1}\,\varphi_2^2\,N_{\text{Av}}\left(\frac{1}{2}-\chi\right)\left(\delta-\frac{h}{2}\right)^2\left(3R+2\delta+\frac{h}{2}\right) \tag{12.10}$$

where k is the Boltzmann constant, T is the absolute temperature, V_1 is the molar volume of the solvent, and N_{Av} is Avogadro's constant.

It is clear from Equation (12.10) that when the Flory–Hugging interaction parameter, χ, is less than 0.5 – that is, the chains are in good solvent conditions – then G_{mix} will be positive and the interaction repulsive, and will increase very rapidly with decreasing h, when the latter is lower than 2δ. This explains the strong repulsion obtained between water droplets surrounded by PHS chains. The latter are highly soluble in the hydrocarbon medium, and any attempt to overlap the chains results in very strong repulsion as a result of the above-mentioned unfavourable mixing.

Equation (12.10) also shows that when $\chi > 0.5$ – that is, when the solvency of the medium for the chains becomes poor – G_{mix} will be negative and the interaction will become attractive. Thus, it is important to ensure that the solvent used to prepare the W/O emulsion is a good solvent for the PHS chains, otherwise flocculation of the water droplets (perhaps followed by their coalescence) may occur. Fortunately, the PHS chains are soluble in most hydrocarbon solvents used in most formulations. The condition $\chi = 0.5$ is referred to as θ-solvent, and this denotes the onset of a change from repulsion to attraction. Thus, to ensure steric stabilisation by the above mechanism it must be ensured that the chains are kept in better than θ-solvent.

The second repulsive force arises from the loss of configuration entropy when the chains overlap to some extent. When the two surfaces of the water droplets are separated at an infinite distance, each chain will have a number of configurations, Ω_∞, that are determined by the volume of the hemisphere swept by the PHS chain. When the two surfaces approach to a distance h that is significantly smaller than the radius of the hemisphere swept by the PHS chain, the volume available to the chain becomes smaller and this results in a reduction in the configurational entropy to a value Ω (that is smaller than Ω_∞). This results in a strong repulsion – an effect which is referred to as entropic, volume restriction or elastic repulsion, and is given by the following expression,

$$G_{\mathrm{el}} = 2\nu \ \ln \frac{\Omega}{\Omega_\infty} \tag{12.11}$$

where ν is the number of polymer chains per unit area of the surface. It should be mentioned that G_{el} is always repulsive in any solvent, and becomes very high on considerable overlap of the PHS chains. This can be illustrated from rheological measurements, as will be discussed later.

Plots of G_{mix}, G_{el} and G_A (the van der Waals energy) versus h are illustrated in Figure 12.9. This figure shows that G_{mix} is positive (when $\chi < 0.5$) and increases very rapidly with a decrease of h as soon as h becomes less than 2δ (~20 nm for the PHS chains). G_{el} increases in magnitude (which is always positive) magnitude with decrease of h, becoming very large at short distances (when h becomes smaller than δ; about 10 nm for PHS).

A combination of G_{mix}, G_{el} and G_A results in the total G_T–h curve (see Figure 12.9), which shows a shallow minimum, G_{min} (weak attraction) at $h \sim 2\delta$; that is, at $h \sim 20$ nm for the present W/O emulsion based on PHS-PEO-PHS block copolymer. When $h < 2\delta$, G_T is increased very rapidly with further decreases in h. The depth of the minimum, G_{min}, will depend on the adsorbed layer thickness. In the present W/O emulsion, based on a PHS layer thickness of about 10 nm, G_{min} is very small (fraction of kT). This shows that, with the present sterically stabilised W/O emulsion, there is only a very weak attraction at a relatively long distance of

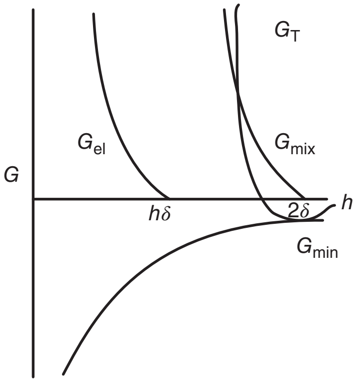

Figure 12.9 Schematic representation of the variation of G_{mix}, G_{el}, G_A, and G_T with h.

separation between the water droplets, and this is overcome by Brownian diffusion (which is on the order of 1 kT). Thus, it can be said that the net interaction is repulsive, which ensures the long-term physical stability of the W/O emulsion (which approaches thermodynamic stability).

Another important use of the PHS-PEO-PHS block copolymer is the formation of a viscoelastic film around water droplets [11, 12]; this results from the dense packing of the molecule at the W/O interface, which leads to an appreciable interfacial viscosity. The viscoelastic film prevents transport of water from the internal water droplets in the multiple emulsion drop to the external aqueous medium, and this ensures the long-term physical stability of the multiple emulsion when using polymeric surfactants. The viscoelastic film can also reduce the transport of any a.i. in the internal water droplets to the external phase. This is desirable in many cases when protection of the ingredient in the internal aqueous droplets is required and release is provided on application of the multiple emulsion.

When the W/O emulsion is emulsified in an aqueous solution containing another polymeric surfactant with a high HLB number, the multiple emulsion drops become surrounded with another polymer surfactant layer. This is illustrated, for example when using Pluronic PEF127 as the secondary polymer emulsifier. This triblock copolymer consists of two PEO chains of ~100 EO units each and a PPO chain of ~55 units. The PPO chain adsorbs relatively strongly at the O/W interface, leaving the two PEO chains in the aqueous continuous phase. The PEO layer thickness is probably larger than 10 nm, and hence at separation distance h between the multiple emulsion drops smaller than ~20 nm, repulsion between the multiple emulsion drops becomes very strong and prevents flocculation and/or coalescence.

It should be emphasised that polymeric surfactants prevent the coalescence of water droplets in the multiple emulsion drops, as well as coalescence of the latter drops themselves. This is due to the interfacial rheology of the polymeric surfactant films. As a result of the strong lateral repulsion between the stabilising chains at the interface (PHS chains at the W/O interface and PEO chains at the O/W interface), these films resist deformation under shear and hence produce a viscoelastic film. On approach of the two droplets, this film prevents deformation of the interface so as to prevent coalescence.

Based on the above discussion, the role of polymeric surfactants in the stabilisation of W/O and W/O/W multiple emulsions can be summarised. First, the polymeric surfactant ensures complete coverage of the droplets and, by virtue of its strong adsorption, displacement of the film on close approach is prevented. This is essential for eliminating coalescence of the emulsion droplets. Second, as the stabilising chains (PHS for the W/O emulsion and PEO for the W/O/W multiple emulsion) are in good solvent conditions, the mixing interaction is positive, which leads to a strong repulsion between the drops on close approach. This, together with the elastic interaction, provides a system that is repulsive at short separation distances and prevents any flocculation and/or coalescence between the drops. The polymeric surfactant chains should be sufficiently long to prevent any weak flocculation, which may result if the depth of the minimum becomes large; that is, when δ becomes small (maybe <5 nm).

As mentioned above, the strong repulsive force between sterically stabilised emulsion droplets can be investigated using rheological measurements, in particular dynamic (oscillatory) measurements. For this, the emulsion is placed in the gap between two concentric cylinders or a cone and plate geometry, after which a sinusoidal strain with small amplitude γ_o is applied to one of the platens (maybe the cup of the concentric cylinder or the plate of the cone-plate geometry). The stress on the other platen is measured simultaneously during the oscillation, and the response in stress of a viscoelastic material subjected to a sinusoidally varying strain is monitored as a function of strain amplitude and frequency. The stress amplitude, τ_o, is also a sinusoidally varying function in time, but in a viscoelastic material it is shifted out of phase with the strain. The phase angle shift between stress and strain, δ, is given by,

$$\delta = \Delta t\, \omega \tag{12.12}$$

where ω is the frequency in radians, s^{-1} ($\omega = 2\pi\nu$, where ν is the frequency in Hertz).

From the amplitudes of stress and strain and the phase angle shift, one can obtain the following viscoelastic parameters,

$$|G^*| = \frac{\tau_o}{\gamma_o} \tag{12.13}$$

$$G' = |G^*| \cos \delta \tag{12.14}$$

$$G'' = |G^*| \sin \delta \tag{12.15}$$

where G^* is the complex modulus, G' is the elastic component of the complex modulus (which is a measure of the energy stored by the system in a cycle), and G'' is the viscous component of the complex modulus (which is a measure of the energy dissipated as viscous flow in a cycle).

In viscoelastic measurements, the viscoelastic parameters are measured as a function of strain amplitude (at a fixed frequency) in order to obtain the linear viscoelastic region. The strain amplitude is gradually increased from the smallest possible value at which a measurement can be made, and the rheological parameters are monitored as a function of the strain amplitude γ_o. Initially, the rheological parameters remain virtually constant and independent of the strain amplitude, but above a critical value of strain amplitude (γ_{cr}) the rheological parameters show a change with further increase in the amplitude above γ_{cr}. The linear viscoelastic region is the range of strain amplitudes below γ_{cr}. Once this region is established, measurements are made as a function of frequency, keeping γ_o below γ_{cr}. By fixing the frequency region, while changing the volume fraction of the emulsion, information can be obtained on the interdroplet interaction.

As an illustration, Figure 12.10 shows the variation of G' and G'' (measured in the linear viscoelastic region and at a frequency of 1 Hz) versus the water volume fraction ϕ.

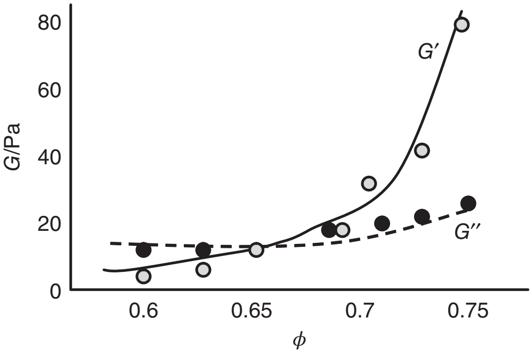

Figure 12.10 Variation of G' and G'' with φ for W/O emulsions stabilised with a block copolymer of PHS-PEO-PHS.

The results show a transition from predominantly viscous to predominantly elastic response as φ exceeds 0.67. This is a direct manifestation of the strong elastic interaction that occurs at and above this critical φ. At this volume fraction, the interdroplet distance is comparable to twice the thickness of PHS chains, resulting in their interpenetration and/or compression. As φ exceeds 0.7, the storage modulus increases very sharply with any further increase in φ, and this is a reflection of the very strong repulsion between the water droplets.

12.8
Examples of Multiple Emulsions Using Polymeric Surfactants

Several examples of W/O emulsions and W/O/W multiple emulsions based on the block copolymer of PHS-PEO-PHS, have been produced. As an illustration, a typical formulation of W/O/W multiple emulsion is described below, using two different thickeners, namely Keltrol (xanthan gum from Kelco) and Carbopol 980 (a crosslinked polyacrylate gel produced by BF Goodrich). These thickeners were added to reduce creaming of the multiple emulsion. A two-step process was used in both cases.

The primary W/O emulsion was prepared using PHS-PEO-PHS. A sample of PHS-PEO-PHS (4 g) was dissolved in 30 g of a hydrocarbon oil; for quick dissolution the mixture was heated to 75 °C. The aqueous phase, which consisted of 65.3 g water, 0.7 g $MgSO_4 \cdot 7H_2O$, and a preservative, was also heated to 75 °C. The aqueous phase was then added slowly to the oil phase while stirring intensively, using a high-speed mixer. The W/O emulsion was homogenised for 1 min and allowed to cool to 40–45 °C, followed by further homogenisation for another minute; stirring was then continued until the temperature reached ambient.

The primary W/O emulsion was emulsified in an aqueous solution containing the polymeric surfactant Pluronic PEF127. A sample of the polymeric surfactant (2 g) was dissolved in 16.2 g water containing a preservative by stirring at 5 °C.

Subsequently, 0.4 g $MgSO_4 \cdot 7H_2O$ was then added to the aqueous polymeric surfactant solution, after which 60 g of the primary W/O emulsion were slowly added to the aqueous PEF127 solution while stirring slowly at 700 rpm (using a paddle stirrer). An aqueous Keltrol solution was prepared by slowly adding 0.7 g Keltrol powder to 20.7 g water, while stirring. The resulting thickener solution was further stirred for 30–40 min until a homogeneous gel was produced. The thickener solution was slowly added to the multiple emulsion while stirring at low speed (400 rpm), and the whole system was then homogenised for 1 min, followed by gentle stirring at 300 rpm until the thickener had completely dispersed in the multiple emulsion (ca. 30 min stirring was sufficient). The final system was investigated using optical microscopy to ensure that the multiple emulsion had been produced. The formulation was left to stand for several months, after which the droplets of multiple emulsion were investigated using optical microscopy. The rheology of the multiple emulsion was also measured at various intervals to ensure that the consistency of the product remained the same on long-term storage.

The above multiple emulsion was prepared under the same conditions except that Carbopol 980 was used as a thickener (gel). In this case, no $MgSO_4$ was added as the carbopol gel was affected by electrolytes. The aqueous PEF127 polymeric surfactant solution was prepared by dissolving 2 g of the polymer in 23 g water; 15 g of 2% master gel of Carbopol were then added to the PEF127 solution while stirring until the Carbopol had completely dispersed. The primary W/O emulsion (60 g) was then slowly added to the aqueous solution of PEF127/Carbopol solution, while stirring thoroughly at 700 rpm. Triethanolamine was added slowly, while gently stirring until the pH of the system reached 6.0–6.5.

12.9
Characterisation of Multiple Emulsions

12.9.1
Droplet Size Measurements

To measure the droplet size distribution of the primary emulsion (W/O in W/O/W or O/W in O/W/O) that has a micron range (with an average radius of 0.5–1.0 μm), a dynamic light-scattering technique (also referred to as photon correlation spectroscopy; PCS) can be applied. Details of this method are described in Chapter 19. Basically, the intensity fluctuation of scattered light by the droplets as they undergo Brownian diffusion is measured; from this, the diffusion coefficient of the droplets can be determined, and in turn the radius can be obtained by using the Stokes–Einstein equation.

To measure the droplet size distribution of the resulting multiple emulsion (with diameters >5 μm), optical microscopy combined with image analysis can be used. An alternative method to measure droplet size distribution is to use light diffraction and then to apply Fraunhofer's diffraction theory. Details of this method are provided in Chapter 19, but basically a laser beam that has been enlarged and made monochromatic by passage through a spatial filter, is allowed to traverse the sample in which all droplets to be measured must be well separated. The droplets diffract the light, and the intensity of the scattered light is a function of the droplets' dimensions.

Detailed information on the size and structure of the multiple emulsion drops can be obtained using electron microscopy and freeze-fracture techniques. The technique consists of four essential steps: (i) cryofixation of the sample by rapid cooling to avoid formation of ice crystals; (ii) fracture and etching of the cryofixed sample; (iii) replication of the exposed surface by coating with platinum–carbon; and (iv) cleaning of the sample by washing with convenient chemicals. Initially, the measurements are carried out using the primary W/O or O/W emulsion to obtain information on the size and structure of the primary droplets, but this is followed by measurements using the W/O/W or O/W/O multiple emulsion.

12.10
Rheological Measurements

Both, steady-state shear stress-shear rate and dynamic (oscillatory) techniques can be applied to study the stability of the multiple emulsions. These techniques are described in detail in Chapter 20. In the steady-state method, the sample is placed in the gap between two concentric cylinders (or a cone-plate geometry) and the inner or outer cylinder (or cone or plate) is subjected to a constant shear rate that can be gradually increased from the lowest value (usually $0.1\,s^{-1}$) to a maximum value of $100–500\,s^{-1}$; the stress is simultaneously measured at each shear rate, and in this way a plot of shear stress and viscosity as a function of shear rate is obtained. The rheological results are analysed using models for non-Newtonian flow to obtain the yield value and viscosity. By following the rheology with time of storage of the multiple emulsion (both at room temperature, lower and higher temperature in the range 10–50 °C), it is possible to obtain information on the stability of the multiple emulsion. For example, if the viscosity and yield value of the system does not show any change with storage time, this indicates a stable multiple emulsion. If, for example, a W/O/W multiple shows a gradual diffusion of water from the external to the internal water droplets, this results in a swelling of the multiple emulsion droplets that is accompanied by a gradual increase of the viscosity and yield value with time until a maximum of the values is reached when maximum swelling occurs. However, when the multiple emulsion droplets breakdown to form O/W emulsion a sudden reduction in viscosity and yield value occurs after a certain storage time.

A more sensitive rheological techniques for following the stability of multiple emulsions is to use oscillatory techniques. In this case, a sinusoidal strain or stress is applied to the sample, which is placed in the gap of the concentric cylinder or cone-and-plate geometry; the resulting stress or strain sine wave is followed at the same time. For a viscoelastic system, as is the case with multiple emulsions, the stress and strain sine waves oscillate with the same frequency, but out of phase.

From the time shift of the stress and strain amplitudes Δt and the frequency ω (rad s^{-1}), the phase angle shift δ is calculated ($\delta = \Delta t\omega$). Them from the amplitudes of stress (σ_o) and strain (γ_o) and δ, the various viscoelastic parameters can be calculated: Complex modulus $G^* = (\sigma_o)/(\gamma_o)$; Storage (elastic) modulus $G' = G^* \cos \delta$; and Loss (viscous) modulus $= G^* \sin \delta$. Two main experiments are carried out. In the first experiment (strain sweep) the frequency is kept constant at 1 Hz or 6.28 (rad s^{-1}), and G^*, G' and G'' are measured as a function of strain amplitude. This allows the linear viscoelastic region to be obtained, where G^*, G' and G'' remain constant and independent of the applied strain. After a critical strain value that depends on the system, G^* and G' start to decrease while G'' starts to increase in line with the increase in applied strain (no-linear response). In the second experiment, the strain is kept constant in the linear region and G^*, G' and G'' are measured as a function of frequency. For a viscoelastic liquid, as is the case with multiple emulsion, both G^* and G' are low at low frequency (long time scale) and gradually increase with increase of frequency, reaching a plateau value at high frequency. In contrast, G'' is high at low frequency but increases with an increase of frequency to reach a maximum at which $G' = G''$, and then decreases with a further increase in frequency. The characteristic frequency ω^* at which $G' = G''$ ($\tan \delta = 1$) is equal to the reciprocal of the relaxation time of the system.

By following the above measurements as a function of storage time, the stability of the multiple emulsion can be assessed. For example, in the case of a W/O/W multiple emulsion whereby the diffusion of water occurs from the outside to the inside water droplets (as a result of osmotic imbalance), a swelling of the multiple emulsion with time results in an increase in the storage time obtained in the linear viscoelastic region, and a shift of the characteristic frequency ω^* to higher values (an increase in the relaxation time of the system). However, after a sudden breakdown of the multiple emulsion droplets, both G' and ω^* will show a sudden decrease with increasing storage time.

References

1. Florence, A.T. and Whitehill, D. (1981) *J. Colloid Interface Sci.*, **79**, 243.
2. Matsumoto, S., Kita, Y., and Yonezawa, D. (1976) *J. Colloid Interface Sci.*, **57**, 353.
3. Aston, M. (1987) PhD Thesis. Reading University.
4. Whorlow, R.W. (1980) *Rheological Techniques*, Ellis Horwood, Chichester.
5. Tadros, Th.F. (1980) *Adv. Colloid Interface Sci.*, **12**, 121.
6. Mewis, J. and Spaul, A.J.B. (1976) *Adv. Colloid Interface Sci.*, **6**, 173.
7. Krieger, I.M. and Dougherty, M. (1959) *Trans. Soc. Rheol.*, **3**, 137.
8. Krieger, I.M. (1972) *Adv. Colloid Interface Sci.*, **3**, 111.
9. Napper, D.H. (1983) *Polymeric Stabilisation of Dispersions*, Academic Press, London.
10. Flory, P.J. (1953) *Principles of Polymer Chemistry*, Cornell University Press, New York.
11. Tadros, Th.F. (1994) *Colloids Surf., A*, **91**, 39.
12. Tadros, Th.F. (1992) *Int. J. Cosmet. Sci.*, **14**, 93.

13
Preparation of Nanosuspensions

13.1
Introduction

Nanosuspensions are solid/liquid (S/L) dispersions with particle diameters in the range of 10 to 100 nm. They can be considered as submicron colloidal dispersions (nanocolloids) as their size falls within the colloid range (1 nm to 1 μm). They are usually stabilised with surfactants and/or polymers that are strongly adsorbed at the S/L interface; the stabilising mechanism can be electrostatic, steric, or a combination of both [1].

Two methods can be applied to the preparation of nanosuspensions:

- The bottom-up approach, which starts with molecular components and the particles are built up by a process of nucleation and growth.
- The top-down process, which starts with the bulk material (which may consist of aggregates and agglomerates) that is dispersed into single particles (using a wetting/dispersing agent); this is followed by a subdivision of the large particles into smaller units that fall within the required nanosize. This process requires the application of intense mechanical energy that can be applied using bead milling, high-pressure homogenisation and/or the application of ultrasonics [1].

Nanosuspensions have wide applications in various industrial fields, among which can be included drug delivery systems of poorly soluble compounds, whereby reducing the particle size to nanoscale dimensions enhances drug bioavailability. This is due to the increase in solubility of the active ingredient on reduction of the particle radius, as given by the Kelvin equation [2]:

$$S(r) = S(\infty)\exp\left(\frac{2\gamma V_m}{rRT}\right) \tag{13.1}$$

where $S(r)$ is the solubility of a particle with radius r and $S(\infty)$ is the solubility of a particle with infinite radius (the bulk solubility), γ is the S/L interfacial tension, R is the gas constant, and T is the absolute temperature.

Equation (13.1) shows a significant increase in solubility of the particle with reduction in particle radius, particularly when the latter becomes significantly smaller than 1 μm.

Formulation of Disperse Systems: Science and Technology, First Edition. Tharwat F. Tadros.

Another important application of nanosuspensions is in the field of cosmetics and personal care products, in particular in sunscreens for UV protection. These systems use semiconductor inorganic particles of titanium dioxide and zinc oxide that are able to absorb UV light, with maximum attenuation being obtained when the particle sizes are in the range of 30–50 nm [3].

Several other applications of nanosuspensions can be listed, such as the preparation of nanopolymer particles, clays and composites, metal nanoparticles, nanotubes and dispersions of carbon black for printing applications. All of these systems must be stabilised against aggregation, Ostwald ripening (crystal growth), and sintering.

In this chapter, the first section will detail the process of nucleation and growth and the control of particle size distribution; this will be followed by descriptions of the various methods that can be applied for bottom-up procedures. A third section will cover the production of nanosuspensions using the top-down process; powder wetting, dispersion and reductions of particle size will be described with particular reference to the role of surfactants (wetting agents) and dispersing agents. As these processes were described in detail in Chapter 9, only a summary will be given here. Finally, the various colloid stabilisation methods that were described in detail in Chapter 9 will be outlined.

13.2
Nucleation and Growth, and Control of Particle Size Distribution

In order to achieve a monodisperse suspension or polydisperse system with particular particle size contribution, it is necessary to control the process of nucleation and particle growth. With most disperse systems, where the particles have some finite solubility, the smaller particles will have higher solubilities than their larger counterparts. With time, molecular diffusion occurs from the smaller to the larger particles, and this results in a shift in the particle size distribution to larger values; this process is referred to as Ostwald ripening.

If a substance becomes less soluble by a change of some parameter, such as a temperature decrease or the addition of a nonsolvent, the solution may enter a metastable state with the formation of some precipitate or nuclei. The classical theory considers the nucleus to consist of a bulk phase containing N_i^s molecules and a shell with N_i^σ molecules which have a higher free energy per molecule than the bulk. This is shown schematically in Figure 13.1. The Gibbs free energy of the nucleus G^s is made of a bulk part and a surface part [4]:

$$G^s = \mu_i^s N_i^s + \sigma A \tag{13.2}$$

where $\mu_i{}^s$ is the chemical potential per molecule, σ is the S/L interfacial tension, and A is the surface area of the nucleus.

In a supersaturated solution, the activity a_i is higher than that of a saturated solution a_i(sat), and as a result molecules will be transferred from the solution to the nucleus surface. The free energy change ΔG^s upon the transfer of a small

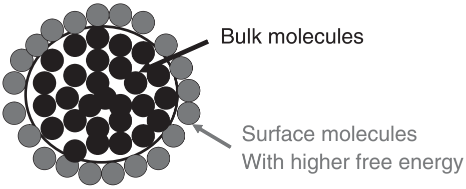

Figure 13.1 Schematic representation of a nucleus.

number N_i from the solution to the particle is made of two contributions from the bulk and the surface,

$$\Delta G^s = \Delta G^s(\text{bulk}) + \Delta G^s(\text{surface}) \tag{13.3}$$

The first term on the right-hand side of Equation (13.3) is negative (it is the driving force), whereas the second term is positive (work must be carried out in expanding the interface). ΔG^s(bulk) is determined by the relative supersaturation, whereas ΔG^s(surface) is determined by the S/L interfacial tension σ and the interfacial area A, which is proportional to $(N_i^s)^{2/3}$

ΔG^s is given by the following expression,

$$\Delta G^s = -N_i kT \ln S + \beta\sigma N_i^{2/3} \tag{13.4}$$

where k is the Boltzmann constant, T is the absolute temperature, and β is a proportionality constant that depends on the shape of the nucleus. S is the relative supersaturation that is equal to a_i/a_i(sat).

For small clusters, the surface area term dominates whereas ΔG^s only starts to decrease due to the bulk term beyond a critical value N^*.

N^*can be obtained by differentiating Equation (13.4) with respect to N and equating the result to 0 ($\mathrm{d}G^s/\mathrm{d}N = 0$)

$$(N^*)^{1/3} = \frac{2\sigma\beta}{3kT \ln S} \tag{13.5}$$

The maximum in the Gibbs energy is given by,

$$\Delta G^* = \frac{1}{3}\beta(N^*)^{2/3} \tag{13.6}$$

Equation (13.5) shows the critical cluster size decreases with increase of the relative supersaturation S or a reduction of σ by the addition of surfactants. This explains why a high supersaturation and/or addition of surfactants favours the formation of small particles. A large S pushes the critical cluster size N^* to smaller values and simultaneously lowers the activation barrier, as illustrated in Figure 13.2, which shows the variation of ΔG with radius at increasing S.

Assuming the nuclei to be spherical, Equation (13.4) can be given in terms of the nucleus radius r

$$\Delta G = 4\pi r^2\sigma - \left(\frac{4}{3}\right)\pi r^3 \left(\frac{kT}{V_m}\right) \ln S \tag{13.7}$$

where V_m is the molecular volume.

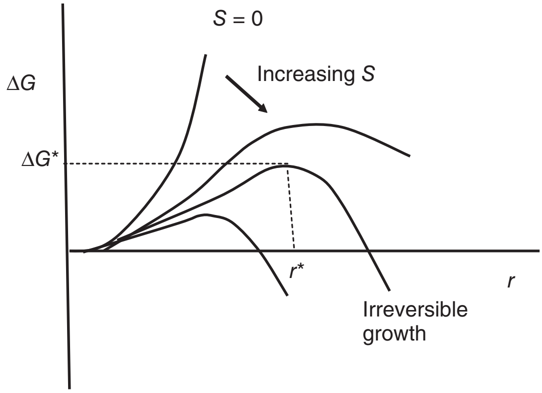

Figure 13.2 Schematic representation of the effect of supersaturation on particle growth.

ΔG^* and r^* are given by,

$$\Delta G^* = \frac{4}{3}\pi (r^*)^2 \sigma \tag{13.8}$$

$$r^* = \frac{2V_m \sigma}{kT \ln S} \tag{13.9}$$

When no precautions are taken, precipitation from a supersaturated solution produces polydisperse particles. This is because the nucleation of new particles and further particle growth overlap in time. The overlap is the consequence of the statistical nature of the nucleation process; near the critical size particles may grow as well as dissolve. To narrow down the particle size distribution as much as possible, nucleation should take place in a short time, followed by equal growth of a constant number of particles. This can be achieved by rapidly creating the critical supersaturation required to initiate homogeneous nucleation, after which particle growth lowers the saturation sufficiently to suppress new nucleation events. Another option is to add nuclei (seeds) to a solution with subcritical supersaturation. A fortunate consequence of particle growth is that, in many cases, the size distribution is self-sharpening.

13.3
Preparation of Nanosuspensions by Bottom-Up Processes

Several methods can be applied for preparation of nanosuspensions using bottom-up processes, of which the following are worthy of mention:

- Precipitation of nanoparticles by addition of a nonsolvent (containing a stabiliser for the particles formed) to a solution of the compound in question.
- Preparation of a nanoemulsion of the substance by using a solvent in which it is soluble following emulsification of the solvent in another immiscible solvent;

this is then followed by removal of the solvent, creating the emulsion droplets by evaporation.

- Preparation of the particles by mixing two microemulsions containing two chemicals that react together when the microemulsion droplets collide with each other.
- Production of polymer nanosuspensions by miniemulsion or suspension polymerisation.

Brief descriptions of each of these processes are provided in the following sections.

13.3.1
Solvent–Antisolvent Method

In this method [5], the substance (e.g., a hydrophobic drug) is dissolved in a suitable solvent, such as acetone. The resulting solution is carefully added to another miscible solvent in which the resulting compound is insoluble, and this results in precipitation of the compound by nucleation and growth. The particle size distribution is controlled by using a polymeric surfactant that is strongly adsorbed onto the particle surface and provides an effective repulsive barrier to prevent aggregation of the particles. The polymeric surfactant is chosen to have a specific adsorption on the particle surface to prevent Ostwald ripening. This method can be adapted for the preparation of low-water solubility drug nanosuspensions, whereby the drug is dissolved in acetone and the resulting solution is added to an aqueous solution of Poloxamer (an A-B-A block copolymer consisting of two A polyethylene oxide (PEO) chains and a B polypropylene oxide (PPO) chain, that is PEO-PPO-PEO). After precipitation of the particles the acetone is removed by evaporation. The main problems with this method are the possibility of forming several unstable polymorphs that will undergo crystal growth, and that the resulting particles may also be of needle-shaped structure although, by correctly choosing the polymeric surfactant the particle morphology and shape can be controlled. Another problem may involve difficulties in removing the solvent after the particles have precipitated.

13.3.2
Use of a Nanoemulsion

In this case, the compound is dissolved in a volatile organic solvent that is immiscible with water, such as methylene dichloride. The oil solution is emulsified in water using a high-speed stirrer, followed by high-pressure homogenisation [6]. A suitable emulsifier for the oil phase is used which has the same HLB number as the oil. The volatile oil in the resulting nanoemulsion is removed by evaporation, and the formed nanosuspension particles are stabilised against aggregation by using an effective polymeric surfactant that can be dissolved in the aqueous phase. The main problem with this technique is the possible interaction between the emulsifier, which may cause the resulting nanosuspension to be destabilised.

However, by carefully selecting the emulsifier/stabilising system it is possible to form a colloidally stable nanosuspension.

13.3.3
Mixing Two Microemulsions

For this method [7], reverse microemulsions lend themselves as suitable ‘‘nonreactors’’ for the synthesis of nanoparticles. Inorganic salts are first dissolved in the water pools of a W/O microemulsion, after which another W/O microemulsion with a reducing agent dissolved in the water pools is prepared. When the two microemulsions are then mixed, the reaction between the inorganic salt and the reducing agent starts at the interface and proceeds towards the centre of the droplet. The rate-limiting step appears to be droplet diffusion. Control of the exchange can be achieved by tuning the film rigidity. This procedure has been applied to the preparation of noble metal particles that could be applied in electronics and catalysis, and also in potential medical systems.

13.3.4
Preparation of Polymer Nanoparticles by Miniemulsion or Minisuspension polymerisation

When preparing polymer in this way [5], the suspension polymerisation process can be adapted to prepare polymer nanoparticles. This is divided into three stages for both polymer soluble (A) and insoluble (B) in its monomer. In the first stage for the A system, when the viscosity of the disperse phase remains low, the bulk monomer phase is dispersed into small droplets due to the shear stress imposed by the stirring conditions. Simultaneously, through the reverse process of coalescence, the drops tend to reverse to the original monomer mass. The droplet size distribution results from a break-up–coalescence dynamic equilibrium. The adsorption of polymeric stabilisers at the monomer droplet–water interface deceases the interfacial tension, and the adsorbed layer prevents coalescence. During the second stage, the viscosity within the droplets increases with increasing conversion, which causes the coalescence to overcome the break-up. However, if the stabiliser is present in sufficient amounts and provides a strong repulsion between the droplets, this coalescence process is delayed and this results in a small increase in particle size. Towards the end of this stage, coalescence is stopped due to the elastic nature of the particle collisions, and after this point the particle size remains virtually constant. The degree of agitation and design of the stirrer/reactor system have a major influence on the dispersion of monomer droplets, as well as on the overall process. An increase in agitation improves the mixing and heat transfer, and promotes the break-up of the droplets. However, a greater agitation increases the frequency of collisions, thus increasing coalescence. These conflicting mechanisms show a reduction in droplet size with increase of speed of agitation, reaching a minimum at an optimum agitation speed followed by increase in droplet size with further increase in stirrer speed due to coalescence. The formation of nanoparticles is also determined by the concentration and nature of the stabiliser. In most cases, a mixture of a polymeric stabiliser such as poly(vinyl alcohol) or Pluronic (an A-B-A block copolymer of PEO, A and PPO) with an anionic surfactant, such as sodium dodecyl sulphate is used. In this case, the stabilising mechanism is the combination of electrostatic and steric mechanism, referred to as electrosteric.

13.4
Preparation of Nanosuspensions Using the Bottom-Down Process

As mentioned above, the top-down process starts with a bulk material (which may consist of aggregates and agglomerates) that is dispersed into single particles (using a wetting/dispersing agent), followed by subdivision of the large particles into smaller units that fall within the required nanosize. This process requires the application of intense mechanical energy that can be applied using bead-milling, high-pressure homogenisation, and/or the application of ultrasonics. Finally, the resulting nanodispersion must remain colloidally stable under all conditions (e.g., temperature changes, vibration) with an absence of flocculation and/or crystal growth. These various processes have been described in detail in Chapter 9, and only a summary is provided here.

13.4.1
Wetting of the Bulk Powder

Most chemicals are supplied as powders consisting of aggregates, where the particles are joined together with their "faces" (compact structures), or agglomerates, where the particles are connected at their corners (loose aggregates). It is essential to wet both the external and internal surfaces (in the pores within the aggregate or agglomerate structures), and this requires the use of an effective wetting agent (surfactant). The wetting of a solid by a liquid (such as water) requires the replacement of the solid/vapour interfacial tension, γ_{SV}, by the solid/liquid interfacial tension, γ_{SL}. The work of dispersion of a powder with surface area A, W_d, is given by:

$$W_d = A(\gamma_{\mathrm{SL}} - \gamma_{\mathrm{SV}}) \tag{13.10}$$

Using the Young's equation,

$$\gamma_{\mathrm{SV}} = \gamma_{\mathrm{SL}} + \gamma_{\mathrm{LV}} \cos\theta \tag{13.11}$$

where γ_{LV} is the liquid/vapour interfacial tension and θ is the contact angle of the liquid drop at the wetting line:

$$W_d = -A\gamma_{\mathrm{LV}} \cos\theta \tag{13.12}$$

Equation (13.12) shows that W_d depends on γ_{LV} and θ, both of which are lowered by the addition of surfactants (wetting agents). If $\theta < 90°$, W_d is negative and dispersion is spontaneous.

Wetting of the internal surface requires penetration of the liquid into channels between and inside the agglomerates. The process is similar to forcing a liquid through fine capillaries. To force a liquid through a capillary with radius r, a pressure p is required that is given by,

$$p = -\frac{2\,\gamma_{\mathrm{LV}}\ \cos\ \theta}{r} = \left[\frac{-2\,(\gamma_{\mathrm{SV}} - \gamma_{\mathrm{SL}}}{r\,\gamma_{\mathrm{LV}}}\right] \tag{13.13}$$

where γSL must be made as small as possible, with a rapid surfactant adsorption to the solid surface, and low θ. When $\theta = 0$, $p \propto \gamma_{\mathrm{LV}}$; thus for penetration into pores a high γLV is required, and the wetting of the external surface requires a low contact angle θ and low surface tension γ_{LV}. Wetting of the internal surface (i.e., penetration through pores) requires a low θ but a high γ_{LV}. However, these two conditions are incompatible and a compromise must be made, with $\gamma_{\mathrm{SV\text{-}SL}}$ being kept at a maximum and γ_{LV} being kept as low as possible, but not too low.

The above conclusions illustrate the problem of choosing the best dispersing agent for a particular powder. This requires measurement of the above parameters, as well as testing the efficiency of the dispersion process.

The contact angle of liquids on solid powders can be measured by application of the Rideal–Washburn equation. For horizontal capillaries (gravity neglected), the depth of penetration l in time t is given by the Rideal–Washburn equation [8, 9]:

$$l = \left[\frac{r\ t\ \gamma_{\mathrm{LV}}\ \cos\ \theta}{2\,\eta}\right]^{1/2} \tag{13.14}$$

To enhance the rate of penetration, γ_{LV} must be made as high as possible, θ as low as possible, and η as low as possible. For dispersion of powders into liquids, surfactants should be used that lower θ but do not reduce γ_{LV} too much; the viscosity of the liquid should also be kept at a minimum. Thickening agents (such as polymers) should not be added during the dispersion process. It is also necessary to avoid foam formation during the dispersion process.

For a packed bed of particles, r may be replaced by K, which contains the effective radius of the bed and a turtuosity factor, which takes into account the complex path formed by the channels between the particles, that is,

$$l^2 = \left(\frac{kt\gamma_{\mathrm{LV}}\cos\theta}{2\eta}\right)t \tag{13.15}$$

Thus, a plot of l^2 versus t will give a straight line, from the slope of which it is possible to obtain θ. The Rideal–Washburn equation can be applied to obtain the contact angle of liquids (and surfactant solutions) in powder beds. For this, K should first be obtained using a liquid that produces a zero contact angle, after which a packed bed of powder is prepared, probably in a tube fitted with a sintered glass at the end (to retain the powder particles). It is essential that the powder is packed uniformly in the tube (a plunger may be used in this case). The tube containing the bed is immersed in a liquid that provides spontaneous wetting (e.g., a lower alkane), as well as a zero contact angle such that cos $\theta = 1$. By measuring the rate of penetration of the liquid (this can be carried out gravimetrically using, for example, a microbalance or a Kruss instrument), K can be obtained. The tube is then removed from the lower-alkane liquid, left to stand for the liquid to evaporate, and then immersed in the liquid in question. The rate of penetration is then measured again as a function of time. By using Equation (13.15), $\cos\theta$ can be calculated and hence θ.

For the efficient wetting of hydrophobic solids in water, a surfactant is needed that lowers the surface tension of water very rapidly (within a few milliseconds) and is quickly adsorbed at the S/L interface. To achieve a rapid adsorption, the wetting agent should be either a branched chain with central hydrophilic group or a short hydrophobic chain with a hydrophilic end group. The most commonly used wetting agents are the following:

Aerosol OT (diethylhexyl sulfosuccinate)

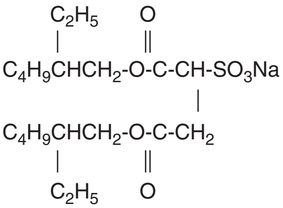

$$\begin{array}{l} C_4H_9\overset{\displaystyle C_2H_5}{\overset{|}{C}}HCH_2\text{-}O\text{-}\overset{\displaystyle O}{\overset{\|}{C}}\text{-}CH\text{-}SO_3Na \\ \qquad\qquad\qquad\qquad\qquad\quad | \\ C_4H_9\underset{\displaystyle C_2H_5}{\underset{|}{C}}HCH_2\text{-}O\text{-}\underset{\displaystyle O}{\underset{\|}{C}}\text{-}CH_2 \end{array}$$

The above molecule has a low critical micelle concentration (cmc) of 0.7 g dm^{-3}, and at and above the cmc the water surface tension is reduced to ~25 mNm^{1} in less than 15 s.

An alternative anionic wetting agent is sodium dodecylbenzene sulphonate, with a branched alkyl chain

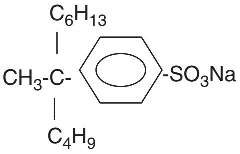

The above molecule has a higher cmc (1 g dm^{-3}) than Aerosol OT, but it is less effective in lowering the surface tension of water, reaching a value of 30 mN m^{-1} at and above the cmc. It is, therefore, not as effective as Aerosol OT for powder wetting.

Several nonionic surfactants, such as the alcohol ethoxylates, can also be used as wetting agents. These consist of a short hydrophobic chain (mostly C_{10}) which is also branched, while a medium chain (PEO) mostly consisting of six EO units or lower may be used. These molecules also reduce the dynamic surface tension within a short time (<20 s), and have a reasonably low cmc.

In all cases, the minimum amount of wetting agent should be used to avoid interference with the dispersant that must be added to maintain colloid stability during dispersion and on storage.

13.4.2
Breaking of Aggregates and Agglomerates into Individual Units

This usually requires the application of mechanical energy. High-speed mixers (which produce turbulent flow) are efficient in breaking-up the aggregates and agglomerates; examples include Silverson and UltraTurrax mixers. The mixing conditions must be optimised, with heat generation at high stirring speeds being avoided in particular. This is especially the case when the viscosity of the resulting dispersion increases during dispersion (note that the energy dissipation as heat is given by the product of the square of the shear rate and the viscosity of the suspension). Foam formation should also be avoided during dispersion; the correct choice of dispersing agent is essential, and antifoams (silicones) may be applied during the dispersion process.

In order to maintain the particles as individual units, it is essential to use a dispersing agent that provides an effective repulsive barrier so as to prevent aggregation of the particles by van der Waals forces. This dispersing agent must be strongly adsorbed onto the particle surface and should not be displaced by the wetting agent. The repulsive barrier may be electrostatic in nature, whereby electrical double layers are formed at the S/L interface [10, 11]. These double layers must be extended (by maintaining low electrolyte concentration), and a strong repulsion occurs on the double layer overlap. Alternatively, repulsion can be created by using nonionic surfactant or polymer layers that remain strongly hydrated (or solvated) by molecules of the continuous medium [12]. As the particles approach a surface-to-surface separation distance that is less than twice the adsorbed layer thickness, a strong repulsion will occur as a result of two main effects: (i) unfavourable mixing of the layers when these are in good solvent conditions; and (ii) a loss of configurational entropy on significant overlap of the adsorbed layers. This process is referred to as steric repulsion. A third repulsive mechanism occurs when the electrostatic and steric repulsions are combined, for example when using polyelectrolyte dispersants.

13.4.3
Wet Milling or Comminution

The primary particles produced after dispersion are subdivided into smaller units by milling or comminution (a process that requires rupture of bonds). Wet milling can be achieved using ball mills, bead mills (ceramic balls or beads are normally used to avoid contamination), or colloid mills. Again, the milling conditions must be adjusted to prevent heat and/or foam formation. The role of the dispersing agent (surfactant) in breaking the primary particles is usually described in terms of the ‘‘Rehbinder’’ effect – that is, the adsorption of dispersing agent molecules onto the surface of the particles (which lowers their surface energy) and in particular in the ‘‘cracks,’’ which facilitates their propagation.

To avoid contamination by products that may be released from the beads, alternative methods have been applied that avoid the need for beads, including sonochemical and cavitation processing. In sonochemical processing, an acoustic cavitation process can generate a transient localised hot zone with extremely high temperature and pressure gradients that leads to destruction of the large particles and the formation of nanoparticles. In hydrodynamic cavitation, nanoparticles are generated through the creation and release of gas bubbles inside the suspension.

13.4.4
Stabilisation of the Resulting Dispersion

The particles of the resulting dispersion may undergo aggregation (flocculation) on standing, as a result of the universal van der Waals attractions. Any two macroscopic bodies (such as particles) in a dispersion will attract each other as a result of the London dispersion attractive energy between the particles, and this attractive energy may become very large at short distances of separation between the particles. This attractive energy, G_A, is given by the following expression:

$$G_A = -\frac{A_{11(2)}\ R}{12\ h} \tag{13.16}$$

where $A_{11(2)}$ is the effective Hamaker constant of two identical particles with Hamaker constant A_{11} in a medium with Hamaker constant A_{22}. The Hamaker constant of any material is given by the following expression,

$$A = \pi^2\ q^2\ \beta \tag{13.17}$$

where q is number of atoms or molecules per unit volume, and β is the London dispersion constant. Equation (13.17) shows that A_{11} has the dimension of energy.

As mentioned above, in order to overcome the everlasting van der Waals attraction energy, it is essential to have a repulsive energy between the particles. The first mechanism is electrostatic repulsive energy, produced by the presence of electrical double layers around the particles and due to charge separation at the S/L interface. The dispersant should be strongly adsorbed onto the particles, produce a high charge (high surface or zeta-potential), and form an extended double layer (that can be achieved at low electrolyte concentration and low valency) [10, 11].

When charged colloidal particles in a dispersion approach each other such that the double layers begin to overlap (when particle separation becomes less than twice the double layer extension), then repulsion will occur. The individual double layers can no longer develop unrestrictedly, as the limited space does not allow complete potential decay [10, 11]. The potential $\psi_{H/2}$ half-way between the plates is no longer zero (as would be the case for isolated particles at $x \rightarrow \infty$). For two spherical particles of radius R and surface potential ψ_o and condition $\kappa R < 3$ (where κ is the reciprocal Debye length), the expression for the electrical double layer repulsive interaction is given by Deryaguin and Landau [10] and Verwey and Overbeek [11],

$$G_{el} = \frac{4\pi\ \varepsilon_r \varepsilon_o\ R^2\ \psi_o^2\ \exp-(\kappa h)}{2R + h} \tag{13.18}$$

where h is the closest distance of separation between the surfaces.

The above expression shows an exponential decay of G_{el} with h. The higher the value of κ (i.e., the higher the electrolyte concentration), the steeper the decay; this means that at any given distance h, the double layer repulsion will decrease with an increase of electrolyte concentration.

One important aspect of the double layer repulsion is the situation during particle approach. If at any stage the assumption is made that the double layers adjust to new conditions, so that equilibrium is always maintained, then the interaction will take place at a constant potential. This would be the case if the relaxation time of the surface charge were to be much shorter than the time that the particles are in each other's interaction sphere as a result of Brownian motion. However, if the relaxation time of the surface charge is appreciably longer than the time particles are in each other's interaction sphere, the charge rather than the potential will be the constant parameter. The constant charge leads to larger repulsion than the constant potential case.

Most qualitative aspects of the "microscopic" theory given by Equations (13.7–13.12) are fully confirmed; the only exception concerns the decay of G_{A} with h at large separations. Owing to the time required for electromagnetic waves to cover the distance between the particles, the h^{-2} dependence in Equation (13.7) gradually changes to h^{-3} dependence at large separations, a phenomenon known as retardation.

The combination of G_{el} and G_{A} results in the well-known theory of stability of colloids (DLVO theory) [8, 10, 11],

$$G_{\mathrm{T}} = G_{\mathrm{el}} + G_{\mathrm{A}} \tag{13.19}$$

A plot of G_{T} versus h is shown in Figure 13.3, which represents the case at low electrolyte concentrations – that is, a strong electrostatic repulsion between the particles. G_{el} decays exponentially with h; that is $G_{\mathrm{el}} \to 0$ as h becomes large. G_{A} is $\infty 1/h$, that is G_{A} does not decay to 0 at large h.

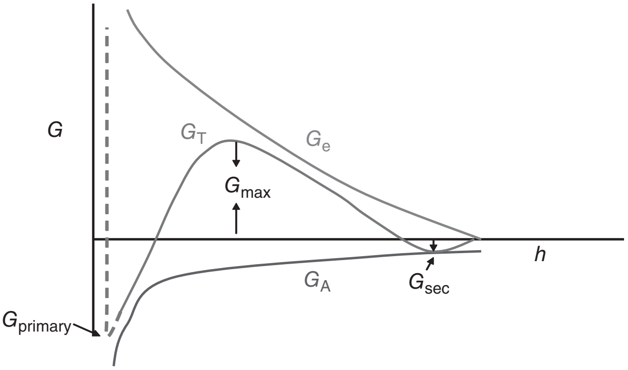

Figure 13.3 Schematic representation of the variation of G_{T} with h, according to DLVO theory.

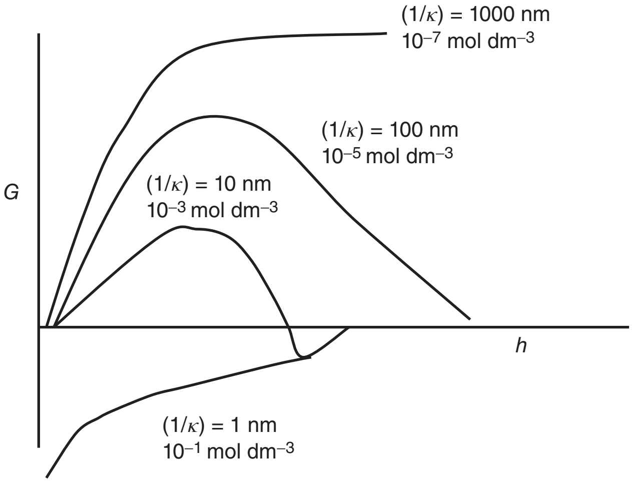

Figure 13.4 Variation of G with h at various electrolyte concentrations.

At long distances of separation, $G_A > G_{el}$, resulting in a shallow minimum (secondary minimum), whereas at very short distances, $G_A \gg G_{el}$, resulting in a deep primary minimum.

At intermediate distances, $G_{el} > G_A$, resulting in energy maximum, G_{max}, the height of which depends on ψ_o (or ψ_d) and the electrolyte concentration and valency.

At low electrolyte concentrations ($<10^{-2}$ mol dm^{-3} for a 1 : 1 electrolyte), G_{max} is high (>25 kT), and this prevents particle aggregation into the primary minimum. The higher the electrolyte concentration (and the higher the valency of the ions), the lower the energy maximum.

Under some conditions (depending on electrolyte concentration and particle size), flocculation into the secondary minimum may occur. This flocculation is weak and reversible. By increasing the electrolyte concentration, G_{max} decreases until, at a given concentration, it vanishes and particle coagulation occurs; this is illustrated in Figure 13.4, which shows the variation of G_T with h at various electrolyte concentrations.

Since approximate formulae are available for G_{el} and G_A, quantitative expressions for $G_T(h)$ can also be formulated. These can be used to derive expressions for the coagulation concentration, which is that concentration that causes every encounter between two colloidal particles to lead to destabilisation. Verwey and Overbeek [11] introduced the following criteria for transition between stability and instability,

$$G_T(= G_{el} + G_A) = 0 \tag{13.20}$$

$$\frac{dG_T}{dh} = 0 \tag{13.21}$$

$$\frac{dG_{el}}{dh} = -\frac{dG_A}{dh} \tag{13.22}$$

Using the equations for G_{el} and G_A, the critical coagulation concentration (ccc) could be calculated, as will be shown below. The theory predicts that the c.c.c. is directly proportional to the surface potential ψ_o and inversely proportional to the Hamaker constant A and the electrolyte valency $\underline{Z}$. The c.c.c is inversely proportional to Z^6 at high surface potential, and inversely proportional to Z^6 at low surface potential.

The second stabilisation mechanism, referred to as steric repulsive energy, is produced by the presence of adsorbed (or grafted) layers of surfactant or polymer molecules. In this case, the nonionic surfactant or polymer (referred to as polymeric surfactant) should be strongly adsorbed onto the particle surface, while the stabilising chain should be strongly solvated (hydrated in the case of aqueous suspensions) by molecules of the medium [12]. The most effective polymeric surfactants are those of the A-B, A-B-A block or BA_n graft copolymer. The ''anchor'' chain B is chosen to be highly insoluble in the medium and to have a strong affinity to the surface, while the A stabilising chain is chosen to be highly soluble in the medium and strongly solvated by the molecules of the medium. For suspensions of hydrophobic solids in aqueous media, the B chain can be polystyrene, poly(methylmethacrylate) or poly(propylene oxide), while the A chain may be poly(ethylene oxide), which is strongly hydrated by the medium.

When two particles each with a radius R and containing an adsorbed polymer layer with a hydrodynamic thickness δ_h, approach each other to a surface–surface separation distance h that is smaller than $2\delta_h$, the polymer layers interact with each other, resulting in two main situations [12]: (i) the polymer chains may overlap with each other; and/or (ii) the polymer layer may undergo some compression. In both cases, there will be an increase in the local segment density of the polymer chains in the interaction region. However, the ''real'' situation is perhaps in between the above two cases – that is, the polymer chains may undergo some interpenetration and some compression.

Provided that the dangling chains (the A chains in A-B, A-B-A block or BA_n graft copolymers) are in a good solvent, this local increase in segment density in the interaction zone will result in strong repulsion as a result of two main effects [12]. First, an increase in the osmotic pressure in the overlap region as a result of the unfavourable mixing of the polymer chains, when these are in good solvent conditions; this is referred to as osmotic repulsion or mixing interaction, and is described by a free energy of interaction G_{mix}. Second, a reduction in the configurational entropy of the chains in the interaction zone; this entropy reduction results from the decrease in the volume available for the chains when these are either overlapped or compressed; this is referred to as volume restriction interaction, entropic or elastic interaction, and is described by a free energy of interaction G_{el}.

The combination of G_{mix} and G_{el} is usually referred to as the steric interaction free energy, G_s, that is,

$$G_s = G_{mix} + G_{el} \tag{13.23}$$

The sign of G_{mix} depends on the solvency of the medium for the chains. If in a good solvent – that is, the Flory–Huggins interaction parameter χ is less than 0.5 – then G_{mix} is positive and the mixing interaction leads to repulsion (see below). In contrast, if $\chi > 0.5$ (i.e., the chains are in a poor solvent condition), then G_{mix} will be negative and the mixing interaction will become attractive. G_{el} is always positive, and hence in some cases stable dispersions can be produced in a relatively poor solvent (this is termed enhanced steric stabilisation).

As mentioned above, the mixing interaction results from the unfavourable mixing of the polymer chains, when these are in a good solvent conditions. Consider two spherical particles with the same radius and each containing an adsorbed polymer layer with thickness δ. Before overlap, in each polymer layer a chemical potential for the solvent $\mu_{\text{i}}{}^{\alpha}$ and a volume fraction for the polymer in the layer ϕ_2 can be defined. In the overlap region (volume element dV), the chemical potential of the solvent is reduced to $\mu_{\text{i}}{}^{\beta}$. This results from the increase in polymer segment concentration in this overlap region. In the overlap region, the chemical potential of the polymer chains is now higher than in the rest of the layer (with no overlap), and this amounts to an increase in the osmotic pressure in the overlap region. As a result, solvent will diffuse from the bulk to the overlap region, thus separating the particles such that a strong repulsive energy arises from this effect. The above repulsive energy can be calculated by considering the free energy of the mixing of two polymer solutions, as for example treated by Flory and Krigbaum [13]. The free energy of mixing is given by two terms: (i) an entropy term that depends on the volume fraction of polymer and solvent; and (ii) an energy term that is determined by the Flory–Huggins interaction parameter,

$$\delta(G_{\text{mix}}) = kT\ (n_1\ \ln\ \varphi_1 + n_2\ \ln\ \varphi_2 + \chi\ n_1\ \varphi_2) \tag{13.24}$$

where n_1 and n_2 are the number of moles of solvent and polymer with volume fractions φ_1 and φ_2, k is the Boltzmann constant, and T is the absolute temperature.

The total change in free energy of mixing for the whole interaction zone, V, is obtained by summing over all the elements in V,

$$G_{\text{mix}} = \frac{2kT\ V_2^2}{V_1}\ \nu_2\ \left(\frac{1}{2} - \chi\right)\ R_{\text{mix}}(h) \tag{13.25}$$

where V_1 and V_2 are the molar volumes of solvent and polymer respectively, ν_2 is the number of chains per unit area and $R_{\text{mix}}(h)$ is geometric function which depends on the form of the segment density distribution of the chain normal to the surface, $\rho(z)$. k is the Boltzmann constant and T is the absolute temperature.

Using the above theory, an expression can be derived for the free energy of mixing of two polymer layers (assuming a uniform segment density distribution in each layer) surrounding two spherical particles as a function of the separation distance h between the particles [12].

The expression for G_{mix} is,

$$G_{\text{mix}} = \left(\frac{2V_2^2}{V_1}\right)\ \nu_2\ \left(\frac{1}{2} - \chi\right)\ \left(\delta - \frac{h}{2}\right)^2\ \left(3R + 2\delta + \frac{h}{2}\right) \tag{13.26}$$

The sign of G_{mix} depends on the value of the Flory–Huggins interaction parameter χ: if $\chi < 0.5$, G_{mix} is positive and the interaction is repulsive; if $\chi > 0.5$, G_{mix} is negative and the interaction is attractive. The condition $\chi = 0.5$ and $G_{mix} = 0$ is termed the θ-condition. The latter corresponds to the case where the polymer mixing behaves as ideal, that is mixing of the chains does not lead to increase or decrease of the free *e*.

The elastic interaction arises from the loss in configurational entropy of the chains on the approach of a second particle. As a result of this approach, the volume available for the chains becomes restricted, and this results in a loss of the number of configurations. This can be illustrated by considering a simple molecule, represented by a rod that rotates freely in a hemisphere across a surface. When the two surfaces are separated by an infinite distance ∞, the number of configurations of the rod is $\Omega(\infty)$, which is proportional to the volume of the hemisphere. When a second particle approaches to a distance h such that it cuts the hemisphere (losing some volume), the volume available to the chains is reduced and the number of configurations become $\Omega(h)$, which is less than $\Omega(\infty)$. For two flat plates, G_{el} is given by the following expression,

$$\frac{G_{el}}{kT} = 2\nu_2 \ln\left[\frac{\Omega(h)}{\Omega(\infty)}\right] = 2\nu_2 R_{el}(h) \tag{13.27}$$

where $R_{el}(h)$ is a geometric function whose form depends on the segment density distribution. It should be stressed that G_{el} is always positive and could play a major role in steric stabilisation. G_{el} becomes very strong when the separation distance between the particles becomes comparable to the adsorbed layer thickness δ.

The combination of G_{mix} and G_{el} with G_A gives the total energy of interaction G_T (assuming that there is no contribution from any residual electrostatic interaction); that is,

$$G_T = G_{mix} + G_{el} + G_A \tag{13.28}$$

A schematic representation of the variation of G_{mix}, G_{el}, G_A and G_T with surface–surface separation distance h is shown in Figure 13.5. G_{mix} increases very sharply with decrease of h, when $h < 2\delta$. while G_{el} increases very sharply with decrease of h, when $h < \delta$. G_T versus h shows a minimum, G_{min}, at separation distances comparable to 2δ, and when $h < 2\delta$, G_T shows a rapid increase with decrease in h. The depth of the minimum depends on the Hamaker constant A, the particle radius R, and the adsorbed layer thickness δ. G_{min} increases with increase of A and R. At given values of A and R, G_{min} increases with a decrease in δ (i.e., with a decrease in the molecular weight, M_w, of the stabiliser). This is illustrated in Figure 13.6, which shows the energy–distance curves as a function of δ/R, and where the larger is the value of δ/R the smaller is the value of G_{min}. In this case, the system may approach thermodynamic stability, as is the case with nanosuspensions.

Several criteria can be established for effective steric stabilisation:

- The particles should be completely covered by the polymer (the amount of polymer should correspond to the plateau value). Any bare patches may cause

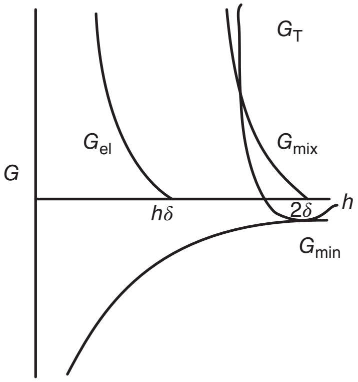

Figure 13.5 Energy–distance curves for sterically stabilised systems.

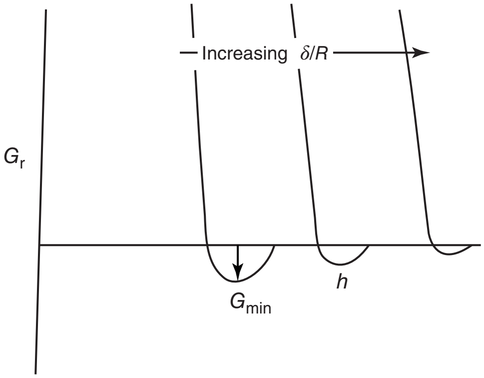

Figure 13.6 Variation of G_{min} with δ/R.

flocculation either by van der Waals attractions (between the bare patches) or by bridging flocculation (whereby a polymer molecule will become simultaneously adsorbed on two or more particles).

- The polymer should be strongly ''anchored'' to the particle surfaces, to prevent any displacement during particle approach; this is particularly important for concentrated suspensions. A-B, A-B-A block and BA_n graft copolymers are the most suitable for this purpose, where the chain B is chosen to be highly insoluble in the medium and has a strong affinity to the surface. Examples of B groups for hydrophobic particles in aqueous media are polystyrene and poly(methylmethacrylate).
- The stabilising chain A should be highly soluble in the medium, and strongly solvated by its molecules. Examples of A chains in aqueous media are poly(ethylene oxide) and poly(vinyl alcohol).
- δ should be sufficiently large (>5 nm) to prevent weak flocculation.

13.4.5
Prevention of Ostwald Ripening (Crystal Growth)

The driving force for Ostwald ripening is the difference in solubility between the small and large particles (the smaller particles have a higher solubility than their larger counterparts). The difference in chemical potential between different sized particles was given by Lord Kelvin [2] [Eq. (13.1)].

For two particles with radii r_1 and r_2 ($r_1 < r_2$),

$$\frac{RT}{V_m} \ln \left[\frac{S(r_1)}{S(r_2)}\right] = 2\sigma \left[\frac{1}{r_1} - \frac{1}{r_2}\right] \tag{13.29}$$

Equation (13.29) shows that, the larger the difference between r_1 and r_2, the higher the rate of Ostwald ripening.

Ostwald ripening can be quantitatively assessed from plots of the cube of the radius versus time t [14, 15],

$$r^3 = \frac{8}{9} \left[\frac{S(\infty)\ \sigma\ V_m\ D}{\rho\ RT}\right] t \tag{13.30}$$

where D is the diffusion coefficient of the disperse phase in the continuous phase.

Several factors affect the rate of Ostwald ripening, and these are determined by surface phenomena, although the presence of surfactant micelles in the continuous phase can also play a major role. Trace amounts of impurities that are highly insoluble in the medium and have a strong affinity to the surface can significantly reduce Ostwald ripening by blocking the active sites on the surface on which the molecules of the active ingredient can be deposited. Many polymeric surfactants – particularly those of the block and graft copolymer types – can also reduce the Ostwald ripening rate by being strongly adsorbed onto the surface of the particles, making the surface inaccessible for molecular deposition. Surfactant micelles that can solubilize the molecules of the active ingredient may enhance the rate of crystal grow by increasing the flux of transport by diffusion.

References

1. Tadros, T. (2012) *Dispersion of Powders in Liquids and Stabilisation of Suspensions*, Wiley-VCH Verlag GmbH, Weinheim.
2. Thompson, W. (Lord Kelvin) (1871) *Philos. Mag.*, **42**, 448.
3. Tadros, T. (2008) *Colloids in Cosmetics and Personal Care*, Wiley-VCH Verlag GmbH, Weinheim.
4. Gibbs, J.W. (1928) *Collected Work*, vol. **1**, Longman, New York, p. 219.
5. I. Capek, in *Encyclopedia of Colloid and Interface Science*, (ed. T. Tadros), (2013) Springer, p. 748.
6. Tadros, T., Izquierdo, P., Esquena, J., and Solans, C. (2004) *Adv. Colloid Interface Sci.*, **108-109**, 303.
7. Eastoe, J., Hopkins Hatzopolous, M., and Tabor, R. (2013) in *Encyclopedia of Colloid and Interface Science* (ed T. Tadros), Springer, p. 688.
8. Rideal, E.K. (1922) *Philos. Mag.*, **44**, 1152.
9. Washburn, E.D. (1921) *Phys. Rev.*, **17**, 273.
10. Deryaguin, B.V. and Landau, L. (1941) *Acta Physicochem. USSR*, **14**, 633.

11. Verwey, E.J.W. and Overbeek, J.T.G. (1948) *Theory of Stability of Lyophobic Colloids*, Elsevier, Amsterdam.

12. Napper, D.H. (1983) *Polymeric Stabilisation of Colloidal Dispersions*, Academic Press, London.

13. Flory, P.J. and Krigbaum, W.R. (1950) *J. Chem. Phys.*, **18**, 1086.

14. Lifshitz, I.M. and Slesov, V.V. (1959) *Sov. Phys. JETP*, **35**, 331.

15. Wagner, C. (1961) *Z. Electrochem.*, **35**, 581.

14
Formulation of Nanoemulsions

14.1
Introduction

Nanoemulsions are transparent or translucent systems mostly covering the size range 50 to 200 nm [1, 2], and may also be referred to as mini-emulsions [3, 4]. Unlike microemulsions (which are also transparent or translucent and thermodynamically stable; see Chapter 15), nanoemulsions are only kinetically stable. However, the long-term physical stability of nanoemulsions (with no apparent flocculation or coalescence) makes them unique and they are sometimes referred to as 'approaching thermodynamic stability'. The inherently high colloid stability of nanoemulsions can be well understood from a consideration of their steric stabilisation (when using nonionic surfactants and/or polymers), and how this is affected by the ratio of the adsorbed layer thickness to droplet radius (this will be discussed below). Unless adequately prepared (to control the droplet size distribution) and stabilised against Ostwald ripening (that occurs when the oil has some finite solubility in the continuous medium), nanoemulsions may lose their transparency with time as a result of increases in droplet size.

The attraction of nanoemulsions for application in personal care products and cosmetics, as well as in healthcare, is due to the following advantages:

- The very small droplet size causes a large reduction in the gravity force, and the Brownian motion may be sufficient for overcoming gravity; this means that no creaming or sedimentation will occur on storage.
- The small droplet size also prevents any flocculation of the droplets. If weak flocculation can be prevented this enables the system to remain dispersed, with no separation.
- The small size of the droplets also prevents their coalescence, as the droplets are nondeformable and hence surface fluctuations are prevented. The significant surfactant film thickness (relative to droplet radius) also prevents any thinning or disruption of the liquid film between the droplets.
- Nanoemulsions are suitable for the efficient delivery of active ingredients through the skin. The large surface area of the emulsion system allows the rapid penetration of active agents.

Formulation of Disperse Systems: Science and Technology, First Edition. Tharwat F. Tadros.

- Due to their small size, nanoemulsions can penetrate the ''rough,'' skin surface and this enhances the penetration of active agents.
- The transparent nature of the system, their fluidity (at reasonable oil concentrations), as well as the absence of any thickeners may give nanoemulsions a pleasant aesthetic character and skin feel.
- Unlike microemulsions (which require a high surfactant concentration, usually in the region of 20% and higher for a 20% microemulsion), nanoemulsions can be prepared using reasonable surfactant concentrations. For a 20% O/W nanoemulsion, a surfactant concentration in the region of 5% may be sufficient.
- The small size of the droplets allows nanoemulsion to be deposited uniformly on substrates. Wetting, spreading and penetration may be also enhanced as a result of the low surface tension of the whole system and the low interfacial tension of the O/W droplets.
- Nanoemulsions can be applied for the delivery of fragrants, which are often incorporated in many personal care products. The same could apply to perfumes, which preferably are formulated alcohol-free.
- Nanoemulsions may be applied as a substitute for liposomes and vesicles (which are much less stable). It is also possible in some cases to build lamellar liquid crystalline phases around the nanoemulsion droplets.

In spite of the above advantages, nanoemulsions have attracted interest only during recent years, for the following reasons:

- Their preparation often requires special application techniques, such as the use of high-pressure homogenisation as well as ultrasound. Such equipment (e.g., the Microfluidizer) has become available only during recent years.
- There is a perception in the personal care products and cosmetic industries that nanoemulsions are expensive to produce; indeed, expensive equipment is required and high concentrations of emulsifiers are used when compared to macroemulsion production.
- There is a lack of understanding of the mechanism of production of submicron droplets and the roles of surfactants and cosurfactants.
- Demonstrations are lacking of the benefits that can be obtained from using nanoemulsions when compared to classic macroemulsion systems.
- A lack of understanding of the interfacial chemistry involved in production of nanoemulsions. For example, few formulations chemists are aware of the concepts of phase inversion composition (PIC) and phase inversion temperature (PIT), and how these can be usefully applied to produce small emulsion droplets.
- A poor knowledge of the mechanism of Ostwald ripening, which is perhaps the most serious instability problem with nanoemulsions.
- A lack of knowledge regarding the ingredients that can be incorporated to overcome Ostwald ripening. For example, the addition of a second oil phase with very low solubility and/or the incorporation of polymeric surfactants that strongly adsorb at the O/W interface (which are also insoluble in the aqueous medium).
- A fear of introducing new systems without fully evaluating the costs and benefits.

In spite of the above difficulties, several companies have introduced nanoemulsions onto the market, and their benefits will be evaluated within the next few years. Nanoemulsions have been used in the pharmaceutical industry as drug-delivery systems [5], although the acceptance by customers of nanoemulsions as a new type of formulation depends on how they are perceived and their efficacy. With the advent of new instruments for high-pressure homogenisation, and the competition between various manufacturers, the cost of nanoemulsion production will surely and may even approach that of classic macroemulsions. Fundamental investigations into the role of surfactants in the process [6, 7] will lead to optimised emulsifier systems such that a more economic use of surfactants will doubtless emerge.

In this chapter, the fundamental principles of emulsification and the role of surfactants, as well as the production of nanoemulsions using high-pressure homogenisation, the PIC and PIT principles, and via the dilution of microemulsions, will be discussed. Subsequently, the theory of steric stabilisation of emulsions and the role of the relative ratio of adsorbed layer thickness to the droplet radius will be described, as will the theory of Ostwald ripening and methods of reducing the process. The latter include the incorporation of a second oil phase with very low solubility and the use of strongly adsorbed polymeric surfactants. Finally, examples will be given of recently prepared nanoemulsions, and of investigations of the above effects on these materials.

14.2
Mechanism of Emulsification

As mentioned in Chapter 10, the preparation of an emulsion requires oil, water, a surfactant, and energy. This can be considered on the basis of the energy required to expand the interface, $\Delta A\gamma$ (where ΔA is the increase in interfacial area when the bulk oil with area A_1 produces a large number of droplets with area A_2; $A_2 \gg A_1$, where γ is the interfacial tension). Since γ is positive, the energy to expand the interface is large and positive. This energy term cannot be compensated by the small entropy of dispersion $T\Delta S$ (which is also positive), and the total free energy of formation of an emulsion, ΔG is positive,

$$\Delta G = \Delta A\gamma - T\Delta S \tag{14.1}$$

Thus, emulsion formation is nonspontaneous and energy is required to produce the droplets. The formation of large droplets (of a few micrometers), as is the case for macroemulsions, is fairly easy and hence high-speed stirrers such as the UltraTurrax or Silverson mixer are sufficient to produce the emulsion. In contrast, the formation of small drops (submicron, as is the case with nanoemulsions) is difficult and this requires a large amount of surfactant and/or energy. The high energy required to form nanoemulsions can be understood by considering the Laplace pressure p (the difference in pressure between inside and outside the droplet,

$$p = \gamma \left(\frac{1}{R_1} + \frac{1}{R_2} \right) \tag{14.2}$$

where R_1 and R_2 are the principal radii of curvature of the drop.

For a spherical drop, $R_1 = R_2 = R$, and

$$p = \frac{2\gamma}{R} \tag{14.3}$$

In order to break up a drop into smaller droplets, it must be strongly deformed and this deformation will increase p; consequently, the stress needed to deform the drop will be higher for a smaller drop. As the stress is generally transmitted by the surrounding liquid via agitation, higher stresses will need a more vigorous agitation, and hence more energy is needed to produce smaller drops [8]. Surfactants play major roles in the formation of nanoemulsions: By lowering the interfacial tension, p is reduced such that the stress needed to break up a drop is also reduced. Surfactants prevent the coalescence of newly formed drops.

When assessing a nanoemulsion formation, the normal approach is to measure the droplet size distribution using dynamic light scattering techniques, including photon correlation spectroscopy (PCS). In this technique, the intensity fluctuation of light scattered by the droplets is measured as they undergo Brownian motion [9]. When a light beam passes through a nanoemulsion, an oscillating dipole moment is induced in the droplets, such that the light is re-radiated. Due to the random position of the droplets, the intensity of the scattered light will, at any instant, appear as a random diffraction or ‘‘speckle’’ pattern. As the droplets undergo Brownian motion, the random configuration of the pattern will, therefore, fluctuate such that the time taken for an intensity maximum to become a minimum (i.e., the coherence time) will correspond exactly to the time required for the droplet to move one wavelength. By using a photomultiplier of which the active area is about the diffraction maximum (i.e., one coherence area), this intensity fluctuation can be measured. The analogue output is digitised using a digital correlator that measures the photocount (or intensity) correlation function of the scattered light. The photocount correlation function $G^{(2)}(\tau)$ is given by the equation:

$$G^{(2)}(\tau) = B(1 + \gamma^2 [g^{(1)}(\tau)]^2) \tag{14.4}$$

where τ is the correlation delay time. The correlator compares $G^{(2)}(\tau)$ for many values of τ. B is the background value to which $G^{(2)}(\tau)$ decays at long delay times, while $g^{(1)}(\tau)$ is the normalised correlation function of the scattered electric field, and γ is a constant (~1).

For monodisperse noninteracting droplets,

$$g^{(1)} = \exp(-\Gamma \tau) \tag{14.5}$$

where Γ is the decay rate or inverse coherence time, that is related to the translational diffusion coefficient D by the equation,

$$\Gamma = DK^2 \tag{14.6}$$

where K is the scattering vector,

$$K = \frac{4\pi n}{\lambda_o} \sin\left(\frac{\theta}{2}\right) \tag{14.7}$$

where λ is the wavelength of light *in vacuo*, n is the refractive index of the solution, and θ is the scattering angle.

The droplet radius R can be calculated from D using the Stokes–Einstein equation,

$$D = \frac{kT}{6\pi \eta_o R} \tag{14.8}$$

where η_o is the viscosity of the medium.

The above analysis is valid for dilute monodisperse droplets. With many nanoemulsions the droplets are not perfectly monodisperse (usually with a narrow size distribution), and the light-scattering results are analysed for polydispersity. For this, the data are expressed as an average size, and a polydispersity index provides information on how they deviate from the average size.

14.3
Methods of Emulsification and the Role of Surfactants

With macroemulsions, several procedures may be applied for emulsion preparation, ranging from simple pipe flow (low agitation energy, L), static mixers and general stirrers (low to medium energy, L-M), high-speed mixers such as the UltraTurrax (M), colloid mills and high-pressure homogenisers (high-energy, H), ultrasound generators (M-H). The method of preparation can be either continuous (C) or batch-wise (B). With nanoemulsions, however, a higher power density is required and this restricts their preparation to the use of high-pressure homogenisation and ultrasound.

An important parameter that describes droplet deformation, Weber number, W_e, provides the ratio of the external stress $G\eta$ (where G is the velocity gradient and η is the viscosity) over the Laplace pressure (see Chapter 10),

$$W_e = \frac{G\eta r}{2\gamma} \tag{14.9}$$

The droplet deformation increases with increases in the Weber number which means that, in order to produce small droplets, high stresses (i.e., high shear rates) are require. In other words, the production of nanoemulsions costs more energy than does the production of macroemulsions [4]. The role of surfactants in emulsion formation has been described in detail in Chapter 10, and the same principles apply to the formation of nanoemulsions. Thus, it is important to consider the effects of surfactants on the interfacial tension, interfacial elasticity, and interfacial tension gradients.

14.4
Preparation of Nanoemulsions

Four methods may be applied to prepare nanoemulsions (covering the droplet radius size range of 50 to 200 nm): high-pressure homogenisation (aided by an appropriate choice of surfactants and cosurfactants); application of the PIC method; application of the PIT concept; and the dilution of a microemulsion.

14.4.1
High-Pressure Homogenisation

The production of small (submicron) droplets requires the application of large amounts of energy, as the process of emulsification is generally very inefficient (as illustrated below).

Simple calculations have shown that the mechanical energy required for emulsification exceeds the interfacial energy by several orders of magnitude. For example, to produce an emulsion at $\varphi = 0.1$ with a $d_{32} = 0.6\,\mu\text{m}$, using a surfactant that gives an interfacial tension $\gamma = 10\,\text{mN m}^{-1}$, the net increase in surface free energy is $A\gamma = 6\varphi\gamma/d_{32} = 10^4\,\text{J m}^{-3}$. The mechanical energy required in a homogeniser is $10^7\,\text{J m}^{-3}$, which represents an efficiency of only 0.1%, with the rest of the energy (99.9%) being dissipated as heat [10].

The intensity of the process or the effectiveness in making small droplets is often governed by the net power density ($\varepsilon(t)$):

$$p = \varepsilon(t)\,\mathrm{d}t \qquad (14.10)$$

where t is the time during which emulsification occurs.

The break-up of droplets will only occur at high ε-values, which means that the energy dissipated at low ε levels is wasted. Batch processes are generally less efficient than continuous processes and this shows why, when using a stirrer in a large vessel, most of the energy applied at low intensity is dissipated as heat. In a homogeniser, p is simply equal to the homogeniser pressure.

Several procedures may be applied to enhance the efficiency of emulsification when producing nanoemulsions. First, the efficiency of agitation should be optimised by increasing ε and decreasing the dissipation time. Second, the emulsion should preferably be prepared at a high volume faction of the disperse phase and diluted afterwards, although very high φ-values may result in coalescence occurring during the emulsification. The addition of more surfactant might create a smaller γ_{eff} and possibly diminish any re-coalescence. A surfactant mixture should be used that shows a greater reduction in γ of the individual components; if possible, the surfactant should be dissolved in the disperse phase rather than in the continuous phase, as the latter approach often leads to smaller droplets.

Notably, it may be useful to emulsify in steps of increasing intensity, particularly with emulsions having a highly viscous disperse phase.

14.4.2
Phase Inversion Composition (PIC) Principle

A study of the phase behaviour of water/oil/surfactant systems showed that emulsification can be achieved via three different low-energy methods, as shown schematically Figure 14.1:

- The stepwise addition of oil to a water–surfactant mixture.
- The stepwise addition of water to a solution of the surfactant in oil.
- Mixing all of the components in the final composition and pre-equilibrating the samples prior to emulsification.

In these studies, the system water/Brij 30 (polyoxyethylene lauryl ether with an average of 4 mol ethylene oxide/decane) was chosen as a model to obtain O/W emulsions. The results showed that nanoemulsions with droplet sizes on the order of 50 nm were formed only when water was added to mixtures of surfactant and oil (method B), whereby an inversion from a W/O emulsion to an O/W nanoemulsion occurred.

14.4.3
Phase Inversion Temperature (PIT) Principle

Phase inversion in emulsions can be one of two types: (i) a transitional inversion, induced by changing factors that affect the HLB of the system, such as temperature and/or electrolyte concentration; and/or (ii) a catastrophic inversion, which is induced by increasing the volume fraction of the disperse phase.

Transitional inversion can also be induced by changing the HLB number of the surfactant at constant temperature, using surfactant mixtures. This is illustrated in Figure 14.2, which shows the average droplet diameter and rate constant for

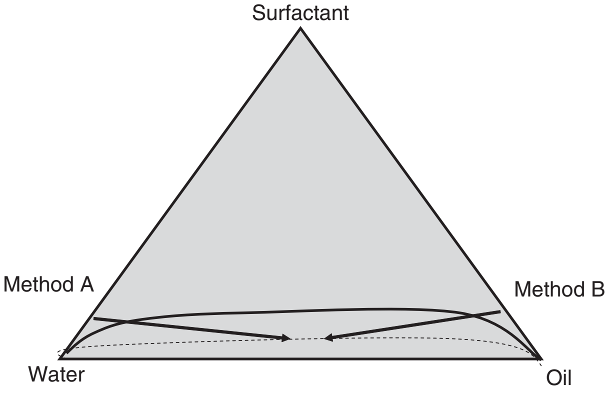

Figure 14.1 Schematic representation of the experimental path in two emulsification methods. Method A, addition of decane to water/surfactant mixture; Method B, addition of water to decane/Brij 30 solutions.

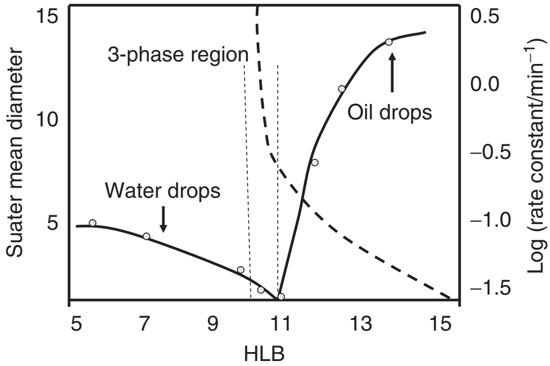

Figure 14.2 Emulsion droplet diameters (circles) and rate constant for attaining steady size (squares) as function of HLB–cyclohexane/nonylphenol ethoxylate.

attaining a constant droplet size as a function of the HLB number. It can be seen that the diameter decreases and the rate constant increases as inversion is approached.

To apply the phase inversion principle, the transitional inversion method should be used, as demonstrated by Shinoda and coworkers [11, 12] when using nonionic surfactants of the ethoxylate type. These surfactants are highly dependent on temperature, becoming lipophilic with increasing temperature due to dehydration of the poly(ethylene oxide) (PEO) chain. When an O/W emulsion that has been prepared using a nonionic surfactant of the ethoxylate type is heated, at a critical temperature – the PIT – the emulsion will invert to a W/O emulsion. At the PIT, the droplet size reaches a minimum and the interfacial tension also reaches a minimum, but the small droplets are unstable and coalesce very rapidly. Rapid cooling of an emulsion that has been prepared close to the PIT results in very stable and small emulsion droplets.

A clear demonstration of the phase inversion that occurs on heating an emulsion was made when studying the phase behaviour of emulsions as a function of temperature. This is illustrated in Figure 14.3, which shows schematically the effect of increasing the temperature [13, 14]. At low temperature, over the Winsor I region, O/W macroemulsions can be formed which are quite stable; however, on increasing the temperature the O/W emulsion stability is decreased and the macroemulsion finally resolves when the system reaches the Winsor III phase region (when both O/W and W/O emulsions are unstable). At higher temperature, over the Winsor II region, the W/O emulsions become stable.

Near the HLB temperature, the interfacial tension reaches a minimum, as illustrated in Figure 14.4. Thus, by preparing the emulsion at a temperature 2–4 °C below the PIT (near the minimum in γ), followed by rapid cooling of the system, nanoemulsions may be produced. The minimum in γ can be explained in terms of the change in curvature H of the interfacial region, as the system changes from O/W to W/O. For an O/W system and normal micelles, the monolayer curves towards the oil such that H has a positive value. However, for a W/O emulsion and inverse micelles the monolayer will curve towards the water and H will be assigned

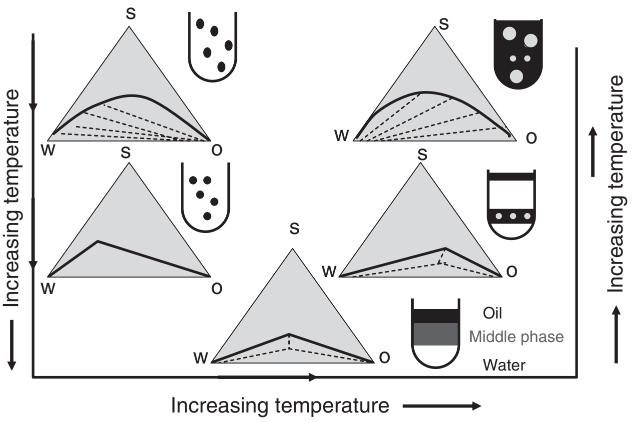

Figure 14.3 The PIT concept.

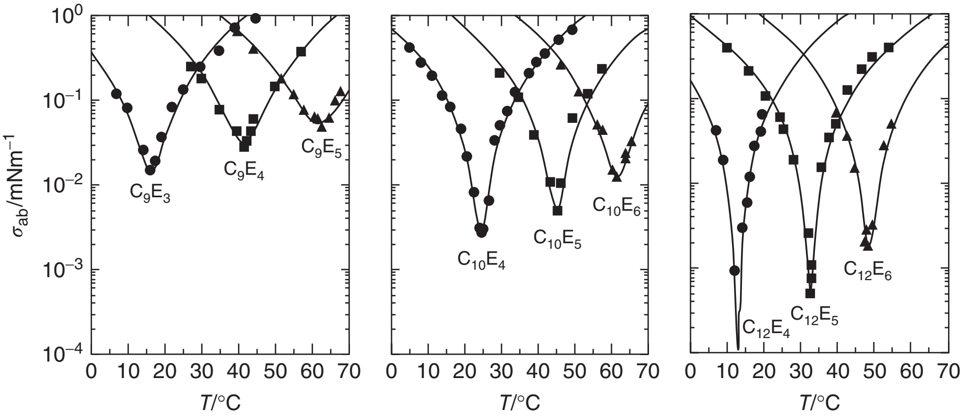

Figure 14.4 Interfacial tensions of *n*-octane against water in the presence of various C_nE_m surfactants above the cmc as a function of temperature.

a negative value. At the inversion point (HLB temperature), H becomes zero while γ reaches a minimum.

14.4.4
Preparation of Nanoemulsions by Dilution of Microemulsions

A common method of preparing nanoemulsions by self-emulsification is to dilute an O/W microemulsion with water. During this process, part of the surfactant and/or cosurfactant will diffuse to the aqueous phase and the droplets will no longer be thermodynamically stable as the surfactant concentration will not be high enough to maintain the ultra-low interfacial tension ($<10^{-4}$ mN m^{-1}) for thermodynamic stability. Hence, the system becomes unstable and the droplets show a tendency to grow by coalescence and/or Ostwald ripening, forming a

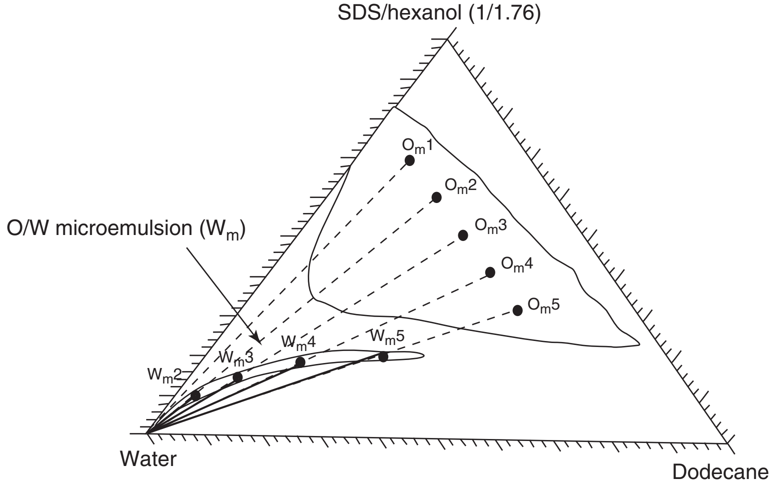

Figure 14.5 Pseudoternary phase diagram of water/SDS/hexanol/dodecane with SDS : hexanol ratio of 1 : 1.76. Solid and dashed lines indicate the emulsification paths followed starting from both O/W (W$_m$) and W/O (O$_m$) microemulsion domains.

nanoemulsion. This is illustrated in Figure 14.5, which shows the phase diagram of the system water/SDS-hexanol (ratio 1 : 1.76)/dodecane.

Nanoemulsions can be prepared starting from microemulsions located in the inverse microemulsion domain, O$_m$, and in the direct microemulsion domain, W$_m$, at different oil : surfactant ratios ranging from 12 : 88 to 40 : 60, and coincident for both types of microemulsion. The water concentration is fixed at 20% for microemulsions in the O$_m$ domain labelled as O$_m$1, O$_m$2, O$_m$3, O$_m$4, and O$_m$5. The microemulsions in the W$_m$ region are accordingly W$_m$2, W$_m$3, W$_m$4, and W$_m$5, and their water content was decreased from W$_m$2 to W$_m$5.

Four main emulsification methods can be applied, including: (i) the addition of a microemulsion into water in one step; (ii) the addition of a microemulsion into water stepwise; (iii) the addition of water into a microemulsion in one step; and (iv) the addition of water into microemulsion stepwise. The final water content is kept constant at 98 wt%.

Starting emulsification from W$_m$ microemulsions, low-polydisperse nanoemulsions with droplet sizes within the range 20–40 nm are obtained, regardless of the emulsification method used. When starting from O$_m$ microemulsions the nanoemulsion formation and properties depended on the emulsification method. For example, from a O$_m$1 microemulsion a turbid emulsion with rapid creaming was obtained, whichever method was used, and in this case the direct microemulsion region W$_m$ was not crossed. However, starting from O$_m$2 to O$_m$5 and using the fourth emulsification method, in which water is gradually added to the microemulsion, the nanoemulsion droplet sizes coincided with those obtained starting from microemulsions in the W_m domain for the corresponding O : S ratio. The first three of the above-described methods produced coarse emulsions.

14.5
Steric Stabilisation and the Role of the Adsorbed Layer Thickness

As most nanoemulsions are prepared using nonionic and/or polymeric surfactants, it is necessary to consider the interaction forces between droplets containing adsorbed layers (steric stabilisation). As this was described in detail in Chapter 10, only a summary will be given here [15, 16].

When two droplets each containing an adsorbed layer of thickness δ approach to a distance of separation h, whereby h becomes less than 2δ, repulsion will occur as a result of two main effects:

- Unfavourable mixing of the stabilising chains A of the adsorbed layers when these are in good solvent conditions; this is referred to as the ‘‘mixing’’ (osmotic) interaction, G_{mix}, and is given by the following expression:

$$\frac{G_{\text{mix}}}{kT} = \frac{4\pi}{3V_1}\phi_2^2\left(\frac{1}{2}-\chi\right)\left(3a+2\delta+\frac{h}{2}\right) \tag{14.11}$$

  where k is the Boltzmann constant, T is the absolute temperature, V_1 is the molar volume of the solvent, φ_2 is the volume fraction of the polymer (the A chains) in the adsorbed layer, and χ is the Flory–Huggins (polymer–solvent interaction) parameter. It can be seen that G_{mix} depends on three main parameters: (i) the volume fraction of the A chains in the adsorbed layer (the more dense the layer is, the higher the value of G_{mix}); (ii) the Flory–Huggins interaction parameter χ (for G_{mix} to remain positive, i.e., repulsive, χ should be $<1/2$); and (iii) the adsorbed layer thickness, δ.
- Reduction in configurational entropy of the chains on significant overlap. This is referred to as ‘‘elastic’’ (entropic) interaction, and is given by the expression:

$$G_{\text{el}} = 2\nu_2 \ln\left[\frac{\Omega(h)}{\Omega(\infty)}\right] \tag{14.12}$$

  where ν_2 is the number of chains per unit area, $\Omega(h)$ is the configurational entropy of the chains at a separation distance h, and $\Omega(\infty)$ is the configurational entropy at infinite distance of separation.
- The combination of G_{mix}, G_{el} with the van der Waals attraction G_A gives the total energy of interaction G_T,

$$G_T = G_{\text{mix}} + G_{\text{el}} + G_A \tag{14.13}$$

Figure 14.6 shows a schematic representation of the variation of G_{mix}, G_{el}, G_A and G_T with h. As can be seen form Figure 14.6, G_{mix} increases very rapidly with a decrease of h, but as soon as $h < 2\delta$, G_{el} increases very rapidly with a decrease of h when $h < \delta$. G_T shows one minimum, G_{min}, and increases very rapidly with decrease of h when $h < 2\delta$.

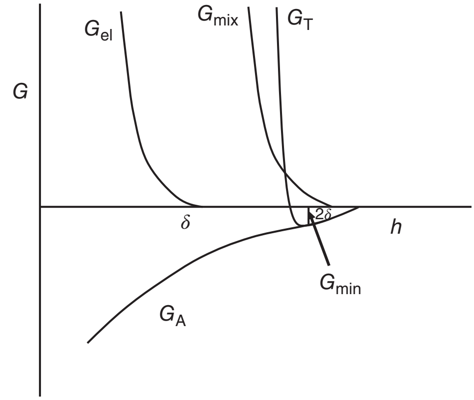

Figure 14.6 Variation of G_{mix}, G_{el}, G_A and G_T with *h*.

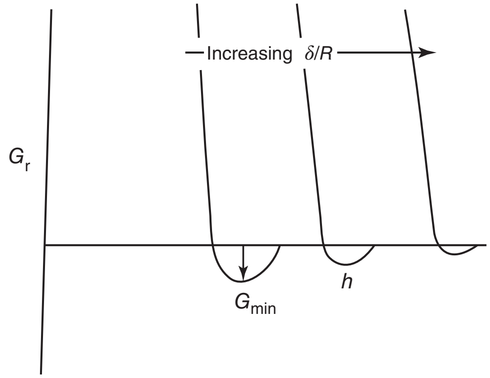

Figure 14.7 Variation of G_T with *h* with increasing δ/R.

The magnitude of G_{min} depends on the following parameters: the particle radius *R*; the Hamaker constant *A*; and the adsorbed layer thickness δ. As an illustration, Figure 14.7 shows the variation of G_T with h at various ratios of δ/R. It can be seen from Figure 14.7 that the depth of the minimum decreases with increasing δ/R, and this is the basis of the high kinetic stability of nanoemulsions. With nanoemulsions having a radius in the region of 50 nm and an adsorbed layer thickness of say 10 nm, the value of δ/R will be 0.2. This high value (when compared to the situation with macroemulsions, where δ/R is at least an order of magnitude lower) results in a very shallow minimum (which could be less than kT).

The above situation results in a very high stability with no flocculation (weak or strong). In addition, the very small size of the droplets and the dense adsorbed layers ensure a lack of deformation of the interface, and a lack of thinning and disruption of the liquid film between the droplets; hence, coalescence is also prevented.

The only instability problem encountered with nanoemulsions is Ostwald ripening, which is discussed below.

14.5.1
Ostwald Ripening

One of the main problems with nanoemulsions is Ostwald ripening which results from differences in solubility between the small and large droplets. The difference in the chemical potential of dispersed phase droplets between different-sized droplets as given by Lord Kelvin [17],

$$c(r) = c(\infty)\,\exp\left(\frac{2\gamma V_\mathrm{m}}{r\,RT}\right) \tag{14.14}$$

where $c(r)$ is the solubility surrounding a particle of radius r, $c(\infty)$ is the bulk phase solubility, and V_m is the molar volume of the dispersed phase.

The quantity $(2\gamma V_\mathrm{m}/RT)$ is termed the characteristic length, and has an order of ~1 nm or less, indicating that the difference in solubility of a 1 μm droplet is on the order of 0.1%, or less.

Theoretically, Ostwald ripening should lead to the condensation of all droplets into a single drop (i.e., phase separation); however, this does not occur in practice as the rate of growth decreases with increases of droplet size.

For two droplets of radii r_1 and r_2 (where $r_1 < r_2$),

$$\left(\frac{RT}{V_\mathrm{m}}\right)\ln\left[\frac{c(r_1)}{c(r_2)}\right] = 2\gamma\left(\frac{1}{r_1} - \frac{1}{r_2}\right) \tag{14.15}$$

Equation (14.15) shows that the larger the difference between r_1 and r_2, the higher the rate of Ostwald ripening.

Ostwald ripening can be quantitatively assessed from plots of the cube of the radius versus time t (the Lifshitz–Slesov–Wagner; LSW) theory [18, 19],

$$r^3 = \frac{8}{9}\left[\frac{c(\infty)\,\gamma\, V_\mathrm{m}\, D}{\rho\, RT}\right] t \tag{14.16}$$

where D is the diffusion coefficient of the disperse phase in the continuous phase and ρ is the density of the disperse phase.

Several methods may be applied to reduce Ostwald ripening [20–22]:

- The addition of a second disperse phase component which is insoluble in the continuous phase (e.g., squalene). In this case, a significant partitioning occurs between different droplets, with the component having a low solubility in the continuous phase expected to be concentrated in the smaller droplets. During Ostwald ripening in a two-component disperse phase system, equilibrium is established when the difference in chemical potential between different-sized droplets (which results from curvature effects) is balanced by the difference in chemical potential resulting from a partitioning of the two components. If the secondary component has zero solubility in the continuous phase, the size distribution will not deviate from the initial one (the growth rate is equal to zero).

In the case of limited solubility of the secondary component, the distribution is the same as governed by Equation (14.16); that is, a mixture growth rate is obtained which is still lower than that of the more soluble component.

- Modification of the interfacial film at the O/W interface. According to Equation (14.15), a reduction in γ will result in a reduction of Ostwald ripening; however, this alone is not sufficient as γ has to be reduced by several orders of magnitude. Walstra [23] suggested that, by using surfactants which are strongly adsorbed at the O/W interface (i.e., polymeric surfactants) and which do not desorb during ripening, the rate could be significantly reduced. An increase in the surface dilational modulus and decrease in γ would be observed for the shrinking drops. The difference in γ between the droplets would balance the difference in capillary pressure (i.e., curvature effects).

To achieve the above effect it is useful to use A-B-A block copolymers that are soluble in the oil phase and insoluble in the continuous phase. The polymeric surfactant should enhance the lowering of γ by the emulsifier. In other words, the emulsifier and the polymeric surfactant should show synergy in lowering γ.

14.5.2
Practical Examples of Nanoemulsions

Several experiments were recently carried to investigate the methods of preparing nanoemulsions, and their stability [24]. In the first method, the PIT principle was applied whereby experiments were carried out using hexadecane and isohexadecane (Arlamol HD) as the oil phase and Brij 30 ($C_{12}EO_4$) as the nonionic emulsifier. The phase diagrams of the ternary system water-$C_{12}EO_4$-hexadecane and water-$C_{12}EO_4$-isohexadecane are shown in Figures 14.8 and 14.9. The main features of the pseudoternary system were as follows: (i) O_m isotropic liquid transparent phase, which extended along the hexadecane-$C_{12}EO_4$ or isohexadecane-$C_{12}EO_4$ axis, corresponding to inverse micelles or W/O microemulsions; (ii) L_α lamellar liquid crystalline phase, which extended from the W-$C_{12}EO_4$ axis towards the oil vertex; (iii) the rest of the phase diagram consisted of two- or three-phase regions: ($W_m + O$) two-liquid-phase region, which appeared along the water-oil axis; ($W_m + L_\alpha + O$) three-phase region, which consisted of a bluish liquid phase (O/W microemulsion), a lamellar liquid crystalline phase (L_α) and a transparent oil phase; ($L_\alpha + O_m$) two-phase region which consisted of an oil and liquid crystalline region; and M_{LC}, a multiphase region which contained a lamellar liquid crystalline phase (L_α).

The HLB temperature was determined using conductivity measurements, whereby 10^{-2} mol dm^{-3} NaCl was added to the aqueous phase (to increase the sensitivity of the measurements). The concentration of NaCl was low and hence had little effect on the phase behaviour.

Figure 14.10 shows the variation of conductivity versus temperature for 20% O/W emulsions at different surfactant concentrations. It can be seen that there is a sharp decrease in conductivity at the PIT or HLB temperature of the system. The HLB temperature then decreases with increases in surfactant concentration,

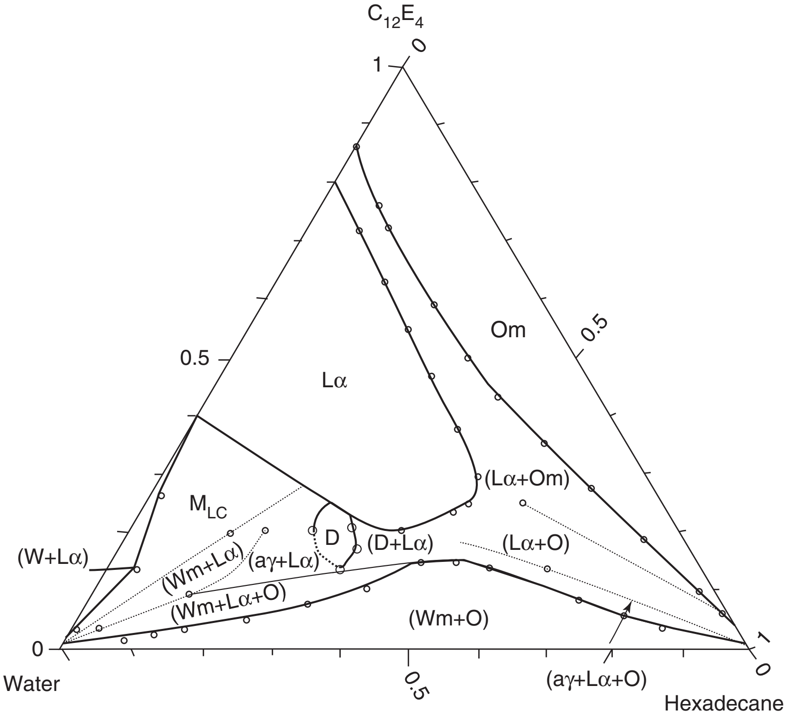

Figure 14.8 Pseudoternary phase diagram at 25 °C of the system water-C$_{12}$EO$_4$-hexadecane.

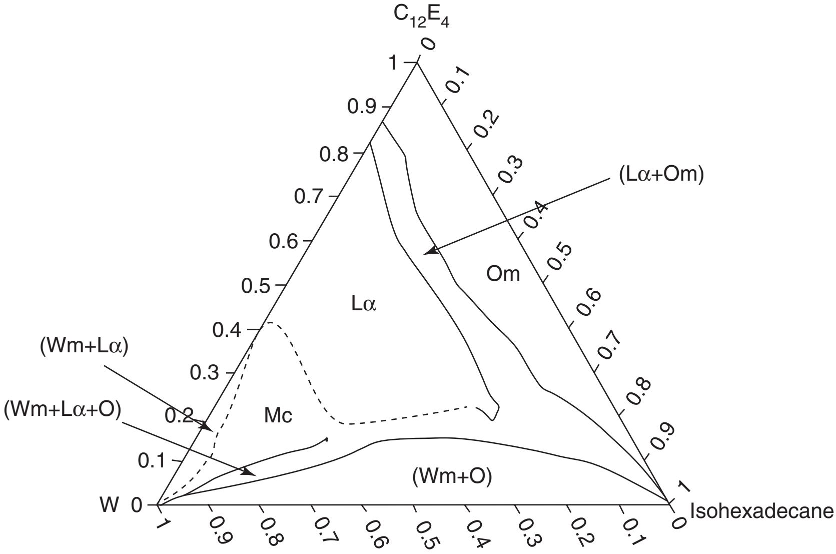

Figure 14.9 Pseudoternary phase diagram at 25 °C of the system water-C$_{12}$EO$_4$-isohexadecane.

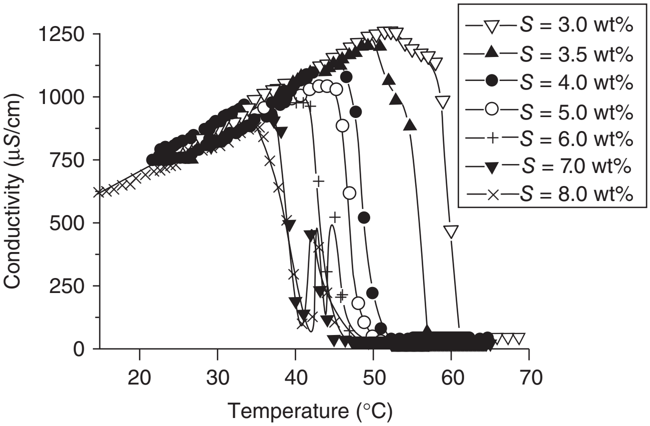

Figure 14.10 Conductivity versus temperature for a 20 : 80 hexadecane : water emulsions at various $C_{12}EO_4$ concentrations.

though this may have been due to the excess nonionic surfactant remaining in the continuous phase. At a concentration of surfactant higher than 5%, however, the conductivity plots showed a second maximum (Figure 14.10) that was attributed to the presence of L_α phase and bicontinuous L_3 or D' phases [25].

Nanoemulsions were prepared by rapid cooling of the system to 25 °C, and the droplet diameter was determined using PCS. The results are summarised in Table 14.1, which shows the exact composition of the emulsions, HLB temperature, z-average radius, and polydispersity index.

O/W nanoemulsions with droplet radii in the range 26–66 nm could be obtained at surfactant concentrations between 4% and 8%. The nanoemulsion droplet size and polydispersity index was shown to decrease with increases in surfactant concentration; this effect was considered due to the to the increase in surfactant interfacial area and the decrease in interfacial tension, γ.

Table 14.1 Composition, HLB temperature (T_{HLB}), droplet radius r and polydispersity index (PI) for the system water-$C_{12}EO_4$-hexadecane at 25 °C.

Surfactant (wt%)	Water (wt%)	Oil/water	T_{HLB} (°C)	r (nm)	PI
2.0	78.0	20.4/79.6	—	320	1.00
3.0	77.0	20.6/79.4	57.0	82	0.41
3.5	76.5	20.7/79.3	54.0	69	0.30
4.0	76.0	20.8/79.2	49.0	66	0.17
5.0	75.0	21.2/78.9	46.8	48	0.09
6.0	74.0	21.3/78.7	45.6	34	0.12
7.0	73.0	21.5/78.5	40.9	30	0.07
8.0	72.0	21.7/78.3	40.8	26	0.08

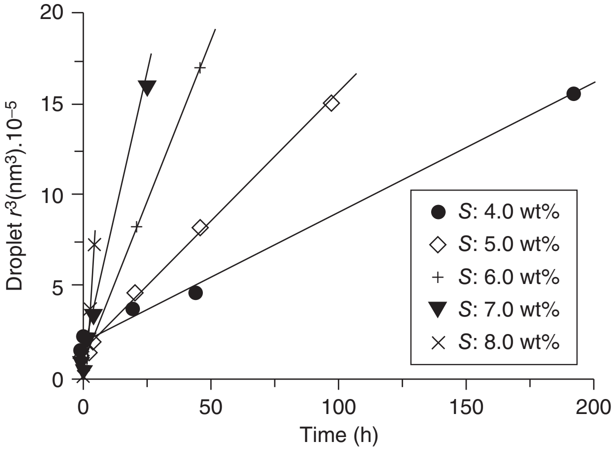

Figure 14.11 r^3 versus time at 25 °C for nanoemulsions prepared using the system water-$C_{12}EO_4$-hexadecane.

As mentioned above, γ reaches a minimum at the HLB temperature, and therefore the minimum in interfacial tension would occur at a lower temperature as the surfactant concentration increased. This temperature would become closer to the cooling temperature as the surfactant concentration increased, and this would result in smaller droplet sizes.

All nanoemulsions showed an increase in droplet size with time, as a result of Ostwald ripening. Figure 14.11 shows plots of r^3 versus time for all the nanoemulsions studied. The slope of the lines gives the rate of Ostwald ripening ω (in m^3 s^{-1}), and this showed an increase from 2 to 39.7×10^{-27} m^3 s^{-1} as the surfactant concentration was increased from 4% to 8 wt%. This increase may have been due to a number of factors:

- The decrease in droplet size increases the Brownian diffusion, and this enhances the rate.
- The presence of micelles, which increases with in line with increases in surfactant concentration. This has the effect of increasing the solubilisation of the oil into the core of the micelles and leads to an increase of the flux J of diffusion of oil molecules from different-sized droplets. Although the diffusion of micelles was slower than the diffusion of oil molecules, the concentration gradient ($\delta C/\delta X$) could be increased by orders of magnitude as a result of solubilisation. The overall effect would be an increase in J, and this may enhance Ostwald ripening.
- The partition of surfactant molecules between the oil and aqueous phases. With higher surfactant concentrations, the molecules with shorter EO chains (i.e., lower HLB number) may accumulate preferentially at the O/W interface. This may result in a reduction of the Gibbs elasticity, which in turn would cause an increase in the Ostwald ripening rate.

Table 14.2 Composition, HLB temperature (T_{HLB}), droplet radius r and polydispersity index (PI) at 25 °C for emulsions in the system water-$C_{12}EO_4$-isohexadecane.

Surfactant (wt%)	Water (wt%)	O/W	T_{HLB} (°C)	r (nm)	PI
2.0	78.0	20.4/79.6	—	97	0.50
3.0	77.0	20.6/79.4	51.3	80	0.13
4.0	76.0	20.8/79.2	43.0	65	0.06
5.0	75.0	21.1/78.9	38.8	43	0.07
6.0	74.0	21.3/78.7	36.7	33	0.05
7.0	73.0	21.3/78.7	33.4	29	0.06
8.0	72.0	21.7/78.3	32.7	27	0.12

The results with isohexadecane are summarised in Table 14.2. As with the hexadecane system, the droplet size and polydispersity index were decreased with increases in surfactant concentration. Nanoemulsions with droplet radii of 25–80 nm were obtained at 3–8% surfactant concentration. It should be noted, however, that nanoemulsions could be produced at lower surfactant concentration when using isohexadecane, when compared to results obtained with hexadecane. This could be attributed to the higher solubility of isohexadecane (a branched hydrocarbon), the lower HLB temperature, and the lower interfacial tension.

The stability of nanoemulsions prepared using isohexadecane was assessed by following the droplet size as a function of time. Plots of r^3 versus time for four

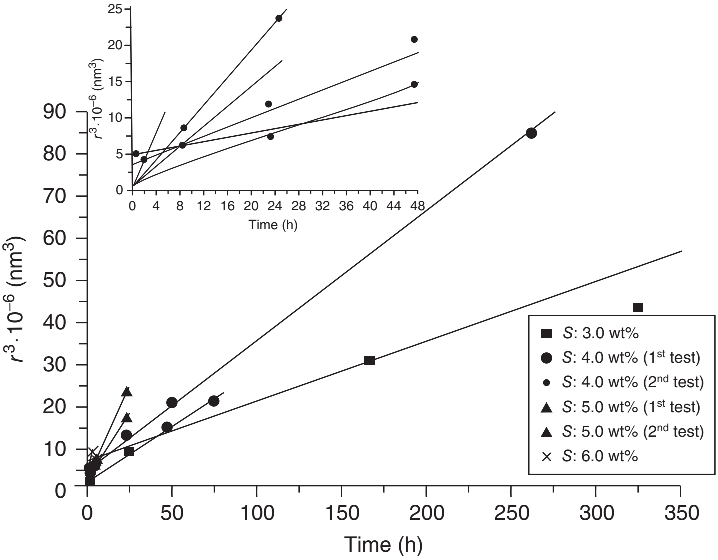

Figure 14.12 r^3 versus time at 25 °C for the system water-$C_{12}EO_4$-isohexadecane at various surfactant concentration; O/W ratio 20/80.

surfactant concentrations (3, 4, 5 and 6 wt%) are shown in Figure 14.12. The results showed an increase in Ostwald ripening rate as the surfactant concentration was increased from 3% to 6% (the ripening rate was increased from 4.1 to $50.7 \times 10^{-27}\ \mathrm{m^3\,s^{-1}}$). The nanoemulsions prepared using 7 wt% surfactant were so unstable that they showed significant creaming after 8 h; however, when the surfactant concentration was increased to 8 wt% a very stable nanoemulsion could be produced with no apparent increase in droplet size over several months. This unexpected stability was attributed to the phase behaviour at such surfactant concentrations. The sample containing 8 wt% surfactant showed birefringence to shear when observed under polarised light. It seemed that the ratio between the phases ($W_m + L_\alpha + O$) may play a key factor in nanoemulsion stability. Attempts were made to prepare nanoemulsions at higher O/W ratios (hexadecane being the oil phase), while keeping the surfactant concentration constant at 4 wt%. When the oil content was increased to 40% and 50%, the droplet radius increased to 188 nm and 297 nm, respectively. In addition, the polydispersity index was increased to 0.95. Whilst these systems became so unstable that they showed creaming within a few hours, this was not too surprising as the surfactant concentration is insufficient to produce nanoemulsion droplets with a high surface area. Similar results were obtained with isohexadecane, but nanoemulsions could be produced using a 30/70 O/W ratio (droplet size 81 nm), but with a high polydispersity index (0.28) the nanoemulsions showed significant Ostwald ripening.

The effect of changing the alkyl chain length and branching was investigated using decane, dodecane, tetradecane, hexadecane, and isohexadecane. Plots of r^3 versus time are shown in Figure 14.13 for a 20/80 O/W ratio and a surfactant concentration of 4 wt%. As expected, by reducing the oil solubility from decane to hexadecane, the rate of Ostwald ripening decreases, and the branched oil isohexadecane also showed a higher Ostwald ripening rate when compared to

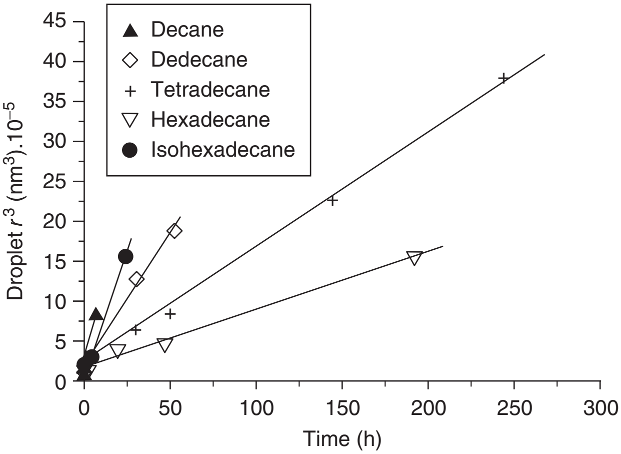

Figure 14.13 r^3 versus time at 25 °C for nanoemulsions (O/W ratio 20/80) with hydrocarbons of various alkyl chain lengths. System water-$C_{12}EO_4$-hydrocarbon (4 wt% surfactant).

Table 14.3 HLB temperature (T_{HLB}), droplet radius r, Ostwald ripening rate ω and oil solubility for nanoemulsions prepared using hydrocarbons with different alkyl chain length.

Oil	T_{HLB} (°C)	r (nm)	ω (10^{27} m^3 s^{-1})	$C(\infty)$ (ml ml^{-1})
Decane	38.5	59	20.9	710.0
Dodecane	45.5	62	9.3	52.0
Tetradecane	49.5	64	4.0	3.7
Hexadecane	49.8	66	2.3	0.3
Isohexadecane	43.0	60	8.0	—

hexadecane. A summary of the results is shown in Table 14.3, which also shows the solubility of the oil $C(\infty)$.

As expected from the Ostwald ripening theory [LSW theory, Eq. (14.16)], the rate of Ostwald ripening decreases as the oil solubility decreases. Isohexadecane has a rate of Ostwald ripening similar to that of dodecane.

As discussed before, it would be expected that the Ostwald ripening of any given oil should decrease on the incorporation of a second oil with a much lower solubility. To test this hypothesis, nanoemulsions were created using hexadecane or isohexadecane, to which various proportions of a less-soluble oil, namely squalene, was added. The results using hexadecane showed a significant decrease in stability on the addition of 10% squalane, but this was considered due to coalescence rather than to an increase in the Ostwald ripening rate. In some cases, the addition of a hydrocarbon with a long alkyl chain can induce instability as a result of change in the adsorption and conformation of the surfactant at the O/W interface.

In contrast to the results obtained with hexadecane, the addition of squalane to the O/W nanoemulsion system based on isohexadecane showed a systematic decrease in Ostwald ripening rate as the squalene content was increased. The results are included in Figure 14.14, which shows plots of r^3 versus time for nanoemulsions containing varying amounts of squalane. The addition of squalane up to 20% based on the oil phase showed a systematic reduction in ripening rate (from 8.0 to 4.1×10^{27} m^3 s^{-1}). It should be noted that when squalane alone was used as the oil phase, the system was very unstable and showed creaming within 1 h. The results also showed that the surfactant used was unsuitable for the emulsification of squalane.

The effect of HLB number on nanoemulsion formation and stability was investigated by using mixtures of $C_{12}EO_4$ (HLB = 9.7) and $C_{12}EO_4$ (HLB = 11.7). Two surfactant concentrations (4 and 8 wt%) were used and the O/W ratio was kept at 20/80. The data in Figure 14.15 showed that the droplet radius remained virtually constant in the HLB range 9.7–11.0, after which there was a gradual increase in line with increases in the HLB number of the surfactant mixture. All nanoemulsions showed an increase in droplet radius with time, except for the sample prepared at 8 wt% surfactant with an HLB number of 9.7 (100% $C_{12}EO_4$). Figure 14.16 shows the variation of Ostwald ripening rate constant ω with the HLB number

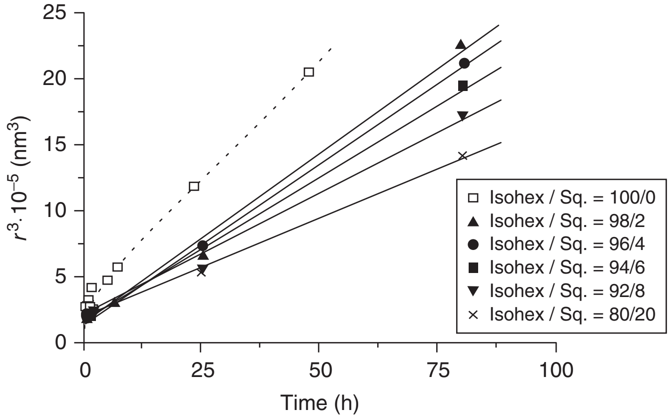

Figure 14.14 r^3 versus time at 25 °C for the system water-$C_{12}EO_4$-isohexadecane-squalane (20/80 O/W ratio and 4 wt% surfactant).

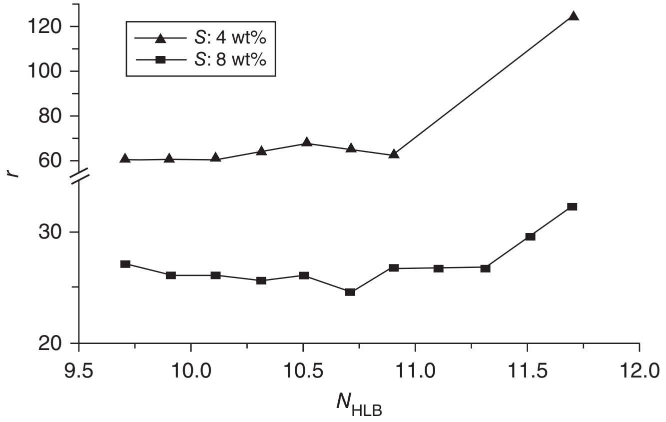

Figure 14.15 *r* versus HLB number at two different surfactant concentrations (O/W ratio 20/80).

of the surfactant. The rate seemed to decrease with an increase of surfactant HLB number such that, when the latter was >10.5 the rate reached a low value ($<4 \times 10^{-27}$ m^3 s^{-1}).

As discussed above, the incorporation of an oil-soluble polymeric surfactant that adsorbs strongly at the O/W interface would be expected to cause a reduction in the Ostwald ripening rate. To test this hypothesis, an A-B-A block copolymer of poly(hydroxystearic acid) (PHS, the A chains) and PEO (the B chain) PHS-PEO-PHS (Arlacel P135) was incorporated in the oil phase at low concentrations (the ratio of surfactant to Arlacel was varied between 99 : 1 and 92 : 8). For the hexadecane system, the Ostwald ripening rate showed a decrease with the addition of Arlacel P135 surfactant at ratios lower than 94 : 6. Although similar results were

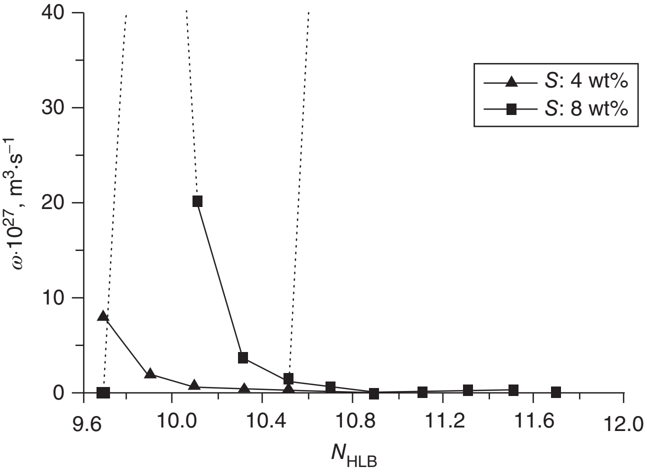

Figure 14.16 ω versus HLB number in the system water-$C_{12}EO_4$-$C_{12}EO_6$-isohexadecane, at two surfactant concentrations.

obtained using isohexadecane, at higher polymeric surfactant concentrations the nanoemulsion became unstable.

As mentioned above, nanoemulsions prepared using the PIT method are relatively polydisperse and generally give higher Ostwald ripening rates when compared to nanoemulsions prepared using high-pressure homogenisation techniques. To test this hypothesis, several nanoemulsions were prepared using a Microfluidizer (that can apply pressures in the range 5000–15 000 psi or 350–1000 bar). Using an oil : surfactant ratio of 4 : 8 and O/W ratios of 20/80 and 50/50, emulsions were prepared first using the UltraTurrax, followed by high-pressure homogenisation (ranging from 1500 to 15 000 psi) The best results were obtained using a pressure of 15 000 psi (one cycle of homogenisation). The droplet radius was plotted versus the oil : surfactant ratio, R(O/S), as shown in Figure 14.17.

For comparison, the theoretical radii values calculated by assuming that all surfactant molecules are at the interface was calculated using the Nakajima equation [1, 2],

$$r = \left(\frac{3M_b}{AN_{\mathrm{Av}}\rho_a}\right)R + \left(\frac{3\alpha M_b}{AN_{\mathrm{Av}}\rho_b}\right) + d \tag{14.17}$$

where M_b is the molecular weight of the surfactant, A is the area occupied by a single molecule, N_{Av} is Avogadro's number, ρ_a is the oil density, ρ_b is the density of the surfactant alkyl chain, α is the alkyl chain weight fraction, and d is the thickness of the hydrated layer of PEO.

In all cases, there was an increase in nanoemulsion radius with increase in the R(O/S). However, when using the high-pressure homogeniser the droplet size could be maintained at values below 100 nm at high R(O/S) values. With the PIT method, there was a rapid increase in r with increase in R(O/S) when the latter exceeded 7.

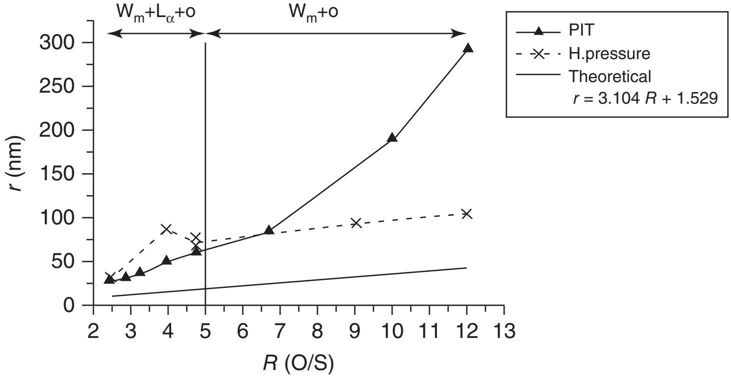

Figure 14.17 r versus R(O/S) at 25 °C for the system water-$C_{12}EO_4$-hexadecane. W_m = micellar solution or O/W microemulsion; L_α = lamellar liquid crystalline phase; O = oil phase.

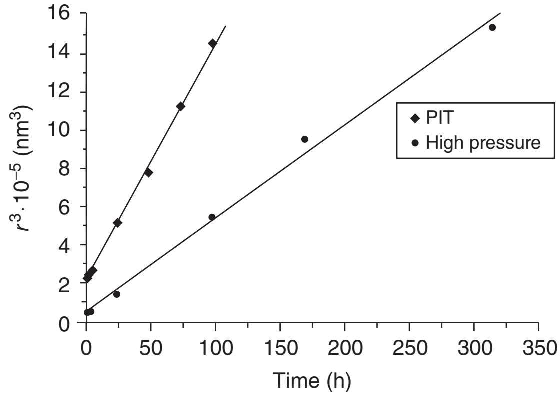

Figure 14.18 r^3 versus time for nanoemulsion systems prepared using the PIT and Microfluidizer. 20/80 O/W ratio and 4 wt% surfactant.

As expected, the nanoemulsions prepared using high-pressure homogenisation showed a lower Ostwald ripening rate when compared to systems prepared using the PIT method. This is illustrated in Figure 14.18, which shows plots of r^3 versus time for the two systems.

14.5.3
Nanoemulsions Based on Polymeric Surfactants

The use of polymeric surfactants to prepare nanoemulsions is expected to significantly reduce Ostwald ripening due to the high interfacial elasticity produced by the adsorbed polymeric surfactant molecules [26]. To test this hypothesis, several nanoemulsions were formulated using a graft copolymer of hydrophobically modified inulin. The inulin backbone consists of polyfructose with a degree of polymerisation > 23; this hydrophilic backbone is hydrophobically modified by attachment of several C_{12} alkyl chains [27]. The polymeric surfactant (trade name INUTEC SP1®) adsorbs with several alkyl chains that may be soluble in the oil phase or become strongly attached to the oil surface, leaving the strongly hydrated hydrophilic polyfructose loops and tails "dangling" in the aqueous phase. These hydrated loops and tails (with a hydrodynamic thickness > 5 nm) provide an effective steric stabilisation.

Oil/water nanoemulsions were prepared using a two-step emulsification process where, in the first step, an O/W emulsion was prepared using a high-speed stirrer (UltraTurrax) [28]. The resulting coarse emulsion was subjected to high-pressure homogenisation (Microfluidizer; Microfluidics, USA) where, in all cases, the pressure used was 700 bar and homogenisation was carried out for 1 min. The *z*-average droplet diameter was determined using PCS measurements, as discussed before.

Figure 14.19 shows plots of r^3 versus t for nanoemulsions of the hydrocarbon oils that were stored at 50 °C. It can be seen that both paraffinum liquidum with low and high viscosities gave almost a zero-slope, indicating the absence of Ostwald ripening in this case. This was not surprising as both oils have a very low solubility and INUTEC SP1® was strongly adsorbed at the interface, giving a high elasticity that reduced both the Ostwald ripening and coalescence. However, with the more soluble hydrocarbon oils (namely isohexadecane) there was an increase in r^3 with

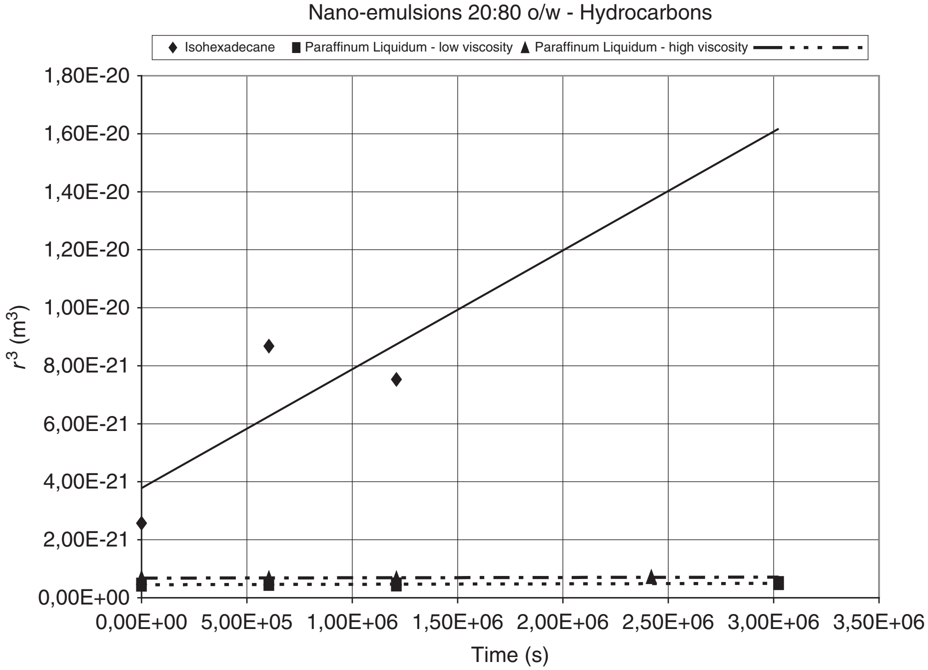

Figure 14.19 r^3 versus t for nanoemulsions based on hydrocarbon oils.

time, giving an Ostwald ripening rate of 4.1×10^{-27} $m^3\ s^{-1}$. The ripening rate for this oil was almost three orders of magnitude lower than that obtained with a nonionic surfactant, namely laureth-4 (C_{12}-alkylchain with 4 mol ethylene-oxide) when stored at 50 °C. This clearly showed the effectiveness of INUTEC SP1® in reducing Ostwald-ripening, an effect that could be attributed to an enhancement of the Gibbs dilational elasticity [26] that resulted from the multipoint attachment of the polymeric surfactant with several alkyl groups to the oil droplets. This resulted in a reduction of the molecular diffusion of the oil from the smaller to the larger droplets.

Figure 14.20 shows the results for the isopropylalkylate O/W nanoemulsions. As with the hydrocarbon oils, there was a significant reduction in the Ostwald ripening rate with increases in the alkyl chain length of the oil. The rate constants were 1.8×10^{-27}, 1.7×10^{-27}, and 4.8×10^{-28} $m^3\ s^{-1}$, respectively.

Figure 14.21 shows the r^3–t plots for nanoemulsions based on natural oils. Although, in all cases, the Ostwald ripening rate was very low, a comparison between squalene and squalane showed the rate to be relatively higher for squalene (unsaturated) than for squalane (lower solubility). The Ostwald ripening rates for these natural oils are listed in Table 14.4.

Figure 14.22 shows the results based on silicone oils. Both, dimethicone and phenyl trimethicone give an Ostwald ripening rate close to zero, whereas cyclopentasiloxane gave a rate of 5.6×10^{-28} $m^3\ s^{-1}$.

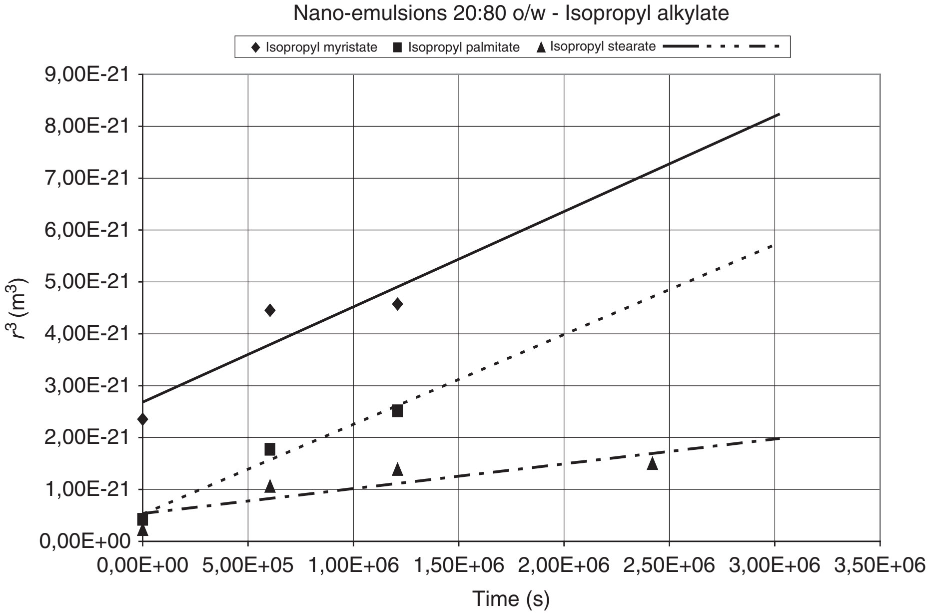

Figure 14.20 r^3 versus t for nanoemulsions based on isopropylalkylate.

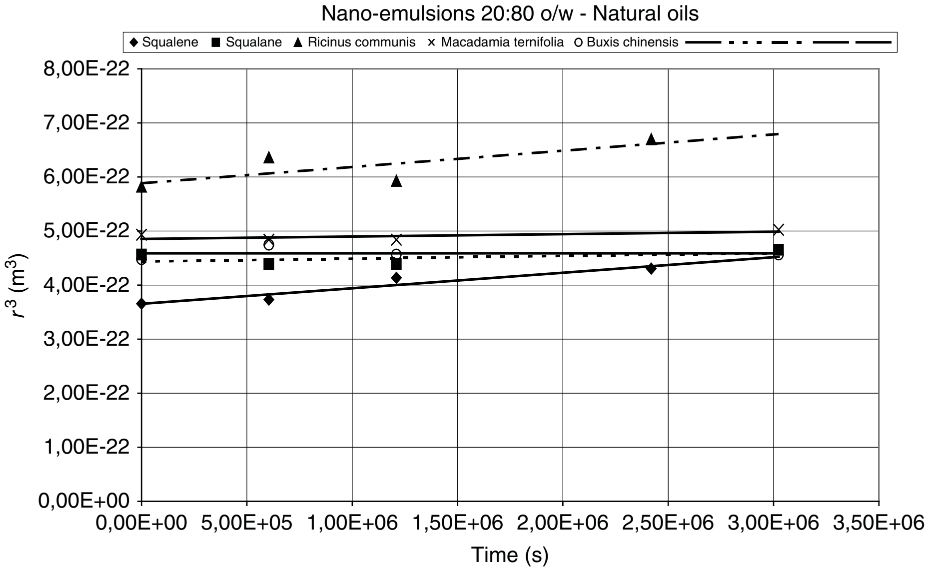

Figure 14.21 r^3 versus t for nanoemulsions based on natural oils.

Table 14.4 Ostwald ripening rates for nanoemulsions based on natural oils.

Oil	Ostwald ripening rate ($m^3\ s^{-1}$)
Squalene	2.9×10^{-28}
Squalane	5.2×10^{-30}
Ricinus communis (castor oil)	3.0×10^{-29}
Macadamia ternifolia (macadamia nut)	4.4×10^{-30}
Buxis chinensis (jojoba)	~0

Figure 14.23 shows the results for nanoemulsions based on esters, and the Ostwald ripening rates are listed in Table 14.5. C_{12-15} alkylbenzoate appeared to give the highest ripening rate.

Figure 14.24 shows a comparison of two nanoemulsions based on polydecene, a highly insoluble nonpolar oil and PPG-15 stearyl ether which is relatively more polar. Polydecene gave a low Ostwald ripening rate of $6.4 \times 10^{-30}\ m^3\ s^{-1}$ which was one order of magnitude lower than that of PPG-15 stearyl ether ($5.5 \times 10^{-29}\ m^3\ s^{-1}$).

The influence of adding glycerol (which is sometimes used in personal care formulations as a humectant) on the Ostwald ripening rate when preparing transparent nanoemulsions was monitored by matching the refractive index of the oil and the aqueous phase (see Figure 14.25). In the case of the more insoluble silicone oil the addition of 5% glycerol did not cause any increase in ripening rate, whereas for the more soluble isohexadecane oil the ripening rate was increased.

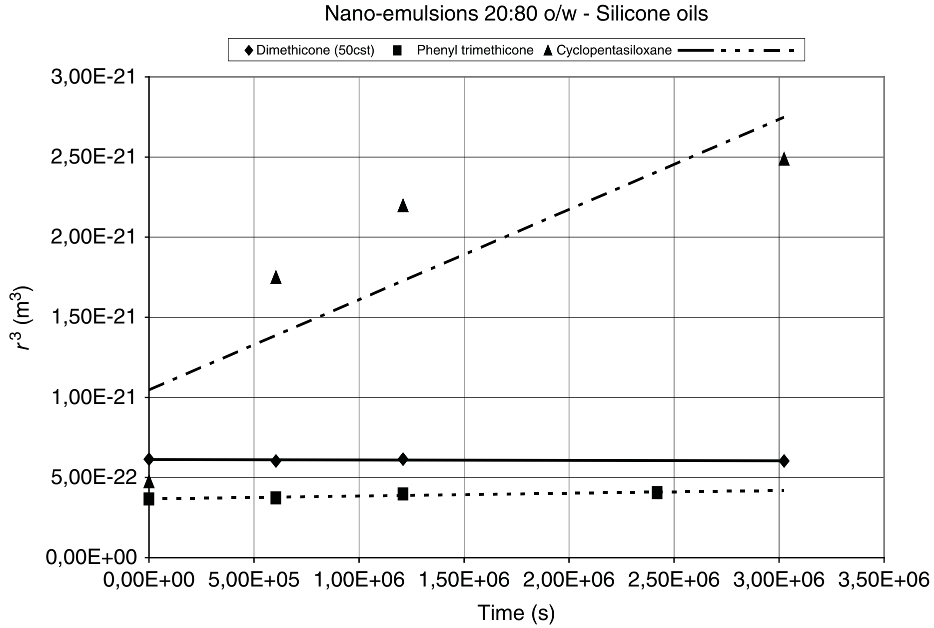

Figure 14.22 r^3 versus t for nanoemulsions based on silicone oils.

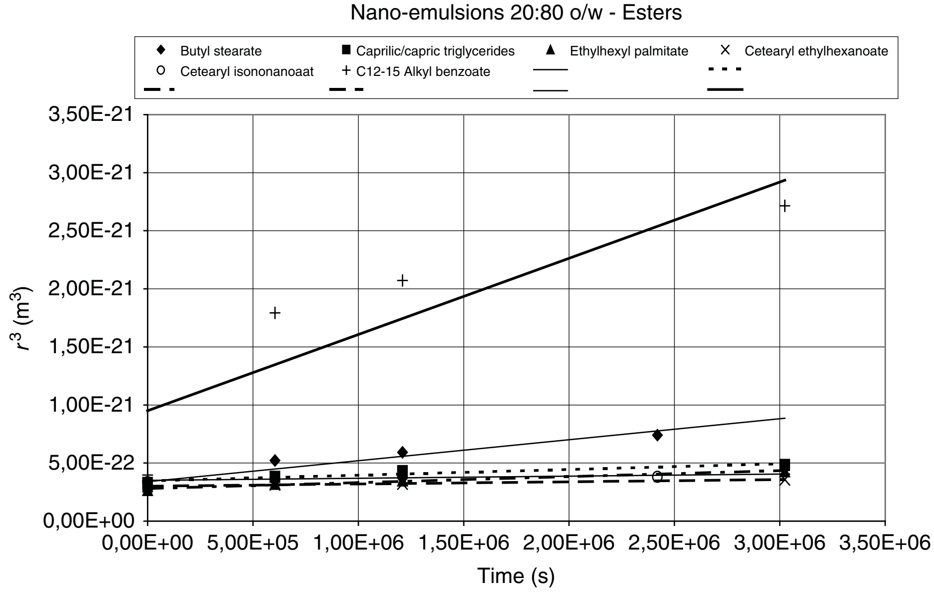

Figure 14.23 r^3 versus t for nanoemulsions based on esters.

Table 14.5 Ostwald ripening rates for nanoemulsions based on esters.

Oil	Ostwald ripening rate ($m^3\ s^{-1}$)
Butyl stearate	1.8×10^{-28}
Caprylic capric triglyceride	4.9×10^{-29}
Cetearyl ethylhexanoate	1.9×10^{-29}
Ethylhexyl palmitate	5.1×10^{-29}
Cetearyl isononanoate	1.8×10^{-29}
$C_{12\text{-}15}$ alkyl benzoate	6.6×10^{-28}

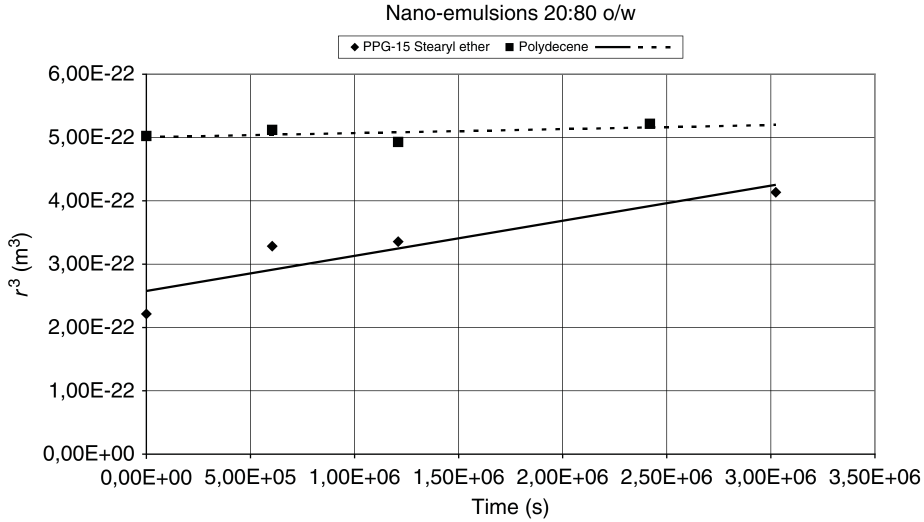

Figure 14.24 r^3 versus t for nanoemulsions based on PPG-15 stearyl ether and polydecene.

The hydrophobically modified inulin (INUTEC SP1®) was shown to reduce the Ostwald ripening rate of nanoemulsions when compared to nonionic surfactants such as laureth-4. This was due to the strong adsorption of INUTEC SP1® at the O/W interface (by multipoint attachment) and an enhancement of the Gibbs dilational elasticity, both of which effects reduced the diffusion of oil molecules from the smaller to the larger droplets. The present study results also showed a major influence of the nature of the oil phase, with the more soluble and more polar oils giving the highest Ostwald ripening rates. However in all cases when INUTEC SP1® was used, the rates were reasonably low, allowing this polymeric surfactant to be applied to the formulation of nanoemulsions for personal care products.

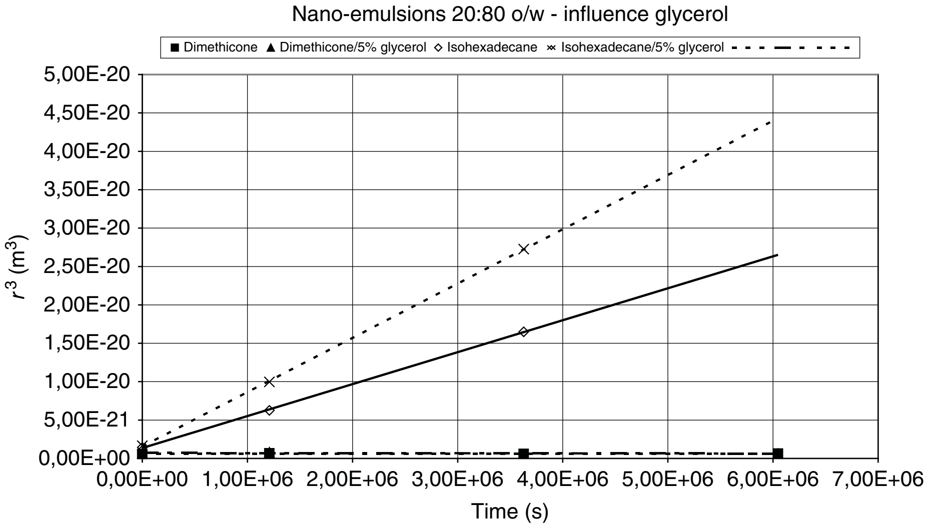

Figure 14.25 Influence of glycerol on the Ostwald ripening rate of nanoemulsions.

References

1. Nakajima, H., Tomomossa, S. and Okabe, M. (1993) First Emulsion Conference, Paris.
2. Nakajima, H. (1997) in *Industrial Applications of Microemulsions* (eds C. Solans and H. Konieda), Marcel Dekker, New York.
3. Ugelstadt, J., El-Aassar, M.S., and Vanderhoff, J.W. (1973) *J. Polym. Sci.*, **11**, 503.
4. El-Aasser, M. (1997) in *Polymeric Dispersions* (ed. J.M. Asua), Kluwer Academic Publishers, Dordrecht.
5. Benita, S. and Levy, M.Y. (1993) *J. Pharm. Sci.*, **82**, 1069.
6. Forgiarini, A., Esquena, J., Gonzalez, J., and Solans, C. (2000) *Prog. Colloid Polym. Sci.*, **115**, 36.
7. Shinoda, K. and Kunieda, H. (1983) in *Encyclopedia of Emulsion Technology* (ed. P. Becher), Marcel Dekker, New York.
8. Walstra, P. (1983) in *Encyclopedia of Emulsion Technology* (ed. P. Becher), Marcel Dekker, New York.
9. Pusey, P.N. (1973) in *Industrial Polymers: Characterisation by Molecular Weights* (eds J.H.S. Green and R. Dietz), Transcripta Books, London.
10. Walstra, P. and Smoulders, P.E.A. (1998) in *Modern Aspects of Emulsion Science* (ed. B.P. Binks), The Royal Society of Chemistry, Cambridge.
11. Shinoda, K. and Saito, H. (1969) *J. Colloid Interface Sci.*, **30**, 258.
12. Shinoda, K. and Saito, H. (1968) *J. Colloid Interface Sci.*, **26**, 70.
13. Brooks, B.W., Richmond, H.N., and Zerfa, M. (1998) in *Modern Aspects of Emulsion Science* (ed. B.P. Binks), Royal Society of Chemistry Publication, Cambridge.
14. Sottman, T. and Strey, R. (1997) *J. Chem. Phys.*, **108**, 8606.
15. Napper, D.H. (1983) *Polymeric Stabilisation of Colloidal Dispersions*, Academic Press, London.
16. Tadros, T.F. (1982) Polymer adsorption and colloid stability, in *The Effect of Polymers on Dispersion Properties* (ed. T.F. Tadros), Academic Press, London.
17. Thompson, W. (Lord Kelvin) (1871) *Philos. Mag.*, **42**, 448.
18. Lifshitz, I.M. and Slesov, V.V. (1959) *Sov. Phys. JETP*, **35**, 331.
19. Wagner, C. (1961) *Z. Electrochem.*, **35**, 581.
20. Kabalnov, A.S. and Shchukin, E.D. (1992) *Adv. Colloid Interface Sci.*, **38**, 69.
21. Kabalnov, A.S. (1994) *Langmuir*, **10**, 680.

22. Weers, J.G. (1998) in *Modern Aspects of Emulsion Science* (ed. B.P. Binks), Royal Society of Chemistry Publication, Cambridge.
23. Walstra, P. (1993) *Chem. Eng. Sci.*, **48**, 333.
24. Izquierdo, P. (2002) Studies on nano-emulsion formation and stability. PhD Thesis, University of Barcelona, Barcelona, Spain.
25. Kuneida, H., Fukuhi, Y., Uchiyama, H., and Solans, C. (1996) *Langmuir*, **12**, 2136.
26. Tadros, T. (2008) *Colloids in Cosmetics and Personal Care*, Wiley-VCH Verlag GmbH, Weinheim.
27. Stevens, C.V., Meriggi, A., Peristerpoulou, M., Christov, P.P., Booten, K., Levecke, B., Vandamme, A., Pittevils, N., and Tadros, T.F. (2001) *Biomacromolecules*, **2**, 1256.
28. Tadros, T.F., Vandamme, A., Levecke, B., Booten, K., and Stevens, C.V. (2004) *Adv. Colloid Interface Sci.*, **108-109**, 207.

15

Formulation of Microemulsions

15.1

Introduction

Microemulsions are a special class of ‘‘dispersions’’(transparent or translucent) which actually have little in common with emulsions, and are better described as ‘‘swollen micelles.’’ The term microemulsion was first introduced by Hoar and Schulman [1, 2] who discovered that the titration of a milky emulsion (stabilised by a soap, such as potassium oleate) with a medium-chain alcohol such as pentanol or hexanol led to the production of a transparent or translucent system. A schematic representation of the titration method adopted by Schulman and coworkers is given below:

$$\begin{array}{ccccc} \text{O/W emulsion} & & \text{Add cosurfactant} & & \text{Transparent} \\ \text{stabilised by} & \rightarrow & \text{e.g. } C_5H_{11}OH & \rightarrow & \text{or translucent} \\ \text{soap} & & C_6H_{13}OH & & \end{array}$$

The final transparent or translucent system is a W/O microemulsion.

A convenient way to describe microemulsions is to compare them with micelles. The latter, which are thermodynamically stable, may consist of spherical units with a radius that is usually less than 5 nm. Two types of micelles may be considered: (i) normal micelles in which the hydrocarbon tails form the core and the polar head groups are in contact with the aqueous medium; and (ii) reverse micelles (formed in nonpolar media) in which the water core contains the polar head groups and the hydrocarbon tails are now in contact with the oil. Normal micelles can solubilise oil in the hydrocarbon core to form O/W microemulsions, whereas reverse micelles can solubilise water to form a W/O microemulsion. A schematic representation of these systems is shown in Figure 15.1.

A rough guide to the dimensions of micelles, micellar solutions and macroemulsions is as follows: Micelles, $R < 5$ nm (they scatter little light and are transparent); macroemulsions, $R > 50$ nm (opaque and milky); micellar solutions or microemulsions, 5–50 nm (transparent, 5–10 nm, translucent 10–50 nm).

The classification of microemulsions based on size is inadequate. Whether a system is transparent or translucent depends not only on the size but also on the difference in refractive index between the oil and the water phases. A microemulsion with small size (in the region of 10 nm) may appear translucent if

Formulation of Disperse Systems: Science and Technology, First Edition. Tharwat F. Tadros.

Normal micelle Inverse micelle

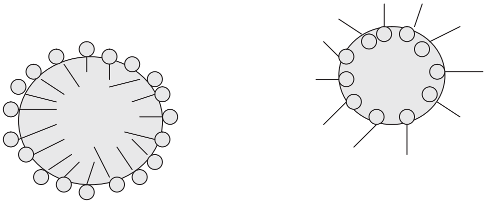

O/W microemulsion W/O microemulsion

Figure 15.1 Schematic representation of microemulsions.

the difference in refractive index between the oil and the water is large (note that the intensity of light scattered depends on the size and an optical constant that is given by the difference in refractive index between oil and water). A relatively large size microemulsion droplet (in the region of 50 nm) may appear transparent if the refractive index difference is very small. The best definition of microemulsions is based on the application of thermodynamics, as discussed below.

15.2
Thermodynamic Definition of Microemulsions

A thermodynamic definition of microemulsions can be obtained from a consideration of the energy and entropy terms for formation of microemulsions. The process of formation of microemulsion from a bulk oil phase (for a O/W microemulsion) or from a bulk water phase (for a W/O microemulsion) is shown schematically in Figure 15.2.

Here, A_1 is the surface area of the bulk oil phase, A_2 is the total surface area of all the microemulsion droplets, and γ_{12} is the O/W interfacial tension. The increase in surface area when going from state I to state II is ΔA [equal to $(A_2 - A_1)$], and

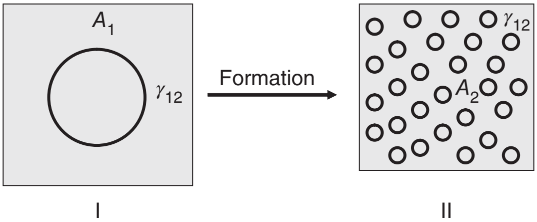

Figure 15.2 Schematic representation of microemulsion formation.

the surface energy increase is equal to $\Delta A\gamma_{12}$. The increase in entropy when going from state I to sate II is $T\Delta S^{\text{conf}}$ (note that state II has higher entropy as a large number of droplets can arrange themselves in several ways, whereas state I with one oil drop has a much lower entropy).

According to the second law of thermodynamics, the free energy of formation of microemulsions ΔG_{m} is given by the following expression,

$$\Delta G_{\text{m}} = \Delta A\gamma_{12} - T\Delta S^{\text{conf}} \tag{15.1}$$

In the case of macroemulsions, $\Delta A\gamma_{12} \gg T\Delta S^{\text{conf}}$ and $\Delta G_{\text{m}} > 0$, and the system is nonspontaneous (i.e., it requires energy for formation of the emulsion drops) and thermodynamically unstable. In the case of microemulsions, $\Delta A\gamma_{12} \leq T\Delta S^{\text{conf}}$ (this is due to the ultralow interfacial tension accompanied with microemulsion formation) and $\Delta G_{\text{m}} \leq 0$; this system is produced spontaneously and is thermodynamically stable.

The above analysis shows the contrast between emulsions and microemulsions. With emulsions, an increase of the mechanical energy and an increase in surfactant concentration usually results in the formation of smaller droplets which become kinetically more stable. With microemulsions, however, neither mechanical energy nor any increase in surfactant concentration can result in their formation. The microemulsion is based on a specific combination of surfactants and specific interaction with the oil and the water phases, and the system is produced at optimum composition.

Thus, microemulsions have nothing in common with macroemulsions, and in many cases it is better to describe the microemulsion system as ''swollen micelles.'' The best definition of microemulsions is as follows [3]: ''System of Water + Oil + Amphiphile that is a single Optically Isotropic and Thermodynamically Stable Liquid Solution.'' Amphiphiles refer to any molecule that consist of a hydrophobic and hydrophilic portions, for example surfactants and alcohols.

The driving force for microemulsion formation is the low interfacial energy which is overcompensated by the negative entropy of dispersion term. The low (ultralow) interfacial tension is produced in most cases by the combination of two molecules, referred to as the surfactant and the cosurfactant (e.g., a medium-chain alcohol).

15.3
Mixed-Film and Solubilisation Theories of Microemulsions

15.3.1
Mixed-Film Theories

The film (which may consist of surfactant and cosurfactant molecules) is considered as a liquid ''two-dimensional'' third phase in equilibrium with both oil and water [4]. Such a monolayer could be a duplex film, with different properties on the water and oil sides. The initial ''flat'' duplex film (see Figure 15.3) has different tensions

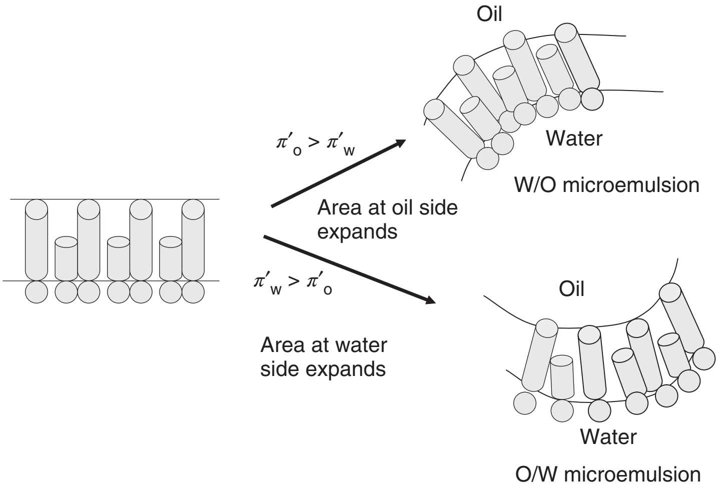

Figure 15.3 Schematic representation of film bending.

at the oil and water sides, due to the different packing of the hydrophobic and hydrophilic groups (these groups have different sizes and cross-sectional areas).

It is convenient to define a two-dimensional surface pressure π,

$$\pi = \gamma_o - \gamma \tag{15.2}$$

where γ_o is the interfacial tension of the clean interface, while γ is the interfacial tension with adsorbed surfactant.

Two values can be defined for π at the oil and water phases, π_o and π_w, which for a flat film are not equal – that is, $\pi'_o \neq \pi'_w$. As a result of the difference in tensions, the film will bend until $\pi_o = \pi_w$. If $\pi'_o > \pi'_w$, the area at the oil side has to expand (resulting in a reduction of π'_o) until $\pi_o = \pi_w$, and in this case a W/O microemulsion is produced. If $\pi'_w > \pi'_o$, the area at the water side expands until $\pi_w = \pi_o$, and in this case an O/W microemulsion is produced. A schematic representation of film bending for the production of W/O or W/O microemulsions is provided in Figure 15.3.

According to the duplex film theory, the interfacial tension γ_T is given by the following expression [5],

$$\gamma_T = \gamma_{(O/W)} - \pi \tag{15.3}$$

and $(\gamma_{o/w})_a$ is the interfacial tension that is reduced by the presence of the alcohol.

The value of $(\gamma_{o/w})_a$ is significantly lower than $\gamma_{o/w}$ in the absence of the alcohol (for example for hydrocarbon/water, $\gamma_{o/w}$ is reduced from 50 to 15–20 mN m^{-1} on the additional of a significant amount of a medium-chain alcohol such as pentanol or hexanol).

Contributions to π are considered to be due to crowding of the surfactant and cosurfactant molecules and penetration of the oil phase into the hydrocarbon chains of the interface. According to Equation (15.3), if $\pi > (\gamma_{o/w)a}$, γ_T becomes negative and this leads to an expansion of the interface until γ_T reaches a small positive value. Since $(\gamma_{o/w})_a$ is of the order of 15–20 mN m^{-1}, surface pressures of this order are required for γ_T to approach a value of zero.

The above duplex film theory can explain the nature of the microemulsion. The surface pressures at the oil and water sides of the interface depend on the interactions of the hydrophobic and hydrophilic potions of the surfactant molecule at both sides, respectively. If the hydrophobic groups are bulky in nature relative to the hydrophilic groups, then for a flat film such hydrophobic groups tend to crowd so as to form a higher surface pressure at the oil side of the interface; this results in bending and expansion at the oil side, forming a W/O microemulsion. An example of a surfactant with bulky hydrophobic groups is Aerosol OT (dioctyl sulphosuccinate). If the hydrophilic groups are bulky, as is the case with ethoxylated surfactants containing more than five ethylene oxide units, crowding will occur at the water side of the interface and this will produce an O/W microemulsion.

15.3.2
Solubilisation Theories

These concepts were introduced by Shinoda and coworkers [6], who considered microemulsions to be swollen micelles that are directly related to the phase diagram of their components.

Consider the phase diagram of a three-component system of water, ionic surfactant and medium-chain alcohol, as described in Figure 15.4. At the water corner and at low alcohol concentration, normal micelles (L_1) will be formed since, in this case, there are more surfactant than alcohol molecules. At the alcohol (cosurfactant corner), inverse micelles (L_2) will be formed since in this region there are more alcohol than surfactant molecules.

Regions L_1 and L_2 are not in equilibrium, but are separated by a liquid crystalline region (a lamellar structure with equal numbers of surfactant and alcohol

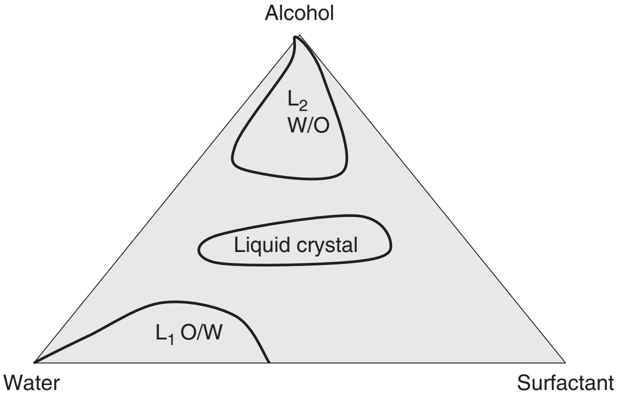

Figure 15.4 Schematic representation of three-component phase diagram.

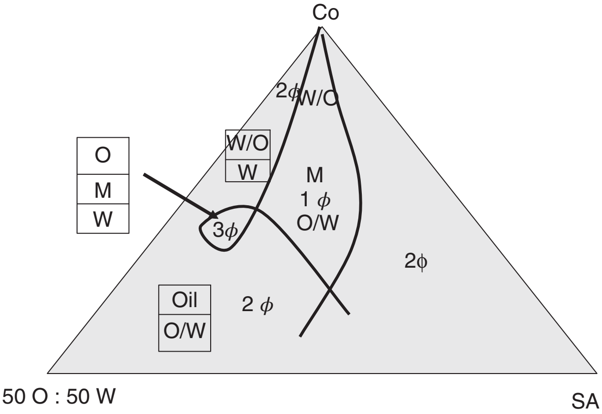

Figure 15.5 Schematic representation of the pseudoternary phase diagram of oil/water/surfactant/cosurfactant.

molecules). The L_1 region may be considered as an O/W microemulsion, and L_2 as a W/O microemulsion.

The addition of a small amount of oil that is miscible with the cosurfactant, but not with the surfactant and water, changes the phase diagram only slightly. The oil may be simply solubilised in the hydrocarbon core of the micelles. The addition of more oil leads to fundamental changes of the phase diagram, as illustrated in Figure 15.5, where 50/50 W/O has been used. To simplify the situation, 50W/50 O is shown on one corner of the phase diagram.

Near the cosurfactant (Co) corner the changes are small compared to the three-phase diagram (Figure 15.5). The O/W microemulsion near the water–surfactant (Sa) axis is not in equilibrium with the lamellar phase, but rather with a noncolloidal oil + cosurfactant phase. If Co is added to such a two-phase equilibrium at fairly high surfactant concentration, all of the oil will be taken up and a one-phase microemulsion will appear. The addition of Co at low Sa concentration may lead to the separation of an excess aqueous phase before all oil is taken up in the microemulsion. As a result, a three-phase system is formed that contains a microemulsion that cannot be clearly identified as W/O or W/O and that presumably is similar to the lamellar phase swollen with oil or to a more irregular intertwining of the aqueous and oily regions (bicontinuous or middle phase microemulsion). The interfacial tensions between the three phases are very low ($0.1–10^{-4}$ mN m^{-1}). Further addition of Co to the three-phase system causes the oil phase to disappear and leaves a W/O microemulsion in equilibrium with a dilute aqueous Sa solution. In the large one-phase region, continuous transitions from O/W to middle phase to W/O microemulsions are found.

Solubilisation can also be illustrated by considering the phase diagrams of nonionic surfactants containing poly(ethylene oxide) (PEO) head groups. Such surfactants do not generally need a cosurfactant for microemulsion formation.

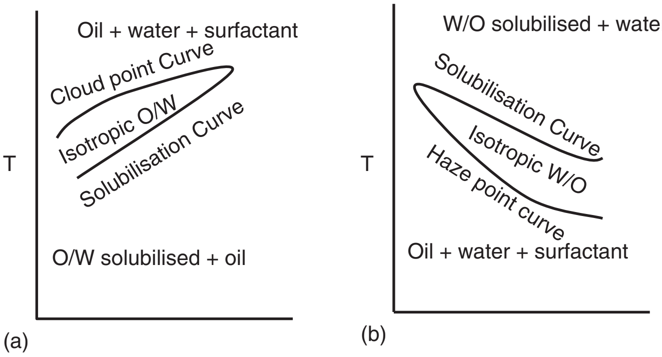

Figure 15.6 Schematic representation of Solubilisation. (a) Oil solubilised in a nonionic surfactant solution; (b) Water solubilised in an oil solution of a nonionic surfactant.

A schematic representation of oil and water Solubilisation by nonionic surfactants is shown in Figure 15.6.

At low temperatures, the ethoxylated surfactant is soluble in water and, at a given concentration, is capable of solubilising a given amount of oil. The oil Solubilisation increases rapidly with increase of temperature near the cloud point of the surfactant. This is illustrated in Figure 15.6, which shows the Solubilisation and cloud point curves of the surfactant. Between these two curves, an isotropic region of an O/W-solubilised system exists. At any given temperature, any increase in the oil weight fraction above the Solubilisation limit will result in oil separation (oil solubilised + oil). At any given surfactant concentration, any increase in temperature above the cloud point will result in separation into oil, water, and surfactant.

When starting from the oil phase with dissolved surfactant and adding water, Solubilisation of the latter will take place and Solubilisation will increase with a reduction of temperature near the haze point. Between the Solubilisation and haze point curves, an isotropic region of W/O solubilised system exists. At any given temperature, any increase in water weight fraction above the Solubilisation limit will result in water separation (W/O solubilised + water), while at any given surfactant concentration any decrease in temperature below the haze point will result in separation to water, oil, and surfactant.

With nonionic surfactants, both types of microemulsions can be formed, depending on the conditions. With such systems, temperature is the most crucial factor as the solubility of surfactant in water or oil is temperature-dependent. Microemulsions prepared using nonionic surfactants will have a limited temperature range.

15.4
Thermodynamic Theory of Microemulsion Formation

The spontaneous formation of a microemulsion with a decrease in free energy can only be expected if the interfacial tension is so low that the remaining free energy of the interface is overcompensated for by the entropy of dispersion of the droplets in the medium [7, 8]. This concept forms the basis of the thermodynamic theory proposed by Ruckenstein and Chi, and Overbeek [7, 8].

15.4.1
Reason for Combining Two Surfactants

Single surfactants lower the interfacial tension γ, but in most cases the critical micelle concentration (cmc) is reached before γ is close to zero. The addition of a second surfactant of a completely different nature (i.e., predominantly oil-soluble, such as an alcohol) then lowers γ further and very small, even transiently negative, values may be reached [9]. This is illustrated in Figure 15.7, which shows the effect of addition of the cosurfactant on the γ–log C_{sa} curve. It can be seen that addition of cosurfactant shifts the whole curve to low γ-values, while the cmc is shifted to lower values.

For a multicomponent system i, each with an adsorption Γ_i (mol m^{-2}, referred to as the surface excess), the reduction in γ (i.e., dγ) is given by the following expression:

$$d\gamma = -\sum \Gamma_i d\mu_i = -\sum \Gamma_i RT \, d\ln C_i \tag{15.4}$$

where μ_i is the chemical potential of component i, R is the gas constant, T is the absolute temperature, and C_i is the concentration (mol dm^{-3}) of each surfactant component.

The reason for the lowering of γ when using two surfactant molecules can be understood from consideration of the Gibbs adsorption equation for multicomponent systems [9]. For two components, sa (surfactant) and co (cosurfactant), Equation (15.4) becomes,

$$d\gamma = -\Gamma_{\text{sa}} RT \, d\ln C_{\text{sa}} - \Gamma_{\text{co}} RT \, d\ln C_{\text{co}} \tag{15.5}$$

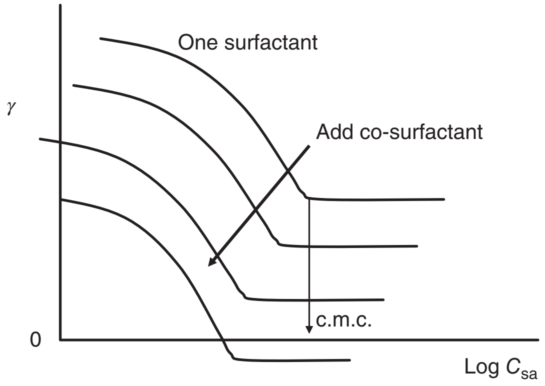

Figure 15.7 γ–log C_{sa} curves for surfactant + cosurfactant.

Integration of Equation (15.5) gives,

$$\gamma = \gamma_\mathrm{o} - \int_0^{C_\mathrm{sa}} \Gamma_\mathrm{sa}\, RT \,\mathrm{dln}\, C_\mathrm{sa} - \int_0^{C_\mathrm{co}} \Gamma_\mathrm{co}\, RT \,\mathrm{dln}\, C_\mathrm{co} \qquad (15.6)$$

which clearly shows that γ_o is lowered by two terms, both from surfactant and cosurfactant.

The two surfactant molecules should adsorb simultaneously and they should not interact with each other, otherwise they lower their respective activities. Thus, the surfactant and cosurfactant molecules should vary in nature, one predominantly water-soluble (e.g., an anionic surfactant) and the other predominantly oil-soluble (e.g., a medium-chain alcohol).

In some cases a single surfactant may be sufficient for lowering γ far enough for microemulsion formation to become possible; examples include Aerosol OT (sodium diethyl hexyl sulphosuccinate) and many nonionic surfactants.

15.4.2
Factors Determining W/O versus O/W Microemulsions

The duplex film theory predicts that the nature of the microemulsion formed depends on the relative packing of the hydrophobic and hydrophilic portions of the surfactant molecule, which determined the bending of the interface. For example, a surfactant molecule such as Aerosol OT,

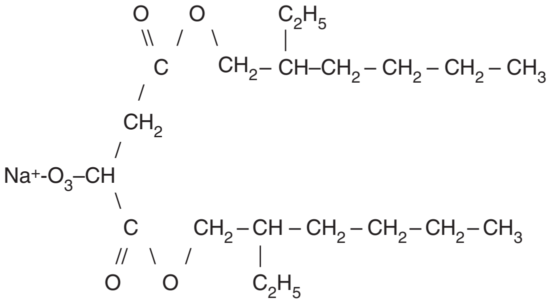

favours the formation of W/O microemulsion, without the need for a cosurfactant. As a result of the presence of a stumpy head group and large volume-to-length (V/l) ratio of the nonpolar group, the interface tends to bend with the head groups facing onwards, thus forming a W/O microemulsion.

The molecule has $V/l > 0.7$, which is considered necessary for the formation of a W/O microemulsion. For ionic surfactants such as SDS, for which $V/l < 0.7$, microemulsion formation requires the presence of a cosurfactant (the latter has the effect of increasing V, without changing l).

The importance of geometric packing was considered in detail by Mitchell and Ninham [10], who introduced the concept of the packing ratio P,

$$P = \frac{V}{l_c\, a_o} \tag{15.7}$$

where a_o is the head group area and l_c is the maximum chain length.

P gives a measure of the hydrophilic–lipophilic balance. For values of $P < 1$ (usually $P \sim 1/3$), normal or convex aggregates are produced (normal micelles), whereas for values of $P > 1$ inverse micelles are produced. P is influenced by many factors, including the hydrophilicity of the head group, the ionic strength and pH of the medium, and temperature.

P also explains the nature of the microemulsion produced using nonionic surfactants of the ethoxylate type: P is increased with increases of temperature (as a result of the dehydration of the PEO chain). A critical temperature (PIT) is reached at which P reaches 1, and above this temperature inversion occurs to form a W/O system.

The influence of surfactant structure on the nature of the microemulsion can also be predicted from thermodynamic theory. The most stable microemulsion would be that in which the phase with the smaller volume fraction forms the droplets (the osmotic pressure increases with increase of ϕ). For a W/O microemulsion prepared using an ionic surfactant such as Aerosol OT, the effective volume (hard-sphere volume) is only slightly larger than the water core volume, as the hydrocarbon tails may penetrate to a certain extent when two droplets come together. For an O/W microemulsion, the double layers may expand to a considerable extent, depending on the electrolyte concentration (the double layer thickness is on the order of 100 nm in 10^{-5} mol dm^{-3} 1 : 1 electrolyte and 10 nm in 10^{-3} mol dm^{-3} electrolyte). Thus, the effective volume of O/W microemulsion droplets can be significantly higher than the core oil droplet volume, which explains the difficulty encountered when preparing O/W microemulsions at high φ-values when using ionic surfactants.

A schematic representation of the effective volume for W/O and O/W microemulsions is shown in Figure 15.8.

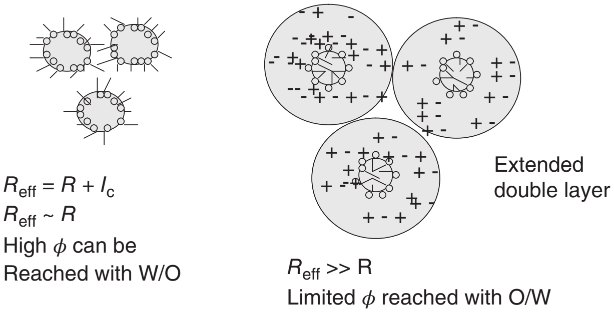

Figure 15.8 Schematic representation of W/O and O/W microemulsion droplets.

15.5
Characterisation of Microemulsions Using Scattering Techniques

Scattering techniques provide the most obvious methods for obtaining information on the size, shape, and structure of microemulsions. The scattering of radiation (including light, neutrons and X-rays) by particles has been applied successfully in the investigation of many systems such as polymer solutions, micelles, and colloidal particles. In all of these methods, measurements can be made at sufficiently low concentrations to avoid complications that might arise from particle–particle interactions. The results obtained can be extrapolated to infinite dilution to obtain the desirable properties, such as the molecular weight and radius of gyration of a polymer coil, and the size and shape of micelles. Unfortunately, this dilution method cannot be applied to microemulsions, which depend on a specific composition of oil, water and surfactants. The microemulsions cannot be diluted by the continuous phase as this will result in a breakdown of the microemulsion; consequently, when applying scattering techniques to microemulsions, the measurements must be made at finite concentrations and the results obtained analysed using theoretical treatments to take into account any droplet–droplet interactions.

Two scattering methods, namely time-average (static) light scattering and dynamic (quasi-elastic) light scattering (also referred to as photon correlation spectroscopy; PCS), will be discussed in the following sections.

15.5.1
Time-Average (Static) Light Scattering

The intensity of scattered light $I(Q)$ is measured as a function of scattering vector Q [11],

$$Q = \left(\frac{4\pi\, n}{\lambda}\right) \sin\left(\frac{\theta}{2}\right) \tag{15.8}$$

where n is the refractive index of the medium, λ is the wave length of light, and θ is the angle at which the scattered light is measured.

For a fairly dilute system, $I(Q)$ is proportional to the number of particles N, the square of the individual scattering units V_p, and some property of the system (material constant) such as its refractive index,

$$I(Q) = [(\text{Material const.})\ (\text{Instrument const.})]\ N\ V_p^2 \tag{15.9}$$

The instrument constant depends on the geometry of the apparatus (the light path length and the scattering cell constant).

For more concentrated systems, $I(Q)$ also depends on the interference effects arising from particle–particle interactions,

$$I(Q) = [(\text{Instrument const.})\ (\text{Material const.})]\ N\ V_p^2\ P(Q)\ S(Q) \tag{15.10}$$

where $P(Q)$ is the particle form factor which allows the scattering from a single particle of known size and shape to be predicted as a function of Q. For a spherical particle of radius R,

$$P(Q) = \left[\frac{(3 \sin QR - QR \cos QR)}{(QR)^3}\right]^2 \tag{15.11}$$

Here, $S(Q)$ is the so-called "structure factor" which takes into account the particle–particle interaction. $S(Q)$ is related to the radial distribution function $g(r)$ (which gives the number of particles in shells surrounding a central particle) [12],

$$S(Q) = 1 - \frac{4\pi N}{Q} \int_0^\infty [g(r) - 1]\, r \sin QR \, dr \tag{15.12}$$

For a hard-sphere dispersion with radius R_{HS} (which is equal to $R + t$, where t is the thickness of the adsorbed layer),

$$S(Q) = \frac{1}{[1 - NC\,(2Q\,R_{HS})]} \tag{15.13}$$

where C is a constant.

Usually, $I(Q)$ is measured at various scattering angles θ, after which the intensity at some chosen angle (usually 90°; i_{90}) is plotted as a function of the volume fraction φ of the dispersion. Alternatively, the results may be expressed in terms of the Rayleigh ratio R_{90},

$$R_{90} = \left(\frac{i_{90}}{I_o}\right) r_s^2 \tag{15.14}$$

where I_o is the intensity of the incident beam and r_s is the distance from the detector.

$$R_{90} = K_o\, M\, C\, P(90)\, S(90) \tag{15.15}$$

where K_o is an optical constant (related to the refractive index difference between the particles and the medium), and M is the molecular mass of scattering units with weight fraction C.

For small particles (as is the case with microemulsions) $P(90) \sim 1$ and,

$$M = \frac{4}{3}\, \pi\, R_c^3\, N_{Av} \tag{15.16}$$

where N_{Av} is Avogadro's constant.

$$C = \varphi_c\, \rho_c \tag{15.17}$$

where ϕ_c is the volume fraction of the particle core and ρ_c is their density.

Equation (15.17) can be written in the simple form,

$$R_{90} = K_1\, \varphi_c\, R_c^3\, S(90) \tag{15.18}$$

where $K_1 = K_o\,(4/3)\, N_{Av}\, \rho_c{}^2$.

Equation (15.18) shows that, in order to calculate R_c from R_{90}, $S(90)$ needs to be known, but this can be calculated using Equations (15.11–15.13).

The above calculations were obtained using a W/O microemulsion of water/xylene/sodium dodecyl benzene sulphonate (NaDBS)/hexanol [11]. The

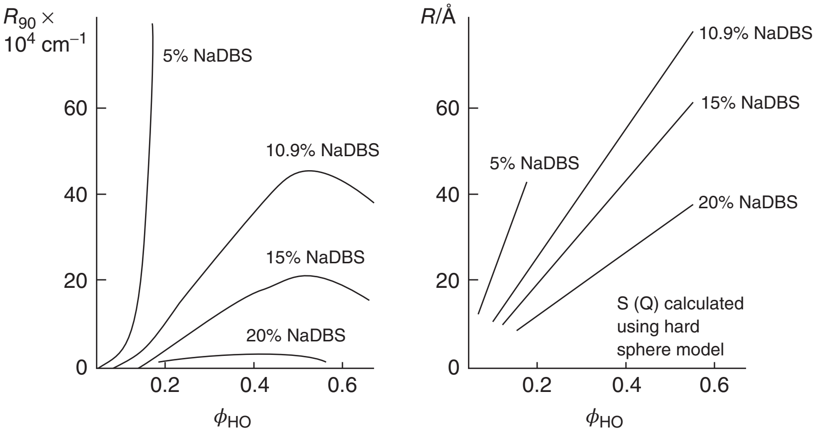

Figure 15.9 Variation of R_{90} and R with the volume fraction of water for a W/O microemulsion based on xylene-water-NaDBS-hexanol.

microemulsion region was established using the quaternary phase diagram. W/O microemulsions were produced at various water volume fractions using increasing amounts of NaDBS (5, 10.9, 15, and 20%).

The results for the variation of R_{90} with the volume fraction of the water core droplets at various NaDBS concentrations are shown in Figure 15.9. With the exception of the 5% NaDBS, all other concentrations showed an initial increase in R_{90} with increase of ϕ, reaching a maximum at a given ϕ, after which R_{90} decreased with further increases in ϕ.

The above results were used to calculate R as a function of φ using the hard-sphere model discussed above [Equation (15.18); this is also shown in Figure 15.9].

It can be seen that with increases in ϕ, at a constant surfactant concentration, R is increased (the ratio of surfactant to water decreases with increase in ϕ). At any volume fraction of water, an increase in surfactant concentration resulted in a decrease in the microemulsion droplet size (the ratio of surfactant to water was increased).

15.5.2
Calculation of Droplet Size from Interfacial Area

If it is assumed that all surfactant and cosurfactant molecules are adsorbed at the interface, it is possible to calculate the total interfacial area of the microemulsion from a knowledge of the area occupied by the surfactant and cosurfactant molecules.

Total interfacial area = Total number of surfactant molecules (n_s) × area per surfactant molecule (A_s) + total number of cosurfactant molecules (n_{co}) × area per cosurfactant molecule (A_{co}).

The total interfacial area A per kilogram of microemulsion is given by the expression,

$$A = \frac{(n_s\, N_{Av}\, A_s + n_{co}\, N_{Av}\, A_{co})}{\varphi} \tag{15.19}$$

where n_s and n_{co} are the number of moles of surfactant and cosurfactant, respectively. A is related to the droplet radius R (assuming that all droplets are of the same size) by,

$$A = \frac{3}{R\,\rho} \tag{15.20}$$

Using reasonable values for A_s and A_{co} (30 Å^2 for NaDBS and 20 Å^2) for hexanol, R was calculated and the results were compared with those obtained using light-scattering results. Two conditions were considered: (i) all hexanol molecules were adsorbed 1A1; and (ii) part of the hexanol was adsorbed to give a molar ratio of hexanol to NaDBS of 2 : 1 (1A2). A good agreement was obtained between the light-scattering data and R calculated from the interfacial area, particularly for 1A2.

15.5.3
Dynamic Light Scattering (Photon Correlation Spectroscopy; PCS)

In this technique, the intensity fluctuation of light that has been scattered by droplets is measured as they undergo Brownian motion [13]. When a light beam passes through a colloidal dispersion, an oscillating dipole movement is induced in the particles, causing the light to be radiated. Due to the random position of the particles, the intensity of the scattered light, at any instant, appears as a random diffraction (“Speckle” pattern). However, as the particles undergo Brownian motion the random configuration of the pattern will fluctuate, such that the time taken for an intensity maximum to become a minimum (the coherence time) will correspond approximately to the time required for a particle to move one wavelength, λ. By using a photomultiplier with an active area about the diffraction maximum (i.e., one coherent area) this intensity fluctuation can be measured. The analogue output is digitised (using a digital correlator) that measures the photocount (or intensity) correlation function of the scattered light.

The photocount correlation function $G^{(2)}\,(\tau)$ is given by,

$$g^{(2)} = B\,[1 + \gamma^2\, g^{(1)}\,(\tau)]^2 \tag{15.21}$$

where τ is the correlation delay time.

The correlator compares $g^{(2)}\,(\tau)$ for many values of τ.

Here, B is the background value to which $g^{(2)}\,(\tau)$ decays at long delay times, $g^{(1)}$ (τ) is the normalised correlation function of the scattered electric field, and γ is a constant (~1).

For monodispersed noninteracting particles,

$$g^{(1)}(\tau) = \exp\,(-\Gamma\,\gamma) \tag{15.22}$$

where Γ is the decay rate or inverse coherence time, that is related to the translational diffusion coefficient D,

$$\Gamma = D\,K^2 \tag{15.23}$$

where K is the scattering vector,

$$K = \left(\frac{4\pi n}{\lambda_o}\right) \sin\left(\frac{\theta}{2}\right) \tag{15.24}$$

The particle radius R can be calculated from D using the Stokes–Einstein equation,

$$D = \frac{kT}{6\pi \eta_o R} \tag{15.25}$$

where η_o is the viscosity of the medium.

The above analysis only applies to very dilute dispersions; with microemulsions which are concentrated dispersions, corrections are needed to take into account the interdroplet interaction. This is reflected in plots of ln $g^{(1)}(\tau)$ versus τ which become nonlinear, implying that the observed correlation functions are not single exponentials.

As with time-average light scattering, there is a need to introduce a structure factor when calculating the average diffusion coefficient. For comparative purposes, the collective diffusion coefficient D can be calculated, and this can be related to its value at infinite dilution D_o by [14],

$$D = D_o (1 + \alpha \varphi) \tag{15.26}$$

where α is a constant that is equal to 1.5 for hard spheres with repulsive interaction.

15.6
Characterisation of Microemulsions Using Conductivity

Conductivity measurements may provide valuable information on the structural behaviour of microemulsions. In the early applications of conductivity measurements, the technique was used to determine the nature of the continuous phase. O/W microemulsions should have a fairly high conductivity (which is determined by that of the continuous aqueous phase), whereas W/O microemulsions should have a fairly low conductivity (determined by that of the continuous oil phase).

To illustrate this point, Figure 15.10 shows the change in electrical resistance (reciprocal of conductivity) with the ratio of water to oil (V_w/V_o) for a microemulsion system prepared using the inversion method [14]. The data in Figure 15.10 indicate the change in optical clarity and birefringence with the ratio of water to oil.

At low V_w/V_o, a clear W/O microemulsion is produced with a high resistance (oil continuous), but as V_w/V_o increases the resistance decreases and, in the turbid region, hexanol and lamellar micelles are produced. Above a critical ratio, inversion occurs and the resistance decreases, producing an O/W microemulsion.

Conductivity measurements were also used to study the structure of the microemulsion, which is influenced by the nature of the cosurfactant. A systematic study of the effect of cosurfactant chain length on the conductive behaviour of W/O microemulsions was carried out by Clausse and coworkers [15]. The cosurfactant chain length was gradually increased from C_2 (ethanol) to C_7 (heptanol),

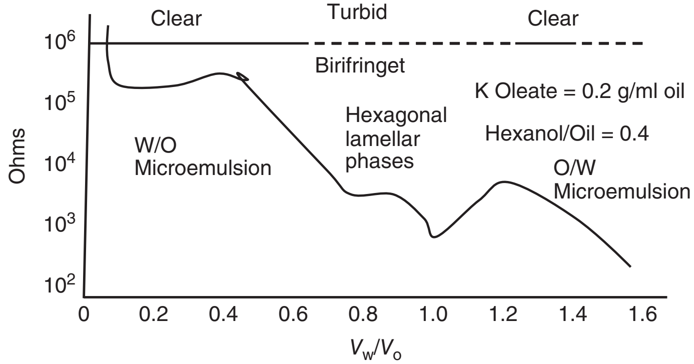

Figure 15.10 Electrical resistance versus V_w/V_o.

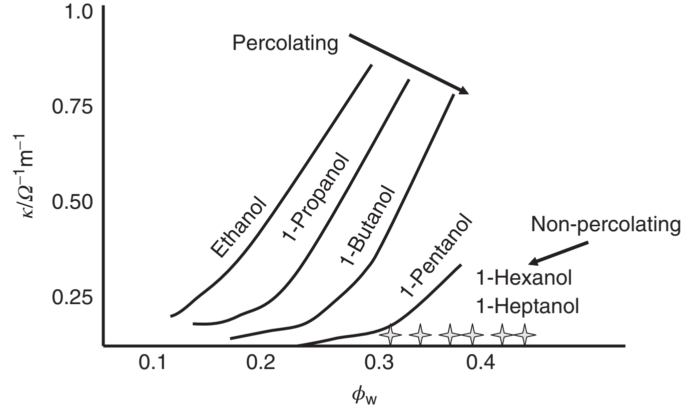

Figure 15.11 Variation of conductivity with water volume fraction for various cosurfactants.

and the results for the variation of κ with ϕ_w are shown in Figure 15.11. With the short-chain alcohols ($C < 5$), the conductivity showed a rapid increase above a critical ϕ value, but with longer chain alcohols (hexanol and heptanol) it remained very low up to a high water volume fraction. With the short-chain alcohols, the system showed percolation above a critical water volume fraction, and under these conditions the microemulsion was "bicontinuous." With the longer-chain alcohols the system was nonpercolating and definite water cores could be defined. This is sometimes referred to as a "true" microemulsion.

15.7
NMR Measurements

Lindman and coworkers [16–18] showed that the organisation and structure of microemulsions can be elucidated from self-diffusion measurements of all components (using pulse-gradient or spin-echo NMR techniques). Within a micelle, the molecular motion of the hydrocarbon tails (translational, reorientation and chain flexibility) is almost as rapid as in a liquid hydrocarbon. In a reverse micelle, water molecules and counterions are also highly mobile. For many surfactant–water systems, there is a distinct spatial separation between the hydrophobic and hydrophilic domains. The passage of species between different regions is an improbable event, and this occurs very slowly.

Thus, self-diffusion – if studied over macroscopic distances – should reveal whether the process is rapid or slow, depending on the geometric properties of the inner structure. For example, a phase that is water-continuous and oil-discontinuous should exhibit a rapid diffusion of hydrophilic components, while the hydrophobic components should diffuse slowly. In contrast, an oil-continuous but water-discontinuous system should exhibit a rapid diffusion of the hydrophobic components. It would be expected that a bicontinuous structure should promote a rapid diffusion of all components.

Using the above principle, Lindman and coworkers [16–18] measured the self-diffusion coefficients of all microemulsion components, with particular emphasis on the role of the cosurfactant. For microemulsions consisting of water, hydrocarbon, an anionic surfactant and a short-chain alcohol (C_4 and C_5), the self-diffusion coefficient of water, hydrocarbon and cosurfactant was quite high (on the order of $10^{-9}\,\mathrm{m^2\,s^{-1}}$), which was two orders of magnitude higher than the value expected for a discontinuous medium ($10^{-11}\,\mathrm{m^2\,s^{-1}}$). This high diffusion coefficient was attributed to three main effects: the presence of bicontinuous solutions; the easy deformability and flexible interface; and the absence of any large aggregates. With microemulsions based on long-chain alcohols (e.g., decanol), the self-diffusion coefficient for water was low, which indicated the presence of definite (closed) water droplets surrounded by surfactant anions in the hydrocarbon medium. Thus, NMR measurements could be used to distinguish clearly between the two types of microemulsion system.

15.8
Formulation of Microemulsions

The formulation of microemulsions or micellar solutions, like that of conventional macroemulsions, is still an art. In spite of exact theories that have explained the formation of microemulsions and their thermodynamic stability, the science of microemulsion formulation has not advanced to a point where an accurate prediction can be made as to what might happen when the various components are mixed. The very much higher ratio of emulsifier to disperse phase which differentiates microemulsions from macroemulsions appears at a first sight that the application of various techniques for formulation to be less critical. However, in the final stages of the formulation it can be realised immediately that the requirements are critical due to the greater number of parameters involved.

The mechanics of microemulsion formation differ from those of macroemulsion formation. The most important difference lies in the fact that exerting more effort in producing a macroemulsion, or increasing the emulsifier, usually improves its stability. However this is not so for microemulsions, the formation of which depends on specific interactions of the molecules of oil, water, and emulsifiers, though the details of these interactions are not exactly known. If such specific interactions are not realised, then no amount of work nor excess emulsifier can produce the microemulsion; however, if the chemistry is ''right,'' then microemulsification will occur spontaneously.

It should be remembered that for microemulsions the ratio of emulsifier to oil is much higher than that used for macroemulsions. This emulsifier used is at least 10% based on the oil, and in most cases it can be as high as 20–30%. The W/O systems are prepared by blending the oil and emulsifier, with some heating if necessary. Water is then added to the oil–emulsifier blend to produce the microemulsion droplets, at which point the resulting system should appear transparent or translucent. If the maximum amount of water that can be microemulsified is not high enough for the particular application, other emulsifiers should be tried in order to reach the required composition.

The most convenient way to produce O/W microemulsion is to blend the oil and emulsifier and then to pour the mixture into water, with mild stirring. In the case of waxes, both the oil–emulsifier blend and the water must be at a higher temperature (above the melting point of the wax). If the melting point of the wax is above the boiling temperature of water, the process can be carried out at high pressure. Another method of mixing the ingredients is to prepare a crude macroemulsion of the oil and one of the emulsifiers. Then, by using small volumes of water a gel can be formed and the system titrated with the coemulsifier until a transparent system is produced. This system may be further diluted with water to produce a transparent or translucent microemulsion.

Four different emulsifier selection methods can be applied to the formulation of microemulsions: (i) the hydrophilic–lipophilic-balance (HLB) system; (ii) the phase-inversion temperature (PIT) method; (iii) the cohesive energy ratio (CER) concept; and (iv) partitioning of the cosurfactant between the oil and water phases. The first three methods are essentially the same as those used for the selection of emulsifiers for macroemulsions. However, with microemulsions attempts should be made to match the chemical type of the emulsifier with that of the oil. A summary of these various methods is given below.

15.8.1
The HLB System

This scale is based on the relative percentage of hydrophilic to lipophilic (hydrophobic) groups in the surfactant molecule [19]. For an O/W microemulsion, a high HLB number (8–18) is required (the molecule is preferentially water-soluble), whereas for a W/O microemulsion a low HLB number (3–6) is required (the molecule is preferentially oil-soluble). The optimum HLB number for O/W or W/O microemulsions depends on the nature of the oil. The HLB number for a given oil is determined by using a mixture of two surfactants, one with a high and one with a low HLB number.

Emulsions are prepared using various ratios of the two surfactants. The total surfactant concentration is kept constant (e.g., 10%) based on the oil phase; typically, for a 50 : 50 emulsion, 5% surfactant is used. The emulsions are placed in cylinders and their stability is assessed by visual inspection (looking for any oil separation), by droplet size analysis (e.g., using a Malvern Master Sizer), and by measuring the interfacial tension. For an O/W emulsion the stability, droplet size and interfacial tension are plotted as a function of the % surfactant with a high HLB number. The stability reaches a maximum at an optimum % of the surfactant with the high HLB number, and at this optimum ratio the droplet size and interfacial tension reach a minimum. For W/O emulsions, the stability droplet size and interfacial tension are plotted versus % surfactant with a low HLB number. The stability reaches a maximum at an optimum % of the surfactant with the low HLB number, and at this optimum ratio the droplet size and interfacial tension reach a minimum.

The average HLB number may be calculated from additivity,

$$\mathrm{HLB}_{\mathrm{av}} = x_1 \mathrm{HLB}_1 + x_2 \mathrm{HLB}_2 \tag{15.27}$$

where x_1 and x_2 are the weight fractions of the two surfactants with HLB_1 and HLB_2, respectively.

Once the HLB number of an oil has been determined, using an arbitrary pair of surfactants, several other surfactant pairs should be investigated to obtain the most effective emulsifier pair. The most effective surfactant pair gives the exact HLB balance for the system (with the lipophilic groups fitting best in the oil phase and hydrophilic groups fitting best in the water phase).

After establishing the optimum HLB for the system, a cosurfactant such as a medium-chain alcohol is added to produce the transparent or translucent microemulsion. The required amount of cosurfactant can be determined by titrating the emulsion with that liquid cosurfactant.

15.8.2
Phase Inversion Temperature (PIT) Method

Shinoda and coworkers [20] found that many O/W emulsions (based on ethoxylated surfactants) undergo a process of inversion to W/O at a critical temperature (PIT). The PIT can be easily measured by following the conductivity of the emulsion as a function of temperature (a small amount of electrolyte, e.g., NaCl is added to increase the sensitivity of measurement). The conductivity of the O/W emulsion increases with increase of temperature until the PIT is reached, above which there is a rapid reduction in conductivity (a W/O emulsion is formed with low conductivity as the continuous phase is now oil). Figure 15.12 shows a schematic representation of the variation of conductivity with temperature increase for an O/W emulsion. At the PIT, the interfacial tension γ reaches a minimum, as illustrated in Figure 15.13 for an O/W emulsion.

From a microemulsion point of view, the PIT has an outstanding feature, in that it can throw light on the chemical nature of the emulsifier needed to match a given oil. The PIT provides information concerning the types of oils, phase–volume

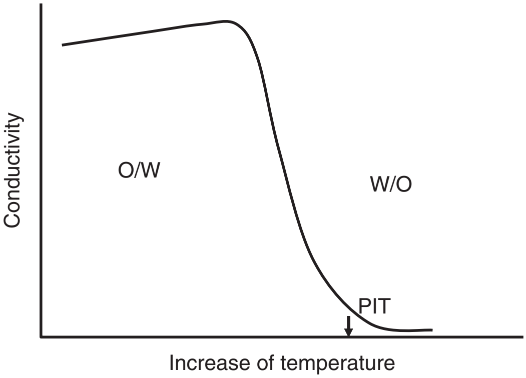

Figure 15.12 Variation of conductivity with temperature for an O/W emulsion.

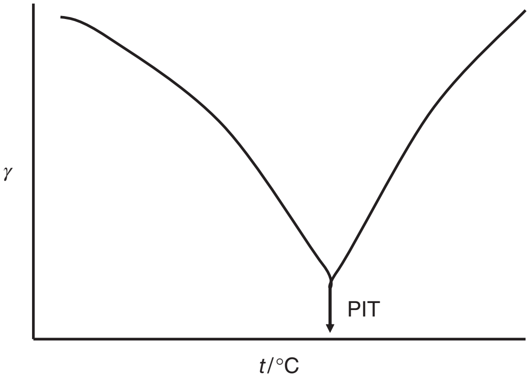

Figure 15.13 Variation of interfacial tension γ with temperature.

relationships and concentration of the emulsifier system. The required HLB values for various oils estimated from the PIT systems compare very favourably with those prepared using the HLB system, as presented in the previous section.

15.8.3
The Cohesive Energy Ratio (CER) Concept

Beerbower and Hills [21] considered the dispersing tendency on the oil and water interfaces of the surfactant or emulsifier in terms of the ratio of the cohesive energies of the mixtures of oil with the lipophilic portion of the surfactant and the water with the hydrophilic portion. For this, the Winsor R_o concept was used, which is the ratio of the intermolecular attraction of oil molecules (O) and lipophilic portion of surfactant (L), C_{LO}, to that of water (W) and hydrophilic portion (H), C_{HW},

$$R_o = \frac{C_{LO}}{C_{HW}} \tag{15.28}$$

C_{LL}, C_{OO}, C_{LO} (at oil side)
C_{HH}, C_{WW}, C_{HW} (at water side)
C_{LW}, C_{HO}, C_{LH} (at the interface)

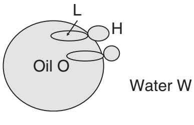

Figure 15.14 The cohesive energy ratio concept.

Several interaction parameters may be identified at the oil and water sides of the interface. Typically, at least nine interaction parameters can be identified, as shown schematically in Figure 15.14.

In the absence of an emulsifier, there will be only three interaction parameters, namely C_{OO}, C_{WW}, C_{OW}, but if $C_{OW} \ll C_{WW}$ the emulsion will break.

The above interaction parameters may be related to the Hildebrand solubility parameter [22] δ (at the oil side of the interface) and the Hansen [23] nonpolar, hydrogen-bonding and polar contributions to δ at the water side of the interface. The solubility parameter of any component is related to its heat of vapourisation ΔH by the expression,

$$\delta^2 = \frac{\Delta H - RT}{V_m} \tag{15.29}$$

where V_m is the molar volume.

Hansen considered δ (at the water side of the interface) to consist of three main contributions: a dispersion contribution, δ_d; a polar contribution, δ_p; and a hydrogen-bonding contribution, δ_h. These contributions have different weighting factors,

$$\delta^2 = \delta_d^2 + 0.25\delta_p^2 + \delta_h^2 \tag{15.30}$$

Beerbower and Hills used the following expression for the HLB number,

$$\text{HLB} = 20\left(\frac{M_H}{M_L + M_H}\right) = 20\left(\frac{V_H\rho_H}{V_L\rho_L + V_H\rho_H}\right) \tag{15.31}$$

where M_H and M_L are the molecular weights of the hydrophilic and lipophilic portions of the surfactants, respectively, and V_L and V_H are their corresponding molar volumes, whereas ρ_H and ρ_L are the densities, respectively.

The cohesive energy ratio was originally defined by Winsor (see Eq. (15.28).

When $C_{LO} > C_{HW}$, $R > 1$ and a W/O emulsion forms; however, if $C_{LO} < C_{HW}$, $R < 1$ and an O/W emulsion will form. If $C_{LO} = C_{HW}$ and $R = 1$, a planer system will result. This denotes the inversion point.

R_o can be related to V_L, δ_L and V_H, δ_H by the expression,

$$R_o = \frac{V_L\delta_L^2}{V_H\delta_H^2} \tag{15.32}$$

Using Equation (15.31),

$$R_o = \frac{V_L\,(\delta_d^2 + 0.25\delta_p^2 + 0.25\delta_h^2)_L}{V_h\,(\delta_d^2 + 0.25\delta_p^2 + 0.25\delta_h^2)_H} \tag{15.33}$$

Combining Equations (15.31) and (15.33), the following general expression for the cohesive energy ratio is obtained,

$$R_o = \left(\frac{20}{\text{HLB}} - 1\right)\frac{\rho_h(\delta_d^2 + 0.25\delta_p^2 + 0.25\delta_h^2)_L}{\rho_L(\delta_d^2 + 0.25\delta_p^2 + 0.25\delta_p^2)_L} \tag{15.34}$$

For an O/W system, HLB = 12–15 and $R_o = 0.58{-}0.29$ ($R_o < 1$); for a W/O system, HLB = 5–6 and $R_o = 2.3{-}1.9$ ($R_o > 1$); for a planar system, HLB = 8–10 and $R_o = 1.25{-}0.85$ ($R_o \sim 1$).

The R_o equation combines both the HLB and cohesive energy densities, and provides a more quantitative estimate of emulsifier selection, while R_o considers HLB, molar volume and chemical match. The success of this approach depends on the availability of data relating to the solubility parameters of the various surfactant portions; some values are provided in the book by Barton [24].

15.8.4
Cosurfactant Partitioning

According to the thermodynamic theory of microemulsion formation, the total interfacial tension of the mixed film of surfactant and cosurfactant must approach zero. The total interfacial tension is given by the following equation,

$$\gamma_T = \gamma_{(O/W)_a} - \pi \tag{15.35}$$

where $\gamma_{(O/W)a}$ is the interfacial tension of the oil in the presence of alcohol cosurfactant and π is the surface pressure. $\gamma(_{O/W})_a$ seems to reach a value of 15 mN m^{-1}, irrespective of the original value of $\gamma_{O/W}$. It seems that the cosurfactant, which is predominantly oil-soluble, distributes itself between the oil and the interface and this causes a change in the composition of the oil, which now is reduced to 15 mN m^{-1}.

Measurement of the partition of the cosurfactant between the oil and the interface is not easy. A simple procedure to select the most efficient cosurfactant is to determine the oil/water interfacial tension $\gamma_{O/W}$ as a function of cosurfactant concentration. In this case, the lower the percentage of cosurfactant required to reduce $\gamma_{O/W}$ to 15 mN m^{-1}, the better is the candidate.

References

1. Hoar, T.P. and Schulman, J.H. (1943) *Nature (London)*, **152**, 102.
2. Prince, L.M. (1977) *Microemulsion Theory and Practice*, Academic Press, New York.
3. Danielsson, I. and Lindman, B. (1983) *Colloids Surf.*, **3**, 391.
4. Schulman, J.H., Stoeckenius, W., and Prince, L.M. (1959) *J. Phys. Chem.*, **63**, 1677.

5. Prince, L.M. (1970) *Adv. Cosmet. Chem.*, **27**, 193.
6. Shinoda, K. and Friberg, S. (1975) *Adv. Colloid Interface Sci.*, **4**, 281.
7. Ruckenstein, E. and Chi, J.C. (1975) *J. Chem. Soc., Faraday Trans. II*, **71**, 1690.
8. Overbeek, J.Th.G. (1978) *Faraday Discuss. Chem. Soc.*, **65**, 7.
9. Overbeek, J.T.G., de Bruyn, P.L., and Verhoeckx, F. (1984) in *Surfactants* (ed. Th.F. Tadros), Academic Press, London, pp. 111–132.
10. Mitchell, D.J. and Ninham, B.W. (1981) *J. Chem. Soc., Faraday Trans. II*, **77**, 601.
11. Baker, R.C., Florence, A.T., Ottewill, R.H., and Tadros, Th.F. (1984) *J. Colloid Interface Sci.*, **100**, 332.
12. Ashcroft, N.W. and Lekner, J. (1966) *Phys. Rev.*, **45**, 33.
13. Pusey, P.N. (1973) in *Industrial Polymers: Characterisation by Molecular Weights* (eds J.H.S. Green and R. Dietz), Transcripta Books, London.
14. Prince, L.M. (1977) *Microemulsions*, Academic Press, New York.
15. Clausse, M., Peyerlasse, J., Boned, C., Heil, J., Nicolas-Margantine, L., and Zrabda, A. (1984) in *Solution Properties of Surfactants*, Vol. 3 (eds K.L. Mittal and B. Lindman), Plenum Press, p. 1583.
16. Lindman, B. and Winnerstrom, H. (1980) in *Topics in Current Chemistry*, Vol. 87 (ed. F.L. Borschke), Springer-Verlag, Heidelberg, pp. 1–83.
17. Winnerstrom, H. and Lindman, B. (1970) *Phys. Rep.*, **52**, 1.
18. Lindman, B., Stilbs, P., and Moseley, M.E. (1981) *J. Colloid Interface Sci.*, **83**, 569.
19. Griffin, W.C. (1949) *J. Cosmet. Chem.*, **1**, 311; **5**, 249 (1954).
20. Shinoda, K. and Saito, H. (1969) *J. Colloid Interface Sci.*, **30**, 258.
21. Beerbower, A. and Hill, M.W. (1972) *Am. Cosmet. Perfum.*, **87**, 85.
22. Hildebrand, J.H. (1936) *Solubility of Non-Electrolytes*, 2nd edn, Reinhold, New York.
23. Hansen, C.M. (1967) *J. Paint Technol.*, **39**, 505.
24. Barton, A.F.M. (1983) *Handbook of Solubility Parameters and Other Cohesive Parameters*, CRC Press, New York.

Further Reading

Cazabat, A.N. and Langevin, D. (1981) *J. Chem. Phys.*, **74**, 3148.

Cebula, D.J., Ottewill, R.H., Ralston, J., and Pusey, P. (1981) *J. Chem. Soc., Faraday Trans. 1*, **77**, 2585.

Lagourette, B., Peyerlasse, J., Boned, C., and Clausse, M. (1969) *Nature*, **281**, 60.

Kilpatrick, S. (1973) *Mod. Phys.*, **45**, 574.

Mooney, M. (1950) *J. Colloid Sci.*, **6**, 162.

Carnahan, N.F. and Starling, K.E. (1969) *J. Chem. Phys.*, **51**, 635.

16
Formulation of Foams

16.1
Introduction

A foam is a disperse system that consists of gas bubbles separated by liquid layers. Because of the significant density difference between the gas bubbles and the medium, the system quickly separates into two layers, with the gas bubbles rising to the top, which may undergo deformation to form polyhedral structures; this process will be discussed in detail below.

Pure liquids cannot foam unless a surface-active material is present. When a gas bubble is introduced below the surface of a liquid, it bursts almost immediately as soon as the liquid has drained away. With dilute surfactant solutions, however, as the liquid/air interface expands and the equilibrium at the surface is disturbed, a restoring force arising from the Gibbs–Marangoni effect (as discussed in Chapter 10) becomes set up and tries to establish the equilibrium. Due to the presence of a surface tension gradient, $d\gamma$ (due to incomplete coverage of the film by surfactant), a dilational elasticity ε is produced (Gibbs elasticity). The surface tension gradient then induces a flow of surfactant molecules from the bulk to the interface, and these molecules carry liquid with them (the Marangoni effect). The Gibbs–Marangoni effect prevents thinning and disruption of the liquid film between the air bubbles, and this in turn stabilises the foam; this process will also be discussed in detail below.

Several surface-active foaming materials may be distinguished, including surfactants (ionic, nonionic and zwitterionic), polymers (polymeric surfactants), particles that accumulate at the air/solution interface, and specifically adsorbed cations or anions from inorganic salts. Many of these substances can cause foaming at extremely low concentrations (as low as $10^{-9}\ \text{mol dm}^{-3}$).

In kinetic terms, foams may be classified as either unstable, transient foams (with a lifetime of seconds), or metastable, permanent foams (with lifetimes of hours or days).

Formulation of Disperse Systems: Science and Technology, First Edition. Tharwat F. Tadros.

16.2
Foam Preparation

Like most disperse systems, foams can be obtained by applying condensation and dispersion methods. The condensation methods for generating foams involves the creation of gas bubbles in the solution by decreasing the external pressure, by increasing temperature, or as a result of chemical reaction. Thus, bubble formation may occur through homogeneous nucleation that occurs at high supersaturation or heterogeneous nucleation (e.g., from catalytic sites) that occurs at low supersaturation. Although the most widely used technique for generating foam is by a simple dispersion technique (mechanical shaking or whipping), this method is unsatisfactory as an accurate control of the amount of air incorporated is difficult to achieve. The most convenient method is to pass a flow of gas (sparging) through an orifice with well-defined radius r_o.

The size of the bubbles (produced at an orifice) r may be roughly estimated from the balance of the buoyancy force F_b with the surface tension force F_s [1],

$$F_b = (4/3)\,\pi\, r^3\, \rho\, g \tag{16.1}$$

$$F_s = 2\,\pi\, r_o\, \gamma \tag{16.2}$$

$$r = \left(\frac{3\,\gamma\, r_o}{2\,\rho\, g}\right)^{1/3} \tag{16.3}$$

where r and r_o are the radii of the bubble and orifice, ρ is the specific gravity of liquid, and g is the acceleration due to gravity.

As the dynamic surface tension of the growing bubble is higher than the equilibrium tension, the contact base may spread, depending on the wetting conditions. Thus, the main problem is the value of γ to be used in Equation (16.3). Another important factor that controls bubble size is the adhesion tension $\gamma\cos\theta$, where θ is the dynamic contact angle of the liquid on the solid of the orifice. With a hydrophobic surface, a bubble develops with a greater size than the hole. A distinction should always be made between the equilibrium contact angle θ and the dynamic contact angle, θ_{dyn} during bubble growth. As the bubble detaches from the orifice, the dimensions of the bubble will determine the velocity of the rise. The subsequent rise of the bubble through the liquid will cause a redistribution of surfactant on the bubble surface, with the top having a reduced concentration and the polar base having a higher concentration than the equilibrium value. This unequal distribution of surfactant on the bubble surface has an important role in foam stabilisation (due to the surface tension gradients). When the bubble reaches the interface, a thin liquid film is produced on its top, the life time of which will depend on many factors including the surfactant concentration, the rate of drainage, surface tension gradient, surface diffusion, and external disturbances.

16.3
Foam Structure

Two main types of foam may be distinguished:

- Spherical foam ("Kugel-Schaum"), consisting of gas bubbles separated by thick films of viscous liquid produced in freshly prepared systems. This may be considered as a temporary dilute dispersion of bubbles in the liquid.
- Polyhedral gas cells produced on aging; thin flat "walls" are produced with junction points of the interconnecting channels (plateau borders). Due to the interfacial curvature, the pressure is lower and the film is thicker in the plateau border. A capillary suction effect of the liquid occurs from the centre of the film to its periphery.

The pressure difference between neighbouring cells, Δp, is related to the radius of curvature (r) of the plateau border by,

$$\Delta p = \frac{2\,\gamma}{r} \tag{16.4}$$

In a foam column, several transitional structures may be distinguished, as illustrated in Figure 16.1.

Near the surface, a high gas content (polyhedral foam) is formed, with a much lower gas content structure near the base of the column (bubble zone). A transition state may be distinguished between the upper and bottom layers. The drainage of excess liquid from the foam column to the underlying solution is initially driven by hydrostatic pressure, which causes the bubble to become distorted. Foam collapse usually occurs from top to bottom of the column, with films in the polyhedral foam being more susceptible to rupture by shock, temperature gradient, or vibration.

Another mechanism of foam instability is due to Ostwald ripening (disproportionation), the driving force for which process is the difference in Laplace pressure between the small and larger foam bubbles. The smaller bubbles have a higher

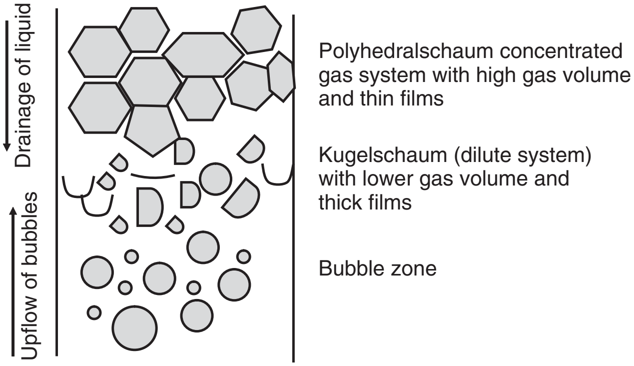

Figure 16.1 Schematic representation of a foam structure in a column.

Laplace pressure than the larger bubbles, but as the gas solubility increases with pressure the gas molecules will diffuse from the smaller to the larger bubbles. This process only occurs with spherical foam bubbles, and may be opposed by the Gibbs elasticity effect. Alternatively, rigid films produced using polymers may resist Ostwald ripening as a result of their high surface viscosity.

In the case of a polyhedral foam with planar liquid lamella, the pressure difference between the bubbles is not large, and consequently Ostwald ripening is not the mechanism for foam instability in this case. With a polyhedral foam, the main driving force for foam collapse is the surface forces that act across the liquid lamella.

To keep the foam stable (i.e., to prevent complete rupture of the film), this capillary suction effect must be prevented by an opposing ‘‘disjoining pressure’’ that acts between the parallel layers of the central flat film (see below). The generalised model for drainage involves the plateau borders forming a ‘‘network’’ through which the liquid flows due to gravity.

16.4
Classification of Foam Stability

All foams are thermodynamically unstable (due to the high interfacial free energy), but for convenience they are classified according to the kinetics of their breakdown:

- Unstable (transient) foams, which have a life time of seconds, are generally produced using ‘‘mild’’ surfactants, for example short-chain alcohols, aniline, phenol, pine oil, and short-chain undissociated fatty acids. Most of these compounds are sparingly soluble and may produce a low degree of elasticity.
- Metastable (‘‘permanent’’) foams, which have a life time of hours or days. These foams are capable of withstanding ordinary disturbances (thermal or Brownian fluctuations), but they may collapse from abnormal disturbances (evaporation, temperature gradients, etc.).

The above metastable foams are produced from surfactant solutions near or above the critical micelle concentration (cmc), and the stability is governed by a balance of the surface forces (see below). The film thickness is comparable to the range of intermolecular forces and, in the absence of any external disturbances, these foams may remain stable indefinitely. They are produced using proteins, long-chain fatty acids or solid particles. Gravity is the main driving force for foam collapse, either directly or indirectly through the plateau border. Thinning and disruption may be opposed by surface tension gradients at the air/water interface. Alternatively, the drainage rate may be decreased by increasing the bulk viscosity of the liquid (e.g., by the addition of glycerol or polymers). Stability may be increased in some cases by the addition of electrolytes that produce a ‘‘gel network’’ in the surfactant film. Foam stability may also be enhanced by increasing the surface viscosity and/or surface elasticity. A high packing of surfactant films (high cohesive forces) may also be produced by using mixed surfactant films or surfactant/polymer mixtures.

In order to investigate foam stability, it is important to consider the role of the plateau border under dynamic and static conditions. Foam films with intermediate life times – that is, between unstable and metastable foams – should also be considered.

16.5
Drainage and Thinning of Foam Films

As mentioned above, gravity is the main driving force for film drainage, and can act either directly on the film or through capillary suction in the plateau borders. As a general rule, the rate of drainage of foam films may be decreased by increasing the bulk viscosity of the liquid from which the foam is prepared. This can be achieved by adding glycerol or high-molecular-weight poly(ethylene oxide). Alternatively, the viscosity of the aqueous surfactant phase can be increased by the addition of electrolytes that form a ‘‘gel’’ network (liquid crystalline phases may be produced). Film drainage can also be reduced by increasing the surface viscosity and surface elasticity; this can be achieved, for example, by the addition of proteins, polysaccharides and even particles. These systems are applied in many food foams.

Most quantitative studies on film drainage have been carried out by Scheludko and coworkers [2–4], who investigated the drainage of small horizontal films using a specially designed measuring system. The film thickness was measured using interferometry, and the drainage time determined and compared with the theoretical value using the Reynold’s equation [5]. The experimental results obtained by Scheludko and coworkers [2–4, 6], produced from dilute solutions of sodium oleate, were in reasonable agreement with the drainage equation. For thinner films, large electrostatic repulsive interactions can reduce the driving force for film drainage and this may lead to stable films. For thick films that contain high surfactant concentrations (>cmc), the micelles present in the film can produce a repulsive structural mechanism.

The drainage of vertical films was investigated by pulling a frame out of a reservoir containing a surfactant solution. Three stages could be identified: (i) an initial formation of the film that is determined by the withdrawal velocity; (ii) drainage of the film within the lamella, which causes thinning with time; and (iii) aging of the film, which may result in the formation of a metastable film. Assuming that the monolayer of the surfactant film at the boundaries of the film is rigid, film drainage may be described by the viscous flow of the liquid under gravity between two parallel plates. As the process proceeds, thinning can also occur by a horizontal mechanism, known as marginal regeneration [7–9], in which the liquid is drained from the film near the border region and exchanged within the low-pressure plateau border. Marginal regeneration is probably the most important cause of film drainage of films with mobile surfaces – that is, at surfactant concentrations above the cmc.

16.6
Theories of Foam Stability

Whilst there is no single theory that can explain foam stability in a satisfactory manner, several approaches have been considered and these are summarised below.

16.6.1
Surface Viscosity and Elasticity Theory

The adsorbed surfactant film is assumed to control the mechanical–dynamical properties of the surface layers by virtue of its surface viscosity and elasticity. This concept may be true for thick films (>100 nm) whereby intermolecular forces are less dominant (i.e., foam stability under dynamic conditions). Surface viscosity reflects the speed of the relaxation process which restores the equilibrium in the system after imposing a stress on it. Surface elasticity is a measure of the energy stored in the surface layer as a result of an external stress.

The viscoelastic properties of the surface layer are important parameters. The most useful technique for studying the viscoelastic properties of surfactant monolayers is surface scattering. When transversal ripples occur, a periodic dilation and compression of the monolayer occurs, and this can be accurately measured, enabling the viscoelastic behaviour of monolayers under equilibrium and nonequilibrium conditions, to be obtained, without disturbing the original sate of the adsorbed layer. Some correlations have been found between surface viscosity and elasticity and foam stability; an example of this is the addition of lauryl alcohol to sodium lauryl sulphate, which tends to increase the surface viscosity and elasticity [10].

16.6.2
The Gibbs–Marangoni Effect Theory

The Gibbs coefficient of elasticity, ε, was introduced as a variable resistance to surface deformation during thinning:

$$\varepsilon = 2\left(\frac{d\gamma}{d\ \ln\ A}\right) = -2\left(\frac{d\gamma}{d\ \ln\ h}\right) \tag{16.5}$$

where d ln h is the relative change in lamella thickness, and ε is the ‘‘film elasticity of compression modulus’’ or ‘‘surface dilational modulus.’’ ε is a measure of the ability of the film to adjust its surface tension in an instant stress, and in general the higher the value of ε, the more stable is the film. ε also depends on surface concentration and film thickness; in order for a freshly produced film to survive, a minimum ε is required.

The main deficiency of the early studies on Gibbs elasticity was that they were applied to thin films and diffusion from the bulk solution was neglected. In other words, the Gibbs theory applies to the case where there is insufficient surfactant molecules in the film to diffuse to the surface and lower the surface tension. This is clearly not the case with most surfactant films. For thick lamella under dynamic conditions, it is important to consider diffusion from the bulk solution – that is, the Marangoni effect – which tends to oppose any rapid displacement of the surface (Gibbs effect) and may provide a temporary restoring force to ''dangerous'' thin films. In fact, the Marangoni effect is superimposed on the Gibbs elasticity, so that the effective restoring force is a function of the rate of extension, as well as the thickness. When the surface layers behave as insoluble monolayers, then the surface elasticity has its greatest value and is referred to as the Marangoni dilational modulus, ε_m.

The Gibbs–Marangoni effect explains the maximum foaming behaviour at intermediate surfactant concentration [6]. This is shown schematically in Figure 16.2 where, at low surfactant concentrations (well below the cmc), the greatest possible differential surface tension will only be relatively small (Figure 16.2a) and minimal foaming will occur. At a very high surfactant concentration (well above the cmc), however, the differential tension relaxes too rapidly because of the supply of surfactant which diffuses to the surface (Figure 16.2c). This provides the restoring force with time to counteract the disturbing forces and produce a dangerously thinner film, so that foaming will be poor. It is the intermediate surfactant concentration range that produces maximum foaming (Figure 16.2b).

16.6.3
Surface Forces Theory (Disjoining Pressure π)

This theory operates under static (equilibrium) conditions in relatively dilute surfactant solutions ($h < 100$ nm). In the early stages of formation, foam films drain under the action of gravitation or capillary forces. Provided that the films remain stable during this drainage stage they may approach a thickness in the range of 100 nm. However, at this stage surface forces come into play; that is, the range of the surface forces now becomes comparable to the film thickness. Deryaguin and coworkers [11, 12] introduced the concept of a disjoining pressure which should remain positive in order to slow down further drainage and film collapse; this is the principle of formation of thin metastable (equilibrium) films.

In addition to the Laplace capillary pressure, three additional forces can operate at surfactant concentration below the cmc, namely electrostatic double layer repulsion π_{el}, van der Waals attractions π_{vdW}, and steric (short-range) forces $\pi_{st,}$

$$\pi = \pi_{el} + \pi_{vdW} + \pi_{st} \tag{16.6}$$

In the original definition of disjoining pressure by Deryaguin [11, 12], only the first two terms on the right-hand side of Equation (16.6) were considered. At low electrolyte concentrations, double layer repulsion predominates and π_{el} can compensate the capillary pressure; that is $\pi_{el} = P_c$. This results in the formation of an equilibrium-free film which is usually referred to as the thick common film CF (~50 nm thickness). This equilibrium-metastable film persists until thermal or mechanical fluctuations cause rupture. The stability of the CF can be described in

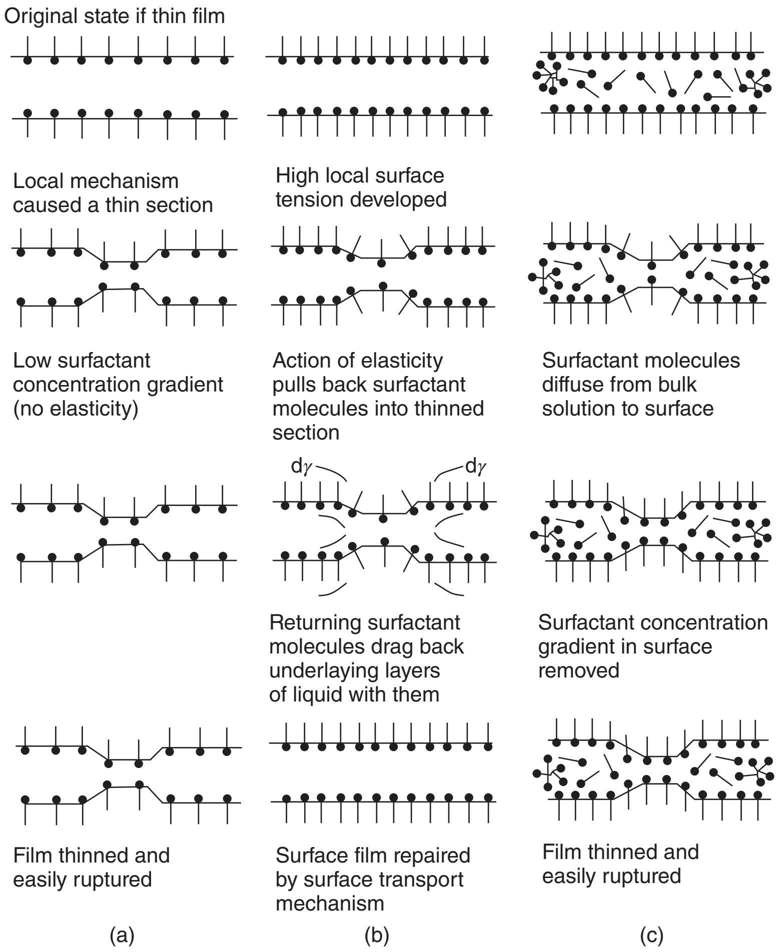

Figure 16.2 Schematic representation of the Gibbs–Marangoni effect. (a) Low surfactant concentration (<cmc); (b) Intermediate surfactant concentration; (c) High surfactant concentration (>cmc).

terms of the theory of colloid stability due to Deryaguin, Landau [13] and Verwey and Overbeek [14] (DLVO theory).

The critical thickness value at which the CF ruptures (due to thickness perturbations) fluctuates, and an average value h_{cr} may be defined. However, an alternative situation may occur as h_{cr} is reached and instead of rupturing a metastable film (high stability) may be formed with a thickness $h < h_{cr}$. The formation of this metastable film can be observed experimentally through the formation of ''islands of spots'' which appear black in light reflected from the surface; consequently, this film is often referred to as ''first black'' or ''common black'' film. The surfactant concentration at which this ''first black'' film is produced may be one to two orders of magnitude lower than the cmc.

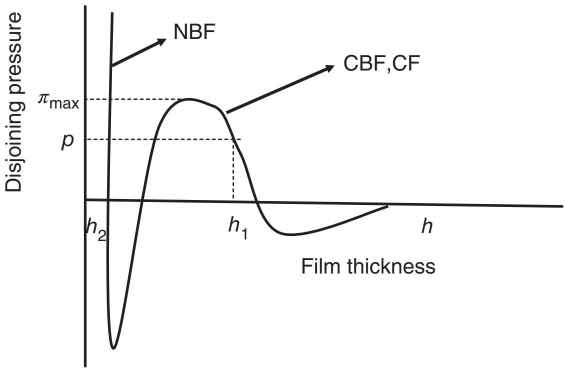

Figure 16.3 Variation of disjoining pressure with film thickness.

Further thinning can cause an additional transformation into a thinner stable region (a stepwise transformation). This usually occurs at high electrolyte concentrations, which in turn leads to a second, very stable, thin black film that usually is referred to as Newton secondary black film, with a thickness in the region of 4 nm. Under these conditions the short-range steric or hydration forces control the stability, and this provided the third contribution to the disjoining press, π_{st}, as described in Equation (16.9).

Figure 16.3 shows a schematic representation of the variation of disjoining pressure π with film thickness h, which shows the transition from the CF to the common black film and to the Newton black film. The common black film has a thickness in the region of 30 nm, whereas the Newton black film has a thickness in the region of 4–5 nm, depending on the electrolyte concentration.

Several investigations were carried out to study the above transitions from CF to common black film, and finally to Newton black film. For sodium dodecyl sulphate, the common black films have thicknesses ranging from 200 nm in very dilute systems to about 5.4 nm. The thickness depends heavily on the electrolyte concentration, while the stability may be considered to be caused by the secondary minimum in the energy distance curve. In cases where the film thins further and overcomes the primary energy maximum, it will fall into the primary minimum potential energy sink where very thin Newton black films are produced. The transition from common black films to Newton black films occurs at a critical electrolyte concentration which depends on the type of surfactant.

The rupture mechanisms of thin liquid films were considered by de Vries [15] and by Vrij and Overbeek [16]. It was assumed that thermal and mechanical disturbances (having a wavelike nature) cause film thickness fluctuations (in thin films), leading to the rupture or coalescence of bubbles at a critical thickness. Vrij and Overbeek [16] carried out a theoretical analysis of the hydrodynamic interfacial force balance, and expressed the critical thickness of rupture in terms of the attractive van der Waals interaction (characterised by the Hamaker constant A), the surface or interfacial tension γ, and the disjoining pressure. The critical wavelength, λ_{crit}, for the perturbation to grow (assuming that the disjoining pressure just exceeds the capillary pressure) was determined. Film collapse occurred when the amplitude of the fast-growing perturbation was equal to the thickness of the film. The critical thickness of rupture, h_{crit}, was defined by the following equation,

$$h_{\mathrm{crit}} = 0.267 \left(\frac{a_{\mathrm{f}}\, A^2}{6\, \pi\, \gamma\, \Delta p} \right)^{1/7} \tag{16.7}$$

where a_{f} is the area of the film.

Many poorly foaming liquids with thick film lamella are easily ruptured, for example pure water and ethanol films (with thickness between 110 and 453 nm). Under these conditions, rupture occurs by growth of disturbances which may lead to thinner sections [17]. Rupture can also be caused by the spontaneous nucleation of vapour bubbles (forming gas cavities) in the structured liquid lamella [18]. An alternative explanation for the rupture of relatively thick aqueous films containing a low level of surfactants is the hydrophobic attractive interaction between the surfaces that may be caused by bubble cavities [19, 20].

16.6.4
Stabilisation by Micelles (High Surfactant Concentrations > cmc)

At high surfactant concentrations (above the cmc), micelles of ionic or nonionic surfactants can produce organised molecular structures within the liquid film [21, 22]. This will provide an additional contribution to the disjoining pressure. Thinning of the film occurs through a stepwise drainage mechanism, referred to as stratification [23]. The ordering of surfactant micelles (or colloidal particles) in the liquid film due to the repulsive interaction provides an additional contribution to the disjoining pressure, and this prevents the thinning of the liquid film.

16.6.5
Stabilisation by Lamellar Liquid Crystalline Phases

This is particularly the case with nonionic surfactants that produce lamellar liquid crystalline structures in the film between the bubbles [24, 25]. These liquid crystals reduce film drainage as a result of the increase in viscosity of the film. In addition, the liquid crystals act as a reservoir of surfactant of the optimal composition to stabilise the foam.

16.6.6
Stabilisation of Foam Films by Mixed Surfactants

It has been found that a combination of surfactants produces a slower drainage and an improved foam stability. For example, mixtures of anionic and nonionic surfactants or anionic surfactant and long-chain alcohol produce much more stable films than the single components, but this could be attributed to several factors. For example, the addition of a nonionic surfactant to an anionic surfactant causes a reduction in the cmc of the anionic. The mixture can also produce a lower surface tension compared to the individual components. The combined surfactant system also has a high surface elasticity and viscosity when compared to the single components.

16.7
Foam Inhibitors

Two main types of inhibition may be distinguished: (i) antifoamers that are added to prevent foam formation; and (ii) defoamers that are added to eliminate an existing foam. For example, alcohols such as octanol are effective as defoamers but ineffective as antifoamers. As the drainage and stability of liquid films is far from being fully understood, it is very difficult at present to explain the antifoaming and foam-breaking action obtained by the addition of substances. The situation is also complicated by the fact that, in many industrial processes, foams are produced by unknown impurities. For these reasons, the mechanism of action of antifoamers and defoamers is far from being understood [26]. However, a summary of the various methods that can be applied to foam inhibition and foam breaking is given below.

16.7.1
Chemical Inhibitors That Lower Viscosity and Increase Drainage

Chemicals that reduce the bulk viscosity and increase drainage can cause a decrease in foam stability. The same applies to materials that reduce surface viscosity and elasticity (swamping the surface layer with excess compound of lower viscosity).

It has been suggested that a spreading film of antifoam may simply displace the stabilising surfactant monolayer. In this case, as the oil lens spreads and expands on the surface, the tension will be gradually reduced to a lower uniform value. This will eliminate the stabilising effect of the interfacial tension gradients – that is, the elimination of surface elasticity.

Reductions in surface viscosity and elasticity may be achieved by the inclusion of low- molecular-weight surfactants; these will reduce the coherence of the layer, for example by the addition of small amounts of nonionic surfactants. These effects depend on the molecular structure of the added surfactant. Other materials, which are not surface-active, can also destabilise the film by acting as cosolvents which reduce the surfactant concentration in the liquid layer. Unfortunately, these non-surface-active materials (e.g., methanol or ethanol) need to be added in large quantities (>10%).

16.7.2
Solubilised Chemicals Which Cause Antifoaming

It has been shown that solubilised antifoamers such as tributyl phosphate and methyl isobutyl carbinol, when added to surfactant solutions such as sodium dodecyl sulphate and sodium oleate, may reduce foam formation [27]. In cases where the oils exceed the solubility limit, the emulsifier droplets of oil can have a great influence on the antifoam action. It has been claimed [27] that the oil solubilised in the micelle causes a weak defoaming action. Mixed micelle formation with extremely low concentrations of surfactant may explain the actions of insoluble fatty acid esters, alkyl phosphate esters, and alkyl amines.

16.7.3
Droplets and Oil Lenses Which Cause Antifoaming and Defoaming

Undissolved oil droplets form in the surface of the film, and this can lead to film rupture. Several examples of oils may be used: alkyl phosphates, diols, fatty acid esters and silicone oils (e.g., polydimethyl siloxane; PDMS).

A widely accepted mechanism for the antifoaming action of oils considers two steps whereby the oil drops enter the air/water interface, and the oil then spreads over the film, causing rupture.

The antifoaming action can be rationalised [28] in terms of the balance between the entering coefficient E and the Harkins [29] spreading coefficient S, which are given by the following equations,

$$E = \gamma_{\mathrm{W/A}} + \gamma_{\mathrm{W/O}} - \gamma_{\mathrm{O/A}} \tag{16.8}$$

$$S = \gamma_{\mathrm{W/A}} - \gamma_{\mathrm{W/O}} - \gamma_{\mathrm{O/A}} \tag{16.9}$$

where $\gamma_{\mathrm{W/A}}$, $\gamma_{\mathrm{O/A}}$ and $\gamma_{\mathrm{W/O}}$ are the macroscopic interfacial tensions of the aqueous phase, oil phase, and interfacial tension of the oil/water interface, respectively.

Ross and McBain [30] suggested that, for efficient defoaming, the oil drop must enter the air/water interface and spread to form a duplex film at both sides of the original film. This leads to a displacement of the original film, leaving an oil film which is unstable and can easily break. Ross [28] used the spreading coefficient [Eq. (16.9)] as a defoaming criterion.

For antifoaming, both E and S should be > 0 for entry and spreading. A schematic representation of oil entry and the balance of the relevant tensions is given in Figure 16.4 [6]. A typical example of this type of spreading/breaking is illustrated for a hydrocarbon surfactant stabilised film. For most surfactant systems, $\gamma_{\mathrm{AW}} = 35\text{–}45\ \mathrm{mN\,m^{-1}}$, and $\gamma_{\mathrm{OW}} = 5\text{–}10\ \mathrm{mN\,m^{-1}}$; hence, for an oil to act as an antifoaming agent γ_{OA} should be less than $25\ \mathrm{mN\,m^{-1}}$. This shows why low-surface-tension silicone oils ($\gamma < 10\ \mathrm{mN\,m^{-1}}$) are effective.

16.7.4
Surface Tension Gradients (Induced by Antifoamers)

It has been suggested that some antifoamers act by eliminating the structure tension gradient effect in foam films by reducing the Marangoni effect. As spreading is driven by a surface tension gradient between the spreading front and the leading edge of the spreading front, thinning and foam rupture can occur by this surface

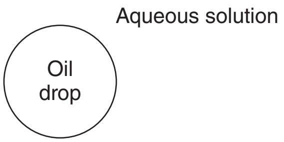

(a) Drop moves towards surface and enters

$E = \gamma_{W/A} + \gamma_{W/O} - \gamma_{O/A}$

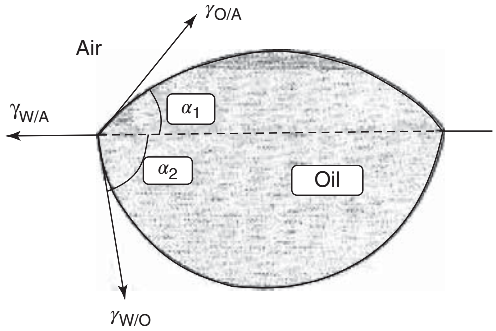

(b) For equilibrium $\gamma_{W/A} = \gamma_{O/A}\cos\alpha_1 + \gamma_{W/O}\cos\alpha_2$

Figure 16.4 Schematic representation of entry of oil droplet into the air/water interface (a) and its further spreading (b).

tension gradient acting as a shear force (dragging the underlying liquid away from the source). This could be achieved by solids or liquids containing surfactant other than that stabilising the foam. Alternatively, liquids which contain foam stabilisers at higher concentrations than are present in the foam may also act by this mechanism. A third possibility would be to use of the adsorbed vapours of surface-active liquids.

16.7.5
Hydrophobic Particles as Antifoamers

Many solid particles with some degree of hydrophobicity have been shown to cause the destabilisation of foams, including hydrophobic silica and poly(tetrafluoroethylene) (PTFE) particles. The PTFE particles exhibit a finite contact angle when adhering to the aqueous interface, and it has been suggested that many such hydrophobic particles can deplete the stabilising surfactant film by rapid adsorption, causing weak spots in the film.

A further mechanism was suggested based on the degree of wetting of the hydrophobic particles [31], and this led to the idea of particle bridging. For large smooth particles (large enough to touch both surfaces and with a contact angle $\theta > 90°$), dewetting can occur; in this case, the Laplace pressure in the film adjacent to the particle initially becomes positive and causes liquid to flow away from the particle, leading to an enhanced drainage and the formation of a ''hole.'' In the case of $\theta < 90°$, the initial situation is the same as for $\theta > 90°$, but as the film drains it attains a critical thickness where the film is planar and the capillary pressure becomes zero. At this point, further drainage reverses the sign of the radii of curvature, causing unbalanced capillary forces that prevent drainage from occurring. This can cause a stabilising effect for certain types of particle, and it means that a critical receding contact angle is required for efficient foam breaking.

With particles containing rough edges, the situation is more complex, as demonstrated by Johansson and Pugh [32], using finely ground quartz particles of different size fractions, the surfaces of which had been hydrophobised by methylation. The results of these studies and others confirmed the importance of the size, shape and hydrophobicity of the particles on foam stability.

16.7.6
Mixtures of Hydrophobic Particles and Oils as Antifoamers

The synergetic antifoaming effect of mixtures of insoluble hydrophobic particles and hydrophobic oils, when dispersed in an aqueous medium, has been well established in the patent literature. These mixed antifoamers are very effective at very low concentrations (10–100 ppm). The hydrophobic particles may be hydrophobised silica and the oil is PDMS.

One possible explanation of this synergetic effect is that the spreading coefficient of the PDMS oil is modified by the addition of hydrophobic particles. It has been suggested that the oil–particle mixtures form composite entities where the particles can adhere to the oil/water interface. Subsequently, the presence of particles adhering to the oil/water interface may facilitate the emergence of oil droplets into the air/water interface, so as to form lenses leading to rupture of the oil–water–air film.

16.8
Physical Properties of Foams

16.8.1
Mechanical Properties

The compressibility of a foam is determined by: (i) the ability of the gas to compress; and (ii) its wetting power, which is determined by the properties of the foaming solution [4]. As with any disperse system, a foam may acquire the properties of a solid body – that is, it can maintain its shape and it possesses a shear modulus (see below).

One of the basic mechanical properties of foams is its compressibility [4] (elasticity), and a bulk modulus E_v may be defined by the following expression,

$$E_v = -\frac{dp_o}{d \ln V} \qquad (16.10)$$

where p_o is the external pressure, causing deformation and V is the volume of the deforming system.

By taking into account the liquid volume V_L, the modulus of bulk elasticity of the "wet" foam E_v' is given by the expression,

$$E_v = \frac{dp_o}{d\ \ln\ V_F} = \frac{V_F\ dp_o}{d\,(V_L + V_G)} = E_v\left(1 + \frac{V_L}{V_G}\right) \tag{16.11}$$

Thus, the real modulus of bulk elasticity ("wet" foam) is higher than E_v ("dry" foam).

16.8.2
Rheological Properties

Like any disperse system, foams produce non-Newtonian systems, and to characterize their rheological properties information must be obtained on the elasticity modulus (the modulus of compressibility and expansion), the shear modulus, yield stress and effective viscosity, and elastic recovery.

It is difficult to study the rheological properties of a foam since, on deformation, its properties are changed. The most convenient geometry to measure foam rheology is to use a parallel plate. The rheological properties could be characterised by a variable viscosity [4],

$$\eta = \eta^*(\dot{\gamma}) + \frac{\tau_\beta}{\dot{\gamma}} \tag{16.12}$$

where γ is the shear rate.

The shear modulus of a foam is given by,

$$G = \frac{\tau_\beta\ \Delta l}{H} \tag{16.13}$$

where Δl is the shear deformation and H is the distance between parallel plates in the rheometer.

Deryaguin [33] obtained the following expression for the shear modulus,

$$G = \frac{2}{5}\ p_\gamma = \frac{2}{5}\left(\frac{2}{3}\gamma\varepsilon\right) \approx \frac{4\gamma}{3\ R_v} \tag{16.14}$$

where R_v is the average volume of the bubble and ε is the specific surface area.

Bikerman [34] obtained the following equation for the yield stress of a foam,

$$\tau_\beta = 0.5\ \frac{N_f}{N_f\text{-}1}\ p_\gamma\ \cos\ \theta \approx \frac{\gamma}{R}\ \cos\ \theta \tag{16.15}$$

where N_f is the number of films contacting the plate per unit area and θ is the average angle between the plate and the film.

Princen [35] used a two-dimensional hexagonal package model to derive an expression for the shear modulus and yield stress of a foam, taking into account the foam expansion ratio and the contact angles,

$$G = 0.525\ \frac{\gamma\ \cos\ \theta}{R}\ \varphi^{1/2} \tag{16.16}$$

$$\tau_\beta = 1.05\,\frac{\gamma\ \cos\ \theta}{R}\,\varphi^{1/2}\,F_{\max} \tag{16.17}$$

where $F_{\max}$ is a coefficient that is equal to 0.1–0.5, depending on the gas volume fraction φ.

For a ‘‘dry’’ foam ($\phi \rightarrow 1$), the yield stress can be calculated from the expression,

$$\tau_\beta = 0.525\,\gamma\ \cos\ \frac{\theta}{R} \tag{16.18}$$

For real foams, the value of τ_β can be expressed by the general expression,

$$\tau_\beta = C\,\frac{\gamma\ \cos\ \theta}{R}\,\varphi^{1/3}\,F_{\max} \tag{16.19}$$

where C is a coefficient that is approximately equal to 1.

16.8.3
Electrical Properties

Only the liquid phase in a foam possesses electrical conductivity. The specific conductivity of a foam, κ_F depends on the liquid content and its specific conductivity κ_L,

$$\kappa_\mathrm{F} = \frac{\kappa_\mathrm{L}}{n\ B} \tag{16.20}$$

where n is the foam expansion ratio and B is a structural coefficient that depends on the foam expansion ratio and the liquid phase distribution between the plateau borders. B changes monotonically from 1.5 to 3 with increase in foam expansion factor.

16.8.4
Electrokinetic Properties

In foams with charged gas/liquid interface, various electrokinetic parameters can be obtained, such as streaming potential and zeta-potential. For example, the relationship between the volumetric flow of a liquid flowing through a capillary or membrane and the zeta-potential can be given by the Smoluchowski equation,

$$Q = \frac{\varepsilon\,\varepsilon_\mathrm{o}\,I}{\eta\,\kappa} = \frac{\varepsilon\,\varepsilon_\mathrm{o}\,r^2}{\eta}\,\frac{\Delta V}{L} \tag{16.21}$$

where ε is the permittivity of the liquid and ε_o is the permittivity of free space, I is the value of the electric current, η is the viscosity of the liquid, r is the capillary radius, L is its length, and ΔV is the potential distance between the electrodes placed at the capillary ends.

The interpretation of electrokinetic results is complicated because of surface mobility and border and films elasticity, which causes large nonhomogeneities in density and border radii at hydrostatic equilibrium and liquid motion.

16.8.5
Optical Properties

The extinction of the luminous flux passing through a foam layer occurs as a result of light scattering (reflection, refraction, interference and diffraction from the foam elements) and light absorption by the solution [4]. In a polyhedral foam there are three structural elements which are clearly distinct by optical properties: films, plateau border, and vertexes.

The optical properties of single foam films have been extensively studied, but those of the foam as disperse system are poorly considered. It has been concluded that the extinction of luminous flux (I/I_o, where I is the intensity of the light passing through the foam and I_o is the intensity of the incident light) is a linear function of the specific foam area. This could be used to determine the specific surface area of a foam.

16.9
Experimental Techniques for Studying Foams

16.9.1
Studies on Foam Films

Most quantitative studies on foams have been carried out using foam films. As discussed above, microscopic horizontal films were studied by Scheludko and coworkers [2–4], when the foam thickness was determined using interferometry. Studies on vertical films were carried out by Mysels and collaborators [6, 7].

One of the most important characteristics of foam films is the contact angle θ that appears where the film makes contact with the bulk phase (solution) from which it is formed. This angle can be obtained using a topographic technique (that is suitable for small contact angles) which is based on determination of the radii of the interference Newton rings when the film is observed in a reflected monochromatic light.

Another technique used to study foam films is α-particle irradiation, which can destroy the film. Depending on the intensity of the α-source, the film will either rupture instantaneously or live for a much shorter time than required for its spontaneous rupture. The lifetime τ_a of a black film subjected to irradiation is considered as a parameter characterizing the destructive effect of α-particles.

A third technique for studying foam films is the fluorescence recovery after photobleaching (FRAP). This techniques was applied by Clarke *et al.* [36] for lateral diffusion in foam films, and involves irreversible photobleaching by intense laser light of fluorophore molecules in the sample. The time of redistribution of probe molecules (which are assumed to be randomly distributed within the constitutive membrane lipids in the film) is monitored. The lateral diffusion coefficient, D, is calculated from the rate of recovery of fluorescence in the bleaching region due to the entry of unbleaching fluoroprobes of adjacent parts of the membranes.

Deryaguin and Titijevskaya [37] measured the isotherms of disjoining pressure of microscopic foam films (common thin films) in a narrow range of pressures. At equilibrium, the capillary p_σ pressure in the flat horizontal foam film is equal to the disjoining pressure π in it,

$$p_\sigma = \pi = p_g - p_L \tag{16.22}$$

where p_g is the pressure in the gas phase and p_L is the pressure in the liquid phase.

Several other techniques have been applied for the measurement of foam films, including ellipsometry, Fourier transform-infrared (FT-IR) spectroscopy, X-ray reflection, and the measurement of gas permeability through the film. These techniques are described in detail in the text by Exerowa and Kruglyakov [4] to which the reader is referred.

16.9.2
Structural Parameters of Foams

The polyhedral foam consists of gas bubbles with a polyhedral shape, the faces of which are flat or slightly bent liquid films, the edges are the plateau borders, and the edge crosspoints are the vortexes. Several techniques can be applied to obtain the analytical dependence of these characteristics and the structural parameters of the foam [4].

The foam expansion ratio can be characterised by the liquid volume fraction in the foam, which is the sum of the volume fractions of the films, plateau borders and vertexes. Alternatively, the foam density can be used as a measure of the foam expansion ratio. The reduced pressure in the foam plateau border can be measured using a capillary manometer [4], while the bubble size and shape distribution in a foam can be determined by microphotography of the foam. Information about the liquid distribution between films and plateau borders is obtained from the data on the border radius of curvature, the film thickness, and the film-to-plateau border number ratio obtained in an elementary foam cell.

16.9.3
Foam Drainage

Following foam formation, the liquid begins to drain out of the foam, with the "excess" liquid draining first into the plateau borders and then flowing down from the upper to the lower foam layers (under gravity) until the gradient of the capillary pressure equalizes the gravity force,

$$\frac{\mathrm{d}p_\sigma}{\mathrm{d}l} = \rho\, g \tag{16.23}$$

where l is a coordinate in the opposite direction to gravity.

Simultaneously with drainage from films into borders, the liquid begins to flow out from the foam when the pressure in the lower foam films outweighs the external pressure. This process is similar to gel syneresis, and is sometimes referred to as "foam syneresis" or "foam drainage."

The rate of foam drainage is determined by the hydrodynamic characteristics of the foam, as well as the rate of internal foam collapse and breakdown of the foam column. Foam drainage is determined by measuring the quantity of liquid that drains from the foam per unit time. Various types of vessel and graduated tubes can be used to measure the quantity of liquid draining from a foam; alternatively, changes in the electrical conductivity of the layer at the vessel mouth can be measured and compared to the electrical conductivity of the foaming solution [4].

16.9.4
Foam Collapse

This can be followed by measuring the bubble size distribution as a function of time, by using microphotography or by counting the number of bubbles. Alternatively, the specific surface area or average bubble size can be measured as a function of time. Other techniques such as light scattering or ultrasound can also be applied.

References

1. Dickinson, E. (1992) *Introduction to Food Colloids*, Oxford University Press.
2. Scheludko, A. (1966) *Colloid Science*, Elsevier, Amsterdam.
3. Scheludko, A. (1971) *Adv. Colloid Interface Sci.*, **1**, 391.
4. Exerowa, D. and Kruglyakov, P.M. (1997) *Foam and Foam Films*, Elsevier, Amsterdam.
5. Reynolds, O. (1886) *Philos. Trans. R. Soc. London, Ser. A*, **177**, 157.
6. Pugh, R.J. (1995) *Adv. Colloid Interface Sci.*, **64**, 67.
7. Mysels, K.J. (1964) *J. Phys. Chem.*, **68**, 3441.
8. Lucassen, J. (1981) *Anionic Surfactants*, (ed. E.H. Lucassen-Reynders), Marcel Dekker, New York, p. 217.
9. Stein, H.N. (1991) *Adv. Colloid Interface Sci.*, **34**, 175.
10. Davies, J.T. (1957) in *Proceedings of the Second International Congress of Surface Activity*, Vol. 1 (ed. J.H. Schulman), Butterworth, London.
11. Deryaguin, B.V. and Churaev, N.V. (1976) *Kolloid Zh.*, **38**, 438.
12. Deryaguin, B.V. (1989) *Theory of Stability of Colloids and Thin Films*, Consultant Bureau, New York.
13. Deryaguin, B.V. and Landua, L.D. (1941) *Acta Physicochim. USSR*, **14**, 633.
14. Verwey, E.J. and Overbeek, J.T.G. (1948) *Theory of Stability of Lyophobic Colloids*, Elsevier, Amsterdam.
15. de Vries, A.J. (1966) *Discuss. Faraday Soc.*, **42**, 23.
16. Vrij, A. and Overbeek, J.T.G. (1968) *J. Am. Chem. Soc.*, **90**, 3074.
17. Radoev, B., Scheludko, A., and Manev, E. (1983) *J. Colloid Interface Sci.*, **95**, 254.
18. Gleim, V.G., Shelomov, I.V., and Shidlovskii, B.R. (1959) *J. Appl. Chem. USSR*, **32**, 1069.
19. Pugh, R.J. and Yoon, R.H. (1994) *J. Colloid Interface Sci.*, **163**, 169.
20. Claesson, P.M. and Christensen, H.K. (1988) *J. Phys. Chem.*, **92**, 1650.
21. Johnott, E.S. (1906) *Philos. Mag.*, **11**, 746.
22. Perrin, J. (1918) *Ann. Phys.*, **10**, 160.
23. Loeb, L. and Wasan, D.T. (1993) *Langmuir*, **9**, 1668.
24. Frieberg, S. (1977) *Mol. Cryst. Liq. Cryst.*, **40**, 49.
25. Perez, J.E., Proust, J.E., and Ter-Minassian Saraga, L. (1988) in *Thin Liquid Films* (ed. I.B. Ivanov), Marcel Dekker, New York, p. 70.
26. Garrett, P.R. (ed) (1993) *Defoaming*, Surfactant Science Series, Vol. 45, Marcel Dekker, New York.
27. Ross, S. and Haak, R.M. (1958) *J. Phys. Chem.*, **62**, 1260.

28. Robinson, J.V. and Woods, W.W. (1948) *J. Soc. Chem. Ind.*, **67**, 361.
29. Harkins, W.D. (1941) *J. Phys. Chem.*, **9**, 552.
30. Ross, S. and Mc Bain, J.W. (1944) *Ind. Chem. Eng.*, **36**, 570.
31. Garett, P.R. (1979) *J. Colloid Interface Sci.*, **69**, 107.
32. Johansson, G. and Pugh, R.J. (1992) *Int. J. Miner. Process.*, **34**, 1.
33. Deryaguin, B.V. (1933) *Kolloid Z.*, **64**, 1.
34. Bickermann, J.J. (1973) *Foams*, Springer-Verlag, New York.
35. Princen, H. (1983) *J. Colloid Interface Sci.*, **91**, 160.
36. Clark, D., Dann, R., Mackie, A., Mingins, J., Pinder, A., Purdy, P., Russel, E., Smith, L., and Wilson, D. (1990) *J. Colloid Interface Sci.*, **138**, 195.
37. Deryaguin, B.V. and Titijevskaya, A.S. (1953) *Kolloidn. Zh.*, **15**, 416.

17
Formulation of Latexes

17.1
Introduction

Emulsion polymers (latexes) are the most commonly used film formers in the coating industry. This is particularly the case with aqueous emulsion paints that are used for home decoration. These aqueous emulsion paints are applied at room temperature, and the latexes coalesce on the substrate to form a thermoplastic film. Occasionally, functional polymers are used for crosslinking in the coating system. The polymer particles are typically submicron (0.1–0.5 μm).

Generally speaking, three methods are available for the preparation of polymer dispersions, namely emulsion, dispersion, and suspension polymerisation:

- In *emulsion polymerisation*, the monomer is emulsified in a nonsolvent (commonly water), usually in the presence of a surfactant. A water-soluble initiator is added, and particles of polymer form and grow in the aqueous medium as the reservoir of the monomer in the emulsified droplets is gradually used up.
- In *dispersion polymerisation* (which is usually applied to the preparation of nonaqueous polymer dispersions, commonly referred to as nonaqueous dispersion polymerisation, NAD), the monomer, initiator, stabiliser (referred to as the protective agent) and solvent initially form a homogeneous solution. The polymer particles precipitate when the solubility limit of the polymer is exceeded, and the particles continue to grow until the monomer is consumed.
- In *suspension polymerisation* the monomer is emulsified in the continuous phase using a surfactant or polymeric suspending agent. The initiator (which is oil-soluble) is dissolved in the monomer droplets and the droplets are converted into insoluble particles, but no new particles are formed.

Descriptions of both emulsion and dispersion polymerisation are given below, with particular reference to the control of their particle size and colloid stability, which is greatly influenced by the emulsifier or dispersant used. Particular emphasis will be placed on the effects of polymeric surfactants that have been recently applied to the preparation of emulsion polymers.

Formulation of Disperse Systems: Science and Technology, First Edition. Tharwat F. Tadros.

17.2
Emulsion Polymerisation

As mentioned above, in emulsion polymerisation the monomer – for example, styrene or methyl methacrylate (MMA) – is insoluble in the continuous phase and is emulsified using a surfactant that adsorbs at the monomer/water interface [1]. The surfactant micelles in bulk solution solubilise some of the monomer. A water-soluble initiator (e.g., potassium persulphate; $K_2S_2O_8$) is then added, and this decomposes in the aqueous phase to form free radicals that interact with the monomers so as to form oligomeric chains. It has long been assumed that nucleation occurs in the ''monomer-swollen micelles,'' the reasoning behind this mechanism being the sharp increase in the rate of reaction above the critical micelle concentration (cmc), and that the number of particles formed (and their size) depends to a large extent on the nature of the surfactant and its concentration (which determines the number of micelles formed). However, this mechanism was later disputed and it was subsequently suggested that the presence of micelles means that excess surfactant is available and the molecules will diffuse readily to any interface.

The most widely accepted theory of emulsion polymerisation is referred to as the coagulative nucleation theory [2, 3]. A two-step coagulative nucleation model has been proposed by Napper and coworkers [2, 3], in which the oligomers first grow by propagation, followed by a termination process in the continuous phase. A random coil is produced which is insoluble in the medium, and this produces a precursor oligomer at the θ-point; the precursor particles subsequently grow, primarily by coagulation, to form true latex particles. Some growth may also occur by further polymerisation. The colloidal instability of the precursor particles may arise from their small size, and the slow rate of polymerisation can be due to reduced swelling of the particles by the hydrophilic monomer [2, 3]. The role of surfactants in these processes is crucial as they determine the stabilising efficiency, and the effectiveness of the surface active agent ultimately determines the number of particles formed. This was confirmed by using surface-active agents of different nature. The effectiveness of any surface-active agent in stabilising the particles was found to be the dominant factor, while the number of micelles formed was relatively unimportant.

A typical emulsion polymerisation formulation contains water, 50% monomer blended for the required glass transition temperature (T_g), surfactant (and often colloid), initiator, pH buffer and fungicide. Hard monomers with a high T_g used in emulsion polymerisation may be vinyl acetate, MMA, and styrene, while soft monomers with a low T_g include butyl acrylate, 2-ethylhexyl acrylate, vinyl versatate, and maleate esters. The most suitable monomers are those with low (but not too-low) water solubility. Other monomers such as acrylic acid, methacrylic acid, and adhesion-promoting monomers may also be included in the formulation. It is important that the latex particles coalesce as the diluent evaporates. The minimum film-forming temperature (MFFT) of the paint is a characteristic of the paint system, and is closely related to the T_g of the polymer, although the latter may be

Table 17.1 Surfactants used in emulsion polymerisation.

Anionic

Carboxylates: $C_nH_{2n+1}\ COO^-\ X$
Sulfates: $C_nH_{2n+1}\ OSO_3{}^-\ X$
Sulfonates: $C_nH_{2n+1}\ SO_3{}^-\ X$
Phosphates: $C_nH_{2n+1}\ OPO(OH)O^-\ X$
With n being the range 8–16 atoms and the counterion X is usually Na^+
Several other anionic surfactants are commercially available such as sulphosuccinates, isothionates and taurates, and these are sometimes used for special applications

Cationic

Alkyl trimethyl ammonium chloride, where R contains 8–18 C atoms, for example dodecyl trimethyl ammonium chloride, $C_{12}H_{25}(CH_3)_3NCl$

Zwitterions

N-alkyl betaines which are derivatives of trimethyl glycine $(CH_3)_3NCH_2COOH$ (that is described as betaine). An example of betaine surfactant is lauryl amido propyl dimethyl betaine $C_{12}H_{25}CON(CH_3)_2CH_2COOH$. These alkyl betaines are sometimes described as alkyl dimethyl glycinates

Nonionic

Alcohol ethoxylates, alkyl phenol ethoxylates, fatty acid ethoxylates, monoalkaolamide ethoxylates, sorbitan ester ethoxylates, fatty amine ethoxylates and ethylene oxide–propylene oxide copolymers (sometimes referred to as polymeric surfactants). Multihydroxy products such as glycol esters, glycerol (and polyglycerol) esters, glucosides (and polyglucosides), sucrose esters
Amine oxides and sulfinyl surfactants (nonionics with a small head group)

affected by other materials present, such as the surfactant and the inhomogeneity of the polymer composition at the surface. High-T_g polymers will not coalesce at room temperature, and in this case a plasticizer (''coalescing agent'') such as benzyl alcohol is incorporated into the formulation to reduce the T_g of the polymer and thus reduce the MFFT of the paint. Clearly, for any paint system it is important to determine the MFFT since, as mentioned above, the T_g of the polymer is greatly affected by the ingredients in the paint formulation.

Several types of surfactant can be used in emulsion polymerisation, and a summary of the various classes is provided in Table 17.1.

The role of the surfactants is two-fold: first, to provide a locus for the monomer to polymerise, and second, to stabilise the polymer particles as they are formed. In addition, surfactants aggregate to form micelles (above the cmc), and these can solubilise the monomers. In most cases a mixture of anionic and nonionic surfactant is used for the optimum preparation of polymer latexes. Cationic surfactants are seldom used, except for specific applications where a positive charge is required on the surface of the polymer particles.

In addition to surfactants, most latex preparations require the addition of a polymer (sometimes referred to as a ''protective colloid'') such as partially hydrolysed polyvinyl acetate (commercially referred to as polyvinyl alcohol; PVA), hydroxyethyl cellulose, or a block copolymer of polyethylene oxide (PEO) and polypropylene oxide (PPO). These polymers can be supplied with various molecular weights or proportions of PEO and PPO. When used in emulsion polymerisation they can be grafted by the growing chain of the polymer being formed; they not only help to control the particle size of the latex but also enhance the stability of the polymer dispersion and control the rheology of the final paint.

A typical emulsion polymerisation process involves two stages: the seed stage and the feed stage. In the feed stage, an aqueous charge of water, surfactant and colloid is raised to the reaction temperature (85–90 °C), at which point 5–10% of the monomer mixture is added along with a proportion of the initiator (a water-soluble persulphate). In the seed stage, the formulation contains monomer droplets stabilised by a surfactant, a small amount of monomer in solution, and also surfactant monomers and micelles. Radicals are formed in solution from the breakdown of the initiator, and these polymerise the small amount of monomer in solution. The oligomeric chains will grow to a critical size, the length of which depends on the solubility of the monomer in water. The oligomers build up to a limiting concentration, and this is followed by a precipitous formation of aggregates (seeds) – a process similar to micelle formation – except in this case the aggregation process is irreversible (unlike surfactant micelles, which are in dynamic equilibrium with monomers).

In the feed stage, the remaining monomer and initiator are fed together, and the monomer droplets become emulsified by the surfactant remaining in solution (or by the extra addition of surfactant). Polymerisation proceeds as the monomer diffuses from the droplets, through the water phase, into the already forming growing particles. At the same time, radicals enter the monomer-swollen particles causing both the termination and reinitiation of polymerisation. As the particles grow, the remaining surfactant from the water phase is adsorbed onto the surface of the polymer particles to aid in their stability. The stabilisation mechanism involves both electrostatic and steric repulsion. The final stage of polymerisation may include a further addition of initiator to complete the conversion.

17.2.1
Mechanism of Emulsion Polymerisation

According to the theory of Smith and Ewart [4] of the kinetics of emulsion polymerisation, the rate of propagation R_p is related to the number of particles N formed in a reaction by the equation,

$$-\frac{\mathrm{d}[M]}{\mathrm{d}t} = R_p \quad k_p \, N \, n_{av} \, [M] \tag{17.1}$$

where $[M]$ is the monomer concentration in the particles, k_p is the propagation rate constant, and n_{av} is the average number of radicals per particle.

According to Equation (17.1), the rate of polymerisation and the number of particles are directly related to each other; that is, an increase in the number of particles will increase the rate. This has been found for many polymerisations, although there are some exceptions. The number of particles is related to the surfactant concentration $[S]$ by the equation [5],

$$N \approx [S]^{3/5} \tag{17.2}$$

Using the coagulative nucleation model, Napper *et al.* [2, 3] found that the final particle number increases with increase in surfactant concentration with a monotonically diminishing exponent, with the slope of $d(\log N_c)/d(\log t)$ varying from 0.4 to 1.2. At a high surfactant concentration, the nucleation time will be long as the new precursor particles will be readily stabilised; as a result of this more latex particles will be formed and eventually these will outnumber the very small precursor particles in the long term. The precursor/particle collisions will then become more frequent and fewer latex particles will be produced. The dN_c/dt will approach zero and at long times the number of latex particles will remain constant. This shows the inadequacy of the Smith–Ewart theory, which predicts a constant exponent (3/5) at all surfactant concentrations, and for this reason the coagulative nucleation mechanism has now been accepted as the most probable theory for emulsion polymerisation. In all cases, the nature and concentration of surfactant used is crucial, and this is very important in the industrial preparation of latex systems.

Most reports on emulsion polymerisation have been limited to commercially available surfactants which, in many cases, are relatively simple molecules such as sodium dodecyl sulphate and simple nonionic surfactants. However, studies on the effects of surfactant structure on latex formation have revealed the importance of the structure of the molecule. Block and graft copolymers (polymeric surfactants) are expected to be better stabilisers when compared to simple surfactants. The use of these polymeric surfactants in emulsion polymerisation and the stabilisation of the resulting polymer particles is discussed below.

17.2.2
Block Copolymers as Stabilisers in Emulsion Polymerisation

Most aqueous emulsion and dispersion polymerisation that have been reported are based on a few commercial products with a broad molecular weight distribution and varying block composition. The results obtained from these studies could not establish the effect that the structural features of the block copolymer would have on their stabilising ability and effectiveness in polymerisation. Fortunately, model block copolymers with well-defined structures can be synthesised, and their roles in emulsion polymerisation have been determined using model polymers and model latexes.

A series of well-defined A-B block copolymers of polystyrene-block-polyethylene oxide (PS-PEO) were synthesised [6] and used for the emulsion polymerisation of styrene. These molecules are ‘‘ideal’’ as the polystyrene (PS) block is compatible with the PS formed, and thus it forms the best anchor chain. The PEO chain (the stabilising chain) is strongly hydrated with water molecules and extends into the aqueous phase where it forms the steric layer necessary for stabilisation.

However, the PEO chain can become dehydrated at high temperatures (due to breakage of hydrogen bonds), which reduces the effective steric stabilisation. Thus, emulsion polymerisation should be carried out at temperatures well below the theta (θ)-temperature of PEO.

Five block copolymers were synthesised [6] with various molecular weights of the PS and PEO blocks. The molecular weight of the PS block and the resulting PS-PEO polymer was determined using gel permeation chromatography. The mol% of ethylene oxide and the percentage of PEO in the block was determined using H^1 NMR spectroscopy. The molecular weight of the blocks varied from $M_n = 1000–7000$ for PS, and $M_w = 3000–9000$ for PEO. When these five block copolymers were used for the emulsion polymerisation of styrene at 50 °C (well below the θ-temperature of PEO), the results indicated that for efficient anchoring, the PS block need not be more than 10 monomer units, and the PEO block should have $M_w \geq 3000$. However, the ratio of the two blocks is very important; for example, if the wt% of PEO is ≤ 3000 the molecule will become insoluble in water (not sufficiently hydrophilic) and no polymerisation would occur when using this block copolymer. In addition, the 50% PEO block could produce a latex but the latter would be unstable and become coagulated at 35% conversion. It became clear from these studies that the % PEO in the block copolymer plays an important role, and this should exceed 75%. However, the overall molecular weight of the block copolymer is also very important; for example, if a PS block with $M_n = 7000$ is used, the PEO molecular weight must be 21 000, which is too high and may result in bridging flocculation, unless a very dilute latex is prepared.

Another systematic study of the effect of block copolymer on emulsion polymerisation was carried out using poly(methylmethacrylate)-block-polyethylene oxide (PMMA-PEO) to prepare PMMA latexes [6]. The ratio and molecular weight of PMMA to PEO in the block copolymer was varied. Ten different PMMA-PEO blocks were synthesised with M_n of PMMA varying between 400 and 2500, and the M_w of PEO varying between 750 and 5000 The recipe for MMA polymerisation consisted of 100 monomer units, 800 g water, 20 g PMMA-PEO block copolymer, and 0.5 g potassium persulphate. The polymerisation was carried out at 45 °C, well below the θ-temperature of PEO, and the rate of polymerisation (R_p) was calculated using latex samples drawn from the reaction mixture at various times (the amount of latex was determined gravimetrically). The particle size of each latex was determined using dynamic light scattering (photon correlation spectroscopy; PCS), and the number of particles (N) in each case was calculated from the weight of the latex and the z-average diameter. The results obtained were used to study the effect of the anchoring group PMMA, molecular weight, the effect of PEO molecular weight, and the effect of the total molecular weight of the block copolymer. The results are summarised in Tables 17.2 and 17.3.

The results showed clearly the effect of these factors on the resulting latex. For example, when using a block copolymer with M_w 400 PMMA and M_w 750 PEO (i.e., containing 65 wt% PEO), the resulting latex had fewer particles when compared to the other surfactants. The most dramatic effect was obtained when the M_w of PMMA was increased to 900 while keeping the of PEO unchanged (750). This block

Table 17.2 Effect of PMMA and PEO molecular weight in the diblock.

M_n PMMA	M_w PEO	Wt% PEO	$R_p \times 10^4$ (mol l^{-1} s^{-1})	D (nm)	$N \times 10^{-13}$ (cm^{-3})
400	750	65	1.3	213	1.7
400	2000	83	1.5	103	14.7
400	5000	93	2.4	116	10.3
900	750	46	**Unstable latex**	—	—
800	2000	71	3.4	92	20.6
800	5000	86	3.2	106	13.5
1300	2000	61	2.4	116	10.3
1200	5000	81	4.6	99	16.6
1900	5000	72	3.4	110	11.4
2500	5000	67	2.2	322	0.4

Table 17.3 Effect of total molecular weight of the PMMA-PEO diblock.

M_w	wt% PEO	$R_p \times 10^4$(mol l^{-1} s^{-1})	D (nm)	$N \times 10^{-13}$ (cm^{-3})
1150	65	1.3	213	1.7
2400	83	1.5	103	14.7
2800	71	3.4	92	20.6
3300	61	2.4	99	16.6
6200	81	4.6	99	16.6
6900	72	3.4	110	11.4
7500	67	2.2	322	0.4

copolymer contained only 46 wt% PEO, and became insoluble in water due to a lack of hydrophilicity. The latex produced was unstable and collapsed at the early stage of polymerisation. The PEO of M_w 750 was insufficient to provide effective steric stabilisation; however, by increasing the M_w of PEO to 2000 or 5000, and keeping the M_w of PMMA at 400 or 800, a stable latex was produced with a small particle diameter and a large number of particles. The best results were obtained by keeping the M_w of PMMA at 800, and that of PEO at 2000. This block copolymer gave the highest conversion rate, the smallest particle diameter, and the largest number of particles (see Table 17.3). It is interesting to note that, by increasing the PEO M_w to 5000 and keeping that of PMMA at 800, the rate of conversion was decreased, the average diameter was increased, and the number of particles was decreased when compared to results obtained using M_w of 2000 for PEO. It seemed that, when the M_w of PEO is increased, the hydrophilicity of the molecule was increased (86 wt% PEO), and this reduced the efficiency of the copolymer. It also seemed that, by increasing the hydrophilicity of the block copolymer and its overall molecular weight, the rate of adsorption of the polymer to the latex particles and its overall adsorption strength may have been decreased. The effect of the overall molecular weight of the block copolymer and its overall hydrophilicity have major effects on latex production (see Table 17.3). An increase in the overall molecular weight of the block copolymer above 6200 resulted in a reduction in the rate of conversion, an increase in the particle diameter, and a reduction in the number of latex particles. The worst results were obtained with an overall molecular weight of 7500 while reducing the PEO wt%; in this case particles of 322 nm diameter were obtained and the number of latex particles was significantly reduced.

The importance of the affinity of the anchor chain (PMMA) to the latex particles was investigated by using different monomers [6]. For example, when using styrene as the monomer the resulting latex was unstable and showed the presence of coagulum. This was attributed to a lack of chemical compatibility of the anchor chain (PMMA) and the polymer to be stabilised, namely PS. The results clearly indicated that block copolymers of PMMA-PEO are unsuitable for the emulsion polymerisation of styrene, but when using vinyl acetate monomer – whereby the resulting poly(vinyl acetate) latex should have strong affinity to the PMMA anchor – no latex was produced when the reaction was carried out at 45 °C. It was speculated that the water solubility of the vinyl acetate monomer would result in the formation of oligomeric chain radicals that could exist in solution without nucleation. Polymerisation at 60 °C, at which particles were nucleated, was found to be controlled by chain transfer of the vinyl acetate radical with the surfactant, resulting in broad molecular weight distributions.

The emulsion polymerisation of MMA using triblock copolymers was carried out using PMMA-block-PEO-PMMA with the same M_w of PMMA (800 or 900) while varying the M_w of PEO from 3400 to 14 000 in order to vary the loop size. Although the rate of polymerisation was unaffected by the loop size, the particles with the smallest diameter were obtained with PEO of M_w 10 000. A comparison of the results obtained using the triblock copolymer with those obtained using diblock copolymer (while keeping the PMMA block M_w unchanged) showed the same rate of polymerisation, but the average particle diameter was smaller and the total number of particles larger when using the diblock copolymer. This clearly showed the higher efficacy of the diblock copolymer when compared to the triblock copolymer.

17.2.3
Graft Copolymers as Stabilisers in Emulsion Polymerisation

The first systematic studies of the effect of graft copolymers were carried out by Piirma and Lenzotti [7], who synthesised well-characterised graft copolymers with different backbone and side-chain lengths. Several grafts of poly(*p*-methylstyrene)-graft-polyethylene oxide ((PMSt)-$(PEO)_n$) were synthesised and used in styrene emulsion polymerisation. Three different PMSt chain lengths (with M_w 750, 2000 and 5000) and three different PEO chain lengths were prepared. In this way, the structure of the amphipathic graft copolymer could be changed in three different ways: (i) three different PEO graft chain lengths; (ii) three different backbone chain lengths with the same wt% PEO; and (iii) four different wt% PEO grafts.

Piirma and Lenzotti [7] investigated the graft copolymer concentration required to produce the highest conversion rate, the smallest particle size and the largest number of latex particles. In this case, the monomer-to-water ratio was kept at 0.15 to avoid overcrowding of the resulting particles, and a concentration of 18 g/100 g monomer (2.7% aqueous phase) was found necessary to obtain the above results. Subsequently, further increases in graft copolymer concentration failed to cause any significant increase in the rate of polymerisation, or increase in the number of particles used. When using a graft copolymer concentration of 2.7% aqueous phase, the results showed an increase in the number of particles with an increase in conversion, reaching a steady value of about 35%. Clearly, before conversion the new particles are still stabilised by the oligomeric precursor particles, but after this all precursor particles are assimilated by the existing particles. The small size of the latex produced, namely 30–40 nm, clearly indicated the efficiency with which this graft copolymer would stabilise the dispersion.

When three different backbone chain lengths of M_n 1140, 4270 and 24 000 were used, while keeping the same wt% of PEO (82%; i.e., equivalent to 3, 10 and 55 PEO chains per backbone, respectively, the results showed the rate of polymerisation, particle diameter and number of particles to be similar for all three cases. Moreover, as the graft copolymer concentration was the same in each case, it could be concluded that one molecule of the highest molecular graft would be as effective as 18 molecules of the lowest molecular weight graft in stabilising the particles.

Four graft copolymers were synthesised with a PMSt backbone with M_w 4540, while increasing the wt% of PEO (68, 73, 82 and 92 wt%, corresponding to 4.8, 6, 10 and 36 grafts per chain). The results showed a sharp decrease (by more than one order of magnitude) in the number of particles as the wt% of PEO was increased from 82% to 94%. The reason for this reduction in particle number was the increased hydrophilicity of the graft copolymer, which could result in desorption of the molecule from the surface of the particle. In addition, a graft with 36 side chains did not leave sufficient space for anchoring by the backbone.

The effect of PEO side chain length on emulsion polymerisation using graft copolymers was studied systematically by maintaining the backbone M_w at 1380 while gradually increasing the M_w of the PEO side chains from 750 to 5000. For example, by increasing the M_w of PEO from 750 to 2000 while keeping the wt% of PEO roughly the same (84% and 82 wt%, respectively) the number of side chains in the graft was decreased from 10 to three. The results also showed a decrease in the rate of polymerisation as the number of side chains in the graft was increased, and this was followed by a sharp reduction in the number of particles produced. These results highlighted the importance of spacing of the side chains to ensure anchoring of the graft copolymer to the particle surface, which is stronger when the graft contains a smaller number of side chains. If the number of side chains for PEO with M_w 2000 was increased from three to nine (93 wt% PEO), the rate of polymerisation and number of particles were each decreased. The use of a PEO chain with M_w 5000 (92 wt% PEO) and three chains per graft gave the same result as the PEO 2000 with three side chains. Any increase in the number of side chains in the graft would result in a reduction in the rate of polymerisation and the number of latex particles produced. This clearly shows the importance of spacing of the side chains of the graft copolymer.

Similar results were obtained using a graft copolymer of poly(methyl methacrylate-*co*-2-hydroxypropyl methacrylate)-graft-polyethylene oxide, PMMA $(PEO)_n$, for the emulsion polymerisation of MMA. As with the PMSt$(PEO)_n$ graft, the backbone molecular weight had little effect on the rate of polymerisation or the number of particles used. The molecular weight of the PEO side chains was varied at constant M_w of the backbone (10 000), and three PEO grafts with M_w of 750, 2000 and 5000 were used. Although the rate of polymerisation was similar for the three graft copolymers, the number of particles was significantly lower with the graft containing PEO 750. These findings indicated that a short PEO chain is insufficient for stabilisation of the particles. The overall content of PEO in the graft also has a major effect. When using the same backbone chain length but changing the wt% of PEO 200, the molecule containing 67 wt% PEO was found to be insufficient for stabilising the particles when compared to a graft containing 82 wt% PEO. These data confirmed that a high concentration of PEO in the adsorbed layer is required for effective steric stabilisation.

The chemical nature of the monomer also plays an important role. For example, stable latexes could be produced using a PMSt$(PEO)_n$ graft but not with a PMMA$(PEO)_n$ graft.

A novel graft copolymer of hydrophobically modified inulin (INUTEC® SP1) has been used in the emulsion polymerisation of styrene, MMA, butyl acrylate, and several other monomers [8]. All lattices were prepared by emulsion polymerisation, using potassium persulphate as initiator, and the *z*-average particle size was determined using PCS; electron micrographs were also recorded.

The emulsion polymerisation of styrene or MMA showed an optimum weight ratio of (INUTEC®)/monomer of 0.0033 for PS particles, and 0.001 for PMMA particles. The (initiator)/(monomer) ratio was kept constant at 0.00125, and the monomer conversion was higher than 85% in all cases. Latex dispersions of PS reaching 50% and of PMMA reaching 40% could be obtained using such low concentrations of INUTEC® SP1. Figure 17.1 shows the variation of particle diameter with monomer concentration.

The stability of the latexes was determined by determining the critical coagulation concentration (ccc) using $CaCl_2$. Although the CCC was low (0.0175–0.05 mol dm^{-3}), it was higher than that for the latex prepared without surfactant. The subsequent addition of INUTEC SP1® resulted in a large increase in the CCC, as illustrated in Figure 17.2, which shows log W–log C curves (where W is the ratio between the fast flocculation rate constant to the slow flocculation rate constant, referred to as the stability ratio) at various additions of INUTEC SP1®.

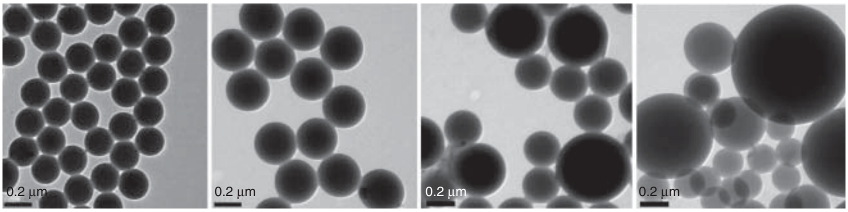

(5 wt%) (10 wt%) (30 wt%) (40 wt%)

(a) PS latexes

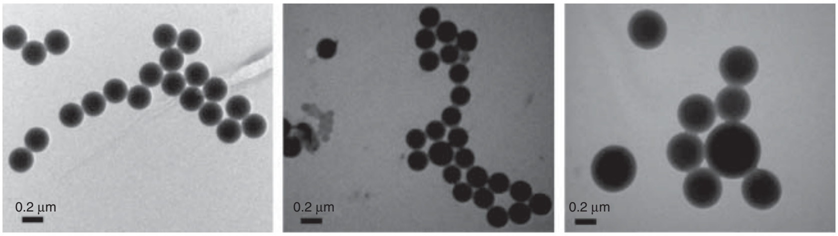

(10 wt%) (20 wt%) (30 wt%)

(b) PMMA latexes

Figure 17.1 (a,b) Electron micrographs of the latexes.

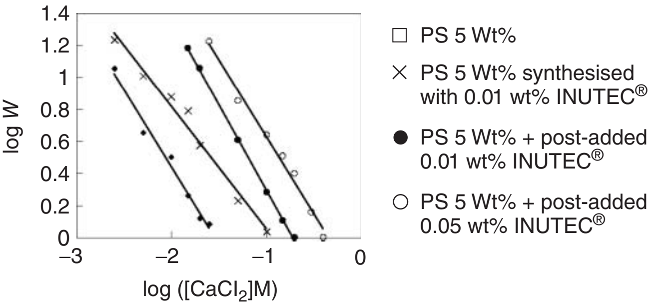

Figure 17.2 Influence of post addition of INUTEC SP1® on latex stability.

As with the emulsions, the high stability of the latex when using INUTEC SP1 is due to the strong adsorption of the polymeric surfactant on the latex particles, and the formation of strongly hydrated loops and tails of polyfructose that provide effective steric stabilisation. Evidence for the strong repulsion produced when using INUTEC SP1® was obtained from atomic force microscopy investigations [9], whereby the force between hydrophobic glass spheres and hydrophobic glass plate, both containing an adsorbed layer of INUTEC SP1®, was measured as a function of the distance of separation, both in water and in the presence of various Na_2SO_4 concentrations. The results are shown in Figures 17.3 and 17.4.

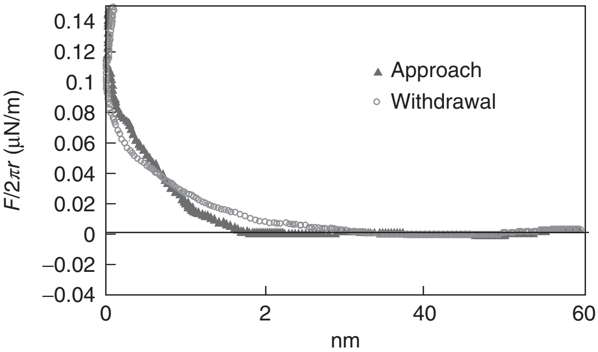

Figure 17.3 Force–distance curves between hydrophobised glass surfaces containing adsorbed INUTEC SP1® in water.

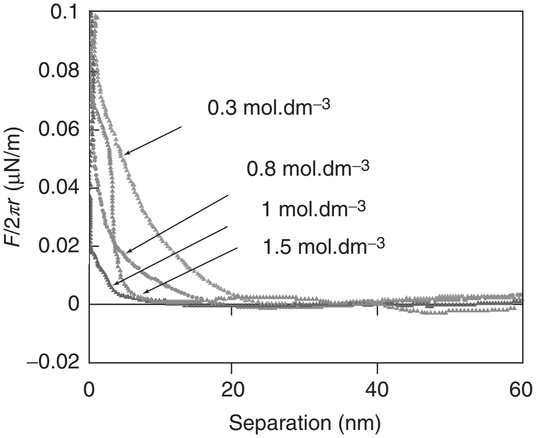

Figure 17.4 Force–distance curves for hydrophobised glass surfaces containing adsorbed INUTEC SP1® at various Na_2SO_4 concentrations.

17.3
Polymeric Surfactants for Stabilisation of Preformed Latex Dispersions

For this purpose, PS latexes were prepared using surfactant-free emulsion polymerisation. Two latexes with *z*-average diameters of 427 and 867 (as measured using PCS) that are reasonably monodisperse were prepared [10]. Two polymeric surfactants, namely Hypermer CG-6 and Atlox 4913 (UNIQEMA, UK) were used; both of these are graft (“comb”) types consisting of a poly(methylmethacrylate)/poly(methacrylic acid) (PMMA/PMA) backbone with methoxy-capped PEO side chains ($M_w = 750$ Da). Hypermer CG-6 is the same graft copolymer as Atlox 4913, but contains a higher proportion of methacrylic acid in the backbone. The average molecular weight of the polymer was ~5000 Da. Figure 17.5 shows a typical adsorption isotherm of Atlox 4913 on the two latexes. Similar

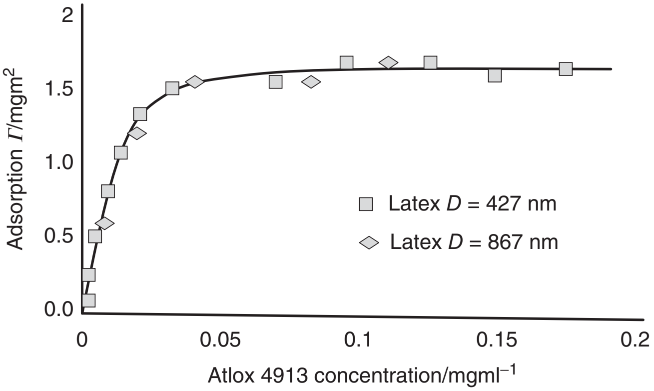

Figure 17.5 Adsorption isotherms of Atlox 4913 on the two latexes at 25 °C.

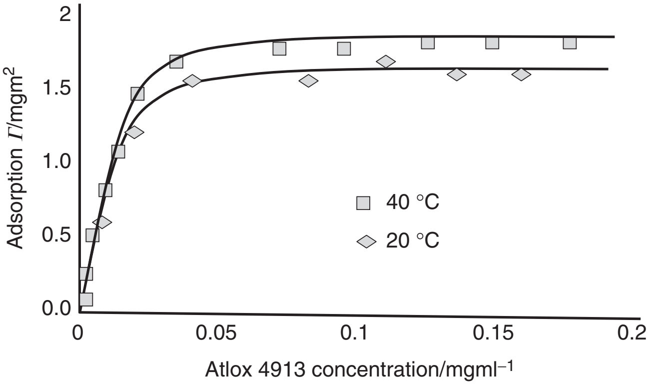

Figure 17.6 Effect of temperature on the adsorption of Atlox 4913 on PS.

results were obtained for Hypermer CG-6, but the plateau adsorption was lower (1.2 mg m^{-2} compared to 1.5 mg m^{-2} for Atlox 4913). It is likely that the backbone of Hypermer CG-6, which contains more PMMA, is more polar and hence less strongly adsorbed. The amount of adsorption was independent of particle size.

The influence of temperature on adsorption is shown in Figure 17.6. The amount of adsorption was shown to increase with increase of temperature, due to the poorer solvency of the medium for the PEO chains. The PEO chains become less hydrated at higher temperatures, and the reduction in solubility of the polymer enhances adsorption.

The adsorbed layer thickness of the graft copolymer on the latexes was determined using rheological measurements. Steady-state (shear stress σ-γ shear rate) measurements were carried out and the results were fitted to the Bingham equation to obtain the yield value σ_β and the high shear viscosity η of the suspension,

$$\sigma = \sigma_\beta + \eta\dot{\gamma} \tag{17.1}$$

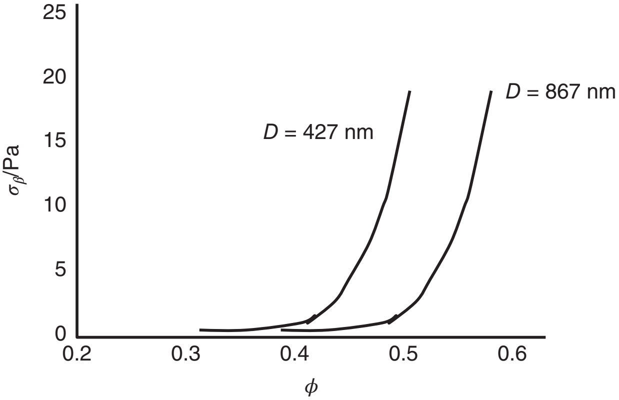

Figure 17.7 Variation of yield stress with latex volume fraction for Atlox 4913.

As an illustration, Figure 17.7 shows a plot of σ_β versus the volume fraction ϕ of the latex for Atlox 4913. Similar results were obtained for latexes stabilised using Hypermer CG-6.

At any given volume fraction, the smaller latex has a higher σ_β when compared to the larger latex. This is due to the higher ratio of adsorbed layer thickness to particle radius, Δ/R, for the smaller latex. The effective volume fraction of the latex ϕ_{eff} is related to the core volume fraction ϕ by the equation,

$$\varphi_{\text{eff}} = \varphi\left[1 + \frac{\Delta}{R}\right]^3 \tag{17.4}$$

As discussed before, ϕ_{eff} can be calculated from the relative viscosity η_r using the Dougherty–Krieger equation,

$$\eta_r = \left[1 - \left(\frac{\varphi_{\text{eff}}}{\varphi_p}\right)\right]^{-[\eta]\varphi_p} \tag{17.5}$$

where ϕ_p is the maximum packing fraction, which can be calculated using the following empirical equation [10]:

$$\frac{(\eta_r^{1/2} - 1)}{\varphi} = \left(\frac{1}{\varphi_p}\right)(\eta^{1/2} - 1) + 1.25 \tag{17.6}$$

The results showed a gradual decrease in the adsorbed layer thickness Δ with increase of the volume fraction ϕ. For the latex with diameter D of 867 nm and Atlox 4913, Δ was decreased from 17.5 nm at $\phi = 0.36$ to 6.5 at $\phi = 0.57$. For Hypermer CG-6 with the same latex, Δ was decreased from 11.8 nm at $\phi = 0.49$ to 6.5 at $\phi = 0.57$. The reduction in Δ with increase in ϕ may be due to overlap and/or compression of the adsorbed layers as the particles come close to each other at higher volume fraction of the latex.

The stability of the latexes was determined using viscoelastic measurements. For this purpose, dynamic (oscillatory) measurements were used to obtain the storage

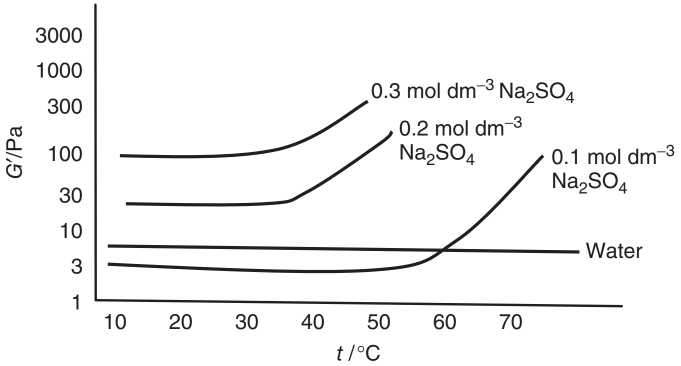

Figure 17.8 Variation of G' with temperature in water and at various Na_2SO_4 concentrations.

modulus G^*, the elastic modulus G' and the viscous modulus G'' as a function of strain amplitude γ_o and frequency ω (rad s^{-1}). The method relies on the application of a sinusoidal strain or stress, and the resulting stress or strain is measured simultaneously. For a viscoelastic system the strain and stress sine waves oscillate with the same frequency, but out of phase. From the time shift Δt and ω, the phase angle shift δ can be obtained.

The ratio of the maximum stress σ_o to the maximum strain γ_o gives the complex modulus $|G^*|$

$$|G^*| = \frac{\sigma_o}{\gamma_o} \tag{17.7}$$

$|G^*|$ can be resolved into two components: (i) the storage (elastic) modulus G', which is the real component of the complex modulus; and (ii) the loss (viscous) modulus G'', which is the imaginary component of the complex modulus. The complex modulus can be resolved into G' and G'' using vector analysis and the phase angle shift δ,

$$G' = |G^*| \cos \delta \tag{17.8}$$

$$G'' = |G^*| \sin \delta \tag{17.9}$$

where G' is measured as a function of electrolyte concentration and/or temperature to assess the latex stability. As an illustration, Figure 17.8 shows the variation of G' with temperature for latex stabilised with Atlox 4913 in the absence of any added electrolyte and in the presence of 0.1, 0.2 and 0.3 mol dm^{-3} Na_2SO_4. In the absence of electrolyte, G' showed no change with temperature up to 65 °C.

In the presence of 0.1 mol dm^{-3} Na_2SO_4, G' remained constant up to 40 °C, above which it was increased with further increases in temperature; this temperature is denoted as the critical flocculation temperature (CFT). The CFT decreases with increases in electrolyte concentration, reaching ~30 °C in 0.2 and 0.3 mol dm^{-3} Na_2SO_4. The reduction in CFT with increases in electrolyte concentration was due to the reduction in solvency of the PEO chains with increase in electrolyte concentrations. The latex stabilised with Hypermer CG-6 gave relatively higher CFT values when compared to that stabilised with Atlox 4913.

17.4
Dispersion Polymerisation

This method is usually applied for the preparation of nonaqueous latex dispersions, and hence is referred to as NAD [5]. The method has also been adapted to prepare aqueous latex dispersions by using an alcohol–water mixture.

In the NAD process, the monomer (normally an acrylic) is dissolved in a nonaqueous solvent (normally an aliphatic hydrocarbon), and an oil-soluble initiator and a stabiliser (to protect the resulting particles from flocculation, sometimes referred to as a ''protective colloid'') is added to the reaction mixture. The most successful stabilisers used in NAD are block and graft copolymers, which are assembled in a variety of ways to provide the molecule with an ''anchor'' chain and a ''stabilising'' chain. The anchor chain should be sufficiently insoluble in the medium and have a strong affinity to the polymer particles produced. In contrast, the stabilising chain should be soluble in the medium and be strongly solvated by its molecules to provide an effective steric stabilisation. The length of the anchor and stabilising chains must be carefully adjusted to ensure a strong adsorption (by multipoint attachment of the anchor chain to the particle surface) and a sufficiently ''thick'' layer of the stabilising chain to prevent close approach of the particles to a distance where the van der Waals attractions become strong. Several configurations of block and graft copolymers are possible, as illustrated in Figure 17.9.

Typical preformed graft stabilisers based on poly(12-hydroxy stearic acid) (PHS) are simple to prepare and effective in NAD polymerisation. Commercial

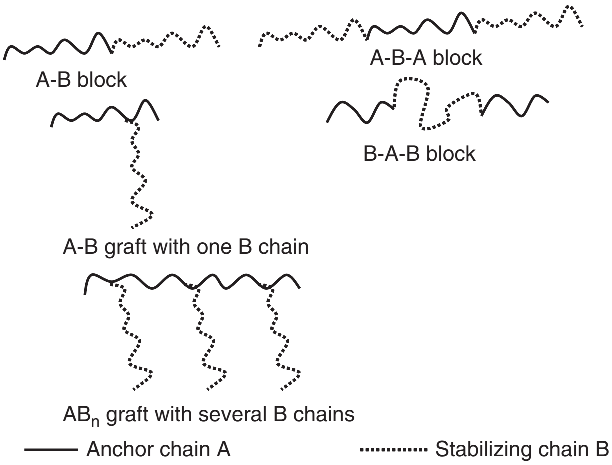

Figure 17.9 Configurations of block and graft copolymers.

Table 17.4 Block and graft copolymers for dispersion polymerisation.

Polymeric surfactant	Continuous phase	Disperse polymer
Polystyrene-block-poly(dimethyl siloxane	Hexane	Polystyrene
Polystyrene-block-poly(methacrylic acid)	Ethanol	Polystyrene
Polybutadiene-graft-poly(methacrylic acid)	Ethanol	Polystyrene
Poly(2-ethylhexyl acrylate)-graft-poly(vinyl acetate)	Aliphatic hydrocarbon	Poly(methyl methacrylate)
Polystyrene-block-poly(*t*-butylstyrene)	Aliphatic hydrocarbon	Polystyrene

12-hydroxystearic acid contains 8–15% palmitic and stearic acids, which limits the molecular weight during polymerisation to an average of 1500–2000. This oligomer may be converted to a "macromonomer" by reacting the carboxylic group with glycidyl methacrylate; the macromonomer is then copolymerised with an equal weight of MMA or similar monomer to produce a "comb" graft copolymer with an average molecular weight of 10 000–20 000. The graft copolymer contains on average 5–10 PHS chains pendent from a polymeric anchor backbone of PMMA; such a graft copolymer can stabilise latex particles of various monomers. The major limitation of the monomer composition is that the polymer produced should be insoluble in the medium used.

Several other examples of block and graft copolymers that are used in dispersion polymerisation are listed in Table 17.4, which also provides details of the continuous phase and disperse polymers that can be used with these polymers.

Two main criteria must be considered in the process of dispersion polymerisation: (i) the insolubility of the formed polymer in the continuous phase; and (ii) the solubility of the monomer and initiator in the continuous phase. Dispersion polymerisation starts as a homogeneous system, but after sufficient polymerisation the insolubility of the resulting polymer in the medium forces them to precipitate. Initially, polymer nuclei are produced which then grow to polymer particles. The latter are stabilised against aggregation by the block or graft copolymer that is added to the continuous phase before the process of polymerisation starts. It is essential to choose the correct block or graft copolymer, which should have a strong anchor chain A and good stabilising chain B, as depicted schematically in Figure 17.9.

Dispersion polymerisation may be considered a heterogeneous process which may include emulsion, suspension, precipitation and dispersion polymerisation. In dispersion and precipitation polymerisation, the initiator must be soluble in the continuous phase, whereas in emulsion and suspension polymerisation the initiator is chosen to be soluble in the disperse phase of the monomer. A comparison of the rates of polymerisation of MMA at 80 °C for the three systems was given by Barrett and Thomas [11], as illustrated in Figure 17.10. The rate of dispersion polymerisation is much faster than either precipitation or solution polymerisation. The enhancement of the rate in precipitation polymerisation over

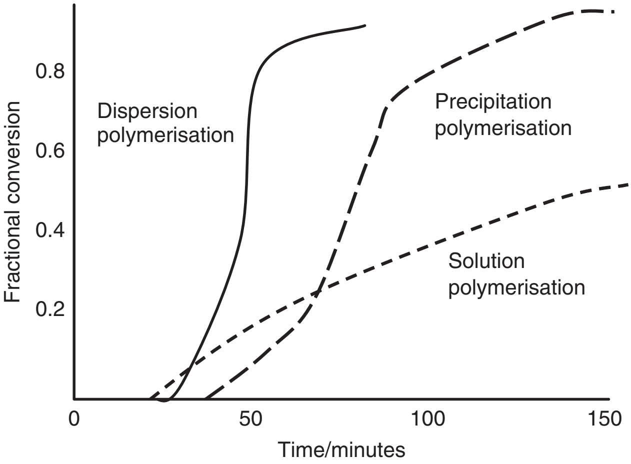

Figure 17.10 Comparison of rates of polymerisation.

solution polymerisation has been attributed to the hindered termination of the growing polymer radicals.

17.4.1
Mechanism of Dispersion Polymerisation

Several mechanisms have been proposed to explain the mechanism of emulsion polymerisation, but no single mechanism can explain all of the happenings. Barrett and Thomas [11] suggested that particles are formed in emulsion polymerisation by two main steps:

- Initiation of the monomer in the continuous phase and subsequent growth of the polymer chains until the latter become insoluble. This process clearly depends on the nature of the polymer and medium.
- The growing oligomeric chains associate with each other, forming aggregates which below a certain size are unstable and become stabilised by the block or graft copolymer added. As mentioned above, this aggregative nucleation theory cannot explain all of the happenings in dispersion polymerisation.

An alternative mechanism based on Napper's theory [4, 5] for aqueous emulsion polymerisation can be adapted to the process of dispersion polymerisation. This theory includes coagulation of the nuclei formed, and not just an association of the oligomeric species. The precursor particles (nuclei), in being unstable, can undergo one of the following events to become colloidally stable: (i) homocoagulation, that is collision with other precursor particles; (ii) growth by propagation, adsorption of stabiliser; and (iii) swelling with monomer. The nucleation-terminating events are the diffusional capture of oligomers and heterocoagulation.

The number of particles formed in the final latex does not depend on particle nucleation alone, as other steps are involved which determine how many of the precursor particles created are involved in the formation of a colloidally stable particle. This clearly depends on the effectiveness of the block or graft copolymer used in stabilising the particles (see below).

17.4.2
Influence of Polymeric Surfactant Concentration and Molecular Weight on Particle Formation

In most cases, an increase in polymeric surfactant concentration (at any given monomer amount) will result in the production of larger numbers of particles with smaller sizes. This is to be expected as the larger number of particles with smaller sizes (i.e., a larger total surface area of the disperse particles) require more polymeric surfactant for their formation. The molecular weight of the polymeric surfactant can also influence the number of particles formed. For example, Dawkins and Taylor [12] found that in the dispersion polymerisation of styrene in hexane, increasing the molecular weight of the block copolymer of polydimethyl siloxane-block-PS resulted in the formation of smaller particles that was attributed to a more effective steric stabilisation by the higher-molecular-weight block.

17.4.3
Effect of Monomer Solubility and Concentration in the Continuous Phase

A systematic study of the effect of monomer solubility and concentration in the continuous phase was carried out by Antl and coworkers [13]. The dispersion polymerisation of MMA in hexane mixed with a high-boiling-point aliphatic hydrocarbon was investigated using a poly(12-hydoxystyearic acid)-glycidyl methacrylate block copolymer. The MMA concentration was found to have a drastic effect on the size of the particles produced; when the monomer concentration was kept below 8.5% very small particles (80 nm) were produced and these remained very stable. However, between 8.5% and 35% monomer, the latex produced was initially stable but flocculated during polymerisation. An increase in monomer concentration from 35% to 50% resulted in the formation of a stable latex, but the particle size was increased sharply from 180 nm to 2.6 μm as the monomer concentration was increased. The authors suggested that the final particle size and stability of the latex was strongly affected by the increased monomer concentration in the continuous phase. The presence of monomer in the continuous phase increases the solvency of the medium for the polymer formed. In a good solvent for the polymer, the growing chain would be capable of reaching a higher molecular weight before being forced to phase-separate and precipitate.

NAD polymerisation is carried out in two steps:

- The seed stage, in which the diluent, a portion of the monomer, a portion of dispersant and the initiator (azo or peroxy type) are heated to form an initial low-concentration fine dispersion.
- The growth stage, in which the remaining monomer, together with more dispersant and initiator, are fed over the course of several hours to complete the

growth of the particles. A small amount of transfer agent is usually added to control the molecular weight.

An excellent control of particle size can be achieved by the correct choice of designed dispersant and correct distribution of dispersant between the seed and growth stages. NAD acrylic polymers are applied in automotive thermosetting polymers, and hydroxy monomers may be included in the monomer blend used.

17.4.4
Stability/Instability of the Resulting Latex

Two main factors must be considered when considering the long-term stability of a nonaqueous polymer dispersion. The first, very important, factor is the nature of the ''anchor chain'' A. As mentioned above, this should have a strong affinity to the produced latex and in most cases it can be designed to be ''chemically'' attached to the polymer surface. Once this criterion is satisfied, the second and important factor in determining the stability is the solvency of the medium for the stabilising chain B. As will be discussed in detail, the solvency of the medium is characterised by the Flory–Huggins interaction parameter χ. Three main conditions can be identified: $\chi < 0.5$ (good solvent for the stabilising chain); $\chi > 0.5$ (poor solvent for the stabilising chain); and $\chi = 0.5$ (referred to as the θ-solvent). Clearly, to maintain stability of the latex dispersion the solvent must be better than a θ-solvent. The solvency of the medium for the B chain is affected by addition of a nonsolvent and/or temperature changes. It is, therefore, essential to determine the critical volume fraction (CVF) of a nonsolvent above which flocculation (sometimes referred to as incipient flocculation) occurs. The CFT should also be determined at any given solvent composition, below which flocculation occurs. The correlation between CVF or CFT and flocculation of the nonaqueous polymer dispersion has been demonstrated by Napper [14], who investigated the flocculation of PMMA dispersions stabilised by PHS or poly(*n*-lauryl methacrylate-*co*-glycidyl methacrylate) in hexane by adding a nonsolvent such as ethanol or propanol and cooling the dispersion. The dispersions remained stable until the addition of ethanol transformed the medium to a θ-solvent for the stabilising chains in solution. However, flocculation did occur under conditions of slightly better than θ-solvent for the chains. The same was found for the CFT which was 5–15 K above the θ-temperature. This difference was accounted for by the polydispersity of the polymer chains. The θ-condition is usually determined by cloud point measurements, and the least-soluble component will precipitate first giving values that are lower than the CVF or higher than the CFT.

17.4.5
Particle Formation in Polar Media

The process of dispersion polymerisation has been applied in many cases using completely polar solvents such as alcohol or alcohol–water mixtures [15]. The results obtained showed completely different behaviours when compared with dispersion polymerisation in nonpolar media. For example, results obtained by Lok and Ober [15] using styrene as monomer and hydroxypropyl cellulose as stabiliser showed a linear increase in particle diameter with increase in the wt% of the monomer. There was no region in monomer concentration where instability occurred (as has been observed for the dispersion polymerisation of MMA in aliphatic hydrocarbons). By replacing water in the continuous phase with 2-methoxyethanol, Lok and Ober were able to grow large, monodisperse particles up to 15 μm in diameter. It was concluded from these results that the polarity of the medium is the controlling factor in the formation of particles and their final size. The authors suggested a mechanism by which the polymeric surfactant molecule would graft to the PS chain, forming a physically anchored stabiliser (nuclei); these nuclei would then grow to form the polymer particles. Paine [16] carried out a dispersion polymerisation of styrene by systematically increasing the alcohol chain length from methanol to octadecanol, and using hydroxypropyl cellulose as stabiliser. In this case, the results showed an increase in particle diameter with increase in number of carbon atoms in the alcohol, reaching a maximum when hexanol was used as the medium, after which there was a sharp decrease in particle diameter with further increase in the number of carbon atoms in the alcohol. Paine explained his results in terms of the solubility parameter of the dispersion medium. The largest particles were produced when the solubility parameter of the medium was closest to those of styrene and hydroxypropyl cellulose.

References

1. Blakely, D.C. (1975) *Emulsion Polymerization*, Elsevier, Applied Science, London.
2. Litchi, G., Gilbert, R.G., and Napper, D.H. (1983) *J. Polym. Sci.*, **21**, 269.
3. Feeney, P.J., Napper, D.H., and Gilbert, R.G. (1984) *Macromolecules*, **17**, 2520**20**, 2922 (1987).
4. Smith, W.V. and Ewart, R.H. (1948) *J. Chem. Phys.*, **16**, 592.
5. Barrett, K.E.J. (ed.) (1975) *Dispersion Polymerization in Organic Media*, John Wiley & Sons, Ltd, Chichester.
6. Piirma, I. (1992) *Polymeric Surfactants*, Marcel Dekker, New York.
7. Piirma, I. and Lenzotti, J.R. (1959) *Br. Polym. J.*, **21**, 45.
8. Nestor, J., Esquena, J., Solans, C., Levecke, B., Booten, K., and Tadros, Th.F. (2005) *Langmuir*, **21**, 4837.
9. Nestor, J., Esquena, J., Solans, C., Luckham, P.F., Levecke, B., and Tadros, Th.F. (2007) *J. Colloid Interface Sci.*, **311**, 430.
10. Liang, W., Bognolo, G., and Tadros, Th.F. (1995) *Langmuir*, **11**, 2899.
11. Barrett, K.E.J. and Thomas, H.R. (1969) *J. Polym. Sci., Part A*, **7**, 2627.
12. Dawkins, J.V. and Taylor, G. (1987) *Polymer*, **20**, 171.
13. Antl, I., Goodwin, J.W., Hill, R.D., Ottewill, R.H., Owen, S.M., Papworth, S., and Waters, J.A. (1986) *Colloids Surf.*, **1**, 67.
14. Napper, D.H. (1983) *Polymeric Stabilisation of Colloidal Dispersions*, Academic Press, London.
15. Lok, K.P. and Ober, C.K. (1985) *Can. J. Chem.*, **63**, 209.
16. Paine, A.J. (1990) *J. Polym. Sci., Part A*, **28**, 2485.

18
Formulation of Pigment and Ink Dispersions

18.1
Introduction

Pigment dispersions find many applications, of which paints, inks and colour cosmetics can be mentioned. The primary pigment particles (normally in the submicron range) are responsible for the opacity, colour and anticorrosive properties. The principal pigment used in paints is titanium dioxide, due to its high refractive index (RI), and this is used to produce white paint in particular. In order to produce maximum scattering, the particle size distribution of titanium dioxide must be controlled within a narrow limit. Rutile with a RI of 2.76 is preferred over anatase, that has a lower RI of 2.55; thus, rutile provides the possibility of a higher opacity than anatase and it is also more resistant to chalking on exterior exposure. To obtain maximum opacity, the particle size of rutile should be within 220–140 nm. Although the surface of rutile is photoactive, its surface can be coated with silica and alumina in various proportions to reduce its photoactivity.

Coloured pigments that are used in paints and inks may consist of inorganic or organic particles. For a black pigment, carbon black, copper carbonate, manganese dioxide (inorganic) or aniline black (organic) can be used, whereas for yellow it is possible to use lead, zinc, chromates, cadmium sulphide, iron oxides (inorganic) or nickel azo yellow (organic). For blue/violet pigments, ultramarine, Prussian blue, cobalt blue (inorganic) or phthalocyanin, indanthrone blue, or carbazol violet (organic) can be used, and for red pigments red iron oxide, cadmium selenide, red lead, chrome red (inorganic) or toluidine red, and quinacridones (organic) can be used.

The colour of a pigment is determined by the selective absorption and reflection of the various wavelengths of visible light (400–700 nm) which impinge on it. For example, a blue pigment appears so because it reflects the blue wavelengths in the incident white light and absorbs the other wavelengths. Black pigments absorb all the wavelengths of incident light almost totally, whereas a white pigment reflects all visible wavelengths.

The primary shape of a pigmented particle is determined by its chemical nature, its crystalline structure (or lack of it), and the way in which the pigment is created in nature or made synthetically. Pigments as primary particles may be

Formulation of Disperse Systems: Science and Technology, First Edition. Tharwat F. Tadros.

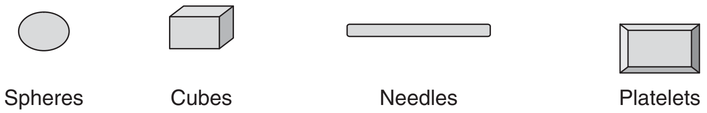

Figure 18.1 Schematic representation of particle shape.

spherical, nodular, needle or rod-like, plate like (lamellar); examples are illustrated in Figure 18.1.

The pigments are usually supplied in the form of aggregates (where the particles are attached at their faces) or agglomerates (where the particles are attached at their corners). When dispersed in the continuous phase, these aggregates and agglomerates must be dispersed into single units, and this requires the use of an effective wetter/dispersant as well as the application of mechanical energy. As this process of dispersion was discussed in Chapter 9, only a brief summary of the process will be given at this point, with particular reference to the measurement of powder wetting, the role of surfactants, and the dynamic processes of adsorption and wetting.

In paint formulations, secondary pigments are also used; these are referred to as extenders, fillers and supplementary pigments. Typically, they are relatively cheaper than the primary pigments and are incorporated in conjunction with the primary pigments for a variety of reasons such as cost-effectiveness, enhancement of adhesion, reduction of water permeability, and enhancement of corrosion resistance. For example, in a primer or undercoat (matt latex paint), coarse particle extenders such as calcium carbonate are added in conjunction with TiO_2 to achieve whiteness and opacity in a matt or semi-matt product. The particle size of extenders ranges from submicron to few tens of microns. Their RI is very close to that of the binder, and hence they do not contribute to the opacity from light scattering. Most extenders used in the paint industry are naturally occurring materials such as barytes (barium sulphate), chalk (calcium carbonate), gypsum (calcium sulphate) and silicates (silica, clay, talc or mica). However, more recently synthetic polymeric extenders have been designed to replace some of the TiO_2. A good example is spindrift, which consists of polymer beads comprising spherical particles (up to 30 μm in diameter) that contain submicron air bubbles and a small proportion of TiO_2. The small air bubbles (<0.1 μm) reduce the effective RI of the polymer matrix, thus enhancing the light scattering of TiO_2.

The RI of any material (primary or secondary pigment) is a key to its performance. As is well known, the larger the difference in RI between the pigment and the medium in which it is dispersed, the greater the opacity effect. A summary of the refractive indices of various extender and opacifying pigments is provided in Table 18.1.

The RI of the medium in which the pigment is dispersed ranges from 1.33 (for water) to 1.4–1.6 (for most film formers). Thus, rutile will give the highest opacity, whereas talc and calcium carbonate will be transparent in fully bound surface coatings. Another important fact that affects light scattering is the particle size; hence, in order to obtain the maximum opacity from rutile an optimum particle

Table 18.1 Refractive indices for extenders.

Extender pigment	RI	Opacifying white pigment	RI
Calcium carbonate	1.58	Zinc sulphide	1.84
China clay	1.56	Zinc oxide	2.01
Talc	1.55	Zinc sulphide	2.37
Barytes	1.64	TiO_2 anatase	2.55
		TiO_2 rutile	2.76

size of 250 nm is required. This explains the importance of a good dispersion of the powder in the liquid, and this can be achieved by using a good wetting/dispersing agent, as well as the application of sufficient milling efficiency.

For coloured pigments, the RI of the pigment in the nonabsorbing (i.e., highly reflecting) part of the spectrum affects the performance as an opacifying material. For example, Pigment Yellow 1 and Arylamide Yellow G give lower opacities than Pigment Yellow 34 Lead Chromate. Most suppliers of coloured pigments attempt to increase the opacifying effect by controlling the particle size.

The nature of the pigment surface plays a very important role in its dispersion in the medium, as well as its affinity to the binder. For example, the polarity of the pigment will determine its affinity for alkyds, polyesters, acrylic polymers and latexes that are commonly used as film formers (see below). In addition, the nature of the pigment surface determines its wetting characteristics in the medium in which it is dispersed (which can be aqueous or nonaqueous), as well as the dispersion of aggregates and agglomerates into single particles. It also affects the overall stability of the liquid paint. Most pigments are surface-treated by the manufacturer to achieve the optimum performance. As mentioned above, the surface of rutile particles is treated with silica and alumina in various proportions to reduce photoactivity. If the pigment is to be used in a nonaqueous paint, its surface is also treated with fatty acids and amines to render it hydrophobic for incorporation in an organic medium. This surface treatment enhances the dispensability of the paint, its opacity and tinting strength and its durability (glass retention, resistance to chalking and colour retention), and it can also protect the binder in the paint formulation.

Dispersion of the pigment powder in a continuous medium requires several processes, namely wetting of the external and internal surfaces of the aggregates and agglomerates, separation of the particles from these aggregates and agglomerates by the application of mechanical energy, the displacement of occluded air, and coating of the particles with the dispersion resin. It is also necessary to stabilise the particles against flocculation, either by electrostatic double layer repulsion and/or steric repulsion. The process of wetting and dispersion of pigments was described in Chapter 9, while the eminence of colloid stability (lack of aggregation) was discussed in Chapters 7 and 8.

Dispersion methods are used to prepare suspensions of preformed particles. The term dispersion refers to the complete process of incorporating the solid into a liquid, such that the final product consists of fine particles distributed throughout the dispersion medium. The role of surfactants (or polymers) in the dispersion can be seen from a consideration of the stages involved [1, 2]. Three stages have been identified [3]: (i) wetting of the powder by the liquid; (ii) breaking of the aggregates and agglomerates; and (iii) comminution (milling) of the resulting particles into smaller units. These three stages are considered below.

18.2
Powder Wetting

Before describing the wetting of powders (that consist of aggregates, where the particles are attached by their ''faces,'' or agglomerated, where the particles are attached by their ''corners''), it is essential to describe the fundamental process of wetting in general, as well as other factors such as the adhesion of liquids to surfaces, the spreading of liquids on substrates, and the importance of the surface energy of the solid. These fundamental principles are briefly described below.

Wetting is a fundamental process in which one fluid phase is displaced completely or partially by another fluid phase from the surface of a solid. A useful parameter to describe wetting is the contact angle θ of a liquid drop on a solid substrate. If the liquid makes no contact with the solid, that is $\theta = 180°$, the solid is referred to as ''nonwettable by the liquid in question''. This may be the case for a perfectly hydrophobic surface with a polar liquid such as water. However, when $180° > \theta > 90°$, this is referred to as ''poor wetting.'' When $0° < \theta < 90°$, partial (incomplete) wetting is the case, whereas when $\theta = 0°$ complete wetting occurs and the liquid spreads onto the solid substrate to form a uniform liquid film. The cases of partial and complete wetting are shown schematically in Figure 18.2, for a liquid on a perfectly smooth solid substrate.

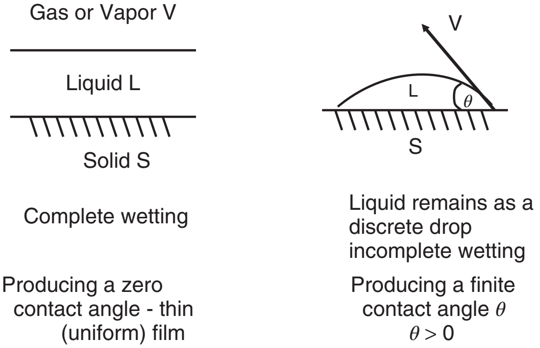

Figure 18.2 Illustration of complete and partial wetting.

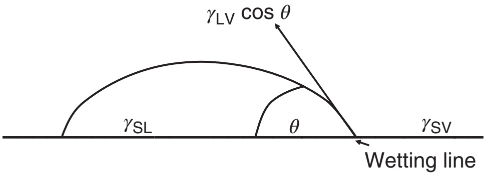

Figure 18.3 Schematic representation of contact angle and wetting line.

The utility of contact angle measurements depends on equilibrium thermodynamic arguments (static measurements) using the well-known Young's equation [4]. The value depends on: (i) the history of the system; and (ii) whether the liquid is tending to advance across or recede from the solid surface (advancing angle θ_A, receding angle θ_R; usually, $\theta_A > \theta_R$).

Under equilibrium, the liquid drop takes the shape that minimizes the free energy of the system. Three interfacial tensions can be identified: γ_{SV}, solid/vapour area $A_{SV;}$ γ_{SL}, solid/liquid area A_{SL}; and γ_{LV}, liquid/vapour area A_{LV}. A schematic representation of the balance of tensions at the solid/liquid/vapour interface is shown in Figure 18.3. The contact angle is that which is formed between the planes tangent to the surfaces of the solid and liquid at the wetting perimeter. Here, solid and liquid are simultaneously in contact with each other and the surrounding phase (air or vapour of the liquid). The wetting perimeter is referred to as the three-phase line or wetting line, and in this region there is an equilibrium between vapour, liquid, and solid.

$\gamma_{SV}\, A_{SV} + \gamma_{SL}\, A_{SL} + \gamma_{LV}\, A_{LV}$ should be a minimum at equilibrium, and this leads to the well-known Young's equation,

$$\gamma_{SV} = \gamma_{SL} + \gamma_{LV}\ \cos\theta \tag{18.1}$$

$$\cos\theta = \frac{\gamma_{SV} - \gamma_{SL}}{\gamma_{LV}} \tag{18.2}$$

The contact angle θ depends on the balance between the solid/vapour (γ_{SV}) and solid/liquid (γ_{SL}) interfacial tensions. The angle which a drop assumes on a solid surface is the result of the balance between the adhesion force between solid and liquid and the cohesive force in the liquid,

$$\gamma_{LV}\ \cos\theta = \gamma_{SV} - \gamma_{SL} \tag{18.3}$$

If there is no interaction between solid and liquid,

$$\gamma_{SL} = \gamma_{SV} + \gamma_{LV} \tag{18.4}$$

that is $\cos\theta = -1$ or $\theta = 180°$.

If there is a strong interaction between solid and liquid (maximum wetting), the latter spreads until Young's equation is satisfied,

$$\gamma_{LV} = \gamma_{SV} - \gamma_{SL} \tag{18.5}$$

that is, $\cos\theta = 1$ or $\theta = 0°$; the liquid is described to spread spontaneously on the solid surface.

There is no direct way by which γ_{SV} or γ_{SL} can be measured, but the difference between γ_{SV} and γ_{SL} can be obtained from contact angle measurements ($=\gamma_{LV}$ $\cos\theta$). This difference is referred to as the wetting tension or adhesion tension [5–7]

$$\text{Adhesion tension} = \gamma_{SV} - \gamma_{SL} = \gamma_{LV}\ \cos\theta \tag{18.6}$$

The work of adhesion is a direct measure of the free energy of interaction between solid and liquid,

$$W_a = (\gamma_{LV} + \gamma_{SV}) - \gamma_{SL} \tag{18.7}$$

Using Young's equation,

$$W_a = \gamma_{LV} + \gamma_{SV} - \gamma_{LV}\cos\theta = \gamma_{LV}(\cos\theta + 1) \tag{18.8}$$

The work of adhesion depends on: γ_{LV}, the liquid/vapour surface tension and θ, the contact angle between liquid and solid.

The work of cohesion, W_c, is the work of adhesion when the two surfaces are the same:

$$W_c = 2\,\gamma_{LV} \tag{18.9}$$

For adhesion of a liquid on a solid, $W_a \sim W_c$ or $\theta = 0°$ ($\cos\theta = 1$).

Harkins [8, 9] defined the spreading coefficient as the work required to destroy unit area of SL and LV and leaves unit area of bare solid SV,

The spreading coefficient, S, is equal to [Surface energy of final state – surface energy of the initial state]:

$$S = \gamma_{SV} - (\gamma_{SL} + \gamma_{LV}) \tag{18.10}$$

Using Young's equation,

$$\gamma_{SV} = \gamma_{SL} + \gamma_{LV}\ \cos\theta \tag{18.11}$$

$$S = \gamma_{LV}\,(\cos\theta - 1) \tag{18.12}$$

If S is zero (or positive), that is $\theta = 0$, the liquid will spread until it completely wets the solid, but if S is negative, that is $\theta > 0$, then only partial wetting will occur. Alternatively, the equilibrium (final) spreading coefficient can be used. For the dispersion of powders into liquids, complete spreading is usually required; that is, θ should be zero.

For a liquid spreading on a uniform, nondeformable solid (idealised case), there is only one contact angle–equilibrium value, but with real systems (practical solids) a number of stable contact angles can be measured. Two relatively reproducible angles can be measured: (i) largest, with an advancing angle θ_A; and smallest, with a receding angle θ_R. Typically, θ_A is measured by advancing the periphery of a drop over a surface (e.g., by adding more liquid to the drop), while θ_R is measured by pulling the liquid back. $(\theta_A - \theta_{R)}$ is referred to as contact angle hysteresis.

There are two main causes of contact angle hysteresis: (i) the penetration of wetting liquid into pores during advancing contact angle measurements; and (ii) surface roughness [10], when the first and rear edges both meet the liquid with some intrinsic angle θ_o (microscopic contact angle). The macroscopic angles θ_A and θ_R vary significantly. θ_o values are determined by contact of the liquid with the "rough" valleys (microscopic contact angle). θ_A and θ_R are determined by contact of the liquid with arbitrary parts on the surface (peak or valley). Surface roughness can be accounted for by comparing the "real" area of the surface A with that of the projected (apparent) area A',

$$r = \frac{A}{A'} \tag{18.13}$$

where A is area of surface taking into account all peaks and valleys, and A' is the apparent area (with the same macroscopic dimensions); $r > 1$.

$$\cos\theta = r\ \cos\theta_o \tag{18.14}$$

where θ is the macroscopic contact angle and θ_o is the microscopic contact angle.

$$\cos\theta = r\ \left[\frac{(\gamma_{SV} - \gamma_{SL})}{\gamma_{LV}}\right] \tag{18.15}$$

If $\cos\theta$ is negative on a smooth surface ($\theta > 90°$), it becomes more negative on a rough surface (θ is larger), and surface roughness reduces wetting; however, if $\cos\theta$ is positive on a smooth surface ($\theta < 90°$) it becomes more positive on a rough surface (θ is smaller) and the roughness enhances wetting.

Another factor that can cause contact angle hysteresis is surface heterogeneity. Most practical surfaces are heterogeneous and consist of "islands" or "patches" with different surface energies. As the drop advances on such a surface, its edge will tend to stop at the boundary of the "island"; the advancing angle will then be associated with the intrinsic angle of the high-contact angle region, while the receding angle will be associated with the low-contact angle region. If the heterogeneities are very small compared to the dimensions of the liquid drop, a composite contact angle can be defined using Cassie's equation [11, 12],

$$\cos\theta = Q_1\ \cos\theta_1 + Q_2\ \cos\theta_2 \tag{18.16}$$

where Q_1 is the fraction of surface having contact angle θ_1, and Q_2 is the fraction of surface having contact angle θ_2. θ_1 and θ_2 are the maximum and minimum possible angles.

A systematic way of characterizing the "wettability" of a surface was introduced by Fox and Zisman [13] where, for a given substrate and for a series of related liquids (e.g., *n*-alkanes, siloxanes and dialkyl ethers), a plot of $\cos\theta$ versus γ_{LV} gives a straight line. This is shown in Figure 18.4.

Extrapolation of the straight line to $\cos\theta = 1$ ($\theta = 0$) gives the critical surface tension of wetting γ_c. Any liquid with $\gamma_{LV} < \gamma_c$ will give $\theta = 0$, that is, it wets the surface completely; γ_c is the surface tension of a liquid that just spreads on the substrate to give complete wetting.

The above linear relationship can be represented by the following empirical equation,

$$\cos\theta = 1 + b\,(\gamma_{LV} - \gamma_c) \tag{18.17}$$

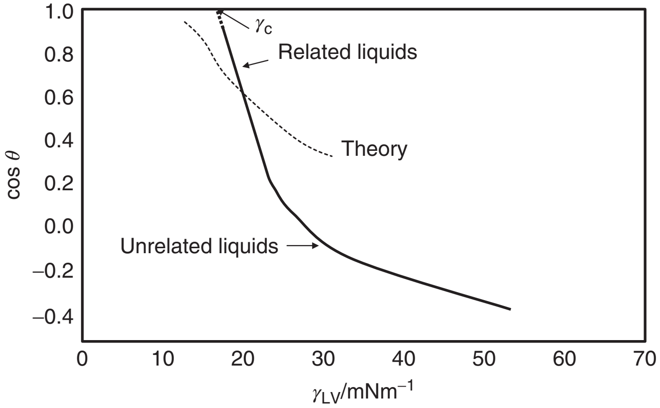

Figure 18.4 Illustration of the wettability of a surface.

High-energy solids (e.g., glass) give high γ_c (>40 mN m^{-1}), while low-energy solids (e.g., hydrophobic surfaces) give lower γ_c (~30 mN m^{-1}). Very low-energy solids such as Teflon (polytetrafluoroethylene; PTFE) give lower γ_c (<25 mN m^{-1}).

18.2.1
Effect of Surfactant Adsorption

Surfactants lower the surface tension of water, γ, and adsorb at the solid/liquid interface. A plot of γ_{LV} versus log C (where C is the surfactant concentration) results in a gradual reduction in γ_{LV} followed by a linear decrease of γ_{LV} with log C (just below the critical micelle concentration; cmc) and when the cmc is reached, γ_{LV} remains virtually constant. This is shown schematically in Figure 18.5.

From the slope of the linear portion of the γ–log C curve (just below the cmc), the surface excess (number of moles of surfactant per unit area at the liquid/air interface) can be obtained. Then, using the Gibbs adsorption isotherm,

$$\frac{\mathrm{d}\gamma}{\mathrm{dlog}\,C} = -2.303\,RT\,\Gamma \tag{18.18}$$

where Γ is the surface excess (mol m^{-2}), R is the gas constant, and T is absolute temperature.

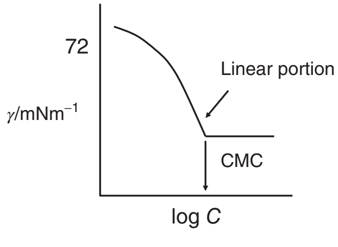

Figure 18.5 Surface tension–log C curves.

From Γ, the area per molecule can be obtained,

$$\text{Area per molecule} = \frac{1}{\Gamma\ N_{\text{Av}}}\ (m^2) = \frac{10^{18}}{\Gamma\ N_{\text{Av}}}\ (nm^2) \tag{18.19}$$

Most surfactants produce a vertically oriented monolayer just below the cmc. The area per molecule is usually determined by the cross-sectional area of the head group. For ionic surfactants containing -OSO_3^- or -SO_3^- head groups, the area per molecule is in the region of 0.4 nm^2, whereas for nonionic surfactants containing several moles (e.g., 8–10) of ethylene oxide (EO) the area per molecule can be much larger (1–2 nm^2). Surfactants will also adsorb at the solid/liquid interface. For hydrophobic surfaces, the main driving force for adsorption is by hydrophobic bonding, which results in a lowering of the contact angle of water on the solid surface. For hydrophilic surfaces, adsorption occurs via the hydrophilic group, for example cationic surfactants on silica. Initially, the surface becomes more hydrophobic and the contact angle θ increases with increase in surfactant concentration. However, at higher cationic surfactant concentration, a bilayer is formed by hydrophobic interactions between the alkyl groups, such that the surface becomes increasingly hydrophilic and eventually the contact angle reaches zero at high surfactant concentrations.

Smolders [14] suggested the following relationship for change of θ with C,

$$\frac{d\gamma_{\text{LV}}\ \cos\theta}{d\ln C} = \frac{d\gamma_{\text{SV}}}{d\ln C} - \frac{d\gamma_{\text{SL}}}{d\ln C} \tag{18.20}$$

Using the Gibbs equation,

$$\sin\theta \left(\frac{d\gamma}{d\ln C}\right) = RT(\Gamma_{\text{SV}} - \Gamma_{\text{SL}} - \gamma_{\text{LV}}\ \cos\theta) \tag{18.21}$$

Since $\gamma_{\text{LV}}\ \sin\theta$ is always positive, then ($d\theta/d\ln C$) will always have the same sign as the RHS of Equation (18.21). Three cases may be distinguished: ($d\theta/d\ln C) < 0$; $\Gamma_{\text{SV}} < \Gamma_{\text{SL}} + \Gamma_{\text{LV}}\cos\theta$, when the addition of a surfactant improves wetting; ($d\theta/d\ln C) = 0$; $\Gamma_{\text{SV}} = \Gamma_{\text{SL}} + \Gamma_{\text{LV}}\ \cos\theta$, when a surfactant has no effect on wetting; and ($d\theta/d\ln C) > 0$; $\Gamma_{\text{SV}} > \Gamma_{\text{SL}} + \Gamma_{\text{LV}}\cos\theta$, when the surfactant causes dewetting.

18.2.2
Wetting of Powders by Liquids

The wetting of powders by liquids is very important in their dispersion, for example in the preparation of concentrated suspensions. The particles in a dry powder form either aggregates or agglomerates, as illustrated in Figure 18.6.

It is essential in the dispersion process to wet both the external and internal surfaces and to displace any air entrapped between the particles. Wetting is achieved by the use of surface-active agents (wetting agents) of the ionic or nonionic type, which are capable of diffusing quickly (i.e., they lower the dynamic surface tension) to the solid/liquid interface and displacing the air entrapped by rapid penetrating the channels between the particles and inside any "capillaries." For the wetting of hydrophobic powders into water, anionic surfactants (e.g., alkyl sulphates or

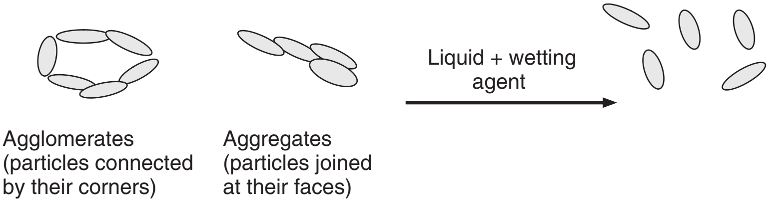

Figure 18.6 Schematic representation of aggregates and agglomerates.

sulphonates) or nonionic surfactants of the alcohol or alkyl phenol ethoxylates are normally used.

A useful concept for choosing wetting agents of the ethoxylated surfactants (see below) is the hydrophilic–lipophilic balance (HLB) concept,

$$\mathrm{HLB} = \frac{\%\text{of hydrophilic groups}}{5} \tag{18.22}$$

Most wetting agents of this class have an HLB number in the range 7–9.

The process of wetting of a solid by a liquid involves three types of wetting: adhesion wetting (W_a); immersion wetting (W_i); and spreading wetting (W_s). However, the work of dispersion wetting (W_d) can be considered as simply resulting from replacement of the solid/vapour interface with the solid/liquid interface.

Dispersion wetting W_d is given by the product of the external area of the powder, A, and the difference between γ_{SL} and γ_{SV}:

$$W_d = A(\gamma_{SL} - \gamma_{SV}) \tag{18.23}$$

Using the Young's equation:

$$W_d = -A\gamma_{LV}\cos\theta \tag{18.24}$$

Thus, wetting of the external surface of the powder depends on the liquid surface tension and contact angle. If $\theta < 90°$, $\cos\theta$ will be positive and the work of dispersion negative, such that wetting is spontaneous. The most important parameter that determines wetting of the powder is the dynamic surface tension, γ_{dynamic} (i.e., the value at short times). As will be discussed later, γ_{dynamic} depends both on the diffusion coefficient of the surfactant molecule and its concentration. As wetting agents are added in sufficient amounts (γ_{dynamic} is lowered sufficiently), spontaneous wetting is the rule rather than the exception.

Wetting of the internal surface requires penetration of the liquid into channels between and inside the agglomerates, a process which is similar to forcing a liquid through fine capillaries. To force a liquid through a capillary with radius r, a pressure p is required that is given by,

$$p = -\frac{2\,\gamma_{LV}\,\cos\theta}{r} = \left[\frac{-2\,(\gamma_{SV} - \gamma_{SL})}{r\,\gamma_{LV}}\right] \tag{18.25}$$

In this case, γ_{SL} must be made as small as possible, and there will be a rapid surfactant adsorption to the solid surface (i.e., low θ). When $\theta = 0$, $p \infty \gamma_{LV}$, and thus for penetration into pores a high γ_{LV} is required. Hence, wetting of the external surface requires a low contact angle θ and a low surface tension γ_{LV}. Wetting of the internal surface (i.e., penetration through the pores) requires a low θ but a high γ_{LV}. Clearly, these two conditions are incompatible and a compromise must be made: $(\gamma_{SV} - \gamma_{SL})$ must be kept at a maximum, while γ_{LV} should be kept as low as possible, but not too low.

The above conclusions illustrate the problem of choosing the best wetting agent for a particular powder. This requires measurement of the above parameters as well as testing the efficiency of the dispersion process.

The rate of penetration of the liquid in a powder aggregate or agglomerate can be applied to measure the contact angle of the liquid on the powder surface. For horizontal capillaries (gravity neglected), the depth of penetration l in time t is given by the Rideal–Washburn equation [15, 16],

$$l^2 = \left[\frac{r\ \gamma_{LV}\ \cos\theta}{2\ \eta}\right] t \tag{18.26}$$

where r is the effective radius. To enhance the rate of penetration, γ_{LV} has to be made as high as possible, θ as low as possible, and η as low as possible. For dispersion of powders into liquids, surfactants should be used that lower θ but do not reduce γ_{LV} too much; the viscosity of the liquid should also be kept at a minimum. Thickening agents (such as polymers) should not be added during the dispersion process. It is also necessary to avoid foam formation during the dispersion process.

For a packed bed of particles, r may be replaced by r/k^2, where the effective radius of the bed and a k is the turtuosity factor, which takes into account the complex path formed by the channels between the particles, that is:

$$l^2 = \left(\frac{r\gamma_{LV}\cos\theta}{2\eta k^2}\right) t \tag{18.27}$$

Thus, a plot of l^2 versus t will give a straight line, from the slope of which θ can be obtained. The Rideal–Washburn equation can be applied to obtain the contact angle of liquids (and surfactant solutions) in powder beds; however, k should first be obtained by using a liquid that produces a zero contact angle. This is discussed below.

18.2.3
Measurement of Wettability of Powders

18.2.3.1 Submersion Test: Sinking Time or Immersion Time

This by far the most simple (but qualitative) method for assessing the wettability of a powder by a surfactant solution. The time for which a powder floats on the surface of a liquid before sinking into the liquid is measured. For this, 100 ml of the surfactant solution is placed in a 250 ml beaker (of internal diameter 6.5 cm), and after 30 min standing an aliquot (0.3 g) of loose powder (previously screened through a 200-mesh sieve) is distributed with a spoon onto the surface of the solution. The time t taken

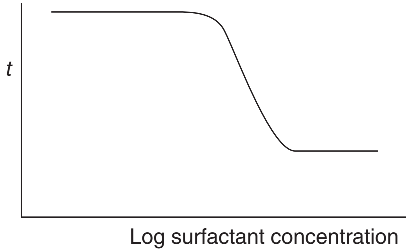

Figure 18.7 Sinking time as a function of surfactant concentration.

for the 1- to 2-mm-thin powder layer to completely disappear from the surface is measured, using a stop watch. Surfactant solutions with different concentrations are used and t is plotted versus surfactant concentration, as illustrated in Figure 18.7.

It can be seen from Figure 18.7 that the sinking time starts to decrease sharply above a critical surfactant concentration, reaching a minimum above this concentration. This procedure can be used to select the most effective wetting agent. The lower the surfactant concentration above which a rapid decrease in sinking time occurs, and the lower the minimum wetting time obtained above this concentration, the more effective is the wetting agent.

18.2.4
Measurement of Contact Angles of Liquids and Surfactant Solutions on Powders

As discussed above, the contact angle θ can be used for the quantitative assessment of a surfactant as a wetting agent for a particular powder. The simplest procedure is to measure the contact angle on a flat surface of the powder. This requires the preparation of a flat surface, for example by using a large crystal of the chemical or by compressing the powder to a thin plate (using high pressure, as commonly used for IR measurements). Unfortunately, this procedure tends to be inaccurate since, by compressing the powder, its surface will be changed and the measured contact angle will not be representative of the powder in question. However, this procedure may be used to compare various wetting agents, with the assumption being made that the lower the surfactant concentration required to reach a zero contact angle, the more effective is the wetting agent.

The contact angle on powders can be more accurately measured by determining the rate of liquid penetration through a carefully packed bed of powder placed in a tube fitted with a sintered glass at the end (to retain the powder particles). It is essential to pack the powder uniformly in the tube (a plunger may be used for this). By plotting l^2 (where l is the distance covered by the liquid flowing under capillary pressure) versus time t, a straight line is obtained [Equation (18.27)], the slope of which is equal to $r\gamma_{\mathrm{LV}}\cos\theta/2\eta k^2$ (where r is the equivalent capillary radius and k is the tortuosity factor, γ_{LV} is the liquid surface tension, and η is the liquid viscosity) (see Figure 18.8). The slope of $\cos\theta$ is obtained, provided that r/k^2 is known.

The tortuosity factor k and the ratio of r/k^2 can be obtained by using a liquid that completely wets the powder, giving a zero contact angle and $\cos\theta = 1$. The powder

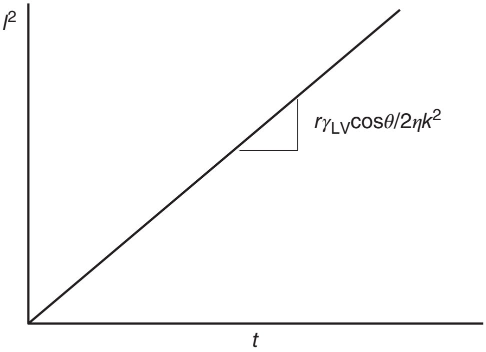

Figure 18.8 Variation of l^2 with t.

is carefully packed into a specially designed cell fitted with a plunger for packing the powder (as supplied by Kruss). The cell is placed on the top of liquid hexane, which gives a zero contact angle with most powders. The rate of hexane penetration through the powder plug is measured by following the increase in weight, ΔW, of the cell with time. After plotting ΔW^2 versus t, r/k^2 can be obtained from the slope of the linear line. The cell is then removed and the hexane allowed to evaporate completely. The same cell with its powder pack is then placed on surfactant solutions of various concentrations, and this allows the contact angle as a function of concentration to be obtained. The most effective wetting agent gives $\theta = 0°$ at the lowest concentration.

18.2.5
Wetting Agents for Hydrophobic Pigments

The most effective wetting agent gives a zero contact angle at the lowest concentration. For $\theta = 0°$ or $\cos\theta = 1$, γ_{SL} and γ_{LV} must be as small as possible, and this requires a quick reduction of γ_{SL} and γ_{LV} under dynamic conditions during powder dispersion (the reduction should normally be achieved in <20 s). To achieve this, a rapid adsorption of the surfactant molecules is required both at the L/V and S/L interfaces.

It should be noted that a reduction of γ_{LV} is not always accompanied by a simultaneous reduction of γ_{SL}, and hence it is necessary to obtain information on both interfacial tensions; this, in turn, means that measurement of the contact angle is essential in the selection of wetting agents. Measurements of γ_{SL} and γ_{LV} should be carried out under dynamic conditions (i.e., within very short times). In the absence of such measurements, the sinking time (as described above) could be applied as a guide for wetting agent selection.

The most commonly used wetting agents for hydrophobic solids are anionic or nonionic surfactants. To achieve a rapid adsorption, the wetting agent should be either a branched chain with a central hydrophilic group, or a short hydrophobic chain with a hydrophilic end group. The most commonly used wetting agent is

Aerosol OT (diethylhexyl sulphosuccinate):

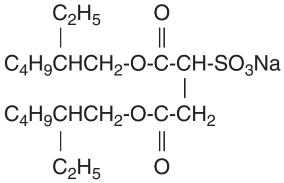

The above molecule has a low cmc of 0.7 g dm^{-3}, at and above which water surface tension is reduced to ~25 mN m^{-1} in less than 15 s.

An alternative anionic wetting agent is sodium dodecylbenzene sulphonate (NaDBS) with a branched alkyl chain.

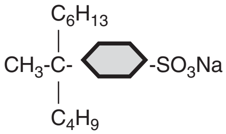

NaDBS has a higher cmc (1 g dm^{-3}) than Aerosol OT, and it is also less effective in lowering the surface tension of water, reaching a value of 30 mN m^{-1} at and above the cmc. It is, therefore, less effective as Aerosol OT for powder wetting.

Several nonionic surfactants, such as the alcohol ethoxylates, can also be used as wetting agents. These molecules consist of a short hydrophobic chain (mostly C_{10}) which is also branched; a medium-chain polyethylene oxide (PEO) mostly consisting of six EO units or fewer is used in this case. The above molecules also reduce the dynamic surface tension within a short time (<20 s) and have reasonably low cmc-values. In all cases, the minimum amount of wetting agent should be used in order to avoid interference with the dispersant that needs to be added to maintain colloid stability during dispersion and storage.

18.2.6
Dynamics of Processing of Adsorption and Wetting

Most processes of powder wetting operate under dynamic conditions, and improvements in their efficiency require the use of surfactants that lower the liquid surface tension γ_{LV} under these circumstances. The interfaces involved (particles separated from aggregates or agglomerates) are freshly formed and have only a small effective age of some seconds, or even less than a millisecond.

The most frequently used parameter to characterize the dynamic properties of liquid adsorption layers is the dynamic surface tension (a time-dependent quantity). Various techniques are available to measure γ_{LV} as a function of time (which ranges from a fraction of a millisecond to minutes and hours or even days).

In order to optimize the use of surfactants, specific knowledge of their dynamic adsorption behaviour rather than their equilibrium properties is of great interest [17]. Hence, it is necessary to describe the dynamics of surfactant adsorption at a fundamental level.

The first physically sound model for adsorption kinetics, which was derived by Ward and Tordai [18], is based on the assumption that the time dependence of a surface or interfacial tension (which is directly proportional to the surface excess Γ, in mol m^{-2}) is caused by diffusion and transport of surfactant molecules to the interface. This is referred to as "diffusion-controlled adsorption kinetics model". The interfacial surfactant concentration at any time t, $\Gamma(t)$, is given by the following expression,

$$\Gamma(t) = 2\left(\frac{D}{\pi}\right)^{1/2}\left(c_o\, t^{1/2} - \int_0^{t^{1/2}} c_o t - \tau\right) \mathrm{d}(\tau)^{1/2} \tag{18.28}$$

where D is the diffusion coefficient, c_o is the bulk concentration, and τ is the thickness of the diffusion layer.

The above diffusion-controlled model assumes transport by diffusion of the surface-active molecules to be the rate-controlled step. The so-called "kinetic controlled model" is based on the transfer mechanism of molecules from solution to the adsorbed state, and vice-versa [17].

A schematic of the interfacial region is provided in Figure 18.9, which shows three main states: (i) adsorption when the surface concentration Γ is lower than the equilibrium value Γ_o; (ii) the equilibrium state when $\Gamma = \Gamma_o$; and (iii) desorption when $\Gamma > \Gamma_o$.

The transport of surfactant molecules from the liquid layer adjacent to the interface (subsurface) is simply determined by molecular movements (in the absence of forced liquid flow). At equilibrium – that is, when $\Gamma = \Gamma_o$ – the flux of adsorption is equal to the flux of desorption. Clearly, when $\Gamma < \Gamma_o$, the flux of adsorption predominates, whereas when $\Gamma > \Gamma_o$, the flux of desorption predominates [17].

In the presence of liquid flow, the situation becomes more complicated due to the creation of surface tension gradients [17]. These gradients, described by the Gibbs dilational elasticity [17], ε, initiate a flow of mass along the interface in direction of a higher surface or interfacial tension (the Marangoni effect). ε is given by the

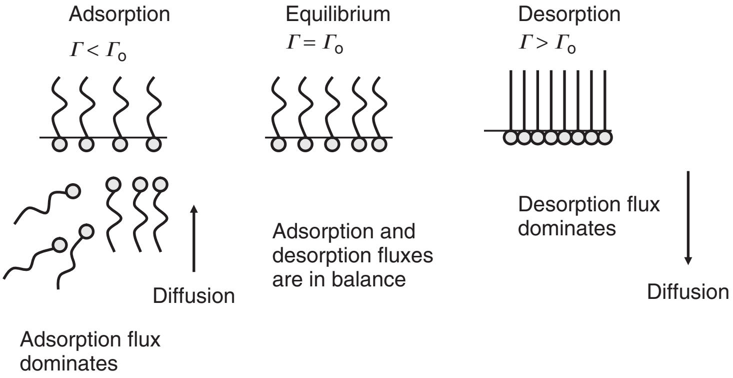

Figure 18.9 Representation of the fluxes of adsorbed surfactant molecules in the absence of liquid flow.

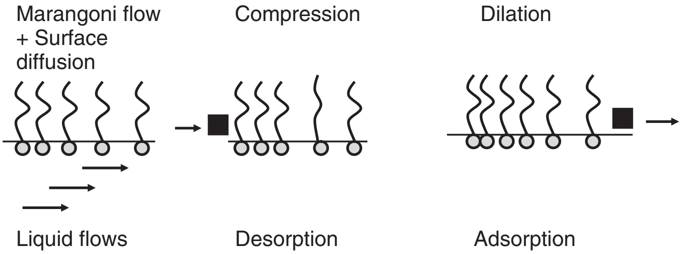

Figure 18.10 Representation of surfactant transport at the surface and in the bulk of a liquid.

following expression,

$$\varepsilon = A\frac{\mathrm{d}\gamma}{\mathrm{d}A} = \frac{\mathrm{d}\gamma}{\mathrm{d}\ln A} \tag{18.29}$$

where $\mathrm{d}\gamma$ is the surface tension gradient and $\mathrm{d}A$ is the change in area of the interface.

The above situation can happen, for example, if an adsorption layer is compressed or stretched, as illustrated in Figure 18.10.

A qualitative model that can describe adsorption kinetics is described by the following equation,

$$\Gamma(t) = c_o \left(\frac{D\,t}{\pi}\right)^{1/2} \tag{18.30}$$

Equation (18.30) provides a rough estimate, and results from Equation (18.28) when the second term on the right-hand side is neglected.

An equivalent equation to Equation (18.30) has been derived by Panaitov and Petrov [19],

$$c(0,t) = c_o - \frac{2}{(D\pi)^{1/2}} \int_0^{t^{1/2}} \frac{d\Gamma\,(t-\tau)}{\mathrm{d}t}\,\mathrm{d}\tau^{1/2} \tag{18.31}$$

Hansen, Miller and Lukenheimer gave numerical solutions to the integrals of Equations (18.28) and (18.31), and obtained a simple expression using a Langmuir isotherm,

$$\Gamma(t) = \Gamma_\infty \frac{c(0,t)}{a_L + c(0,t)} \tag{18.32}$$

where a_L is the constant in the Langmuir isotherm (mol m^{-3}).

The corresponding equation from the variation of surface tension γ with time is as follows (Langmuir–Szyszkowski equation):

$$\gamma = \gamma_o + RT\Gamma_\infty \ln\left(1 - \frac{\Gamma\,(t)}{\Gamma_\infty}\right) \tag{18.33}$$

Calculations based on Equations (18.30–18.33) are given in Figure 18.11, with different values of c_o/a_L [17].

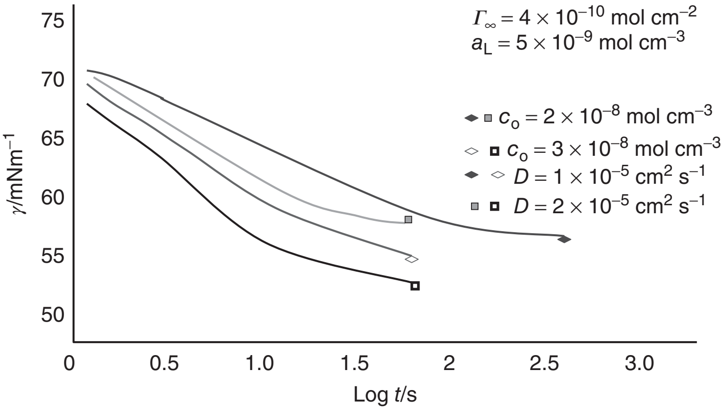

Figure 18.11 Surface tension γ–log t curves calculated on the basis of Equations (18.30–18.33).

Surfactants form micelles above the critical cmc of different sizes and shapes, depending on the nature of the molecule, the temperature, and electrolyte concentration. The dynamic nature of micellisation can be described by two main processes; that is, complete dissolution into main relaxation processes, τ_1 (the life time of a monomer in a micelle) and τ_2 (the life time of the micelle, that is complete dissolution into monomers). The presence of micelles in equilibrium with monomers influences the adsorption kinetics remarkably. When a fresh surface has been formed, surfactant monomers are adsorbed and this results in a concentration gradient of the monomers. Subsequently, the gradient will be equalised by diffusion to re-establish a homogeneous distribution. Simultaneously, the micelles will no longer be in equilibrium with monomers within the range of concentration gradient, and this will lead to a net process of micelle dissolution or rearrangement to re-establish the local equilibrium. As a consequence, a concentration gradient of micelles will result that is equalised by diffusion of micelles [17].

Based on the above concepts, it would be expected that the ratio of monomers c_1 to micelles c_m, the aggregation number n, and the rates of micelle formation k_f, and micelle dissolution k_d, would influence the rate of the adsorption process. A schematic image of the kinetic process in the presence of micelles is shown in Figure 18.12. The data in the figure show that, to describe the kinetics of adsorption, the diffusion of monomers and micelles must be taken into account, as well as the kinetics of micelle formation and dissolution. Several processes may take place, and these are represented schematically in Figure 18.13. Three main mechanisms may be considered, namely formation–dissolution (Figure 18.13a), rearrangement (Figure 18.13b), and stepwise aggregation–dissolution (Figure 18.13c). To describe the effect of micelles on adsorption kinetics, it is important to know several parameters, such as the micelle aggregation number and the rate constants of micelle kinetics [17].

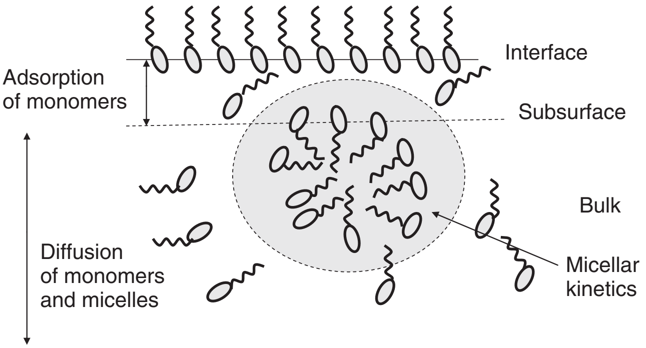

Figure 18.12 Representation of the adsorption process from a micellar solution.

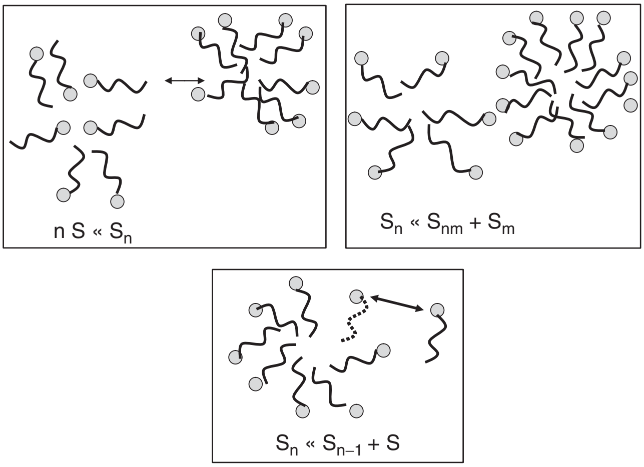

Figure 18.13 Scheme of micelle kinetics.

18.2.7
Experimental Techniques for Studying Adsorption Kinetics

The most suitable technique for studying adsorption kinetics and dynamic surface tension is the maximum bubble pressure method, which allows measurements to be obtained in the millisecond range, particularly if correction for the so-called "dead time," τ_d. The dead time is simply the time required to detach the bubble after it has reached its hemispherical shape. A schematic representation of the principle of maximum bubble pressure is shown in Figure 18.14, which describes the evolution of a bubble at the tip of a capillary. The figure also shows the variation of pressure p in the bubble with time.

At $t = 0$ (initial state), the pressure is low (note that the pressure is equal to $2\gamma/r$; since r of the bubble is large, p will be small). At $t = \tau$ (the smallest bubble radius that is equal to the tube radius), p reaches a maximum, whilst at $t = \tau_b$

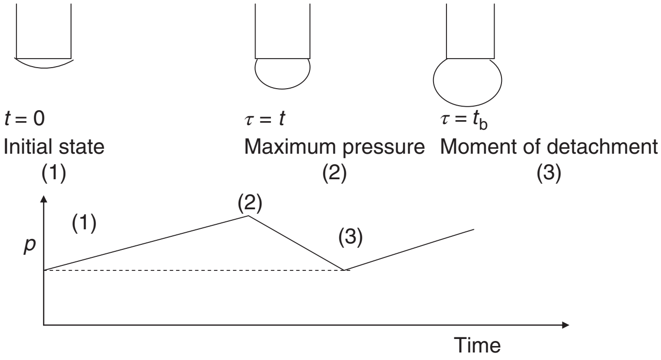

Figure 18.14 Scheme of bubble evolution and pressure change with time.

(detachment time), p will decrease as the bubble radius increases. The design of a maximum bubble pressure method for high bubble formation frequencies (short surface age) requires the following: (i) the measurement of bubble pressure; (ii) the measurement of bubble formation frequency; and (iii) an estimation of the surface lifetime and effective surface age.

The first problem can be easily solved if the system volume (which is connected to the bubble) is large enough in comparison to the bubble separating from the capillary. In this case, the system pressure is equal to the maximum bubble pressure. The use of an electric pressure transducer to measure bubble formation frequency presumes that pressure oscillations in the measuring system are distinct enough, and that this satisfies condition (ii). Estimation of the surface lifetime and effective surface age (condition (iii)) requires estimation of the dead time τ_d. A schematic representation of the set-up for measuring the maximum bubble pressure and surface age is shown in Figure 18.15. In this case, the air from a microcompressor flows first through the flow capillary, with the flow rate being determined by measuring the pressure difference at both ends of the flow capillary with the electric transducer PS_1. Thereafter, the air enters the measuring cell and the excess air pressure in the system is measured by a second electric sensor, PS_2. A sensitive microphone is placed in the tube which leads the air to the measuring cell.

The measuring cell, which is equipped with a water jacket for temperature control, simultaneously holds the measuring capillary and two platinum electrodes, one of which is immersed in the liquid under study while the second is situated exactly opposite to the capillary and controls the size of the bubble. The electric signals from the gas flow sensor PS_1 and pressure transducer PS_2, the microphone and the electrodes, as well as the compressor, are connected to a personal computer which operates the apparatus and acquires the data.

The value of τ_d, equivalent to the time interval necessary to form a bubble of radius R, can be calculated using Poiseuille's law,

$$\tau_d = \frac{\tau_b\, L}{K\, p}\left(1 + \frac{3r_{ca}}{2R}\right) \tag{18.34}$$

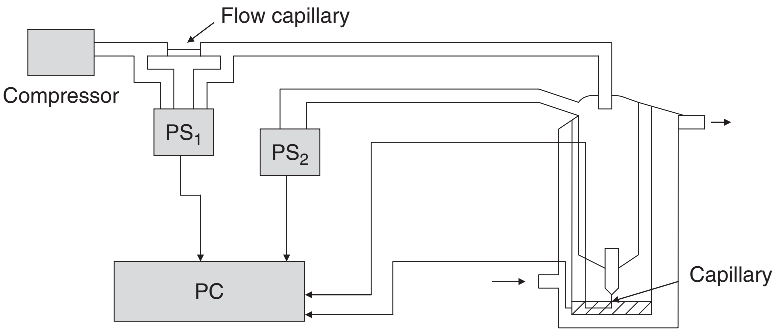

Figure 18.15 Maximum bubble pressure apparatus.

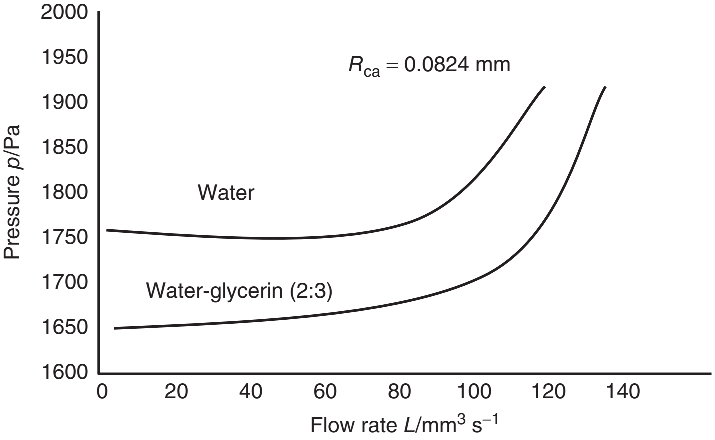

Figure 18.16 Dependence of p on gas flow rate L at 30 °C.

K is given by Poiseuille's law,

$$K = \frac{\pi\, r^4}{8\, \eta\, l} \tag{18.35}$$

where η is the gas viscosity, l is the length, L is the gas flow rate, and r_{ca} is the radius of the capillary. The calculation of dead time τ_d can be simplified when taking into account the existence of two gas flow regimes for the gas flow leaving the capillary: the bubble flow regime when $\tau > 0$, and the jet regime when $\tau = 0$; hence, $\tau_b = \tau_d$. A typical dependence of p on L is shown in Figure 18.16.

At the right-hand side of the critical point, the dependence of p on L is linear, in accordance with Poiseuille's law. Under these conditions,

$$\tau_d = \tau_b\, \frac{L\, p_c}{L_c\, p} \tag{18.36}$$

where L_c and p_c are related to the critical point, and L and p are the actual values of the dependence left from the critical point.

The surface lifetime can be calculated from,

$$\tau = \tau_b - \tau_d = \tau_b \left(1 - \frac{L\,p_c}{L_c\,p}\right) \tag{18.37}$$

The critical point in the dependence of p and L can be easily located, and is included in the software of the computer program.

The surface tension value in the maximum bubble pressure method is calculated using the Laplace equation,

$$p = \frac{2\,\gamma}{r} + \rho\,h\,g + \Delta p \tag{18.38}$$

where ρ is the density of the liquid, g is acceleration due to gravity, h is the depth the capillary is immersed in the liquid, and Δp is a correction factor to allow for hydrodynamic effects.

18.3
Breaking of Aggregates and Agglomerates (Deagglomeration)

As mentioned above, all pigments are supplied as powders that consist of either aggregates (where the particles are connected by their surfaces) or agglomerates (where the particles are connected by their corners). For example, pigmentary titanium dioxide mostly exists in powder form as loose agglomerates of several tens of micrometers in diameter. These pigments are surface-coated by the manufacturer for two main reasons. First, the surface coating reduces the cohesive forces of the powder, thus assisting the deagglomeration process. Second, the coating (SiO_2 and Al_2O_3) deactivates the surface rutile pigment (by reducing the photochemical activity), which otherwise would accelerate degradation of the resin on weathering.

The ''grinding stage'' in mill-based manufacture is not a comminution stage but rather a dispersion process of the pigment agglomerates, whereby the latter are separated into ''single'' primary particles. However, some of the primary particles may consist of sinters of TiO_2 crystals produced during the surface-coating stage. To separate the particles in an aggregate or agglomerate, the use of a wetting/dispersing system is required. As mentioned above, the wetting agent (which is usually a short-chain surfactant molecule) can seldom prevent reaggregation of the primary particles after the dispersion process. Thus, in order to prevent reaggregation of the particles, a dispersing agent is required, and this may either replace the wetting agent at the S/L interface or become coadsorbed with the wetting agent. On close approach of the particles, the dispersant produces an effective repulsive barrier that is particularly important for concentrated pigment dispersions (which may contain more than 50% by volume of solids).

The main criteria for an effective dispersant are:

- A strong adsorption or ''anchoring'' to the particle surface.
- A high repulsive barrier. The stabilising chain A of the dispersant must provide an effective repulsive barrier to prevent flocculation by van der Waals attractions.

Three main mechanisms of stabilisation can be considered: (i) electrostatic, as produced by ionic surfactants; (ii) steric, as produced by nonionic polymeric surfactants of the A-B, B-A-B, A-B-A or AB_n graft copolymers (where A is the ‘‘anchor’’ chain and B is the ‘‘stabilising’’ chain; and (iii) electrosteric, as produced by polyelectrolytes.

- Strong solvation of the stabilising B chain, which should be in a good solvent condition, be highly soluble in the medium, and strongly solvated by its molecules. Solvation of the chain by the medium is determined by the chain/solvent (Flory–Huggins) interaction parameter χ. In good solvent conditions $\chi < 0.5$ and hence the mixing or osmotic interaction is positive (repulsive). χ should be maintained at <0.5 under all conditions, for example low and high temperature, in the presence of electrolytes and other components of the formulation such as addition of antifreeze (mostly propylene glycol).
- A reasonably thick adsorbed layer. The adsorbed layer thickness of the B chains, which is usually described by a hydrodynamic value δ_h (i.e., the thickness δ plus any contribution from the solvation shell), should be sufficiently large to prevent the formation of a deep minimum which may result in flocculation (although reversible) and an increase in the viscosity of the suspension. A value of $\delta_h > 5$ nm is usually sufficient to prevent the formation of a deep minimum.

18.4
Classification of Dispersants

18.4.1
Surfactants

Anionic, for example sodium dodecyl sulphate (SDS) $C_{12}H_{25}OSO_3Na$. Sodium dodecylbenzenesulphonate (NaDBS). $C_{12}H_{25}$--SO_3Na. Cationic, for example dodecyl trimethyl ammonium chloride $C_{12}H_{25}$ $N(CH_3)_3Cl$.Amphoteric, for example betaines; lauryl amido propyl dimethyl betaine $C_{12}H_{25}CON(CH_3)_2CH_2COOH$. Nonionic surfactants: The most common nonionic surfactants are the alcohol ethoxylates R-O- $(CH_2\text{-}CH_2\text{-}O)n\text{-}H$, for example $C_{13/15}(EO)_n$ with n being 7, 9, 11, or 20. These surfactants are not the most effective dispersants as their adsorption by the C $_{13/15}$ chain is not very strong. To enhance the adsorption on hydrophobic surfaces a polypropylene oxide (PPO) chain is introduced into the molecule, giving R-O- $(PPO)_m$- $(PEO)_n$-H. A more effective nonionic surfactant with a strong adsorption is obtained by using a tristyrylphenol with PEO, for example

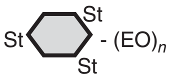

The tristyrylphenol hydrophobic chain adsorbs strongly onto a hydrophobic surface; this is due to the poor ‘‘anchor’’ of the chain to the surface and the high solubility of the polymer in water.

18.4.2
Polymeric Surfactants

Homopolymers consisting of the same repeating units such as PEO or poly(vinylpyrrolidone) are not good dispersants for hydrophobic solids in aqueous media. This is due to the poor ‘‘anchor’’ of the chain to the surface, and the high solubility of the polymer in water. In most cases these homopolymers do not adsorb at all on the particles, since the loss in configurational entropy on adsorption is not compensated by an adsorption energy (the adsorption energy per segment χ_s is very low).

As mentioned above, the most effective polymeric surfactants as dispersants are those of the A-B, B-A-B block and AB_n or BA_n graft types. In the case of A, the ‘‘anchor’’ chain is chosen to be highly insoluble in the medium, and has a strong affinity to the surface. Examples of A chains for hydrophobic solids are polystyrene (PS), poly(methylmethacrylate) (PMMA), PPO or alkyl chains, provided that these have several attachments to the surface. The B stabilising chain has to be soluble in the medium and strongly solvated by its molecules. The B chain/solvent interaction should be strong, giving a Flory–Huggins χ-parameter <0.5 under all conditions. Examples of B chains are PEO, polyvinyl alcohol (PVA) and polysaccharides (e.g., polyfructose). Several examples of commercially available B-A-B block copolymers are available: B-A-B Block copolymers of PEO and PPO. Pluronics: Several molecules of PEO-PPO-PEO are available with various proportions of PEO and PPO. The commercial name is followed by a letter L (Liquid), P (Paste), and F (Flake); this followed by two numbers that represent the composition. The first digit represents the PPO molar mass and the second digit represents the % PEO. Hence, Pluronic F68 (PPO molecular mass 1508–1800 + 80% or 140 mol EO); Pluronic L62 (PPO molecular mass 1508–1800 + 20% or 15 mol EO). In many cases, two Pluronics with high and low EO contents are used together to enhance the dispersing power.

Graft copolymers of the AB_n type are also available, for example AB_n graft copolymers based on a PMMA backbone (with some polymethacrylic acid) on which several PEO chains (with average molecular weight 750) are grafted:

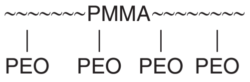

$$\begin{array}{c}
\sim\sim\sim\sim\sim\sim\sim \text{PMMA} \sim\sim\sim\sim\sim\sim\sim\sim \\
\begin{array}{cccc} | & | & | & | \\ \text{PEO} & \text{PEO} & \text{PEO} & \text{PEO} \end{array}
\end{array}$$

This is a very effective dispersant, particularly for high-solids-content suspensions. The graft copolymer is strongly adsorbed onto hydrophobic surfaces with several attachment points by the small PMMA loops of the backbone, and a strong steric barrier is obtained by the highly hydrated PEO chains in aqueous solutions.

A novel BA_n graft has been recently synthesised, namely INUTEC SP1 (by Orafti in Belgium) consisting of inulin (a linear polyfructose chain A with degree of polymerisation >23), onto which several alkyl chains have been grafted:

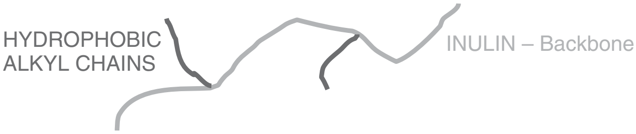

The polymeric surfactant adsorbs with multipoint attachment with several alkyl chains.

Another commercially available “blocky”’ copolymer is partially hydrolysed polyvinyl acetate (PVAc), which is commercially referred to as polyvinyl alcohol. The molecule contains short blocks of PVAc which form the anchor chains to the hydrophobic surface, leaving several loops and tails of PVA chains which are strongly hydrated to give an effective steric barrier:

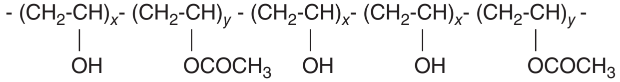

$$\begin{array}{ccccc} -(CH_2\text{-}CH)_x- & (CH_2\text{-}CH)_y- & (CH_2\text{-}CH)_x- & (CH_2\text{-}CH)_x- & (CH_2\text{-}CH)_y- \\ | & | & | & | & | \\ OH & OCOCH_3 & OH & OH & OCOCH_3 \end{array}$$

Several commercial PVA grades are available with molecular weights in the range 20 000–100 000 and acetate content in the range 4–12%. The molecule is designated by two numbers representing the degree of hydrolysis and viscosity of a 4% solution (this gives a rough estimate of molecular weight). For example, Moviol 88/10 refers to a degree of hydrolysis of 88% (12% acetate groups) and a viscosity of 10 mPa·s of a 4% solution.

18.4.3
Polyelectrolytes

Naphthalene formaldehyde sulphonated condensate:

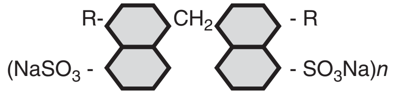

Here, *n* varies between 2 and 9 units; that is, the molecule has a wide distribution of molecular weights.

Another group of commercially available dispersants are the lignosulphonates. These are isolated from the waste liquor of wood pulping by the sulphite process, during which lignin is sulphonated. They are also produced by sulphonating lignin in the alkaline pulping of wood by the Krafft process. Lignosulphonates as dispersants are mixtures of polyelectrolytes with molecular weights ranging from 2000 to 10 000. The exact structure of lignosulphonates is not completely known, but guaiacylpropyl groups with the sulphate groups attached to the aliphatic chains of lignin have been identified. The degree of sulphonation varies from 0.3 to 1.0 per phenyl unit. The commercial products, namely Polyfon (Wesvaco) and Ufoxane (Borregard), are described by their degree of sulphonation per 840 units of lignin. For example, Polyfon H has a degree of sulphonation of 0.5, whereas Polyfon T has a degree of 2.0. The most effective lignosulphonates for hydrophobic solids in aqueous solution are those with a lower degree of sulphonation that give a higher adsorption.

18.4.4
Assessment and Selection of Dispersants

18.4.4.1 Adsorption Isotherms

These are by far the most quantitative methods for the assessment of dispersing power. Known amounts of solids (in grams) with a surface area A (m^2 g^{-1}) are equilibrated at a constant temperature with dispersant solutions of various concentrations, C_1. The bottles containing the various dispersions are rotated for several hours until equilibrium is reached, after which the particles are removed from the dispersant solution by centrifugation and/or filtration through Millipore filters. The dispersant concentration in the supernatant liquid, C_2, is analytically determined by a suitable technique that can measure low concentrations.

The amount of adsorption Γ (mg m^{-2} or mol m^{-2}) is calculated:

$$\Gamma = \frac{(C_1 - C_2)}{mA} \tag{18.39}$$

A plot of Γ versus C_2 gives the adsorption isotherm. Two types of isotherms can be distinguished: a Langmuir type for reversible adsorption of surfactants (Figure 18.17); and a high-affinity isotherm (Figure 18.18) for the irreversible adsorption of polymeric surfactants.

In both cases a plateau adsorption value Γ_∞ is reached at a given value of C_2. In general, the value of Γ_∞ is reached at a lower C_2 for polymeric surfactant adsorption when compared to small molecules. The high-affinity isotherm obtained with polymeric surfactants implies that the first added molecules are virtually

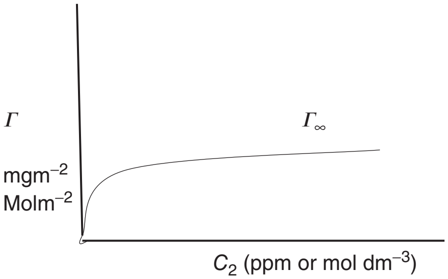

Figure 18.17 Langmuir-type adsorption isotherm.

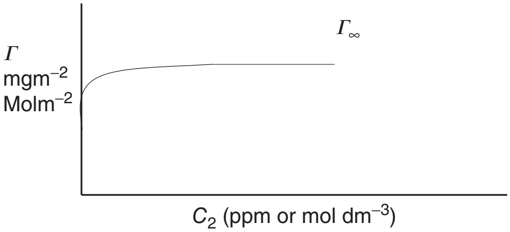

Figure 18.18 High-affinity isotherm.

completely adsorbed and that such a process is irreversible. The irreversibility of adsorption is checked by carrying out a desorption experiment. For this, the suspension at the plateau value is centrifuged and the supernatant liquid replaced by water. After redispersion, the suspension is re-centrifuged and the concentration of the polymeric surfactant in the supernatant liquid is determined. If there is a lack of desorption the above concentration will be very small, indicating that the polymer has remained on the particle surface.

18.4.4.2 Measurement of Dispersion and Particle Size Distribution

An effective dispersant should result in complete dispersion of the powder into single particles. In addition, on wet milling (comminution) a smaller particle distribution should be obtained. The efficiency of dispersion and reduction of particle size can be understood from the behaviour of the dispersant. Strong adsorption and an effective repulsive barrier will prevent any aggregation occurring during the dispersion process. It is necessary in this case to include the wetting agent (which should be kept at the optimum concentration). Adsorption of the dispersant at the solid/liquid interface results in a lowering of γ_{SL}, and this in turn reduces the energy required for breaking the particles into smaller units. In addition, crack propagation may occur (the Rehbinder effect) due to adsorption in crystal defects, and this can result in the production of smaller particles.

Several methods may be applied for measuring particle size distribution, and these will be described in detail in Chapter 19.

18.4.4.3 Wet Milling (Comminution)

The primary dispersion (sometimes referred to as the mill base) may then be subjected to a bead milling process to produce the nanoparticles that are essential for some coating applications. Subdivision of the primary particles into much smaller units in the nanosize range (10–100 nm) requires the application of intense energy. In some cases, high-pressure homogenisers (such as the Microfluidizer, USA) may be sufficient to produce nanoparticles, and this is particularly the case with many organic pigments. In some cases, high-pressure homogenisation is combined with the application of ultrasound to produce nanoparticles.

Milling or comminution (the generic term for size reduction) is a complex process, and very little fundamental information is available on its mechanism. For the breakdown of single crystals or particles into smaller units, mechanical energy is required, and in a bead mill this energy is supplied by impaction of the glass or ceramic beads with the particles. As a result, permanent deformation of the particles and crack initiation will most likely occur, and this will eventually lead to the fracture of particles into smaller units. As the milling conditions are random, some particles will receive impacts far in excess of those required for fracture, whereas others will receive impacts that are insufficient to cause fracture. This makes the milling operation grossly inefficient, and only a small fraction of the applied energy is used in comminution, the remainder being dissipated as heat, vibration, sound, and interparticulate friction.

The role of surfactants and dispersants on the grinding efficiency is far from being understood. In most cases, the choice of surfactants and dispersant is made by trial and error until a system is found that gives the maximum grinding efficiency. When Rehbinder and colleagues investigated the role of surfactants in the grinding process, surfactant adsorption at the solid/liquid interface caused the surface energy at the boundary to be reduced, and this facilitated the processes of deformation or destruction. The adsorption of surfactants at the solid/liquid interface in cracks may facilitate crack propagation; this mechanism is referred to as the Rehbinder effect.

Several factors affect the efficiency of dispersion and milling, including the volume concentration of the dispersed particles (i.e., the volume fraction); the nature of the wetting/dispersing agent; and (iii) the concentration of the wetting agent/dispersant (which determines the adsorption characteristics).

In order to optimize the dispersion/milling process, the above parameters need to be investigated systematically. From the wetting performance of a surfactant, evaluated via the sinking time or contact angle measurements, it is possible to establish the nature and concentration of the wetting agent. The nature and concentration of the dispersing agent is also required, and can be determined by adsorption isotherm and rheological measurements (see Chapter 20).

When the concentration of wetting/dispersing agent has been established, dispersions are prepared at various volume fractions, keeping the ratio of the wetting/dispersing agent to the solid content constant. Each system is then subjected to dispersion/milling process, again keeping all parameters constant: (i) the speed of the stirrer (normally a lower speed is used at first and is increased incrementally at fixed times); (ii) the volume and size of the beads relative to the volume of the dispersion (an optimum value is required); and (iii) the speed of the milling.

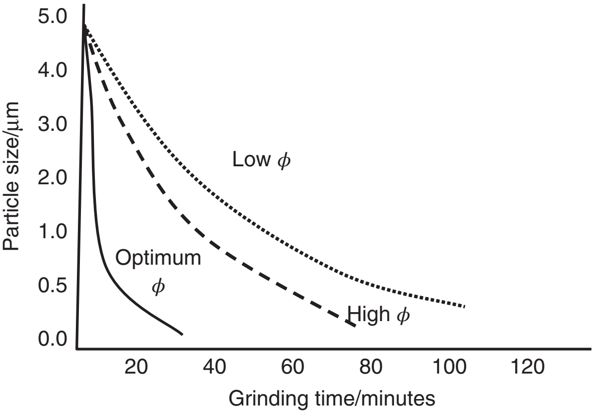

Figure 18.19 Variation of particle size with grinding time in a typical bead mill.

The change in average particle size with time of grinding is established using, for example, the Master Sizer. Figure 18.19 shows a schematic representation of the reduction of particle size with grinding time (in minutes), using a typical bead mill (see below) at various volume fractions. The data in Figure 18.19 are not based on experimental findings, but rather demonstrate the expected trend. When the volume fraction ϕ is below the optimum (in this case, the relative viscosity of the dispersion is low), a long time is needed to achieve size reduction, and the final particle size may be large and outside the nanometre range. However, when ϕ is above the optimum value the dispersion time will be prolonged (due to the relatively high relative viscosity of the system), the grinding time will be longer, and the final particle size will be larger than that obtained at the optimum ϕ. At the optimum ϕ, both the dispersion and grinding time will be shorter and the final particle size will be smaller.

18.4.4.4 **Bead Mills**

When preparing nanodispersions, bead mills are commonly used. The beads are mostly made from glass or ceramics (these are preferred due to minimum contamination), and the operating principle is to pump the premixed, preferably predispersed (using a high-speed mixer), mill base through a cylinder containing a specified volume of (probably) ceramic beads that are normally 0.5–1 mm diameter to achieve nanosize particles. The dispersion is agitated by a single or multidisc rotor, and the disc may be either flat or perforated. The mill base passing through the shear zone is then separated from the beads by a suitable screen located at the opposite end of the feedport.

Generally speaking, bead mills may be classified as two types: (i) vertical mills with an open or closed top; and (ii) horizontal mills with closed chambers. The horizontal mills are more efficient, and the most commonly used are produced by Netzsch (Germany) and Dyno Mill (Switzerland). These bead mills are available in various sizes, ranging from 0.5 to 500 litres in volume. The factors that affect the general dispersion efficiency are known reasonably well (from the manufacturer), but selecting the correct diameter of the beads is important for maximum utilisation. In general, the smaller the size of the beads, the higher will be their density and the more efficient the milling process.

The principle of operation of a bead mill involves a centrifugal force being transmitted to the grinding beads at the tip of the rotating disc, such that a greater shear force can be applied to the mill base (this explains why smaller, more dense beads are more efficient for grinding). The speed transmitted to the individual chambers of the beads at the tip of the disc assumes that speed and the force can be calculated.

The applied centrifugal force, F, is given by

$$F = \frac{v^2}{rg} \tag{18.40}$$

where v is the velocity, r is the radius of the disc, and g is acceleration due to gravity.

References

1. Blake, T.B. (1984) Wetting, in *Surfactants* (ed. Th.F. Tadros), Academic Press, London.
2. Parfitt, G.D. (1977) *Dispersion of Powders in Liquids*, Applied Science, London.
3. Tadros, T. (2010) *Dispersion of Powders in Liquids and Stabilisation of Suspensions*, Wiley-VCH Verlag GmbH, Weinheim.
4. Young, T. (1805) *Philos. Trans. R. Soc. (London)*, **95**, 65.
5. Gibbs, J.W. (1928) *The Collected Work of J. Willard Gibbs*, vol. **1**, Longman-Green, New York.
6. Everett, D.H. (1980) *Pure Appl. Chem.*, **52**, 1279.
7. Johnson, R.E. (1959) *J. Phys. Chem.*, **63**, 1655.
8. Harkins, W.D. (1937) *J. Phys. Chem.*, **5**, 135.
9. Harkins, W.D. (1952) *The Physical Chemistry of Surface Films*, Reinhold, New York.
10. Wenzel, R.N. (1936) *Ind. Eng. Chem.*, **28**, 988.
11. Cassie, A.B.D. and Dexter, S. (1944) *Trans. Faraday Soc.*, **40**, 546.
12. Cassie, A.B.D. (1948) *Discuss. Faraday Soc.*, **3**, 361.
13. Zisman, W.A. (1964) *Adv. Chem. Ser.*, **43**, 1.
14. Smolders, C.A. (1960) *Rec. Trav. Chim.*, **80**, 650.
15. Rideal, E.K. (1922) *Philos. Mag.*, **44**, 1152.
16. Washburn, E.D. (1921) *Phys. Rev.*, **17**, 273.
17. Dukhin, S.S., Kretzscmar, G., and Miller, R. (1995) *Dynamics of Adsorption at Liquid Interfaces*, Elsevier Publishers, Amsterdam.
18. Ward, A.F.H. and Tordai, L. (1946) *J. Phys. Chem.*, **14**, 453.
19. Panaitov, I. and Petrov, J.G. (1968/1969) *Ann. Univ. Sofia, Fac. Chem.*, **64**, 385.

19
Methods of Evaluating Formulations after Dilution

19.1
Introduction

For full characterisation of the properties of suspensions, three main types of investigation are needed:

- Fundamental investigation of the system at the molecular level. This requires investigations of the structure of the solid/liquid interface, namely the structure of the electrical double layer (for charge-stabilised suspensions), adsorption of surfactants, polymers and polyelectrolytes and conformation of the adsorbed layers (e.g., the adsorbed layer thickness). It is important to know how each of these parameters changes with the conditions, such as temperature, solvency of the medium for the adsorbed layers, and the effect of addition of electrolytes.
- Investigation of the state of suspension on standing, namely flocculation rates, flocculation points with sterically stabilised systems, spontaneity of dispersion on dilution, and Ostwald ripening or crystal growth. All of these phenomena require an accurate determination of the particle size distribution as a function of storage time.
- Bulk properties of the suspension. This is particularly important for concentrated systems, and requires measurement of the rate of sedimentation and equilibrium sediment height. More quantitative techniques are based on assessing the rheological properties of the suspension (without disturbing the system; that is, without its dilution and measurement under conditions of low deformation) and how these are affected by long-term storage. This subject is discussed in detail in Chapter 20.

In this chapter, a summary of the methods that can be applied to assess the structure of the solid/liquid interface will first be provided, followed by details of assessing sedimentation, flocculation, and Ostwald ripening. In the latter cases (flocculation and Oswald ripening), information is needed on the particle size distribution, and several techniques are available to obtain this from diluted systems. It is essential to dilute the concentrated suspension with its own dispersion medium in order not to affect the state of the dispersion during examination. The dispersion medium can be obtained by centrifuging the suspension, when the supernatant liquid will be produced at the top of the centrifuge tube in the case

Formulation of Disperse Systems: Science and Technology, First Edition. Tharwat F. Tadros.

of suspensions, or at the bottom for most emulsions. Care should be taken when diluting the concentrated system with its supernatant liquid (i.e., with minimum shear).

19.2
Assessment of the Structure of the Solid/Liquid Interface

19.2.1
Double Layer Investigation

19.2.1.1 Analytical Determination of Surface Charge

The surface charge on a solid surface can be obtained by determining the adsorption of potential-determining ions at various potentials of the interface [1]. For example, in the case of a silver iodide sol the adsorption of Ag^+ and I^- ions is determined at various concentrations of Ag^+ and I^- ions in bulk solution. Similarly, for an oxide the adsorption of H^+ and OH^- ions (Γ_{H+} and Γ_{OH-}, respectively) is determined as a function of the pH of the suspension. In this case, the surface charge density σ_o is given by,

$$\sigma_o = F(\Gamma_{H+} - \Gamma_{OH-}) \tag{19.1}$$

whereas the surface potential ψ_o is given by the Nernst equation,

$$\psi_o = \frac{RT}{F} \ln \frac{a_{H+}}{(a_{H+})_{pzc}} \tag{19.2}$$

where R is the gas constant, T is the absolute temperature, F is the Faraday constant, a_{H+} is the activity of H^+ ions in bulk solution, and $(a_{H+})_{pzc}$ is the value at the point of zero charge.

σ_o can be directly determined by titration of an oxide suspension in an aqueous solution of indifferent electrolyte (e.g., KCl) using a cell of the type,

E_1| Oxide suspension | E_2

where E_1 is an electrode reversible to H^+ and OH^- ions, such as glass electrode, and E_2 is a reference electrode such as Ag-AgCl. From knowledge of the amount of H^+ and OH^- ions added, and the amount remaining in solution (which can be calculated from a knowledge of the electrical potential of the above cell), Γ_{H+} and Γ_{OH-} can be determined from material balance and knowledge of the surface area of the oxide. The latter can be determined from gas adsorption using the BET method. In order to calculate the absolute values of Γ_{H+} and Γ_{OH-} it is necessary to know the pzc; this can be located from the common intersection point of the titration curve at various electrolyte concentrations, if there is no specific adsorption of ions.

As an illustration of the direct surface charge determination, the results obtained on precipitated silica are shown in Figure 19.1, where σ_o is plotted versus pH at four different KCl concentrations [2]. There is a common intersection point at pH ~ 3,

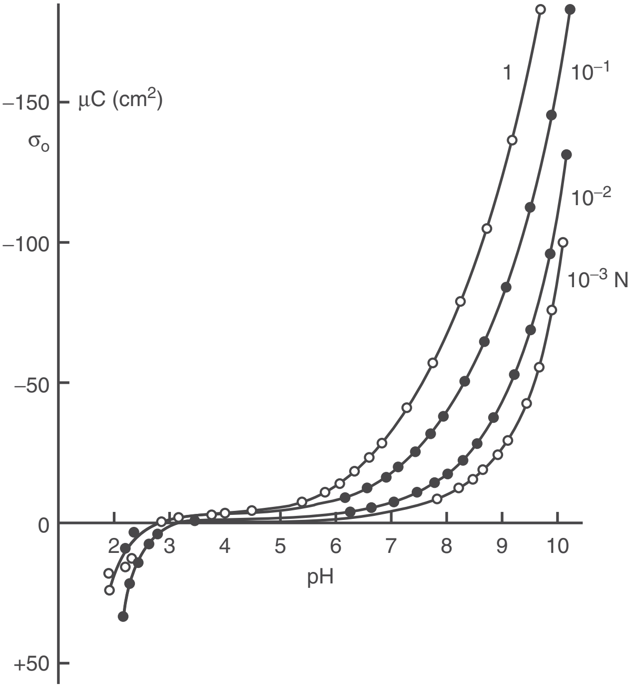

Figure 19.1 σ_o–pH isotherms for precipitated silica at four KCl concentrations.

which is the pzc, indicating an absence of specific adsorption of K^+ or Cl^- ions. The charge increases progressively with increasing pH, reaching very high values at high pH and electrolyte concentrations. However, this high surface charge is not reflected in a high zeta-potential, and the silica dispersions are not particularly stable even at high pH. This shows clearly that measurement of the surface charge alone cannot be used as an indication of the stability of the silica dispersion.

19.2.1.2 **Electrokinetic and Zeta-Potential Measurements**

The principles of electrokinetic phenomena and measurement of the zeta-potential were discussed in detail in Chapter 5. There are essentially two techniques to measure electrophoretic mobility and zeta-potential, namely the ultramicroscopic method and laser velocimetry. As an illustration, Figure 19.2 shows plots of zeta-potential versus pH for goethite FeO(OH) at three electrolyte concentrations [3]. It is clear that below pH 6.9 the particles are positively charged and the zeta-potential increases in magnitude with a further decrease in the pH. Above pH 6.9, however, the particles are negatively charged and the zeta-potential increases with further increase in pH. At pH 6.9, the particles are uncharged and this denotes the isoelectric point (i.e.p.) of goethite. Below and above the i.e.p., the zeta-potential decreases with increase in electrolyte concentration as a result of double layer compression. In this case, the stability of goethite is directly correlated with its

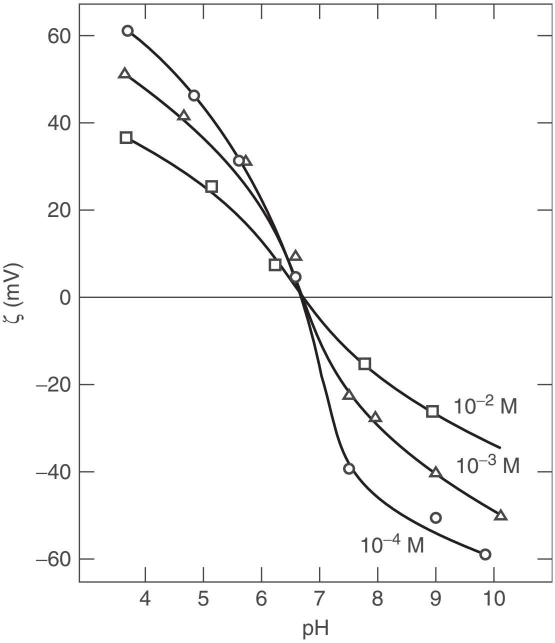

Figure 19.2 Zeta-potential as a function of pH for goethite.

zeta-potential value, in that the higher the zeta-potential the more stable is the suspension. A rapid flocculation of goethite suspensions occurs at the i.e.p.

19.2.2
Measurement of Surfactant and Polymer Adsorption

As discussed in detail in Chapters 6 and 7, surfactant and polymer adsorption are key to understanding how these molecules affect the stability/flocculation of a suspension. The various techniques that may be applied to obtain information on surfactant and polymer adsorption were described in Chapters 6 and 7. Surfactant (both ionic and nonionic) adsorption is reversible, and the process of adsorption can be described using the Langmuir isotherm [4]. Basically, representative samples of the solid with mass m and surface area A ($m^2\,g^{-1}$) are equilibrated with surfactant solutions covering various concentrations C_1 (a wide concentration range from values below and above the critical micelle concentration; cmc). The particles are dispersed in the solution by stirring and then left to equilibrate (preferably overnight while being stirred over rollers); the particles are then removed by centrifugation and/or filtration (using Millipore filters). The concentration in the supernatant solution C_2 is determined using a suitable analytical method, but the analysis used must be sensitive enough to determine very low surfactant concentrations. The surface area of the solid can be determined using gas adsorption and application

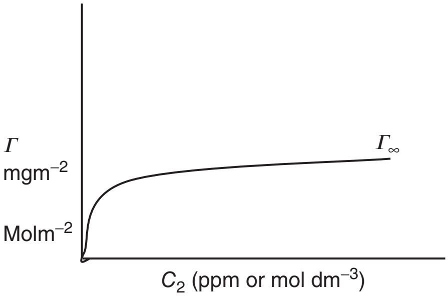

Figure 19.3 Langmuir-type adsorption isotherm.

of the BET equation. Alternatively, the surface area of the "wet" solid (which may be different from that of a dry solid) can be determined using dye adsorption [1].

By knowing C_1, C_2, m and A, it is possible to calculate the extent of adsorption Γ (mg m^{-2} or mol m^{-2}) as a function of the equilibrium concentration C_2 (ppm or mol dm^{-3}),

$$\Gamma = \frac{C_1 - C_2}{mA} \tag{19.3}$$

With most surfactants, a Langmuir-type isotherm is obtained, as illustrated in Figure 19.3, where Γ increases gradually with increase of C_2 and eventually reaches a plateau value Γ_∞ which corresponds to saturation adsorption.

The results of Figure 19.3 can be fitted to the Langmuir equation,

$$\Gamma = \frac{\Gamma_\infty b C_2}{1 + bC_2} \tag{19.4}$$

where b is a constant that is related to the free energy of adsorption ΔG_{ads},

$$b = \exp(-\Delta G_{\text{ads}}/RT) \tag{19.5}$$

A linearised form of the Langmuir equation may be used to obtain Γ_∞ and b, as illustrated in Figure 19.4,

$$\frac{1}{\Gamma} = \frac{1}{\Gamma_\infty} + \frac{1}{\Gamma_\infty b C_2} \tag{19.6}$$

A plot of $1/\Gamma$ versus $1/C_2$ gives a straight line (Figure 19.4) with intercept $1/\Gamma_\infty$ and slope $1/\Gamma_\infty\, b$, from which both Γ_∞ and b can be calculated.

From Γ_∞ the area per surfactant ion or molecule can be calculated,

$$\text{Area/molecule} = \frac{1}{\Gamma_\infty N_{av}}(m^2) = \frac{10^{18}}{\Gamma_\infty N_{\text{Av}}}(nm^2) \tag{19.7}$$

As discussed in Chapter 5, the area per surfactant ion or molecule gives information on the orientation of surfactant ions or molecules at the interface. This information is relevant for the stability of the suspension. For example, for the vertical orientation of surfactant ions (e.g., dodecyl sulphate anions), which is essential to produce a high surface charge (and hence an enhanced electrostatic

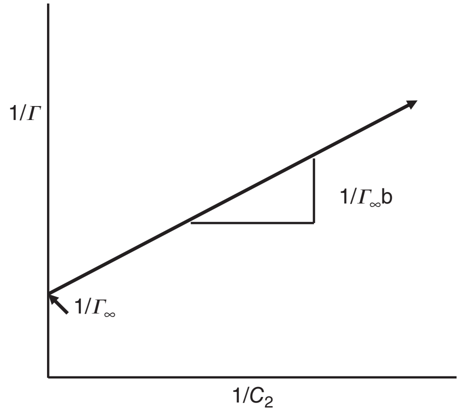

Figure 19.4 Linearised form of the Langmuir equation.

stability), the area per molecule is determined by the cross-sectional area of the sulphate group, which is in the region of 0.4 nm^2 With nonionic surfactants consisting of an alkyl chain and a poly(ethylene oxide) (PEO) head group, adsorption onto a hydrophobic surface is determined by the hydrophobic interaction between the alkyl chain and the hydrophobic surface. For the vertical orientation of a monolayer of surfactant molecules, the area per molecule will depend on the size of the PEO chain, which is in turn directly related to the number of ethylene oxide (EO) units in the chain. If the area per molecule is smaller than that predicted from the size of the PEO chain, the surfactant molecules may associate on the surface to form bilayers and hemimicelles (as discussed in detail in Chapter 5). This information can be related directly to the stability of the suspension.

The adsorption of polymers is more complex than surfactant adsorption, since the various interactions (chain–surface, chain–solvent and surface–solvent) must be considered, as well as the conformation of the polymer chain on the surface [5]. As discussed in Chapter 6, complete information on polymer adsorption may be obtained if the segment density distribution can be determined – that is, the segment concentration in all layers parallel to the surface. However, such information is generally unavailable, and therefore three main parameters must be determined, namely the amount of adsorption Γ per unit area, the fraction p of segments in direct contact with the surface (i.e., in trains), and the adsorbed layer thickness δ.

The amount of adsorption Γ can be determined in the same way as for surfactants, although in this case the adsorption process may take a long equilibrium time. Most polymers show a high-affinity isotherm, as is illustrated in Figure 19.5.

This implies that the first added molecules are completely adsorbed and the isotherm cuts the y-axis at $C_2 = 0$. For desorption to occur, the polymer concentration in the supernatant liquid must approach zero, and this implies irreversible adsorption. As discussed in Chapter 6, the magnitude of saturation adsorption will

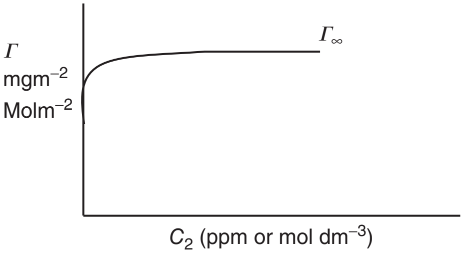

Figure 19.5 High-affinity isotherm.

depend on the molecular weight of the polymer, the temperature, and the solvency of the medium for the chains.

The fraction of segments p in trains can be determined using spectroscopic techniques such IR, electron spin resonance (ESR) and NMR. As discussed in Chapter 6, p depends on surface coverage, the polymer molecular weight and the solvency of the medium for the chains.

Several techniques may be applied for determination of the adsorbed layer thickness δ, and these were described in detail in Chapter 6.

19.3
Assessment of Sedimentation of Suspensions

As mentioned in Chapter 9, most suspensions undergo sedimentation on standing due to gravity and the density difference $\Delta\rho$ between the particles and the dispersion medium; this applies particularly when the particle radius exceeds 50 nm and when $\Delta\rho > 0.1$. In this case, the Brownian diffusion cannot overcome the gravity force and sedimentation occurs, resulting in an increasing particle concentration from the top to the bottom of the container. As discussed in Chapter 10, in order to prevent particle sedimentation, ‘‘thickeners’’ (rheology modifiers) are added in the continuous phase. The sedimentation of the suspension is characterised by the sedimentation rate, sediment volume, the change in particle size distribution during settling, and the stability of the suspension to sedimentation. The assessment of sedimentation of a suspension depends on the force applied to the particles in the suspension, namely gravitational, centrifugal, and electrophoretic. The sedimentation processes are complex and subject to various errors in sedimentation measurements [6]. A suspension is usually agitated before measuring sedimentation, to ensure an initially homogeneous system of particles in random motion. However, vigorous agitation or the use of ultrasonic cavitation must be avoided to prevent any breakdown of aggregates and change in the particle size distribution.

Several physical measurements can be applied to assess sedimentation, and these methods have been described in detail by Kissa [6]. The simplest method is to measure the density of the settling suspension at a known depth, using a hydrometer, but unfortunately this method is highly invasive due to disturbance of the suspension by the hydrometer. A more accurate method is to use a sedimentation balance, whereby the sediment accumulated at the base of the sedimentation column is collected and weighed. Manometric methods that use a capillary side-arm to measure the difference between the densities of the pure sedimentation fluid and that of the suspension can also be applied. Several electrical methods can be used to assess sedimentation, as most suspensions have complex electrical permittivities; however, it may require the measurement of both capacitance and conductivity to determine the solid volume fraction at depth h and time t. This method has the advantage of being noninvasive, as the sensing electrodes do not have to be in direct contact with the dispersion. A more convenient method is to use ultrasound probes at various heights from the top to the bottom of the sedimentation tube. The ultrasound velocity and attenuation depends on the volume fraction of the suspension, and this allows the solids content to be obtained as a function of height in the sedimentation tube. An alternative optical technique is to measure the back-scattering of near-IR radiation at various heights of the sedimentation tube; a commercially available apparatus, the Turboscan, can be used for this purpose.

Several other techniques have been designed to monitor the sedimentation of suspensions, of which photosedimentation, X-ray sedimentation and laser anemometry are worthy of mention. The simplest sedimentation test is based on the visual observation of settling, whereby the turbidity of a suspension is estimated visually, or the height of the sediment and sediment volume are recorded as a function of time. Although this visual estimation of sedimentation is only qualitative, it is adequate for many practical situations.

The characterisation of suspensions and the determination of particle size distribution requires quantitative sedimentation methods, however, and in this respect instrumental techniques have been developed to measure the turbidity of the suspension as a function of time, either by monitoring the turbidity of the bulk suspension or by withdrawing a sample at a given height of the settling suspension. The earlier instruments used for measuring the turbidity of suspensions, called nephelometers, have evolved into instruments with a more sophisticated optical system. Photosedimentometers monitor gravitational particle sedimentation by the photoelectric measurement of incident light under steady-state conditions. For this, a horizontal beam of parallel light is projected through a suspension in a sedimentation column to impact a photocell. Double-beam photosedimentometers using matched photocells – one for the sample and the other for the reference beam – were later developed. A more sophisticated method was also introduced which used a linear charge-coupled photodiode array as the image sensor to convert the light intensity attenuated by the particles into an electric signal. The output of each of the photodetectors is handled by a computer, independently, such that the settling distance between any point in the liquid and the surface of the liquid can be measured accurately, without using a mechanical device. As a consequence, the particle measurement is rapid, requiring only about 5 min to determine the particle size distribution. More recently, the use of fibre optics has allowed the scanning of sedimentation columns without moving parts, or with a fibre optic probe that can be moved inside the sedimentation column.

Laser anemometry, also described as laser Doppler velocity (LDV) measurement, is a sensitive technique that can extend the range of photosedimentation methods. It has been applied in a sedimentometer to measure particle sizes as small as 0.5 μm.

X-ray sedimentometers measure X-ray absorption to determine concentration gradients in sedimenting suspensions. The use of X-ray and γ-rays has been proposed as transmittance probes that correlate transmitted radiation with the density of suspension. In this case, the X-ray transmittance T is directly related to the weight of particles by an exponential relationship, analogous to the Lambert–Beer law governing the transmittance of visible radiation,

$$\ln T = -A\varphi_{\mathrm{s}} \tag{19.8}$$

where A is a particle-, medium- and equipment constant, and ϕ_{s} is the volume fraction of particles in the suspension.

The concentration of particles remaining in the liquid at various sedimentation depths is determined by using a finely collimated beam of X-rays, while the time required for sedimentation measurements can be reduced by continuously changing the effective sedimentation depth. The concentration of particles remaining at various depths is measured as a function of time. X-ray sedimentometers can be used for particles containing elements with atomic numbers above 15 and, therefore, the method cannot be applied to measure the sedimentation of organic pigments.

It should be mentioned that gravitational sedimentation is often too slow, particularly if the particles are small and have a density that is not appreciably higher than that of the medium. The application of a centrifugal force accelerates sedimentation, allowing results to be obtained within a reasonable time, although data obtained by centrifugation do not always correlate with those resulting from settling under gravity. This is particularly the case with suspensions that are weakly flocculated, where the loose structure may break-up on application of a centrifugal force. The interaction between the particles may also change when a high gravitational force is applied, and this casts doubt on the use of centrifugation as an accelerated test for the prediction of sedimentation.

19.4
Assessment of Flocculation and Ostwald Ripening (Crystal Growth)

The assessment of flocculation and Ostwald ripening of a suspension requires measurement of the particle size and shape distribution as a function of time. Several techniques may be applied for this purpose, and these are summarised below [6].

19.4.1
Optical Microscopy

This is by far the most valuable tool for the qualitative or quantitative examination of suspensions. Information on the size, shape, morphology and aggregation of particles can be conveniently obtained, with minimum time required for sample preparation. As individual particles can be directly observed, and their shape examined, optical microscopy is considered to be the only absolute method for particle characterisation. Unfortunately, however, optical microscopy has some limitations. First, the minimum size that can be detected; the practical lower limit for the accurate measurement of particle size is 1.0 μm, although some detection may be obtained down to 0.3 μm. Second, the image contrast may be insufficient for observations, particularly when using a video camera (mostly for convenience). The contrast can be improved by reducing the aperture of the iris diaphragm, but this will also reduce the resolution. The image contrast will depend on the refractive index of the particles relative to that of the medium; hence, contrast can be improved by increasing the difference between the refractive index of the particles and the immersion medium. Unfortunately, changing the medium of the suspension is not practical as this may affect the state of the dispersion. Fortunately, water with a refractive index of 1.33 is a suitable medium for most organic particles, which normally have a refractive index > 1.4.

The ultramicroscope, by virtue of dark-field illumination, extends the useful range of optical microscopy to small particles not visible in a bright-light illumination. Dark-field illumination utilizes a hollow cone of light at a large angle of incidence, and the image is formed by light scattered from the particles against a dark background. As a consequence, particles which are about 10-fold smaller than those visible by bright light illumination can be detected. However, the image obtained is abnormal and the particle size cannot be accurately measured. For that reason, the electron microscope (see below) has largely displaced the ultramicroscope, except in dynamic studies using flow ultramicroscopy.

Three main variants of optical microscopy are available, and these will be described in the following sections.

19.4.1.1 Phase-Contrast Microscopy

This utilizes the difference between the diffracted waves from the main image and the direct light from the light source. The specimen is illuminated with a light cone, and this illumination is within the objective aperture. The light illuminates the specimen and generates zero-order and higher orders of diffracted light. The zero-order light beam passes through the objective and a phase plate which is located at the objective back focal plane. The difference between the optical path of the direct light beam and that of the beam diffracted by a particle causes a phase difference. The constructive and destructive interferences result in brightness changes which enhance the contrast, and this produces sharp images that allow particle size measurements to be obtained more accurately. The phase contrast microscope has a plate in the focal plane of the objective back focus. In addition, instead of a conventional iris diaphragm the condenser is equipped with a ring that is matched in its dimensions to the phase plate.

19.4.1.2 Differential Interference Contrast (DIC) microscopy

This provides a better contrast than the phase-contrast method by utilizing a phase difference to improve contrast. However, separation and recombination of the light beam into two beams is accomplished using prisms. DIC microscopy generates interference colours, and the contrast effects indicate the refractive index difference between the particle and medium.

19.4.1.3 Polarised Light Microscopy

This illuminates the sample with linearly or circularly polarised light, either in a reflection or transmission mode. One polarising element, located below the stage of the microscope, converts the illumination to polarised light, while a second polariser is located between the objective and the ocular and is used to detect polarised light. Linearly polarised light cannot pass the second polariser in a crossed position, unless the plane of polarisation has been rotated by the specimen. Various characteristics of the specimen can be determined, including anisotropy, polarisation colours, birefringence, and polymorphism.

19.4.1.4 Sample Preparation for Optical Microscopy

A drop of suspension is placed on a glass slide and covered with a coverslip. If the suspension has to be diluted, then the dispersion medium (obtained by centrifugation and/or filtration of the suspension) must be used as a diluent in order to avoid aggregation. At low magnification, the distance between the objective and the sample is usually adequate for manipulating the sample, but at high magnification the objective may be too close to the sample. An adequate working distance can be obtained, while maintaining high magnification, by using a more powerful eyepiece with a low-power objective. For suspensions encountering Brownian motion (when the particle size is relatively small), microscopic examination of moving particles can become difficult. In this case, the image can be recorded on a photographic film or video tape or disc (using computer software).

19.4.1.5 Particle Size Measurements Using Optical Microscopy

The optical microscope can be used to observe dispersed particles and flocs. Particle sizing can be carried out using manual, semiautomatic or automatic image analysis techniques. In the (rather tedious) manual method, the microscope is fitted with a minimum of 10× and 43× achromatic or apochromatic objectives, equipped with high-numerical apertures (10×, 15× and 20×), a mechanical XY stage, a stage micrometer, and a light source. The direct measurement of particle size is aided by a linear scale or globe-and-circle graticules in the ocular. The linear scale is useful mainly for spherical particles, with a relatively narrow particle size distribution. The globe-and-circle graticules are used to compare the projected particle area with a series of circles in the ocular graticule. The size of spherical particles can be expressed by the diameter, but for irregularly shaped particles various statistical diameters are used. One difficulty with evaluating dispersions by optical microscopy is the quantification of data, as the number of particles in at least six different size ranges must be counted to obtain a distribution. However, this problem can be alleviated by using automatic image analysis, which can also give an indication of the floc size and its morphology.

19.4.2
Electron Microscopy

Electron microscopy utilizes an electron beam to illuminate the sample. The electrons behave as charged particles which can be focused by annular electrostatic or electromagnetic fields surrounding the electron beam. Due to the very short wavelength of electrons, the resolving power of an electron microscope exceeds that of an optical microscope about 200-fold. The resolution depends on the accelerating voltage, which in turn determines the wavelength of the electron beam; indeed, magnifications as high as ×200 000 can be reached with intense beams, though this may damage the sample. In general, the accelerating voltage is kept below 100–200 kV and the maximum magnification obtained is below ×100 000. The main advantage of electron microscopy is the high resolution, sufficient for resolving details separated by only a fraction of a nanometre. The increased depth of field, usually by about 10 μm or about 10-fold that of an optical microscope, is another important advantage of electron microscopy. Nevertheless, electron microscopy has certain disadvantages, including sample preparation, selection of the area viewed, and interpretation of the data acquired. The main drawback of electron microscopy is the potential risk of altering or damaging the sample, perhaps introducing artefacts and causing possible aggregation of the particles during sample preparation. The suspension must be dried or frozen, and removal of the dispersion medium may alter the distribution of the particles. If the particles do not conduct electricity, the sample must be coated with a conducting layer such as gold, carbon or platinum, in order to avoid negative charging by the electron beam. The two main types of electron microscopy are transmission electron microscopy and scanning electron microscopy.

19.4.2.1 Transmission Electron Microscopy

Transmission electron microscopy (TEM) displays an image of the specimen on a fluorescent screen, and the image can be recorded on a photographic plate or film. TEM can be used to examine particles in the range of 0.001 to 5 μm. The sample is deposited on a Formvar (polyvinyl formal) film which rests on a grid to prevent the sample from becoming charged. The sample is usually observed as a replica by coating with an electron-transparent material (e.g., gold or graphite). Sample preparation for TEM may alter the state of dispersion and cause aggregation, and consequently freeze-fracturing techniques have been developed to avoid some of the changes that may occur during sample preparation. Freeze-fracturing allows dispersions to be examined without dilution, and replicas can be made of dispersions containing water. In TEM it is essential to have a high cooling rate in order to avoid the formation of ice crystals in the sample.

19.4.2.2 Scanning Electron Microscopy

Scanning electron microscopy (SEM) can show particle topography by scanning a very narrowly focused beam across the particle surface. The electron beam is directed either normally or obliquely at the surface, after which the back-scattered or secondary electrons are detected in a raster pattern and displayed on a monitor screen. The image provided by secondary electrons exhibits good three-dimensional detail. The back-scattered electrons, which are reflected from the incoming electron beam, indicate regions of high electron density. Most SEM instruments are equipped with both types of detector, and the resolution of the microscope will depend on the energy of the electron beam (which does not exceed 30 kV), and hence the resolution is lower than that obtained with TEM. One very important advantage of SEM is elemental analysis using energy-dispersive X-ray analysis (EDX). If the electron beam impinging on the specimen has sufficient energy to excite atoms on the surface, then the sample will emit X-rays. The energy required for X-ray emission is characteristic of a given element and, since the emission is related to the number of atoms present, a quantitative determination will be possible.

Scanning transmission electron microscopy (STEM), coupled with EDX, has been used to determine metal particle sizes. The specimens for STEM are prepared by dispersing the sample ultrasonically in methanol and placing one drop of the suspension onto a Formvar film supported on a copper grid.

19.4.3
Confocal Laser Scanning Microscopy

Confocal laser scanning microscopy (CLSM) is a very useful technique for the identification of suspensions. It uses a variable pinhole aperture or variable-width slit to illuminate only the focal plane by the apex of a cone of laser light. Out-of-focus items are dark and do not distract from the contrast of the image. As a result of extreme depth discrimination (optical sectioning), the resolution is considerably improved (by up to 40% compared to optical microscopy). The CLSM technique acquires images by laser scanning or uses computer software to subtract out-of-focus details from the in-focus image. The images are stored as the sample is advanced through the focal plane in increments as small as 50 nm. Three-dimensional images can be constructed to show the shape of the particles.

19.4.4
Scanning Probe Microscopy

Scanning probe microscopy (SPM) can be used to measure the physical, chemical and electrical properties of the sample by scanning the particle surface with a tiny sensor of high resolution. The scanning probe microscope does not measure a force directly; rather, the deflection of a cantilever which is equipped with a tiny stylus (the tip) functioning as the probe is measured. The deflection of the cantilever is monitored by: (i) a tunneling current; (ii) laser deflection beam from the reverse side of the cantilever; (iii) optical interferometry; (iv) the laser output, controlled by the cantilever used as a mirror in the laser cavity; and (v) a change in capacitance. SPM generates a three-dimensional image and allows calibrated measurements in three (x,y,z) coordinates. SPM not only produces a highly magnified image, but also provides valuable information on sample characteristics. Unlike electron microscopy, which requires vacuum for its operation, SPM can be operated under ambient conditions and, with some limitation, in liquid media.

19.4.5
Scanning Tunneling Microscopy

In scanning tunneling microscopy (STM), an electric current is measured that flows through a thin insulating layer (vacuum or air) separating two conductive surfaces. The electrons are visualised to ‘‘tunnel’’ through the dielectric and generate a current, I, that depends exponentially on the distance, s, between the tiny tip of the sensor and the electrically conductive surface of the sample. The STM tips are usually prepared by etching a tungsten wire in an NaOH solution until the wire forms a conical tip; Pt/Ir wire has also been used. In the contrast current imaging mode, the probe tip is raster-scanned across the surface and a feedback loop adjusts the height of the tip in order to maintain a constant tunnel current. When the energy of the tunneling current is sufficient to excite luminescence, the tip–surface region emits light and functions as an excitation source of subnanometre dimensions. *In situ* STM has revealed a two-dimensional molecular lamellar arrangement of long-chain alkanes adsorbed onto the basal plane of graphite. The thermally induced disordering of adsorbed alkanes was studied using variable-temperature STM, and an atomic-scale resolution of the disordered phase was claimed by studying the quenched high-temperature phase

19.4.6
Atomic Force Microscopy

Atomic force microscopy (AFM) allows the topography of a sample to be scanned by using a very small tip made from silicon nitride. The tip is attached to a cantilever that is characterised by its spring constant, resonance frequency, and a quality factor. The sample rests on a piezoceramic tube which can be moved horizontally (x,y motion) and vertically (z motion). Displacement of the cantilever is measured by the position of a laser beam reflected from the mirrored surface on the top side of the cantilever, whereby the reflected laser beam is detected by a photodetector. AFM can be operated in either contact or a noncontact mode. In contact mode the tip travels in close contact with the surface, whereas in noncontact mode the tip hovers 5–10 nm above the surface.

19.5
Scattering Techniques

These are by far the most useful methods for characterizing suspensions, and in principle they can provide quantitative information on the particle size distribution, floc size, and shape. The only limitation of the methods is the need to use sufficiently dilute samples to avoid interference such as multiple scattering, which makes the interpretation of results difficult. However, back-scattering methods have recently been designed to allow samples to be measure without dilution. In principle, any electromagnetic radiation can be used such as light, X-ray or neutrons, but in most industrial laboratories only light scattering is applied (using lasers).

19.5.1
Light-Scattering

Light-scattering techniques can be conveniently divided into the following classes: (i) time-average light scattering; (ii) static or elastic scattering; (iii) Turbidity measurements, which can be carried out using a simple spectrophotometer; (iv) light diffraction techniques; and (v) dynamic light scattering (DLS) and quasi-elastic light scattering (QELS), that usually is referred to as photon correlation spectroscopy (PCS). This is a rapid technique that is very suitable for measuring submicron particles or droplets (nanosize range). A further category includes back-scattering techniques that are suitable for measuring concentrated samples. The application of any of these methods will depend on the information required and the availability of the instrumentation.

19.5.1.1 Time-Average Light Scattering

In this method the dispersion that is sufficiently diluted to avoid multiple scattering is illuminated by a collimated light (usually laser) beam, and the time-average intensity of scattered light is measured as a function of the scattering angle θ. Static light scattering is termed elastic scattering. Three regimes can be identified.

Rayleigh Regime In the Rayleigh regime, the particle radius R is smaller than $\lambda/20$ (where λ is the wavelength of the incident light). The scattering intensity is given by the equation,

$$I(Q) = [\text{Instrument constant}][\text{Material constant}]\ N\ V_{\text{p}}^{2} \tag{19.9}$$

where Q is the scattering vector that depends on the wavelength of light λ used, and is given by,

$$Q = \left(\frac{4\pi n}{\lambda}\right)\sin\left(\frac{\theta}{2}\right) \tag{19.10}$$

where n is the refractive index of the medium.

The material constant depends on the difference between the refractive index of the particle and that of the medium. N is the number of particles and V_{p} is the volume of each particle. Assuming that the particles are spherical, the average size can be obtained using Equation (19.9).

The Rayleigh equation reveals two important relationships: (i) the intensity of scattered light increases with the square of the particle volume and, consequently, with the sixth power of the radius R; hence, scattering from larger particles may dominate scattering from smaller particles; and (ii) the intensity of scattering is inversely proportional to λ^4, and hence a decrease in wavelength will substantially increase the scattering intensity.

19.5.1.2 **Rayleigh–Gans–Debye Regime (RGD) $\lambda/20 < R < \lambda$**

The Rayleigh-Gans-Debye (RGD) regime is more complicated than the Rayleigh regime, and the scattering pattern is no longer symmetrical about the line corresponding to the 90° angle but favours forward scattering ($\theta < 90°$) or back-scattering ($180° > \theta > 90°$). Since the preference of forward scattering increases with increasing particle size, the ratio $I_{45}°/I_{135}°$ can indicate the particle size.

Mie Regime $R > \lambda$ In this case, the scattering behaviour is more complex than the RGD regime, and the intensity exhibits maxima and minima at various scattering angles, depending on the particle size and refractive index. The Mie theory for light scattering can be used to obtain the particle size distribution using numerical solutions. Information can also be obtained on the particle shape.

19.5.2
Turbidity Measurements

Turbidity (total light-scattering technique) can be used to measure particle size, flocculation and particle sedimentation. This technique is simple and easy to use, employing either a single- or double-beam spectrophotometer or a nephelometer.

For nonabsorbing particles the turbidity τ is given by

$$\tau = (1/L)\ln(I_o/I) \tag{19.11}$$

where L is the path length, I_o is the intensity of incident beam, and I is the intensity of the transmitted beam.

The particle size measurement assumes that light scattering by a particle is singular and independent of other particles, and that any multiple scattering will complicate the analysis. According to the Mie theory, the turbidity is related to the particle number N and their cross-section πr^2 (where r is the particle radius) by

$$\tau = Qpr^2N \tag{19.12}$$

where Q is the total Mie scattering coefficient. Q depends on the particle size parameter α (which in turn depends on particle diameter and wavelength of incident light λ) and the ratio of refractive index of the particles and medium m.

Q depends on α in an oscillatory mode and exhibits a series of maxima and minima, the positions of which depend on m. For particles with $R < (1/20)\ \lambda$, $\alpha < 1$ and Q can be calculated by using the Rayleigh theory. For $R > \lambda$, Q approaches

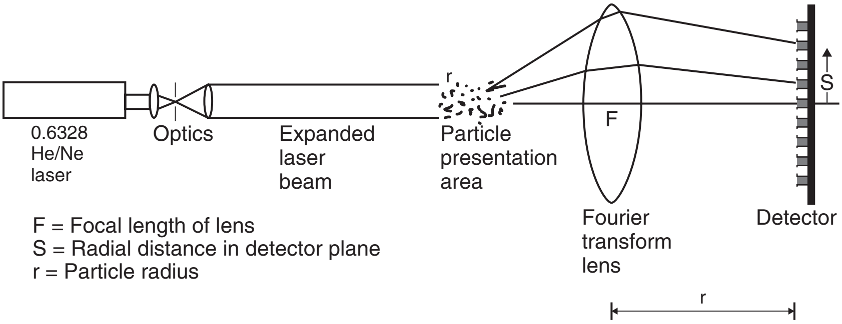

Figure 19.6 Schematic illustration of light-diffraction particle sizing system.

2 and between these two extremes, and the Mie theory is used. If the particles are not monodisperse (as is the case with most practical systems), the particle size distribution must be taken into account. By using this analysis the particle size distribution can be established, using numerical solutions.

19.5.3
Light-Diffraction Techniques

This is a rapid and nonintrusive technique for the determination of particle size distribution in the range 2 to 300 μm, with good accuracy for most practical purposes. Light diffraction provides an average diameter over all particle orientations as randomly oriented particles pass the light beam A collimated and vertically polarised laser beam illuminates a particle dispersion and generates a diffraction pattern with the undiffracted beam in the centre. The energy distribution of the diffracted light is measured by a detector which consists of light-sensitive circles separated by isolating circles of equal width. The angle formed by the diffracted light increases with decreasing particle size. The angle-dependent intensity distribution is converted by Fourier optics into a spatial intensity distribution $I(r)$, after which the spatial intensity distribution is converted into a set of photocurrents and the particle size distribution is calculated using a computer. Several commercial instruments are available, including the Malvern Master Sizer (Malvern, UK), Horriba (Japan), and the Coulter LS Sizer (USA). A schematic illustration of the set-up is shown in Figure 19.6

In accordance with the Fraunhofer theory (which was introduced by Fraunhofer over 100 years ago), the special intensity distribution is given by,

$$I(r) = \int_{X_{\min}}^{X_{\max}} N_{\text{tot}} q_{\text{o}}(x) I(r, x) dx \tag{19.13}$$

where $I(r,x)$ is the radial intensity distribution at radius r for particles of size x, N_{tot} is the total number of particles, and $q_{\text{o}}(x)$ describes the particle size distribution.

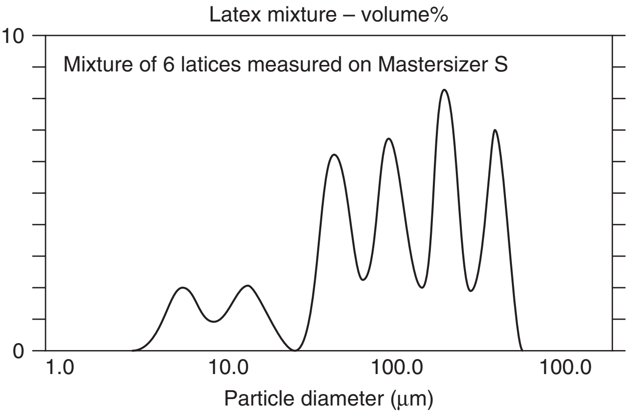

Figure 19.7 Single measurement of a mixture of six standard lattices using the Master Sizer.

The radial intensity distribution $I(r,x)$ is given by,

$$I(r,x) = I_o \left(\frac{\pi x^2}{2f} \right)^2 \left(\frac{J_i(k)}{k} \right)^2 \tag{19.14}$$

with $k = (pxr)/(\mathrm{l}f)$

where r is the distance to the centre of the disc, λ is the wavelength, f is the focal length, and J_i is the first-order Bessel function.

The Fraunhofer diffraction theory applies to particles whose diameter is considerably larger than the wavelength of illumination. As shown in Figure 19.6, a He/Ne laser is used with $\lambda = 632.8$ nm for particle sizes mainly in the 2 to 120 µm range. In general, the diameter of the sphere-shaped particle should be at least four times the wavelength of the illumination light. The accuracy of particle size distribution determined by light diffraction is not very good if a large fraction of particles with diameter <10 µm is present in the suspension. For small particles (diameter <10 µm), the Mie theory is more accurate if the necessary optical parameters such as the refractive index of particles and medium and the light absorptivity of the dispersed particles, is known. Most commercial instruments combine light diffraction with forward light scattering to obtain a full particle size distribution covering a wide range of sizes. As an illustration, Figure 19.7 shows the result of particle sizing using a six-component mixture of standard polystyrene lattices (using a Master Sizer).

Most practical suspensions are polydisperse and generate a very complex diffraction pattern. The diffraction pattern of each particle size overlaps with diffraction patterns of other sizes, while the particles of different sizes diffract light at different angles and the energy distribution becomes a very complex pattern. However, the manufacturers of light-diffraction instruments (such as Malvern, Coulters and Horriba) have developed numerical algorithms relating diffraction patterns to particle size distribution.

Several factors can affect the accuracy of Fraunhofer diffraction: (i) particles smaller than the lower limit of Fraunhofer theory; (ii) nonexistent ''ghost'' particles in particle size distribution obtained by Fraunhofer diffraction applied to systems containing particles with edges, or a large fraction of small particles (below 10 μm); (iii) computer algorithms that are unknown to the user and vary with the manufacturer's software version; (iv) the composition-dependent optical properties of the particles and dispersion medium; and (v) if the density of all particles is not the same, the result may be inaccurate.

19.5.4
Dynamic Light Scattering (DLS): Photon Correlation Spectroscopy (PCS)

DLS is a method that measures the time-dependent fluctuation of scattered intensity, and is also referred to as quasi-elastic light scattering or photon correlation spectroscopy. The latter term is the most commonly used for describing the process, since most dynamic scattering techniques employ autocorrelation.

In PCS, Brownian motion is used to measure the particle size. As a result of Brownian motion of dispersed particles, the intensity of the scattered light undergoes fluctuations that are related to the velocity of the particles. As larger particles move less rapidly than their smaller counterparts, the intensity fluctuation (intensity versus time) pattern will depend on particle size, as illustrated in Figure 19.8. The velocity of the scatterer is measured in order to obtain the diffusion coefficient.

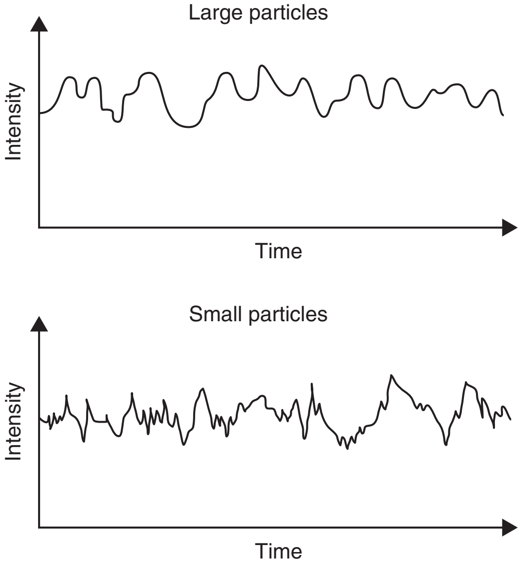

Figure 19.8 Schematic representation of the intensity fluctuation for large and small particles.

In a system where the Brownian motion is not interrupted by sedimentation or particle–particle interaction, the movement of particles is random. Hence, the intensity fluctuations observed after a large time interval do not resemble those fluctuations observed initially, but rather represent a random distribution of particles. Consequently, the fluctuations observed at a large time delay are not correlated with the initial fluctuation pattern. However, when the time differential between the observations is very small (a nanosecond or a microsecond), both positions of particles are similar and the scattered intensities will be correlated, and when the time interval is increased then the correlation will be decreased. The decay of correlation is particle size-dependent; that is, the smaller the particles the faster the decay.

The fluctuations in scattered light are detected by a photomultiplier and recorded; the data containing information on particle motion are then processed by a digital correlator. The latter compares the intensity of scattered light at time t, $I(t)$, to the intensity at a very small time interval τ later, $I(t+\tau)$, and constructs the second-order autocorrelation function $G_2(\tau)$ of the scattered intensity,

$$G_2(\tau) = < I(t)I(t+\tau) > \tag{19.15}$$

The experimentally measured intensity autocorrelation function $G_2(\tau)$ depends only on the time interval τ, and is independent of t, the time when the measurement started.

PCS can be measured in a homodyne where only scattered light is directed to the detector. It can also be measured in heterodyne mode where a reference beam split from the incident beam is superimposed on scattered light. The diverted light beam functions as a reference for the scattered light from each particle.

In the homodyne mode, $G_2(\tau)$ can be related to the normalised field autocorrelation function $g_1(\tau)$ by,

$$G_2(\tau) = A + Bg_1^2(\tau) \tag{19.16}$$

where A is the background term designated as the baseline value and B is an instrument-dependent factor. The ratio B/A is regarded as a quality factor of the measurement or the signal-to-noise ratio, and is expressed sometimes as the % merit.

The field autocorrelation function $g_1(\tau)$ for a monodisperse suspension decays exponentially with τ,

$$g_1(\tau) = \exp(-\Gamma\tau) \tag{19.17}$$

where Γ is the decay constant (s^{-1}).

The substitution of Equation (19.17) into Equation (19.16) yields the measured autocorrelation function,

$$G_2(\tau) = A + B\exp(-2\Gamma\tau) \tag{19.18}$$

The decay constant Γ is linearly related to the translational diffusion coefficient D_T of the particle,

$$\Gamma = D_T q^2 \tag{19.19}$$

The modulus q of the scattering vector is given by,

$$q = \frac{4\pi n}{\lambda_o} \sin\left(\frac{\theta}{2}\right) \tag{19.20}$$

where n is the refractive index of the dispersion medium, θ is the scattering angle, and λ_o is the wavelength of the incident light in vacuum.

PCS determines the diffusion coefficient, and the particle radius R is obtained using the Stokes–Einstein equation,

$$D = \frac{kT}{6\pi\eta R} \tag{19.21}$$

where k is the Boltzmann constant, T is the absolute temperature, and η is the viscosity of the medium.

The Stokes–Einstein equation is limited to noninteracting, spherical and rigid spheres. The effect of particle interaction at relatively low particle concentration, c, can be taken into account by expanding the diffusion coefficient into a power series of concentration,

$$D = D_o(1 + k_D c) \tag{19.22}$$

where D_o is the diffusion coefficient at infinite dilution and k_D is the virial coefficient that is related to particle interaction. D_o can be obtained by measuring D at several particle number concentrations and extrapolating to zero concentration.

For polydisperse suspensions, the first-order autocorrelation function is an intensity-weighted sum of autocorrelation function of particles contributing to the scattering,

$$g_1(\tau) = \int_0^\infty C(\Gamma) \exp(-\Gamma\tau) \mathrm{d}\Gamma \tag{19.23}$$

where $C(\Gamma)$ represents the distribution of decay rates.

For a narrow particle size distribution the cumulant analysis is usually satisfactory. The cumulant method is based on the assumption that, for monodisperse suspensions $g_1(\tau)$ is monoexponential. Hence, the log of $g_1(\tau)$ versus τ yields a straight line with a slope equal to Γ,

$$\ln g_1(\tau) = 0.5 \ln(B) - \Gamma\tau \tag{19.24}$$

where B is the signal-to-noise ratio.

The cumulant method expands the Laplace transform about an average decay rate,

$$< \Gamma > = \int_0^\infty \Gamma C(\Gamma) \mathrm{d}\Gamma \tag{19.25}$$

The exponential in Equation (19.24) is expanded about an average and integrated term,

$$\ln g_1(\tau) = \langle \Gamma \rangle \tau + (\mu_2 \tau^2)/2! - (\mu_3 \tau^3)/3! + ... \tag{19.26}$$

An average diffusion coefficient is calculated from $<\Gamma>$ and the polydispersity (termed the polydispersity index) is indicated by the relative second moment,

$\mu_2/\langle\Gamma\rangle^2$. A constrained regulation method (CONTIN) yields several numerical solutions to the particle size distribution, and this is normally included in the software of the PCS machine.

PCS is a rapid, absolute, nondestructive and rapid method for particle size measurements, but it does have some limitations. The main disadvantage is the poor resolution of particle size distribution, and it also suffers from the limited size range (absence of any sedimentation) that can be accurately measured. Several instruments are commercially available, for example by Malvern, Brookhaven, and Coulter. The most recently developed instrument that is convenient to use is HPPS, supplied by Malvern (UK). This allows the particle size distribution to be measured without the need for too much dilution (which may cause some particle dissolution).

19.5.5
Back-Scattering Techniques

This method is based on the use of fibre optics, and is sometimes referred to as fibre optic dynamic light scattering (FODLS). The method allows measurements to be made at high particle number concentrations by employing either one or two optical fibres (fibre bundles may also be used). The exit port of the optical fibre (optode) is immersed in the sample, and the scattered light in the same fibre is detected at a scattering angle of 180° (i.e., back-scattering).

The above technique is suitable for on-line measurements during the manufacture of a suspension or emulsion, and several commercial instruments are currently available (e.g., Lesentech, USA).

19.6
Measurement of Rate of Flocculation

Two general techniques may be applied for measuring the rate of flocculation of suspensions, both of which can only be applied to dilute systems. The first method is based on measuring the scattering of light by the particles. For monodisperse particles with a radius that is less than $\lambda/20$ (where λ is the wavelength of light), the Rayleigh equation can be applied whereby the turbidity, τ_o, is given by,

$$\tau_o = A'\, n_o\, V_1^2 \tag{19.27}$$

where A' is an optical constant (which is related to the refractive index of the particle and medium and the wavelength of light) and n_o is the number of particles, each with a volume V_1.

By combining the Rayleigh theory with the Smoluchowski–Fuchs theory of flocculation kinetics [7, 8], the following expression can be obtained for the variation of turbidity with time,

$$\tau = A'\, n_o\, V_1^2 (1 + 2 n_o k t) \tag{19.28}$$

where k is the rate constant of flocculation.

The second method for obtaining the rate constant of flocculation is by direct particle counting as a function of time. For this purpose, optical microscopy or image analysis may be used, provided that the particle size is within the resolution limit of the microscope. Alternatively, the particle number may be determined using electronic devices such as the Coulter counter or flow ultramicroscopy.

The rate constant of flocculation is determined by plotting $1/n$ versus t, where n is the number of particles after time t, that is,

$$\left(\frac{1}{n}\right) = \left(\frac{1}{n_o}\right) + kt \tag{19.29}$$

The rate constant k of slow flocculation is usually related to the rapid rate constant k_o (the Smoluchowski rate) by the stability ratio W,

$$W = \left(\frac{k}{k_o}\right) \tag{19.30}$$

Usually, log W is plotted versus log C (where C is the electrolyte concentration) to obtain the critical coagulation concentration (c.c.c.), which is the point at which log $W = 0$.

One very useful approach to measuring flocculation is to use the single-particle optical method. The particles of a suspension that are dispersed in a liquid will flow through a narrow, uniformly illuminated cell, but if the suspension is made sufficiently dilute (using the continuous medium) then the particles will pass through the cell individually. A particle passing through the light beam that is illuminating the cell will generate an optical pulse that can be detected by a sensor. Hence, if the particle size is greater than the wavelength of light (>0.5 μm), the peak height will depend on the projected area of the particle. If the particle size is <0.5 μm, the scattering will dominate the response, but for particles >1 μm a light obscuration (also called blockage or extinction) sensor can be used. For particles smaller than 1 μm, a light-scattering sensor will be more sensitive.

The above method can be used to determine the size distribution of aggregating suspensions. In this case, the aggregated particles pass individually through the illuminated zone and generate a pulse which is collected at a small angle (<3°). At sufficiently small angles, the pulse height will be proportional to the square of the number of monomeric units in an aggregate, and independent of the aggregate shape or its orientation.

19.7
Measurement of Incipient Flocculation

This can be achieved for sterically stabilised suspensions, when the medium for the chains becomes a θ-solvent. This occurs, for example, on heating an aqueous suspension stabilised with PEO or poly(vinyl alcohol) chains. Above a certain temperature (the θ-temperature), which depends on the electrolyte concentration, flocculation of the suspension will occur, and the temperature at which this occurs is defined as the critical flocculation temperature (CFT).

This process of incipient flocculation can be followed by measuring the turbidity of the suspension as a function of temperature. Above the CFT, the turbidity of the suspension rises very sharply.

For the above purpose, the cell in the spectrophotometer that is used to measure turbidity is placed in a metal block that is connected to a temperature-programming unit, which allows the temperature to be increased at a controlled rate.

19.8
Measurement of Crystal Growth (Ostwald Ripening)

Ostwald ripening is the result of the difference in solubility S between small and large particles. Typically, smaller particles have a larger solubility than larger particles, and the effect of particle size on solubility can be described by the Kelvin equation [9],

$$S(r) = S(\infty) \exp\left(\frac{2\sigma V_{\mathrm{m}}}{rRT}\right) \tag{19.31}$$

where $S(r)$ is the solubility of a particle with radius r, $S(\infty)$ is the solubility of a particle with infinite radius, σ is the solid/liquid interfacial tension, V_{m} is the molar volume of the disperse phase, R is the gas constant, and T is absolute temperature.

For two particles with radii r_1 and r_2,

$$\frac{RT}{V_{\mathrm{m}}} \ln\left(\frac{S_1}{S_2}\right) = 2\sigma\left(\frac{1}{r_1} - \frac{1}{r_2}\right) \tag{19.32}$$

where R is the gas constant, T is absolute temperature, M is the molecular weight, and ρ is the density of the particles.

To obtain a measure of the rate of crystal growth, the particle size distribution of the suspension is followed as a function of time, using either a Coulter counter, a Master Sizer or an optical disc centrifuge. Usually, the cube of the average radius is plotted versus time; this gives a straight line from which the rate of crystal growth can be determined (the slope of the linear curve),

$$r^3 = \frac{8}{9}\left[\frac{S(\infty)\ \sigma\ V_{\mathrm{m}}\ D}{\rho\ RT}\right] t \tag{19.33}$$

where D is the diffusion coefficient of the disperse phase in the continuous phase and ρ is the density of the particles.

19.9
Bulk Properties of Suspensions: Equilibrium Sediment Volume (or Height) and Redispersion

For a "structured" suspension, obtained by "controlled flocculation" or the addition of "thickeners" (such polysaccharides, clays or oxides), the "flocs" sediment at a rate depending on their size and porosity of the aggregated mass. After this initial sedimentation, compaction and rearrangement of the floc structure occurs, a phenomenon which is referred to as consolidation.

Normally, in sediment volume measurements, the initial volume V_o (or height H_o) is compared with the ultimately reached value V (or H). A colloidally stable suspension gives a ''close-packed'' structure with relatively small sediment volume (dilatant sediment, referred to as clay). A weakly ''flocculated'' or ''structured'' suspension gives a more open sediment, and hence a higher sediment volume. Thus, by comparing the relative sediment volume V/V_o or height H/H_o, it is possible to distinguish between a clayed and flocculated suspension.

References

1. Lyklema, J. (1987) in *Solid/Liquid Dispersions*, Chapter 3 (ed. Th.F. Tadros), Academic Press, London.
2. Tadros, Th.F. and Lyklema, J. (1968) *J. Electroanal. Chem.*, **17**, 267.
3. Hunter, R.J. (1981) *Zeta Potential in Colloid Science: Principles and Application*, Academic Press, London.
4. Parfitt, G.D. and Rochester, C.H. (eds) (1983) *Adsorption from Solution at the Solid/Liquid Interface*, Academic Press, London.
5. Fleer, G.J., Cohen-Stuart, M.A., Scheutjens, J.M.H.M., Cosgrove, T., and Vincent, B. (1993) *Polymers at Interfaces*, Chapman & Hall, London.
6. Kissa, E. (1999) *Dispersions, Characterisation, Testing and Measurement*, Marcel Dekker, New York.
7. von Smoluchowski, M. (1916) *Phys. Z.*, **17** (557), 585.
8. Fuchs, N. (1936) *Z. Phys.*, **89**, 736.
9. Thompson, W. (Lord Kelvin) (1871) *Philos. Mag.*, **42**, 448.

20
Evaluating Formulations without Dilution: Rheological Techniques

20.1
Introduction

Evaluation of the stability/instability of suspensions without any dilution (which can cause significant changes in the structure of the system) requires carefully designed techniques that should cause as little disturbance to the structure. The most powerful techniques that can be applied in any industrial laboratory are rheological measurements [1–7]. These provide accurate information on the state of the system, such as sedimentation and flocculation, and may also be applied to predict the long-term physical stability of the suspension. The various rheological techniques that can be applied and the measurement procedures are listed below.

- *Steady state shear stress σ-shear rate γ measurements*: This requires the use of a shear rate-controlled instrument, and the results obtained can be fitted to models to obtain the yield value σ_β and the viscosity η as a function of shear rate. Time effects (thixotropy) can also be investigated.
- *Constant stress (creep) measurements*: A constant is stress is applied to the system and the strain γ or compliance J (γ/σ) is followed as a function of time. By measuring creep curves at increasing stress values, it is possible to obtain the residual (zero-shear) viscosity $\eta(o)$ and the critical stress σ_{cr}; that is, the stress above which the structure starts to break down. σ_{cr} is sometimes referred to as the ''true'' yield value.
- *Dynamic (oscillatory) measurements*: A sinusoidal stress or strain with amplitudes σ_o and γ_o is applied at a frequency ω (rad s^{-1}), and the stress and strain are measured simultaneously. For a viscoelastic system, as is the case with most formulations, the stress and strain amplitudes oscillate with the same frequency, but out of phase. The phase angle shift δ is measured from the time shift of the strain and stress sine waves. From σ_o, γ_o and δ, it is possible to obtain the complex modulus $|G^*|$, the storage modulus G' (the elastic component), and the loss modulus G'' (the viscous component). The results are obtained as a function of strain amplitude and frequency.

Formulation of Disperse Systems: Science and Technology, First Edition. Tharwat F. Tadros.

20.2
Steady-State Measurements

Most suspensions, and particularly those with a high volume fraction and/or containing rheology modifiers, do not obey Newton's law. This can be clearly shown from plots of shear stress σ versus shear rate, as illustrated in Figure 20.1. Five different flow curves can be identified: (a) Newtonian; (b) Bingham Plastic; (c) Pseudoplastic (shear thinning); (d) Dilatant (shear thickening); and (e) Yield stress and shear thinning. The variation of viscosity with shear rate for the above five systems is shown in Figure 20.2. Apart from the Newtonian flow (a), all other systems show a change of viscosity with applied shear rate.

20.2.1
Rheological Models for Analysis of Flow Curves

20.2.1.1 Newtonian Systems

$$\sigma = \eta\dot{\gamma} \tag{20.1}$$

where η is independent of the applied shear rate, for example simple liquids and very dilute dispersions.

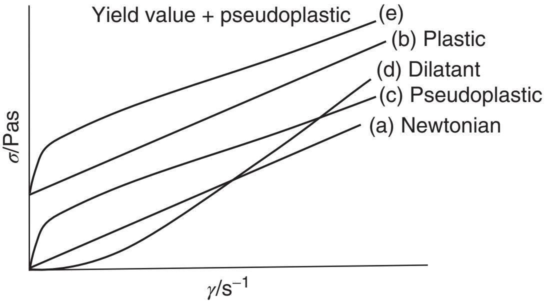

Figure 20.1 Flow curves for various systems.

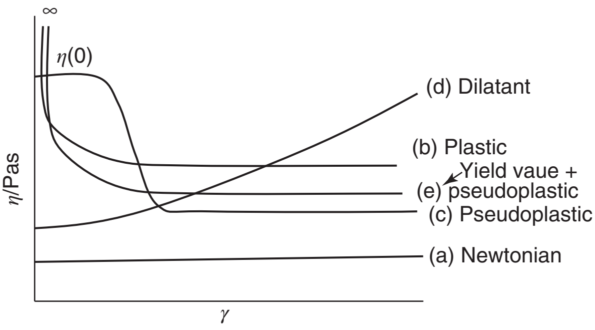

Figure 20.2 Viscosity–shear rate relationship.

20.2.1.2 Bingham Plastic Systems

$$\sigma = \sigma_\beta + \eta_{\text{pl}} \dot{\gamma} \tag{20.2}$$

The system shows a (dynamic) yield stress σ_β that can be obtained by extrapolation to zero shear rate [8]. Clearly, at and below σ_β the viscosity $\eta \to \infty$. The slope of the linear curve gives the plastic viscosity η_{pl}. Some systems, such as clay suspensions, may show a yield stress above a certain clay concentration.

The Bingham equation describes the shear stress/shear rate behaviour of many shear thinning materials at low shear rates. Unfortunately, the value of σ_β obtained depends on the shear rate ranges used for the extrapolation procedure.

20.2.1.3 Pseudoplastic (Shear Thinning) System

In this case, the system does not show a yield value; rather, it shows a limiting viscosity $\eta(\text{o})$ at low shear rates (that is referred to as residual or zero shear viscosity). The flow curve can be fitted to a power law fluid model (Ostwald de Waele)

$$\sigma = k\dot{\gamma}^n \tag{20.3}$$

where k is the consistency index and n is the shear thinning index ($n < 1$).

By fitting the experimental data to Equation (20.3), k and n can be obtained, and the viscosity at a given shear rate can be calculated:

$$\eta = \frac{\sigma}{\dot{\gamma}} = \frac{k\dot{\gamma}^n}{\dot{\gamma}} = k\dot{\gamma}^{n-1} \tag{20.4}$$

As the power law model [Equation (20.3)] fits the experimental results for many non-Newtonian systems over two or three decades of shear rate, this model is more versatile than the Bingham model, although care should be taken when applying this model outside the range of data used to define it. In addition, the power law fluid model fails at high shear rates, whereby the viscosity must ultimately reach a constant value – that is, the value of n should approach unity.

20.2.1.4 Dilatant (Shear Thickening) System

In some cases the very act of deforming a material can cause rearrangement of its microstructure such that the resistance to flow increases with an increase of shear rate. In other words, the viscosity increases with applied shear rate and the flow curve can be fitted with the power law, Equation (20.3), but in this case $n > 1$. The shear thickening regime extends over only about a decade of shear rate. In almost all cases of shear thickening, there is a region of shear thinning at low shear rates.

Several systems can show shear thickening, such as wet sand, corn starch dispersed in milk and some polyvinyl chloride sols. Shear thickening can be illustrated when somebody walks on wet sand such that some water is "squeezed out" and the sand appears dry. The deformation applied by the feet causes a rearrangement of the close-packed structure produced by the water motion, and this process is accompanied by a volume increase (hence the term dilatancy) as a result of "sucking in" of the water. The process amounts to a rapid increase in the viscosity.

20.2.1.5 Herschel–Bulkley General Model

Many systems show a dynamic yield value followed by a shear thinning behaviour [9]. The flow curve can be analysed using the Herschel–Bulkley equation:

$$\sigma = \sigma_\beta + k\dot{\gamma}^n \tag{20.5}$$

When $\sigma_\beta = 0$, Equation (20.14) reduces to the Power Fluid Model, but when $n = 1$, Equation (20.14) reduces to the Bingham model. When $\sigma_\beta = 0$ and $n = 1$, Equation (20.15) becomes the Newtonian equation. The Herschel–Bulkley equation fits most flow curves with a good correlation coefficient, and hence is the most widely used model.

Several other models have been suggested, of which the following is worthy of mentioning.

20.2.1.6 The Casson Model

This is a semi-empirical linear parameter model that has been applied to fit the flow curves of many paints and printing ink formulations [10],

$$\sigma^{1/2} = \sigma_C^{1/2} + \eta_C^{1/2}\dot{\gamma}^{1/2} \tag{20.6}$$

Thus, a plot of $\sigma^{1/2}$ versus γ should give a straight line from which σ_C and η_C can be calculated from the intercept and slope of the line. Care must be taken when using the Casson equation, since straight lines are only obtained from the results above a certain shear rate.

20.2.1.7 The Cross Equation

This can be used to analyse the flow curve of shear thinning systems that show a limiting viscosity $\eta(\mathrm{o})$ in the low shear rate regime and another limiting viscosity $\eta(\infty)$ in the high shear rate regime [11]. These two regimes are separated by a shear thinning behaviour, as shown schematically in Figure 20.3.

$$\frac{\eta - \eta(\infty)}{\eta(0) - \eta(\infty)} = \frac{1}{1 + K\dot{\gamma}^m} \tag{20.7}$$

where K is a constant parameter with dimension of time and m is a dimensionless constant.

An equivalent equation to Equation (20.7) is,

$$\frac{\eta_o - \eta}{\eta - \eta_\infty} = (K\dot{\gamma}^m) \tag{20.8}$$

20.2.2
Time Effects during Flow: Thixotropy and Negative (or Anti-) Thixotropy

When a shear rate is applied to a non-Newtonian system, the resulting stress may not be achieved simultaneously. First, the molecules or particles will undergo spatial rearrangement to follow the applied flow field. Second, the structure of the

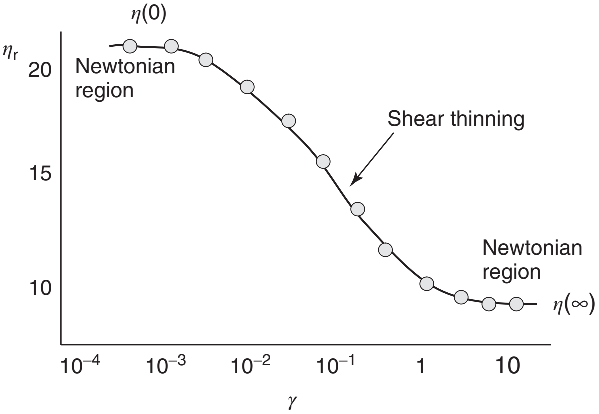

Figure 20.3 Viscosity versus shear rate for a shear thinning system.

system may change by the breaking of weak bonds, the alignment of irregularly shaped particles, and the collision of particles to form aggregates.

The above changes are accompanied with s decrease or increase of viscosity with time at any given shear rate. These changes are referred to as thixotropy if the viscosity decreases with time, or as negative thixotropy or anti-thixotropy if the viscosity increases with time.

- *Thixotropy*: This refers to the reversible time-dependent decease of viscosity. When the system is sheared for some time the viscosity decreases, but when the shear is stopped (the system is left to rest) the viscosity of the system is restored. Practical examples of systems that show thixotropy include paint formulations (sometimes referred to as thixotropic paints), tomato ketchup, and some hand creams and lotions.
- *Negative thixotropy or antithixotropy*: When the system is sheared for some time the viscosity increases, but when the shear is stopped (the system is left to rest) the viscosity decreases. A practical example of the above phenomenon is corn starch suspended in milk.

Generally speaking, two methods can be applied to study thixotropy in a suspension. The first, and the most commonly used, procedure is the ‘‘loop test,’’ whereby the shear rate is increased continuously and linearly in time from zero to some maximum value and then decreased to zero in the same way; this is illustrated in Figure 20.4.

The main problem with the above procedure is the difficulty of interpreting the results. The nonlinear approach used is not ideal for developing loops because, by decoupling the relaxation process from the strain, the recovery of the material is not allowed. However, the loop test does provide a qualitative behaviour of the suspension thixotropy.

An alternative method for studying thixotropy is to apply a step change test, whereby the suspension is suddenly subjected to a constant high shear rate and

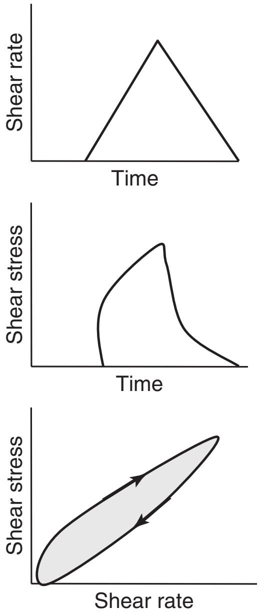

Figure 20.4 Loop test for studying thixotropy.

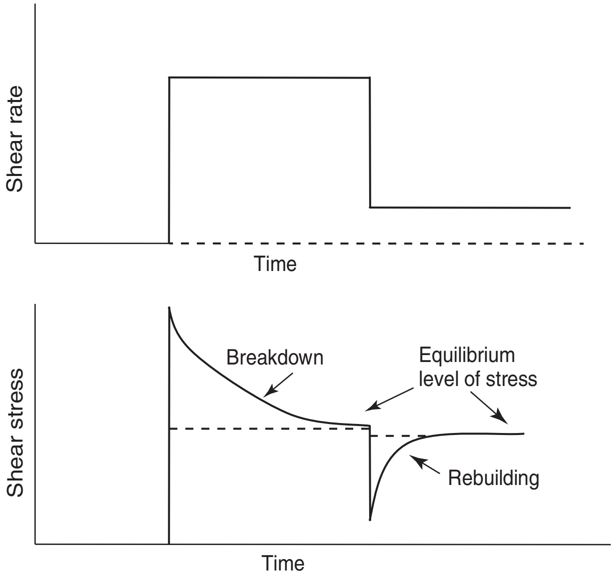

Figure 20.5 Step change for studying thixotropy.

the stress is followed as a function of time, whereby the structure breaks down and an equilibrium value is reached. The stress is further followed as a function of time to evaluate the rebuilding of the structure. A schematic representation of this procedure is shown in Figure 20.5.

20.3
Constant Stress (Creep) Measurements

A constant stress σ is applied on the system (that may be placed in the gap between two concentric cylinders or a cone and plate geometry) and the strain (relative deformation) γ or compliance J ($=\gamma/\sigma$, Pa^{-1}) is followed as a function of time for a period of t. At $t=t$, the stress is removed and the strain γ or compliance J is followed for another period t [1].

The above procedure is referred to as "creep measurement." From the variation of J with t when the stress is applied, and the change of J with t when the stress is removed (in this case J changes sign), it is possible to distinguish between viscous, elastic, and viscoelastic responses, as illustrated in Figure 20.6.

- *Viscous response*: In this case, the compliance J shows a linear increase with increase of time, reaching a certain value after time t. When the stress is removed after time t, J remains the same; that is, no creep recovery occurs.
- *Elastic response*: In this case, the compliance J shows a small increase at $t=0$ and this remains almost constant for the whole period t. When the stress is removed, J changes sign and reaches 0 after some time t; that is, complete creep recovery occurs.
- *Viscoelastic response*: At $t=0$, J shows a sudden increase and this is followed by slower increase for the time applied. When the stress is removed, J changes sign and shows an exponential decrease with increase of time (creep recovery), but it does not reach 0, as is the case for an elastic response.

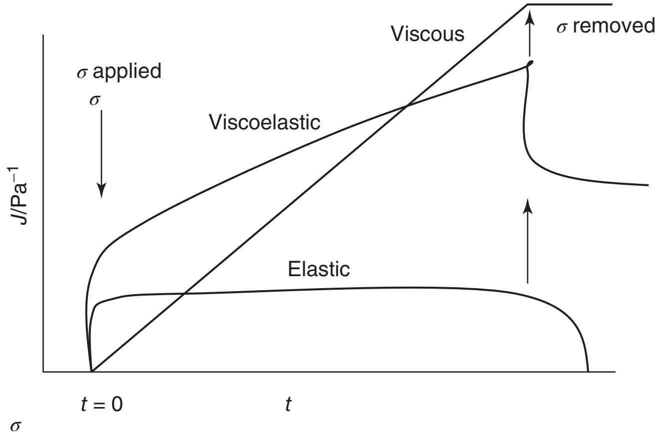

Figure 20.6 Creep curves for viscous, elastic, and viscoelastic responses.

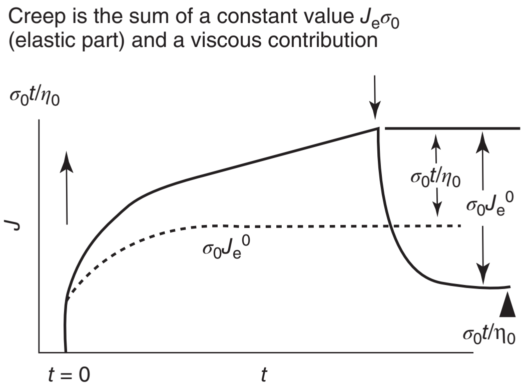

Figure 20.7 Creep curve for a viscoelastic liquid.

20.3.1
Analysis of Creep Curves

20.3.1.1 Viscous Fluid

The linear curve of J versus t gives a slope that is equal to the reciprocal viscosity

$$J(t) = \frac{\gamma}{\sigma} = \frac{\dot{\gamma} t}{\sigma} = \frac{t}{\eta(0)} \tag{20.9}$$

20.3.1.2 Elastic Solid

The increase of compliance at $t = 0$ (rapid elastic response), $J(t)$, is equal to the reciprocal of the instantaneous modulus $G(0)$.

$$J(t) = \frac{1}{G(0)} \tag{20.10}$$

20.3.2
Viscoelastic Response

20.3.2.1 Viscoelastic Liquid

Figure 20.4 shows the case for a viscoelastic liquid whereby the compliance $J(t)$ is given by two components: (i) an elastic component J_e that is given by the reciprocal of the instantaneous modulus; and (ii) a viscous component J_v that is given by $t/\eta(o)$

$$J(t) = \frac{1}{G(0)} + \frac{t}{\eta(0)} \tag{20.11}$$

Figure 20.7 also shows the recovery curve which gives $\sigma_o J_e{}^o$; when this is subtracted from the total compliance, it gives $\sigma_o t/\eta(o)$.

The driving force for relaxation is spring, and the viscosity controls the rate. The Maxwell relaxation time τ_M is given by,

$$\tau_M = \frac{\eta(0)}{G(0)} \tag{20.12}$$

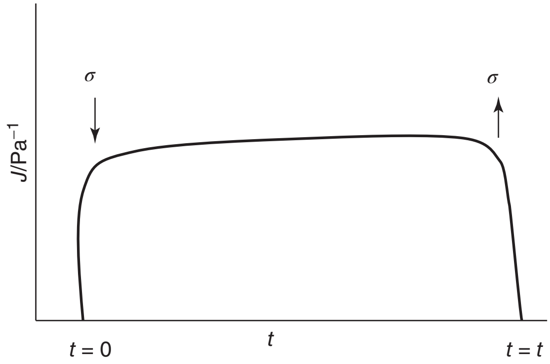

Figure 20.8 Creep curve for a viscoelastic solid.

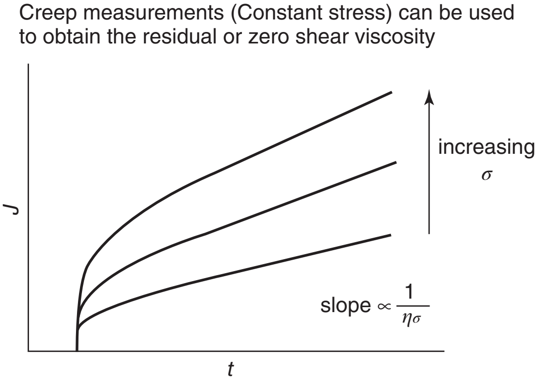

Figure 20.9 Creep curves at increasing applied stress.

20.3.2.2 **Viscoelastic Solid**

In this case complete recovery occurs, as illustrated in Figure 20.8. The system is characterised by a Kelvin retardation time τ_k that is also given by the ratio of $\eta(o)/G(0)$.

20.3.3
Creep Procedure

Creep experiments start with a low applied stress (below the critical stress σ_{cr}, see below) at which the system behaves as a viscoelastic solid with complete recovery, as illustrated in Figure 20.8. The stress is gradually increased and several creep curves are obtained. Above σ_{cr}, the system behaves as a viscoelastic liquid showing only partial recovery, as illustrated in Figure 20.7. Figure 20.9 shows a schematic representation of the variation of compliance J with time t at increasing σ (above σ_{cr}).

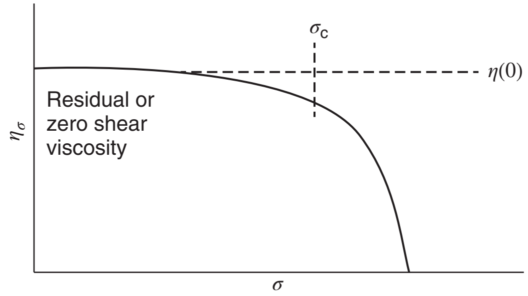

Critical stress is a useful parameter (related to yield stress) as denotes the stress at which structure "breaks down".

Figure 20.10 Variation of viscosity with applied stress.

From the slopes of the lines, the viscosity η_σ can be obtained at each applied stress. A plot of η_σ versus σ is shown in Figure 20.10, which shows a limiting viscosity $\eta(\text{o})$, while below σ_{cr} and above σ_{cr} the viscosity shows a sharp decrease with further increase in σ. $\eta(\text{o})$ is referred to as the residual or zero shear viscosity, which is an important parameter for predicting sedimentation. σ_{cr} is the critical stress above which the structure "breaks down"; this is sometimes referred to as the "true"' yield stress.

20.4
Dynamic (Oscillatory) Measurements

This is the response of the material to an oscillating stress or strain [1]. When a sample is constrained in, say, a cone and plate or concentric cylinder assembly, an oscillating strain at a given frequency ω (rad s^{-1}) ($\omega = 2\nu\pi$, where ν is the frequency in cycles s^{-1} or Hz) can be applied to the sample. After an initial start-up period, a stress develops in response of the applied strain; that is, it oscillates with the same frequency. The change of the sine waves of the stress and strain with time can be analysed to distinguish between elastic, viscous, and viscoelastic response. An analysis of the resulting sine waves can be used to obtain the various viscoelastic parameters, as discussed below.

Three cases can be considered:

- *Elastic response*: This occurs when the maximum of the stress amplitude is at the same position as the maximum of the strain amplitude (no energy dissipation). In this case, there is no time shift between the stress and strain sine waves.
- *Viscous response*: This occurs when the maximum of the stress is at the point of maximum shear rate (i.e., the inflection point), where there is maximum energy dissipation. In this case, the strain and stress sine waves are shifted by $\omega t = \pi/2$ (referred to as the phase angle shift, δ, which in this case is 90°).

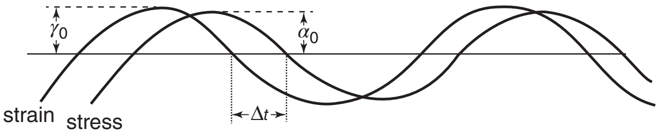

Δt = time shift for sine waves of stress and strain.

$\Delta t\omega = \delta$ phase angle shift

ω = frequency in radian s^{-1}

$\omega = 2\pi\upsilon$

Perfectly elastic solid	$\delta = 0$
Perfectly viscos liquid	$\delta = 90°$
Viscoelastic system	$0 < \delta < 90°$

Figure 20.11 Strain and stress sine waves for a viscoelastic system.

- *Viscoelastic response*: In this case the phase angle shift δ is greater than 0, but less than 90°.

20.4.1
Analysis of Oscillatory Response for a Viscoelastic System

Consider the case of a viscoelastic system, for which the sine waves of strain and stress are shown in Figure 20.11. The frequency ω is in rad s^{-1}, and the time shift between the strain and stress sine waves is Δt. The phase angle shift δ is given by (in dimensionless units of radians).

$$\delta = \omega \Delta t \tag{20.13}$$

As discussed before:

Perfectly elastic solid	$\delta = 0$
Perfectly viscous liquid	$\delta = 90°$
Viscoelastic system	$0 < \delta < 90°$

The ratio of the maximum stress σ_o to the maximum strain γ_o gives the complex modulus $|G^*|$

$$|G^*| = \frac{\sigma_o}{\gamma_o} \tag{20.14}$$

The complex modulus can be resolved into G' (the storage or elastic modulus) and G'' (the loss or viscous modulus), using vector analysis, and the phase angle shift δ, as shown below.

20.4.2
Vector Analysis of the Complex Modulus

$$G' = |G^*| \cos \delta \tag{20.15}$$

$$G'' = |G^*| \sin \delta \tag{20.16}$$

$$\tan \delta = \frac{G''}{G'} \tag{20.17}$$

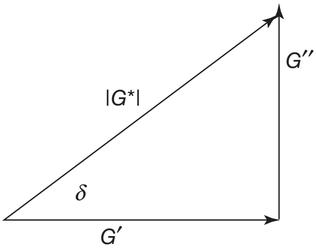

20.4.2.1 Dynamic viscosity η'

$$\eta' = \frac{G''}{\omega} \tag{20.18}$$

Note that $\eta \to \eta(o)$ as $\omega \to 0$

Both, G' and G'' can be expressed in terms of frequency ω and Maxwell relaxation time τ_{m} by,

$$G'(\omega) = G\frac{(\omega\tau_{\mathrm{m}})^2}{1 + (\omega\tau_{\mathrm{m}})^2} \tag{20.19}$$

$$G''(\omega) = G\frac{\omega\tau_m}{1 + (\omega\tau_m)^2} \tag{20.20}$$

In oscillatory techniques, two types of experiment must be carried out:

- *Strain sweep*: In which the frequency ω is kept constant and G^*, G' and G'' are measured as a function of strain amplitude.
- *Frequency sweep*: In which the strain is kept constant (in the linear viscoelastic region) and G^*, G' and G'' are measured as a function of frequency.

20.4.2.2 Strain Sweep

The frequency is fixed say at 1 Hz (or 6.28 rad s^{-1}) and G^*, G' and G'' are measured as a function of strain amplitude γ_o; this is illustrated in Figure 20.12, where G^*, G' and G'' are seen to remain constant up to a critical strain γ_{cr} . This is the linear viscoelastic region where the moduli are independent of the applied strain. Above γ_{cr}, however, G^* and G' start to decrease whereas G'' starts to increase with further increase in γ_o; this is the nonlinear region.

γ_{cr} may be identified with the critical strain above which the structure starts to "break down." It can also be shown that, above another critical strain, G'' becomes higher than G', a situation sometimes referred to as the "melting strain," when the system becomes more viscous than elastic.

20.4.2.3 Frequency Sweep

The strain γ_o is fixed in the linear region (taking a midpoint, i.e., not a too-low strain, where the results may show some "noise" and far from γ_{cr}). G^*, G' and G'' are then measured as a function of frequency (a range of 10^{-3} to 10^2 rad s^{-1} may be chosen, depending on the instrument and operator patience). Figure 20.13 shows

Fixed frequency (0.1 or 1 Hz) and follow G^*, G' and G'' with strain amplitude γ_0

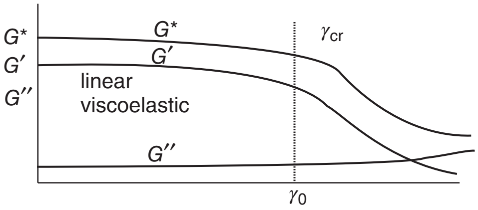

Linear viscoelastic region

G^*, G' and G'' are independent of strain amplitude

γ_{cr} is the critical strain above which system shows non-linear response (break down of structure)

Figure 20.12 Schematic representation of strain sweep.

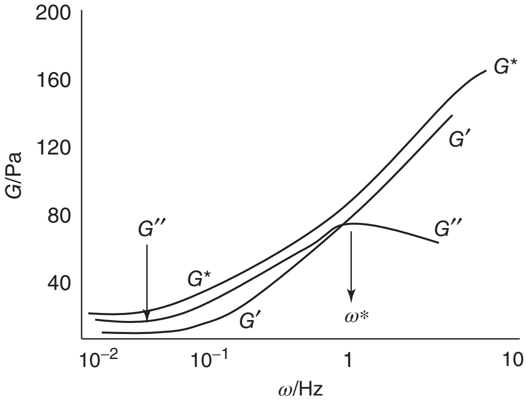

Figure 20.13 Schematic representation of oscillatory measurements for a viscoelastic liquid.

a schematic representation of the variation of G^*, G' and G'' with frequency ω (rad s^{-1}) for a viscoelastic system that can be represented by a Maxwell model. Here, a characteristic frequency ω^* can be identified at which $G' = G''$ (the "cross-over point"), which can be used to obtain the Maxwell relaxation time τ_m

$$\tau_m = \frac{1}{\omega^*} \tag{20.21}$$

In the low-frequency regime, $\omega < \omega^*$ and $G'' > G'$; this corresponds to a long-term experiment (time is reciprocal of frequency), and hence the system can dissipate energy as viscous flow. In the high-frequency regime, $\omega > \omega^*$, $G' > G''$; this corresponds to a short-term experiment where energy dissipation is reduced. At a sufficiently high frequency, $G' \gg G''$. At such high frequency $G'' \to 0$ and $G' \sim G^*$; the high-frequency modulus $G'(\infty)$ is sometimes referred to as the "rigidity modulus" where the response is mainly elastic.

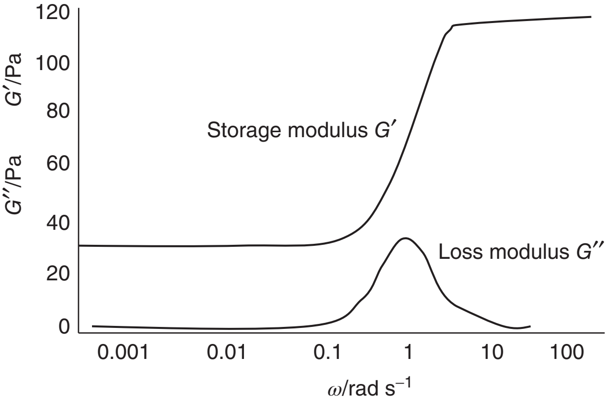

Figure 20.14 Schematic representation for oscillatory measurements for a viscoelastic solid.

For a viscoelastic solid G' does not become zero at low frequency, but G'' still shows a maximum at intermediate frequency, as illustrated in Figure 20.14.

20.4.3
The Cohesive Energy Density E_c

The cohesive energy density, which is an important parameter for identifying the "strength" of the structure in a dispersion, can be obtained from the change of G' with γ_o (see Figure 20.9).

$$E_c = \int_0^{\gamma_{cr}} \sigma d\gamma \tag{20.22}$$

where σ is the stress in the sample that is given by,

$$\sigma = G''\gamma \tag{20.23}$$

$$E_c = \int_0^{\gamma_{cr}} G''\gamma_{cr} d\gamma = \frac{1}{2}\gamma_{cr}^2 G' \tag{20.24}$$

Note that E_c is given in J m^{-3}.

20.4.4
Application of Rheological Techniques to Assess and Predict the Physical Stability of Suspensions

20.4.4.1 Rheological Techniques to Assess Sedimentation and Syneresis

As mentioned in Chapter 9, sedimentation is prevented by the addition of "thickeners" that form a "three-dimensional elastic" network in the continuous phase [3].

If the viscosity of the elastic network, at shear stresses (or shear rates) comparable to those exerted by the particles or droplets, exceeds a certain value, then sedimentation is completely eliminated.

The shear stress, σ_{p}, exerted by a particle (force/area) can be simply calculated,

$$\sigma_{\mathrm{p}} = \frac{(4/3)\pi R^3 \Delta\rho g}{4\pi R^2} = \frac{\Delta\rho R g}{3} \tag{20.25}$$

Hence, for a 10 μm radius particle with a density difference $\Delta\rho$ of 0.2 g cm^{-3}, the stress is equal to,

$$\sigma_{\mathrm{p}} = \frac{0.2 \times 10^3 \times 10 \times 10^{-6} \times 9.8}{3} \approx 6 \times 10^{-3}\,\mathrm{Pa} \tag{20.26}$$

For smaller particles, smaller stresses are exerted. Thus, in order to predict sedimentation it is necessary to measure the viscosity at very low stresses (or shear rates). These measurements can be carried out using a constant stress rheometer (Carrimed, Bohlin, Rheometrics, Haake or Physica). Usually, a good correlation is obtained between the rate of creaming or sedimentation, v, and the residual viscosity $\eta(0)$, as will be described in Chapter 21. Above a certain value of $\eta(0)$, v becomes equal to 0. Clearly, in order to minimize sedimentation it is necessary to increase $\eta(0)$; an acceptable level for the high shear viscosity η_∞ must be achieved, depending on the application. In some cases, a high $\eta(0)$ may be accompanied by a high η_∞ (which may not be acceptable for application, for example if spontaneous dispersion on dilution is required). If this is the case, the formulation chemist should seek an alternative thickener.

Another problem encountered with many dispersions is that of "syneresis"; this is the appearance of a clear liquid film at the top of the container, and it occurs with most "flocculated" and/or "structured" dispersions (i.e., those containing a thickener in the continuous phase). Syneresis may be predicted from measurements of the yield value (using steady-state measurements of shear stress as a function of shear rate) as a function of time, or by using oscillatory techniques (whereby the storage and loss modulus are measured as a function of strain amplitude and frequency of oscillation). The oscillatory measurements are perhaps more useful, since to prevent separation the bulk modulus of the system should balance the gravity forces that is given by $h\rho\Delta g$ (where h is the height of the disperse phase, $\Delta\rho$ is the density difference, and g is acceleration due to gravity). The bulk modulus is related to the storage modulus G'. A more useful predictive test is to calculate the cohesive energy density of the structure E_{c} that is given by Equation (20.24).

The separation of a formulation decreases with increase in E_{c}, as will be discussed in Chapter 21. The value of E_{c} required to stop complete separation depends on the particle or droplet size distribution, the density difference between the particle or droplet and the medium, as well as on the volume fraction ϕ of the dispersion.

20.4.4.2 Role of Thickeners

As mentioned above, thickeners reduce creaming or sedimentation by increasing the residual viscosity $\eta(\mathrm{o})$, which must be measured at stresses compared to those exerted by the droplets or particles (mostly less than 0.1 Pa). At such low stresses, $\eta(o)$ increases very rapidly with increases in ''thickener'' concentration. The fact that this rapid increase is not observed at high stresses illustrates the need for measurements to be made at low stresses (using constant stress or creep measurements); this point will be highlighted in Chapter 21.

20.4.5
Assessment of Flocculation Using Rheological Techniques

Steady-state rheological investigations may be used to investigate the state of flocculation of a dispersion. Weakly flocculated dispersions usually show thixotropy, and the change of thixotropy with applied time may be used as an indication of the strength of this weak flocculation. These methods are only qualitative and the results cannot be used in a quantitative manner. This is due to a possible breakdown of the structure when the formulation is transferred to the rheometer, and also during the uncontrolled shear experiment. Better techniques for studying the flocculation of a formulation are constant stress (creep) or oscillatory measurements. By carefully transferring the sample to the rheometer (with minimum shear), the structure of the flocculated system may be maintained.

One very important point that must be considered in any rheological measurement is the possibility of ''slip'' during the measurements. This is particularly the case with highly concentrated dispersions, whereby the flocculated system may form a ''plug'' in the gap of the platens, leaving a thin liquid film at the walls of the concentric cylinder or cone-and-plate geometry. This behaviour is caused by some syneresis of the formulation in the gap of the concentric cylinder or cone and plate. In order to reduce ''slip,'' roughened walls should be used for the platens; an alternative method would be to use a vane rheometer.

Steady-state shear stress-shear rate measurements are by far the most commonly used method in many industrial laboratories. Basically, the dispersion is stored at various temperatures and the yield value σ_β and plastic viscosity η_{pl} are measured at various intervals of time. Any flocculation in the formulation should be accompanied by an increase in σ_β and η_{pl}. One rapid technique for studying the effect of temperature changes on the flocculation of a formulation is to perform temperature sweep experiments, running the samples from perhaps 5 to 50 °C. Any trend in the variation of σ_β and η_{pl} with temperature can quickly provide an indication of the temperature range at which a dispersion will remain stable, since during that temperature range σ_β and η_{pl} will remain constant.

If Ostwald ripening occurs simultaneously, σ_β and η_{pl} may change in a complex manner with storage time. Ostwald ripening results in a shift of the particle size distribution to higher diameters, and this has the effect of reducing σ_β and η_{pl}. If flocculation occurs simultaneously (having the effect of increasing these rheological parameters), the net effect may be an increase or decrease of the rheological parameters. This trend depends on the extent of flocculation relative to Ostwald ripening and/or coalescence. Therefore, to follow σ_β and η_{pl} with storage time requires a knowledge of Ostwald ripening. Only in the absence of these latter breakdown processes use rheological measurements be used as a guide for the assessment of flocculation.

Constant stress (creep) experiments are more sensitive for following flocculation. As mentioned before, a constant stress σ is applied to the system and the compliance J (Pa^{-1}) is plotted as a function of time. These experiments are repeated several times, increasing the stress in small increments from the smallest possible value (that can be applied by the instrument), to produce a set of creep curves at various applied stresses From the slope of the linear portion of the creep curve (when the system has reached a steady state), the viscosity at each applied stress, η_σ, is calculated. As noted above, a plot of η_σ versus σ allows the limiting (or zero shear) viscosity $\eta(0)$ and the critical stress σ_{cr} (which may be identified with the ''true'' yield stress of the system) to be obtained. The values of $\eta(0)$ and σ_{cr} may be used to assess the flocculation of the dispersion on storage. If flocculation does occur on storage (without any Ostwald ripening), the values of $\eta(0)$ and σ_{cr} may show a gradual increase with increase of storage time. As discussed in the previous section (on steady-state measurements), the trend becomes complicated if Ostwald ripening occurs simultaneously, as both have the effect of reducing $\eta(0)$ and σ_{cr}.

The above measurements should be supplemented by particle size distribution measurements of the diluted dispersion (ensuring that no flocs are present after dilution) to assess the extent of Ostwald ripening. Another complication may arise from the nature of the flocculation which, if it occurs in an irregular fashion (producing strong and tight flocs), may cause $\eta(0)$ to be increased while σ_{cr} may show some decrease, and this will complicate the analysis of the results. Yet, in spite of these complications, constant stress measurements may provide valuable information on the state of the dispersion on storage.

To perform creep experiments and ensure that a steady state is reached can be time-consuming. Typically, a stress sweep experiment would be carried out whereby the stress would be gradually increased (within a predetermined time period to ensure that the steady state is not too far away) and plots of η_σ versus σ would be established. These experiments are carried out at various storage times (perhaps every two weeks) and temperatures. From the changes of $\eta(0)$ and σ_{cr} with storage time and temperature, information can be obtained on the degree and the rate of flocculation of the system. Clearly, interpretation of the rheological results requires an expert knowledge of rheology and measurements of particle size distribution as a function of time.

A major problem in carrying out the above experiments is sample preparation. When a flocculated dispersion is removed from the container, care must be taken not to cause too much disturbance to the structure (minimum shear should be applied on transferring the formulation to the rheometer). It is also advisable to use separate containers for assessing flocculation; a relatively large sample is prepared and this is then transferred to a number of separate containers. Each sample should be used separately at a given storage time and temperature. Care must be taken when transferring the sample to the rheometer; if any separation does occur in the formulation the sample can be gently mixed by placing it on a roller. It is advisable to use as minimum shear as possible when transferring the sample from the container to the rheometer (the sample is preferably transferred using a ''spoon'' or by simple pouring from the container). The experiment should be carried out without an initial pre-shear.

An alternative rheological technique for assessing flocculation involves oscillatory measurements which, as noted above, can include two sets of experiments, namely strain and oscillatory sweep measurements.

20.4.5.1 **Strain Sweep Measurements**

In this case, the oscillation is fixed (e.g., at 1 Hz) and the viscoelastic parameters are measured as a function of strain amplitude. G^*, G' and G'' remain virtually constant up to a critical strain value, γ_{cr} (this region is the linear viscoelastic region), but above γ_{cr}, G^* and G' starts to fall, whereas G'' starts to increase (this is the nonlinear region). The value of γ_{cr} may be identified with the minimum strain above which the ''structure'' of the dispersion starts to break down (e.g., the breakdown of flocs into smaller units and/or the breakdown of a ''structuring'' agent).

From γ_{cr} and G', it is possible to obtain the cohesive energy E_c (J m^{-3}) of the flocculated structure, using Equation (20.24). Subsequently, E_c may be used in a quantitative manner as a measure of the extent and strength of the flocculated structure in a dispersion; the higher the value of E_c, the more flocculated is the structure. Clearly, E_c depends on the volume fraction of the dispersion as well as the particle size distribution (which determines the number of contact points in a floc). Therefore, for a quantitative comparison between various systems, it must be ensured that the volume fraction of the disperse particles is the same and that the dispersions have a very similar particle size distribution. E_c also depends on the strength of the flocculated structure – that is, the energy of attraction between the droplets – and this in turn depends on whether the flocculation is in the primary or secondary minimum. Flocculation in the primary minimum is associated with a large attractive energy, and this leads to higher values of E_c when compared to values obtained for secondary minimum flocculation (weak flocculation). For a weakly flocculated dispersion, such as the case with secondary minimum flocculation of an electrostatically stabilised system, the deeper the secondary minimum the higher will be the value of E_c (at any given volume fraction and particle size distribution of the dispersion). With a sterically stabilised dispersion, weak flocculation can also occur when the thickness of the adsorbed layer decreases. Again, the value of E_c can be used as a measure of the flocculation; the higher the value of E_c, the stronger the flocculation. If incipient flocculation occurs (on reducing the solvency of the medium for the change to worse than θ-condition), a much deeper minimum is observed and this is accompanied by a much larger increase in E_c.

In order to apply the above analysis, an independent method must be available for assessing the nature of the flocculation. Rheology is a bulk property that can provide information on the interparticle interaction (whether repulsive or attractive), and to apply it in a quantitative manner it is necessary to know the nature of these interaction forces. However, rheology can also be used in a qualitative manner to follow changes in the formulation on storage. Provided that the system does not undergo any Ostwald ripening, the change of the moduli with time – and, in particular, the change of the linear viscoelastic region – may be used as an indication of flocculation. Strong flocculation is usually accompanied by a rapid increase in G', and this may be accompanied by a decrease in the critical strain above which the ''structure'' breaks down. This may be used as an indication of the formation of ''irregular'' and tight flocs which become sensitive to the applied strain. The floc structure will entrap a large amount of the continuous phase, and this will lead to an apparent increase in the volume fraction of the dispersion, and hence an increase in G'.

20.4.5.2 **Oscillatory Sweep Measurements**

In this case, the strain amplitude is kept constant in the linear viscoelastic region (usually, a point is taken far from γ_{cr} but not too low – that is in the midpoint of the linear viscoelastic region) and measurements are carried out as a function of frequency. Both, G^* and G' are increased with an increase in frequency and ultimately, above a certain frequency, they reach a limiting value and show little dependence on frequency. G'' is higher than G' in the low-frequency regime; it also increases with increase in frequency and at a certain characteristic frequency ω^* (which depends on the system) it becomes equal to G' (this is usually referred to as the cross-over point), after which it reaches a maximum and then shows a reduction with further increase in frequency.

From ω^*, the relaxation time τ of the system can be calculated:

$$\tau = \frac{1}{\omega^*} \tag{20.27}$$

The relaxation time may be used as a guide for the state of the dispersion. For a colloidally stable dispersion (at a given particle size distribution), τ increases with increase of the volume fraction of the disperse phase, ϕ. In other words, the cross-over point shifts to lower frequency with increase in ϕ. For a given dispersion, τ increases with increase in flocculation, provided that the particle size distribution remains the same (i.e., no Ostwald ripening).

The value of G' also increases with increase in flocculation, since aggregation of the particles usually results in liquid entrapment and the effective volume fraction of the dispersion will show an apparent increase. With flocculation, the net attraction between the particles also increases, and this results in an increase in G'. The latter is determined by the number of contacts between the particles and the strength of each contact (which is determined by the attractive energy).

It should be mentioned that, in practice, the full curve may not be obtained due to the frequency limit of the instrument, and also that measurements at low frequency are time-consuming. In fact, only part of the frequency dependence of G′ and G″ is usually obtained, and in most cases the system will be more elastic than viscous.

Most disperse systems used in practice are weakly flocculated, and they also contain ''thickeners'' or ''structuring'' agents to reduce sedimentation and to acquire the correct rheological characteristics for applications, such as handcreams and lotions. The exact values of G' and G'' required will depend on the system and its application, but in most cases a compromise must be made between the correct rheological characteristics for application and the optimum rheological parameters for long-term physical stability. Clearly, the application of rheological measurements to achieve these conditions requires a great deal of skill and understanding of the factors that affect rheology.

References

1. Ferry, J.D. (1980) *Viscoelastic Properties of Polymers*, John Wiley & Sons, Inc., New York.
2. Mackosko, C.W. (1994) *Rheology, Principles, Measurement and Applications*, Wiley-VCH Verlag GmbH, New York.
3. Tadros, Th.F. (2010) *Rheology of Dispersions*, Wiley-VCH Verlag GmbH, Weinheim.
4. Goodwin, J.W. and Hughes, R.W. (1992) *Adv. Colloid Interface Sci.*, **42**, 303.
5. Tadros, Th.F. (1996) *Adv. Colloid Interface Sci.*, **68**, 97.
6. Goodwin, J.W. and Hughes, R.W. (2000) *Rheology for Chemists*, Royal Society of Chemistry Publication, Cambridge.
7. Wohrlow, R.W. (1980) *Rheological Techniques*, John Wiley & Sons, Inc., New York.
8. Bingham, E.C. (1922) *Fluidity and Plasticity*, McGraw-Hill, New York.
9. (a) Herschel, W.H. and Bulkley, R. (1926) *Proc. Am. Soc. Test Mater.*, **26**, 621; (b) Herschel, W.H. and Bulkley, R. (1926) *Kolloid Z.*, **39**, 291.
10. Casson, N. (1959) in *Rheology of Disperse Systems* (ed. C.C. Mill), Pergamon Press, New York, pp. 84–104.
11. Cross, M.M. (1965) *J. Colloid Interface Sci.*, **20**, 417.

Further Reading

Buscall, R., Goodwin, J.W., Ottewill, R.H., and Tadros, Th.F. (1982) *J. Colloid Interface Sci.*, **85**, 78.

Hunter, R.J. and Nicol, S.K. (1968) *J. Colloid Interface Sci.*, **28**, 250.

Neville, P.C. and Hunter, R.J. (1974) *J. Colloid Interface Sci.*, **49**, 204.

21
Assessment and Prediction of Creaming, Sedimentation, Flocculation, and Coalescence of Formulations

21.1
Assessment and Prediction of Creaming and Sedimentation

21.1.1
Introduction

Most formulations undergo creaming or sedimentation as a result of the density difference between disperse phase particles and medium [1]. This situation is particularly the case with most practical systems that contain particles with radii R that are large (>1 μm), whereby the Brownian diffusion is not sufficient to overcome the gravity force, that is

$$kT \ll (4/3)\pi R^3 \Delta\rho g L$$

where k is the Boltzmann constant, T is the absolute temperature, R is the particle radius, $\Delta\rho$ is the density difference between the disperse phase and the medium, g is acceleration due to gravity, and L is the height of the container.

21.1.2
Accelerated Tests and Their Limitations

Several tests have been designed to accelerate the process of sedimentation or creaming, the most commonly used methods being based on increasing the temperature or subjecting the suspension or emulsion to high g-forces (using a high-speed centrifuge).

With increasing temperature the viscosity of the system usually decreases, and hence sedimentation or creaming is accelerated. The assumption is usually made that if a suspension or emulsion does not show any sedimentation, creaming or separation at 50 °C for say one month, then the system will show no separation at ambient temperatures for more than one year.

The above method is only valid if the formulation viscosity η follows the Arrhenius equation, which predicts a linear increase in $\ln\eta$ with $(1/T)$, where T is the absolute temperature. Most practical formulations do not follow such a plot due to the possible phase changes or flocculation that may occur at high temperatures. With many surfactant systems, such phase changes may result in

Formulation of Disperse Systems: Science and Technology, First Edition. Tharwat F. Tadros.

the formation of liquid crystalline phases that have a higher viscosity at high temperatures and hence no separation will result at high temperatures, although that could occur at ambient conditions.

21.1.3
Application of High-Gravity (g) Forces

This method, if carefully studied, may offer a better accelerated method and has been particularly applied to emulsions. The assumption is also made here that, by increasing the *g*-force, the rate of sedimentation or creaming is significantly increased, and that this could be applied to predict the process from measurement at short time periods.

In a centrifuge, the gravitational force is given by,

$$g = \omega^2 x \tag{21.1}$$

where x is the mean distance of the centrifuge tube from the axis of rotation and ω is the angular velocity ($\omega = 2\pi\nu$, where ν is the number of revolutions per second). Note that if the centrifuge tube is not small compared to x, then the applied centrifugal field cannot be considered to be uniform over the length of the tube.

Modern analytical ultracentrifuges allow the separation of emulsions to be followed in a quantitative manner. With typical oil-in water (O/W) emulsions, three layers are generally observed: (i) a clear aqueous phase; (ii) an opaque phase consisting of distorted polyhedral oil droplets; and (iii) a clear separated oil phase, resulting from coalescence of the polyhedra.

The degree of emulsion stability may be taken as the volume of the opaque phase remaining after time t. Alternatively, the volume of oil separated at infinite time may be used as an index of stability.

A simple expression may be used to treat the data in a quantitative manner,

$$\frac{t}{V} = \frac{1}{bV_\infty} + \frac{1}{V_\infty} \tag{21.2}$$

where V is the volume of oil separated at time t, V_∞ is the extrapolated volume at infinite time, and b is a constant.

A plot of t/V versus t should give a straight line from which b and V_∞ may be calculated. These two parameters may be taken as indices of emulsion stability.

A more rigorous procedure to study emulsion stability using the ultracentrifuge is to observe the system at various speeds of rotation. At relatively low centrifuge speeds, the expected opaque cream layer may be observed, but at sufficiently high speeds a coalesced oil layer and a cream layer may be observed that are separated by an extra layer of deformed oil droplets. This deformed layer resembles a ‘‘foam’’; that is, it consists of oil droplets separated by thin aqueous films.

For certain emulsions, increasing the centrifuge speed will not necessarily cause the ‘‘foam’’/cream layer boundary to move. Indeed, under conditions where there is an equilibrium between the ‘‘foam’’/cream layer, it may be concluded that there is no barrier to be overcome in forming the foam layer from the cream layer.

This implies that, in the foam layer, the aqueous film separating two oil droplets thins to a "black" film under the action of van der Waals attraction forces. The boundary between the foam layer and the coalesced layer is associated with a force (or pressure) barrier.

In this way, the minimum centrifuge speed necessary to produce a visible amount of coalesced oil after, say 30 min of centrifugation, can be determined. This centrifuge speed can then be used to calculate the "critical pressure" that must be applied to induce coalescence.

21.1.4
Rheological Techniques for Prediction of Sedimentation or Creaming

Sedimentation or creaming is prevented by the addition of "thickeners" that form a "three-dimensional elastic" network in the continuous phase. If the viscosity of the elastic network, at shear stresses (or shear rates) comparable to those exerted by the particles or droplets, exceeds a certain value, then creaming or sedimentation is completely eliminated.

As mentioned in Chapter 20, the shear stress, σ_p, exerted by a particle (force/area) can be simply calculated,

$$\sigma_p = \frac{(4/3)\pi R^3 \Delta\rho g}{4\pi R^2} = \frac{\Delta\rho R g}{3} \tag{21.3}$$

For a 10 μm radius particle with a density difference $\Delta\rho$ of 0.2 g cm^{-3}, the stress is equal to:

$$\sigma_p = \frac{0.2 \times 10^3 \times 10 \times 10^{-6} \times 9.8}{3} \approx 6 \times 10^{-3}\,\text{Pa} \tag{21.4}$$

For smaller particles smaller stresses are exerted.

Thus, to predict creaming or sedimentation, it is necessary to measure the viscosity at very low stresses (or shear rates), and these measurements can be carried out using a constant stress rheometer (e.g., Carrimed, Bohlin, Rheometrics, Haake or Physica).

Usually, a good correlation is obtained between the rate of creaming or sedimentation ν and the residual viscosity $\eta(o)$; this is illustrated in Figure 21.1. Above a certain value of $\eta(o)$, ν becomes equal to 0, and to minimize creaming or sedimentation it is clearly necessary to increase $\eta(o)$; an acceptable level for the high shear viscosity η_∞ must be achieved, depending on the application. In some cases, a high $\eta(o)$ may be accompanied by a high η_∞ (which may not be acceptable for application, for example if spreading of a dispersion on the skin is required). If this is the case, the formulation chemist should seek an alternative thickener.

21.1.5
Separation of Formulation ("Syneresis")

Another problem encountered with many dispersions is that of "syneresis"; that is, the appearance of a clear liquid film at the bottom (if creaming is the case)

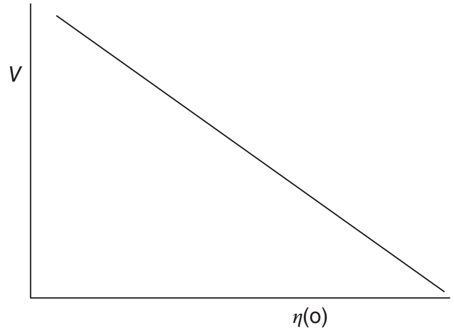

Figure 21.1 Variation of creaming or sedimentation rate with residual viscosity.

or the top (if sedimentation is the case) of the container. Syneresis occurs with most "flocculated" and/or "structured" (i.e., those containing a thickener in the continuous phase) dispersions.

Syneresis may be predicted from measurement of the yield value (using steady-state measurements of shear stress as a function of shear rate) as a function of time, or by using oscillatory techniques whereby the storage and loss modulus are measured as a function of strain amplitude and frequency of oscillation.

The oscillatory measurements are perhaps more useful, since to prevent separation the bulk modulus of the system should balance the gravity forces that is given by $h\rho\Delta g$, where h is the height of the disperse phase, $\Delta\rho$ is the density difference, and g is acceleration due to gravity.

The bulk modulus is related to the storage modulus G'. A more useful predictive test is to calculate the cohesive energy density of the structure E_c, which is given by the following equation (see Chapter 20):

$$E_c = \int_0^{\gamma_{cr}} G'\gamma \mathrm{d}\gamma = \frac{1}{2}G'\gamma_{cr}^2 \tag{21.5}$$

The separation of a formulation decreases with increase in E_c. This is illustrated in Figure 21.2, which shows schematically the reduction in percentage separation with increase in E_c. The value of E_c required to stop complete separation depends on the particle or droplet size distribution, the density difference between the particle or droplet and the medium, as well as on the volume fraction ϕ of the dispersion.

21.1.6
Examples of Correlation of Sedimentation or Creaming with Residual (Zero Shear) Viscosity

21.1.6.1 Model Suspensions of Aqueous Polystyrene Latex

The sedimentation rate is a complex function of the volume fraction ϕ. This was tested using polystyrene (PS) latex suspensions with radius $R = 1.55$ μm in 10^{-3} mol dm^{-3} NaCl [2].

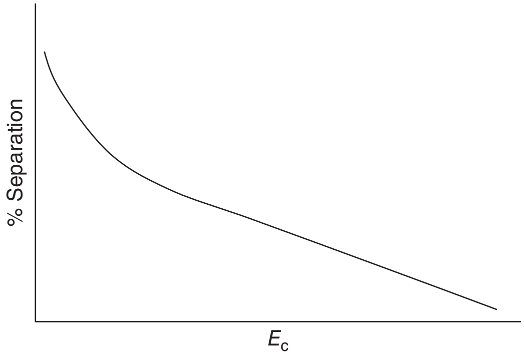

Figure 21.2 Schematic representation of the variation of % separation with E_c.

It may be possible to correlate the change in the rate of sedimentation with increasing φ with the viscosity of the suspension, as predicted by the Dougherty–Krieger equation [3],

$$\frac{v}{v_o} \propto \frac{\eta_o}{\eta} \tag{21.6}$$

$$\frac{v}{v_o} = \alpha \frac{\eta_o}{\eta} \tag{21.7}$$

where α is a constant.

$$\frac{v}{v_o} = \left[1 - \left(\frac{\varphi}{\varphi_p}\right)\right]^{-[\eta]\varphi_p} \tag{21.8}$$

where ϕ_p is the maximum packing fraction and $[\eta]$ is the intrinsic viscosity.

Equation (21.8) was tested for polystyrene dispersions, as illustrated in Figure 21.3.

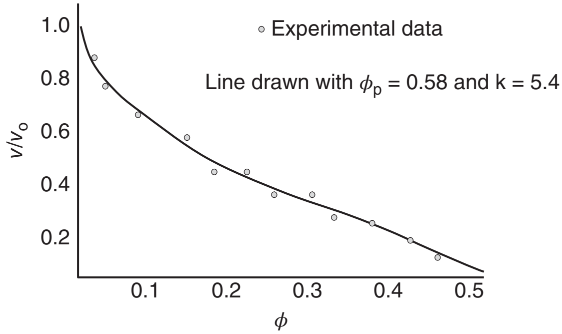

Figure 21.3 Variation of sedimentation rate with volume fraction for polystyrene dispersions.

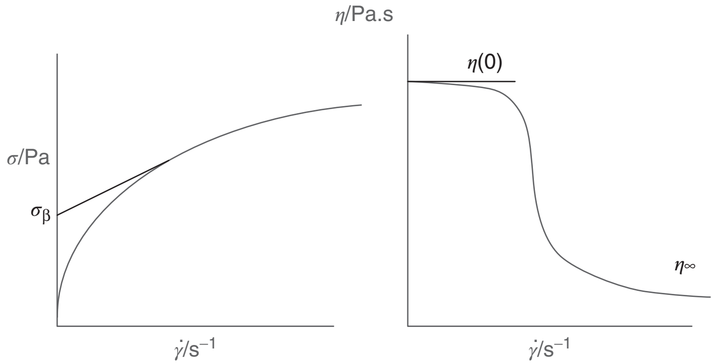

Figure 21.4 Flow behaviour of ''thickeners.''

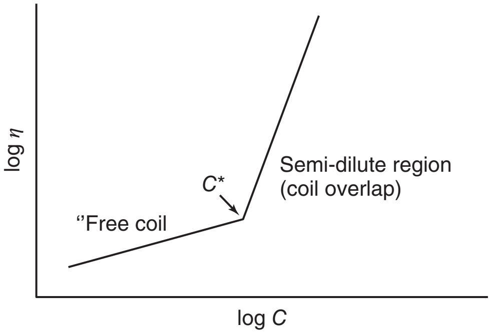

Figure 21.5 Variation of log η with log C.

21.1.6.2 Sedimentation in Non-Newtonian Liquids

To reduce sedimentation, a high-molecular-weight material is usually added, such as hydroxyethyl cellulose or xanthan gum (Kelzan, Keltrol or Rhodopol). Above a critical concentration, C^*, such polymer solutions show non-Newtonian flow in aqueous solution; this is illustrated in Figure 21.4, which shows the variation of shear stress and viscosity with shear rate [1].

Figure 21.5 shows the variation of log η with log C to illustrate the onset of free coil overlap. Here, before overlap $\eta \propto C$, whereas after overlap $\eta \propto C^{3.4}$. Two limiting Newtonian viscosities are identified: (i) residual (zero shear) viscosity $\eta(0)$; and (ii) Newtonian high shear rate viscosity η_∞. $\eta(0)$ may be several order of magnitude (10^3–10^5) higher than η_∞, and such as high $\eta(0)$ can significantly reduce creaming or sedimentation.

21.1.6.3 Role of Thickeners

As mentioned above, thickeners reduce creaming or sedimentation by increasing the residual viscosity $\eta(0)$, which must be measured at stresses compared to those exerted by the droplets or particles (mostly less than 0.1 Pa). At such low stresses, $\eta(0)$ increases very rapidly with increase in ''thickener'' concentration;

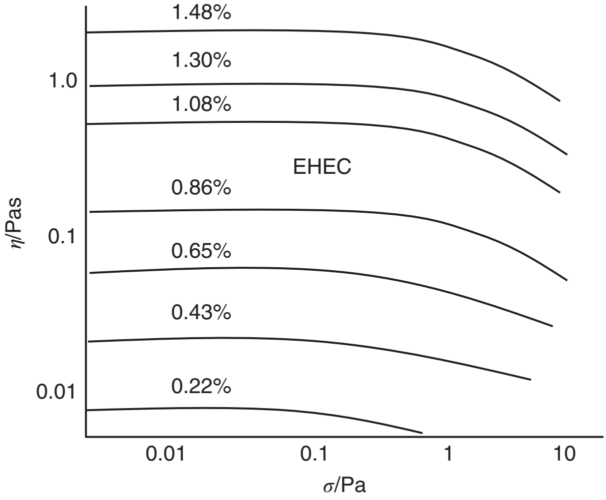

Figure 21.6 Constant stress (creep) measurements for PS latex dispersions as a function of EHEC concentration.

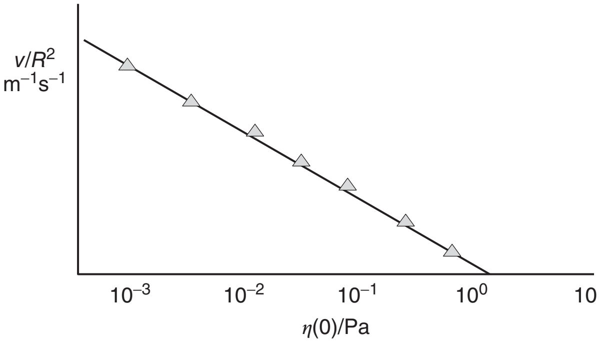

Figure 21.7 Sedimentation rate versus $\eta(0)$.

however, this rapid increase is not observed at high stresses, illustrating the need for measurement at low stresses (using constant stress or creep measurements). As an illustration of this, Figure 21.6 shows the variation of η with applied stress σ for ethyl hydroxyethyl cellulose (EHEC), a thickener that is applied in some formulations [2].

It can be seen that the limiting residual viscosity increases rapidly with increase in EHEC concentration. A plot of sedimentation rate for 1.55 μm PS latex particles versus $\eta(o)$ is shown in Figure 21.7 which shows an excellent correlation [2], in which case a value of $\eta(o) \geq 10$ Pa·s is sufficient for reducing the rate of sedimentation to 0.

21.1.6.4 **Prediction of Emulsion Creaming**

For the above purpose, some model emulsions were prepared using mixtures of oils and commercial surfactants. The oil phase of the emulsion consisted of 10 parts Arlamol HD (Isohexadecane; supplied by UNIQEMA, ICI), two parts of Estol 3603 (Caprylic/capric triglyceride, supplied by UNIQEMA), one part sunflower oil (Florasen 90, *Helianthus annus*; supplied by Florateck) and one part of Avocado oil (*Persea gratissima*; supplied by Mosselman).

Two emulsifier systems were used for the preparation of O/W emulsions. The first emulsifier was Synperonic PEF 127, an A-B-A block copolymer of poly(ethylene oxide), PEO (the A chains, were about 100 EO units each) and propylene oxide PPO (the B chain was about 55 PO units), supplied by UNIQEMA. The second emulsifier system was Arlatone V-100 (supplied by UNIQEMA), a nonionic emulsifier system composed of a blend of Steareth-100 (stearyl alcohol with 100 EO units), Steareth-2 (stearyl alcohol with 2 EO units), glyceryl stearate citrate, sucrose, and a mixture of two polysaccharides, namely mannan and xanthan gum (Keltrol F, supplied by Kelco). In some emulsions, xanthan gum was used as a thickener. All emulsions contained a preservative (Nipaguard BPX).

The rate of creaming and cream volume was measured using graduated cylinders. The creaming rate was assessed by comparing the cream volume V_c with that of the maximum value V_∞ obtained when the emulsion was stored at 55 °C. The time $t_{0.3}$ taken to reach a value of $V_c/V_\infty = 0.3$ (i.e., 30% of the maximum rate) was calculated [4].

All rheological measurements were carried out using a Physica UDS 200 (Universal Dynamic Spectrometer), using a cone-and-plate geometry with a cone angle of 2°. The emulsions were also investigated using optical microscopy and image analysis.

Figure 21.8 shows the results for creaming rates obtained at various temperature, using a 20/80 O/W emulsion stabilised with Synperonic PEF 127. It is clear from these data that $t_{0.3}$ decreases with the increase in temperature.

21.1.6.5 **Creep Measurements for Prediction of Creaming**

The most useful method for predicting creaming is to use constant stress (creep) measurements, from which the residual (zero shear) viscosity $\eta(0)$ can be obtained.

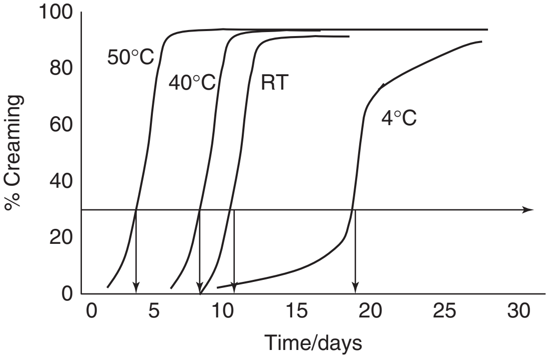

Figure 21.8 Percentage creaming versus time at various temperatures.

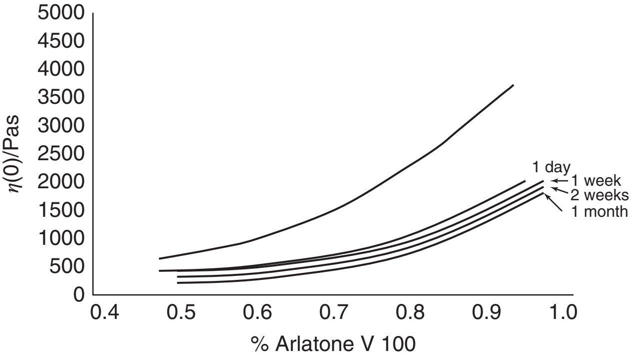

Figure 21.9 Variation of residual viscosity with Arlatone V-100 concentration at various storage times.

Results were obtained for 20/80 (v/v,%) emulsions as a function of Arlatone V-100 concentration, and are shown in Figure 21.9 after several periods of storage (1 day, 1 week, 2 weeks and 1 month). $\eta(0)$ showed a large decrease after one day which might have been due to equilibration of the structure, but the results after one and two and one month were close to each other. There was a significant increase in $\eta(0)$ when the Arlatone V-100 concentration was increased above 0.8 %. The creaming rate of the emulsion also showed a sharp decrease above 0.8% Arlatone V-100, indicating a correlation between $\eta(0)$ and creaming rate.

21.1.6.6 Oscillatory Measurements for Prediction of Creaming

One very useful method to predict creaming is to measure the cohesive energy density, as given by Equation (21.9),:

$$E_c = \frac{1}{2}\gamma_{cr}^2 G' \tag{21.9}$$

As an illustration of this, Figure 21.10 shows the variation of cohesive energy density E_c with Arlatone V-100 concentration. The results show clearly a rapid

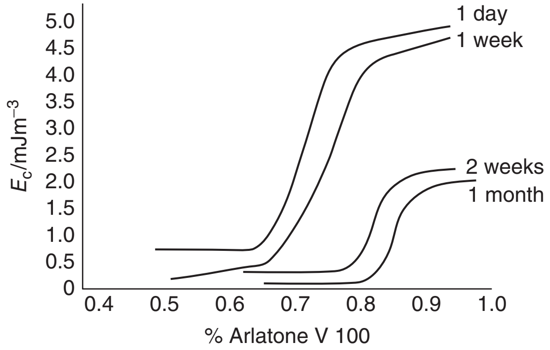

Figure 21.10 Variation of E_c with % Arlatone V-100 in the emulsion.

increase in E_c above 0.8% Arlatone V-100, with E_c seeming to show a decrease in value after storage for two weeks. This may have been due to a small increase in droplet size (as a result of some coalescence), which in turn resulted in a reduction in the cohesive energy density. Unfortunately, this small increase in droplet size could not be detected by microscopy as the change was very small.

21.2
Assessment and Prediction of Flocculation Using Rheological Techniques

21.2.1
Introduction

Steady-state rheological investigations may be used to investigate the state of flocculation of a dispersion. As mentioned in Chapter 10, weakly flocculated dispersions usually show thixotropy, and the change of thixotropy with applied time may be used as an indication of the strength of a weak flocculation. Unfortunately, as these methods are only qualitative the results cannot be used in a quantitative manner. This is due to the possible breakdown of the structure on transferring the formulation to the rheometer, and also during the uncontrolled shear experiment. Better techniques for studying the flocculation of a formulation include constant stress (creep) or oscillatory measurements. The structure of the flocculated system may be maintained by carefully transferring the sample to the rheometer, with minimum shear.

21.2.2
Wall Slip

As mentioned in Chapter 20, one very important point that must be considered in any rheological measurement is the possibility of ''slip'' during the measurements. This is particularly the case with highly concentrated dispersions, whereby the flocculated system may form a ''plug'' in the gap of the platens so as to leave a thin liquid film at the walls of the concentric cylinder or cone-and-plate geometry. This behaviour is caused by some syneresis of the formulation in the gap of the concentric cylinder or cone and plate. In order to reduce slip, roughened walls should be used for the platens, and a vane rheometer may also be used.

21.2.3
Steady-State Shear Stress-Shear Rate Measurements

This is by far the most commonly used method in many industrial laboratories. Basically, the dispersion is stored at various temperatures and the yield value σ_β and plastic viscosity η_{pl} are measured at various intervals. Any flocculation in the formulation should be accompanied by an increase in σ_β and η_{pl}.

A rapid technique for studying the effect of temperature changes on the flocculation of a formulation is to perform temperature sweep experiments, running the samples from perhaps 5 to 50 °C. The trend in the variation of σ_β and η_{pl} with temperature can rapidly provide an indication of the temperature range at which a dispersion will remains stable (over the same temperature range, σ_β and η_{pl} will remain constant).

21.2.4
Influence of Ostwald Ripening and Coalescence

If Ostwald ripening and/or coalescence occur simultaneously, σ_β and η_{pl} may change in a complex manner with storage time. Ostwald ripening and/or coalescence result in a shift of the particle size distribution to higher diameters, which has the effect of reducing σ_β and η_{pl}. If flocculation occurs simultaneously (this has the effect of increasing these rheological parameters), then the net effect may be either an increase or a decrease in the rheological parameters.

The above trend depends on the extent of flocculation relative to Ostwald ripening and/or coalescence. Therefore, the monitoring of σ_β and η_{pl} with storage time requires knowledge of Ostwald ripening and/or coalescence. Only in the absence of these latter breakdown processes can rheological measurements be used as a guide for assessing flocculation.

21.2.5
Constant Stress (Creep) Experiments

Basically, a constant stress σ is applied on the system and the compliance J (Pa^{-1}) is plotted as a function of time (see Chapter 20). These experiments are repeated several times, increasing the stress in small increments from the smallest possible value that can be applied by the instrument). A set of creep curves is produced at various applied stresses, and from the slope of the linear portion of the creep curve (when the system has reached steady state) the viscosity at each applied stress, η_σ, can be calculated. A plot of η_σ versus σ allows the limiting (or zero shear) viscosity $\eta(o)$ and the critical stress σ_{cr} (which may be identified with the "true" yield stress of the system) to be obtained (see also Chapter 4). The values of $\eta(o)$ and σ_{cr} may be used to assess the flocculation of the dispersion on storage.

If flocculation occurs on storage (without any Ostwald ripening or coalescence), the values of $\eta(o)$ and σ_{cr} may show a gradual increase with increase in storage time. As discussed in the previous section on steady-state measurements, the trend becomes complicated if Ostwald ripening and/or coalescence occur simultaneously, as both have the effect of reducing $\eta(o)$ and σ_{cr}.

The above measurements should be supplemented by particle size distribution measurements of the diluted dispersion (ensuring that no flocs are present after dilution) to assess the extent of Ostwald ripening and/or coalescence. Another complication may arise from the nature of the flocculation, however. If the latter occurs in an irregular fashion, so as to produce strong and tight flocs, $\eta(o)$ may increase while σ_{cr} may show some decrease, and this complicates the analysis of the results. In spite of these complications, constant stress measurements may provide valuable information on the state of the dispersion on storage.

To carry out creep experiments and ensure that a steady state is reached can be time-consuming. Typically, a stress sweep experiment is carried out whereby the stress is gradually increased within a predetermined time period to ensure that the steady state is almost attained, after which plots of η_σ versus σ can be established.

The above experiments are carried out at various storage times (perhaps every two weeks) and temperatures. From the change in $\eta(0)$ and σ_{cr} with storage time and temperature, information may be obtained on the degree and the rate of flocculation of the system. Clearly, the interpretation of these rheological results requires an expert knowledge of rheology, as well as measurements of particle size distribution as a function of time.

One major problem in carrying out the above experiments is sample preparation. When a flocculated dispersion is removed from the container, care must be taken not to disturb the structure, with minimum shear being applied when transferring the formulation to the rheometer. It is also advisable to use separate containers when assessing flocculation; in this case, a relatively large sample can be prepared and transferred to several separate containers, with each sample being used at a given storage time and temperature. Care must also be taken when transferring the sample to the rheometer, although if any separation does occur in the formulation, the sample can be gently mixed by placing it on a roller. It is advisable to use as minimum shear as possible when transferring a sample from the container to the rheometer; the preferred method is to use a ‘‘spoon,’’ or simply to pour it from the container. The experiment should be carried out without an initial pre-shear.

21.2.6
Dynamic (Oscillatory) Measurements

In oscillatory measurements, two sets of experiments are carried out, namely strain sweep measurements and oscillatory sweep measurement.

21.2.6.1 Strain Sweep Measurements

In this case, the oscillation is fixed (e.g., at 1 Hz) and the viscoelastic parameters are measured as a function of strain amplitude (see Chapter 20). G^*, G' and G'' remain virtually constant up to a critical strain value, γ_{cr}; this region is termed linear viscoelastic. Above γ_{cr} , G^* and G' start to fall whilst G'' starts to increase; this is termed the nonlinear region. The value of γ_{cr} may be identified with the minimum strain above which the ‘‘structure’’ of the dispersion starts to break down (e.g., the breakdown of flocs into smaller units and/or the breakdown of a ‘‘structuring’’ agent). From γ_{cr} and G', it is possible to obtain the cohesive energy E_c (in J m^{-3}) of the flocculated structure, using Equation (21.9). E_c may be used in a quantitative manner as a measure of the extent and strength of the flocculated structure in a dispersion; the higher the value of E_c the more flocculated is the structure.

Clearly, E_c depends on the volume fraction of the dispersion, as well as the particle size distribution (which determines the number of contact points in a floc). Therefore, for quantitative comparison between various systems, it must be ensured that the volume fraction of the disperse particles is the same, and that the dispersions have very similar particle size distributions. E_c also depends on the strength of the flocculated structure – that is, the energy of attraction between the droplets – and this in turn depends on whether the flocculation is in the primary or secondary minimum. Flocculation in the primary minimum is associated with a large attractive energy, and this leads to higher values of E_c when compared to values obtained for secondary minimum flocculation (weak flocculation). For a weakly flocculated dispersion, as is the case for the secondary minimum flocculation of an electrostatically stabilised system, the deeper the secondary minimum the higher the value of E_c (at any given volume fraction and particle size distribution of the dispersion).

With a sterically stabilised dispersion, weak flocculation can also occur when the thickness of the adsorbed layer decreases. Again, the value of E_c can be used as a measure of the flocculation; the higher the value of E_c, the stronger the flocculation. If incipient flocculation occurs (on reducing the solvency of the medium for the change to worse than θ-condition), a much deeper minimum is observed and this is accompanied by a much larger increase in E_c.

To apply the above analysis, an independent method must be available for assessing the nature of the flocculation. Rheology is a bulk property that can provide information on interparticle interaction (whether repulsive or attractive), and in order to apply it in a quantitative manner it is necessary to know the nature of these interaction forces. However, rheology can also be used in a qualitative manner to follow change in the formulation on storage.

Provided that the system does not undergo any Ostwald ripening and/or coalescence, the change in the moduli with time – and, in particular, the change in the linear viscoelastic region – may be used as an indication of flocculation. Strong flocculation is usually accompanied by a rapid increase in G', and this may be accompanied by a decrease in the critical strain above which the "structure" breaks down. This may be used as an indication of the formation of "irregular" and tight flocs which become sensitive to the applied strain. The floc structure will entrap a large amount of the continuous phase, and this leads to an apparent increase in the volume fraction of the dispersion, and hence an increase in G'.

21.2.6.2 **Oscillatory Sweep Measurements**

In this case, the strain amplitude is kept constant in the linear viscoelastic region (normally, a point far from γ_{cr}, but not too low, is taken; that is, in the midpoint of the linear viscoelastic region) and measurements are carried out as a function of frequency. Both, G^* and G' increase with increase in frequency such that ultimately, above a certain frequency, they reach a limiting value and show little dependence on frequency. G'' is higher than G' in the low-frequency regime, and it also increases with increase in frequency such that, at a certain characteristic frequency ω^* (which depends on the system) it becomes equal to G' (this is usually referred to as the cross-over point), after which it reaches a maximum and then shows a reduction with further increase in frequency.

From ω^*, the relaxation time τ of the system can be calculated:

$$\tau = \frac{1}{\omega^*} \tag{21.10}$$

The relaxation time may be used as a guide for the state of the dispersion. For a colloidally stable dispersion (at a given particle size distribution), τ increases with increases in the volume fraction of the disperse phase, ϕ. In other words, the cross-over point shifts to lower frequency with an increase in ϕ. For a given dispersion, τ increases with increase in flocculation, provided that the particle size distribution remains the same (i.e., no Ostwald ripening and/or coalescence).

The value of G' also increases with increase in flocculation, since the aggregation of particles usually results in liquid entrapment such that the effective volume fraction of the dispersion shows an apparent increase. With flocculation, the net attraction between the particles also increases, and this results in an increase in G'. The latter is determined by the number of contacts between the particles and the strength of each contact (which is determined by the attractive energy).

It should be mentioned that, in practice, it may not be possible to obtain the full curve due to the frequency limits of the instrument; measurements at low frequency are also time-consuming. Usually, part of the frequency dependence of G' and G'' is obtained, but in most cases the system is more elastic than viscous.

Most disperse systems used in practice are weakly flocculated and also contain ‘‘thickeners’’ or ‘‘structuring agents’’ to reduce creaming or sedimentation, and also to acquire the correct rheological characteristics for application; examples include handcreams and lotions. The exact values of G' and G'' required depend on the system and its application. In most cases a compromise must be made between acquiring the correct rheological characteristics for application and the optimum rheological parameters for long-term physical stability. The application of rheological measurements to determine these conditions requires a great deal of skill and an understanding of the factors that affect rheology.

21.2.7
Examples of the Application of Rheology for Assessment and Prediction of Flocculation

21.2.7.1 Flocculation and Restabilisation of Clays Using Cationic Surfactants

Hunter and Nicol [5] studied the flocculation and restabilisation of kaolinite suspensions using rheology and zeta-potential measurements. Figure 21.11 shows plots of the yield value (σ_β) and electrophoretic mobility (μ) as a function of cetyl trimethyl ammonium bromide (CTAB) concentration at pH = 9. σ_β increases in line with increases in CTAB concentration, reaching a maximum at the point where the mobility reaches zero (the isoelectric point, i.e.p., of the clay), and then decreases with further increases in CTAB concentration. This trend can be explained on the basis of flocculation and restabilisation of the clay suspension.

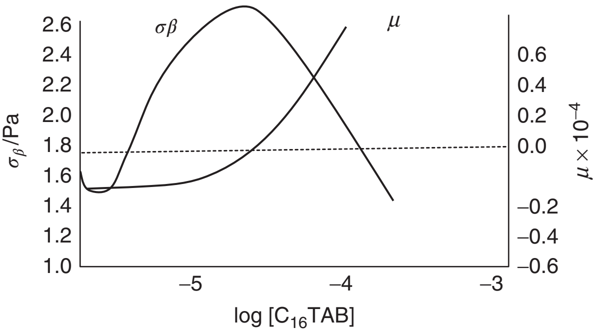

Figure 21.11 Variation of yield value σ_β and electrophoretic mobility μ with C_{16}TAB concentration.

The initial addition of CTAB caused a reduction in the negative surface charge of the clay (by the adsorption of CTA^+ on the negative sites of the clay), and this was accompanied by reduction in the negative mobility of the clay. When complete neutralisation of the clay particles occurred (at the i.e.p.), maximum flocculation of the clay suspension occurred and this was accompanied by a maximum in σ_β. On further increases in CTAB concentration, a further adsorption of CTA^+ occurred, and this resulted in charge reversal and restabilisation of the clay suspension. This was accompanied by a reduction in σ_β.

21.2.7.2 **Flocculation of Sterically Stabilised Dispersions**

Neville and Hunter [6] studied the flocculation of poly(methylmethacrylate) (PMMA) latex stabilised with poly(ethylene oxide) (PEO). Flocculation was induced by the addition of electrolyte and/or an increase in temperature. Figure 21.12 shows the variation of σ_β with increase of temperature at constant electrolyte concentration. In the figure, it can be seen that σ_β increased with increases of temperature, reaching a maximum at the critical flocculation temperature (CFT), and then decreased with further increase in temperature. The initial increase was due to the flocculation of the latex with increase of temperature, as the result of a reduction in solvency of the PEO chains with the increase in temperature. The

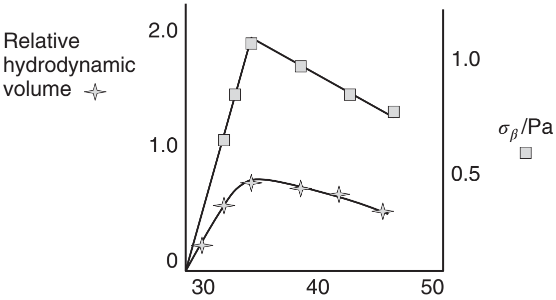

Figure 21.12 Variation of σ_β and hydrodynamic volume with temperature.

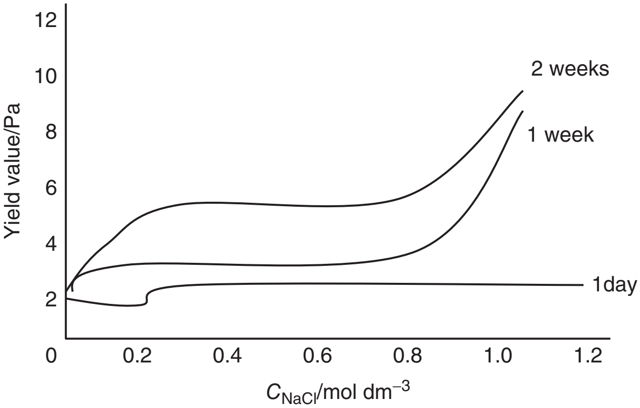

Figure 21.13 Variation of yield value with NaCl concentration.

reduction in σ_β after the CFT was due to a reduction in the hydrodynamic volume of the dispersion.

21.2.7.3 Flocculation of Sterically Stabilised Emulsions

Emulsions were prepared using an ABA block copolymer of poly(ethylene oxide)-poly(propylene oxide)-poly(ethylene oxide) PEO-PPO-PEO (Synperonic F127). Flocculation was induced by the addition of NaCl. Figure 21.13 shows the variation of the yield value, calculated using the Herschel–Bulkley model, as a function of NaCl concentration at various storage times. In the absence of NaCl the yield value did not change with storage time over a period of one month, indicating an absence of flocculation. However, in the presence of NaCl the yield value was increased with increases in storage time, and this change was very significant when the NaCl concentration was increased above 0.8 mol dm^{-3}.

The above increase in yield value indicated flocculation of the emulsion, and this was confirmed with optical microscopy. The smaller increase in yield value below 0.8 mol dm^{-3} NaCl was indicative of weak flocculation, and this could be confirmed by a redispersion of the emulsion by gently shaking. Above 0.8 mol dm^{-3} NaCl, the flocculation was strong and irreversible, and in this case the solvency of the medium for the PEO chains became poor, resulting in incipient flocculation.

Further evidence of flocculation was also obtained from dynamic (oscillatory) measurements. Figure 21.14 shows the variation of G' with NaCl concentration at various storage times. Below 0.8 mol dm^{-3} NaCl, G' showed a modest increase with storage time over a period of two weeks, indicating weak flocculation. However, above 0.8 mol dm^{-3} NaCl, G' showed a rapid increase in storage time, indicating a strong flocculation. This strong (incipient) flocculation was considered due to the reduction in solvency of the PEO chains (worse than θ-solvent), and this resulted in a strong attraction between the droplets, which were difficult to redisperse.

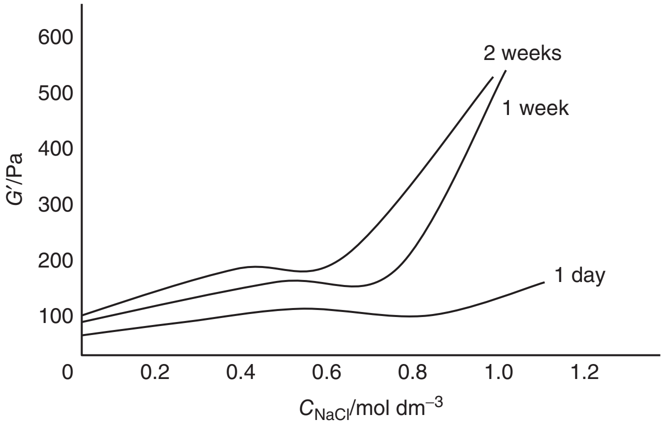

Figure 21.14 Variation of G' with NaCl concentration.

21.3
Assessment and Prediction of Emulsion Coalescence Using Rheological Techniques

21.3.1
Introduction

The driving force of emulsion coalescence is the thinning and disruption of the liquid film between the droplets [7–10]. When two emulsion droplets come into contact – perhaps in a cream layer or a floc, or even during Brownian collision – the liquid film between them undergoes some fluctuation in thickness such that the thinnest part of the film will have the highest van der Waals attractions, and this is the region where coalescence starts. Alternatively, the surfaces of the emulsion droplets may undergo fluctuation producing waves which may grow in amplitude; the strongest van der Waals attractions occur at the apices of these fluctuations, and coalescence occurs by further growth of the fluctuation. One may define a critical film thickness below which coalescence occurs.

21.3.2
Rate of Coalescence

The rate of coalescence is determined by the rate at which the film thins, and this usually follows a first-order kinetics,

$$N = N_o \exp(-Kt) \tag{21.11}$$

where N is the number of droplets after time t, N_o is the number at zero time, and K is the rate constant of coalescence.

Alternatively, the average droplet diameter d can be measured as a function of time:

$$d = d_o \exp(Kt) \tag{20.12}$$

Provided that the emulsion does not undergo any flocculation, the coalescence rate can be measured simply by following the number of droplets or average diameter as a function of time. For this, a given volume of the emulsion is carefully diluted into the Isotone solution of the Coulter counter, and the number of droplets is measured. The average diameter can be obtained using laser diffraction methods (e.g., with the Master Sizer). By following this procedure at various time periods, the coalescence rate constant K can be obtained.

Usually, log N or log d is plotted versus t, and the slope of the line in the initial period gives the rate of coalescence, K. Clearly, the higher the value of K the higher the coalescence of the emulsion. An accelerated test may be used by subjecting the system to higher temperatures; usually, the rate of coalescence increases with an increase of temperature (though this is not always the case). Care must be taken during the dilution procedure, particularly if the oil is significantly soluble (e.g., $>$10 ppm) in the Isotone solution or in the tank of the Master Sizer. In this case, the solution should be saturated with the oil before diluting the concentrated emulsion for droplet counting or sizing.

21.3.3
Rheological Techniques

21.3.3.1 Viscosity Measurements

In the absence of any flocculation, the coalescence of an emulsion results in a reduction of its viscosity. At any given volume fraction of oil, an increase in droplet size will result in a reduction of viscosity, and this is particularly the case for concentrated emulsions. Thus, by following the decrease in emulsion viscosity with time, information may be obtained on its coalescence. However, care should be exercised when applying simple viscosity measurements, particularly if flocculation occurs simultaneously (as this results in an increased viscosity). It is possible – at least in principle – to predict the extent of viscosity reduction on storage by combining the results of droplet size analysis (or droplet number) as a function of time with the reduction in viscosity during the first few weeks.

Freshly prepared emulsions with various droplet sizes are prepared by controlling the speed of the stirrer used for emulsification. The emulsifier concentration in these experiments should be kept constant, and care taken that there is no excess of emulsifier in the continuous phase. When the viscosity of these freshly prepared emulsions is plotted against the average droplet diameter, a master curve is produced that relates the emulsion viscosity to the average droplet size. The viscosity is seen to decrease monotonically with increases in the average droplet size.

By using the Coulter counter or Master Sizer, the rate of coalescence can be determined by plotting log of the average droplet diameter versus time in the first few weeks. This allows a prediction of the average droplet diameter over a longer period (e.g., 6–12 months); the predicted average droplet diameter can then be used to measure the viscosity reached on storage, using the master curve of viscosity versus average drop size.

The above procedure is useful for setting the limit of viscosity that might be reached on storage as a result of coalescence. With many creams, the viscosity of the system is not allowed to drop below an acceptable limit (which is important for application). However, the limit that may be reached after one year of storage can be predicted from viscosity and rate constant measurements made over the first few weeks.

21.3.3.2 Measurement of Yield Value as a Function of Time

As the yield value σ_β of an emulsion depends on the number of contacts between the droplets, any coalescence should be accompanied by a reduction in the yield value. However, this trend is only observed if no flocculation occurs (as this causes an increase in σ_β).

The above change was recently measured using O/W emulsions that were stabilised with an A-B-A block copolymer of poly(ethylene oxide) (A); poly(propylene oxide) (B); Synperonic NPE 127 (UNIQEMA). O/W emulsions (60/40) were prepared using 0.5, 1.0, 1.5, 2.0, 3, 4, and 5% emulsifier. Figure 21.15 shows the variation in droplet size with time at various Synperonic PEF 127 concentrations. At an emulsifier concentration > 2%, there was no change in droplet size with time, indicating an absence of coalescence; however, below 2% the droplet size was increased with time, indicating coalescence.

21.3.3.3 Measurement of Storage Modulus G′ as a Function of Time

This is perhaps the most sensitive method for predicting coalescence. G' is a measure of the contact points of the emulsion droplets, as well as their strength. Provided that no flocculation occurs (which would cause an increase in G'), any reduction in G' on storage indicates the presence of coalescence.

The above trend was confirmed using the emulsions described above. Emulsions containing <3% Synperonic PEF 127 showed a rapid reduction in G' compared to those containing > 3%, in which virtually no change in G' occurred over a two-week period (see Figure 21.16).

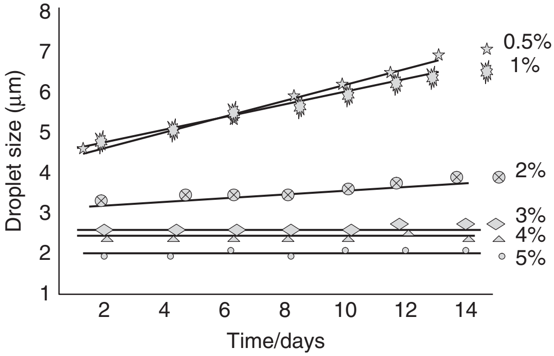

Figure 21.15 Variation of droplet size with time at various Synperonic PEF 127 concentrations.

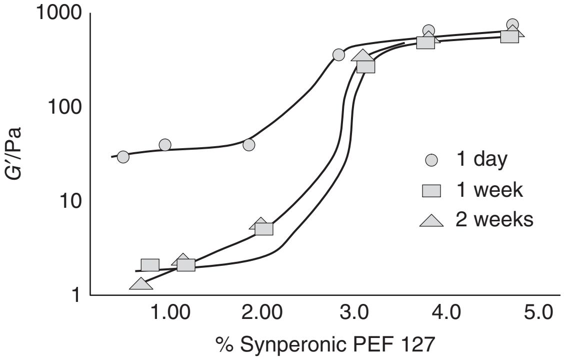

Figure 21.16 Variation of G' with Synperonic PEF 127 concentration at various storage times.

21.3.4
Correlation between Elastic Modulus and Coalescence

The correlation between the emulsion elastic modulus and coalescence rate can be easily represented by calculating the relative decrease in G' after two weeks,

$$\text{Relative decrease of } G' = \left(\frac{(G_{\text{initial}} - G_{\text{after 2 weeks}}}{G_{\text{initial}}}\right) \times 100 \tag{21.13}$$

Figure 21.17 shows the variation in the relative decrease of G' and relative increase in droplet size with Synperonic PEF127 concentration. The correlation between the relative decrease in G' and relative increase in droplet size as a result of coalescence is now very clear.

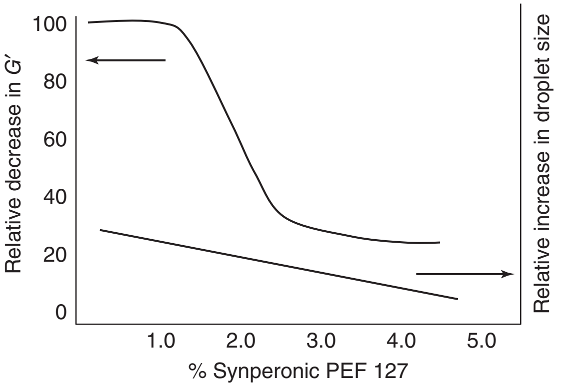

Figure 21.17 Correlation of relative decrease in G' with relative increase in droplet size.

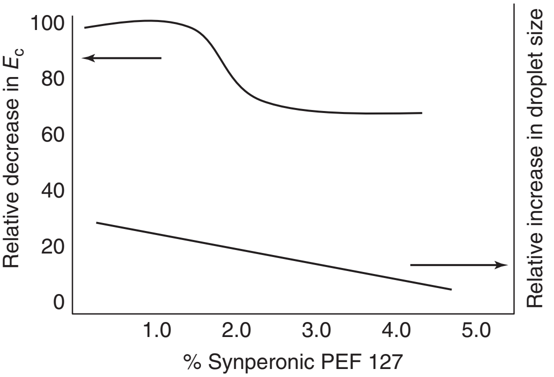

Figure 21.18 Correlation of relative decrease in E_c with relative increase in droplet size.

21.3.5
Cohesive Energy E_c

The cohesive energy E_c is the most sensitive parameter for assessment of coalescence,

$$E_c = (1/2)G'\gamma_{cr}^2 \tag{21.14}$$

where γ_{cr} is the critical strain above which the linear response (where G' is independent on the applied strain) changes to a nonlinear response. Any coalescence results in a decrease in the number of contact points, and causes a reduction in E_c.

Using the above-mentioned emulsions, E_c was found to decrease with an increase of droplet size (as a result of coalescence). However, at and above 3% Synperonic PE 127, E_c remained virtually constant, indicating an absence of coalescence. Figure 21.18 shows the variation of relative decrease of E_c with relative increase in droplet size; the correlation is clear.

References

1. Tadros, Th.F. (2012) *Dispersions of Powders in Liquids and Stabilisation of Suspensions*, Wiley-VCH Verlag GmbH, Weinheim.
2. Buscall, R., Goodwin, J.W., Ottewill, R.H., and Tadros, Th.F. (1982) *J. Colloid Interface Sci.*, **85**, 78.
3. Krieger, I.M. (1972) *Adv. Colloid Interface Sci.*, **3**, 111.
4. Salager, J.L. (2000) *Pharmaceutical Emulsions and Suspensions*, Marcel Dekker, New York.
5. Hunter, R.J. and Nicol, S.K. (1968) *J. Colloid Interface Sci.*, **28**, 250.
6. Neville, P.C. and Hunter, R.J. (1974) *J. Colloid Interface Sci.*, **49**, 204.
7. Tadros, Th.F. and Vincent, B. (1983) in *Encyclopedia of Emulsion Technology*, Vol. 1, Chapter 3 (ed. P. Becher), Marcel Dekker, New York.
8. Tadros, Th.F. (1994) *Colloids Surf., A*, **91**, 39.
9. Tadros, Th.F. (ed.) (2013) *Emulsion Formation and Stability*, Wiley-VCH Verlag GmbH, Weinheim.
10. Tadros, Th.F. (2004) *Adv. Colloid Interface Sci.*, **108–109**, 227.

Index

Formulation of Disperse Systems: Science and Technology, First Edition. Tharwat F. Tadros.